Harnessing demographic data for cross-scale analysis of forest dynamics



Jessica Needham

New College

University of Oxford

A thesis submitted for the degree of

Doctor of Philosophy

Trinity 2016

Acknowledgements

I have to begin by expressing my enormous gratitude to Sean McMahon who has been the most amazing mentor throughout my DPhil. Thank you for getting me onboard with this project even when I knew next to nothing of forest demography or programming, and for continuing to work with me despite the logistic challenges of different continents and time zones. I've learnt so much over the last three years and much of it would not have been possible without your continued support, enthusiasm and humour. Thank you for reminding me to think big at times when I was lost in the details of a problem.

Next, I would like to say thank you to my supervisors, Roosa Leimu-Brown, Jess Metcalf and Nick Brown for getting me started on my DPhil, and for giving me support and advice but also the freedom to explore and make mistakes before finding my 'niche'. Thank you to Andy Hector for stepping in as a supervisor in the last two years, and to the Hector-Turnball Ecology lab for providing an ecological community within the department. Thanks also to Keith Kirby for showing me Wytham Woods and for all the tea room discussions of its history and ecology.

Thank you to Joan Webber and everybody at Forest Research, where I spent several months during my first year. I had a lot of fun at FR and learnt to appreciate how incredible trees really are.

I would like to give special thanks to Cory Merow for interesting discussions and extensive, and often hilarious, comments on two of my manuscripts. Your guidance while I was writing my first paper was hugely appreciated.

None of this work would be possible without the CTFS-ForestGEO network. I had such an incredible time at the meetings in China; there were so many inspiring talks and meal time conversations that I cannot thank everyone individually. However, I'd like to mention Chia-Hao Chang-Yang, Dan Jonson and Marco Visser who have all shared ideas and contributed to my thinking.

A huge thank you to the PIs of the Wytham and BCI plots for allowing me to use the data. Especially the Wytham PIs, Nathalie Butt, Mike Morecroft,

Yadvinder Malhi and Toby Marthews–your enthusiasm for the Wytham projects and your feedback has been incredibly valuable. Huge thanks must also go to the field workers who collected all of the data that made this project possible.

I would like to thank Hal Caswell and his group in Amsterdam for contributing work on the matrix side of this project. Both trips out to visit were hugely productive and a lot of fun!

Thank you to the Gatsby Plant Science Network for inspiring me to study plants in the first place, and for the incredibly helpful training throughout my DPhil.

I would also like to thank Matthew Smith, Drew Purves and everyone in the Computational Biology group at Microsoft Research, Cambridge. I spent a fantastic three months there during my third year and learnt an enormous amount.

I have to say a huge thank you to Lynn and John Pilgrim for all of your kindness and friendship during my time in Oxford and for looking after me when I needed a break from the city.

The four years of my DPhil have been some of my happiest and for that I have to thank all of my incredible friends. A special mention to all of my wonderful and talented friends at New College and to two sets of fantastic housemates. I could not have dreamed of more lovely people to spend these four years with.

I would like to thank everyone in the Department of Plant Sciences, and especially Gem Toes, for help and support and for creating such a friendly environment to work in. Thank you to the Kellangdale lab for allowing a random ecologist to join you for cake and lab christmas lunches.

An especially big thank you goes to Emily Seward, Tom Hughes, Olga Sedelnikova, Michael Dunne, Ross Hendron, El Jaskowska, David Emms and Ellis O'Niell for being the absolute best group of people to share an office/next door office with. It has been a barrel of laughs.

I thoroughly enjoyed my viva and am grateful to my examiners Prof. David Coomes and Prof. Tim Coulson for excellent suggestions for future work.

I must give sincere thanks to Julia Bouska, without whom I would not be here.

Finally, I have to thank my family for their unwavering love and support. I could not have done this without you.

Harnessing demographic data for cross-scale analysis of forest dynamics

Jessica Needham
New College

Doctor of Philosophy, Trinity 2016

Forests are a critical biome but are under threat from unprecedented global change. The need to understand forest dynamics across spatial, temporal and biological scales has never been greater. Critical to this will be understanding how the demographic rates of individuals translate into patterns of species diversity, biomass and carbon turnover at much larger scales.

In this thesis, I present a modelling framework focussed on demography. In Chapter 2, I introduce methods for translating forest inventory data into population models that account for the size-dependency of vital rates and persistent differences in individual performance.

Outbreaks of forest pest and pathogens are increasing in frequency and severity, with consequences for biodiversity and forest structure. In Chapter 3, I explore the impact of ash dieback on the community dynamics of a British woodland, describing a spatially explicit individual based model that captures the effect of an opening of the canopy on local competitive interactions.

Chapter 4 introduces methods to infer the impact of historical deer herbivory on the juvenile survival of forest trees. The approach is generalisable and could be applied to any forest in which patterns of regeneration and community structure have been impacted by periodic disturbance (e.g. forest fires).

Finding meaningful ways of incorporating species diversity into global vegetation models is increasingly recognised as a research priority. In Chapter 5, I explore the diversity of demographic rates in a tropical forest community and identify groups of species with similar life history strategies. I discuss the potential of integrating demographic and physiological traits as a way to aggregate species for inclusion in global models.

In summary, translating measurements of individuals into population dynamics provides opportunities to both explore small-scale community responses to disturbance events, and to feed into much larger scale vegetation models.

Contents

1 Introduction **1**

1.1 The importance of forests and global threats 1

1.2 Forest Models 2

1.3 Thesis outline 6

2 A cross-scale demographic approach to forest dynamics **10**

2.1 Chapter Introduction 10

2.1.1 Authors 10

2.1.2 Author Contributions 10

2.2 Introduction 13

2.2.1 Forests and forest demographic models 13

2.2.2 Fine-scale demographic information for large scale inference . . . 13

2.2.3 A way forward through vital rates 14

2.3 Methods 15

2.3.1 Vital Rate Models 15

2.3.1.1 Growth 15

2.3.1.2 Survival 17

2.3.1.3 Fecundity 18

2.3.2 Integrating vital rates and filling in missing data 19

2.3.2.1 IPMs 19

2.3.2.2 Inverse modelling with IPMs 24

2.3.3 Sensitivity to transition probabilities between growth distributions 25

2.3.4 Site and species descriptions 26
2.4 Results 27
2.4.1 Two and three distribution growth models 27
2.4.2 Size-dependent survival models 27
2.4.3 Size-dependent fecundity models 29
2.4.4 Population level statistics 29
2.4.5 Sensitivity analysis: transition probabilities between growth classes 33
2.4.6 Recommendations for IPM specifications 33
2.5 Discussion 35
2.5.1 Towards scalable inference in forest dynamic models 35
2.5.2 Vital rates as biological and statistical processes 35
2.5.3 Validation of model outputs 38
2.5.4 Evolution, biodiversity, and carbon 39
2.5.5 Conclusions 40

3 Forest community response to invasive pathogens: the case of ash dieback in a British woodland 42

3.1 Chapter Introduction 42
3.1.1 Authors 42
3.1.2 Author Contributions 42
3.2 Summary 44
3.3 Introduction 45
3.3.1 Ash Dieback 46
3.3.2 Forecasting Forest Dynamics 46
3.4 Materials and Methods 47
3.4.1 Data 47
3.4.2 Models and simulations 49
3.4.3 Experimental design and analysis 56
3.5 Results 59

3.6 Discussion . . . 65
3.6.1 Conclusions . . . 70
3.7 Acknowledgements . . . 71
3.8 SUPPORTING INFORMATION . . . 71

4 The ghost of Bambi past: Inferring deer impacts from forest demography 74

4.1 Chapter Introduction . . . 74
4.1.1 Authors . . . 74
4.1.2 Author Contributions . . . 74
4.2 Introduction . . . 77
4.3 Methods . . . 78
4.3.1 Site Descriptions . . . 78
4.3.2 Data collection . . . 79
4.3.3 Vital Rates . . . 79
4.3.4 Population Projections . . . 81
4.4 Results . . . 85
4.4.1 Vital Rates . . . 85
4.4.2 Population Projections . . . 85
4.5 Discussion . . . 87
4.5.1 Conclusions . . . 88
4.6 Acknowledgements . . . 89

5 Diversity of demographic rates in tropical tree species 94

5.1 Chapter Introduction . . . 94
5.1.1 Authors . . . 94
5.1.2 Author Contributions . . . 94
5.2 Introduction . . . 97
5.3 Methods . . . 99

5.3.1 Site Descriptions . . . 99
5.3.2 Data collection . . . 100
5.3.3 Vital Rates . . . 100
5.3.4 Integral Projection Models . . . 102
5.3.5 Clustering of species into demographic types . . . 104
5.4 Results . . . 105
5.4.1 Overview of results . . . 105
5.4.2 Vital Rates . . . 105
5.4.3 Demographic Metrics . . . 107
5.5 Discussion . . . 108
5.5.1 Axes of life history . . . 109
5.5.2 Impact of El Niño on demographic rates . . . 110
5.5.3 Functional versus demographic traits . . . 111
5.5.4 Potential applications in large scale vegetation models . . . 112
5.5.5 Conclusions . . . 113

6 Discussion **120**

6.1 Demography for local and global analysis . . . 120
6.2 A novel demographic framework . . . 121
6.2.1 Vital rate models that can handle species diversity and individual differences . . . 121
6.2.2 Individuals to populations–accounting for persistent individual differences . . . 124
6.3 Future Directions . . . 124
6.3.1 Scaling up . . . 124
6.3.2 Integrating different data sources . . . 127
6.3.3 Linking demographic traits to functional types . . . 127
6.4 Conclusions . . . 128

A Chapter 2: Supplementary material **130**

A.1 Transition probabilities for three distribution growth model 130

A.2 Sensitivity to matrix size 130

A.2.1 Matrix size sensitivity results 131

A.3 Eviction of individuals from IPMs 132

B Chapter 2: Matrix calculations **143**

B.1 Notation 143

B.2 Occupancy times 144

B.2.1 Mixed distributions 145

B.3 Survivorship 145

B.3.1 Mixed distributions 145

B.4 Longevity Statistics 146

B.5 Passage Times 146

B.6 R code 147

B.6.1 Occupancy times 147

B.6.2 Survivorship 150

B.6.3 Longevity Statistics 151

B.6.4 Passage Times 152

C Chapter 2: Worked example **154**

C.1 Introduction 154

C.2 Data - loading and cleaning 155

C.2.1 Formatting 155

C.2.2 Correcting measurement errors 159

C.3 Vital rates 162

C.3.1 Growth 162

C.3.2 Survival 167

C.4 Transitions between growth classes 170

C.5 Recruit size and growth classes . . . 172
C.6 Vec-permutation IPM . . . 174
C.7 Inverse modelling fecundity . . . 178
C.8 IPM diagnostics . . . 186
C.8.1 Occupancy times . . . 186
C.8.2 Survivorship . . . 189
C.8.3 Longevities . . . 190
C.8.4 Passage Times . . . 191
C.9 Functions . . . 192
C.9.1 Data processing functions . . . 192
C.9.2 Diagnostic functions . . . 199
C.9.3 Growth functions . . . 205
C.9.4 Survival functions . . . 207
C.9.5 IPM construction functions . . . 208
C.9.6 Particle filter functions . . . 211
C.10 Stan files . . . 217
C.10.1 Growth . . . 217
C.10.2 Survival . . . 218

D Chapter 3: Supplementary material 220

D.0.1 Vital rates parameters . . . 238
D.0.2 Population sizes . . . 240
D.0.3 Basal areas . . . 243

E Chapter 4: Supplementary material 246

E.1 Vital rate parameter values for abundant Wytham species . . . 246
E.2 Inferred effect of deer on abundant Wytham species . . . 246

F Chapter 5: Supplementary material **248**

F.1 Diversity of growth and survival across species and through time 248

F.2 Shifts in demographic metrics through time 270

F.3 Vital rate parameter tables for 134 BCI species 292

F.4 Demographic metrics for 134 BCI species 301

Bibliography **309**

List of Figures

2.1 Simulated and observed *C. longifolium* individual trajectories 23

2.2 Two and three distribution growth models for three BCI species 28

2.3 Size-dependent survival models for three BCI species 30

2.4 Size-dependent fecundity models for three BCI species 31

2.5 Passage times and life expectancies for three BCI species 32

2.6 Sensitivity of passage times to transition probabilities between growth classes 34

3.1 Schematic of the individual based model 55

3.2 Stem maps of the Wytham plot at the start of example hypotheses tests . 57

3.3 BA of Wytham canopy species under each ash dieback mortality scenario 60

3.4 Population size of Wytham canopy species under each ash dieback mortality scenario 61

3.5 BA and population size of Wytham canopy species under each spatial scenario 63

3.6 BA and population size of Wytham canopy species under each abundance scenario 64

4.1 Periodicity of deer herbivory 83

4.2 Size-dependent survival model fit to abundant Wytham species 90

4.3 Two distribution growth model fit to abundant Wytham species 91

4.4 Inferred impact of deer browsing on juvenile survival of Wytham species . 92

4.5 Simulations results of Wytham populations with inferred levels of deer browsing 93

5.1 Parameter loadings from PCA on vital rate parameters of 134 BCI species 114

5.2 Eigenvalues from PCA on vital rate parameters of 134 BCI species 115
5.3 Positions of 134 BCI species in PCA space according to vital rate parameters 116
5.4 Mean vital rates from each demographic cluster 117
5.5 Position of 134 BCI species in PCA space in each census interval, clustered by demographic similarity 118
5.6 Life history trade-offs of 134 BCI species 119

A.1 DBH increment data for 134 BCI species 133
A.2 Sensitivity analysis of simulated populations to inversely estimated fecundity parameters 134
A.3 Population growth rates and stable size distributions for three BCI species 135
A.4 Occupancy times in size class and growth distribution combinations for three BCI species 136
A.5 Sensitivity analysis of passage times and life expectancies to transitions between growth distributions 137
A.6 Matrix size analysis: *P. copaifera* 138
A.7 Matrix size analysis: *C. longifolium* 139
A.8 Matrix size analysis: *G. intermedia* 140

D.1 Size distribution of Wytham species 220
D.2 Wytham weather data 221
D.3 Schematic of the size-dependent survival function 222
D.4 Survival function of each Wytham species 223
D.5 Histogram of DBH increment data from all Wytham species combined . . 224
D.6 Modelled growth distributions for each Wytham species 225
D.7 Inversely estimated size-dependent fecundity for each Wytham species . . 226
D.8 Schematic of size and growth IPM 227
D.9 Schematic of light environment transitions 228
D.10 Changes to BA of sub-canopy species in each mortality scenario 229
D.11 Changes to population size of sub-canopy species in each mortality scenario 230

D.12 Changes to BA and population size of sub-canopy species in each spatial test 231

D.13 Changes to BA and population size of sub-canopy species in each abundance test 232

D.14 Sensitivity analysis to fecundity parameters - BA and population size of canopy species 233

D.15 Sensitivity analysis to fecundity parameters - BA and population size of sub-canopy species 234

D.16 BA of canopy species separated by recruits and existing trees 235

F.1 Size-dependent survival models: 134 BCI species 259

F.2 Two distribution growth models: 134 BCI species 270

F.3 Passage times: 134 BCI species 281

F.4 Life expectancies: 134 BCI species 292

List of Tables

1.1 Summary of forest models 4

5.1 Parameter loadings from PCA on vital rate parameters of 134 BCI species 107

A.1 Analysis of *C. longifolium* pathways through the life cycle: two distribution growth model 132

A.2 Analysis of *C. longifolium* pathways through the life cycle: three distribution growth model 141

A.3 Two distribution growth model parameters for three BCI species 141

A.4 Three distribution growth model parameters for three BCI species 141

A.5 Survival parameters for three BCI species 141

A.6 Fecundity parameters for three BCI species 141

A.7 AIC values for two and three distribution growth models 142

D.1 Information on Wytham species 236

D.2 Relationship between competition and DBH increment for Wytham species 237

D.3 Survival parameters for Wytham species 238

D.4 Growth parameters for Wytham species 238

D.5 Fecundity parameters for Wytham species 239

D.6 Population size for each Wytham species in the 0% mortality scenario . . 240

D.7 Population size for each Wytham species in the 25% mortality scenario . 240

D.8 Population size for each Wytham species in the 50% mortality scenario . . 241

D.9 Population size for each Wytham species in the 75% mortality scenario . . 241

D.10 Population size for each Wytham species in the 100% mortality scenario . . 241

D.11 Population size for each Wytham species in the spatial test including *F. excelsior* in spatial randomisation 241

D.12 Population size for each Wytham species in the spatial test excluding *F. excelsior* from spatial randomisation 242

D.13 Population size for each Wytham species in the abundance test with equal starting abundances of *A. pseudoplatanus* and rare 'canopy' species . . . 242

D.14 Population size for each Wytham species in the abundance test with low starting abundance of *A. pseudoplatanus* 242

D.15 Population size for each Wytham species in the abundance test with *A. pseudoplatanus* absent 242

D.16 BA of each Wytham species in the 0% mortality scenario 243

D.17 BA of each Wytham species in the 25% mortality scenario 243

D.18 BA of each Wytham species in the 50% mortality scenario 243

D.19 BA of each Wytham species in the 75% mortality scenario 244

D.20 BA of each Wytham species in the 100% mortality scenario 244

D.21 BA of each Wytham species in the spatial test including *F. excelsior* in spatial randomisation 244

D.22 BA of each Wytham species in the spatial test excludig *F. excelsior* from spatial randomisation 244

D.23 BA of each Wytham species in the abundance test with equal start sizes of *A. pseudoplatanus* and 'rare canopy' species 245

D.24 BA of each Wytham species in the abundance test with reduced start size of *A. pseudoplatanus* 245

D.25 BA of each Wytham species in the abundance test with *A. pseudoplatanus* absent 245

E.1 Survival parameters: abundant Wytham species 246

E.2 Growth parameters: abundant Wytham species 246

E.3 Estimates of historic deer impacts on abundant Wytham species 247

F.1 BCI survival parameters: 134 species 292

F.2 BCI growth parameters: 134 species 296

F.3 BCI Passage Times: 134 species 301
F.4 BCI Passage Times and Life Expectancies: 134 species 306

Chapter 1

Introduction

1.1 The importance of forests and global threats

Forests are a critical ecosystem Forests cover 31% of global land area (Keenan *et al.*, 2015), host the majority of terrestrial biodiversity, and are fundamental to many critical ecosystem services from water regulation to soil formation (Millennium Ecosystem Assessment, 2005). At least 10 million people depend on forests for direct employment, a figure predicted to rise as the world's population increases and there is an increase in demand for wood and non-wood forest products (FAO, 2010). Further, the response of forests to anthropogenic-driven environmental change will be critical to determining future climates (Friedlingstein *et al.*, 2006).

Threats to forests Globally, forests are under threat from land use change (Hurtt *et al.*, 2006), invasive pests and pathogens (Hicke *et al.*, 2012) and a rapidly changing climate (Van Mantgem & Stephenson, 2007). Between 2000 and 2012, there was a net loss of 1.5 million square kilometres of forest across the globe, with the largest losses from tropical regions (Hansen *et al.*, 2013). Results from a meta-analysis of 138 studies show that the consequences of forest conversion and degradation for tropical biodiversity are overwhelmingly negative, with degraded forests having lower biodiversity compared with primary forest for nearly all regions and taxonomic groups studied (Gibson *et al.*, 2011).

There are feedbacks between the different threats facing forests; outbreaks of forest pests and pathogens have risen sharply in the last few decades, e.g. (Kurz *et al.*, 2008; Cobb *et al.*, 2012), and will likely continue to rise due to global trade of forest products (Brasier, 2008) and the impact of climate on both pests and forests. Increased temperatures across much of the Earth has already led to range shifts in a number of insect herbivores, e.g. (Jepsen *et al.*, 2008; Cudmore *et al.*, 2010) along with documented cases of increased

winter survival (Battisti *et al.*, 2005) and expected additional generations per year in some species (Bale *et al.*, 2002). Targeted tree species may also be more susceptible to pest and pathogen attack due to lowered resilience from climate induced stress (Jactel *et al.*, 2012), exacerbating the effects of pest and pathogen outbreaks. The cumulative impact of land use change, climate, and the rise in invasive pests and pathogens could be enough to drive forests to tipping points beyond which structure and functioning are irreversibly altered (Reyer *et al.*, 2015).

As sessile organisms with long generation times, responses to these challenges will be determined in large part by demographic rates e.g. adult survival (Williams *et al.*, 2013), and the ability of seeds and seedlings to successfully recruit (Walck *et al.*, 2011). A demographic approach is therefore required to predict how forests will respond to global change. It is essential that we understand how forest communities are organised; the impact of species differences in demography on competitive interactions, how these interactions play out to determine patterns of biodiversity, and the effect of biodiversity on biogeochemical cycling over large spatial and temporal scales.

This thesis presents a novel workflow for bridging the gap between descriptions of individual-level vital rates and population projections; something that will be critical for predicting how forests will respond to global change (land use change, climate change and the increase in disturbance from pests and pathogens) and the impact on biodiversity and future climates. Before introducing the work of this thesis, I give a brief overview of forest modelling, describing some of the important breakthroughs over the years and the current state of the field.

1.2 Forest Models

A brief history: from yield tables to Global Vegetation Models Due to the scales of interest and the difficulty of experimentation in natural systems, models are frequently used to explore ecological principles underlying forest structure and to predict responses of forest systems to future global change.

There is a long history of forest models, beginning more than a century ago with forest managers predicting yields in monocultures right up to the current generation of Global Vegetation Models (GVMs).

Stand models Models of tree growth were initially developed by forest managers to predict yields of economically important timber species. These were often simple yield

tables based on predicted growth rates for same-aged single-species stands (e.g. Payandeh & Papadopol, 1994).

But increased computational power in the later half of the 20th century allowed models of mixed age/species stands to be developed, enabling an exploration of the ecological principles underlying forest dynamics. For example, distributional models track the change in the distribution of sizes within a stand, either treating time as continuous via regressions (Alder & Silva, 2000), or discrete via matrix models (Kolbe *et al.*, 1999; Zuidema *et al.*, 2009). Integral Projection Models (IPMs) (cf. Easterling *et al.*, 2000; Merow *et al.*, 2014a) use discrete time steps but treat the distribution of sizes as continuous (for applications to forest trees see Zuidema *et al.* (2010); Metcalf *et al.* (2009)).

Other stand models include spatial structure, dividing the stand into a series of subplots, each of which has a spatial location and its own dynamics. Subplots transition to different states (e.g. total basal area (BA)) based on probabilities relating to the state of neighbouring subplots (e.g. Wissel, 1992; Frelich *et al.*, 1993).

Gap models The 1970's saw the introduction of JABOWA, the first gap model (Botkin *et al.*, 1972), which simulates the fates of individual stems through stochastic models of survival, growth and recruitment.

JABOWA led to the development of a whole range of new individual based models which became increasingly complex as computational power and understanding of physiological processes increased (e.g. Pacala *et al.*, 1993, 1996). While initial gap models were applied to temperate forests, Doyle (1981) applied the FORICO model to 36 common species in Puerto Rico. Later, the FORMIND model was developed which aggregates species into plant functional types in order to model whole communities in tropical forests (Köhler & Huth, 1998; Fischer *et al.*, 2016). For a summary of some of the important innovations in gap models see table 1.1.

Table 1.1: Summary of forest models

Model	Citation	Modelling Unit	Geography	Approach
JABOWA	Botkin *et al.* (1972)	Individual trees	North America	Canonical gap model–horizontally homogeneous gaps of large tree size in which large individuals shade smaller individuals
FORICO	Doyle (1981)	Individual trees	Puerto Rico	One of the first gap models applied to a tropical system–modelled 36 common species
FORSKA	Prentice & Leemans (1990)	Individual trees	Europe	More realistic representation of crown structure–flat discs replaced with cylinders
FORMIX	Bossel & Krieger (1991)	Cohorts in vertical layers	Malaysia	First cohort approach with canopy classes–cohorts are a mix of species
ZELIG	Urban *et al.* (1991)	Individual trees	Temperate North American forests and circumpolar boreal forests	First gap model to introduce interactions between gaps–trees can shade other trees in neighbouring patches. Applied to large geographic regions
SORTIE	Pacala *et al.* (1993, 1996)	Individual trees	North America	Individuals have explicit coordinates allowing detailed representation of light environments
FORMIX2	Bossel & Krieger (1994)	Cohorts in vertical layers	Malaysia	Vertically and horizontally structured distance dependent model used to evaluate management practices
ForClim	Bugmann (1994)	Cohorts	Europe	Stochasticity in recruit size is removed so that all individuals of the same species that recruit in a given year are identical, and since growth is deterministic they remain the same allowing cohorts rather than individuals to be modelled. Used to model sensitivity to climate change
ARCADIA	Williams (1996)	Individual trees	North America	Process based model with patches occupied by single trees whose dynamics are determined by their C budgets (photosynthesis, partitioning, etc.)
FORMIX3	Huth *et al.* (1998)	Cohorts in vertical layers	Malaysia	Interactions between patches through the death of a large tree causing damage to trees in neighbouring patches. Species are grouped into functional types

Continued on next page

Table 1.1 –continued from previous page

Model	Citation	Modelling Unit	Geography	Approach
FORMIND	Köhler & Huth (1998); Fischer *et al.* (2016)	Cohorts	Tropical forests	Models cohorts as individuals grouped by size and functional group using a mechanistic approach that includes carbon fixation and respiration rates
Ecosystem Demography (ED) Model	Moorcroft *et al.* (2001)	Cohorts	South America	Size and age structured approximation of a stochastic ecosystem model allows scaling up to large regions without simulating individual stems
PPA/IDT	Strigul *et al.* (2008); Purves & Pacala (2008); Purves *et al.* (2007); Adams *et al.* (2007)	Individual trees	North America	Trees divided into understory and canopy based on species specific height thresholds. Canopy crowns fill all available space
ED v.2	Medvigy *et al.* (2010)	Cohorts	North America	Coupled to a climate model to explore how environmental variability impacts carbon dynamics and community composition

Global Vegetation Models The link between climate and vegetation has been recognised for over a century (von Humboldt, 1849) but models combining vegetation dynamics with biogeochemistry and biophysics were not developed until the late 1980's when the integration of these fields led to Dynamic Global Vegetation Models (DGVMs) or Terrestrial Biosphere Models (TBMs) (e.g. Foley *et al.*, 1996). Despite much progress in the field over the last two decades, even current models diverge widely in how they predict the feedback between vegetation and climate will play out to influence future climate (Cramer *et al.*, 2001; Friedlingstein *et al.*, 2006; Sitch *et al.*, 2008; Galbraith *et al.*, 2010; Friend *et al.*, 2014). Since the end of the 20th century the threat of climate change has made decreasing the uncertainty in these models a research priority.

Divergences in DGVM predictions of future climate are partly due to the differences in the way that models treat intermediate levels of organisation, i.e. how they scale from physiological processes in individuals to biogeochemical cycling across large geographic areas. Until recently, DGVMs have typically modelled biogeochemical cycling with little consideration of biodiversity or its impact on ecosystem functioning e.g. (King *et al.*, 1997; Cox, 2001). The inclusion of demography in DGVMs has been highlighted as one way to reduce uncertainty in model outcomes (Moorcroft, 2006; Purves & Pacala, 2008).

1.3 Thesis outline

This thesis presents flexible and generalisable methods for modelling forest dynamics from a demographic perspective. Using commonly available forest inventory data I present novel vital rate models, and methods to combine them into analytically tractable models of population dynamics. While these methods have many potential applications, in this thesis I present two case studies; an exploration of the impact of host specific pathogens on community dynamics, and a study examining our ability to infer historic levels of deer browsing using only data from recent forest plot censuses. Finally, the methods are applied to over 100 tropical forest species to explore the diversity in life history strategies and to identify groups of demographically similar species.

Making best use of available data As outlined above, one of the challenges currently facing forest ecologists is how to scale up from measurements at the individual level to an understanding of forest dynamics at the population level. Models need to encompass the entire life cycle and yet data on crucial ontogenic stages are often scarce or missing. This is particularly true in the tropics where the majority of species occur at low densities. And yet, to project entire communities forward in time we need to include all stems.

Developing methods that deal with incomplete data sets and account for rare species is therefore critical for a robust, demographic approach to vegetation modelling.

Two data sets are introduced in this thesis. The first is the permanent 50 ha forest plot on Barro Colorado Island (BCI), Panama, in which all individuals greater than 1 cm diameter at breast height (DBH) within the plot have been mapped and measured beginning in 1981-1983 and then every five years from 1985 onwards. BCI is a part of the Smithsonian's Center for Tropical Forest Science-Forest Global Earth Observatory (CTFS-ForestGEO) network of plots. There are currently 63 plots located in 24 countries across the world. However, BCI is the oldest plot; many plots in the CTFS-ForestGEO network, and other similar networks, have data for less than two decades, which is only a small fraction of the potential life span of many forest species.

The other data set used in this thesis is more typical of the data usually available for studies of forest dynamics. Wytham Woods, UK, is a more recent addition to the CTFS-ForestGEO network. The plot was established in 2008 and has had only one other census, completed two years later in 2010. As a result of this short census interval, few mortality events were recorded, especially for larger stems, which complicates attempts to model population dynamics. However, while temporally limited, it includes measurements for nearly 20,000 stems located in a single contiguous 18 ha plot, making it possible to develop spatially explicit models that include local competitive interactions.

Bridging the scales in forest modelling Chapter 2 presents the methods for scaling from individuals to populations. It begins with descriptions of vital rate models which are used to capture growth, survival and fecundity in biologically meaningful ways, using only DBH measurements from forest inventory data. I then show how to combine vital rate models into IPMs which capture critical temporal correlations in individual vital rates. Population models need to encompass all life cycle stages but this can be difficult when, as mentioned previously, even the longest running forestry data sets do not capture the full life cycle of many long-lived tree species. Further, tracking individual seed production and/or the germination and survival of seeds is extremely challenging logistically, given the high fecundity and high seedling mortality common among tree species. IPMs can be used to inverse model parts of the life cycle that are informed by few data. In an inverse model, model parameters are adjusted based on the fit of model outputs to observed data. In chapter 2, I show how to inverse model fecundity when data on seeds and seedlings are missing. This involves using population level output from IPMs to infer per capita rates of reproduction. However, the method can also be used for other parts of the life cycle, such as adult senescence which is described in Chapter 3.

Finally, I demonstrate analysis of these IPMs, showing how to extract key population level outputs such as passage times to key life cycle stages, expected longevities, population growth rates and stable size distributions. These metrics are useful not only for answering questions relating to ecological and evolutionary theory, but also as a way of validating model outputs and informing management and conservation policies. Methods in this chapter are applied to data for three abundant species from the permanent forest plot on BCI.

Projections of a woodland community faced with ash dieback disease Chapter 3 is an application of the workflow exploring the impact of disease disturbance on local community dynamics. Using data from a British woodland in Oxfordshire (the Wytham Woods data set), I show possible outcomes of an epidemic of ash dieback. This disease, caused by the fungal pathogen *Hymenoscyphus fraxineus*, threatens common ash, *Fraxinus excelsior*, across much of its European distribution. In this chapter I use vital rate parameters inferred from inverse modelling with IPMs to parameterise a spatially explicit individual based model (IBM) that can model the interactions of multiple species within the community. Results are of interest from a management and conservation perspective, since *F. excelsior* is locally dominant across much of Britain and parts of Europe. However, the work also demonstrates how we can use models to explore the effect of community structure–species abundances and spatial associations–on outcomes of succession. Given the global increase in pest and pathogen disturbance events, it is important to understand the mechanisms determining community response.

Using models to infer unmeasured variables Grazing by large herbivores has the potential to alter community composition and forest structure through its impact on regeneration and survival of juvenile trees. In Chapter 4, I show how to infer the historic impact of deer grazing on demographic rates using recent census data from Wytham Woods. I construct IPMs for the most abundant species which can be used for population projections. By assuming a simple model of deer herbivory in which juvenile survival is reduced in proportion to 'deer effect', I project initial populations forward 50 years and infer the sequence of deer browsing effects most likely to have given rise to the observed populations recorded in the census data. For all but one species the simulated populations are a good match to the observed populations, suggesting the potential of this method to infer many unknown historic disturbance events, from cyclones to fire regimes.

Demography as traits In attempts to explain patterns of species richness and coexistence mechanisms, much previous work has explored how species are distributed across a continuum of life history strategies resulting from variation in functional traits. In Chapter 5, I treat demographic rates as traits. I firstly explore the diversity of life history strategies across 134 species from BCI, fitting growth and survival models and then obtaining life expectancies and passage times to key life cycle stages for each species. Both the variation across species and the temporal variation within a species are described. Finally I use principal component analysis to identify groups of demographically similar species and discuss how this approach to aggregating species might be one way in which demographic models at small scales can inform large scale vegetation models.

Discussion In the discussion, I bring together the work from previous chapters to discuss how we can use demographic data from forest inventories for inference across geographic and temporal scales. At the local scale, we can explore forest response to disturbances, either projecting whole communities forward in time under various disturbance scenarios, or inferring the impacts of historic disturbance events using patterns in the current data. At larger scales, we can compare the vital rates of species from across forest types and identify groups of demographically similar species. Clustering species in this way might be one approach to incorporating species diversity into global vegetation models.

Chapters are written using the collective pronoun 'we' since the work for these chapters was carried out in collaboration with co-authors. An author contribution section is provided at the start of each chapter. As chapters are written as stand-alone papers for publication, there is some repetition of material.

Chapter 2

A cross-scale demographic approach to forest dynamics

2.1 Chapter Introduction

In this chapter I introduce the modelling framework that forms the basis for work in subsequent chapters. I explain the need for the inclusion of demography in forest modelling but also some of the difficulties in capturing the full life cycle of long-lived, slow-growing organisms. I then present methods that address some of these difficulties. By combining biologically informed vital rates models, fit to simple forest census data, I demonstrate how to construct population level models that encompass the full life cycle, and, critically, the persistent variation between individuals that drives community structure. The methods are demonstrated for three species from Barro Colorado Island, Panama, and a complete worked example with R code is provided in Appendix C.

2.1.1 Authors

Jessica Needham, Cory Merow, Chia-Hao Chang-Yang, Hal Caswell & Sean M. McMahon

2.1.2 Author Contributions

JN and SM conceived of the study. JN carried out the analysis. CHCY contributed code for the Stan MCMCs. HC provided detailed notes on the matrix algebra which JN translated into Appendix B and Appendix C. JN wrote the manuscript. CM and SM provided detailed comments on the manuscript.

At the time of thesis submission this manuscript was about to be submitted.

Abstract

Forests drive much of the Earth's terrestrial carbon cycle and host the majority of terrestrial biodiversity. Models that predict the future of Earth's forests largely rely on coarse approximations of biodiversity, with species rich ecosystems often reduced to a small number of vegetation types. Building models that incorporate information on individuals, populations, and communities, however, is challenging due to features of the data collected, a miss-match between mechanisms and scales, and the sensitivities of output to model assumptions and behaviours.

Methods We present a modelling framework that enables critical variation both between and within species to be incorporated into population projections. Our models are analytically tractable, producing population level demographic metrics with minimal computational effort. We employ a survival model that accounts for the different patterns of size-dependent mortality in small and large individuals by fitting two separate curves. Similarly, our growth model includes multiple distributions, which enables us to construct Integral Projection Models (IPMs) that move individuals between sizes and growth distributions. Unlike traditional IPMs, these IPMs capture the temporal autocorrelation in individual variation critical to structuring forest communities. We demonstrate our methods for three tropical forest species with distinct life-history strategies, and provide a fully worked example with complete code in Appendix C.

Results Vital rate models capture the higher growth rates and survival probabilities of the two canopy species along with the high turnover of individuals in the understory species. From the IPMs we extract expected longevities, passage times to, and occupancy time in, key life cycle stages, conditional on starting size and growth rate. We show how population-level metrics from IPMs are sensitive to IPM dimensions and estimates of transition probabilities between growth distributions.

Implications By combining biological knowledge with well-established features of a modelling platform, we demonstrate that information at fine scales can be retained and appropriately applied at higher scales of organisation, answering questions about populations and communities from individual stem demography. Scaling up from the individual to the ecosystem via intermediate levels of organisation will be crucial for reducing uncertainty in predictions generated by terrestrial biosphere models.

2.2 Introduction

2.2.1 Forests and forest demographic models

Forests store 30% of terrestrial carbon, provide important resources for humans (FAO, 2010), and are home to two thirds of terrestrial biodiversity (Millennium Ecosystem Assessment, 2005). Yet globally, forests are under threat from human land use change, native and non-native pests and pathogens, and a shifting climate. The need to understand forest dynamics across spatial, temporal, and biological scales has never been greater (Purves & Pacala, 2008). Large datasets are increasingly available to develop understanding across biomes, but translating those measurements into insights regarding current and future forest dynamics remains a daunting challenge. Demographic models are a promising way forward, as they take advantage of these large datasets and can build larger-scaled understanding of forest dynamics while retaining important local-scale mechanisms in their structures.

Although data relevant to demographic change in forests are most commonly collected at the scale of the individual and can be extensive, efforts to extrapolate local mechanisms to larger scales need to address the challenge of information gaps in these data. Although, taking robust data on the most common species with complete knowledge of life-history suffices for questions regarding biomass, this approach will not answer the pressing questions concerning diversity and community composition. Rare species comprise the majority of the diversity in most systems, and poorly measured long-lived and large trees drive regeneration, carbon fluxes, and other key ecosystem properties.

A potential pathway towards successfully modelling complete communities would be through building demographic models from extensive permanent plot data, where individual stems are tagged, mapped and measured. Challenges to using these data, however, are that sampling uncertainty occurs, the data are often highly skewed to common species of small sizes, and large gaps exist in information about critical life-history stages. Moreover, the scale of inference sought–that of populations, communities, and biomes–are emergent properties of the action of individuals in local neighbourhoods (Clark *et al.*, 2014).

2.2.2 Fine-scale demographic information for large scale inference

To move forward, we need to scale up our knowledge of the mechanisms governing vital rates in individuals to species, community and ecosystems.

For example, we have a good understanding of the molecular mechanisms of photosynthesis in a single leaf and how changes in CO_2 concentration influence photosynthetic rates at the level of the leaf or individual (Liang *et al.*, 2001). But what does this mean for whole forests faced with climate change? The biggest source of uncertainty in global climate models comes from vegetation dynamics. Current models diverge widely in how they predict the feedback between vegetation and rising CO_2 and temperature will play out (Cramer *et al.*, 2001; Friedlingstein *et al.*, 2006; Friend *et al.*, 2014). One of the major problems with current models is that they move from physiology to global dynamics with very little or no consideration of any of the scales in between; in many models highly diverse ecosystems are reduced to just a few plant functional types (e.g. (Friend *et al.*, 2014) and references therein). We need models that take into account how individual level processes scale to demographic rates, the differences in demography between species, how these differences influence community composition and turnover, and how climate change, through its effect on physiology will impact all of these processes, ultimately impacting the biogeochemical dynamics of entire regions. Here we focus on demography, addressing the critical link between individuals, populations and communities.

2.2.3 A way forward through vital rates

Demographic vital rates offer both direct mechanisms that drive forest dynamics (e.g., exogenous responses to disturbance events through mortality) and indirect measurements of the impact of unknown processes (e.g., growth and mortality changes due to pathogen loads, nutrient availability, or stress). We demonstrate how to use widely available permanent plot data (e.g. CTFS-ForestGEO network of plots (Condit, 1998), USDA forest inventory program, (McRoberts *et al.*, 2005)) to fit vital rate models that capture the changing probability of survival through ontogeny and the highly skewed distribution of individual growth rates. These models can be combined into Integral Projection Models (IPMs) (cf. Easterling *et al.*, 2000; Merow *et al.*, 2014a); population models that track the change in the size distribution of a population through time. The IPMs presented here do not model individuals explicitly, yet take into account persistent individual differences in performance, which enables us to avoid computationally expensive individual simulations. The easy parameterisation of these models, combined with straightforward analytic tractability offers the potential for spatial and temporal scaling.

We developed our methods to work with any data set in which there are repeated measurements of individual stems through time. To demonstrate the general applicability of our methods we demonstrate the basic workflow for three tropical forest tree species with different life history strategies, *Garcinia intermedia*–an understory tree species,

Calophyllum longifolium–a fast growing canopy species and *Prioria copaifera*–an emergent species. Data for these three species comes from a permanent forest plot on Barro Colorado Island, Panama. More details on the site and the example species are given at the end of the methods. A worked example with full code is provided in Appendix C.

2.3 Methods

2.3.1 Vital Rate Models

2.3.1.1 Growth

The success of an individual stem in an intact or light-limited forest is largely determined by whether it can outgrow its neighbours and gain access to critical resources such as light and nutrients. The outcome of these local competitive interactions determine larger patterns of community composition and ecosystem functioning, since only the minority of fastest growing individuals make it to the canopy (Brienen & Zuidema, 2006).

It is important that demographic models capture the skew in growth data. Using just the population mean growth rate can give a significant underestimate of passage times to key life cycle events–e.g. reproduction–with consequences for population dynamics. In order to accurately capture forest dynamics, it is therefore essential that we move away from models that focus on population averages, towards a framework that accounts for individual differences and temporal correlations in vital rates, using structured population models.

To capture asymmetry in growth data we fit multiple distributions to characterise multiple modes of growth present in forest trees. For each species we define a size threshold (explained below) and assume that all individuals above this size are in the 'fast' growth distribution, while individuals below this size are in the 'slow' distribution. In closed canopy forests such as those we study here, this is mostly to reflect access to light–widely accepted to be a key determinant of growth rates (Purves *et al.*, 2008). However, we also allow the fastest 5% of individuals below the size threshold to contribute to the fast growth distribution since there will be some 'lucky' understory trees that are expected to be located in gaps. Five percent was chosen based on rough estimates of gap frequency in closed canopy forests (van der Meer & Bongers, 1996). The assumption that growth rates relate to light environment is not critical to the model, since even light intolerant species are expected to show skewed increment data, with only a subset of faster growing individuals. And again, this will still likely scale with size as larger individuals have access to increased resources due to, for example, larger rooting systems.

The size threshold for fast growth could be found using species- or site-specific allometric equations to find the DBH at which a stem would be tall enough to have reached the canopy, but here we use 200 mm for canopy species and the 0.8^{th} quantile of size for species with a maximum observed DBH < 500 mm. The 200 mm threshold was chosen to reflect the approximate size at which an individual of a canopy species would reach the canopy. In Condit *et al.* (1993) the annual absolute growth rates of *P. copaifera* increased markedly in the size category from 160-319 mm.

For understory species, the 0.8^{th} quantile of the size distribution reflects the fact that larger individuals will tend to grow faster and ensures sufficient sample sizes to parameterise each distribution.

We model growth classes with a mixture of gamma distributions:

$$z \sim \begin{cases} \text{Gamma}(\alpha_1, \beta_1) & \text{for q}x < thresh_g, \\ \text{Gamma}(\alpha_2, \beta_2) & \text{for all } x \geq thresh_g \\ & (1-q)x < thresh_g \end{cases} \tag{2.1}$$

where z is increment growth, x is DBH, q is the proportion of understory individuals in the slow growth class, α and β are the distribution shape and rate parameters with subscripts 1 and 2 referring to the slow and fast distributions respectively, and $thresh_g$ is the DBH threshold for inclusion in the fast growth distribution. An individual's growth is therefore determined by its growth class as oppose to its size, i.e. this is not a regression of increment against size. This makes sense biologically, since trees of similar sizes can grow at very different rates for a number of reasons (see Fig. A.1 for the increment data plotted against DBH for over 100 abundant BCI species). Categorising trees into growth classes enables variation in growth rates of same-sized individuals and, when used to construct IPMs, allows us to capture temporal correlations in growth rates. Gamma distributions proved a good fit to the increment growth data, effectively capturing the observed right skew of slow growers and the more symmetric distribution of fast growers, with only two free parameters per distribution.

Our growth model can theoretically be extended to any number of distributions, but this risks over fitting if few data are available to parameterise each distribution. Further, the time taken for analysis of these IPMs increases as a function of the number of growth distributions. In this paper, we limit our analyses to growth models with just two or three distributions. With three distributions, the rule set for defining the distributions is as above, only with an additional 'very fast' class consisting of the fastest 0.02 quantile of all individuals.

We fit both growth and survival models for the three BCI species using Bayesian MCMC analysis implemented in R (R Core Team, 2014) and RStan (http://mc-stan.org).

2.3.1.2 Survival

Models of North American forest communities have indicated that differences in performance between species are primarily due to differences in mortality as opposed to growth rates (Purves *et al.*, 2008). Fitting robust models that capture species differences as well as changes in survival through ontogeny is therefore critical for capturing community dynamics and predicting the outcome of succession.

One difficulty in modelling whole-life-history survival is how to capture senescence in large individuals when the data are dominated by small stems which show the opposite pattern of size dependent mortality (i.e. capturing the bathtub-shaped mortality curve (Metcalf *et al.*, 2009)). Clark *et al.* (2010) use a non-parametric survival model to better capture steep regions of this relationship. We chose to retain parametric functions but to combine then in a way that provides the necessary flexibility to capture changing size-survival relationships over ontogeny. As parametric models they are better behaved across many species, hierarchical models, and their extension to predictive models with covariates is relatively straightforward.

To take advantage of parametric models, we fit two separate regressions of survival probability against size, one for small individuals in which survival probability increases with size, and one for larger individuals in which survival probability decreases with size. The two curves meet at a species-specific (or pre-determined) size threshold.

Survival in our framework is given by:

$$s = \left(L_1 + \frac{K_1 - L_1}{1 + \left(\frac{1}{e^{-r_1(x-p_1)}} \right)} \right)^t \quad \text{for all } x < thresh_s \tag{2.2}$$

$$s = \left(L_2 + \frac{K_2 - L_2}{1 + \left(\frac{1}{e^{-r_2(x-p_2)}} \right)} \right)^t \quad \text{for all } x \geq thresh_s \tag{2.3}$$

where s is survival probability, L and K are the lower and upper asymptotes of the curves, r and p are the rate of change and inflection point in the curves respectively, t is the time in years between censuses, x is DBH and $thresh_s$ is a species specific size threshold at which the two curves meet. Subscripts 1 and 2 denote parameters for the small and large survival curves respectively.

We made the size threshold equal to the size threshold for fast growth for each species. Fixing the size threshold has little influence on the curve since survival probabilities are constant with size (at K) across much of the size range. However, for species where this is not the case, or in instances where different data sets are being used to fit juvenile and adult portions of the survival curve, it may be necessary to use smoothing functions over a size interval where the two regressions meet, see Merow *et al.* (2014b) for an example of this approach. Priors were used during Bayesian parameter estimation in order to constrain r_2 negative to ensure decreasing survival with increasing size in large trees.

To reduce problems of with identifiability, we fixed the lower asymptotes ($L1$ and $L2$) at 0 so that the increases and decreases in survival with size were determined by the inflection point and rate of change. The curves are therefore reduced to

$$s = \left(\frac{K}{1 + \left(\frac{1}{e^{-r(x-p)}} \right)} \right)^t \tag{2.4}$$

leaving just five free parameters in total.

2.3.1.3 Fecundity

Seed and seedling dynamics have important implications for patterns of adult abundance and spatial distributions (Umaña *et al.*, 2016; Comita *et al.*, 2007). Further, given that these stages are often the most sensitive in the lifecycle to abiotic conditions (Dobrowski *et al.*, 2015), the impact of climate change on population dynamics will largely be determined by the ability of each species to regenerate given environmental change (Walck *et al.*, 2011).

Due to the abundance and high mortality of seedlings in the forest understory, combined with difficulties in species and individual identification, monitoring of seed and seedling stages presents an important logistical challenge (Umaña *et al.*, 2016). As a result, forest inventories commonly use 1 cm or even 10 cm diameter at breast height (DBH) as the threshold for inclusion of stems in a census. Where data on seedling stages are available, it is not always clear that they captures the full dynamics that give rise to observed patterns of larger individuals. For instance, in absolute terms, the few seedlings produced by rare species are often swamped by the seedlings of more abundant species, meaning that without huge surveying efforts the recorded fecundity of these rare species might be near zero. In addition, masting events can skew estimates of reproductive rates unless sampling is over a long enough time period to capture the periodicity of such rare events (Chang-Yang *et al.*, 2013).

To illustrate our methods for cases where no data on seed or seedling dynamics are available, we introduce a very simple fecundity function in this section and then describe how to parameterise it using population statistics from IPMs in section 2.3.2.2.

We assume that individual fecundity scales linearly with basal area (BA). The number of offspring, b, produced by individuals each year is given by

$$b = \begin{cases} \pi \left(\frac{x}{2}\right)^2 f & \text{for all } x \geq thresh_f, \\ 0 & \text{for all } x < thresh_f \end{cases} \tag{2.5}$$

where x is DBH, f is a species specific fecundity parameter, and $thresh_f$ is a size threshold for reproduction. For canopy species (those with a maximum observed DBH $\geq$ 500 mm) we set the size threshold to 0.5 times the maximum observed DBH. Visser *et al.* (2016) show that this is a good predictor of the size at which 50% of individuals will be reproductive. For understory species we assume no size threshold since many species will begin reproduction at sizes <10 mm DBH.

2.3.2 Integrating vital rates and filling in missing data

2.3.2.1 IPMs

Capturing persistent individual differences In traditional IPMs (cf. Easterling *et al.*, 2000; Merow *et al.*, 2014a), growth at each size is modelled by a distribution of possible increments such that same-sized individuals can grow at different rates. However, these differences are not autocorrelated through time and as a result, an individual growing slowly one year might grow fast the next. Over a longer simulated period (or asymptotic analytical solution) the average growth will trend toward the mean. We know that this does not reflect how trees typically grow; for a range of reasons, including genetics, pathogen load and microsite conditions, fast growers usually remain fast growing and slow growers remain slow growing for extended periods (Brienen & Zuidema, 2006).

In forests, the small proportion of individuals that make it to the canopy are those that grew consistently faster than the trees around them (Obrien *et al.*, 1995). These 'winners' contribute disproportionately to the population growth rate (Zuidema *et al.*, 2009) and define the structure, biomass and carbon dynamics of the forest.

Models of growth at the population level, therefore need to incorporate the way that multiple factors (access to resources, herbivory etc.) act on individuals through time, giving rise to temporally correlated variation in the population. However, individual level data on any or all of these factors is rarely available. Previous work has explored the

impact of using the local competition around a focal tree as a proxy for light availability (Lichstein *et al.*, 2010; Grote *et al.*, 2013; Uriarte *et al.*, 2010). Here we take a different approach that can be implemented even when spatial data is unavailable (as in many national forest inventories (Tomppo *et al.*, 2010)).

We use our vital rate models to construct IPMs (cf. Easterling *et al.*, 2000; Merow *et al.*, 2014a). We use a vec-permutation approach (Caswell, 2012) with the IPMs to describe the transitions of individuals between size and growth distributions. It is the transitions between growth distributions that determine the degree of temporal correlation in our models. Low probabilities of transitioning between growth distributions results in high temporal correlation, i.e. fast growers remaining fast growing and slow growers remaining slow growing, and vice versa.

The vec-permutation approach for constructing size-growth IPMs Matrix construction using a vec-permutation method has already been presented in detail in Caswell (2012) and Caswell & Salguero-Gómez (2013), and therefore we give just a brief overview of the methods here, indicating any differences between the age-stage approach described in Caswell (2012) and the size-growth approach presented here.

Although throughout this paper we refer to matrices, it is worth noting that these are IPM matrices, with transition probabilities between size classes given by the vital rates regression models (in our case regressions of survival and fecundity against size, and the two or three growth distributions). Size is treated as continuous in these regression/distribution models and is only discretised in order to numerically calculate the integration of transition probabilities between sizes (Easterling *et al.*, 2000).

The full IPM is constructed by combining matrices describing transitions of individuals between sizes *within* each growth distribution, and matrices describing the probability of transitions *between* growth distributions at each size.

We begin by making matrices which describe the probability of growth from every size to every other size, combined with the survival probability at each size. There is a growth and survival matrix, $\mathbf{U}$, for every growth distribution. If we have discretised size into S size bins, and there are G growth distributions then we have $\mathbf{U}_1$, $\mathbf{U}_2 \ldots \mathbf{U}_G$ with each $\mathbf{U}$ matrix of dimensions S x S (note that our G growth distributions replace the i age classes used in Caswell (2012)). These $\mathbf{U}_{1\ldots G}$ matrices are arranged in a block diagonal matrix $\mathbb{U}$.

$$\mathbb{U} = \begin{pmatrix} \mathbf{U}_1 & 0 & \dots & 0 \\ 0 & \mathbf{U}_2 & \dots & 0 \\ \vdots & \vdots & \ddots & \vdots \\ 0 & 0 & \dots & \mathbf{U}_G \end{pmatrix}$$

To describe the transition probabilities of individuals *between* growth classes we construct a G x G matrix, C for every size bin S and arrange them in a block diagonal matrix $\mathbb{M}$, of dimensions GS x GS (in Caswell (2012) this is referred to as $\mathbb{D}_U$).

We assumed that transition probabilities from slow to fast increase, and from fast to slow decrease, with size up until the size threshold for fast growth, beyond which individuals are fixed in the fast growth distribution. This allowed us to capture the fact that stems generally grow faster as they increase in size, while still accounting for the substantial variation at each size.

Estimating these transition probabilities from data is impossible because of the overlap in the growth distributions. We therefore came up with transition probabilities based on estimates of gap duration (van der Meer & Bongers, 1996) and then tested the sensitivity of population outputs to changes in these probabilities (see below). Since gaps in closed canopy tropical forests have been estimated to last approximately 15 years on average, we found the transition probability of moving from fast to slow such that after 15 years individuals at the smallest size would have a probability of 0.1 of remaining in the fast distribution, and those at the size below the size threshold for automatic fast growth, would have a probability of 0.9 of remaining in fast growth.

The annual probability of moving from slow to fast was assumed to range from 0.02 at the smallest size, up to 0.1 for the size below the size threshold.

When we simulated individuals using these rule sets, and the growth and survival models as defined above, the distribution of consecutive years spent in the fast growth distribution matched expectations of gap duration (tables A.1, A.2).

Transition probabilities for the smallest size class are therefore:

$$C_{1,1} = \begin{pmatrix} 0.98 & 0.14 \\ 0.02 & 0.86 \end{pmatrix},$$

while the transition probabilities for the size class below the size threshold for fast growth are:

$$C_{1,thresh_{g-1}} = \begin{pmatrix} 0.90 & 0.01 \\ 0.10 & 0.99 \end{pmatrix}.$$

We define the matrix, C_2 for all sizes $\geq$ the size threshold $thresh_g$. In the case of $G = 2$

$$C_2 = \begin{pmatrix} 0 & 0 \\ 1 & 1 \end{pmatrix},$$

since individuals remain in the slow growth class with probability 0, and move to fast growth class with probability 1.

$\mathbb{M}$ has the sequence of size dependent C_1s on the diagonal until $\mathbb{M}_{thresh_g, thresh_g}$, and then C_2 on remaining diagonals.

In the three distribution growth model, transitions were as above but with the transition probability of moving into the very fast distribution–from both the slow and fast distributions–set at 0.005 for all sizes below the size threshold, and transition probabilities of moving into the fast distribution reduced by 0.005. From the very fast distribution, we assumed transition probabilities back to fast distribution ranging from 0.4 to 0.2 and to the slow distribution from 0.1 to 0.07, as size increased from the smallest size to the size threshold, see A.1.

We next make K, the vec permutation matrix. K is of dimension GS x GS and consists of 1s and 0s. It rearranges a column vector holding the size distribution of the population, $\tilde{\mathbf{n}}$, from (in the case of $G = 2$, shown here transposed)

$$\tilde{\mathbf{n}}_t = \left(n_{1,1},\ n_{2,1}, \ldots n_{S,1} \middle| n_{1,2},\ n_{2,2} \ldots n_{S,2}\right)^T$$

where individuals are arranged as sizes within growth classes, to

$$\mathbf{K}\tilde{\mathbf{n}}_t = \left(n_{1,1},\ n_{1,2} \middle| n_{2,1},\ n_{2,2} \middle| \ldots \middle|\ n_{S,1},\ n_{S,2}\right)^T$$

where individuals are arranged by growth classes within size classes.

The final growth and transition matrix $\tilde{\mathbf{U}}$ is given by

$$\tilde{\mathbf{U}} = K^T \mathbb{M} K \mathbb{U}. \tag{2.6}$$

Reading (2.6) from right to left, $\mathbb{U}$ first moves individuals between size classes within a growth class. K rearranges the population vector so that $\mathbb{M}$ can move individuals between growth classes. Finally K^T rearranges the population vector back to its original orientation.

IPMs do not explicitly keep track of individuals. Therefore, to visualise individual trajectories, and analyse the number of consecutive years each individual spent in each

growth distribution, we simulated populations, keeping track of individual sizes and growth classes, (Fig. 2.1). Each year of the simulation, we applied the growth and survival functions and then moved individuals between growth classes according to the transition probabilities defined above. From these simulations we found the mean, variance and range in the number of consecutive years understory and canopy individuals spent in each growth distribution.

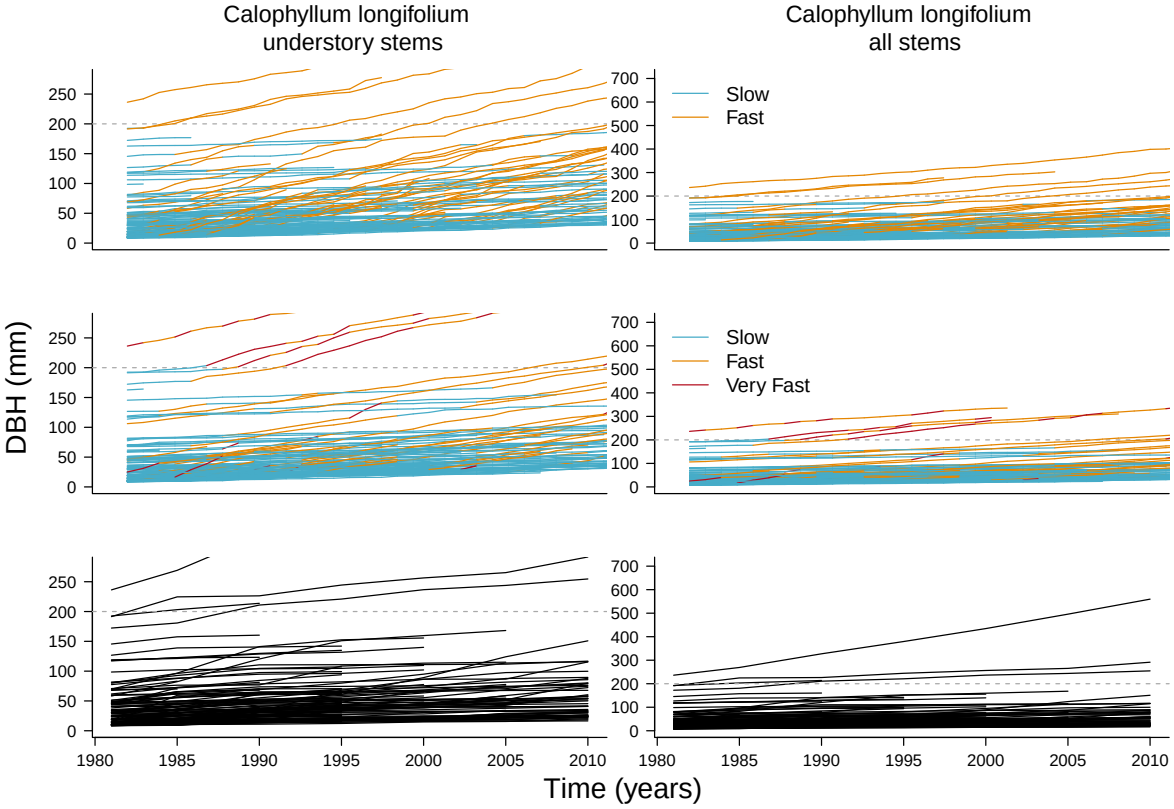


Figure 2.1: Simulated trajectories for *C. longifolium* individuals using the two and three distribution growth model. Left hand panels show a sample of 100 understory stems as they grow up to the size threshold for fast growth, while right hand panels show a sample of 200 individuals of all sizes. These simulations did not include reproduction and only the first 30 years are shown to make results comparable to the trajectories of observed trees shown in the bottom row. Simulated populations using the two distribution model more closely match the observed trajectories of this species.

$\tilde{\mathbf{U}}$ is sufficient to enable analysis of cohort dynamics, such as calculating passage time to a certain size or expected longevity of each size class. However, to model the full population dynamics we need $\tilde{\mathbf{F}}$, the fecundity matrix.

$\tilde{\mathbf{F}}$ is constructed much as $\tilde{\mathbf{A}}$, with a series of $\mathbf{F}$ matrices, $\mathbf{F}_1$, $\mathbf{F}_2$ $\ldots \mathbf{F}_G$, describing production of offspring of each size by adults of each size, in each growth class G. These are arranged in a block diagonal matrix $\mathbb{F}$. The distribution of offspring into each growth

class, by adults in each growth class, is given by $\mathbb{D}$. We assumed that the probabilities of offspring recruiting into the slow and fast distributions were 0.95 and 0.05 respectively. In the three distribution model, the probability of recruiting into fast and very fast distributions were 0.04 and 0.01 respectively. Since it is rare to be able to attribute seeds and seedlings to individual adult trees, we assumed that parent growth class had no affect on offspring growth distribution.

The $\tilde{\mathbf{F}}$ matrix is given by

$$\tilde{\mathbf{F}} = K^T \mathbb{D} K \mathbb{F}. \tag{2.7}$$

Finally $\tilde{\mathbf{A}}$, the full IPM matrix describing growth, survival and fecundity, along with movement of individuals between growth classes is given by

$$\tilde{\mathbf{A}} = \tilde{\mathbf{U}} + \tilde{\mathbf{F}}. \tag{2.8}$$

For each BCI species we constructed IPMs for both two and three growth distributions, using $S = 1500$. For each size, conditional on starting growth class, we used $\tilde{\mathbf{U}}$s to calculate passage times to the size threshold for fast growth, i.e. the number of years an individual of each size and starting growth class would be expected to take to grow to $thresh_g$, conditional on it surviving, and expected longevity i.e. the expected number of years until death. We also calculated the expected occupancy time in each growth distribution for stems above and below the size threshold for fast growth. See Appendix B for more details on how these metrics are calculated.

We used $\tilde{\mathbf{A}}$s to calculate population growth rates (λ, the dominant eigenvalue) and the stable size distributions (w, the dominant right eigenvector) i.e the proportion of the population in each size class.

Along with providing a rough validation of IPM outputs (e.g. comparison of life expectancies to tree ring data or passage times to know ages at certain sizes), these metrics allow us to make comparisons of life history strategies amongst different species, and ask questions relating to niche theory and phylogenetic conservation of demographic rates. In addition, population growth rates give an indication of whether a population is increasing or in decline and are therefore of interest from a conservation perspective.

2.3.2.2 Inverse modelling with IPMs

Inverse modelling describes the process of adjusting model parameters based on comparisons of model output and observed data (Hartig *et al.*, 2014). Population summary

statistics from IPMs can be used to inverse model vital rates parameters which could not be inferred from available data. In our examples we used inverse models to estimate fecundity parameters. To find the likelihood of a given fecundity parameter, we first constructed $\tilde{\mathbf{A}}$. Next, using the census data from 1995 as a starting point we projected the population forward fifteen years through iterative multiplication with $\tilde{\mathbf{A}}$. Following González *et al.* (2016), the likelihood of a given fecundity parameter was found by comparing the population size distribution and the number of individuals from the simulated population with the census data from 2000, 2005 and 2010. Size distributions were compared with a multinomial distribution which gives the log likelihood of observing n individuals of size x, with probabilities given by the normalised population size distribution from the simulation. The log likelihood of the observed population size of N was found from a Poisson distribution with λ as the number of individuals in the simulated population. These log likelihoods were summed to give the final log likelihood of the proposed fecundity parameter.

For inverse modelling we used Approximate Bayesian Computation Sequential Monte Carlo (ABC SMC) methods (sometimes referred to as a particle filter) as described in Beaumont (2010). This involves sampling parameters from the prior distribution and using each sampled parameter to get summary statistics and log likelihoods (of the data given the model with that parameterisation). Only those parameters with a log likelihood above a certain threshold are accepted. In each subsequent iteration, accepted parameters are perturbed slightly, re-sampled with importance weights, and again, only those with log likelihoods above the acceptance threshold are accepted. As the acceptance threshold is updated with each iteration, sampling is increasingly focused in areas of high likelihood. A more in depth discussion of this, and related techniques, is beyond the scope of this paper, but we recommend Beaumont (2010) and Hartig *et al.* (2011).

We can sample from the posterior distribution of fecundity parameters to get uncertainty around our estimates, along with the sensitivity of population summary statistics and log likelihoods to changes in fecundity. We drew 1000 samples from the posterior distribution of fecundity parameters for *C. longifolium* with two growth distributions, and found the associated summary statistics and log likelihoods for each sampled parameter. Results are shown in Fig. A.2.

2.3.3 Sensitivity to transition probabilities between growth distributions

Multiple factors influence growth rates (light, nutrients, disease status etc.). The differential impact of these factors on individuals is represented in our models by the proportion of

individuals in each growth class. Further, the timeframe over which these various factors act is represented by the probabilities of individuals moving between growth classes. In order to explore how these estimates might impact results we tested the impact of changing the proportion of individuals in each growth class, and the transition probabilities between growth classes, on passage times and longevities, specifically the passage time from the smallest size to the size threshold for fast growth, and longevity at the smallest size.

Since we were interested in the impact of different combinations of proportions and transition probabilities, we calculated transition probabilities such that each proportion would stay fixed through time (i.e. the number of individuals moving from slow to fast each year would match the number of individuals moving from fast to slow). For this analysis we also assumed that transition probabilities were size independent up to the size threshold for fast growth (unlike in our other IPMs in which transition probabilities between growth classes change with size). If q is the quantile of individuals in the slow growth class, the rule sets are therefore as follows:

(SF = slow to fast, SS = slow to slow, FS = fast to slow and FF = fast to fast):

$SS + SF = 1$
$FF + FS = 1$
$qSF = (1 - q)FS$
$SF = \frac{(1-q)}{q} FS$

For each value of q from 0.5 to 0.95 in increments of 0.05, we tested FF from 1 to 0.1 in increments of 0.1 and the corresponding FS, SF and SS values. For these IPMs we used S=1500.

We next kept the quantile of individuals in the slow distribution fixed at 0.95 and tested the sensitivity of passage times to changes in combinations of slow to fast and fast to slow transitions. The probability of transitioning from the slow to fast growth distribution ranged from 0.1 to 1, while the probability of transitioning back from fast to slow ranged from 0 to 0.9. Again, we compared passage times from the smallest size up to the size threshold for fast growth and assumed that transitions were size independent. Sensitivities to transition probabilities were tested with *C. longifolium* data.

We also tested the sensitivity of population outputs for all three species to a range of IPM dimensions, see Appendix A for details.

2.3.4 Site and species descriptions

To demonstrate our methods we used census data from a 50 ha forest plot located on Barro Colardo Island (BCI), Panama (9°9'N, 79°51'W) (Hubbell & Foster, 1983; Hubbell

et al., 1999). The BCI plot consists of moist, tropical forest, of which 48 ha is undisturbed old growth forest and 2 ha is 100 year old secondary forest (Foster & Brokaw, 1982). More detailed descriptions of the geography and vegetation of BCI are available in Croat (1978); Leigh *et al.* (1982); Leigh (1999).

Within the 50 ha plot all stems $\geq$ 1 cm DBH are mapped, measured and identified to species level following a standardised protocol (Condit, 1998). The first censuses were conduced in 1981, 1983, 1985 and then every five years. In this paper, we use the most recent census to fit vital rates models for IPM construction and use censuses from 1995, 2000, 2005 and 2010 for inverse models.

To illustrate the general applicability of our methods we chose three species of varying life history strategies, *Garcinia intermedia*, an understory species, *Calophyllum longifolium*, a canopy species, and *Prioria copaifera* an emergent. More information on these three species can be found in Condit *et al.* (1993) and Lim (2012). Over the four censuses, excluding stems missing in any of the censuses, we had 2349 stems of *C. longifolium*, 5741 stems of *G. intermedia* and 1539 stems of *P. copaifera*.

2.4 Results

2.4.1 Two and three distribution growth models

Prioria copaifera and *C. longifolium* had faster growth rates than *G. intermedia*. In the two distribution model, the fast distribution is more distinct for *C. longifolium* than *P. copaifera* but the introduction of a third distribution allowed a subset of very fast *P. copaifera* to be distinguished, (Fig. 2.2, tables A.3, A.4). The *G. intermedia* growth distributions were more overlapped than in the other species, which matches expectations for an understory species that never reaches the canopy and therefore never experiences release from light competition unless situated in a gap.

2.4.2 Size-dependent survival models

The upper asymptote of the survival curve was 0.99 for *P. copaifera* and there were only small declines in survival probability at small and large sizes, (Fig. 2.3). These results are consistent with findings from other studies in BCI (Condit *et al.*, 1993). *Calophyllum longifolium* had lower overall survival with an upper asymptote of 0.97 and more distinct senescence. However, the highly skewed size distribution in *C. longifolium* means that senescence is determined by just a few data points, and the death of the largest individual

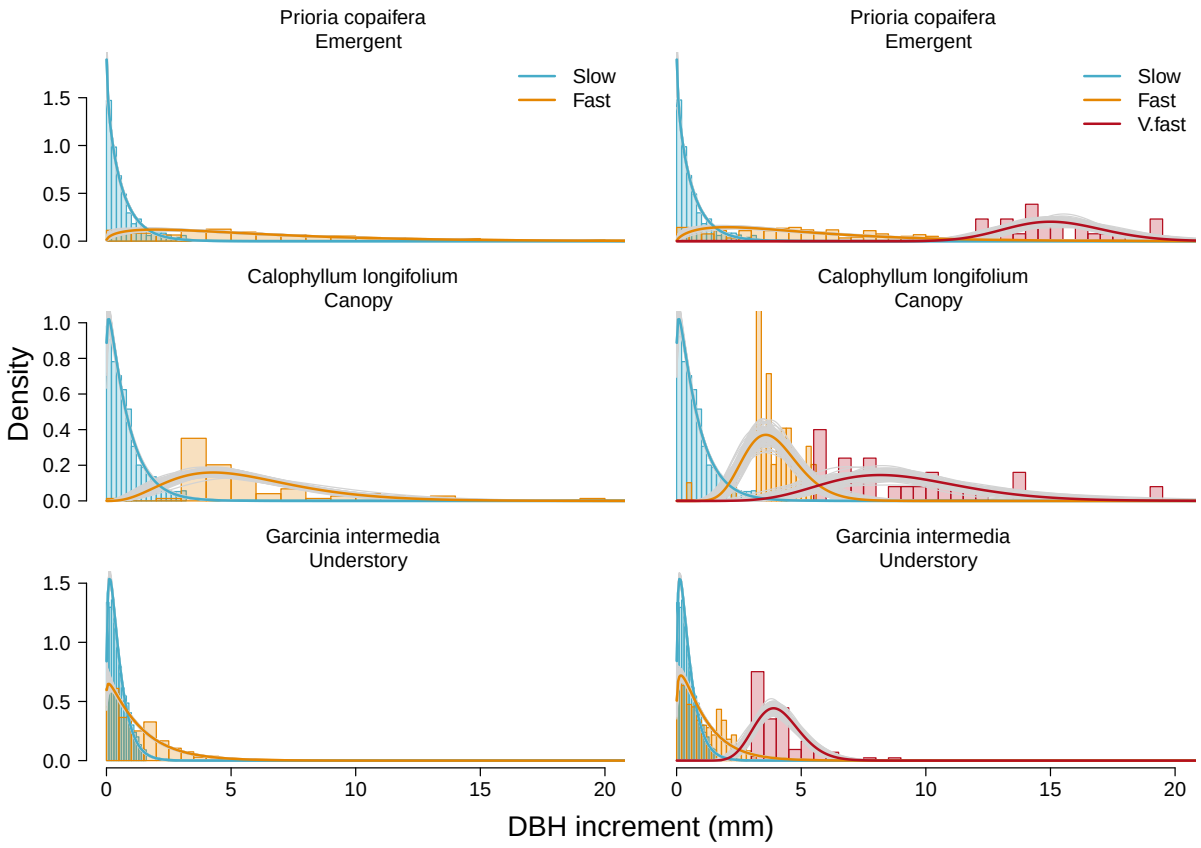


Figure 2.2: Growth models with two distributions (left) and three distributions (right). To clearly show the shape of each distribution the height of each curve does not scale with the number of individuals in each growth class. Grey lines show parameter uncertainty from the MCMC joint posterior distribution and bars show histograms of individuals in each growth distribution, again each distribution is on a different scale. In the two distribution model *C. longifolium* had the highest growth rates, but the introduction of a third distribution distinguished a subset of very fast *P. copaifera* individuals.

in the dataset contributes a lot to the inferred senescence. This is reflected by the higher uncertainty in survival probability at large sizes for *C. longifolium*. *Garcinia intermedia* had an upper asymptote at 0.98 and also showed only minor decreases in survival probability at the smallest sizes (table A.5).

2.4.3 Size-dependent fecundity models

We used an inverse model to estimate fecundity parameters for the three BCI species, using the framework given in Beaumont (2010). Using 0.5*max(observed DBH) as the reproductive size threshold for canopy species and 0 for species with max(observed DBH) < 500, resulted in a reproductive size threshold of 404 mm for *C. longifolium*, 699 mm for *P. copaifera* and 0 mm for *G. intermedia*. *Garcinia intermedia* had the highest fecundity parameter (Fig. 2.4) which also translated into the highest reproductive output of the three species once population size structure and reproductive size thresholds were accounted for (table A.6).

The uncertainty around fecundity parameter estimates is given by the posterior distributions from the inverse models. We took 1000 samples from the posterior distribution of *C. longifolium* fecundity parameters, and from the inverse model found the simulated size distributions, population size and the log likelihood of simulated summary statistics. The results are plotted in Fig. A.2. Although changes to the fecundity parameters had little influence on the size distribution of the simulated population, the population size after a 15 year simulation ranged from 1367 to 2266 with fecundity parameters ranging from 3.67 to 7.76 annual offspring per unit basal area.

2.4.4 Population level statistics

We constructed IPMs for each species and used them to calculate population level statistics. For each species we compared results from the two and three growth distribution models.

Population growth rates did not vary more than 0.008 between the two and three growth distribution models (Fig. A.3). Stable size distributions, given by the dominant right eigenvector, w, were also insensitive to the number of growth distributions used (Fig. A.3).

Fig. 2.5 shows the passage times to the size threshold for fast growth and life expectancies for each BCI species conditional on starting growth distribution. Patterns of size- and growth-dependent passage times for *P. copaifera* and *C. longifolium* are very similar albeit slightly longer for the former. In contrast, while life expectancies are also qualitatively similar in both species, they are more than three times higher for *P. copaifera* than *C.*

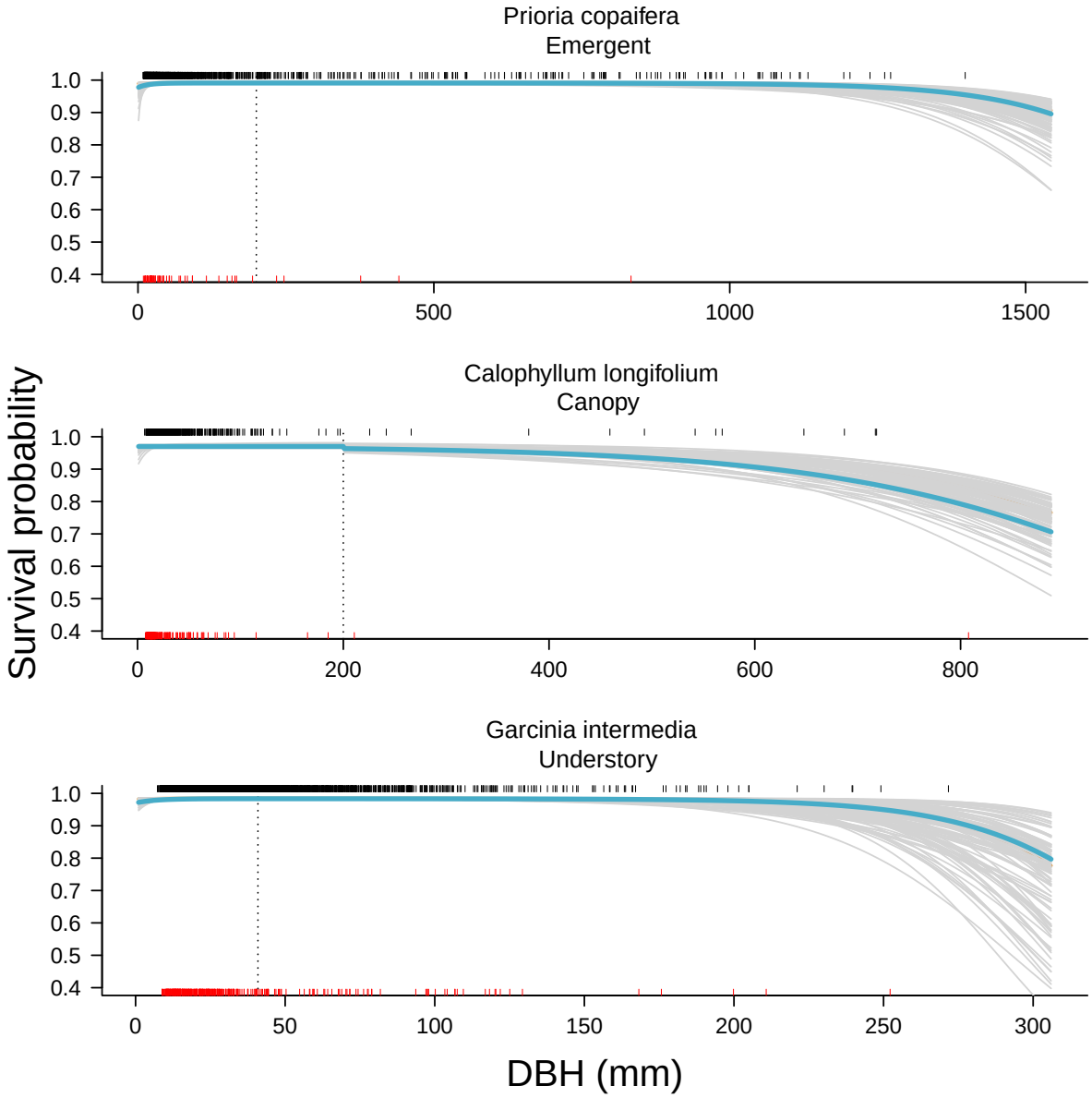


Figure 2.3: Survival models for each BCI species. Rugs along the top and bottom axis show survival and mortality data while dashed lines show the size threshold where the two logistic regressions meet. Survival probability was above 0.97 for all species across much of the observed size range. Grey lines around each curve show parameter uncertainty from the MCMC joint posterior distribution.

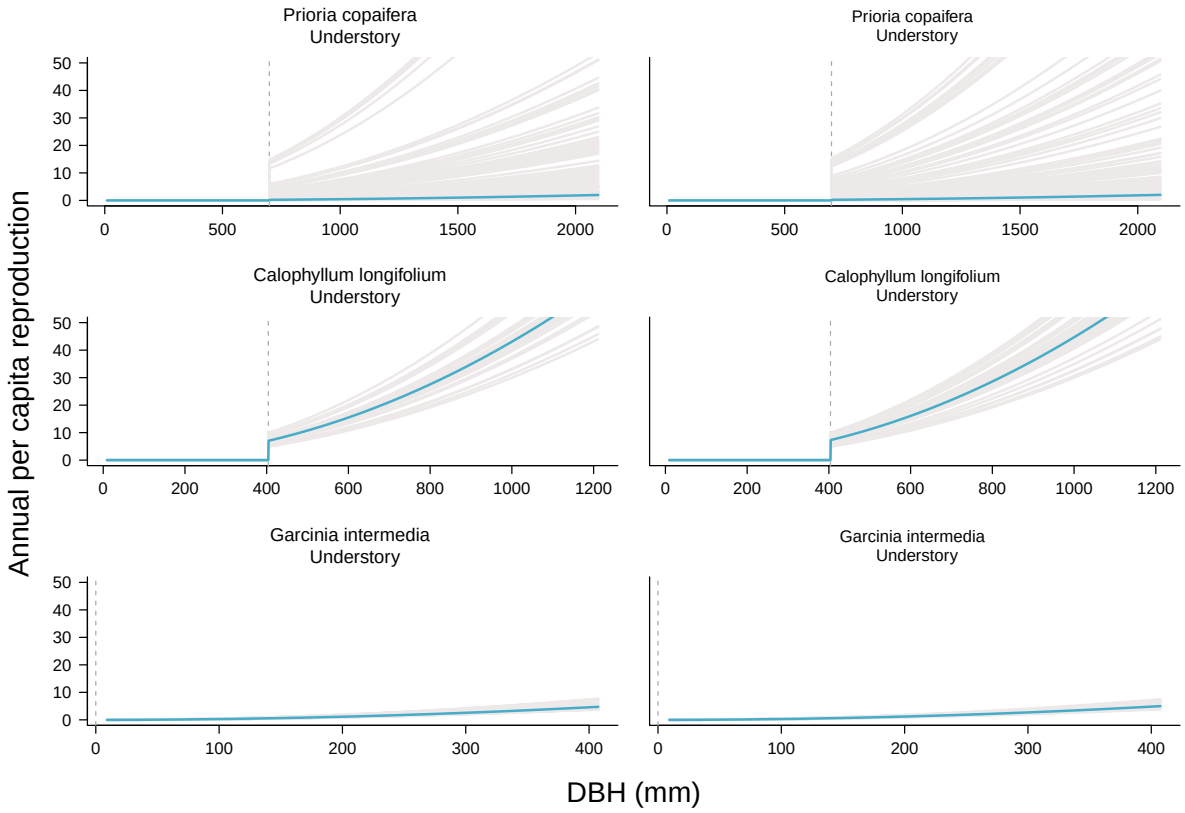


Figure 2.4: Fecundity model for each BCI species. There is a fecundity size threshold (0 for understory species) below which individuals do not reproduce, shown by the dotted vertical lines. Parameter uncertainty, shown with grey lines, was much greater for larger species than for the understory shrub *G. intermedia* due to the longer reproductive life spans of these species and therefore the bigger impact of changes in fecundity parameters on changes in individual reproductive outputs.

longifolium at the smallest size, and show a more gradual decrease with size. This mostly reflects the larger maximum size of *P. copaifera* as well as the higher juvenile mortality rates in *C. longifolium*. In fact, the high juvenile mortality of *C. longifolium* resulted in life expectancies being higher in the understory shrub *G. intermedia* than in *C. longifolium* at the smallest sizes. However, life expectancies declined much more rapidly with size for *G. intermedia*, as expected for an understory species. These results demonstrate the ability of our models to capture a range of life history strategies.

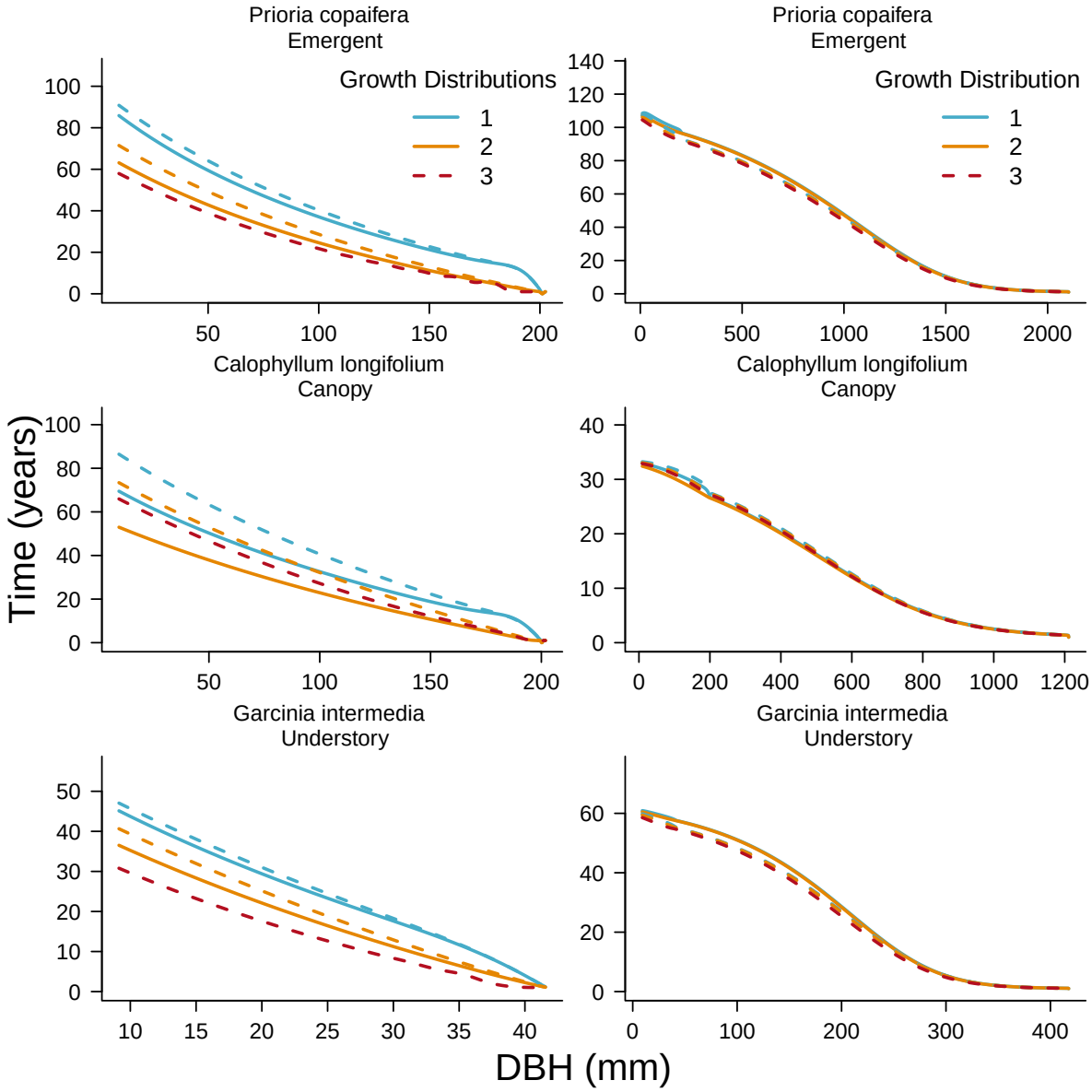


Figure 2.5: Passage times to the size threshold for fast growth (left) and life expectancies (right) for the BCI species, conditional on starting growth distribution. Due to high juvenile mortality *C. longifolium* has lower life expectancy in the smallest size classes than the understory shrub *G. intermedia*.

Occupancy times below and above the size threshold for fast growth are shown in Fig. A.4. Size dependent patterns of expected occupancy were similar for all three species, although quantitatively different, with occupancy times of *P. copaifera* being approximately double those of the other two species. This reflects differences in the size threshold for fast growth along with differences in growth rates. Because our IPMs have no memory, survival probability is size but not age dependent. Occupancy times above the size threshold for fast growth are therefore not influenced by starting growth distribution. In reality, it is possible that individuals which take longer to reach the canopy might have lower survival once there, due to factors such as accumulated pathogen load and herbivore damage.

2.4.5 Sensitivity analysis: transition probabilities between growth classes

We tested sensitivity of population statistics to the individual transition probabilities between growth classes and the proportion of the population in each growth class, using vital rates parameters from *C. longifolium* data, with $G = 2$ and $S = 1500$. Fig. 2.6 shows the passage times from 10 mm to 200 mm and the life expectancy of 10 mm stems conditional on starting growth class. As expected, passage times for individuals starting life in the fast growth class are shortest when the probability of remaining in the fast growth class and the proportion of individuals in the fast growth class are high. The pattern of passage times for individuals starting in the slow growth class is qualitatively the same but passage times are higher. Fast growers reach senescence faster resulting in lower life expectancies when the proportion of the population in the fast growth distribution increased.

When we tested the sensitivity of passage times to different combinations of transition probabilities between growth classes we found greater sensitivity to fast to slow transitions than slow to fast transitions (Fig. A.5).

2.4.6 Recommendations for IPM specifications

Decisions regarding IPM dimensions and the number of growth distributions to use depend on the study species and the available data. Species with larger maximum sizes will generally need larger IPMs in order to have sufficient resolution to capture variation in growth rates. Based on our sensitivity analysis to matrix size (see A.2), we suggest approximately 1000 size bins for a canopy species such as *C. longifolium* and *P. copaifera*. Further discretisation would lead to much greater computational costs with little gains in accuracy. For an understory species such as *G. intermedia*, with a maximum observed

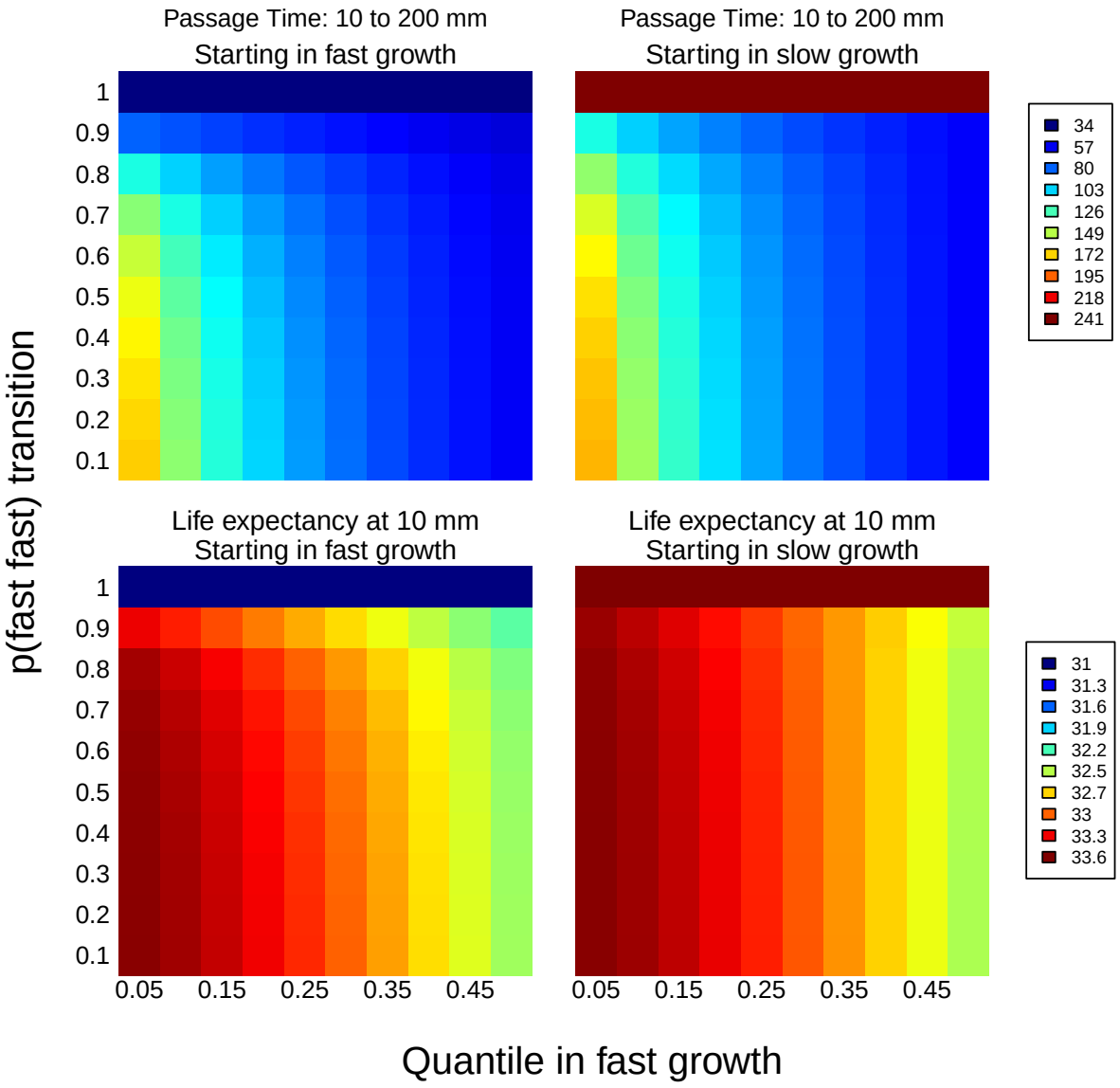


Figure 2.6: Sensitivity of passage time from 10 mm to 200 mm, (top) and the life expectancy of 10 mm stems (bottom), to the quantile determining the proportion of individuals in each growth distribution and the transition probabilities between growth distributions. Passage times to this threshold are fastest when a high proportion of individuals are in the fast growth class and the probability of remaining in fast growth is high. Life expectancies decrease as the quantile of individuals in fast growth increases. Both passage times and life expectancies are more sensitive to the proportion of the population in each distribution than to transition probabilities between distributions.

DBH of 272 mm, our results suggest as few as 600 size bins would be sufficient to accurately estimate population level demographic metrics.

Regarding the number of growth distributions, we generally recommend sticking to two distributions. Transition probabilities between growth distributions are difficult to estimate but have a substantial impact on results. Since the number of transitions to estimate is the square of the number of growth distributions, unnecessary distributions should be avoided. Two distributions make sense biologically, and since results were generally insensitive to whether a two or three distribution model was used (Figs A.3, 2.5) there seems to be little reason to increase the number of parameters to estimate and the computational cost of analysing the IPM.

2.5 Discussion

2.5.1 Towards scalable inference in forest dynamic models

Capturing demographic rates and their impact on community composition and turnover is a critical step in furthering understanding of how vegetation dynamics will respond to global change. In this paper we present a flexible and generalisable workflow for modelling the dynamics of forest trees using demographic data–specifically growth and survival. We show how to use these commonly collected measurements at the level of the individual, and scale up to population-level inference. By making use of readily available inventory data, we produce models that are easily parameterised across large geographic regions. Further, the analytic tractability of the models makes inference possible at large temporal and spatial scales without huge computational effort.

2.5.2 Vital rates as biological and statistical processes

Forest inventory data, in which the DBH of individual stems are recorded through time, are available from all the major forest biomes globally e.g. (Condit, 1998; Malhi *et al.*, 2002; Smith, 2002; McRoberts *et al.*, 2005; Anderson-Teixeira *et al.*, 2015). These simple data allow statistical descriptions of size-dependent vital rates (e.g. Condit *et al.*, 2006). Although ideally we would fit mechanistic models based on detailed understanding of the physiological process that govern individual growth, survival and reproduction, the data necessary to parameterise such models are not available across the scales of interest. Furthermore, recent studies have found that gap models with simple representations of vital rates are able to reproduce the dynamics predicted by more complex models (Purves *et al.*, 2008). In the workflow presented here, the vital rate models are simple

to parameterise, relying only on measurements of DBH from inventory data. However, the functional forms, although simple, capture the important biology that produces the patterns observed in the data. In addition, while the methods can be implemented using only inventory data, the modular nature of the workflow makes it easy to extend any or all of the vital rate models.

Growth: temporal correlations and competition for light The aims of our growth model were twofold: 1) to capture the dependency of growth rates on light availability without explicit inclusion of light or spatial data, and 2) to capture autocorrelation in growth rates.

Light is widely accepted to be a key determinant of annual growth rates in forest trees (Adams *et al.*, 2007) and many forest model include complex representations of light environment, e.g. Markov models describing movement through crown illumination classes (Metcalf *et al.*, 2009), or resource sub-models that account for species specific crown architecture, light attenuation through the canopy, and seasonal and diurnal fluctuations in light availability (Pacala *et al.*, 1996). However, the realised light environment of individual stems is known to be very difficult to approximate (except, perhaps, through fine measurements of growth) (Rüger *et al.*, 2011). Previous studies have looked at using spatial coordinates to calculate competition indices as proxies for direct measurements of light at the individual level (Lichstein *et al.*, 2010), but again this depends upon spatial data that are not always available.

In the Perfect Plasticity Approximation (PPA) (Purves & Pacala, 2008; Strigul *et al.*, 2008) or Ideal Tree Distribution (ITD) model (Adams *et al.*, 2007; Purves *et al.*, 2007), individuals are either in or out of the canopy, depending on whether they are above or below a species specific height threshold Z^*. A version of the gap model SORTIE (Pacala *et al.*, 1993; Hurtt *et al.*, 1998) with the perfect plasticity approximation and a much simpler sub-model of light was able to recreate the dynamics of the full SORTIE model (Strigul *et al.*, 2008). Further, despite its simplicity, the PPA model does well at matching chronosequences of stand development in North American forests on different soil types (Purves *et al.*, 2008), illustrating that simple but biologically meaningful representations of competition for light might be sufficient to capture forest dynamics. As in the PPA/ITD model, we define species specific size thresholds in order to distinguish between small and large trees in which the balance of factors limiting growth can be substantially shifted.

IPMs crucially fail to capture differences between individuals that persist through time. When dealing with long-lived organisms such as trees, this presents a critical problem, since it results in a population which evolves from a mean-field operation on individual

level mechanisms, when in reality, population dynamics are largely defined by the small minority of fast-growing, reproductive individuals (Brienen & Zuidema, 2006).

Previous attempts to account for autocorrelation in individual growth rates have focused on second-order matrix models (Picard *et al.*, 2003), and either size-growth (Pfister & Wang, 2005) or size-age (Zuidema *et al.*, 2009) matrix models. While a size-age model performs well at capturing the size distribution of a tropical tree (Zuidema *et al.*, 2009), it depends on estimates of individual age, which are not commonly available.

Our approach differs in that growth rates are determined by distributions which are independent of size (i.e. not classic regressions of growth against size), but which individuals transition in and out of in a size dependent manner. As a result, while the majority of understory individuals are slow growing, they have the potential to grow fast, either through the long tail of the slow growth distribution or by the increasing probability of transitioning into the fast distribution. These differences enable us to capture temporal correlations in individual variation–resulting in more biologically realistic models of pathways through the lifecycle.

Survival Survival rates can determine species ranges (Purves, 2009), responses to climate change (Van Mantgem & Stephenson, 2007), and have important consequences for community composition (Purves *et al.*, 2007). However, fitting survival models can be challenging; due to the long lifespan of canopy trees, extensive data sets are needed to parameterise models of survival in large individuals, especially for the majority of species that have low population densities. Previous descriptions of mortality have varied in the level of mechanism included. Lines *et al.* (2010) fit models to 21 species across the Eastern US with multiple abiotic covariates. In contrast, (Coomes & Allen, 2007) describe the development of *Nothofagus solandri* stands in New Zealand, using simple logistic functions to describe mortality, with initial size as the only explanatory variable. In the FORENA gap model (Solomon, 1986), two years of poor growth leads to a reduction in survival probability.

The function presented here was designed to be simple to parameterise, but with the ability to capture the important features of size-dependent mortality and the potential to be extended in applications where additional data are available. Unlike the FORENA model (Solomon, 1986), our framework does not include any interaction between growth and survival rates. However, it would be straightforward to incorporate interactions into future iterations of the model, simply by fitting survival functions to fast and slow growing individuals and then making the survival function in the IPM dependent on growth distribution. Further, the inclusion of either species- or stand-specific covariates

into the survival function itself is also straightforward. Similar to the study by Purves (2009) this could allow an exploration of how mortality changes across species ranges or environmental gradients.

Inverse models to fill in the life cycle In order to address issues of few or missing data, we describe inverse methods for estimating vital rates parameters using outputs from IPMs. Inverse modelling involves using model outcome to inform model inputs (Wood, 1987). These methods have been successfully applied primarily in individual-based ecological studies (cf. (Grimm & Railsback, 2005)), for instance in an individual based model of marine ecosystems (Duboz *et al.*, 2010), and a model of observed tree line formation in mountain ecotones (Martínez *et al.*, 2011). Inverse models are broadly applicable, even to stochastic, process-based models with complex heterogeneous data structures (Hartig *et al.*, 2012, 2014).

Here we show how to use population-level summary statistics obtained from IPMs to infer vital rate parameters for forest tree species. Our likelihood function is based on the method described in (González *et al.*, 2016), comparing the number of individuals and population size structure of simulated populations to time series data. This approach allows the incorporation of vital rates parameters estimated independently from forward models. For example, when working with forest inventory data, growth rates are relatively easy to estimate directly from changes in recorded DBH measurements. These growth models can be used in the construction of IPMs from which other vital rate parameters are inversely estimated. For example, along with fecundity parameters, senescence of large individuals could be inversely estimated. Examples of this approach are found in Needham *et al.* (2016) or see A.3 for more details. In this way inverse models provide another method for translating across scales from individuals to populations, even when data are incomplete.

2.5.3 Validation of model outputs

Validating predictions of passage times and life expectancies is challenging given that few, if any, data sets extend over the full life cycle of a canopy tree. However, tree ring analysis provides estimates of age at given size and can be used for independent validation of passage times from demographic models. While tree ring data is not available from BCI, it has been collected from other tropical forests. Brienen & Zuidema (2006) used tree ring data to study lifetime growth patterns of six species from a Bolivian rain forest and found considerable variation both within and between species, with the average age at 60 cm varying by threefold between species and two-three fold within a species. While

a direct comparison of results is not possible given the differences in site and species, our estimates of passage times to 20 cm fall within the range of those estimated by (Brienen & Zuidema, 2006) and show similar variances.

Obrien *et al.* (1995) estimate age at given heights for eight species from BCI, including *P. copaifera*, one of the species used in this paper. They estimate an age of 130 years for a 20 m tall *P. copaifera* individual. Passage times to the corresponding DBH of 27.3 cm (based on the allometries provided in Obrien *et al.* (1995)) from our models were 75 and 98 years for stems starting in the fast and slow growth distributions respectively. Passage times from our IPMs are conditional on survival to the target size, with size-dependent survival estimated at a very fine resolution. This might explain the discrepancy between estimates, since Obrien *et al.* (1995) estimate passage times based on measurements of growth in just six size classes, albeit taking growth 1 SD above the mean for each size class to account for the higher survival rates of fast growers.

Metcalf *et al.* (2009) combine IPMs with a Markov model of transitions through light environments for nine species from a rainforest in Costa Rica. Estimates of passage time to 30 cm are 96 and 76 years for stems of the emergent species *Lecythis* starting the dark and light respectively. While again, this is a different species in a different site, results are remarkably similar to our estimates of passage time for the emergent *P. copaifera* (98 and 75 years to reach 27 cm, conditional on starting in the slow and fast growth distribution).

There is clearly a need for more data to be collected that can validate model outputs such as those generated here. Eventually, as data from permanent forest plots accumulates, it will be possible to validate estimates of passage time and life expectancy directly. In the meantime, tree ring data and dendrochronology data are important resources for ensuring our modelling efforts produce biologically plausible outputs.

2.5.4 Evolution, biodiversity, and carbon

Global Vegetation Models (GVMs) diverge widely in how they predict the feedback between climate and vegetation dynamics will play out (Cramer *et al.*, 2001; Friedlingstein *et al.*, 2006) resulting in vegetation dynamics constituting one of the largest sources of uncertainty in predictions of future climate (Medvigy *et al.*, 2010; Friend *et al.*, 2014).

Current GVMs translate knowledge of physiological processes into ecosystem dynamics, often with no consideration of processes acting at intermediate scales. Highly diverse communities are frequently reduced to just a few plant functional types (Köhler & Huth, 1998; Cox, 2001), such that any effect of interspecific differences on demographic rates is lost. Given that differences in demography influence size distributions, biomass, carbon

cycling dynamics, and the ability of species to respond to environmental change, it is important that future models take species differences in demography into account (Purves & Pacala, 2008). For example, a study of mortality rates in tree species across the USA found wide regional variation in species mortality rates that resulted from both regional variation in community composition and the effect of environmental conditions on mortality rates within species (Lines *et al.*, 2010). The authors conclude that including variation in mortality rates in GVMs could help reduce uncertainty in climate change predictions. While it may be possible to model individual species in temperate and boreal regions, in the tropics, where species richness is considerably higher (Lee *et al.*, 2002), it will be necessary to find biologically sensible ways to aggregate species.

In the last two decades, a new generation of model, derived from traditional gap models, has been developed. These models are underpinned by macroscopic equations describing the dynamics of forest plots, making them mathematically tractable and computationally efficient (Moorcroft *et al.*, 2001; Strigul *et al.*, 2008). As a result these models have the potential to be scaled up to large regions without the need to simulate millions of individual stems.

Outputs from the IPMs presented here could feed into large scale vegetation models in two ways. First they could providing benchmarks to validate outputs from large scale models. IPMs can be easily analysed using simple matrix algebra in order to infer population dynamics. Because construction and parameterisation of the IPMs is relatively straightforward, relying on simple forest inventory data, IPM outputs could be used for independent validation of results from large scale vegetation models, at scales for which we have available data. Small scale validation based on empirical evidence will be necessary for assessing uncertainty in large scale predictions (Moorcroft, 2006). Second, by providing an efficient way to analyse the demographic rates of hundreds of species, IPMs could be used to aggregate species into 'demographic types', enabling the incorporation of biodiversity into GVMs which cannot be parameterised at a species level.

2.5.5 Conclusions

Species differences in demographic rates are critical to determining the outcome of local competitive interactions. Over wide areas these competitive interactions determine species range shifts and shape community composition. Yet, moving from data at the level of the individual, through descriptions of vital rates and population models to an understanding of forest dynamics across large geographic and temporal scales remains an important challenge facing ecologists. By proposing simple models of vital rates that capture the

critical processes shaping populations, we make best use of increasingly available forest inventory data to translate knowledge of individuals into an understanding of dynamics at the population and community level. This demographic approach will be essential for reducing uncertainty in predictions of how forests will respond to global change.

Although we present our methods in the context of modelling forest trees, the techniques for building multi-state IPMs and using them to inverse model missing vital rate parameters are generally applicable to organisms with a range of life history strategies. Further, the framework presented here can be used to explore a range of ecological and evolutionary questions from optimal life history strategies to range shifts and community responses to disturbance.

Chapter 3

Forest community response to invasive pathogens: the case of ash dieback in a British woodland

3.1 Chapter Introduction

Outbreaks of forest pests and pathogens are increasing in frequency and severity with consequences for forest composition and ecosystem functioning. In this chapter I explore community dynamics in an 18 ha plot in Wytham Woods in response to a simulated outbreak of ash dieback disease. I demonstrate how the methods in the previous chapter can be combined with a spatially explicit individual based model that enables local competitive interactions to drive regeneration following ash mortality.

3.1.1 Authors

Jessica Needham, Cory Merow, Nathalie Butt, Toby Marthews, Yadvinder Malhi, Michael Morecroft & Sean M. McMahon

3.1.2 Author Contributions

JN and SM conceived of the study. JN carried out the analysis. JN wrote the manuscript. CM provided detailed comments on two drafts of the manuscript. SM, NB, YM, TM and MM provided data and feedback on the manuscript.

This paper was published in the Journal of Ecology (citation below) and the copy in this thesis, other than minor formatting changes is the same as the published manuscript.

Needham, J., Merow, C., Butt, N., Malhi, Y., Marthews, T.R., Morecroft, M. & McMahon, S.M. (2016). Forest community response to invasive pathogens: the case of ash dieback in a British woodland. *Journal of Ecology*, 104, 315?330.

3.2 Summary

1. Large-scale mortality events in forests are increasing in frequency and intensity and can lead to both intermediate and long-term changes in these systems. Specialist pests and pathogens are unique disturbances, as they commonly target individual species that are relatively prevalent in the community.

2. Understanding the consequences of pathogen-caused mortality requires using sometimes limited available data to create statistical models that can forecast future community states.

3. In the last two decades, ash dieback disease has swept through Europe causing widespread mortality of *Fraxinus excelsior* L. (European ash) across much of its distribution. In the UK, *F. excelsior* is an abundant and ecologically important species.

4. Using demographic data from an 18 ha plot in Wytham Woods, Oxfordshire, we built models that forecast the response of this forest plot to the loss of *F. excelsior*. We combine Integral Projection Models (IPM) and Individual Based Models (IBM) to link models of growth, survival, and fecundity to population dynamics. We demonstrate likely responses in Wytham by comparing projections under different levels of *F. excelsior* mortality. To extrapolate results to other systems, we test hypotheses regarding the role of abundance, spatial structure and demographic differences between species in determining community response to disease disturbance.

5. We show that the outcome of succession is determined largely by the differing demographic strategies and starting abundances of competing species. Spatial associations between species were shown to have little effect on community dynamics at the spatial scale of this plot.

6. *Synthesis*: Host-specific pests and pathogens are an increasingly important type of disturbance. We have developed a framework that makes use of forest inventory data to forecast changes in the population dynamics of remaining species and the consequences for community structure. We use our framework to predict how a typical British woodland will respond to ash dieback disease and show how vital rates, spatial structure and abundance impact the community response to the loss of a key species.

Key-words: Bayesian inference, disease disturbance, forest demography, Individual Based Models, Integral Projection Models, inverse models, plant population and community dynamics

3.3 Introduction

Global change driven by anthropogenic activities has resulted in a rising threat to forests from both native and introduced pests and pathogens (Brasier, 2008). Pests and pathogens that cause high mortality rates in the host species can have a profound impact on forest structure and function (Logan & Powell, 2001). The most recent Forest Resources Assessment (FRA) indicates that close to 40 million hectares of forested land were adversely affected by disease or insect outbreaks in 2005 (FAO, 2010).

Not surprisingly, the negative impact of forest pathogens is predicted to be greatest when the target is a dominant species (Ellison *et al.*, 2005; Loo, 2009). The ecosystem effects of epidemics in dominant tree species are well documented and include changes to ecosystem processes (Hicke *et al.*, 2012) and declines in populations of dependent species (Tingley *et al.*, 2002). Further, the loss of a dominant species can have a cascading impact on the forest as large mortality events can lead to other disturbances, such as increased fire risk, or the facilitation of an aggressive, non-native species. The loss of a dominant species from an ecosystem provides the opportunity to study the role of a single species in structuring community dynamics and regulating ecosystem processes, as well as determining the successional changes that take place upon its removal.

The decline in eastern hemlock, *Tsuga canadensis*, from North America due to the hemlock woolly adelgid, *Adelges tsugae*, has led to substantial changes in the microenvironment of the forest understory and a dramatic increase in the abundance of invasive plant species (Eschtruth *et al.*, 2006; Ford *et al.*, 2012). Another example is the mountain pine beetle *Dendroctonus ponderosae*, which has caused widespread mortality in *Pinus contorta* and *Pinus ponderosa* forests throughout the Rocky Mountains from Mexico to Canada. The reduction of carbon uptake and the increase in wood decomposition is great enough to have converted the affected region from a net carbon sink to a carbon source (Kurz *et al.*, 2008). The focus of this study, *Fraxinus excelsior* (European ash), is a dominant species in many woodlands across Britain (National Forest Inventory, 2012) and its expected decline due to the pathogen *Hymenoscyphus fraxineus* is likely to have important consequences for forest composition and biodiversity (Mitchell *et al.*, 2014).

3.3.1 Ash Dieback

Ash dieback disease is a current epidemic in Europe, caused by the fungal pathogen *Hymenoscyphus fraxineus* (Gross *et al.*, 2014). Significant numbers of diseased *F. excelsior* were first recorded in Poland in the early 1990's (Przybyl, 2002) and since then the fungus has spread rapidly causing widespread mortality of *F. excelsior* across its entire European distribution (McKinney *et al.*, 2014). The pathogen targets all size classes, although symptoms and eventual mortality progress more rapidly in smaller individuals (Keßler *et al.*, 2012). Progeny trials in Scandanavia predict that just 1% of natural populations will have resistance (Kjær *et al.*, 2012). However, while infection rates are high across Europe, there is substantial variation in mortality rates (Vasaitis & Lygis, 2008; Pliura *et al.*, 2011; Kirisits & Freinschlag, 2012; McKinney *et al.*, 2014).

3.3.2 Forecasting Forest Dynamics

How can we predict community responses in the aftermath of a dramatic disturbance? Classic theory on succession predicts that pioneer species will benefit from the disturbance caused by the loss of a dominant species, for example due to pest and pathogens or selective harvesting (Whitmore, 1998). However, spatial structure and pre-disturbance abundances are also important (Frelich & Reich, 1995). The spatial and temporal patterns of mortality influence the size and frequency of gap formation, with different gap sizes being associated with recruitment by different species (Kneeshaw & Bergeron, 1998). In addition, the initial abundance of each species can influence community trajectories following disturbance. Abundant species may have an initial recruitment advantage because they produce more seeds or are closer, on average, to gaps. But in the presence of superior competitors with faster growth rates or higher survival and fecundity, this advantage may be quickly lost and even abundant species can decline in relative dominance (Clebsch & Busing, 1989).

Fraxinus excelsior is ecologically important in a variety of forest and non-forest settings. Nevertheless, the consequences of ash dieback disease on forest ecosystems have not been well documented (but see Jönsson & Thor (2012); McKinney *et al.* (2012)). Throughout Europe, *F. excelsior* plays a keystone role in riparian forest ecosystems (Pautasso *et al.*, 2013). It is especially abundant in Britain, making up 14% of broadleaved forest standing volume nationally (National Forest Inventory, 2012), and is often dominant at smaller spatial scales. In many countries *F. excelsior* was clear-felled either upon infection by *H. fraxineus* or pre-emptively. Studies from clear-felled natural forest sites suggest very little *F. excelsior* regeneration and a shift towards increased abundance of other species (Lygis *et al.*, 2014). However, we predict that succession will play out differently where

the epidemic is left to run its course, as the time scale over which mortality occurs among different size classes differentially impacts regeneration across species.

Here, we develop a predictive framework to test hypotheses about responses to the anticipated loss of *F. excelsior* due to ash dieback disease. We combine population and community level models to forecast succession in our study plot and similar woodlands, and address the following hypotheses:

H1: The severity of *F. excelsior* mortality will determine the post-disturbance dynamics. Specifically, we expect the *F. excelsior* population to show limited or no recovery once the population is reduced beyond a certain threshold. As a result, we expect remaining tree species to show short-term regeneration when *F. excelsior* mortality is low, and more sustained increases in BA and population size when *F. excelsior* mortality is high.

H2: Increases in population size and BA of remaining species will depend on demographic rates, as oppose to initial abundances. Thus, *A. pseudoplatanus* will be capable of significant increases even when it starts with a small population size.

H3: Spatial associations between *F. excelsior* and other species will determine patterns of regeneration.

H4: Under all mortality scenarios, the total BA and total number of trees of all species will recover to pre-disturbance levels within 100 years, although the size structure will shift as the gaps left by the mortality of large *F. excelsior* trees get filled by smaller recruits.

We conclude by generalising our insights to other forest ecosystems faced with disturbance from pests or pathogens.

3.4 Materials and Methods

3.4.1 Data

Site Description

Our study area is the 18 ha permanent plot in Wytham Woods, Oxfordshire, UK (51.77N, -1.34W). For details on Wytham Woods and its management history see Savill *et al.* (2010); Morecroft *et al.* (2008). Wytham Woods is typical of southern England, with a temperate climate that rarely experiences either snow or temperatures above 30 °C (Butt *et al.*, 2009). The plot lies in an area of disturbed, ancient, semi-natural woodland with a small section of secondary woodland and an abandoned small scale-plantation.

Data from 164 100 m^2 monitoring plots across Wytham showed that since 1974 the occurrence and basal area (BA) of *Acer pseudoplatanus* and other canopy species such

as *Quercus robur* and *Fagus sylvatica* has been relatively stable while *F. excelsior* has increased in both frequency and basal area (Kirby *et al.*, 2014). As is typical in other woodlands (Waters & Savill, 1992), *F. excelsior* has also dominated regeneration in Wytham in the last few decades (accounting for 75% of seedlings in 2012), while *Q. robur* and *F. sylvatica* show virtually no regeneration (Kirby *et al.*, 2014). High mortality of *F. excelsior* could therefore leave significant canopy gaps and an opening of the understory. The fungal pathogen, *H. fraxineus* has been observed in nearby woodlands, but not yet in Wytham Woods (http://chalaramap.fera.defra.gov.uk/). We expect it to arrive in the next few years.

Data

The forest plot is part of the Smithsonian Institution's Forest Global Earth Observatory network of plots (http://www.forestgeo.si.edu/), and data collection follows a standardized protocol (Condit, 1998). The 18 ha plot is arranged as a 6 ha x 3 ha grid, with each hectare further divided into 25 20 m x 20 m subplots. In the plot, all woody stems greater than 1 cm diameter at breast height (DBH) are measured, identified, and mapped. Measurements of DBH were at a marked point of measure. This census was conducted twice, in 2008 and 2010. In total, more than 20300 stems of 24 different species were recorded over the two censuses (Butt *et al.*, 2009). The plot lies in an area of relatively young growth ($<$ 150 years) with few very large trees relative to the large number of smaller stems (see Fig. D.1 in Supporting Information).

We used observations of 16188 individuals from censuses two years apart. This census interval is relatively short compared with the lifespan of a canopy tree. The census years were representative of the climate over the 30 preceding years (Fig. D.2) with the exception of November 2009, which had 86 mm more precipitation than average, and December 2010 which was 3.3 °C colder than average (CRU CL 2.0). Building models from such a short census interval represents a critical challenge in managing forests under global change. Even censuses 1-2 decades apart represent a short window in the lifespan of most trees, and with many forests worldwide uncensussed, the prospect of obtaining data over longer intervals is extremely limited.

Species groupings

The four most abundant species were treated separately and the remaining species were pooled into either sub-canopy or canopy groupings according to life-form (table D.1). The four most abundant species, which together made up 94% of stems, were *Acer pseudoplatanus* (sycamore), *Fraxinus excelsior* (European ash), both canopy species, *Crataegus monogyna* (hawthorn) and *Corylus avellana* (hazel), both sub-canopy species. Remaining species had too few individuals across the size distribution to infer vital rates

parameters at the species level. Pooled rare species are referred to as 'rare sub-canopy' and 'rare canopy'.

3.4.2 Models and simulations

Simulation overview

The workflow proceeds in three stages. In the "Vital Rate Models", we first develop novel functions to describe individual vital rates, and use Bayesian MCMC methods (Hastings, 1970; Gelman & Hill, 2007; Gelman *et al.*, 2013) to estimate species specific parameters directly from the census data. In "Inverse Estimation from Integral Projection Models (IPMs)", we take an inverse modelling approach to estimate vital rate parameters that could not be inferred from the census data (fecundity and several survival parameters). For each species or pooled species group, this involves a second Bayesian MCMC analysis in which we use population-level summary statistics from IPMs to estimate 'missing' individual-level vital rates parameters. Finally, in "Forward projection with an Individual Based Model (IBM)" we use vital rates parameters derived from the IPM analysis to drive spatially explicit IBMs that test how different mechanisms–spatial structure, ash dieback severity and interspecific demographic variation–differentially influence forest dynamics within our study plot (Fig. 3.1).

Vital Rates Models

Survival: A mixture of logistic functions

Survival between censuses was recorded as a binary variable. For each species, survival probability was modelled as a function of individual size x using two five-parameter logistic functions that meet at a species-specific size threshold k (equation 3.1). This approach is similar to a generalised additive model, and captures the high mortality of small trees, followed by the increase and plateau in survival before a gradual senescence at larger sizes. The five-parameter form offers a flexible way of adjusting the lower and upper asymptotes of survival probability along with the rate and symmetry of change and the size at which it occurs (Fig. D.3). By splicing together two logistic functions, we ensure that the many observations at small sizes do not influence parameter estimates at sizes that have fewer data due to the numerical dominance of small individuals. The survival function takes the form:

$$\text{logit}(s) = \left(L_1 + \frac{K_1 - L_1}{1 + \left(\frac{1}{\theta_1 e^{-r_1\left(\frac{x-p_1}{\theta_1}\right)}} \right)^{\theta_1}} \right)^t \quad \text{for all } x < k \tag{3.1}$$

$$\text{logit}(s) = \left(L_2 + \frac{K_2 - L_2}{1 + \left(\frac{1}{\theta_2 e^{-r_2\left(\frac{x-p_2}{\theta_2}\right)}} \right)^{\theta_2}} \right)^t \quad \text{for all } x \geq k \tag{3.2}$$

where L and K are the lower and upper asymptotes of the survival curve respectively, θ, r and p are the symmetry, rate and inflection point of the curve respectively, x is DBH, t is time in years between census intervals and k is the size threshold at which the curves meet. For small individuals, r_1 is constrained positive, such that survival probability increases with increasing size. For large adults, r_2 is constrained negative so that survival probability decreases with increasing size. K_1 is always equal to K_2 to ensure the two curves meet without sharp changes in survival probability with size. The parameters for each curve, and the size threshold at which the curves meet, were all inferred using Bayesian MCMC analysis (Fig. D.4 and table D.3).

Growth: Distributional models with flexible variance structure

Growth increment was based on absolute change in DBH. We assumed that the apparent dramatic shrinkage (> 6mm) or growth (> 50mm) of a number of trees was due to measurement error and these trees (29) were removed from further analysis. We corrected for smaller measurement errors following the method described by (Rüger & Condit, 2012).

We assumed that growth was determined by the light environment of each individual. The growth increment data collected at Wytham was highly right-skewed with the majority of individuals growing very little each year and a small minority having much larger increments (Fig. D.5). We therefore fit two distributions to the growth data for each species; a lognormal distribution describing the low mean and right skew of the majority of growth increments, $z \sim \text{lognorm}(\mu, \sigma)$ and a truncated normal describing the higher mean and more symmetric distribution of the fastest growers, $z \sim \text{truncnorm}(\mu, \sigma, \alpha, \beta)$, where z is increment in mm, μ and σ are the species-specific mean and standard deviation of each distribution, and α and β are 0 and ∞, respectively, to prevent negative growth.

We assumed that the slow-growing individuals were those experiencing low light conditions, and the fast-growing individuals were those experiencing high light conditions; either

in gaps or because they were tall enough to reach the canopy. Indirectly inferring light environment in this way is a critical step for capturing crucial individual-level variation that drives forest dynamics by taking advantage of typical census data where environmental covariates are unavailable.

For each species, we fit the lognormal distribution to the slowest 95% of increment data and the truncated normal to the fastest 5% of increment data. This reflects the general probability that non-canopy individuals have access to high light during the year. For the three species with the potential to reach canopy height (*A. pseudoplatanus*, *F. excelsior* and 'rare canopy') we also defined a size threshold of 250 mm DBH, where growth from individuals above this size also contributed to the "fast" growth distribution. This step is based on the assumption that individuals with a DBH above 250 mm are tall enough to have reached the canopy and are therefore in high light and not subject to the constraints of low-light environments. These individuals do, however, contribute a few small increments to the fast growth distribution. Species specific parameters were inferred using Bayesian MCMC methods (Fig. D.6 and table D.4).

Inverse Estimation from Integral Projection Models (IPMs)

Key limitations in available data create challenges to predicting whole forest dynamics, especially for projection where all life-history stages need to be included in the model. Common monitoring protocols often lack data on seed production and germination and seedling transitions due to logistical constraints (Comita *et al.*, 2007). Further, once trees escape high seedling and sapling mortality, they generally have high survival throughout their lifetimes (>97% survival per annum). Mortality events are rare and highly stochastic, meaning that few deaths of larger individuals or rare species are recorded in a typical short census interval. These challenges led us to the use of inverse models.

Inverse models use simulation output to describe parameters that have no *a priori* likelihood (Hartig *et al.*, 2014). We fit inverse models to infer demographic transitions without direct observation of those transitions (Wood, 1987). For example, population size is the outcome of survival, growth, and reproduction, and can be used to infer parameter values for each of these vital rates in stage structured models (González & Martorell, 2013) or in unstructured models (Besbeas *et al.*, 2003). Using the survival and growth parameters inferred above, which derive from extensive data, along with initial estimates of fecundity parameters, we inferred a fecundity value for all species groups that would 1) reflect approximate long-term recruitment so that the species had the potential to contribute to forest structure, and 2) demonstrate low overall sensitivity of dynamics to this estimated recruitment component. To do this, we constructed integral projection models (IPMs; (Easterling *et al.*, 2000; Merow *et al.*, 2014a) to project populations with

continuous stage structure (e.g. individual size) forward in time based on a transition 'kernel' that describes the size dependence of survival, growth and offspring production (analogous to matrix population models described by Caswell (2000); Morris & Doak (2002)), and used the output of these IPMs to determine population growth rate, λ. This enables us to run an inverse estimation of recruitment that maintained a general population stability across the forest community. The proposed 'missing' parameters are accepted or rejected in a Bayesian MCMC analysis based on the fit of the eigenvalues from the IPMs to $\lambda = 1$. In this way, population summary statistics feedback to inform individual level parameters which could not be estimated directly from the census data (fecundity, and *p1*, *p2*, *r1* and *r2*) (see Hartig *et al.* (2014) and Beaumont (2010) for a more comprehensive description of inverse models and approximate Bayesian computation methods).

As in Cobb *et al.* (2012), in our inverse models, we make the assumption that the population is stable (population growth rate, λ, equal to one) to infer fecundity and missing survival parameters. There are two apparent drawbacks to this approach. Firstly, there are multiple combinations of parameters that can give rise to a megamatrix with $\lambda = 1$. However, since the growth parameters and the majority of survival parameters are fixed, we are only finding a limited number of parameters that, in combination with these fixed parameters, give a λ =1, and this greatly reduces the parameter space that needs to be searched and the possible values that can be inferred.

Second, the assumption of $\lambda =$ itself could be seen as problematic given that the populations in Wytham are surely not at equilibrium. However, it is important to note that these parameters are for IPMs which model each species in isolation. These IPMs are a tool to enable us to parameterise a spatially explicit IBM in which interactions between species, including competition and density dependence, combine with spatially dependent processes such as seed dispersal, in order to determine community dynamics. A species with parameters giving it a λ =1 in the IPM is unlikely to be stable in the IBM when these other processes operate. Crucially, it enables us to infer fecundity and survival parameters which could not be directly estimated without decades of further data collection.

Fecundity

To construct IPMs that model the full life history of a population, we need a fecundity function describing the production of offspring and the distribution of offspring sizes. We made three assumptions about the probability of reproduction by each individual: 1) there is a reproductive size threshold below which individuals cannot reproduce, 2) the probability of producing offspring scales with basal area, and 3) the probability of reproduction by trees is different in low and high light environments (equation 3.3).

The number of recruits, r, produced per individual of DBH x is given by:

$$b = \begin{cases} \pi \left(\frac{x}{2}\right)^2 f_i j & \text{for all } x \geq D_i, \\ 0 & \text{for all } x < D_i \end{cases} \tag{3.3}$$

Where f_{ij} is the fecundity parameter corresponding to the species i in light environment j (j = high or low) and D_i is the reproductive size threshold for species i.

We estimated D as the 0.8^{th} quantile of DBH measurements for each species, with the exception of 'rare canopy' species where we capped D at 250 mm (due to an ageing population of *Quercus robur* the 0.8^{th} DBH quantile of 'rare canopy' species was 620 mm–much larger than known reproductive size). Further, for the three species where individuals have the potential to reach the canopy, we assumed that only those individuals in the fast growth distribution corresponding to high light would be reproductive (Fig. D.7 and table D.5). We modelled the distribution of offspring sizes as 10 mm plus one year's increment from the slow growth distribution.

IPMs with multiple light environments

To construct IPMs that move individuals between light environments characterized by high and low growth and fecundity functions, we follow the method of Caswell (2012), adapting an age by stage modelling framework to environment by stage and replacing standard population matrices with IPM matrices. This results in so-called 'megamatrices', in which each element of a megamatrix describes the product of the transitions between environmental conditions and the integral projection kernel describing the full life history of the species (Fig. D.8).

In our models, the megamatrix described transitions between low and high light environments, similar to those used by Metcalf *et al.* (2009), who modelled the trajectories of individuals based on continuous growth determined by transitions between nine different light environments. However, whereas Metcalf *et al.* (2009) had direct observations of the transitions between light environments, these are lacking for Wytham. We therefore calculated transition probabilities from the overlap of each growth distribution with the increment threshold that is used to delimit the two distributions (corresponding to the 0.95^{th} quantile of increment data) (Fig. D.9). In other words, the proportion of the lognormal distribution (describing slow growth in low light) that is above the increment corresponding to the 0.95^{th} quantile of all increment data was used as the transition probability from low light to high light. Likewise, the proportion of the truncated normal (describing fast growth in high light) that was below the 0.95^{th} quantile of all increment data, described the transition probability from high light to low light. The distribution

of offspring into high and low light environments matched the transition probabilities between light environments by adult trees of that species, regardless of parent size or light environment.

Forward Projection with an Individual Based Model (IBM)

To combine the dynamics of multiple species we used parameters from the IPMs in spatially explicit Individual Based Models (IBMs). Our IPMs ignore individual differences, except as far as they are captured by the individual size and light environment state variables. However, spatial structure can be key to determining community dynamics, and can only be described at the individual level. Hence we adopted an IBM framework that allowed us to use the vital rate models fitted with the inverse model to simulate forest dynamics while reflecting individual-level spatial structure.

For each year of projection, the IBM involves six steps (Fig 3.1):

1. Survival of each tree is simulated from a binomial distribution with probability taken from the fitted survival function at the appropriate size.

2. Survivors grow according to the distribution corresponding to their light environment and species identity. The light environment for each individual is determined by its competition index, calculated before starting the IBM and again at the end of each year (step 5).

3. The BA of each individual above the reproductive size threshold is multiplied by the species specific fecundity parameter (describing the number of recruits per unit BA) corresponding to its light environment to give a per capita contribution to recruitment. Summing across all reproductive individuals gives the total number of recruits per species.

4. Recruits are distributed according to the BA of reproductive adults in each subplot, representing seed dispersal. We enforce density dependence by limiting the number of recruits that enter the plot each year to 0.05 times the starting plot population. Recruits have a higher probability of removal in the density dependence step if located in subplots with high recruit density, representing thinning at the seedling stage, and/or high total BA, representing the increased likelihood of survival in gaps.

5. Competition is recalculated to take into account the growth of existing trees and the addition of new recruits (see below).

6. Return to step 1.

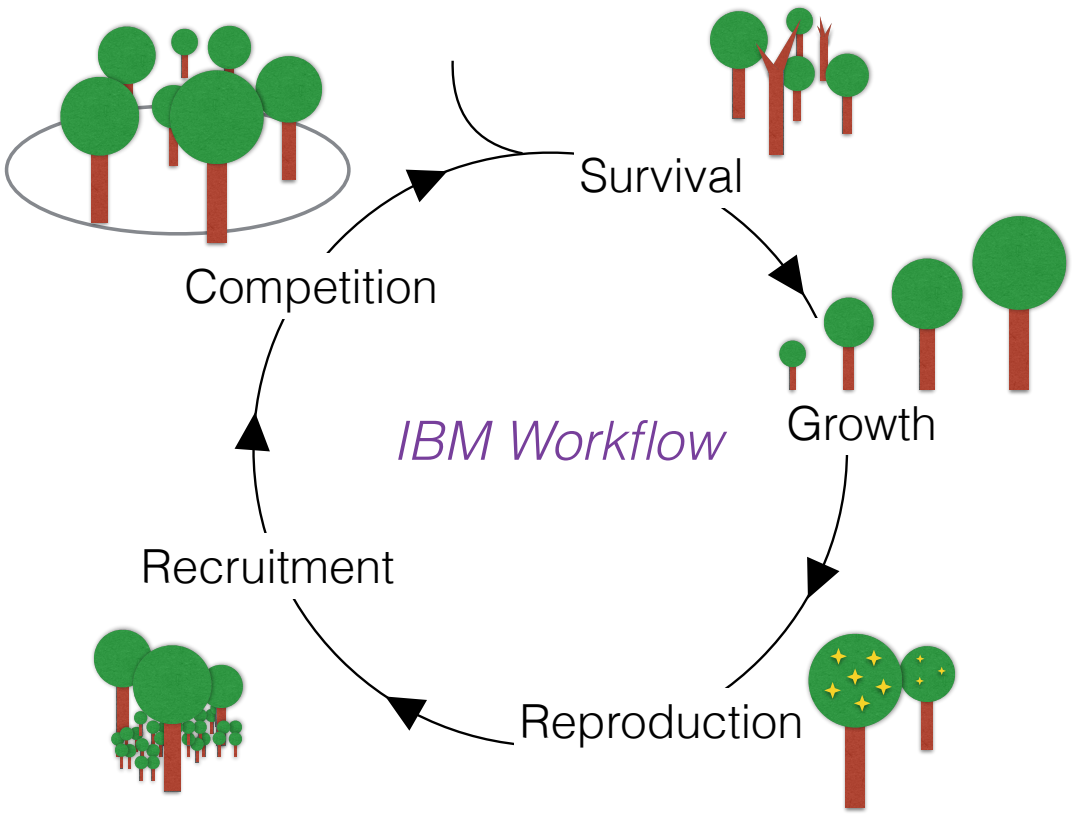


Figure 3.1: Schematic of the individual-based model. Each year trees survive or die as a function of their diameter at breast height (d.b.h). Surviving trees grow with an increment drawn from a distribution dependent on their species and light environment. Individuals with d.b.h. above a reproductive threshold produce offspring. During the recruitment stage offspring are distributed between subplots based on the basal area (BA) of reproductive adults. Density dependence thins the new recruits, removing recruits from areas with a high density of recruits and a high BA of all trees. Competition is recalculated each year and determines the light environment of each individual. The individual-based model is parameterised from a mix of vital rates models fit to census data, and inverse models which infer parameter values for which there were no data.

Competition

In the IBM, we allow competition to determine the light environment of every tree. Since height scales with DBH, competition is calculated by defining a circle with a 10 m radius around each individual and summing the BA of larger neighbours. We tested the assumption that competition is a good predictor of light, and hence growth, with a linear model of increment growth against competition for each species. There was a statistically significant negative relationship between competition and increment growth for all six species (table D.2.).

We use the 5^{th} percentile of competition indices from the 2010 census as the fixed threshold for high light in all years of the IBM; all individuals with competitive indices below this value are assumed to be in high light, while those with competitive indices above this value are assumed to be in low light. In this way, an increase in the number of gaps in the plot results in a higher proportion of individuals included in the high light environment due to competition indices below the fixed threshold.

3.4.3 Experimental design and analysis

Simulating Ash dieback

At the time of writing, ash dieback had not yet arrived in Wytham Woods, thus its effects on mortality at this location was still unknown. To test hypotheses H1 and H4 we explored four possible mortality scenarios with the IBM. In each scenario, we killed *F. excelsior* at a constant rate for the first ten years of the simulation to bring its population down to either 0%, 25%, 50%, or 75% of the initial population size. After ten years, pathogen-driven mortality was no longer included in the simulations, to allow for the possibility of survival and regeneration of resistant *F. excelsior* individuals. As a baseline we included a scenario with no ash dieback. For each scenario, we ran 10 stochastic replicated projections for 100 years each. *Fraxinus. excelsior* stems were randomly removed each year irrespective of size. We tested a wide range of mortality scenarios to reflect the substantial variation in estimated mortality rates across Europe (e.g. (Vasaitis & Lygis, 2008; Kirisits & Freinschlag, 2012)). While some of these scenarios are at the high end of mortality predictions, they are useful to illustrate more generally the potential impacts of host-specific pests and pathogens, and also reflect an observed "worst case scenario" for *F. excelsior*.

Spatial location

To test whether spatial structure determines regeneration patterns (H3), and allow better extrapolation of results to other forests without the pattern of species distributions observed

in our plot, we mixed the locations of stems by sampling without replacement from the observed paired coordinates (Fig 3.2b). This enabled us to break down associations between *F. excelsior* and other species while still preserving species' size distributions. We implemented two spatial tests. In one test, *F. excelsior* was included in the spatial randomisation, and in the second it was excluded. This changed whether there were many widespread smaller gaps versus fewer large gaps left from the removal of clusters of *F. excelsior*. Gaps of different sizes have been shown to favour recruitment by different species (Kneeshaw & Bergeron, 1998) and the different tests were therefore expected to lead to different successional outcomes.

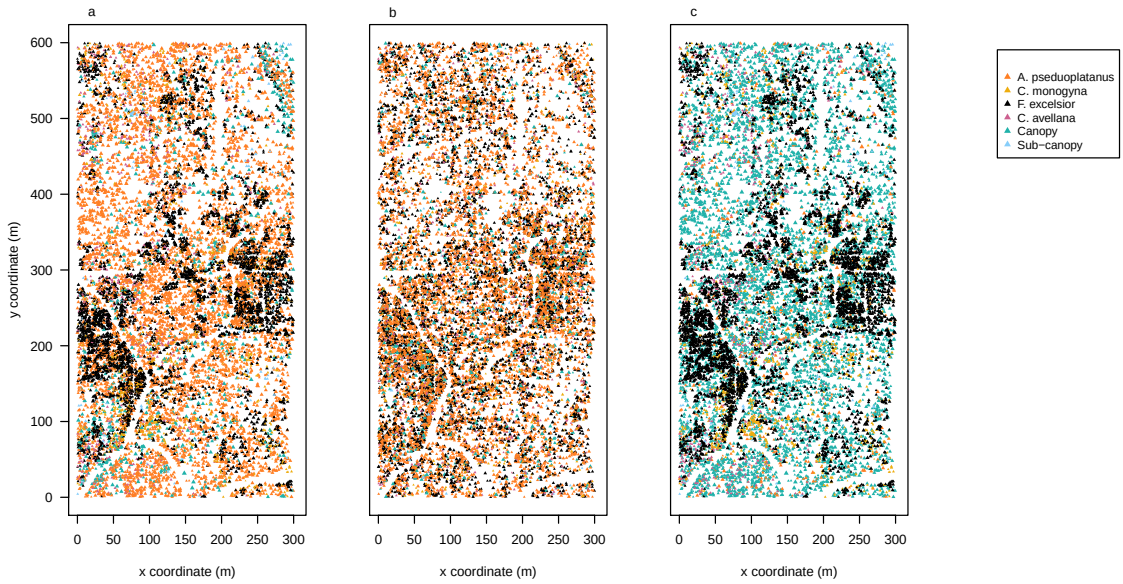


Figure 3.2: Maps showing the distribution of individuals at the start of example hypotheis tests, (a) mortality scenarios, (b) spatial randomisation including Fraxinus excelsior in the mixing and (c) abundance test iwth low *Acer pseudoplatanus* starting population. In (c), the ratio of *A. pseudoplatanus* to rare canopy species was changed to 1:9 to test the invasion potential of *A. pseudoplatanus*. Spatial and abundance test were run at 75% *F. excelsior* mortality. Points are scaled by diameter at breast height.

Abundance

To test the effect of pre-dieback abundance on the ability of species to colonise the gaps left by *F. excelsior* (H2), we ran the IBM while changing the initial population size of *A. pseudoplatanus* and 'rare-canopy' species (Fig 3.2c). These projections were compared to the IBMs with observed starting abundances, and differences in population dynamics were interpreted as the effect of initial population sizes. We kept the starting abundance of *F. excelsior* constant so as not to change the amount of gaps produced. The total number of individuals of canopy species remained the same, only the proportions of each species

changed, enabling us to maintain a realistic size and spatial structure in the plot while also changing the starting population sizes.

Our main interest was in the effect of starting abundance on the non-native *A. pseudoplatanus* (sycamore) since it is the most abundant species in the 18 ha plot. The different treatments were therefore as follows:

a) *Acer pseudoplatanus* and 'rare canopy' started with equal abundance. Other species started at their observed abundances.

b) Acer pseudoplatanus started at 10% and 'rare canopy' at 90% of canopy species (excluding *F. excelsior*). Other species started at their observed abundances.

c) *Acer pseudoplatanus* started at 0% and 'rare canopy' at 100% of canopy species (excluding *F. excelsior*). Other species started at their observed abundances.

We tested both the spatial and abundance hypotheses at 75% *F. excelsior* mortality and ran 10 simulations of each treatment for 100 years. We chose this mortality level as it is similar to observed mortality rates in parts of Europe where ash dieback has been established for several decades (Vasaitis & Lygis, 2008). It is also high enough to result in many new gaps being formed and thus allowed us to more easily explore the effects of succession.

Demography

The effect of demography was implicitly tested in the hypotheses tests above. After accounting for initial abundances and spatial structure, we were able to determine how much community structure was influenced by differences in demographic strategies. If species were able to invade despite low starting abundances, this was due to highly competitive life history strategies i.e. high fecundity, growth rates and/or survival. On the other hand, if a species increased in the standard mortality simulations significantly more than in a simulation in which spatial associations had been broken down, we could conclude that a spatial association with *F. excelsior*, and therefore proximity to gaps left by ash dieback, was partially responsible for its success following *F. excelsior* mortality.

Sensitivity Analysis

Fecundity parameters for use in the IBM were inferred from the inverse model based on the assumption that the population growth rate of each species was stable during the census interval ($\lambda = 1$), which is unlikely to have been the case. To test the sensitivity of our results to this assumption we ran the IBM with either altered fecundity parameters (0.5 or 1.5 times the values inferred from the inverse model), or with fecundity parameters from the inverse model (those that give $\lambda = 1$), but varying levels of density dependence

(the number of new recruits each year limited to 0.01 or 0.1 times the starting total plot population). These tests were again run with ash dieback mortality at 75%, similar to mortality rates observed in Europe so far (Vasaitis & Lygis, 2008) and high enough to allow easy interpretation of the effect of fecundity parameters and the strength of density dependence in determining the response to the loss of *F. excelsior*.

All work was carried out in R 3.1.2 (R Core Team, 2014), using the Matrix (Bates & Maechler, 2015), SpatialTools (French, 2014) and igraph (Csardi & Nepusz, 2006) packages.

3.5 Results

Mortality Scenarios

The plot's population size and BA, recovered from the loss of a dominant species within 100 years (Figs 3.3, 3.4). In all mortality scenarios, the total BA and population size of the plot initially decreased as the *F. excelsior* population was reduced but remaining canopy species responded to the loss of *F. excelsior* with rapid increases in population size, and after a short lag, increases in BA, such that within a century the total plot BA and population size were above pre-disturbance levels, even in the 100% mortality scenario (see also tables D.6, D.7, D.8, D.9, D.10 and tables D.16, D.17, D.18, D.19, D.20). 'Rare canopy' species showed the greatest increase in population size in all mortality scenarios, from 856 to 7144 after 100 years in the 75% mortality scenario, but *A. pseudoplatanus* showed the greatest response to the loss of *F. excelsior*, i.e. a greater increase relative to its trajectory in the no dieback scenario (Fig 3.4). For example, after 100 years the *A. pseudoplatanus* population had 2124 more individuals in the 75% mortality scenario than in the no dieback scenario, while the 'rare canopy' population had 1134 more individuals in the 75% mortality scenario compared with the no dieback scenario. After 100 years, the total plot population size in all mortality scenarios had reached the levels predicted in the no dieback control. However, due to the large increase in BA of *F. excelsior* in the no dieback control, total BA m^2 ha^{-1} was still lower in each mortality scenario than in the no dieback control.

Spatial Tests

The spatial tests had little effect on the plot dynamics (Fig. 3.5). The *F. excelsior* population recovered marginally better from 75% mortality when there was no mixing of any species compared with either spatial test. 'Rare canopy' species also performed better when spatial distributions were as observed, with a population of 7144 after 100

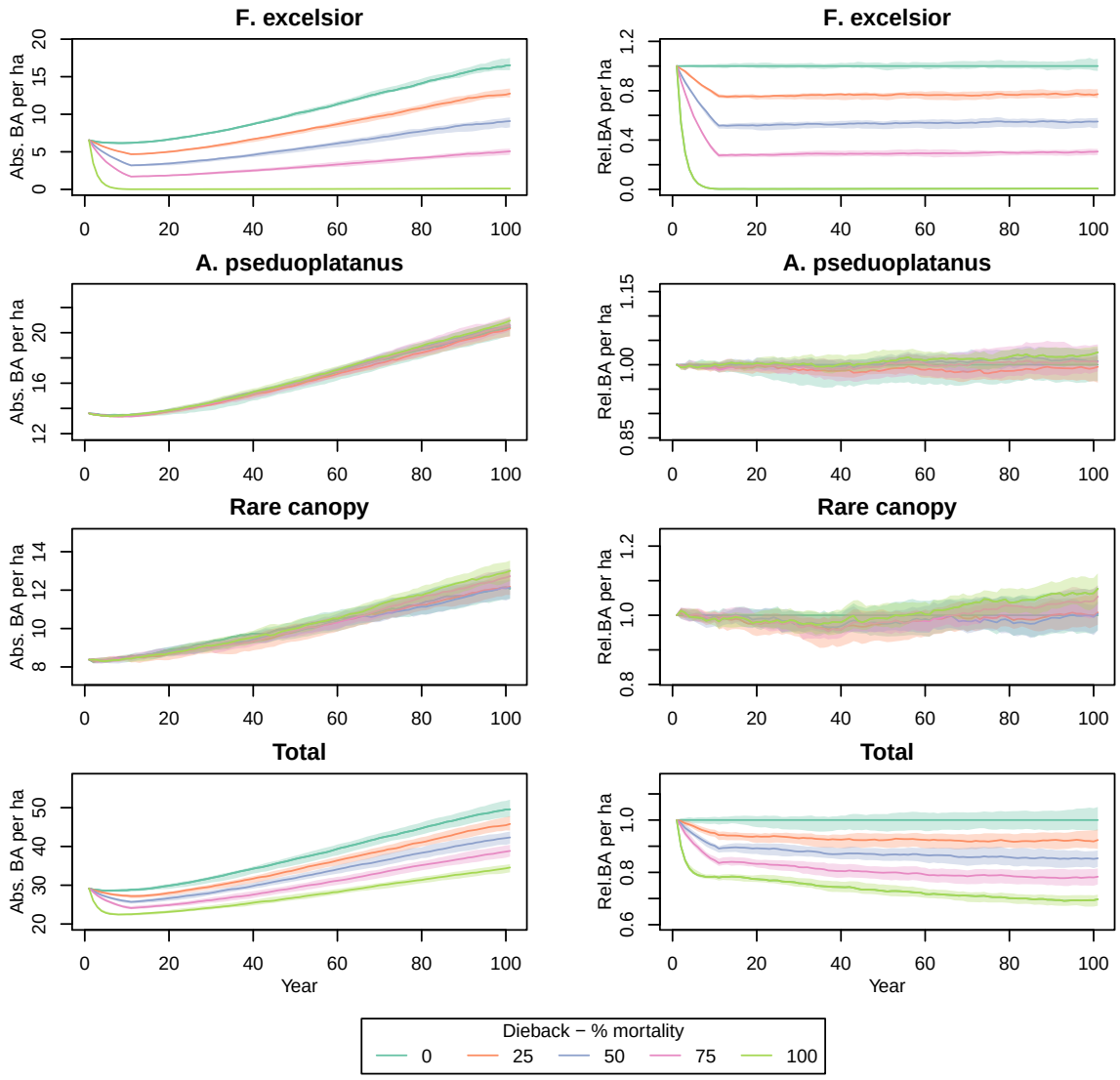


Figure 3.3: Basal area (BA m^2 ha^{-1}) of the canopy species and the total BA m^2 ha^{-1} through time, under each mortality scenario. Left-hand panels show absolute BA m^2 ha^{-1}, while right-hand panels show BA m^2 ha^{-1} relative to the 0% mortality scenario (i.e. mortality scenario/0% mortality). Shading depicts 5th and 95th percentiles from 10 simulations at each mortality level. Medians are shown by the darker lines. Both *Acer pseudoplatanus* and rare canopy species increased in BA m^2 ha^{-1} throughout all simulations but increases were greatest in higher dieback scenarios. The BA of *Fraxinus excelsior* recovered well and after 100 years was nearly at pre-disturbance levels even in the 75% mortality scenario.

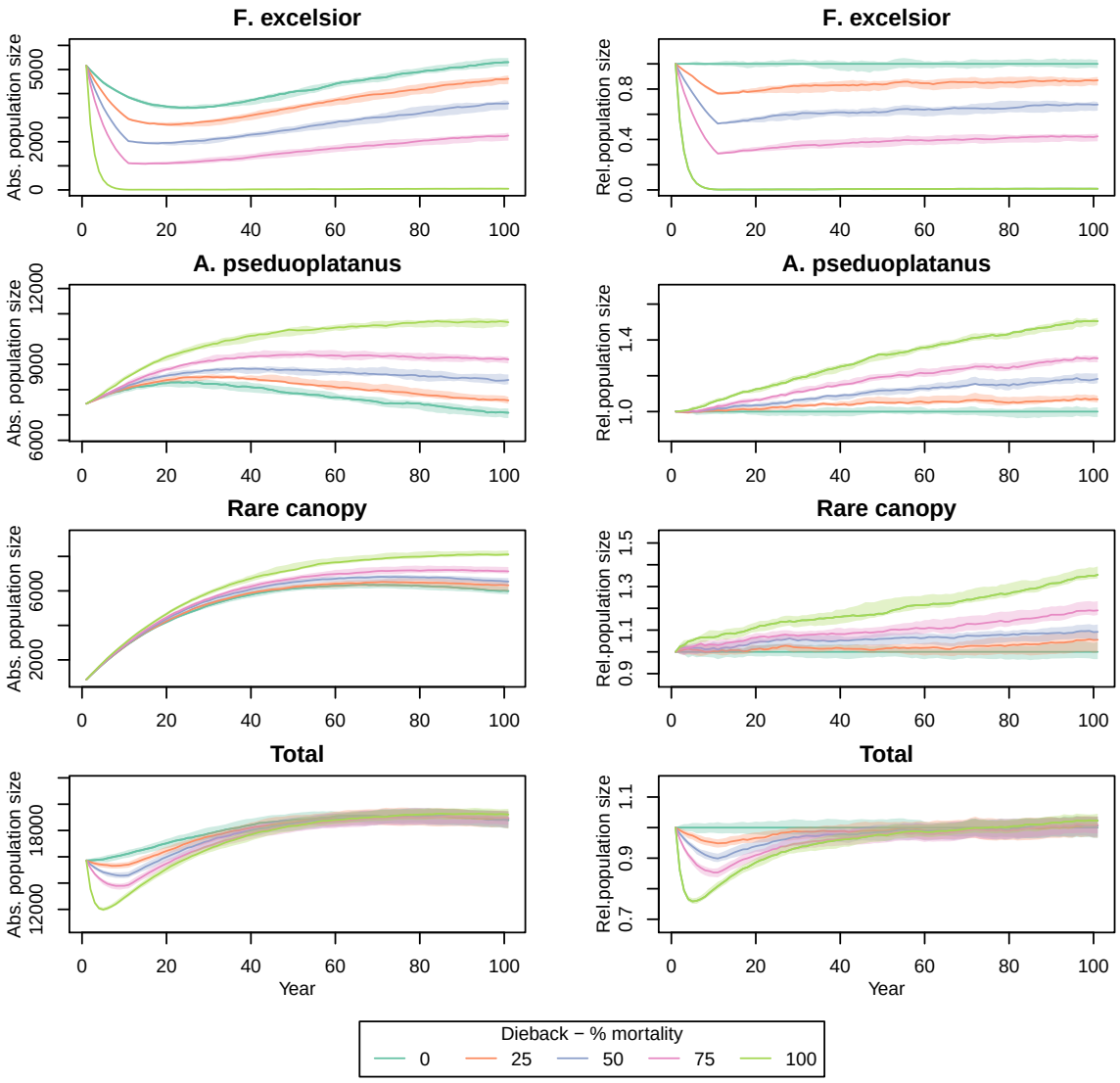


Figure 3.4: Population size of canopy species through time, under each mortality scenario. Left hand panels show absolute population size while right hand panels show population size relative to the 0% mortality scenario (i.e. scenario / 0% mortality). Shading depicts the 5th and 95th percentiles from 10 simulations of each scenario. Medians are shown by darker lines. Rare canopy species showed the greatest overall increase in population size whereas *Acer pseudplatanus* showed the greatest increase in recruitment in response to increasing *Fraxinus excelsior* mortality. The *F. excelsior* population was able to persist in all but the 100% mortality scenario, although it took 100 years for the population to reach pre-disturbance level in the 25% mortality scenario.

years in the 75% mortality scenario compared with 6856 and 6780 in the spatial tests including and excluding *F. excelsior* respectively (tables D.9, D.11, D.12). In contrast, *A. pseudoplatanus* had the highest recruitment in the spatial test excluding *F. excelsior* from the mixing. After 100 years its population was 9358 when all species bar *F. excelsior* were shuffled, compared with 9273 when *F. excelsior* was included in the mixing and 9224 when spatial structure was left as observed in the census. Differences in BA between the two spatial tests and the comparison 75% mortality scenario were small for every species (tables D.19, D.21, D.22).

Abundance Tests

When the starting population size of *A. pseudoplatanus* was decreased and made equal to 'rare canopy' species, it was still able to increase rapidly. After approximately 25 years, the population followed the same trajectory as in the 75% mortality scenario, where starting abundances were not manipulated (Fig. 3.6; tables D.19, D.23, D.9, D.13). However, when the ratio of *A. pseudoplatanus* stems to 'rare canopy' stems was 1:9, *A. pseudoplatanus* failed to increase to the same extent (tables D.24, D.14). After 100 years, the BA of *A. pseudoplatanus* was 3.19 m^2 ha^{-1} when it started rare, compared with 15.29 m^2 ha^{-1} when it started at the same abundance as 'rare canopy' species. 'Rare canopy' species showed a much greater increase in population size and BA when *A. pseudplatanus* was rare. The total forest population size was also higher in the treatments with *A. pseudoplatanus* low or absent, a result of the increased fecundity of 'rare canopy' species relative to *A. pseudoplatanus*.

Sensitivity Analysis

Results from the sensitivity analysis show that density dependence had more effect on the IBM results than fecundity parameters (Figs D.14, D.15). The fecundity parameters were inferred in our inverse model based on the assumption of a starting population at equilibrium, i.e. with a population growth rate (λ =1). In our sensitivity analysis we ran the IBM with fecundity parameters from the inverse model either increased or decreased by 50%. We also ran IBMs in which we changed the strength of density dependence by limiting the number of recruits that enter the plot each year to either 0.01 or 0.1 times the starting total plot population. Changing the strength of density dependence had a much greater effect on the dynamics of the majority of species than altering the fecundity parameters. Qualitatively, the results from the IBMs with altered fecundity parameters were very similar to the IBMs in which we used parameters inferred from inverse model. The sensitivity analysis therefore suggests, that our IBM results are robust to the necessary inverse model assumption of starting populations at equilibrium.

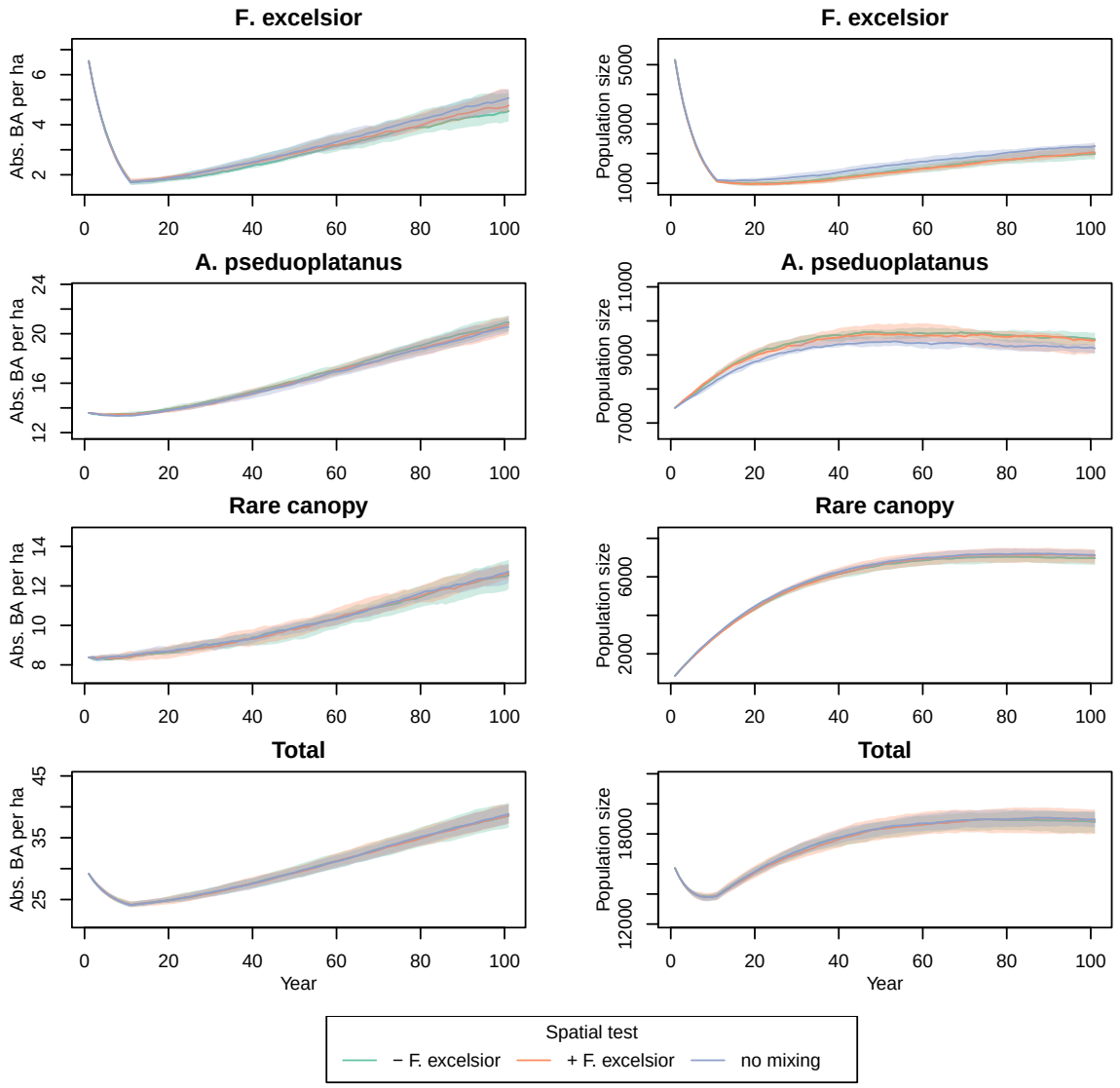


Figure 3.5: Results of the spatial randomisation tests showing basal area BA m^2 ha^{-1} (left hand panels) and population size (right hand panels) of canopy species through time. Spatial randomisation involved reassigning paired coordinates to each stem, with *Fraxinus excelsior* either included (+ *F. excelsior*) or excluded (- *F. excelsior*) from the mixing. Shading depicts the 5th and 95th percentiles from 10 simulations of each scenario. Medians are shown by darker lines. The spatial tests were run at 75% *F. excelsior* mortality which is also plotted for comparison (no mixing). Overall, spatial tests had very little effect on forest dynamics, although *Acer pseudoplatanus* increased more in randomisation tests than in the no mixing scenario, while the opposite was true for *F. excelsior*.

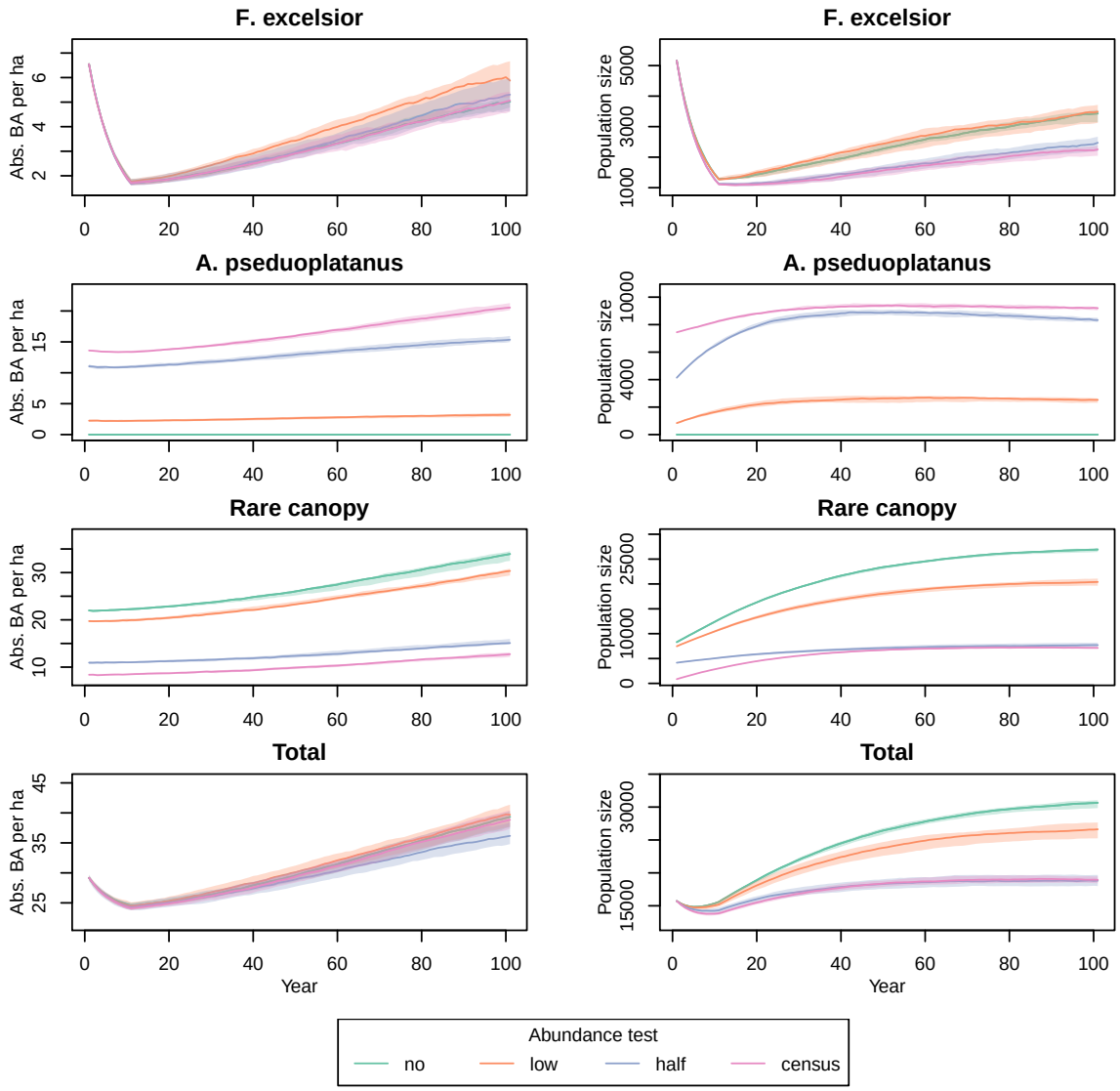


Figure 3.6: Results of the abundance tests showing basal area (BA m^2 ha^{-1}) (left hand panel) and population size (right hand panel) of canopy species through time. The coordinates of stems remained unchanged from the census data in order to maintain the size and spatial distribution of the forest but the species identity of *Acer pseudoplatanus* and rare canopy species were mixed in various proportions to test the invasion potential of *A. pseudoplatanus*, no (0:1), low (1:9) or half (1:1). The abundance tests were run at 75% *F. excelsior* mortality, which is also plotted for comparison (census). Shading depicts the 5th and 95th percentiles from 10 simulations of each scenario. Medians are shown by darker lines. The population of *A. pseudoplatanus* increases rapidly in the 1:1 treatment and follows the expected trajectory of the census population, although the regeneration cannot make up the BA in 100 years. In contrast the population remains much smaller when it starts out low.

3.6 Discussion

Host-specific pathogens that target a dominant forest tree species can cause significant changes to community dynamics including shifts in the size distribution of the host (Peterken & Mountford, 1998), changes in the relative abundance of remaining species (Fajvan & Wood, 1996), and altered forest biomass (Kurz *et al.*, 2008). In our study of the community response to ash dieback in a British woodland, we found that the level of mortality in the host, *F. excelsior* (European ash), determined the extent to which the *F. excelsior* population recovered and the extent of recruitment in remaining species. Further, we found that the starting abundance of each species was an important factor influencing succession. In contrast, spatial associations at this scale (18 ha) had very little impact on the dynamics of remaining species. Our simulations suggest that the *F. excelsior* population could be resilient to mortality even up to 75%. Results indicate that the response of sub-canopy species to the loss of *F. excelsior* will be limited but that *A. pseudoplatanus* and other canopy species will increase in population size, and to a lesser extent BA, as a result of *F. excelsior* decline.

***Fraxinus excelsior* dynamics**

We found that the long-term *F. excelsior* population dynamics in our plot were extremely sensitive to short-term pathogen-induced mortality. We tested several mortality scenarios with the IBM, killing different percentages of the *F. excelsior* population in the first decade and then allowing the population to recover. We predicted that the *F. excelsior* population would recover from low but not severe mortality scenarios, and that this would impact on the dynamics of remaining species (H1). As expected the *F. excelsior* population showed greater recovery from the lower mortality scenarios. After 100 years the population size had recovered to near pre-disturbance level in the lowest mortality scenario. However, contrary to predictions, the *F. excelsior* population showed substantial increases, even from a population reduction of 75%. Our results suggest that, provided there is a high enough proportion of individuals that are resistant or escape infection, the UK *F. excelsior* population will be able to recover from even high rates of mortality, although recovery to pre-disturbance abundance may take over 100 years. Our results are contrary to observations from natural forests that have experienced high *F. excelsior* mortality (Lygis *et al.*, 2014). However, it is worth noting that in those sites *F. excelsior* was clear-felled, and had resistant adults remained, the level of regeneration may have differed.

The dynamics of the host species following pest or pathogen disturbance depends on a number of factors, such as the level of resistance in the population (King & Lively, 2012;

Ennos, 2015), the number and size distribution of remaining individuals and reservoir hosts, (Cobb *et al.*, 2012), and the evolution and dynamics of the pathogen (Brasier & Buck, 2001). The beetle vector of the Dutch elm disease pathogen preferentially targets larger individuals (Seconca & Leisse, 1994), which in places has resulted in the differentiation of *Ulmus* spp. into large sub-populations of small individuals with high regeneration and high mortality and small, isolated sub-populations of larger individuals (Peterken & Mountford, 1998). The ash dieback situation is somewhat different, with potentially high mortality across all size classes (Vasaitis & Lygis, 2008) but symptoms developing faster in smaller individuals (Keßler *et al.*, 2012). The dynamics of the *F. excelsior* population in British woodlands will largely depend on the level of host resistance which is still largely unknown (but see http://oadb.tsl.ac.uk for ongoing research into the genomics of ash dieback resistance), and the evolution of the *H. fraxineus* pathogen . In this study we assumed that individuals remaining after 10 years of ash dieback either avoided infection or were resistant and produced resistant offspring. Under these circumstances our results suggest that recovery of *F. excelsior* will be high. However, it is worth noting that if the pathogen persists in the environment and continues to target non-resistant individuals, or evolves to overcome genetic resistance in *F. excelsior*, then eventual mortality rates might be much higher. Although we test a range of mortality scenarios, pathogen dynamics can be complex and unpredictable (Brasier & Buck, 2001) and we therefore do not attempt to model all possible outcomes. Resistance is also relative rather than absolute and varying levels of sensitivity of different genotypes will provide an additional complication.

Dynamics of remaining species

Epidemics in dominant forest species are normally accompanied by changes in community composition. Fajvan & Wood (1996) report that the death of mature canopy oak trees following defoliation by *Lymantria dispar* (gypsy moth) resulted in increases in subdominant *Acer rubrum* (red maples) and *Acer saccharum* (sugar maples). Likewise, since the late 1980's, high mortality due to Dutch elm disease in a temperate Swedish forest has led to increases in species such as *F. excelsior* and *F. sylvatica* (Brunet *et al.*, 2014). The main 'winners' in our study were *A. pseudoplatanus* and the 'rare canopy' species, both of which increased in population size and BA, especially when *F. excelsior* mortality was high. In contrast, the sub-canopy species showed little response to *F. excelsior* mortality. These results are consistent with general expectations given the life history strategies of canopy and sub-canopy species. In order to eventually reach the canopy, seedlings and saplings of canopy species must be capable of rapid growth when they find themselves in gaps and access to high light (Canham, 1988). In contrast, sub-canopy species are adapted to the lower light levels of the understory and while they might respond to an opening of

the canopy, it will not be to the same extent as canopy species. In support of this, the parameters for the fast growth distribution that were inferred from the census data, were generally lower for the sub-canopy species. It is worth noting that due to our method of pooling rare species, the increases seen by 'rare canopy' can be attributed to increases in ten different species. For example, we did not have the data to model *F. sylavtica* at the species-level, but it could play the role of *A. pseudoplatanus* in other areas of Wytham where *A. pseudoplatanus* is less abundant.

Despite shifts in community composition, European forests generally show high resilience to the decline of a dominant species. For example, in the West-Carpathian fir-beech forests a 50% decline in the population size and BA of the *Abies alba* (fir) population was accompanied by increased recruitment and growth of remaining species, such that total BA and population size of observed forest stands stabilised within a few decades (Vrška *et al.*, 2009). Similar ecosystem resilience was observed following the dieback of *Quercus robur* (pedunculate oak) in Central European alluvial hardwood forests (Janik *et al.*, 2008).

As expected, remaining canopy species in our simulations showed increases in BA and population size in response to the loss of *F. excelsior* (H1), and after 100 years the total plot BA and population size were actually higher than the pre-dieback levels (H4). However, *F. excelsior* is known to have high growth rates (Fraxigen, 2005) and was predicted to increase rapidly in BA in our no-dieback simulation. Although in the different mortality scenarios, remaining species filled the gaps left by *F. excelsior* with new recruits, the BA of these small stems could not match the predicted rapid growth of larger *F. excelsior* stems in the no-dieback scenario. These results suggest that the structure of the plot will change in response to ash dieback. In the short-term, an opening of the canopy will lead to the understory becoming denser due to the increased number of recruits. Overtime, gaps in the canopy will be filled by the growth of existing individuals and the new recruits, such that the BA of the plot recovers to pre-disturbance levels. However, the size structure of the forest will remain more highly skewed towards smaller individuals than it might otherwise have been in a disturbance-free forest.

The role of spatial structure, starting abundances and demographic rates in determining succession

We predicted that demographic strategy would be more important than starting abundance in determining which species responded most to the loss of *F. excelsior*, and that consequently, *A. pseudoplatanus* would dominate succession even with a reduced starting population (H2). Results supported our hypothesis to an extent, but also showed that

with a very low initial starting population *A. pseudoplatanus* recruitment was limited and the population was unable to dominate the plot.

Results provided little support for H3, that spatial associations between species would determine patterns of succession. We broke down spatial associations between species by reassigning locations to stems, either including or excluding *F. excelsior* in the mixing. Contrary to predictions, the different size and distribution of gaps that this created had little effect on the plot dynamics, with results being very similar between two tests and the comparison mortality scenario. While both *F. excelsior* and 'rare canopy' species showed slightly reduced population increases in the spatial tests, *A. pseudoplatanus* appeared to benefit from the spatial randomisation, but only when *F. excelsior* was excluded from spatial mixing. *Fraxinus excelsior* has a clustered distribution in our study plot meaning that high mortality results in gaps that are larger than those normally associated with the loss of a single canopy individual. In plots where *F. excelsior* shows a less clustered distribution gaps will be smaller and more spatially distributed. Our simulation results suggest that *A. pseudoplatanus* will be less successful in such cases. However, with the effect being so small, the spatial tests overall suggest that in this plot, demographic rates influence short-mid term dynamics more than the spatial distribution of species.

Additional considerations

The time-frame of transient dynamics in these simulations are important to keep in mind because we know that other factors such as drought and wind-damage influence forest dynamics (Peterken & Jones, 1987), and the longer the period before simulated stabilisation, the more likely these other stochastic factors will be to alter the course of the forest. For example, an important consideration that may influence the outcome of succession is the drought sensitivity of *A. pseudoplatanus*. Climate projections from Murphy *et al.* (2009) indicate the climate in the south east of England is likely to become hotter and drier with decreased rainfall in the summer months. *Acer pseudoplatanus* has been shown to be particularly sensitive to water stress (Lemoine *et al.*, 2001; Tissier *et al.*, 2004), including at Wytham (Morecroft *et al.*, 2008) and this may limit its ability to dominate over the long-term, despite its success in the transient dynamics forecast here. More generally, models of forest response to pest and pathogen disturbance in areas undergoing rapid climate change or land use change should account for the possibility of much greater impacts due to the increased susceptibility of hosts and the reduced resilience of the whole community (Reyer *et al.*, 2015).

Another important consideration is alternation of regeneration by *F. excelsior* and *A. pseudoplatanus.* In a study of six British woodlands, (Waters & Savill, 1992) observed that both *F. excelsior* and *A. pseudoplatanus* showed higher recruitment under the canopy of the

other species than under a canopy of adults of the same species. A possible consequence of alternation of regeneration is the loss of *F. excelsior* in the canopy limiting regeneration of *A. pseudoplatanus*. However, the study of Waters & Savill (1992) specifically selected sites where reproductive adults of both *A. pseudoplatanus* and *F. excelsior* could contribute seeds to the study plots. Thus, under the *A. pseudoplatanus* canopy the main competitors to *A. pseudoplatanus* seedlings were *F. excelsior* seedlings. In our study plot, there are areas where *A. pseudoplatanus* is abundant despite *F. excelsior* being nearly absent. This suggests that without competition from *F. excelsior* seedlings, *A. pseudoplatanus* can still have high recruitment under its own canopy. In line with this, our results showed increases in *A. pseudoplatanus* recruitment in response to *F. excelsior* mortality. Morecroft *et al.* (2008) showed that *A. pseudoplatanus* has colonised areas of Wytham where the canopy has been opened up through historical management but has not colonised areas where the canopy has remained closed. This is consistent with our results. It is possible that in the much longer term *A. pseudoplatanus* would decline under closed canopy conditions, especially if this were exacerbated by drought sensitivity.

Modelling advances

To predict the dynamics of complex forest communities, ecologists must rely on mechanistic models that combine available data to make scenario-based predictions. Our predictive framework combines these tools to forecast host-specific disease disturbance. The problem of trying to project a whole community forward, based on parameters inferred from just two years' worth of data required an inverse modelling approach to overcome limitations of the short time series available. An example from our analyses highlights an insight that was only possible with the available data by virtue of inverse modelling. We initially used an inverse model that matched the stable size structure from the IPM megamatrix (the normalised dominant right eigenvector) to the observed size distributions from the census data. However, it is clear that due to grazing pressure from fluctuating populations of deer (Perrins & Overall, 2001), few of the tree populations in Wytham have a stable size structure. The number of fallow deer (*Dama dama*) and muntjac (*Muntiacus reevesi*) has increased markedly since the 1970's (Perrins & Overall, 2001), and the observed tree size distributions have a paucity of smaller size classes (due to grazing) that simply cannot reflect asymptotic dynamics (Fig. S1). Instead we maximised the likelihood of vital rates models to give a $\lambda = 1$. Although this also assumes that the long term population growth rate is stable, with an associated stable size structure, it allows the stable size structure to depart from the observed size distribution. Loosening the constraints of the inverse model in this way meant that fecundity parameters producing small individuals did not have a low likelihood in the MCMC analysis, and the resulting parameters are more biologically

plausible. In other systems, where population structure is not so heavily influenced by external forces, such as severe herbivory, the use of the stable size distribution from the IPM megamatrix in the inverse modelling framework could further decrease uncertainty in inference of vital rates parameters.

While there is a rapidly growing repository of global forest inventory data, sites with data over long time series are rare. The ability to make inferences about future forest dynamics based upon short time series data is therefore critical to enable informed forest management decisions to be made in the majority of areas where long time series of data are unavailable and field experiments are impractical. We have developed a method that makes such inferences possible, and allows evaluation of the assumptions needed to connect imperfect data to forecasts. Competitive interactions between individuals are important processes shaping population and community scale patterns. The use of data from a large contiguous plot allowed us to infer these competitive interactions and include them in our simulations of forest dynamics. Our forecasting platform can be readily extended to incorporate other data types such as remote sensing, via inverse modelling, and can explore a wide range of scenario-based forecasts that include different management scenarios.

3.6.1 Conclusions

Wytham Woods is typical of many woodlands in the south of England in terms of its species composition and turnover during the last few decades. As in many forests, *F. excelsior* has increased in abundance while the population of *Quercus robur*, English oak, has aged with limited recruitment (Kirby *et al.*, 2014). Changes in Wytham following ash dieback are therefore likely to reflect changes occurring on a much larger scale. One of the likely successors of *F. excelsior* in Wytham, and many other woodlands across the UK, is *A. pseudoplatanus,* although local patterns of species abundances, size distributions and demographic strategies will influence regeneration in response to ash dieback.

In summary, our modelling results show that forest recovery following epidemics of host-specific pests and pathogens depends on a myriad of factors, but is likely to be dominated by the importance of different demographic strategies which may allow some species to capitalise on a sudden increase in resources.

3.7 Acknowledgements

The 18-ha Long-Term Forest Monitoring Plot is a collaborative project between the University of Oxford, the Centre for Ecology and Hydrology, and the Smithsonian Institution CTFS Forest-GEO (HSBC Climate Partnership). Thanks go to Prof. Hal Caswell for assistance with the megamatrix construction. Much of the early work on this project was carried out at a CTFS Forest-GEO meeting for which JN received a travel grant from the Department of Plant Sciences, Oxford. SMM and CM were partially funded by the USA National Science Foundation (NSF 640261 to SMM). This work forms part of JN's DPhil which is funded by a Clarendon Scholarship, a New College Scholarship and the BBSRC. JN would like to give special thanks to Dr. Roosa Leimu-Brown, Dr. Charlotte Metcalf and Dr. Nick Brown for their valuable supervisory support throughout her DPhil.

The authors declare no conflict of interests.

Data Accessibility

The data are archived in the Smithsonian Institution's Forest Global Earth Observatory site and can be accessed by request from:

http://ctfs.si.edu/Public/plotdataaccess/index.php

3.8 SUPPORTING INFORMATION

Figure S1 *Density plots showing the size distribution of each species.*

Figure S2 *Mean monthly temperatures and precipitation for Wytham Woods for the thirty years up to, and including the census interval.*

Figure S3 *Schematic of the survival function showing the effect of altering each parameter.*

Figure S4 *Survival probability for each species.*

Figure S5 *Histogram of the annual growth increment data from the Wytham census data.*

Figure S6 *Growth distributions for each species.*

Figure S7 *Fecundity function for each species.*

Figure S8 *Schematic of the megamatrix that moves individuals between sizes and light environments.*

Figure S9 *Schematic of the transition probabilities between the light environments, used to construct the megamatrix.*

Figure S10 *Basal area of the sub-canopy species through time under each mortality scenario.*

Figure S11 *Population size of sub-canopy species through time under each mortality scenario.*

Figure S12 *Results of the spatial randomisation tests showing basal area and population size of sub-canopy species through time.*

Figure S13 *Results of the abundance test showing basal area and population size of sub-canopy species through time.*

Figure S14 *Results of the sensitivity analysis showing the basal area and population size of canopy species through time.*

Figure S15 *Results of the sensitivity analysis showing the basal area and population size of sub-canopy species through time.*

Figure S16 *Basal area of the canopy species under each mortality scenario separated by recruits and existing individuals.*

Table S1 *Population sizes and species groupings.*

Table S2 *Slopes and statistical significance of the relationship between competition and growth for each species.*

Table S3 *Survival parameters for each species.*

Table S4 *Growth parameters for each species.*

Table S5 *Fecundity parameters for each species.*

Table S6 *Population size of each species every 25 years in the 0 % mortality scenario.*

Table S7 *Population size of each species every 25 years in the 25% mortality scenario.*

Table S8 *Population size of each species every 25 years in the 50% mortality scenario.*

Table S9 *Population size of each species every 25 years in the 75% mortality scenario.*

Table S10 *Population size of each species every 25 years in the 100% mortality scenario.*

Table S11 *Population size of each species every 25 years in the spatial randomisation test including F. excelsior in the mixing.*

Table S12 *Population size of each species every 25 years in the spatial randomisation test excluding F. excelsior from the mixing.*

Table S13 *Population size of each species every 25 years in the abundance test with equal starting population sizes of A. pseudoplatanus and 'rare canopy' species.*

Table S14 *Population size of each species every 25 years in the abundance test with A. pseudoplatanus and 'rare canopy' species starting in the ratio 1:9.*

Table S15 *Population size of each species every 25 years in the abundance test with A. pseudoplatanus absent.*

Table S16 *Basal area of each species every 25 years in the 0 % mortality scenario.*

Table S17 *Basal area of each species every 25 years in the 25% mortality scenario.*

Table S18 *Basal area of each species every 25 years in the 50% mortality scenario.*

Table S19 *Basal area of each species every 25 years in the 75% mortality scenario.*

Table S20 *Basal area of each species every 25 years in the 100% mortality scenario.*

Table S21 *Basal area of each species every 25 years in the spatial randomisation test including F. excelsior in the mixing.*

Table S22 *Basal area of each species every 25 years in the spatial randomisation test excluding F. excelsior from the mixing.*

Table S23 *Basal area of each species every 25 years in the abundance test with equal starting population sizes of A. pseudoplatanus and 'rare canopy' species.*

Table S24 *Basal area of each species every 25 years in the abundance test with A. pseudoplatanus and 'rare canopy' species starting in the ratio 1:9.*

Table S25 *Basal area of each species every 25 years in the abundance test with A. pseudoplatanus absent.*

Table S26 *Summary of each effect tested, the F. excelsior mortality level and the hypothesis it relates to.*

Chapter 4

The ghost of Bambi past: Inferring deer impacts from forest demography

4.1 Chapter Introduction

Similar to the previous chapter, this chapter uses the methods developed in Chapter 2 to explore the impact of disturbance on forest dynamics. However, while Chapter 3 used the current size distributions of Wytham populations to project forward in time, here I do the opposite, recreating the current size distributions by inversely estimating the effect of deer herbivory on juvenile survival over the last fifty years. The results are of interest given the significant impact grazing pressure from large herbivores can have on forest diversity and structure. However, the approach of inferring previous sequences of disturbance events using only current census data is of interest more generally, and could be applied to a range of sites shaped by anything from herbivores to fire dynamics. Having inferred the impact that these disturbances can have, it becomes possible to explore how future sequences of events might impact the forest community.

4.1.1 Authors

Jessica Needham, Chia-Hao Chang-Yang, Nathalie Butt, Yadvinder Malhi, Michael Morecroft & Sean M. McMahon

4.1.2 Author Contributions

JN and SM conceived of the study. JN carried out the analysis. CHCY provided code for the Stan MCMCs. JN wrote the manuscript. NB, YM and MM provided data and

feedback on the manuscript.

Abstract

1. Large herbivores can have a significant impact on forest dynamics through their impact on seed and seedling survival rates. In places, high levels of browsing have caused an almost complete lack of recruitment in some or all tree species, resulting in shifts in community assemblage and forest structure.
2. We use data from a permanent forest plot in Wytham Woods, Oxfordshire, to infer past levels of deer herbivory based on the current size distributions of the most abundant tree species. Deer are modelled implicitly through their impact on juvenile survival rates by the construction of sequences of Integral Projection Models in which juvenile survival varies in relation to fluctuations in a proposed deer population. We calculate likelihoods for each proposed pattern of deer browsing by comparing the population size and size distribution of the simulated tree population to the current observed population. Using Sequential Monte Carlo (SMC) methods we estimate the most likely pattern of deer browsing.
3. Our model performs well at recreating the current population sizes and size distributions for four of the five most abundant tree species in the Wytham Woods plot, especially the understory species *Corylus avellana* (hazel) and the canopy species *Fraxinus excelsior* (ash).
4. The inferred periodicity and amplitude of fluctuations in deer browsing impact differed between tree species, suggesting that deer show feeding preferences which may shift through time in response to vegetation availability.
5. Using only the most recent census data we are able to estimate the likely patterns of previous browsing that led to the current community composition. Our modelling framework is flexible and generalisable and could be used to infer a range of historic disturbance events, from fire regimes to typhoons.

4.2 Introduction

Importance of forests Forests are a critical biome, hosting the majority of terrestrial biodiversity (Millennium Ecosystem Assessment, 2005), playing an important role in climate regulation (Friedlingstein *et al.*, 2006) and providing important resources for human populations (FAO, 2010). However, forests are under threat from anthropogenic driven global change, including land use change, climate change and subsequent shifts in biotic interactions e.g. from invasive organisms, insect pests and large herbivores. Understanding forest responses to these challenges will be critical to predicting future climates and patterns of biodiversity.

Impact of large herbivores Large herbivores have influenced forest dynamics for thousands of years, with herbivore abundances and feeding preferences determining forest regeneration and patterns of species abundances across large regions. However, in many parts of the world a combination of human activities, such as land use change, control or elimination of large predators, and livestock grazing, has led to shifts in large herbivore populations such that remaining forested areas are subject to unprecedented grazing pressure (Weisberg & Bugmann, 2003). This has led to an almost complete lack of regeneration in some forest tree species (Putman *et al.*, 1989), and subsequent shifts in community composition (Rooney & Waller, 2003; Husheer *et al.*, 2003). Changes to communities as a result of herbivory can be in terms of species identities, as some species are driven to local extinction and new more resistant species move in, or the physical structure of the forest as the understory is thinned and the size distributions of trees are shifted towards larger individuals.

Management practices for dealing with large herbivores vary across regions and according to forestry aims (e.g. production versus promoting biodiversity), but have largely focussed on the control of herbivore numbers within the area of interest. However, there is an increasing awareness that due to the numerous interacting factors that determine forest dynamics and the spatial and temporal scales involved, a focus on a single management strategy is unlikely to be effective (Bugmann & Weisberg, 2003). For example, the lack of regeneration in North American hardwood stands could only be explained by accounting for browsing by white-tailed deer (*Odocoileus virginianus*), along with light regimes and the effects of competition in the understory (Sage *et al.*, 2003). Herbivore-vegetation interactions operate over a range of timescales, from seasonal variations in vegetation availability, through annual fluctuations in herbivore abundances, to long term turnover in forest structure. Likewise, while local interactions are important, landscape connectivity determines whether herbivores can move freely through a mosaic of forest patches or are

confined to certain patches where they might build up to high abundances. The landscape at a regional scale therefore needs to be taken into account when considering ecological dynamics and potential management strategies.

Modelling herbivore damage While experiments over large temporal and spatial scales are rarely feasible, models provide a mechanism by which we can test hypotheses relating to ecological and evolutionary theory and management practices at the scales of interest. Many models of herbivory impacts on forest dynamics are based on gap models such as JABOWA (Botkin *et al.*, 1972), with the inclusion of herbivore dynamics as sub-models that vary in complexity.

Paper outline In this paper we present an inverse approach to infer historic levels of deer herbivory for a forest plot in Wytham Woods, Oxfordshire, UK. In our framework deer are not modelled explicitly; instead we model the impact of deer on target tree populations by assuming that herbivory lowers juvenile survival rates. We infer the most likely pattern of deer herbivory during the last fifty years by fitting growth and survival models to census data and combining these into Integral Projection Models (IPMs), which enable population level projections to be made. Using sequences of IPMs with different survival probabilities for juvenile trees, we can simulate population dynamics under different deer browsing scenarios. The population size distribution at the end of each fifty year simulation is compared to the observed population size distribution in 2010 in order to assess the likelihood of each deer browsing scenario. Using Sequential Monte Carlo (SMC) methods we infer the most likely pattern of historic grazing.

4.3 Methods

4.3.1 Site Descriptions

We used data from a permanent 18 ha plot in Wytham Woods, Oxfordshire (1°20W, 51°47N) (Butt *et al.*, 2009). The plot is largely classified as disturbed ancient woodland, i.e. continuous forest cover since at least the 1600's, with former management as coppice with standards and some timber extraction but no clear felling. Smaller areas are classified as secondary forest which have reverted from grasslands to closed canopy forest over the last 200 years, along with a small section of former plantation (Morecroft *et al.*, 2008).

The plot in Wytham is dominated by *Acer pseudoplatanus* (sycamore), *F. excelsior* (European ash) and *Quercus robur* (English oak) with an understory of *Crataegus mongyna* (hawthorn) and *C. avellana* (hazel).

Deer browsing in Wytham has been linked to changes in the understory vegetation (Morecroft *et al.*, 2001) and subsequent declines in bird populations (Perrins & Overall, 2001). While there are no quantitative records of deer population size in Wytham over the entire period modelled here, three species inhabit the woods, *Capreolus capreolus* (roe deer), *Dama dama* (fallow deer) and *Muntiacus reevesi* (muntjac). *Capreolus capreolus* remains scarce, but populations of the other two species have increased markedly from the 1960s and 1970s respectively. Annual culls began in the 1990s and Perrins & Overall (2001) provide the number of deer removed each year from 1990 until 2000. Culling has limited the increase in deer numbers in recent years and although there are signs of increases in some understory species such as *C. avellana* (Kirby *et al.*, 2014), the impact on recruitment in many tree species is still apparent.

4.3.2 Data collection

The plot in Wytham Woods is part of the Center for Tropical Forest Science-Forest Global Earth Observatory (CTFS-ForestGEO) network of research forest plots, and data collection follows a standardised protocol (Condit, 1998). In brief, every stem ≥ 10 mm DBH is mapped, measured and identified to species, or in some cases genus level. The plot was established in 2008, with the second census in 2010 (Butt *et al.*, 2009). For this study we modelled the three dominant canopy species (*A. pseudoplatanus*, *F. excelsior* and *Q. robur*) and two major understory species (*C. monogyna* and *C. avellana*). Remaining species had fewer than 200 individuals, making uncertainty in parameter estimates too high for robust conclusions to be drawn from population models.

4.3.3 Vital Rates

Survival To capture the different pattern of size dependent survival in small and large individuals, we model survival by splicing together two logistic regressions that meet at a predefined size threshold. For species with a maximum observed DBH ≥ 500 mm we set the size threshold to 200 mm DBH, and for those with smaller maximum sizes we use the 0.8^{th} quantile of the size distribution. Survival is given by:

$$s = \left(\frac{K}{1 + \left(\frac{1}{e^{-r_1(x-p_1)}} \right)} \right)^t \text{ for all } x < thresh_s \tag{4.1}$$

$$s = \left(\frac{K}{1 + \left(\frac{1}{e^{-r_2(x-p_2)}} \right)} \right)^t \text{ for all } x \geq thresh_s \tag{4.2}$$

where s is survival probability, K the upper asymptote of the two curves, r and p are the rate of change and inflection point in the curves respectively, t is the time in years between censuses, x is DBH and $thresh_s$ is the size threshold at which the two curves meet. Subscripts 1 and 2 denote parameters for the small and large survival curves respectively. To ensure senescence in large individuals we constrain r_2 to be negative.

We fit vital rate models to Wytham species for the 2008 – 2010 census interval. For both and survival and growth we fit models using Bayesian MCMCs implemented in R (R Core Team, 2014) and RStan (http://mc-stan.org).

Growth For each species, we divide individuals into two growth classes ('slow' and 'fast') and fit separate gamma distributions to each growth class. The 'slow' growth class consists of the slowest 95% of understory individuals, i.e. those below a size threshold, while the 'fast' growth class consists of the fastest 5% of understory individuals and all individuals over the size threshold. Again, for species with a maximum observed DBH $\geq$ 500 mm we set the size threshold to 200 mm DBH, and for those with smaller maximum sizes we use the 0.8^{th} quantile of the size distribution. Dividing up the data in this way enables us to capture both the slow growth of the majority of individuals and the faster growth of individuals able to escape the high competition of the understory, either due to increased height or location in a gap.

The change in DBH for each individual is therefore given by

$$z \sim \begin{cases} \text{Gamma}(\alpha_1, \beta_1) & \text{for q}x < thresh_g, \\ \text{Gamma}(\alpha_2, \beta_2) & \text{for all } x \geq thresh_g \\ & (1-q)x < thresh_g \end{cases} \tag{4.3}$$

where z is increment in mm, q is the quantile for dividing understory individuals into fast and slow growth classes (fixed at 0.95), x is DBH, $thresh_g$ is the size threshold for automatic inclusion in the fast growth class, and α and β are the shape and rate parameters of each gamma distributions, with subscripts 1 and 2 denoting the slow and fast distributions respectively.

Autocorrelation in growth rates Temporal autocorrelation in individual growth rates is critical to explaining the population dynamics of forest trees. We include this in the modelling framework by combining the multiple growth classes for each species with estimates of the movement of individuals between them. While the slow and fast growth distributions themselves are size independent, we assume that annual transitions between distributions are size dependent. The transition probabilities of moving from slow to fast increase with size up until the size threshold for automatic inclusion in the fast distribution, and the probabilities of moving from fast back to slow decrease with size up until the size threshold. This is described in more detail in the section below.

4.3.4 Population Projections

The vec-permutation approach We made population projections by combining growth and survival models using Integral Projection Models (IPMs). IPMs track the change in a state variable, in this case DBH, in a population through time (cf. Easterling *et al.*, 2000; Merow *et al.*, 2014a) without the need to explicitly simulate individuals. Because of the structure of our growth model, we use a vec-permutation approach (described briefly below) to construct IPMs that move individuals between size and growth classes. The construction of these IPMs is described in detail in Caswell (2012) and Chapter 2.

Briefly, we define a size range that extends beyond the observed size range of the data and then divide it into a large number of discrete size bins, S. For each growth distribution, G, we make a matrix of dimensions S x S which describes the probability of individuals growing from every size at time t, to every other size at time $t+1$, combined with the probability of survival at each size. These matrices are arranged in a block diagonal matrix $\mathbb{U}$. For each size class, 1 to S, we construct a G x G matrix describing the transition probabilities between growth classes at that size. For sizes up until the size threshold the probability of moving from slow to fast increases from 0.01 to 0.2, while the probability of moving from fast back to slow decreases from 0.6 to 0.1. The corresponding probabilities of remaining in slow or fast therefore range from 0.99 to 0.8 and 0.4 to 0.9 as size increases up until the size threshold for fast growth. Beyond this threshold the transition matrix is simply

$$\begin{pmatrix} 0 & 0 \\ 1 & 1 \end{pmatrix}, \tag{4.4}$$

since individuals are moved to the fast distribution and stay there.

These matrices describing transitions between growth classes are arranged in a block diagonal matrix $\mathbb{M}$.

Finally, we make a vec-permutation matrix K, of dimensions GS x GS. K rearranges the population size vector from being organised as sizes within growth classes to growth classes within size classes, i.e.

$$\tilde{\mathbf{n}}_t = \Big(n_{1,1},\ n_{2,1}, \ldots n_{S,1} \big| n_{1,2},\ n_{2,2} \ldots n_{S,2}\Big)^T$$

to

$$\mathbf{K}\tilde{\mathbf{n}}_t = \Big(n_{1,1},\ n_{1,2} \big| n_{2,1},\ n_{2,2} \big| \ldots \big|\ n_{S,1},\ n_{S,2}\Big)^T.$$

With K, $\mathbb{U}$ and $\mathbb{M}$ we can build the matrix which describes the movement of individuals between growth and size classes, $\tilde{\mathbf{U}}$.

$$\tilde{\mathbf{U}} = K^T \mathbb{M} K \mathbb{U}. \tag{4.5}$$

Recruitment As is common at most sites, detailed descriptions of seed and seedling dynamics are not available for Wytham and we therefore kept models of recruitment very simple. We assumed that the distribution of recruit sizes would be equal to the smallest modelled size plus one year's worth of growth from the slow growth distribution. We also assumed that 95% of recruits would enter the model in the slow growth distribution while 5% would enter in the fast distribution. This assumption was based on rough estimates of gap frequency, i.e. the number of breaks in the canopy that allow light to reach down to the forest floor. Although the minimum size in the census data was 10 mm, we extrapolated our growth and survival models down to 1 mm. This allowed us to keep the number of new recruits fixed through time, by assuming that seed rain would be unaffected by deer browsing and instead allow deer to act on juvenile survival probabilities. For each species, fifty new recruits entered the population each year.

Deer browsing We inferred the impact of deer browsing on the demographic rates of Wytham species, using 50 year simulations of each population, from 1960 – 2010. We modelled deer herbivory with a sine wave, with possible values of periodicity, d, ranging from 5 to 250 years and possible amplitudes, b, from 0.02 to 0.45. This was given by $\text{deer}_t = b + b\Big(sin(x + \frac{2\pi}{d} + 5)\Big)$, where deer_t is the effect of deer at time t (Fig. 4.1). Each year of the simulation we calculated the inflection point of the survival curve that would give a survival probability of the smallest size equal to 1 - deer_t, meaning survival at the smallest size could potentially range from 0.1 to 1, and when the effect of deer is

high, juvenile survival is low and vice versa. However, to prevent immortality, we capped survival at the upper asymptote, K, inferred from the survival model fit to the census data. We also assumed a size threshold of 100 mm, above which deer browsing would fail to impact tree survival. Above this size, survival was as inferred from the model fit to census data. The addition of 5 to the equation above ensured that deer started low in 1960, the beginning of simulations. Different combinations of periodicity, d, and deer effect, b, were evaluated using SMC methods as described below.

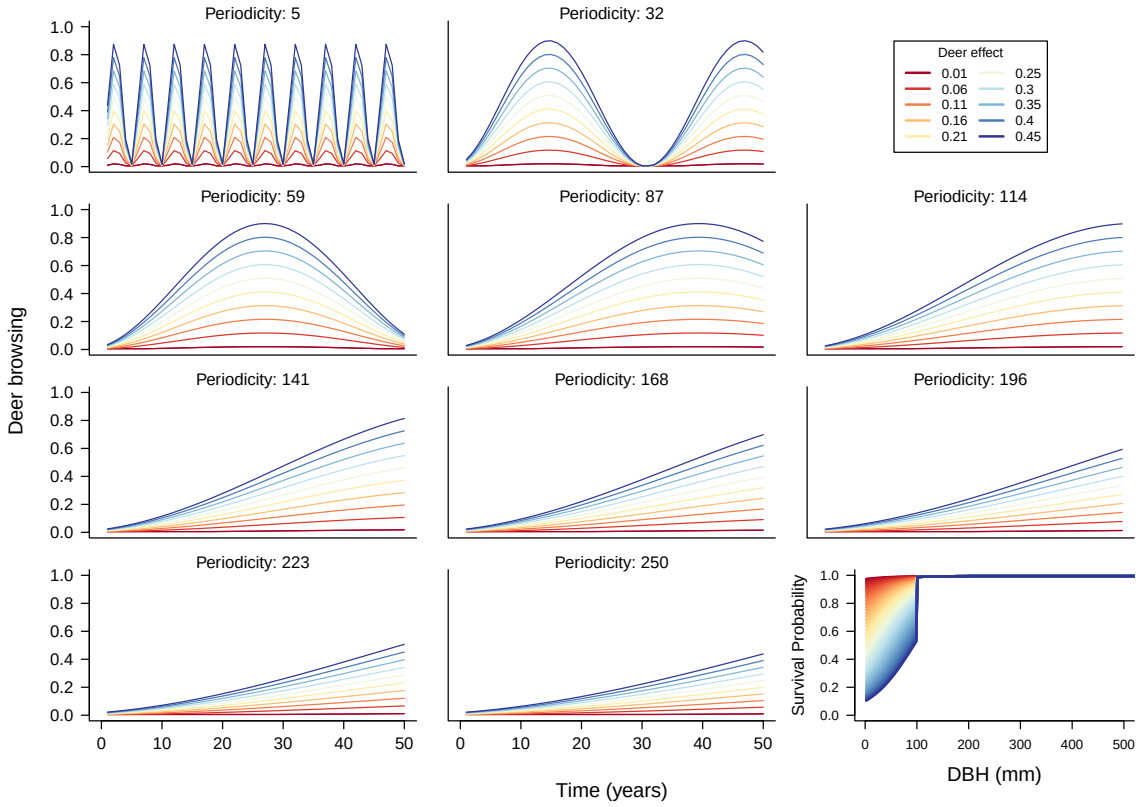


Figure 4.1: The range of deer effects tested in the inverse model. The impact of deer was modelled with a sine wave with periodicity ranging from 5 to 250 and an amplitude ranging from 0.002 to 0.45. Juvenile survival each year was inversely proportional to the deer effect (shown in the bottom right panel). Sequential Monte Carlo (SMC) methods were used to estimate the combination of periodicity and amplitude that led to the simulated population best matching the observed population following 50 years of forward projection.

Starting size distributions Since the size distribution of Wytham tree populations in 1960 is unknown, for the starting population for each species we set the number of individuals in each size class to the -2 power of DBH, since this has been shown to be a

good descriptor of size distributions in forest communities across the globe, irrespective of sampling area or species diversity (Enquist & Niklas, 2001).

Inverse models Inverse models are a way in which outputs from a model can feedback to inform model parameters informed by few data (Wood, 1987). Generally, summary statistics from the model are calculated and compared to summary statistics of the observed data, giving a likelihood by which model parameters are assessed (Hartig *et al.*, 2011).

To estimate deer browsing parameters (b and d), we use SMC methods (sometimes referred to as a particle filter), following Beaumont (2010). This approach involves generating a large number of possible parameter combinations from the prior distribution of each parameter. Each of these parameter combinations (particles) is used in the model to generate a likelihood value and only the particles with the highest likelihoods are selected. At each iteration, particles are perturbed slightly and resampled and only those with likelihoods above an increasingly stringent threshold are retained, thus ensuring sampling is focussed in areas of parameter space with the highest likelihoods. For a more complete description we recommend Beaumont (2010).

A commonly used summary statistic with which to compare model outcome and observed data (and generate a likelihood value) is the size distribution of the study organism (Dislich *et al.*, 2009; González *et al.*, 2016). As in González *et al.* (2016) we compare the size distribution from simulated populations with observed size distributions from inventory data. However, due to the short census interval in Wytham we only match simulated populations to the 2010 census data, unlike (González *et al.*, 2016) who use longer time series.

In complex models there are potentially many parameter combinations that could give rise to the observed data (e.g. high fecundity and juvenile mortality or low fecundity and juvenile mortality might give similar numbers of recruits). Ideally therefore, multiple orthogonal likelihoods are used to compare model and data, thereby reducing problems of parameter identifiability. As in González *et al.* (2016), we also compare the number of individuals in the simulated and observed populations. This is slightly problematic given that the starting population sizes are unknown for the Wytham species, and the final population size in 2010 will be dependent on starting population size. We assumed that the starting population size was equal to that observed in 2010 (taking into account the different minimum sizes) and, after projecting forward 50 years, compared both size distributions and population size to the 2010 census data.

Although populations are rarely in equilibrium, results from Kirby *et al.* (2014) (table 3), show that numbers of individuals of each of the species modelled here have actually remained fairly constant from 1974 to 2012 based on records from 164 10 m x 10 m quadrats across Wytham. We therefore assumed that between 1960 (the starting year for our simulations) and 1974, populations did not change significantly.

4.4 Results

4.4.1 Vital Rates

Survival Survival rates varied between species (Fig. 4.2, table E.1) but was generally high for all species across the entire size distribution. *Fraxinus excelsior* was the only species to show significant juvenile mortality, with an annual survival probability of the smallest size of just 0.84. Due to the short census interval few mortality events were captured in the data and as a result senescence is largely defined by priors.

Growth Wytham species were slow growing with expected annual increments (given by α/β) ranging and from 0.34 to 1.20 mm for the slow distribution and 1.85 to 5.32 mm for the fast growth distribution (Fig. 4.3, table E.2). *Fraxinus excelsior* had the fastest growth rates, which matches expectations for this species.

4.4.2 Population Projections

Deer impacts The inversely estimated impact of deer on juvenile survival varied between species (Fig. 4.4). Periodicity ranged from 14 years (*Q. robur*) to 183 years (*A. pseudoplatanus*), while the estimated impact on juvenile survival resulted in the annual probability of survival at the smallest size ranging from 0.11 (*Q. robur*) to 0.77 (*F. excelsior* and *A. pseudoplatanus*). These results are mostly consistent with surveys of seedling numbers in Wytham (Butt unpublished data) which show that *F. excelsior* seedlings vastly outnumber the seedlings of other species, while *Q. robur* had no recruitment during the sampling period (summer 2010 to spring 2011).

We might initially have expected the temporal dynamics of deer impact to be consistent across species, due to changes in deer numbers resulting in qualitatively similar impacts on juvenile survival in all species. However, deer show vegetation preferences, and as one tree species is heavily browsed this might allow regeneration or increased growth of competing species. That is, until deer numbers rise so high, and the preferred species is

so reduced, that the deer are forced to change their diet, and tree species which initially benefited begin to suffer increased mortality. Therefore, while the inferred impact of deer on *A. pseudoplatanus* is close to expectation, in line with deer numbers in Wytham, the alternating oscillations in juvenile survival in the other species could reflect switches in deer browsing habits.

Simulated populations The inverse models performed reasonably well at recreating current size distributions for populations in Wytham Woods (Fig. 4.5). Particularly for the understory species, *C. avellana* and the canopy species *F. excelsior*, the size distribution of the populations projected forward from 1960 to 2010 were a close fit the observed size distributions from the 2010 census data. The simulated population size in 2010 was also very close for these two species, with the number of individuals (N) equal to 1384 and 4543 for the simulated populations compared with N = 1308 and 5332 for the two observed populations respectively.

In the case of the canopy species *A. pseudoplatanus*, the simulated population correctly captured the lack of individuals in the smallest size classes and the shift in the size distribution towards larger individuals. However, the simulated population size was lower than the recorded number of individuals (4135 compared with 7647) due to too few stems of intermediate and large size. This likely results from underestimates of growth rates; in the 50 years of projection, too few individuals were able to grow fast enough to escape high juvenile mortality rates and reach the larger size classes. Estimates of transitions probabilities between growth classes that were used to construct the IPMs were probably responsible for this mismatch between model and data for this species. It is difficult to estimate these transitions from data due to the overlap in the two growth distributions and the difficulty associated with accurately estimating the realised light environment of forest trees. Our estimates were based on estimates of gap duration from a tropical forest (van der Meer & Bongers, 1996), which are typically denser and faster growing than temperate forests. As a result we may have underestimated the slow-to-fast transitions and overestimated the fast-to-slow transitions.

The model performed poorly at recreating the population size distribution of *Q. robur*, most likely as as a result of the smaller sample size for this species and the most extreme shift in the size distribution towards larger stems. Due to a lack of data on starting size distributions, for each species we used a starting distribution that was highly skewed towards smaller individuals as this is typically what we would expect for forest tree species. However, for *Q. robur* this was probably not appropriate, given that recruitment has been low in this species for many years, and therefore even in 1960 the population was already

shifted towards larger individuals (Kirby *et al.*, 2014). While the inferred amplitude of deer impact was highest for *Q. robur*, reflecting the lack of observed recruitment, with the starting size distribution that we used here, individuals were unable to grow fast enough to reach the sizes observed in the 2010 census.

4.5 Discussion

We used inverse models to recreate the current size distributions of tree populations in a British woodland that has experienced heavy deer browsing during the last 50 years. Using recent census data we fitted models of growth and survival to the most abundant canopy and understory tree species and then inferred past recruitment and survival rates by comparing simulated populations with the most recent observed populations. For four out of five species the inverse approach was successful in that the simulated population size and size distribution after fifty years of projection were good fits to the observed population.

Our methods failed to capture the size distribution of *Q. robur*, most likely because the ageing population has resulted from processes other than deer browsing. Recruitment in *Q. robur* has been low in Wytham, and UK woodlands more generally, for several decades. In many places the high contribution of *Q. robur* to total basal area results from relatively few, large individuals which may be several hundred years old (National Forest Inventory, 2012). Results from Kirby *et al.* (2014) show that in 1974 the majority of *Q. robur* stems across Wytham were already > 60 cm DBH. To better capture the dynamics of this species we would need to account for this in our estimates of the starting size distribution.

Previous models exploring the impact of herbivory on vegetation dynamics have often incorporated browsing into individuals based models of stand dynamics. For example, both Kienast *et al.* (1999) and the FORest GRAzing model FORGRA (Jorritsma *et al.*, 1999) build on the JABOWA forest gap model. While Kienast *et al.* (1999) incorporate herbivory through data on site- and species-specific browsing percentages, the FORGRA model explicitly includes herbivory through submodels of understory vegetation (tree seed and seedlings as well as herbaceous species) and herbivore feeding dynamics, with different herbivore species have different vegetation preferences (Jorritsma *et al.*, 1999).

Our approach is most similar to Kienast *et al.* (1999) in that we model deer implicitly through its effect on survival rates. However, unlike both models above, the inverse method makes it possible to infer deer impact even when site-specific information on browsing is unavailable. This is especially advantageous when the aim is to simulate the impacts of deer over large areas, since we can simply combine estimates of growth and

survival with current size distributions in order to infer the impact of deer in each region. Scaling up from the stand to landscape level will be important, since the impact of large herbivores on any particular forest will be dependent on the availability of suitable habitat in surrounding areas.

Further, in many places herbivores have an impact on vegetation not only through direct grazing but also through interactions with other forces such as forest fires which operate across much larger spatial scales. Kramer *et al.* (2006) use the FORSPACE model which combines a classic gap model with mechanistic representation of herbivory and a stochastic model of fire dynamics to model forest dynamics under different management strategies at the landscape scale. Their study suggests that fire management strategies have a much greater impact on regeneration than deer browsing.

While this study focussed on a small forest plot, the approach has the potential to be applied to much larger regions. IPMs are analytically tractable and can be parameterised using simple demographic data from forest inventories. This makes it relatively straightforward to construct IPMs for a species across large areas, fitting models of vital rates at whatever spatial and temporal scales are permitted by the available data. These IPMs can then be used to infer both historic and current levels of herbivory, but also to simulate vegetation dynamics under different future scenarios.

Didion *et al.* (2009) use the gap model ForClim v2.9.5 to explore how oscillations in ungulate populations can alter forest dynamics, and how this compares to the dynamics when populations are held constant–the target for most management strategies. Similar analysis would be straightforward with the models presented here.

Furthermore, the combination of IPMs with an inverse approach is not restricted to exploring deer herbivory on forest demographic rates. The modelling framework presented here could be applied to other forest systems to infer the impact of unmeasured environmental variables, both biotic, e.g. outbreaks of forest pests, and abiotic e.g. typhoons, forest fires and El Niño events.

4.5.1 Conclusions

Browsing by large herbivores has the potential to significantly alter the dynamics of forest tree species through its effect on survival and recruitment. In the UK, as in many other countries, browsing by deer has severely limited regeneration in many tree species, leading to shifts in community composition and forest structure. Here we show how to use the shifted size distribution captured in forest census data to infer historic patterns of deer browsing. Our approach is successful for all but one of the five species included

in our study. The combination of easily parameterised and analytically tractable IPMs with inverse models could potentially be used to address a whole range of ecological and evolutionary questions.

4.6 Acknowledgements

The 18-ha Long-Term Forest Monitoring Plot is a collaborative project between the University of Oxford, the Centre for Ecology and Hydrology, and the Smithsonian Institution CTFS Forest-GEO (HSBC Climate Partnership).

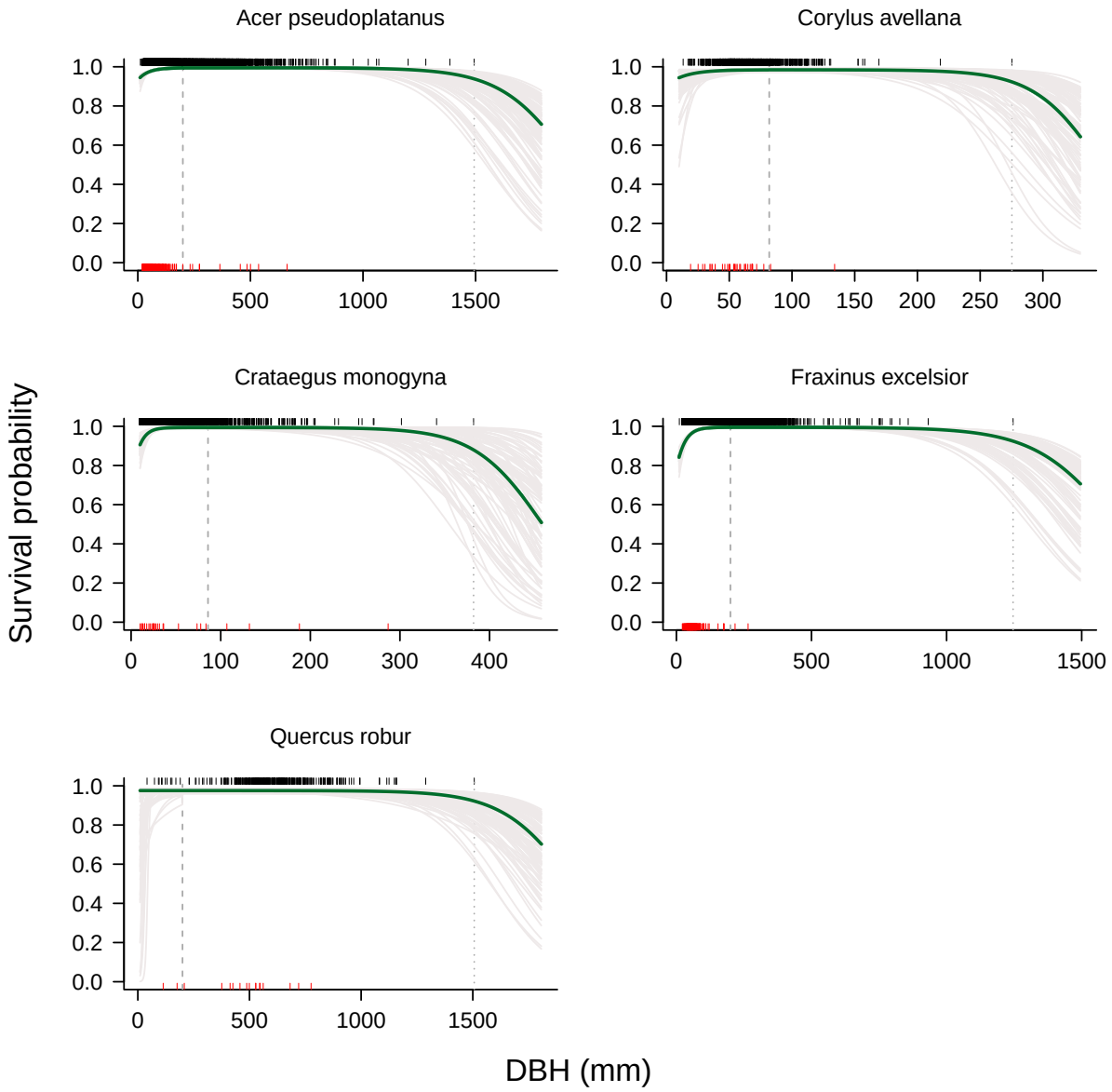


Figure 4.2: Survival functions fit to the census data for the most abundant species in Wytham Woods. Survival was modelled with two logistic regressions that meet at a specific size threshold, with five free parameters in total. Grey lines show uncertainty in parameter estimates. Survival rates are high for most species across the entire size range, with the exception of *F. excelsior* which has lower survival at the smallest sizes.

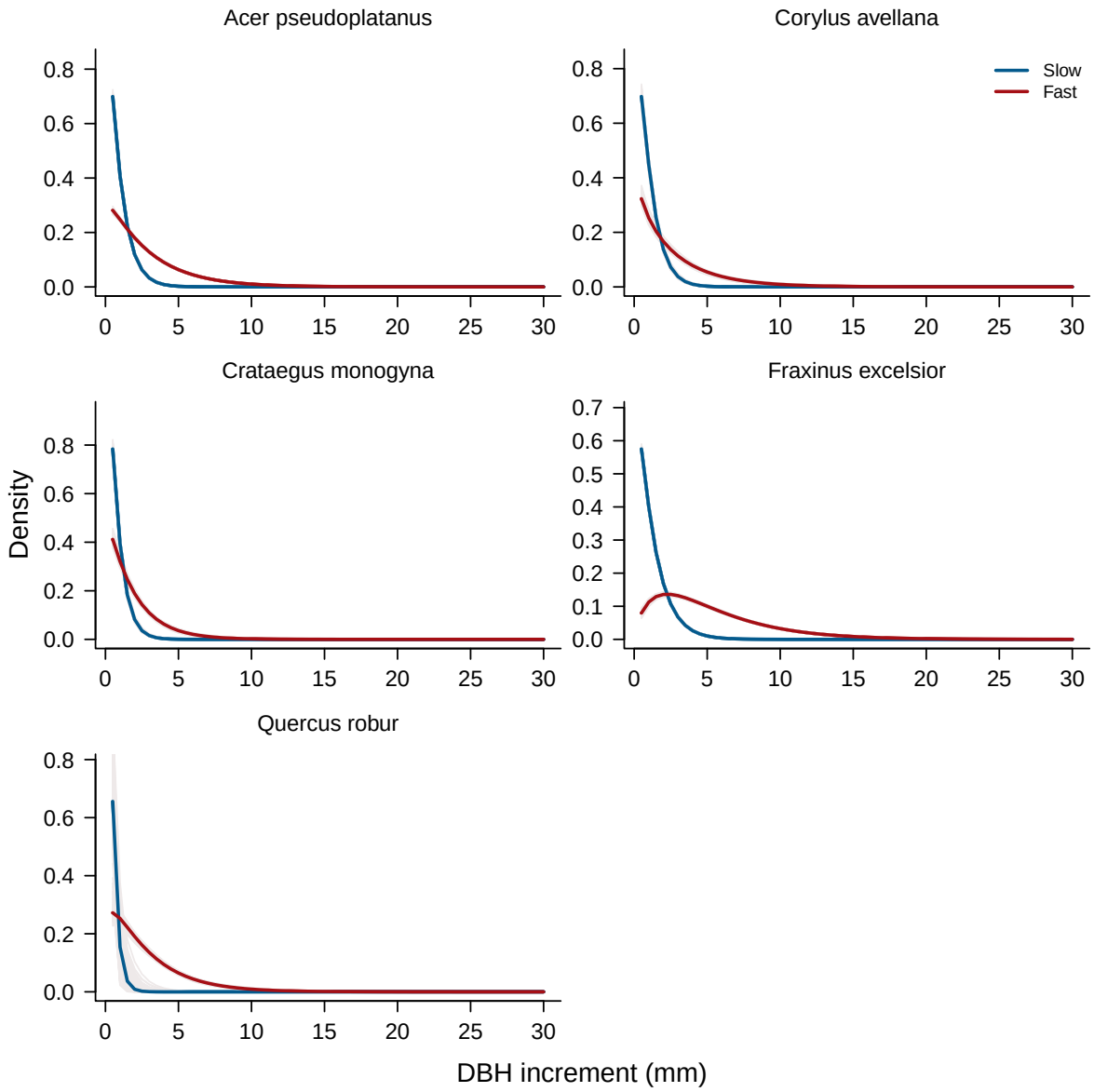


Figure 4.3: Growth distributions fit to the increment data for the most abundant species in Wytham Woods. Uncertainty around parameter estimates is shown with grey lines. Annual growth rates were generally low, with *F. excelsior* having the fastest growth rates.

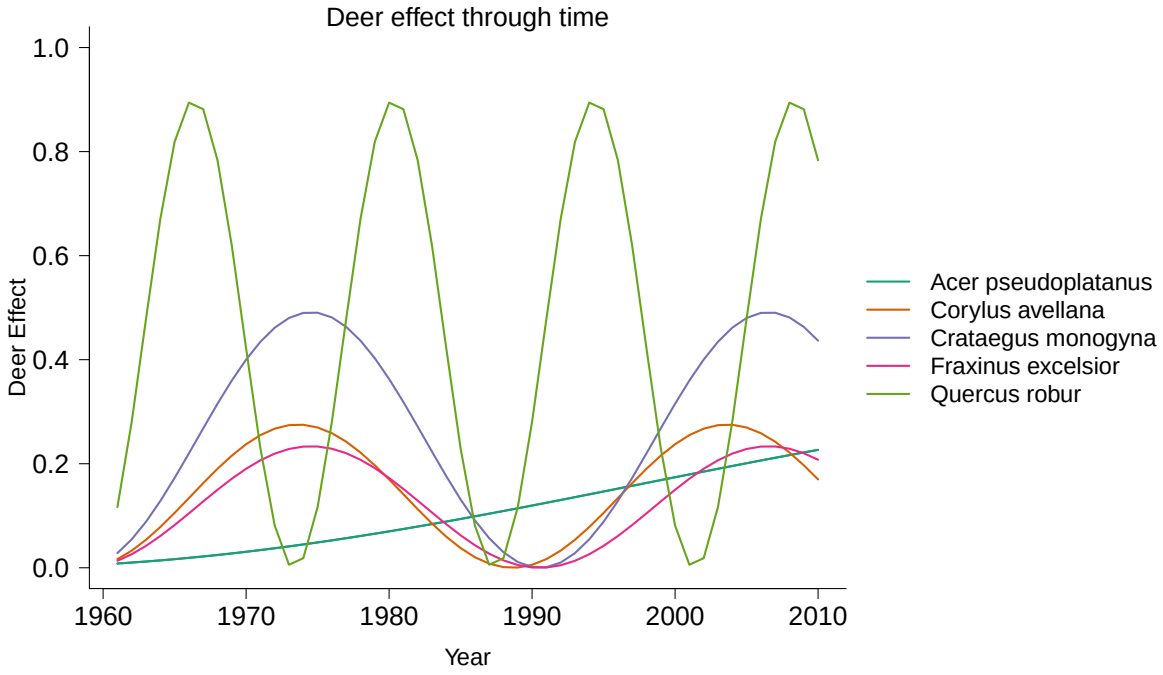


Figure 4.4: Estimates of the effect of deer on juvenile survival over the last fifty years for the most abundant species in Wytham. Periodicity of the deer impact varied between species, as did the estimated effect of deer on juvenile survival. The effect of deer was estimated to be strongest for *Q. robur* and lowest for *F. excelsior* and *A. pseudoplatanus*.

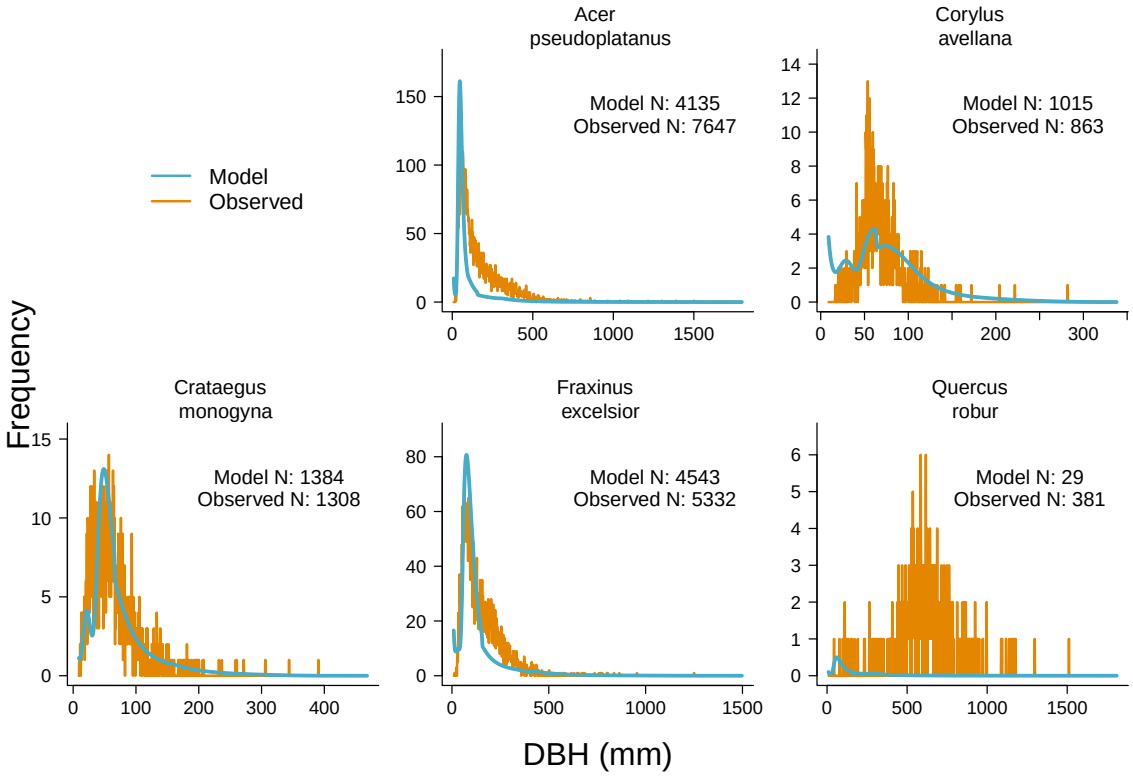


Figure 4.5: Results from the population simulations in which the effect of deer on juvenile survival varied through time. For each species we used the match between the modelled and observed population size and size distribution to infer what the effect of deer herbivory must have been during the last five decades. There was a good match between the model and observed populations for both *C. monogyna* and *F. excelsior*, while the model underestimated the number of intermediate sizes in remaining species.

Chapter 5

Diversity of demographic rates in tropical tree species

5.1 Chapter Introduction

After the previous two chapters, this chapter is a departure from Wytham and a return to the tropical forest of Barro Colorado Island. With the modelling framework established and its utility demonstrated in two applied studies, this chapter presents the bigger picture of how we can take a demographic perspective to study the diversity of forest trees and the processes that shape communities. I fit vital rate models to 134 species with a range of life forms and compare the variation between species and within a species between years. I explore whether temporal variation can be linked to an El Niño event in the first census interval and whether clusters of demographically similar species show similar temporal trends in demographic rates.

5.1.1 Authors

Jessica Needham, Daniel Johnson & Sean M. McMahon

5.1.2 Author Contributions

JN and SM conceived of the study. JN carried out the analysis. DJ provided feedback during the analysis. JN wrote the manuscript.

Abstract

1. Significant effort has gone into studying interspecific variation in functional traits as a means of explaining differences in species performance and species co-existence. However, recent work has questioned the utility of functional traits as proxies for life-history strategy due to variation in functional traits within species, across environments and at different stages of the life cycle.
2. We propose a shift in focus towards studies that explore the diversity of demographic traits within communities. Large-scale patterns of diversity, biomass and carbon turnover are driven by the growth, mortality and recruitment of individuals at a local-scale. Widely available demographic data therefore offers a direct link between individual measurements and the ecosystem processes of interest.
3. We present growth and survival models that account for the size-dependency of vital rates and individual variation in performance. Making use of data from a 50 ha permanent forest dynamics plot on Barro Colorado Island, Panama, we explored the demographic diversity of a tropical tree community by fitting these growth and survival models to 134 species with a range of life forms and population densities.
4. We identified groups of demographically similar species and related these groups to life history strategies. Although we found evidence of a slow fast continuum in life history strategies, we also found that many of the fastest growing species are long-lived canopy and emergent species, and that the majority of species are slow-growing, mid-story species that have high maximum long-term survival but senesce before reaching the canopy. These findings emerge from our vital rate models, which have the flexibility to distinguish subsets of fast growers within species and can account for changes in survival probability through ontogeny.
5. Using 15 years of census data we explored temporal variation in demographic rates, hypothesising that shifts in growth and mortality would be

driven by environmental conditions. However, contrary to predictions, we found no effect of the 1998 El Niño event on community wide demographic rates.

6. Combining vital rate models, we constructed Integral Projection Models (IPMs) that account for persistent individual differences in growth. IPMs provide analytic solutions for estimating size-dependent life expectancies and passage times to key life cycle stages. Across all 134 species we found a positive correlation between life expectancies and passage times to a range of sizes, suggesting the existence of a trade-off between growth and survival.

7. In order to include biodiversity in large scale vegetation models it is necessary to aggregate species in biologically meaningful ways. Functional traits provide the mechanistic link between physiology and demography, making it possible to predict how demographic rates will change in response to changing environments. On the other hand, demographic traits can be assessed across thousands of individuals providing a straightforward approach for scaling up from individuals to populations and communities. A promising way forward would be to combine functional and demographic traits in order to define vegetation types that reflect the physiological mechanisms underlying life history strategies and the consequences of demography for ecosystem functioning.

5.2 Introduction

Functional Traits Functional traits, (cf. McGill *et al.*, 2006), are measurable properties of organisms that strongly influence performance. Ecologists have been measuring plant functional traits for many decades in order to explain variation in individual performance (reviewed inViolle *et al.* (2012)), the diversity of life history strategies across species (Poorter & Bongers, 2006), and the patterns of coexistence that shape communities (Ackerly, 2003; Kraft *et al.*, 2008; McMahon *et al.*, 2011). Functional traits have been shown to be good predictors of the outcome of competitive interactions between individuals (Lasky *et al.*, 2014) and the variation between species (Poorter *et al.*, 2006). As a result, functional traits can be mapped to life history strategies and used to classify species into 'functional types' (Poorter *et al.*, 2006), which can be critical for exploring forest dynamics across large geographic regions (Díaz & Cabido, 1997), especially in the tropics where a community can comprise of thousands of species (Condit *et al.*, 2006). Finally, because functional traits relate to resource acquisition and allocation strategies, they can be used to study the evolution of life history strategies (McMahon *et al.*, 2011).

Potential problems with functional traits Despite these successes, the relevance of a given trait to fitness and the mechanisms shaping communities is not always obvious. For example, Paz *et al.* (2005) found no evidence of a relationship at the species level between seed mass and recruitment in seven species of *Psychotria*, suggesting other factors are responsible for determining recruitment success in this study system. Further, some traits show substantial variation within, as well as between species (Clark, 2010; Paine *et al.*, 2011) and along environmental gradients (Jung *et al.*, 2010). Sampling of these traits needs to occur over a wide enough geographic area, and include sufficient individuals of each species, to accurately estimate trait diversity. Other traits are variable through ontogeny and may have differential impacts on fitness according to life cycle stage. For example, in a study of over 100 tropical tree species Visser *et al.* (2016) found that while seed mass and adult stature are important predictors of success early in life, wood density becomes more important post-establishment. Therefore, although a trait might appear to show no relation to fitness or patterns of community assemblage, it could be that sampling is too limited spatially or temporally.

Demographic rates as traits In this paper we take the view that demographic rates can be treated as functional traits. Ultimately, it is differences in demographic rates which determine patterns of species abundances, community composition and forest structure (Russo *et al.*, 2005). Although demographic rates are themselves determined by functional

traits, the link between physiology and demography is not always clear. Multiple functional traits combine to drive growth, survival and reproduction, with the relative importance of each trait changing through ontogeny (Visser *et al.*, 2016). Further, demographic rates result not just from the functional traits of the individual, but also the functional traits of its neighbours and the way in which individual differences determine the outcome of local competitive interactions (Kraft *et al.*, 2014). Rather than collecting data on functional traits that may or may not be relevant to fitness, directly measuring demographic rates is a simpler route to assessing the link between intra- and inter-specifc variation and patterns of community assemblage.

The increasing availability of demographic data Data on demography is increasingly available over large spatial and temporal scales, due to investment in national forest inventories (Tomppo *et al.*, 2010) and networks of permanent forest dynamics plots (Malhi *et al.*, 2002; Anderson-Teixeira *et al.*, 2015). While significant time and effort is required to collect forest census data, the measurements themselves are relatively straightforward; usually the species identity and diameter at breast height (DBH) for all stems over some threshold (typically 1 or 10 cm) are recorded periodically for all stems within a given area. Demographic data is now available for all major forest biomes across the globe, providing the information necessary to compare the dynamics of highly diverse forest types (Malhi *et al.*, 2002; Condit *et al.*, 2006; Anderson-Teixeira *et al.*, 2015).

Useful metrics from demographic data From these simple data on individually tracked stems, we can construct demographic models that enable us to scale up to populations and communities. Increasing computational power and sophisticated statistical methods enable us to move beyond descriptions of annual growth and mortality in abundant species, to models of whole communities–including rare species–and to combine descriptions of each vital rate into models that encompass the whole life cycle and enable population projections to be made. For example, making use of hierarchical models (cf. Gelman & Hill, 2007) we can include all species in analyses by finding community-level parameters and allowing species-level parameters to deviate based on population sizes (Condit *et al.*, 2006). Further, inverse models, in which model parameters are adjusted based on the fit of model output to data (Hartig *et al.*, 2012, 2014), allow us to infer vital rate parameters informed by few data by comparing population summary statistics (e.g. size distributions) from models, to summary statistics from census data (Martínez *et al.*, 2011; González *et al.*, 2016). Finally, the range of demographic metrics which can be extracted from population models is extensive (including for example, life expectancies, passage times to critical life cycle events and population growth rates) and allows us to address a whole

range of questions relating to ecological and evolutionary theory along with conservation and ecosystem management strategies (Caswell, 2000) .

Paper Outline Using data from a 50 ha tropical forest plot, we compared growth and survival rates for 134 species with a range of life forms and abundances. We used data spanning 15 years in order to compare temporal variation in vital rates between species. We then constructed Integral Projection Models (cf. Easterling *et al.*, 2000; Merow *et al.*, 2014a) for each species as a way of efficiently calculating important demographic metrics such as life expectancies and passage times to key life cycle stages.

We used clustering algorithms to identify groups of demographically similar species and related these to life history strategies and trade-offs between vital rates.

Specific hypotheses were:

- H1: As a diverse tropical forest, BCI would contain species with a range of demographic strategies, but it would be possible to cluster species into 'demographic types'.
- H2: Species clusters would relate to the ecological roles of species, demonstrating the existence of clear life-history strategies and possible trade-offs between vital-rates.
- H3: It would be possible to attribute temporal variation in demographic rates to environmental conditions such as El Niño events. Specifically we expected faster growth rates and higher mortality rates in the census interval that spanned a severe El Niño event.
- H4: Species would differ with respect to temporal variation in vital rates, but demographically similar species would be more likely to show similar trends in vital rates through time.

5.3 Methods

5.3.1 Site Descriptions

Data for this analysis came from a 50 ha permanent forest dynamics plot located on Barro Colorado Island (9°9'N, 79°51'W), a 1567 ha island of tropical rainforest located in the Panama Canal. The temperature on BCI is consistently warm but the island experiences a wet season between April and November. The plot consists mostly of undisturbed

old-growth forest with 2 ha of 100 year old secondary forest. More detailed descriptions of BCI can be found in Croat (1978), Leigh *et al.* (1982) and Leigh (1999).

5.3.2 Data collection

BCI is part of the Center for Tropical Forest Science-Forest Global Earth Observatory (CTFS-ForestGEO) network of research forest plots. The first census was completed between 1981–1983 and subsequent censuses took place every five years from 1985 until the present. In each census all stems $\geq$ 1 cm diameter breast height (DBH) (1.3 m above the ground) are mapped, identified to species and measured. Data collection follows a standardised protocol described in Condit (1998). For this analysis we used censuses from 1995–2010. We included all species with $\geq$ 200 individuals over the four censuses which amounted to 134 species, with abundances ranging from 203 to 43709. These species had a range of life history strategies with the maximum observed DBH of each species ranging from 42 mm to 1498 mm.

5.3.3 Vital Rates

For each of the 134 species, we estimated survival and growth rates in each of the three census intervals from 1995 to 2010, allowing us to explore the diversity in demographic rates both across species, and through time. To prevent estimated parameters being influenced by too few data, we excluded species/census interval combinations where a species had fewer than 50 individuals in the first census. Models were fit using Bayesian MCMCs implemented in R (R Core Team, 2014) and Rstan (http://mc-stan.org).

Survival In forest trees, the pattern of size-dependent mortality changes qualitatively through ontogeny. During early life, survival probability tends to increase as seedlings and saplings escape the high mortality environment of the understory where competition for resources is fierce (Clark & Clark, 1992). Once established, the survival probability for most species remains high for the majority of the life cycle, until eventually, at the largest sizes, it might decrease through accumulation of pathogen load or structural damage.

Capturing the different patterns of size-dependent mortality is further complicated by skews in the size distribution of most species. Mortality in large stems is rare and stochastic and without large sample sizes, or long census intervals, it is possible that few mortality events in large trees will be recorded. This makes it challenging to prevent estimates of survival in large individuals being influenced by the fundamentally different patterns of survival in small stems, which numerically dominate the data.

Our solution is to model survival probability with two logistic regressions that meet at a fixed size threshold.

Survival is given by:

$$s = \left(\frac{K}{1 + \left(\frac{1}{e^{-r_1(x-p_1)}} \right)} \right)^t \text{ for all } x < thresh_s \tag{5.1}$$

$$s = \left(\frac{K}{1 + \left(\frac{1}{e^{-r_2(x-p_2)}} \right)} \right)^t \text{ for all } x \geq thresh_s \tag{5.2}$$

where s is survival probability, K is the upper asymptotes of the two curves, r and p are the rate of change and inflection point in the curves respectively, t is the time in years between censuses, x is DBH and $thresh_s$ is the size threshold at which the two curves meet. Subscripts 1 and 2 denote parameters for the small and large survival curves respectively. To ensure senescence in large individuals we constrain r_2 negative. The size threshold is set to 200 mm for species in which the maximum observed sizes is $\geq$ 500 mm DBH, and the 0.8^{th} quantile of size otherwise. Since K is the same for both curves there are just five free parameters to estimate.

Combining two logistic functions in this way results in a very flexible survival model that can capture a range of survival patterns across ontogeny.

Growth The increment data from forest inventories, i.e. annual change in DBH for each stem, is usually highly skewed in that the majority of individuals grow very slowly and a small subset have much faster growth rates. This could be for a number of reasons, such as asymmetries in soil nutrients, pathogen or liana load, or herbivore pressure. Consequently, while larger trees generally grow faster as a result of increased abilities to acquire resources, there is often high variability in growth rates for same-sized individuals.

We capture the individual variation in growth rates using two gamma distributions. The 'fast' distribution was fit to individuals above a fixed size threshold along with the fastest 5% of individuals below the size threshold. The 'slow' distribution was fit to remaining individuals. We used the same size threshold as in the survival model, i.e. 200 mm for species with a maximum size $\geq$ 500 mm and the 0.8^{th} quantile of the size distribution otherwise.

The change in DBH for each individual is therefore given by

$$z \sim \begin{cases} \text{Gamma}(\alpha_1, \beta_1) & \text{for q} * x < thresh_g, \\ \text{Gamma}(\alpha_2, \beta_2) & \text{for all } x \geq thresh_g \\ & (1-q) * x < thresh_g \end{cases} \tag{5.3}$$

where z is DBH increment in mm, q is the quantile for dividing understory individuals into fast and slow growth classes (fixed at 0.95), x is DBH, $thresh_g$ is the size threshold for automatic inclusion in the fast growth class, and α and β are the shape and rate parameters of each gamma distributions with subscripts 1 and 2 referring to the slow and fast distributions respectively.

5.3.4 Integral Projection Models

Life history strategies are shaped by the interplay between growth and survival rates. We therefore combined our models of growth and survival for each species into population models which can be used to obtain important, population-level demographic metrics such as longevities and passage times to key life cycle stages. We use Integral Projection Models (cf. Easterling *et al.*, 2000; Merow *et al.*, 2014a), which describe population dynamics by tracking the change in the distribution of a state variable (commonly size) in a population through time. This is achieved by combining regression models of vital rates (growth and survival) into a kernel which describes the transitions from every size to every other size.

$$n(y, t+1) = \int_w p(y, x) n(x, t)\, \mathrm{d}x \tag{5.4}$$

where $n(y, t+1)$ is the number of individuals at size y at time $t+1$, $p(y, x)$ is the probability of moving from size x to size y in the time interval between t and $t+1$ and w is the range of possible sizes to be integrated over. To numerically solve the integration the size range is divided into a large number of discrete size bins to give a very large matrix of transition probabilities. Therefore, although we refer to matrices in the next section, it is important to remember that these transitions derive from regression models in which size is treated as continuous, rather than direct observations of the movement of individuals between classes, as in matrix population models.

The vec-permutation approach Due to the structure of our growth model, our IPMs describe transition probabilities not only between sizes but also between growth distributions. We therefore use the vec-permutation approach described in detail by Caswell (2012) and in Chapter 2.

Briefly, if S and G define the number of size bins (here 1000) and growth distributions (here 2), then we define G, S x S matrices that contain transition probabilities between sizes, with one such matrix for each growth distribution.

We next define a series of G x G matrices, one for each size class S, that describe the size-dependent probabilities of transitioning between growth distributions. For sizes up to the threshold for automatic fast growth, $thresh_g$, we assume that the probability of moving into the fast growth distribution increases, while the probability of moving back to the slow distribution decreases. This reflects the assumption that light is the biggest determinant of growth rates and that the probability of having access to light increases with size. Above the size threshold the probability of moving to fast is 1 and the probability of moving back to slow is 0.

Both sets of matrices, the G, S x S matrices describing transitions between sizes *within* a growth distribution, and the S, G x G matrices describing transitions *between* growth distributions for each size, are arranged in block diagonal matrices, $\mathbb{U}$ and $\mathbb{M}$ respectively. These are then multiplied by a vec-permutation matrix K to give the final size-by-growth matrix $\tilde{\mathbf{U}}$ as

$$\tilde{\mathbf{U}} = K^T \mathbb{M} K \mathbb{U}. \tag{5.5}$$

When $\tilde{\mathbf{U}}$ is multiplied by a population vector containing the number of individuals in each size and growth class, then, reading from right to left, $\mathbb{U}$ first moves individuals between sizes, K rearranges the population vector so that individuals are arranged by growth distribution within size class, $\mathbb{M}$ moves individuals between growth distributions and finally K^T rearranges the population vector back to its original orientation.

Demographic Metrics Passage times and life expectancies provide information on, for example, time taken to reach the canopy and time to reproductive size, along with life expectancy across sizes. Further, using our size-by-growth IPMs we can estimate demographic metrics conditional on current growth distribution. This permits us to ask questions such as how time taken to reach the canopy differs between slow or fast growers, and how recruitment into a gap (fast growing) might influence life expectancy. This kind of demographic information is essential for estimating rates of forest turnover and generation times, the latter being necessary for evolutionary analysis. And since IPMs are analytically tractable, it is straightforward to obtain these population-level demographic metrics with minimal computational effort.

We calculated the life expectancy at each size, conditional on growth distribution for each species in each census interval. We also calculated expected passage times from the smallest size class to 100, 150 and 200 mm, and the passage time to the size threshold for fast growth if it differed from 200 mm, again conditional on growth distribution.

Detailed descriptions on how to obtain passage times and life expectancies are provided in Appendix B.

5.3.5 Clustering of species into demographic types

To identify groups of demographically similar species we first carried out Principal Component Analysis (PCA) on vital rate parameters and then performed hierarchical clustering on principal components (HCPC) using the `prcomp` and `hcluster` functions in the `stats` package in R.

Biological interpretation of vital rate parameters The vital rate functions presented here have biologically interpretable parameters making it possible to compare life history strategies across species through direct comparison of growth and survival parameters. For example, different combinations of r_1 and p_1 from the survival function can result in high juvenile mortality, with rapid increases in survival probability with size, as might be expected in species with high fecundity and strong density dependence. Alternatively, they could describe more gradual increases in survival probability with size, that might, for instance result from herbivore browsing. Likewise, senescence can be either abrupt or gradual and occur early or late with respect to the maximum size, depending on r_2 and p_2, while the overall survival rate could be low or high as determined by K.

To make interpretation of the PCA easier, we used the expectation of growth from each gamma distribution, given by α/β, rather than α and β themselves. Although we lose some information regarding the variance in each distribution, a measure of population-level variance in growth is retained as the difference in expected growth between the two distributions.

Using PCA to test hypotheses PCA allows us to find orthogonal axes of variation between species in terms of their life history strategies. We can assess how much each vital rate parameter contributes to the axes of variation, along with the percent of the variation between species that is explained by each axis.

Interpretation of the PCA and HCPC allows us to address each hypothesis in turn. We can find clusters of demographically similar species using HCPC (H1), and relate positions

of clusters on PCA dimensions to life history strategies (H2). In order to get an initial idea of shifts in vital rates between census intervals, we compared the upper asymptotes of the survival curves and the expectation of the growth distributions for each species across census intervals (H3). We then used the results of the PCA and HCPC to determine whether or not species fell into the same clusters in each census interval, and whether, within a cluster, species showed similar movement around PCA space (H4).

5.4 Results

5.4.1 Overview of results

MCMC chains converged for all species/census interval combinations in which there were sufficient individuals (≥ 50). There was variation in vital rates within species and across census intervals (H1) and we consequently identified five demographic types relating to different life history strategies (H2). We found no qualitative effect of the 1998 El Niño event on growth and survival at either the community level (H3) or within clusters of demographically similar species (H4). The position of species in PCA space indicated that although there are trade-offs between growth and survival, not all species fall along the slow-fast life history continuum, and in fact many of the fastest growing species are long-lived canopy and emergent species.

5.4.2 Vital Rates

Survival There was considerable variation in survival rates across species, as well as temporal variation within some species (Fig. F.1, table F.1).

In terms of juvenile survival, some species had consistently very high survival rates at small sizes, e.g. *Virola surinamensis*, while others showed significant variation between censuses, e.g. *Oenocarpus mapora*. Patterns of senescence showed similar variation, being abrupt in some species, e.g. *Aliberia edulis*, gradual in others *Apeiba membranacea*, or a mix depending on census interval e.g. *Inga pezizifera*. In some species survival was high across most of the size range, e.g. *A. blackiana* $K = 0.995$, while in others the upper asymptote was as low as 0.735 in some census intervals, e.g. *Piper cordulatum*. The biggest difference in K between census intervals was in *Palicourea guianensis*, where K went from 0.746 in the interval from 1995–2000 to 0.932 in the interval from 2005–2010.

Contrary to expectations (H3), there was no decrease in the mean of maximum long term survival, K, across all species in the interval from 1995–2000 during which there

was an extreme El Niño event. In fact, the difference in mean longterm survival between the first and second census intervals was very small (0.001) and the largest change was actually between the second and third census intervals during which mean K across species increased from 0.966 to 0.973. Fifty six species did show the expected decrease in maximum longterm survival during the interval from 1995–2000 compared with the other two census intervals (e.g. *P. guianensis*). However, even amongst those species, K was only on average 0.008 lower in the El Niño interval than the others. We did not conduct formal significance tests for differences between census intervals either at the community, cluster or species level. However, it would be possible to test mean differences with, for example, ANOVA or directional statistics.

Growth The diversity of growth rates was less than that of survival, both across species and between census intervals (Fig. F.2, table F.2).

Growth rates were generally low and many species showed little differentiation between the slow and fast growth distributions. Notably fast growing species included *Calophyllum longifolium*, *Simarouba amara* and *Tachigali versicolor*.

Many species showed very little variation in growth rates between census intervals, e.g. *Tabernaemontana arborea* but there were more pronounced differences in some species, e.g. *Croton billbergianus* and *Inga acuminata*.

The mean expectation of both the slow and fast distributions was lowest in the second interval between 2000–2005 and highest in the third interval between 2005–2010. There was therefore no clear impact of the El Niño event on growth rates of all species combined (H3). Fifty three species did show the expected pattern of increased growth during the El Niño interval, but differences were generally small.

Principle Component Analysis of vital rates and species clusters The first two principal components separate parameters relating to juvenile survival and senescence in one plane, and growth versus longterm maximum survival in another, suggesting the existence of trade-offs between vital rates, and the partitioning of species along axes of life history strategies (table 5.1, Fig. 5.1). The first two dimensions together account for 66% of variation between species, across all three census intervals, and over 90% of variation is captured by the first five dimensions (Fig. 5.2). Although some dimensions explain very little of the overall variation, they may be important for distinguishing the strategies of certain species.

We retained five clusters from the HCPC, shown in Fig. 5.3. Example survival and growth curves plotted with the mean parameters from each cluster are shown in Fig. 5.4. Although

	PC1	PC2	PC3	PC4	PC5
K	0.16	0.66	0.52	-0.45	0.23
p1	-0.40	0.01	0.45	0.56	0.39
r1	-0.38	-0.26	-0.29	-0.53	0.64
p2	0.46	0.17	-0.32	-0.02	0.08
r2	0.42	0.13	-0.22	0.42	0.59
ex.slow	0.30	-0.57	0.52	-0.16	0.05
ex.fast	0.44	-0.36	0.15	-0.04	0.14

Table 5.1: Parameter loadings in the PCA. ex.slow and ex.fast are the expectation of growth for each gamma distribution given by α/β

the majority of species were in the same cluster in all three census intervals, 31 were in two different clusters and one (*Cordia alliodora*) was in three clusters, suggesting that although the majority of species had relatively stable vital rates through time, others had much greater temporal fluctuations (Fig. 5.5). In some cases this might be down to demographic stochasticity; especially in small populations the death of a few large individuals can have significant impact on the mean population parameters. However, contrary to expectations, within each cluster species did not show similar variation in vital rates through time (H4) (Fig. 5.5). This probably reflects the fact that there were not major changes in demographic rates between census intervals, i.e. the majority of species showed little variation in vital rates through time. The pattern that we see is what we would expect in an undisturbed forest. However, given that 1998 was one of the most extreme El Niño events of the century (Condit *et al.*, 2004), it is surprising that there was no discernible effect on vital rates, even in just a subset of species with similar life history strategies.

5.4.3 Demographic Metrics

Variation in Passage Times and Life Expectancies To explore how temporal variation in vital rates leads to changes in population dynamics through time, we used vital rates from each census interval to construct IPMs and calculated life expectancy at the smallest size and the expected passage time from the smallest size to the growth threshold, conditional on starting growth distribution, see Figs F.3, F.4 and table F.3.

Passage times from the smallest size to the size threshold for fast growth ranged from 460 years for *Astrocaryum standleyanum* stems starting slow, to just 7 years for *Palicourea guianensis* stems starting fast. However, it is worth noting that this reflects differences in the size threshold as well as variation in growth rates.

Generally, starting growth distribution had little effect on passage times, with the difference in passage time between individuals starting in the fast and slow distributions ranging from -2 to 26 years with a mean of 5 years. Negative numbers indicate that individuals starting in the slow distribution had faster passage times than those in the fast distribution–these were mostly *Cercropia* spp. and other light demanding understory species. *Cercropia insignis* and *C. obtusifoloia* only recruit into high light environments, being extremely shade intolerant, and therefore there was little differentiation between the fast and slow growth distributions simply because the only individuals in the census data were fast growing–those that were in low light having died.

Some species had considerable variation in passage times between years. For example, the passage time for *Sloanea terniflora* stems starting in the slow growth distribution, ranged from 197 years between 2000–2005 to 330 years between 2005–2010. However, across all species, the mean difference in passage time between census intervals was 18 and 17 years for stems starting in the slow and fast growth distributions respectively, again suggesting that demographic rates were relatively stable for the majority of species.

Life expectancies for 9 mm stems ranged from 119 years, *Swartzia simplex* var. *grandiflora* stems in the fast growth distribution, to 3 years, *Bactris major* stems in the slow growth distribution. The mean difference in life expectancy between stems starting in the slow distribution versus the fast distribution was just 1 year, with a range from -2 (*Hampea appendiculata*) to 14 (*Aspidosperma spruceanum*). Negative numbers indicate that individuals starting in the slow distribution had longer life expectancies than those starting the fast distribution.

Life History Trade-Offs We then examined potential trade offs between growth and survival rates by looking at the relationship between life expectancies and passage times for a range of sizes (Fig. 5.6, table F.4). There was a clear positive correlation between life expectancy and passage time–i.e. species that had longer life expectancies also tended to have longer passage times, suggesting a trade-off between growth and survival. Understory species (those with a maximum size < 500 mm) also generally had lower life expectancies for the same given passage times, suggesting that while these species do not necessarily grow faster, they have shorter life cycles.

5.5 Discussion

We found substantial variation in the demographic rates of 134 tropical tree species from a 50 ha plot on BCI, Panama. However, although a range of growth and survival rates

were observed, it was possible to group species according to life history strategy. These clusters support the hypothesis of species being partitioned along axes of life history variation and the existence of trade-offs between vital rates. However, along with the classic 'live-fast, die-young' and 'grow-slow but live-long' strategies emerging, we found that many long-lived canopy species are also fast growing, and that the majority of species in the plot are slow growing, mid-story species. The ability to detect these community-wide patterns results from biologically meaningful models of growth and survival that account for individual differences and changes in vital rates through ontogeny.

5.5.1 Axes of life history

The growth and survival functions presented here, while being robust to small sample sizes, are still sufficiently flexible to capture a range of growth distributions and size-dependent survival patterns. As predicted (H1), there was clearly substantial diversity between species as well as some temporal variation within species. We used PCA and HCPC to identify 5 groups of demographically similar species (H1).

Clusters of demographically similar species clearly relate to different life history strategies (H2). At one extreme there are the long-lived, canopy and emergent species, also characterised by their high expected growth rates in the 'fast' growth distribution. These are the species with a subset of fast growing stems that make it to the canopy. At the other extreme are the classic 'live fast, die young' species, which have high expected growth rates in both the slow and fast distributions but low overall survival and early senescence. However, the latter consisted of relatively few species. The majority of species fell into a mid-story group characterised by slow growth, relatively high maximum survival, and senescence at intermediate sizes. Our results therefore suggest that while there is a clear axis defining fast growth versus high survival, the fastest growers are in fact often the long-lived canopy and emergent species and many small and shrubby species grow slowly and die small.

This result emerges as a consequence of our approach to fitting growth models with multiple distributions and survival models that account for changes in survival probability through ontogeny. Instead of focussing on population mean growth rates, which miss the crucial within species variation, we are able to capture the subset of fast growers in the long-lived species. Further, we can include maximum, longterm survival in our comparison of species which prevents results being influenced solely by the fact that smaller statured species will naturally have higher mean mortality rates as a result of their smaller maximum sizes.

5.5.2 Impact of El Niño on demographic rates

Counter to expectations (H3), the El Niño event in the first census interval did not affect growth and survival rates at the community level. Hypothesis 3 was based on observations of growth and mortality in BCI during previous El Niño events. Condit *et al.* (1992) report that approximately two thirds of species in BCI had increased mortality in the interval from 1982–1985 compared with the interval from 1985–1990, due to an El Niño event in 1983. The greatest difference was seen in canopy species (maximum height at least 20 m) which had annualised mortality rates 31.8% higher in the first interval compared with the second. Forest wide growth rates were also elevated during the drought period that accompanied the 1983 El Niño event, possibly due to survivors having decreased competition as a result of the increased mortality rates.

An analysis of 205 species from BCI, over the same census intervals, reports overall mortality to be 50% higher ($\approx 3\%$) from 1983–1985 compared with 1985–1990 ($\approx 2\%$) (Condit *et al.*, 1995). Again, despite shrubs having higher overall mortality, canopy species had a greater increase in mortality during the El Niño drought. Contrary to the authors predictions, species associated with moist microhabitats did not suffer more severely than other species. Likewise, gap colonisers and generalists (defined by the ratio of recruits in gaps and non-gaps) did not show significant differences in drought response, suggesting that life form may be a better predictor of a species response to environmental perturbation than either habitat preference or simple definitions of life history strategy.

Our finding of no overall increase in mortality during the 1995–2000 census interval, although contrary to the studies above, is consistent with Condit *et al.* (2004), who also found no clear effect of the 1998 El Niño drought on mortality in ten species from BCI. Condit *et al.* (2004) report elevated growth rates during the El Niño event which we did not find in this study. However, we included 134 species in this analysis while Condit *et al.* (2004) focus on just ten. Further, Condit *et al.* (2004) had higher temporal resolution, comparing the intervals from 1995–1998 (before), 1998–1999 (during) and 1999–2000 (after) the El Niño event, whereas our analysis is based on five year census intervals.

Our results are surprising given that the 1998 El Niño was accompanied by the second most severe dry season since 1930 (Condit *et al.*, 2004). Only the 1982–1983 dry season had less rain, which might explain why signatures of drought were found in the vital rates of species in studies covering that interval (Condit *et al.*, 1992, 1995) and not in this study. However, the longer census interval in this study may also be an explanation for the discrepancy. It seems likely that the 1998 El Niño event had no forest wide impact on either growth or survival of BCI species, that was detectable with 5 year census intervals.

However, there was clearly variation in how individual species responded, highlighting, once again, the need to move away from community wide descriptors of vital rates towards studies that account for between and within species variation.

Contrary to expectations, species within clusters did not show similarities in temporal variation (H4) (Fig. 5.5). This contrasts the patterns seen by (Condit *et al.*, 1995) in the 1993 El Niño, where species with different life forms were differentially impacted by the El Niño drought. However, given that we saw no strong impact of the 1998 El Niño event, this result is perhaps not surprising.

5.5.3 Functional versus demographic traits

The potential of functional traits to explain patterns of co-existence and community assemblage has received increasing interest in ecology recently. A large number of studies have explored the diversity of functional traits within and between communities and attempted to relate traits to abiotic conditions (Buzzard *et al.*, 2016), phylogenies (Uriarte *et al.*, 2010) and mechanisms of co-existence (Westoby *et al.*, 2002; McGill *et al.*, 2006).

However, the relationship between functional traits, demography and community functioning is not always straightforward. Firstly, plants are highly plastic and their trait values can vary along environmental gradients (Jung *et al.*, 2010) and through ontogeny (Iida *et al.*, 2014; Visser *et al.*, 2016). Second, some functional traits are difficult to measure in certain environments. For example, collecting sun leaves from trees in a tropical forest is extremely difficult due to the height of the canopy or the fact that some species are only ever shaded (Kraft *et al.*, 2008). Finally, the low population densities of many tropical trees makes it difficult to obtain large samples for many traits. For some traits this may not be a problem as variation between species outweighs variation within a species (Hulshof & Swenson, 2010; Powers & Tiffin, 2010). For other traits, which show large variation between individuals (Lasky *et al.*, 2014) or through ontogeny (Iida *et al.*, 2014; Visser *et al.*, 2016), it is not clear that mean trait values from small samples accurately represent the true mean value for a population or species.

A number of studies have highlighted the difficulty in linking functional traits to demography. In a study of 240 species from five neotropical forests Poorter *et al.* (2008) found that although wood density, seed volume and adult stature were good predictors of growth and survival, the relationship between specific leaf area (SLA), commonly used as an indicator of life history strategy, and growth and survival was unclear. Likewise, in a study of 50 tropical trees, Hérault *et al.* (2011), found that interspecific variation in growth was explained by traits related to stem economics and adult stature, but that seed size and

leaf economic traits had no significant relationship with growth parameters. A global analysis relating size-standardised relative height growth rates (SGR) to traits in 278 species from 27 sites found that wood density, SLA and seed mass explained only 3.1% of interspecific variation in SGR, leading the authors to conclude that functional traits may be unsuitable for predicting juvenile growth rates at broad scales (Paine *et al.*, 2015). Likewise, in a study examining the potential of using leaf habit to predict plant functional types, Powers & Tiffin (2010) found that across 87 species, leaf habit had no relationship with ten other functional traits, suggesting that functional types based on single traits may be uninformative.

The attraction of functional traits is that they offer mechanistic insight into how physiological features relate to demography and ecological functioning. Demographic rates alone do not allow us to predict how species will respond to changing environments. It is of course possible to characterise vital rates across an environmental gradient (e.g. Purves, 2009) but the relationship is still phenomenological and does not provide information on how a species might respond to conditions outside the range of those observed. Integrating functional trait and demographic data, with careful consideration of the whole life cycle and the variation across environments will be necessary to predict species and community responses to environmental change.

5.5.4 Potential applications in large scale vegetation models

In the last decade there has been growing appreciation of the need to more accurately represent biodiversity and differences in species demography in global vegetation models (Moorcroft, 2006; Purves & Pacala, 2008). Current global vegetation models typically represent the world's vegetation with just a few plant functional types (Friend & White, 2000; Sitch *et al.*, 2003; Woodward & Lomas, 2004; Clark *et al.*, 2011; Pavlick *et al.*, 2013; Schaphoff *et al.*, 2013), and due to the spatial resolutions of these models, this can result in highly biodiverse tropical communities being represented by just a single plant functional type. Friend *et al.* (2014) compared climate predictions from seven different global vegetation models and showed that divergences in model predictions largely stemmed from uncertainties in carbon residence time, leading the authors to recommend that future research focus not only on primary productivity, but also on structural dynamics and demographic processes.

Incorporating demography into large scale models is now possible due to the increasing availability of demographic data. Networks of permanent plots extend across all of the major forest biomes and contain the information needed for characterising the vital rates

and life history strategies of hundreds of individual species (Malhi *et al.*, 2002; Anderson-Teixeira *et al.*, 2015). It is these patterns of growth, mortality and recruitment that determine forest turnover, biomass and carbon residence time.

This paper presents one possible approach to aggregating species. We have demonstrated the ability of our models to capture a range of growth and survival patterns from 134 tropical species with very different life forms and population densities. Our vital rate models capture heterogeneity at the individual level which, when scaled up to the population level, more accurately captures the variance in life expectancies and passage times through the life cycle. This matters when we consider that few individuals make it to the canopy, and yet the canopy defines the structure of the forest, determines the light environment for smaller stems, holds the majority of biomass and regulates important ecosystem functions. To model vegetation-atmosphere feedback we therefore need to properly capture the dynamics of canopy trees. By fitting demographic models to individual species and then clustering species according to their demographic similarities, we can account for variation at the individual level and its consequences for community dynamics and ecosystem functioning. Linking demographic types to the functional traits of species will further enable a mechanistic link to be made between physiology, demography and consequences for ecosystem functioning.

5.5.5 Conclusions

We fit growth and survival models to 134 tree species from a 50 ha forest dynamics plot on BCI, Panama and identify groups of demographically similar species. While we find evidence of a 'slow-fast' continuum in life-history strategies, species do not all partition along this one axis. Rather, we find that many of the fastest growing species are long-lived canopy species, while fast-growing, low-survival species actually account for relatively few species. Many slow-growing species also have high mortality. Our results indicate that at the individual level, competition for resources has a large impact on growth and survival, and that correctly accounting for individual heterogeneity in population models is necessary to capture the ecological process shaping communities. Although species showed changes in demographic rates through time, there was no clear impact of the 1998 El Niño event on growth and survival rates in the majority of species. We propose that aggregating species based on a combination of functional and demographic traits is a useful strategy for incorporating biodiversity into large scale vegetation models.

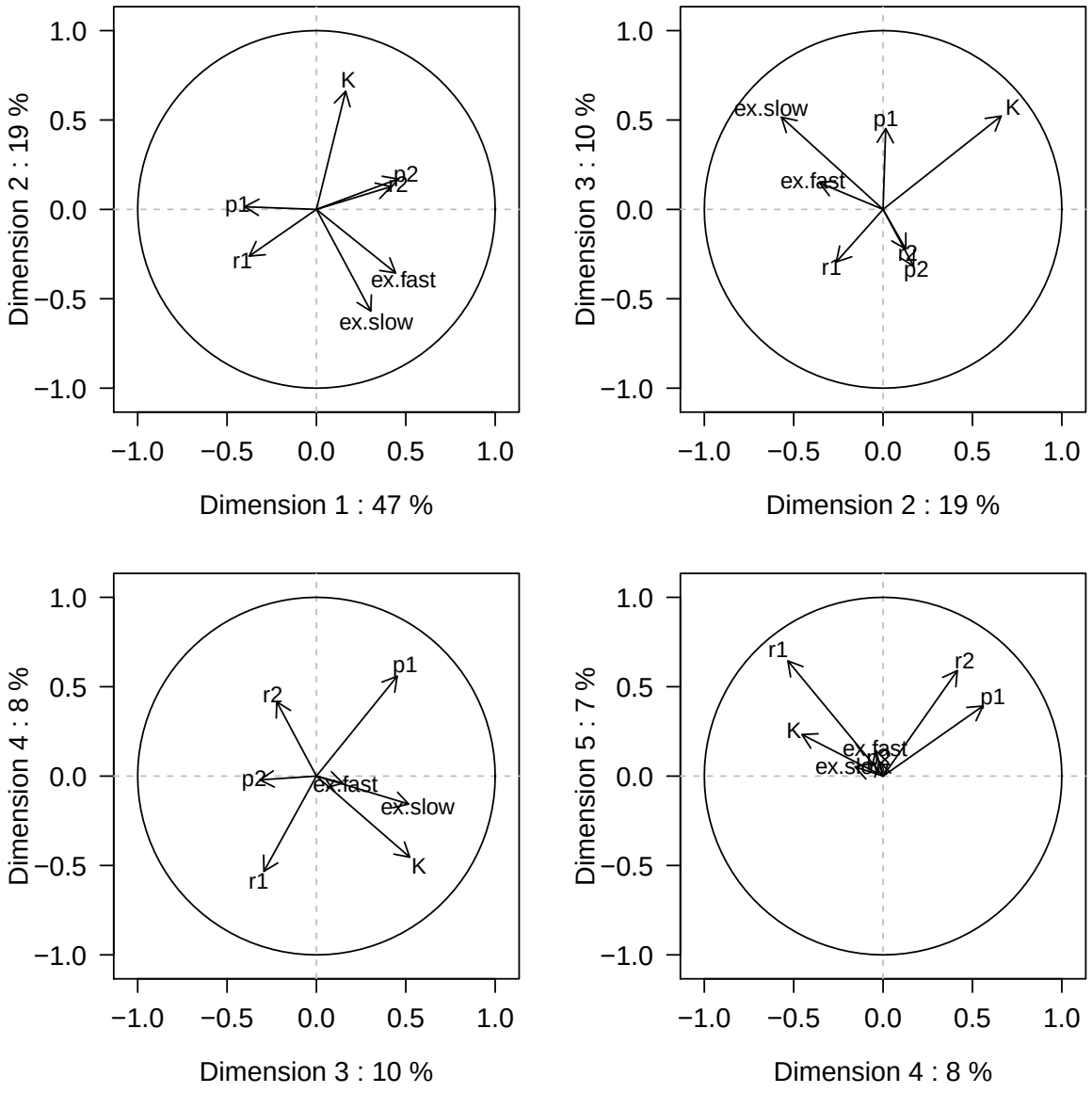


Figure 5.1: Parameter loadings in the PCA. Parameters relating to juvenile survival and senescence oppose each other, suggesting that species with high juvenile mortality also tend to have early senescence. Long term maximum survival (K) and growth parameters oppose each other in dimension 2, providing evidence of a trade-off between fast growth and high overall survival.

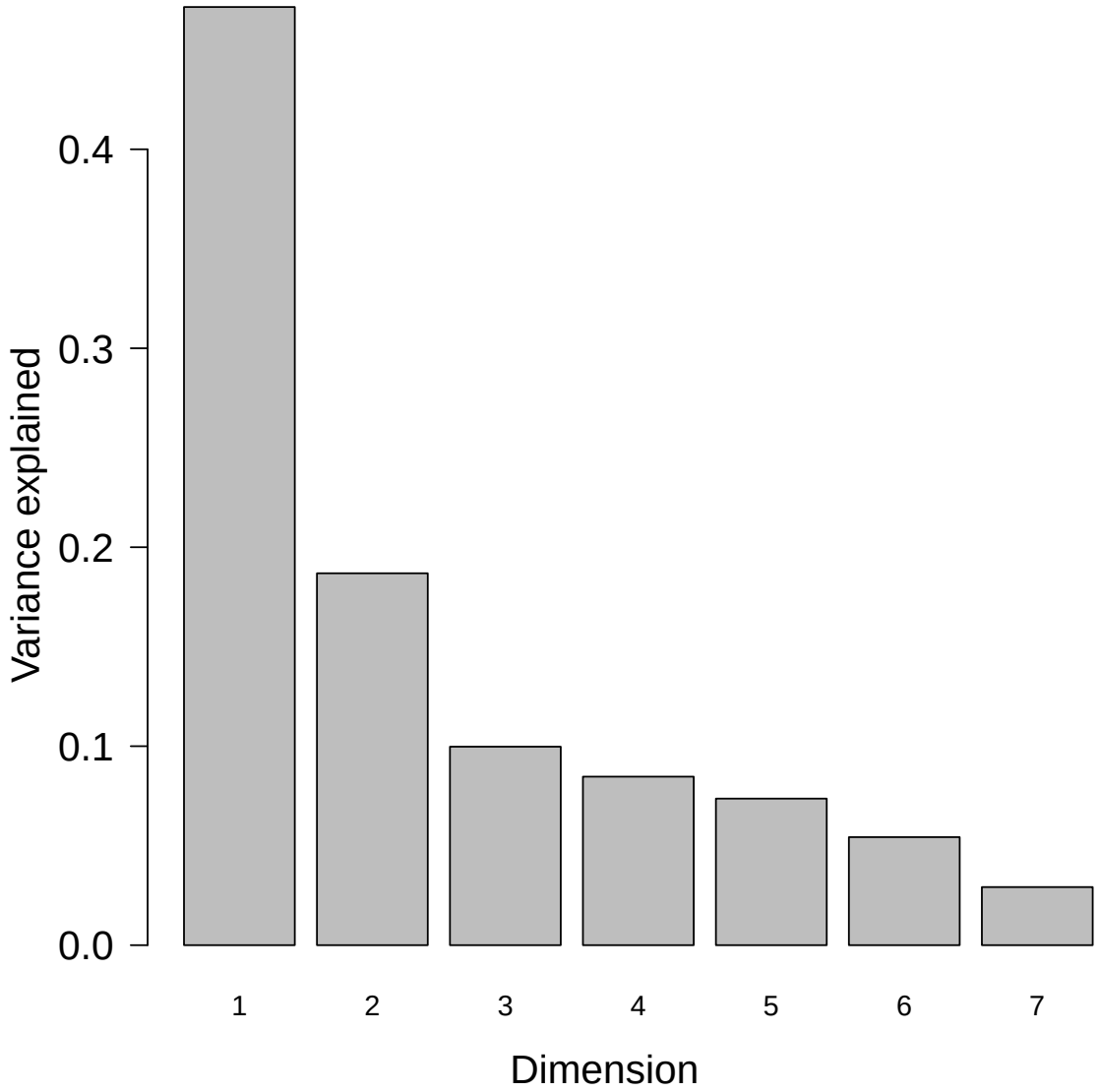


Figure 5.2: The variation between species growth and survival strategies explained by each dimension of the PCA. The first two dimensions together explain 66% of variation.

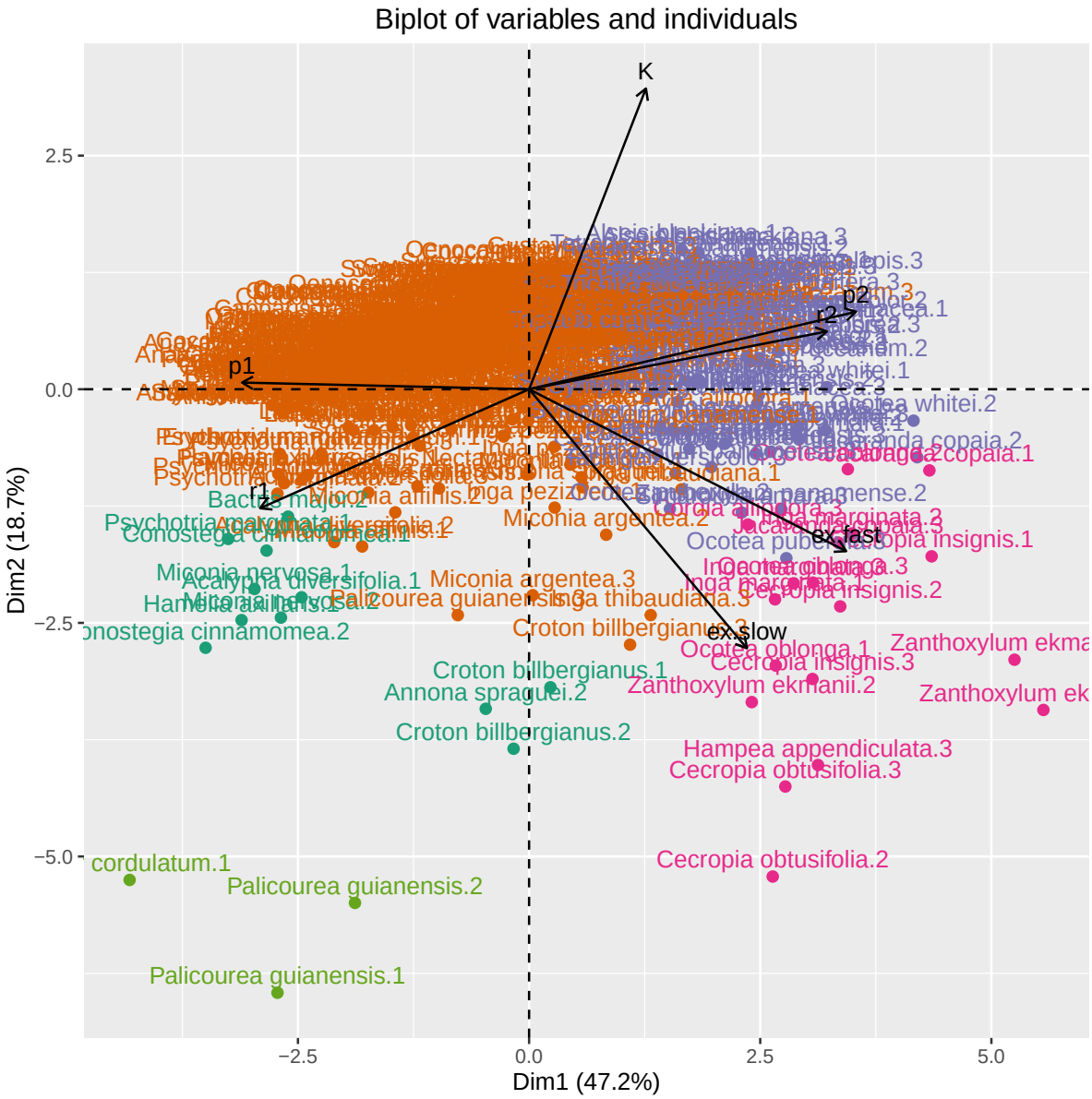


Figure 5.3: Species positions in PCA space, according to the first two PCA dimensions, and the variable loadings on each dimension. Species/census combinations are colour coded by cluster. The majority of species are slow growing mid-story species (shown in orange).

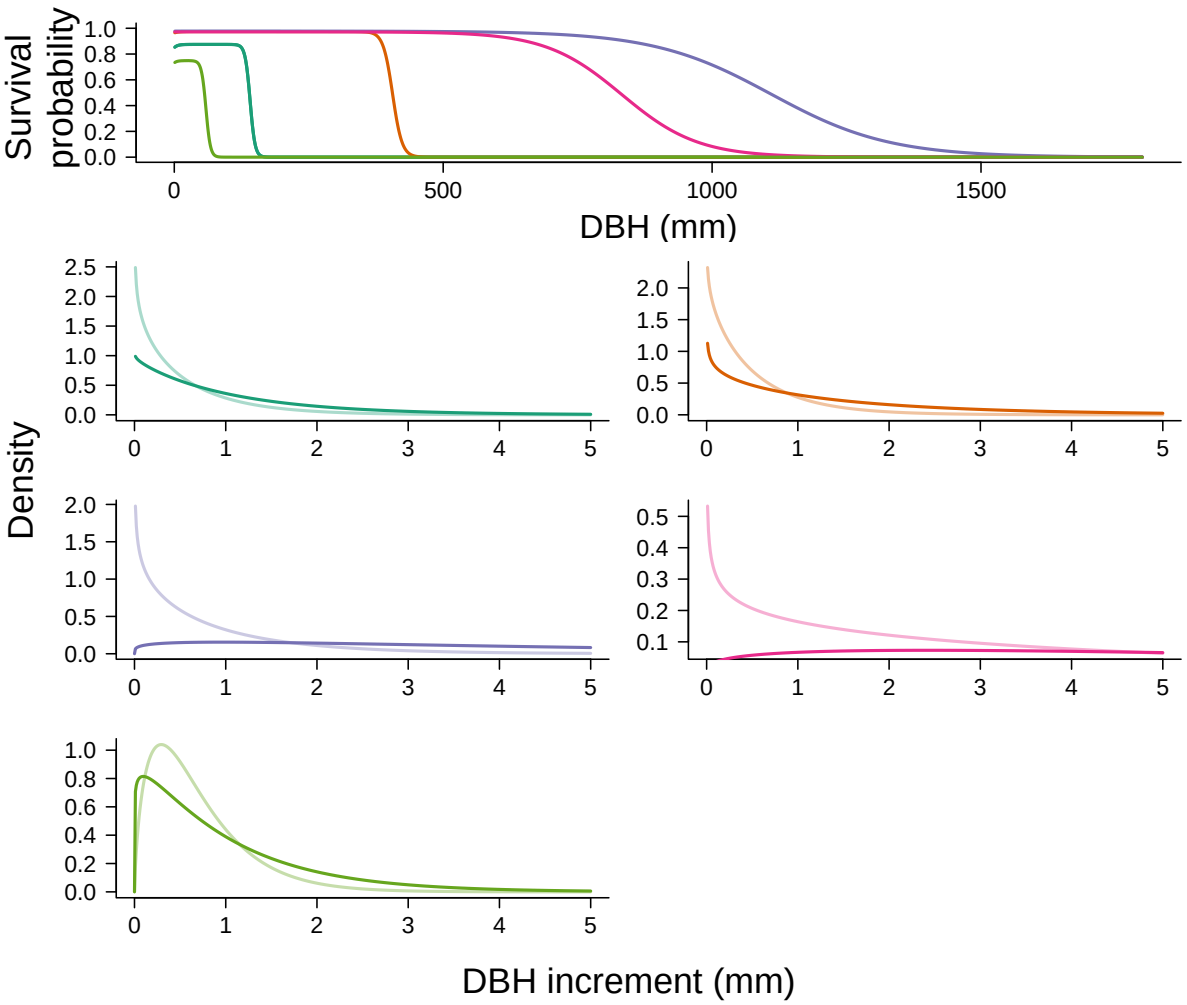


Figure 5.4: Survival and growth curves were plotted using the mean parameter values for species within each cluster. Results suggest that small statured species tend to be slow growing while potentially long-lived canopy species have faster growth rates. The exception is the light green cluster which has high expected increments in both growth distributions but very low overall survival. However, this cluster was informed by very few species.

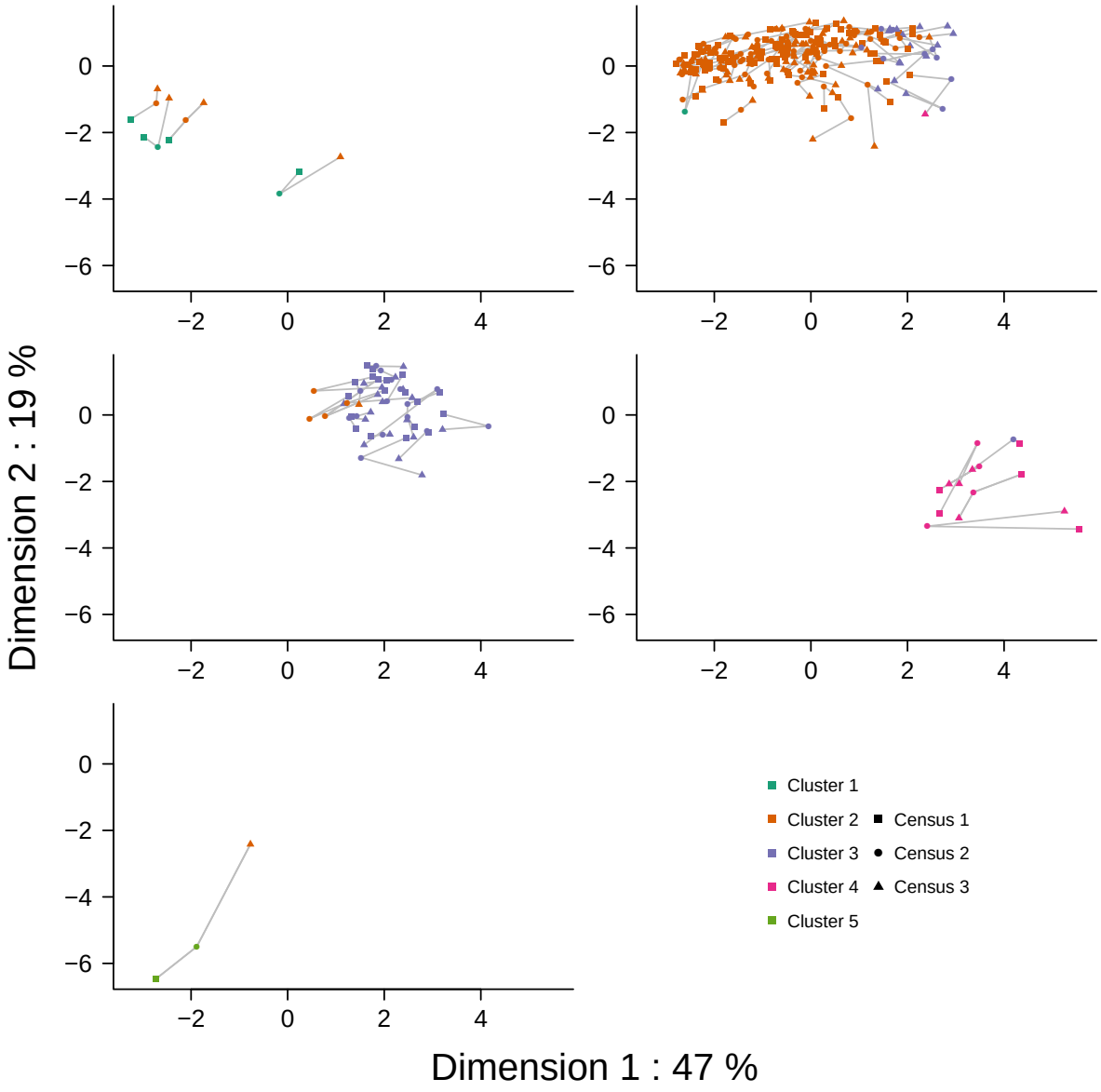


Figure 5.5: Species positions in PCA space, showing which cluster they fall into in each census interval. Species showed more temporal movement along dimension 2 than dimension 1, suggesting greater variability in overall survival and growth than in juvenile survival or senescence. There is no qualitative evidence that within each cluster species show similar temporal variation.

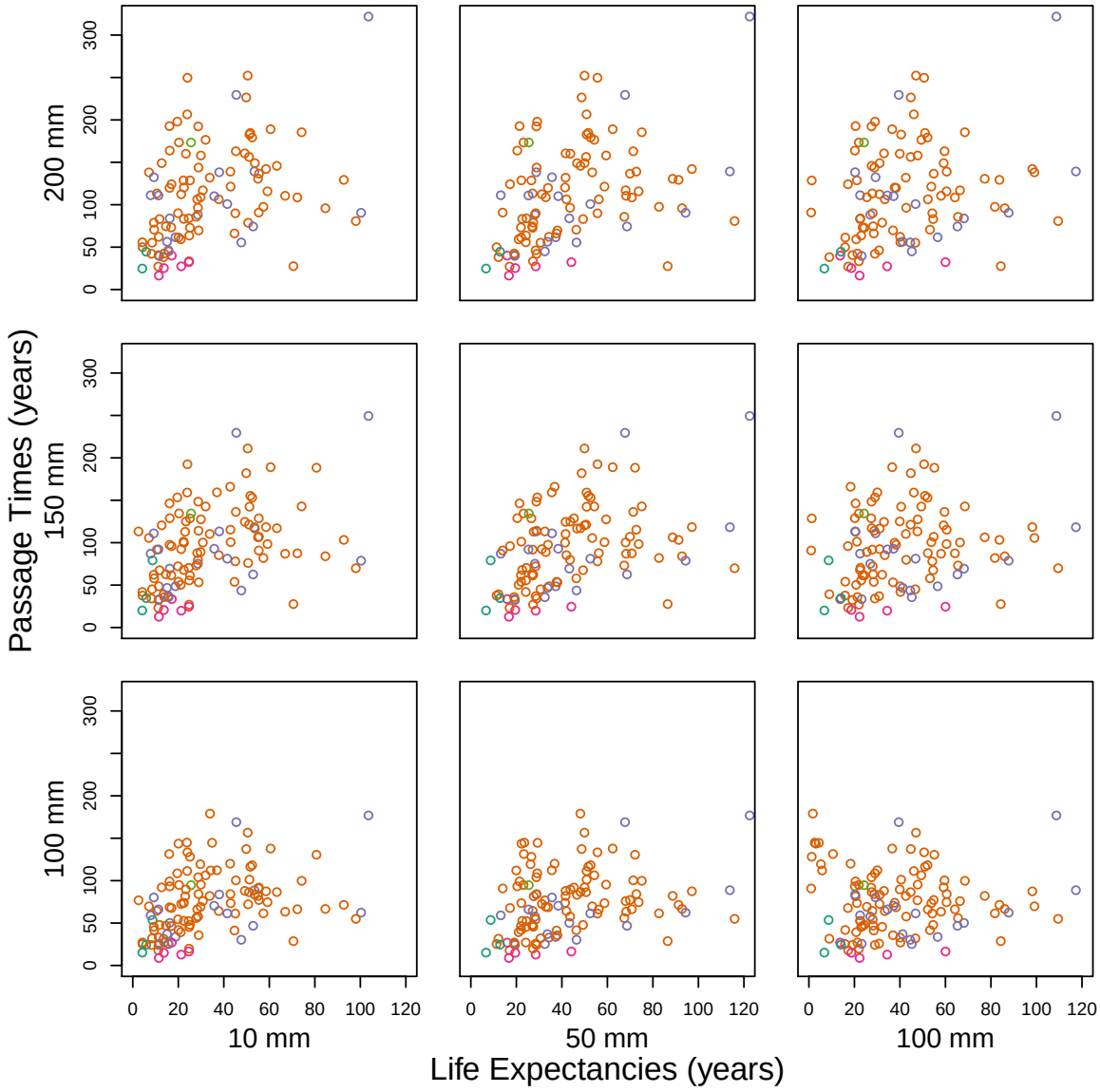


Figure 5.6: Passage time against life expectancy for each of the 134 BCI species, with individuals starting in the slow growth distribution. Species are coloured according to their cluster from the HCPC carried out on vital rate parameters. There is a positive correlation between long life expectancies and longer passage times, suggesting long lived species are slow growing.

Chapter 6

Discussion

6.1 Demography for local and global analysis

Forests are faced with unprecedented global change, including rapidly changing climates, increased herbivore pressure and more severe and frequent outbreaks of pests and pathogens (Reyer *et al.*, 2015). How forests respond to these challenges will be largely determined by the demographic rates of individual species. To understand forest dynamics at both local and global scales we therefore need to appreciate how differences in demographic rates across species shape community composition and forest turnover. For instance, adult trees have been shown to be particularly sensitive to drought (Bennett *et al.*, 2015) while the sensitivity of seeds and seedlings to environmental conditions may limit recruitment and range shifts of many species (Walck *et al.*, 2011; Zhu *et al.*, 2014). At a local scale, regeneration following pest or pathogen outbreaks will be strongly influenced by the growth rates and fecundity of both targeted and non-targeted species (Brunet *et al.*, 2014). Likewise, the vegetation preferences of herbivores, and the response of vegetation to herbivory are both strongly linked to vegetation growth rates (Augustine & McNaughton, 1998). In fact, the impact of all types of disturbance, and succession following disturbance are both directly related to the demographic rates of species in the community. Further, these processes playing out at the local scale determine patterns of diversity and forest turnover across much larger scales, making an understanding of local demography critical to understanding forest dynamics at the landscape level.

Until fairly recently the inclusion of demography in forest models was surprisingly all or nothing. Vital rates of individual stems are described in gap models with increasingly complex mechanistic models of physiological processes, e.g. (Botkin *et al.*, 1972; Pacala *et al.*, 1993; Bugmann *et al.*, 1997; Jorritsma *et al.*, 1999). Early global vegetation models (GVMs) however, moved from cellular processes to global dynamics with no inclusion of

species or their demographic rates, relying instead on coarse representations of vegetation types (Cao & Woodward, 1998). Within the last decade the need for demography at all scales of forest modelling has been recognised (Purves & Pacala, 2008; Friend *et al.*, 2014). There has been much progress in describing the diversity of demographic rates in forests across the globe (Malhi *et al.*, 2002; Condit *et al.*, 2006) as well as integrating demography into large scale vegetation models and highlighting the importance of this integration for accurately describing ecosystem functioning (Moorcroft *et al.*, 2001; Medvigy *et al.*, 2010). However, more work is needed to combine these two areas, i.e. finding meaningful ways of including the full diversity of demographic rates in broad scale vegetation models.

6.2 A novel demographic framework

In this thesis I have presented a novel modelling framework that allows information collected at the level of the individual to be translated into community dynamics with implications for larger scales. This is an important step towards the overarching goal of moving from physiological processes at the leaf scale to global dynamics, and one that has the potential to improve our understanding of forest dynamics at multiple levels. Firstly, individual level data is relatively straightforward to collect and as such is increasingly available from forests across the globe (Malhi *et al.*, 2002; Anderson-Teixeira *et al.*, 2015). Second, making use of individual-level demographic data enables a wide range of questions to be addressed, ranging from the impact of soil moisture on seedling success (Rawal *et al.*, 2015) to the mechanisms maintaining species diversity (Nakashizuka, 2001). Third, at this level of biological organisation it is possible to include data at finer and broader resolutions depending on the question at hand. For instance, environmental covariates can be included in models of survival (Lines *et al.*, 2010) or forest inventory data can be integrated with remotely sensed data to explore the link between forest structure and demographic rates (Stark *et al.*, 2015).

6.2.1 Vital rate models that can handle species diversity and individual differences

The modelling framework presented here is underpinned by vital rate models that allow us to make best use of available data while being robust to biases in the data, flexible enough to handle the huge diversity of life forms encountered in temperate and tropical forests, and with biologically interpretable parameters.

Growth Previous attempts to model growth rates of forest trees have usually focussed on regressions of increment against size (Davies, 2001; Enquist *et al.*, 2007), or simply summarising growth into a single metric for populations as a whole (Condit *et al.*, 2006; Poorter *et al.*, 2008) or divided into size classes (Clark & Clark, 1992; Alvarez-Buylla & Martinez-Ramos, 1992).

Both approaches can be problematic given that there is huge variation in growth rates within a population, even between individuals of the same size. The metabolic scaling theory predicts that growth scales to the 1/3 power of DBH (Enquist *et al.*, 2007). However, this fails to account for asymmetries in competition between individuals. Tests of the metabolic scaling theory have shown it not to be a good match to growth data in both tropical (Coomes & Allen, 2009; Rüger & Condit, 2012) and temperate sites (Ishihara *et al.*, 2016). Rüger *et al.* (2011) found that light was a better predictor of growth rates than individual size, but that both size and light environment together accounted for only 12% of the population level variation in growth rates for 247 species of tropical trees. Other factors such as genetics, pathogen load and herbivore pressure are clearly important.

How to account for the general trend of increasing growth with size, while allowing for substantial individual variation is therefore one of the challenges that needs to be addressed if we are to successfully capture the processes that lead to observed forest structure. The growth models presented in Chapter 2 and applied throughout this thesis offer one solution. Although the binary nature of the two distributions may at first seem arbitrary, it makes biological sense as all species, regardless of whether their dynamics are driven by light requirements, will have a majority of slow growing individuals and a small subset of faster growing trees. The assumption that the distributions link to individual light environments is convenient but not essential. Fitting the distributional growth models to 134 species from the 50 ha plot in BCI, Panama, demonstrated the ability of this approach to capture the diversity of growth strategies that exist in a tropical community. Further, the combination of the distributional growth model with estimates of transition probabilities between distributions enabled us to feature critical temporally correlated individual differences into population models.

In Chapter 3, I demonstrated how these growth models can be linked to spatial data to model the outcome of disturbance events at a local scale. Following a severe epidemic of a forest pest or pathogen, forest structure can be significantly disrupted, changing the proportion of individuals situated in gaps. Allowing a measure of neighbourhood basal area to act as a competition index dictating the growth distribution of each individual

allows us to capture successional dynamics and regeneration following an opening of the canopy.

In the IPM framework used in other chapters, movement between growth distributions is conditional on size as oppose to neighbourhoods. These transition probabilities are difficult to estimate from inventory data and more work is needed to quantitatively characterise the variance in individual pathways through the lifecycle. Work by Brienen & Zuidema (2006) has made important steps in this direction but tree ring analysis is problematic given its bias towards large trees. Using dendrometers to accurately track annual and interannual variation in growth rates of stems across the size distribution of a species might be another way forward.

The distributional approach to modelling growth therefore offers a way of capturing asymmetries in individual trajectories through the life cycle in an ecologically interpretable manner. However, although the distributions themselves are straightforward to parameterise using available forest inventory data, more work is needed to constrain estimates of movement between distributions.

Survival Mortality of large stems play an important role in determining forest biomass, hydrology and the physical structure of the forest; the latter in turn determining understory light levels and therefore the dynamics of smaller stems. Modelling mortality of large stems, however, is complicated by the fact that canopy trees are long lived and morality is a rare and stochastic event. Preventing estimates of senescence being influenced by the qualitatively different pattern of survival shown by the numerically dominant small stems is important if we are to produce survival models that can lead to realistic population level outcomes.

The survival model presented in this thesis is one solution, providing the flexibility to capture size dependent patterns of mortality across a range of species. Separating the data in this way allows questions relating to particular ontogenic stages to be addressed. For instance, in Chapter 3 the combination of forward and inverse models allowed us to better constrain estimates of senescence for species with only two years of data. On the other hand, in Chapter 4, we could infer the impact of deer herbivory on juvenile survival rates by projecting populations through sequences of IPMs with different parameters dictating juvenile survival.

Incorporating the impact of disturbance events on patterns of tree mortality is fundamentally important to predicting how forests will respond to global change. The inverse approach used in Chapter 4 is one way to infer the impact of historic events on tree survival and might provide clues to how species will respond to future patterns of disturbance.

Another interesting way forward would be to look at how survival strategies differ between sites in response to abiotic conditions and disturbance histories. Chapter 5 demonstrated the success of the survival model in capturing the range of survival patterns exhibited by 134 species in BCI and how these changed through time. While there was no strong signature of the El Niño event in this plot, it would be interesting to look at other plots where fire and typhoons may have left more distinct, community wide shifts in survival probabilities through time. While we expect to see the full range of survival strategies represented in forests across the globe, it is possible that some sites may be dominated by species with particular life history strategies as a result of the environmental conditions or disturbance histories in those sites.

6.2.2 Individuals to populations–accounting for persistent individual differences

Incorporating the distributional growth model and the size-dependent survival function into IPMs using the vec-permutation approach (cf. Caswell, 2012) allows us to characterise the asymmetries in individual performance and the consequences for population dynamics. A large body of theory already exists describing the analysis of IPMs and Matrix Population Models (much of which is applicable to IPMs) and their applications to range of organisms and ecological and evolutionary questions (e.g. (Easterling *et al.*, 2000; Caswell, 2000; Childs *et al.*, 2003; Ellner & Rees, 2006; Merow *et al.*, 2014a)). Applying this theory to the size-by-growth IPMs described in this thesis (and the papers herein) enables us to find life expectancies, passage times, population growth rates and stable size distributions, and explore evolutionary stable strategies and life history trade-offs. Further, we can cluster species according to these population level demographic metrics and assess the match between these clusters and the functional types as defined by functional traits. This is discussed further in the 'Future Directions' section below.

6.3 Future Directions

6.3.1 Scaling up

Alternatives to gap models are needed if we are to scale up from individuals to landscape and global vegetation models. The individual based gap model approach is unfeasible for modelling vegetation across large geographic and temporal scales. Firstly there are too many stems to make this computationally efficient, and secondly, most gap models have complex parameterisation, requiring data on individual access to resources that are not

available for most forests, e.g. (Pacala *et al.*, 1993). Forest inventory data on the other hand, is increasingly available and holds the individual level information that could feed into broad scale population models.

There has been significant work in the last decade developing Structured Ecosystem Models (SEMs) that account for important individual and species level variation while being potentially scalable to large geographic regions. Mostly this has involved characterising the average behaviour of stochastic models in order to create mathematically tractable models which can reveal ecosystem properties without the need to simulate thousands or millions of individual stems. For instance, Moorcroft *et al.* (2001) used the average behaviour of a stochastic, individual-based gap model (the Ecosystem Demography (ED) model) to derive macroscopic equations describing ecosystem dynamics. The dynamics of the individual based model were reproduced using a size- and age-structured (SAS) approximation in which the equations for the individual based model became terms in a system of partial differential equations. When the SAS approximation was used to implement ED across a large region of South America, it performed reasonably well at capturing regional dynamics (vegetation and soil carbon, and mean annual NPP). However, there were areas of high disagreement between model predictions and observed dynamics, in part because many of the model inputs were not available at the regional scale.

Similarly, the macroscopic equations presented by Strigul *et al.* (2008) are derived directly from the models describing growth and mortality of individual stems. These macroscopic equations are coupled to the Perfect Plasticity Approximation (PPA) - an integral equation that describes the effect of height structured competition for light on vital rates. Together these equations were able to reproduce the dynamics of the individual based gap model SORTIE (Pacala *et al.*, 1993) when SORTIE was adapted to include the assumption of PPA. Further, by parameterising this framework with FAI data, Purves *et al.* (2008) were able to match chronosequences of stand development for North American forests on different soil types.

The Integral Projection Models presented in this thesis (and the papers herein) offer a different approach to achieving the same aims. IPMs, like the macroscopic equations described by Strigul *et al.* (2008), do not explicitly model individuals, but are underpinned by vital rate models that describe conditional probabilities of individual growth, survival and fecundity given size. They are therefore able to produce population level dynamics that result from individual vital rates, without the need for simulations of thousands of stems. However, although the models of Moorcroft *et al.* (2001), Strigul *et al.* (2008), Adams *et al.* (2007) and Purves *et al.* (2008) are based upon gap models of whole communities, and therefore integrate the dynamics of multiple species, IPMs are species specific. This is

not a problem when we are studying communities in their current states, since interactions between species are implicit in the vital rate models that underpin the IPMs. However, as communities respond to global change and new combinations of species come together as a result of range shifts and invasions, the interactions between species need to be modelled explicitly. Finding ways to incorporate species interactions more directly into IPMs will be necessary if they are to feature in large scale vegetation models.

Species specific outputs from IPMs could be used as benchmarks against which DGVM results are compared. The aims of DGVMs and Earth System Models (ESMs) are to make predictions regarding vegetation dynamics and climate over large geographic regions and timeframes. However, in order to give credibility to predictions at these broad scales, we need to validate model predictions at the scales for which we can collect empirical evidence (Moorcroft, 2006). IPM predictions of population dynamics of common species are based on growth and survival observations from thousands of individual stems. Before scaling up to larger regions, DGVMs should be able to reproduce the dynamics of forest ecosystems at the plot scale, and IPMs offer an efficient way of generating benchmarks for these comparisons.

Finally, the functional types identified by clustering species according to demographic outputs from IPMs could be used to inform the ways in which ESMs handle species diversity, especially in tropical regions. Until recently the number of plant functional types represented in ESMs was typically small, and due to coarse representations of spatial heterogeneity, entire biomes were often described by the dynamics of a single functional type, e.g. (Foley *et al.*, 1996; Cox, 2001). However, even more recent models frequently represent vegetation with just a few functional types. For instance, a recent study by Friend *et al.* (2014) compared predictions from seven global vegetation models, of which five included less than 10 plant types (Friend & White, 2000; Clark *et al.*, 2011; Sitch *et al.*, 2003; Schaphoff *et al.*, 2013; Woodward & Lomas, 2004), and one used randomly generated growth strategies (Pavlick *et al.*, 2013). The study by Friend *et al.* (2014) found large variation in predictions of carbon change between the seven models, in large part due to uncertainties in carbon residency times. Carbon residence times are determined by patterns of growth and mortality, and Friend *et al.* (2014) conclude that the inclusion of demographic processes in DGVMs should be a research priority. By identifying groups of species with similar life history strategies through analysis of demographic traits, IPMs provide a mechanism by which important demographic diversity could be meaningfully represented at large scales.

6.3.2 Integrating different data sources

Central to scaling from individuals through populations and communities to global vegetation dynamics is the ability to incorporate information from different spatial and temporal scales. This could involve data collected at a finer resolution, such as by incorporating physiological processes into the vital rate models in order to move from phenomenological to mechanistic descriptions of growth, survival and fecundity. Although this makes parameterisation more difficult, it will be necessary to predict species responses to climate change, for example elevated CO_2 or increased temperatures. The vital rates functions in this thesis are all designed to be flexible and could easily incorporate environmental covariates.

Alternatively, demographic rates could be linked to canopy structure using remotely sensed data, such as airborne-LiDAR data, as in Stark *et al.* (2015). Remote sensing technologies are becoming increasingly important for monitoring forest dynamics at the landscape scale and there is great potential for using remotely sensed data to extrapolate demographic rates from forest plots across large geographic regions. Stark *et al.* (2015) demonstrated that tree size distributions in Amazonian forests could be predicted from LiDAR remote sensing of vertical canopy components. Further, demographic rates of forest trees could be linked to light environments inferred from models of forest structure. This connection raises the possibility that growth rates could be parameterised at the regional scale, by first calibrating models using forest inventory data and then extrapolating using remotely sensed data.

Finally, measurements of carbon, water and energy exchange between the canopy and the atmosphere are available from the global eddy-flux tower network (https://fluxnet.ornl.gov). Relating these data to the demographic rates of forest trees will make it possible to predict biosphere-atmosphere feedbacks in response to shifts in demographic rates driven by climate change.

6.3.3 Linking demographic traits to functional types

Current approaches to modelling forest dynamics over large scales involve aggregating species into functional types based on either broad descriptions (Foley *et al.*, 1996; Cox, 2001), e.g. 'tropical broadleaf evergreen', or on combinations of physiological traits (e.g. specific leaf area, seed size, wood density) (Díaz & Cabido, 1997). These coarse descriptions however, fail to capture the diversity of tropical plots and the impact that species differences will have on ecosystem functioning, while physiological traits can be difficult to link to life history strategies due to variation between individuals and

through ontogeny (Visser *et al.*, 2011). A more direct route to assessing the similarities and differences between species in terms of life history strategies is to model vital rates themselves. Combining functional traits with vital rate models such as those presented here will enable a mechanistic interpretation of the role of physiology in structuring communities, while taking into account shifts in the importance of traits through the life cycle and the variation between individuals and environments.

Work in Chapter 5 showed how we can identify groups of demographically similar species in a 50 ha tropical plot in Panama. An interesting next step would be to map these demographic groups to functional types identified previously to assess whether functional traits are indeed good indicators of the functional role of species in the community. This analysis could then be extended geographically to explore how vital rates, along with population level metrics, such as size-dependent life expectancies, are distributed across both local and global environmental gradients. Would the clusters of demographically similar species identified in BCI be reproduced in other forests or would different life history strategies dominate other forest types? If so, could differences in demography be linked to environmental conditions and disturbance histories?

6.4 Conclusions

This thesis presents a modelling framework that translates individual stem data from forest inventories into population and community level models. The ability to translate understanding across biological, geographic and temporal scales is critical for predicting how forests will respond to environmental change. The models presented here allow us to explore the impact of disturbances on community dynamics at a local scale, either through projecting communities forward in time under various disturbance scenarios, or by inferring how past disturbances may have impacted populations in order to give rise to the present day communities. Vital rate models that account for individual differences enable us to explore the diversity of demographic strategies within and between forests. Finding ways to aggregate species for inclusion in global vegetation models will be critical for reducing uncertainty in these models. Since large-scale patterns of biomass and carbon turnover are driven by growth, mortality and recruitment at local scales, aggregating species based on demographic models such as those presented here, would be a straightforward and ecologically meaningful approach. This work makes use of abundant demographic data in order to address critical questions relating to forest dynamics, from local plot disturbances to how we can account for biodiversity in large-scale vegetation models.

Appendices A to F on pages 130–308 are provided with the electronic version of this thesis.

Appendix A

Chapter 2: Supplementary material

A.1 Transition probabilities for three distribution growth model

Transition probabilities for the smallest size class are:

$$C_{1,1} = \begin{pmatrix} 0.980 & 0.140 & 0.100 \\ 0.015 & 0.855 & 0.400 \\ 0.005 & 0.005 & 0.500 \end{pmatrix},$$

while the transition probabilities for the size class below the size threshold for fast growth are:

$$C_{1,thresh_g-1} = \begin{pmatrix} 0.900 & 0.010 & 0.070 \\ 0.095 & 0.985 & 0.20 \\ 0.005 & 0.005 & 0.730 \end{pmatrix}.$$

We define the matrix, C_2 for all sizes above the size threshold $thresh_g$ as

$$C_2 = \begin{pmatrix} 0 & 0 & 0 \\ 1 & 0.9 & 0.5 \\ 0 & 0.1 & 0.5 \end{pmatrix}.$$

A.2 Sensitivity to matrix size

The dimensions of IPMs determine the accuracy with which we can estimate population statistics. In IPMs, the state variable (size) against which vital rates are regressed is treated as continuous, but numerical integration involves discretisation of the size variable into a large number of discrete bins. Because trees typically grow a very small amount each

year, relative to their potential maximum size, a large number of size bins are needed to capture individual heterogeneity in growth and prevent the unrealistically fast movement of some individuals through the size classes (Zuidema *et al.*, 2010). However, the time taken to analyse a matrix increases with the size of the matrix. In multi-state IPMs, such as our size by growth IPMs, the dimensions of the matrix are given by the product of the number of classes in each state, for example the number of size classes, multiplied by the number of growth distributions. Increasing the number of state variables, and the number of classes in each, can quickly make calculating metrics such as the population growth rate–the dominant eigenvalue–prohibitively slow. We therefore test the sensitivity of population level outputs from our size-growth IPMs to the number of size classes, since a reduced number of size classes increases the efficiency with which further state variables can be added to the IPMs.

We tested the sensitivity of population statistics in all three BCI species to the number of size bins (S), by constructing IPMs from $S = 200$, to $S = 2000$ in increments of 200 (corresponding to class widths ranging from 6.01 mm to 0.60 mm for *C. longifolium*,10.48 mm to 1.05 mm for *P. copaifera* and 2.04 mm to 0.20 mm for *G. intermedia*). From these IPMs we calculated longevities, and passage times to the size threshold for fast growth (200 mm), conditional on starting growth distribution, along with the population growth rate and stable size distribution from each sized IPM.

A.2.1 Matrix size sensitivity results

Estimates of passage time for a 9 mm *P. copaifera* stem, starting in the slow growth class, to reach 200 mm varied from 237 to 124 years when size bins ranged from 200 to 2000, figure A.6. Life expectancies were insensitive to IPM size, going from 113 to 112 years for a 9 mm stem in slow growth, as the size bins increased from 200 to 2000. This most likely reflects the fact that survival probability was relatively constant across much of the observed size range.

Calophyllum longifolium was less sensitive to IPM dimensions than *P. copaifera*, figure A.7. Demographic metrics stabilised for both species with size bins ≥ 1000. For the understory species, *G. intermedia*, increasing the number of size bins above 600 had little effect on results, figure A.8.

A.3 Eviction of individuals from IPMs

Eviction of individuals from IPMs occurs when the range of sizes dictated by the IPM is less than the maximum that can be obtained through the interplay between the growth and survival models. This results in abrupt death of anything still in the final size bin, as by growing out of the IPM, they disappear from the population. This sudden mortality limit can lead to underestimates of population growth rates (Williams *et al.*, 2012), and failure to capture senescence of large individuals. To ensure that the rate of senescence results in individuals dying before reaching the maximum size, either the modelled size range can be extended, priors can be used when fitting the survival curve, or the survival parameters determining senescence can be sampled in an inverse model. As in the inverse model described above for estimating fecundity parameters, in this inverse modelling approach, the likelihood function compares simulated and observed size distributions and penalises parameters that allow individuals to survive beyond the sizes observed in the data set.

In our example, results from an inverse model would likely be similar to extrapolation from the forward model through extension of the size range, as the survival curve fit to the observed sizes has a slight dip in survival probability, which, when extrapolated, leads to senescence in sizes beyond the observed size range. When data are more limited and few mortality events are observed in large size classes, inverse modelling might be necessary to avoid high rates of survival leading to too many individuals surviving beyond the observed size range.

	Slow small	Fast small	Fast big
Mean	14.29	8.37	24.22
Variance	198.01	50.65	406.12
Min	1.00	1.00	1.00
Max	89.00	37.00	97.00

Table A.1: Distribution of number of consecutive years spent in each growth class from simulations of *C. longifolium* with two growth classes. Small and big refer to individuals below and above the size threshold for automatic inclusion in the fast growth class

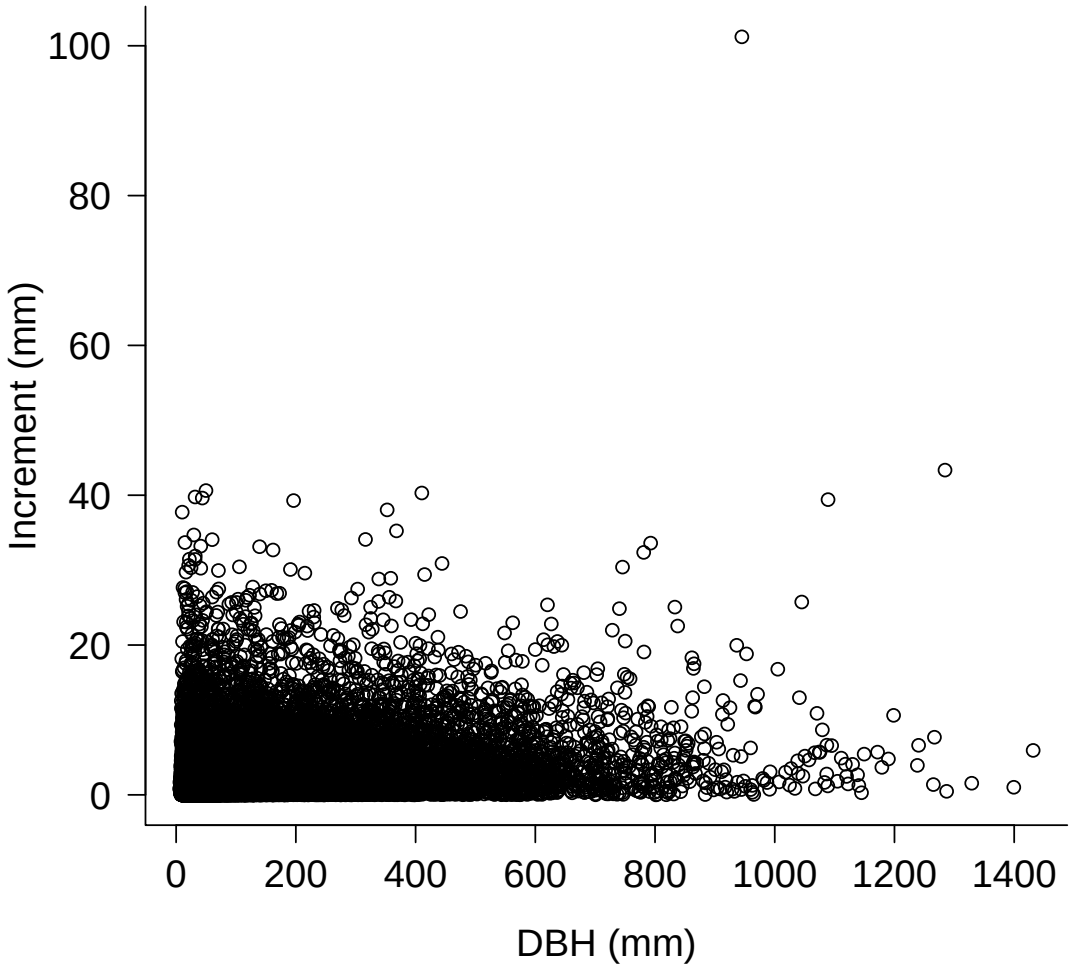


Figure A.1: Annual increment data from the census interval 2005 - 2010, for all BCI species with more than 200 individuals during the interval 1995 to 2010. There is significant variation in increment at all sizes.

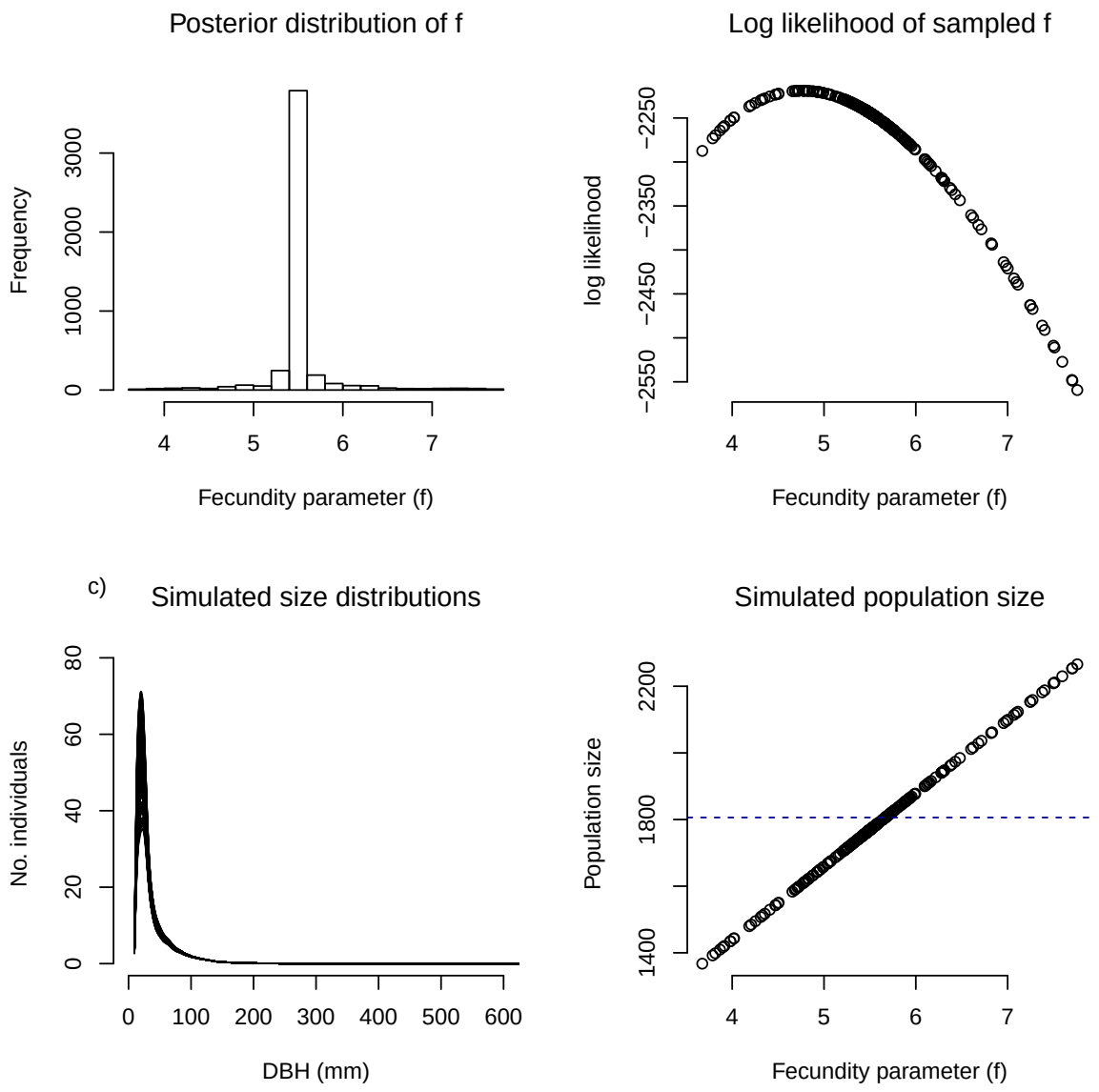


Figure A.2: Posterior distribution of fecundity parameters for *C. longifolium* (a) and the associated log likelihoods (b), simulated size distributions (c) and simulated population sizes (d) of 1000 randomly sampled parameters from the posterior. Small changes to the fecundity parameter resulted in large changes to the population size of the simulated population although the size structure was constant.

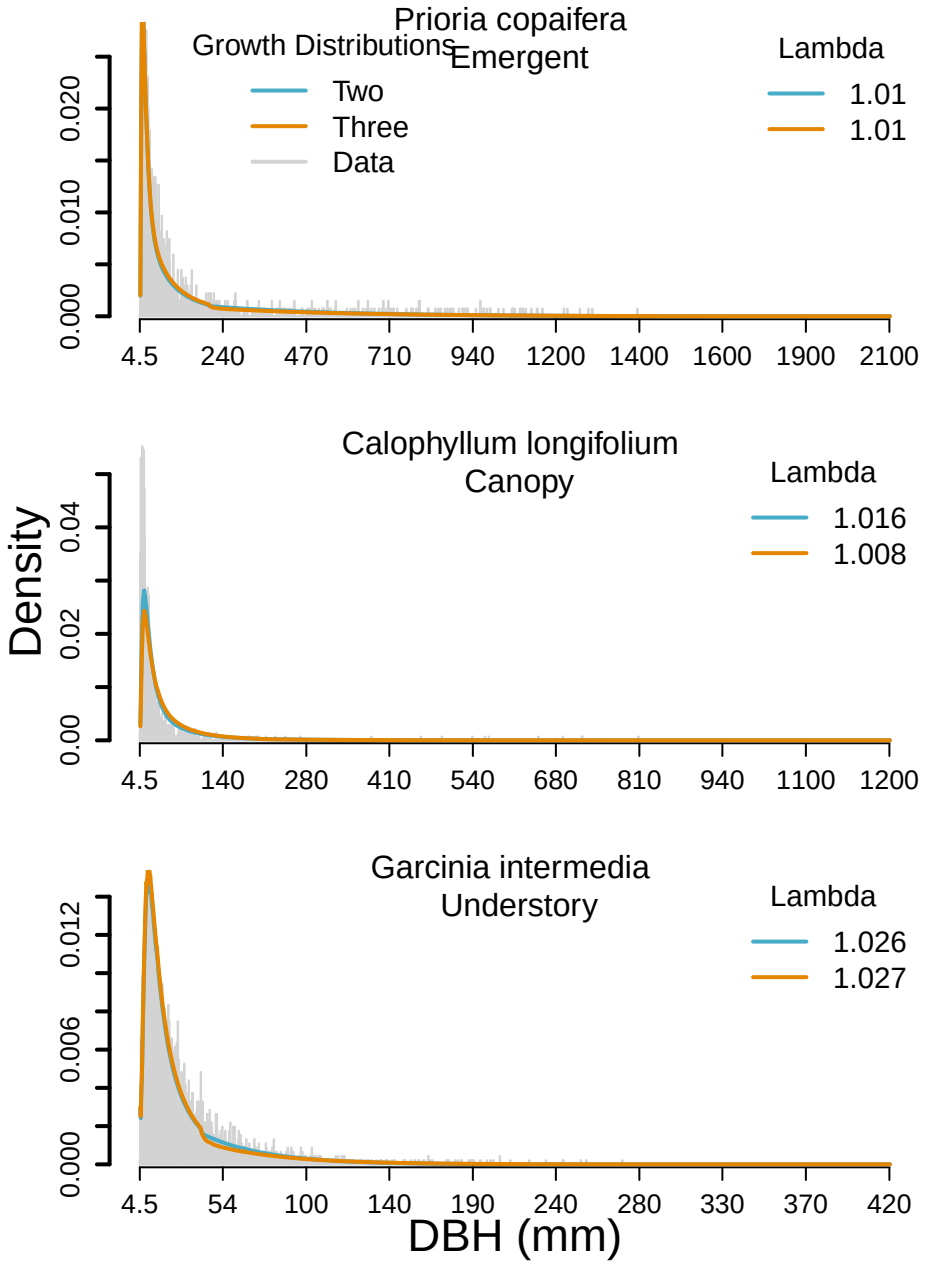


Figure A.3: Stable size distribution and population growth rate (λ) of the BCI species. The stable size distributions show the expected size structure of the population in the long term, given the inferred vital rates parameters and all else remaining constant. The difference in stable size distributions between the two and three distribution growth models were very small. Population growth rates were also similar irrespective of the number of growth distributions.

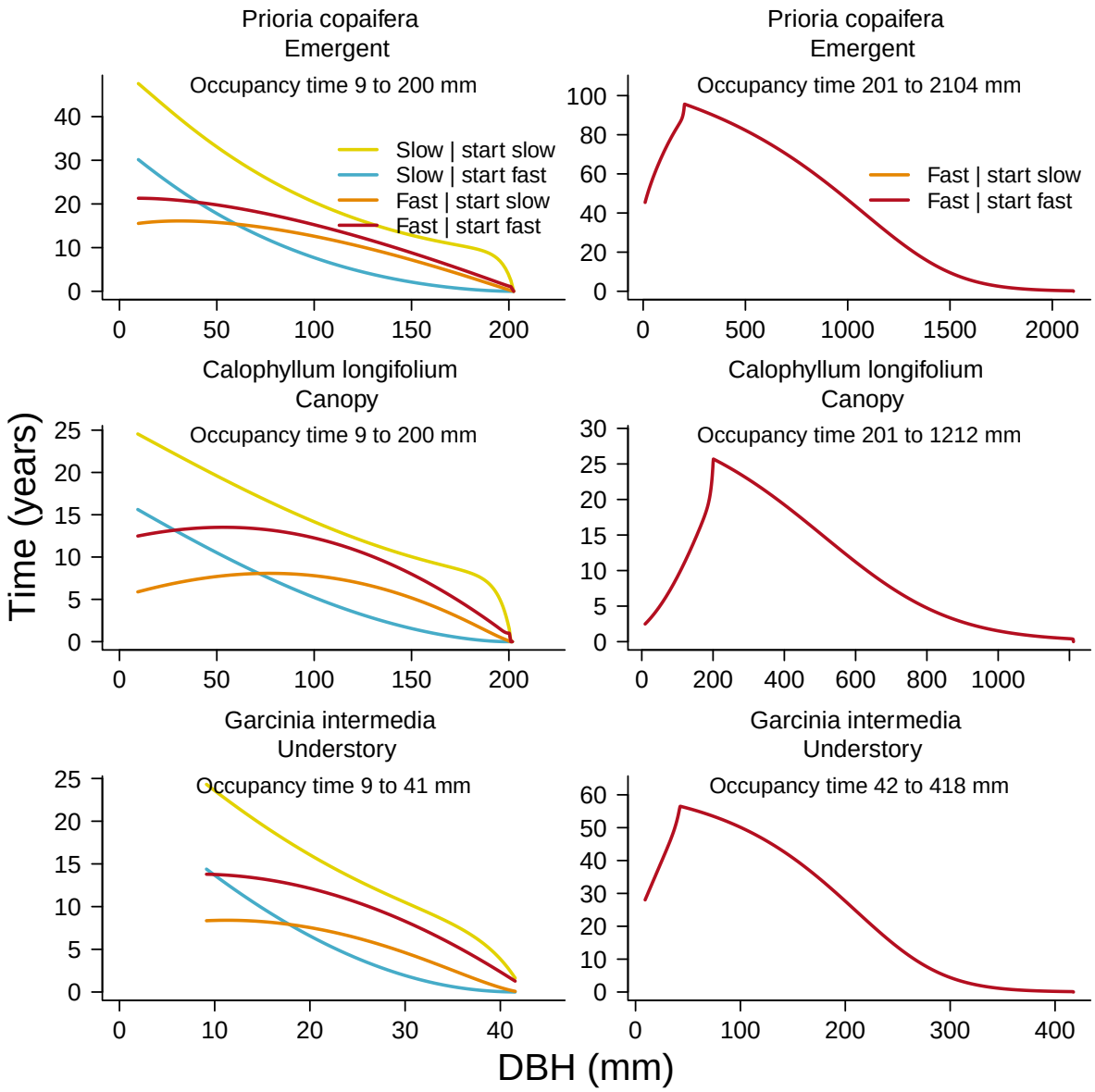


Figure A.4: Occupancy times for each BCI species below (left) and above (right) the threshold for fast growth, conditional on starting growth distribution. Once over the size threshold individuals are automatically in the fast growth distribution, and since the IPMs have no memory of how individuals got there, occupancy times are equal for individuals that started slow or fast.

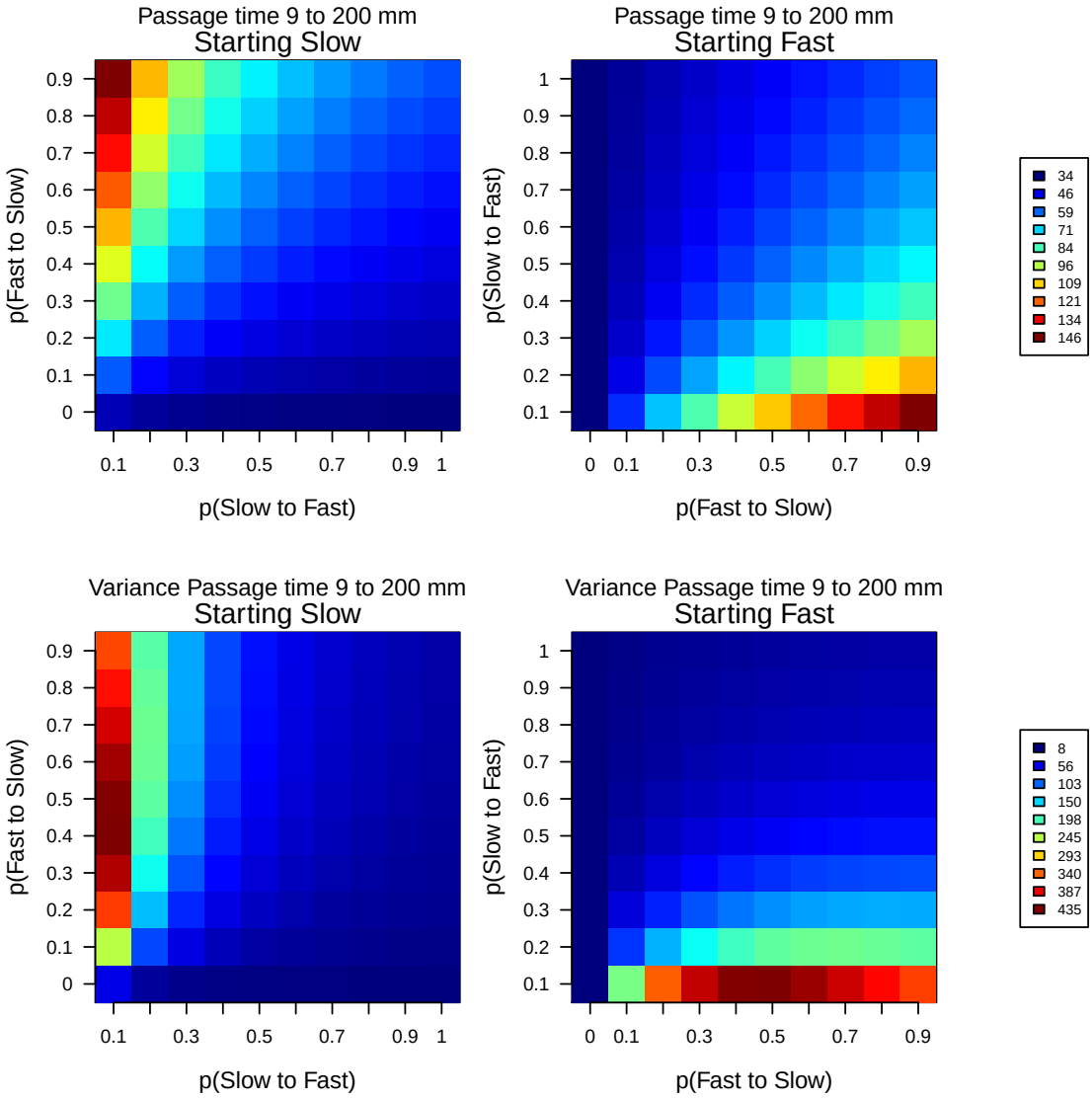


Figure A.5: Heat maps showing the sensitivity of *C. longifolium* passage time from 10 mm to 200 mm (top) and the variance in these passage times (bottom), to different combinations of transition probabilities between growth distributions, conditional on starting growth distribution. Passage times show more sensitivity to fast to slow transitions than to slow to fast transitions.

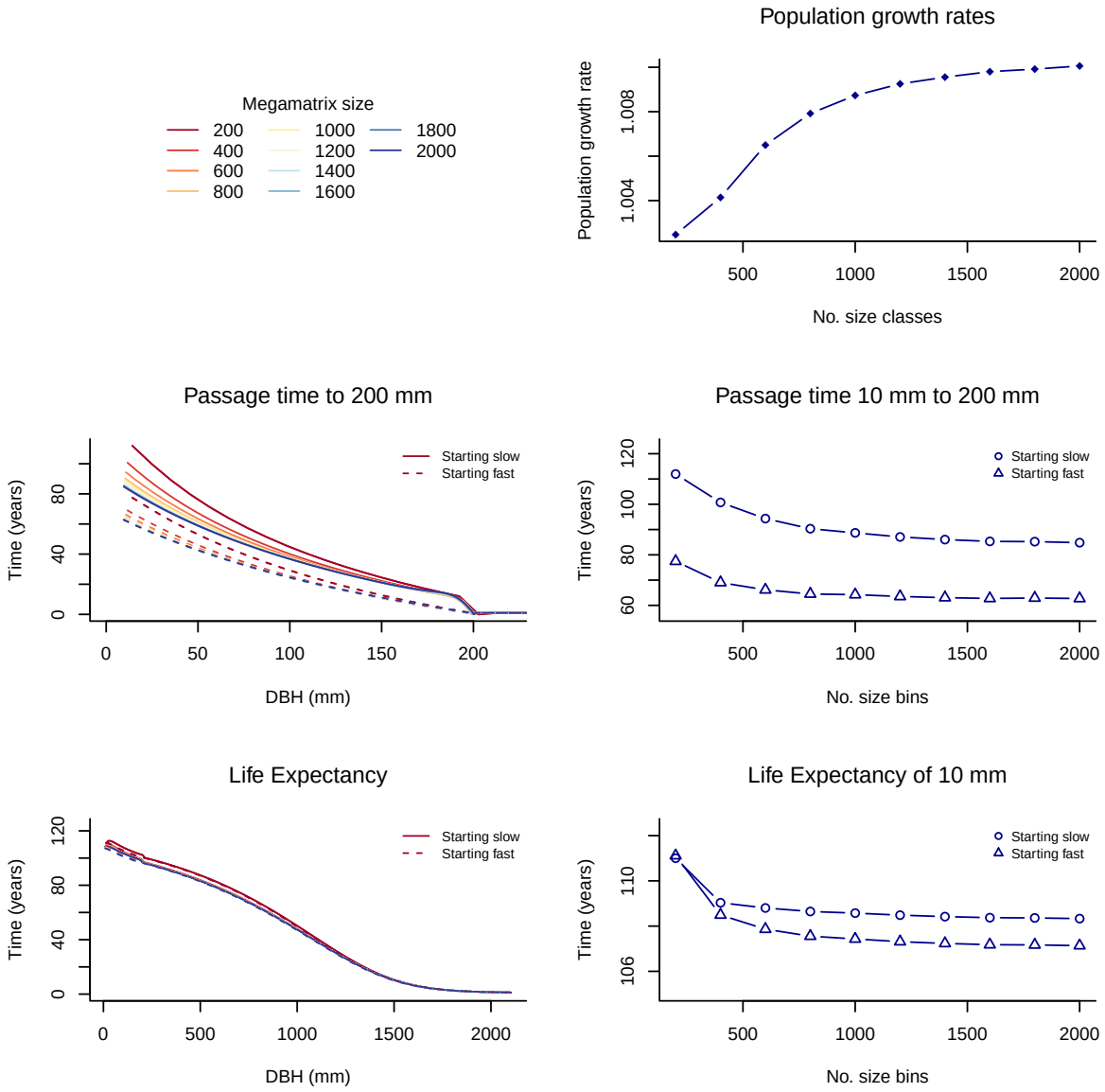


Figure A.6: Sensitivity of *P. copaifera* population growth rates (top right), passage times (middle) and life expectancies (bottom) to different IPM dimensions. Passage times decreased with increasing IPM dimensions resulting in small increases in population growth rate. Increasing the number of size bins above 1000 had little impact on demographic metrics.

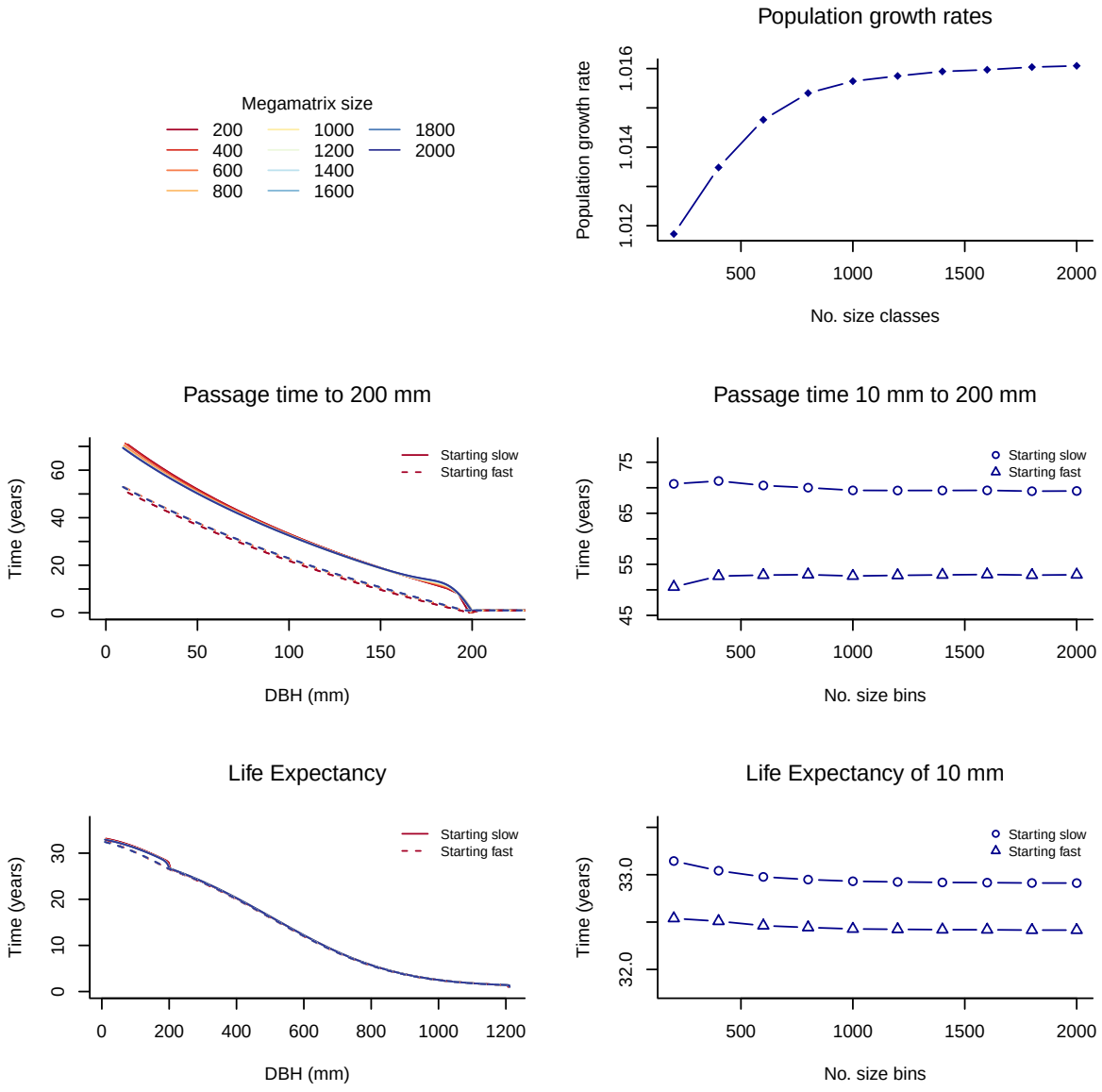


Figure A.7: Sensitivity of *C. longifolium* population growth rates (top right), passage times (middle) and life expectancies (bottom) to different IPM dimensions. Passage times decreased with increasing IPM dimensions resulting in small increases in population growth rate. Longevities were mostly insensitive to IPM dimensions. Increasing the number of size bins above 1000 had little impact on demographic metrics.

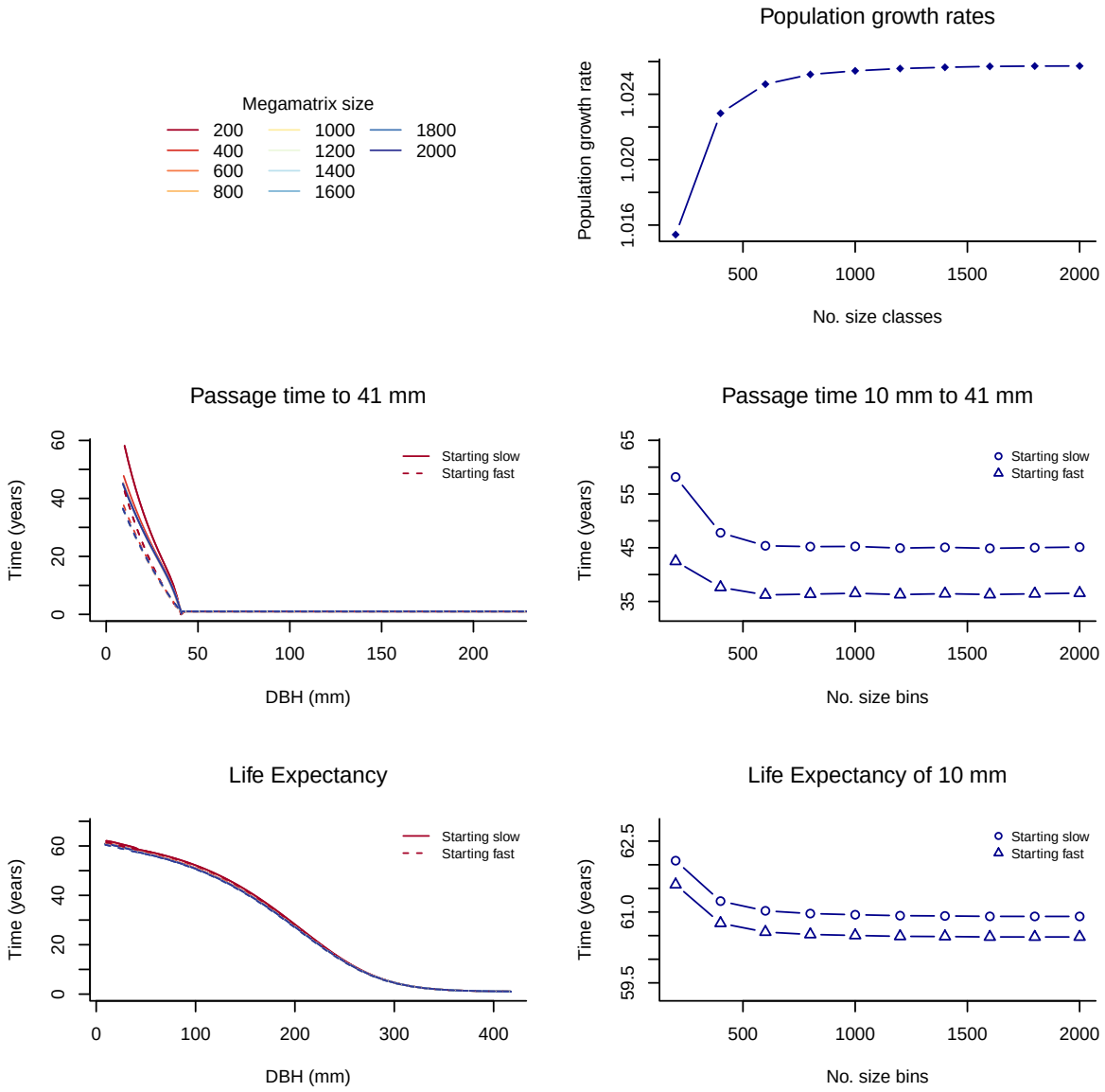


Figure A.8: Sensitivity of *G. intermedia* population growth rates (top right), passage times (middle) and life expectancies (bottom) to different IPM dimensions. Passage times decreased with increasing IPM dimensions resulting in small increases in population growth rate. Longevities were mostly insensitive to IPM dimensions. Increasing the number of size bins above 600 had little impact on demographic metrics.

	Slow small	Fast small	V.fast small	Fast big	V.fast big
Mean	15.20	8.25	2.01	7.88	1.78
Variance	200.95	60.10	4.94	212.45	2.77
Min	1.00	1.00	1.00	1.00	1.00
Max	100.00	44.00	15.00	102.00	13.00

Table A.2: Distribution of number of consecutive years spent in each growth class from simulations of *C. longifolium* with three growth classes. Small and big refer to individuals below and above the size threshold for automatic inclusion in the fast growth class

	alpha1	beta1	alpha2	beta2	threshold	log likelihood
Prioria copaifera	0.91	1.39	1.49	0.25	200.00	-1311.13
Calophyllum longifolium	1.12	1.40	4.08	0.72	200.00	-1059.51
Garcinia intermedia	1.37	2.87	1.07	0.81	40.90	-2088.93

Table A.3: Parameter values for the two distribution growth model and the log likelihood of the data given these parameters. Alpha and beta refer to the shape and rate parameters for gamma distributions. Threshold is the size threshold for automatic inclusion in the fast growth distribution

	alpha1	beta1	alpha2	beta2	alpha3	beta3	threshold	log likelihood
Prioria copaifera	0.91	1.39	1.68	0.34	59.09	3.87	200.00	-1245.42
Calophyllum longifolium	1.12	1.40	12.21	3.13	9.97	1.10	200.00	-1020.25
Garcinia intermedia	1.37	2.87	1.19	1.10	19.82	4.84	40.90	-1890.38

Table A.4: Parameter values for the three distribution growth model and the log likelihood of the data given these parameters. Alpha and beta refer to the shape and rate parameters for gamma distributions. Threshold is the size threshold for automatic inclusion in the fast growth distribution

	K1	p1	r1	K2	p2	r2	threshold
Prioria copaifera	0.99	-84.39	0.07	0.99	1888.26	-0.01	200.00
Calophyllum longifolium	0.97	-114.23	0.15	0.97	1081.54	-0.01	200.00
Garcinia intermedia	0.98	-30.61	0.20	0.98	344.60	-0.03	40.90

Table A.5: Survival parameters. K = upper asymptote, p = inflection point, r = rate. 1 and 2 denote the curves for sizes below and above the survival size threshold respectively. The lower asymptote for both curves was fixed at 0. Threshold is the size threshold at which the two curves meet

	f.param	normalised reproduction (x10^10)	size threshold
Prioria copaifera	0.06	0.19	698.92
Calophyllum longifolium	5.48	0.02	403.87
Garcinia intermedia	3.64	31.52	0.00

Table A.6: Fecundity parameters. f.param refers to the parameter which is multiplied by BA to get per capita reproduction. The normalised fecundity values allow comparison of fecundity among the three species once the size structure and size threshold for reproduction have been accounted for

	Growth 2	Growth 3	IPM 2	IPM 3
Prioria copaifera	13025.36	16476.96	6090.94	7952.92
Calophyllum longifolium	13521.43	20130.74	12184.51	6672.25
Garcinia intermedia	43782.36	33902.14	31836.94	13874.10

Table A.7: AIC values for the two and three distribution growth models and the corresponding IPMs constructed using these growth models

Appendix B

Chapter 2: Matrix calculations

B.1 Notation

Matrices are denoted by bold uppercase letters, e.g. $\mathbf{A}$. The entries of matrices are donated by corresponding lower case letters with subscripts for row and column indices, e.g. a_{ij} is the value in the i^{th} row and j^{th} column of the matrix $\mathbf{A}$. $\mathbf{A}_{[i,.]}$ are the rows of $\mathbf{A}$, and $\mathbf{A}_{[.,j]}$ are the columns of $\mathbf{A}$. Vectors are denoted by bold lowercase letters and indexed with subscripts, e.g. v_i is the i^{th} entry of the vector $\mathbf{v}$. Vec-permutation matrices for describing size-growth structured populations are denoted with a tilde, e.g. $\tilde{\mathbf{A}}$.

Other relevant points:

- $\mathbf{A}^{\mathrm{T}}$ is the transpose of the matrix $\mathbf{A}$.
- $\mathbf{A}^{-1}$ is the inverse of the matrix $\mathbf{A}$.
- $\mathbf{I}_i$ is an identity matrix of dimensions i.
- $\mathbf{A} \otimes \mathbf{B}$ is the Kronecker product of the matrices $\mathbf{A}$ and $\mathbf{B}$.
- $\mathbf{A} \circ \mathbf{B}$ is the Hadamard, or element-by-element, product of the matrices $\mathbf{A}$ and $\mathbf{B}$.
- S is the number of growth classes.
- G is the number of size classes.

B.2 Occupancy times

To find the expected occupancy time of each state (i.e. size and growth class combinations) we first define the fundamental matrix, $\tilde{\mathbf{N}}$, of $\tilde{\mathbf{U}}$.

$$\tilde{\mathbf{N}} = (\mathbf{I}_{SG} - \tilde{\mathbf{U}})^{-1} \tag{B.1}$$

This returns an SG x SG matrix, the entries of which give the expected occupancy time in state i, given starting in state j:

$$\tilde{\mathbf{v}}_{ij} = E(\text{occupancy of state } i | \text{ current state } j) \tag{B.2}$$

It is also possible to find the expected occupancy times in a set of states. If $\mathbf{c}_s$ is an S x 1 vector with 1s indicating the starting size classes of interest and 0s elsewhere then

$$\tilde{\mathbf{N}}(\mathbf{c}_S) = (\mathbf{I}_G \otimes \mathbf{c}_S^{\mathrm{T}})\tilde{\mathbf{N}} \tag{B.3}$$

where $\tilde{\mathbf{N}}(\mathbf{c}_S)$ is a G x SG matrix, in which columns are the starting states, arranged from left to right as sizes within growth classes, and rows correspond to growth classes. Thus, $\tilde{\mathbf{N}}(\mathbf{c}_S)_{ij}$ is the expected occupancy time in G_i summed over the size classes of interest, given starting in size-growth state j.

Likewise, the expected occupancy time in each size for the growth classes of interest is given by

$$\tilde{\mathbf{N}}(\mathbf{c}_G) = (\mathbf{I}_S \otimes \mathbf{c}_G^{\mathrm{T}})\tilde{\mathbf{N}} \tag{B.4}$$

where $\mathbf{c}_G$ is a G x 1 vector indicating growth classes of interest and $\tilde{\mathbf{N}}(\mathbf{c}_G)$ is an S x SG matrix in which $\tilde{\mathbf{N}}(\mathbf{c}_G)_{ij}$ is the expected occupancy time in S_i, summed over the growth classes of interest, given starting in size-growth state j.

Finally, combining the two, we get the expected occupancy time in each size and growth class of interest, $\mathbf{c}_S$ and $\mathbf{c}_G$, for each starting state.

$$\tilde{\mathbf{N}}(\mathbf{c}_S, \mathbf{c}_G) = (\mathbf{c}_G^{\mathrm{T}} \otimes \mathbf{c}_S^{\mathrm{T}})\tilde{\mathbf{N}} \tag{B.5}$$

B.2.1 Mixed distributions

To find the occupancy times for a cohort of individuals that are mixed among sizes and/or growth groups we first define the SG x 1 vector, $\tilde{\mathbf{n}}$ which holds the distribution of states in the population, arranged as sizes within growth groups e.g. for the case of G = 2

$$\tilde{\mathbf{n}}_t = \left(\begin{array}{c} n_{1,1} \\ n_{2,1} \\ \vdots \\ n_{S,1} \\ \hline n_{1,2} \\ n_{2,2} \\ \vdots \\ n_{S,2} \end{array}\right)$$

The occupancy times of this cohort in each state is found by multiplying $\tilde{\mathbf{n}}$ by the fundamental matrix $\tilde{\mathbf{N}}$

$$\tilde{\mathbf{N}}(\tilde{\mathbf{n}}) = \tilde{\mathbf{N}}\tilde{\mathbf{n}} \tag{B.6}$$

B.3 Survivorship

The survivorship of an initial cohort after x years is given by

$$\tilde{\mathbf{l}}(x) = (1_{SG}^{\mathrm{T}}\tilde{\mathbf{U}}^x)^{\mathrm{T}} \tag{B.7}$$

where $\tilde{\mathbf{l}}$ is an SG x 1 vector in which the i^{th} entry is the survivors to age x of a cohort starting in state i.

B.3.1 Mixed distributions

To find survivorship for a cohort with a mixed distribution of starting states we define $\mathbf{n}$, a vector with the size distribution of the cohort (not separated by growth group). The survivorship of all sizes within each growth group after x years is given by:

$$\tilde{\mathbf{l}}(x|\mathbf{n}) = (\mathbf{I}_G \otimes \mathbf{n}_s)^{\mathrm{T}}\tilde{\mathbf{l}} \tag{B.8}$$

B.4 Longevity Statistics

The mean, variance and skew of longevity can be calculated from the fundamental matrix $\tilde{\mathbf{N}}$.

Since $\tilde{\mathbf{N}}$ gives the expected number of visits to each state i, from state j, the column sums of $\tilde{\mathbf{N}}$ give the mean longevity of each starting state j.

$$\tilde{\eta}_1^{\mathrm{T}} = 1_{SG}^{\mathrm{T}}\tilde{\mathbf{N}} \tag{B.9}$$

The second moment of longevity is given by

$$\tilde{\eta}_2^{\mathrm{T}} = \tilde{\eta}_1^{\mathrm{T}}(2\tilde{\mathbf{N}} - I_{SG}) \tag{B.10}$$

which leads to the variance in longevity

$$1_{SG}^{\mathrm{T}}(2\tilde{\mathbf{N}}^2 - \tilde{\mathbf{N}}) - 1_{SG}^{\mathrm{T}}\tilde{\mathbf{N}} \circ 1_{SG}^{\mathrm{T}}\tilde{\mathbf{N}} \tag{B.11}$$

The third moment of longevity, which measures the skewness in the distribution of longevities, is given by

$$\tilde{\eta}_3^{\mathrm{T}} = \tilde{\eta}_1^{\mathrm{T}}(6\tilde{\mathbf{N}}^{\mathbf{2}} - 6\tilde{\mathbf{N}} + I_{SG}) \tag{B.12}$$

Finally, we can compute the full probability distribution of longevities for each state as

$$p(\eta = n|\text{ start in } i) = [1_{SG}^{\mathrm{T}}(I - \mathbf{U})\mathbf{U}^{n-1}]^{\mathrm{T}} \tag{B.13}$$

B.5 Passage Times

To calculate passage times to states of interest, $\Re$, we create a Markov chain in which states of interest are absorbing states, and transition probabilities into those states are conditional on survival to those states. The transition matrix of the conditional Markov chain is given by

$$\tilde{\mathbf{P}} = \left(\begin{array}{c|c} \tilde{\mathbf{U}}' & 0 \\ \hline \tilde{\mathbf{M}}' & 1 \end{array}\right)$$

$\tilde{\mathbf{U}}'$ is equal to $\tilde{\mathbf{U}}$ but with 0s in the rows and columns of $\Re$, since transitions into these states means absorption has already occured.

$\tilde{\mathbf{M}}'$ is a 2 x SG matrix. The first row holds the probabilities of death before reaching the absorbing states of interest, i.e. $1 - \sum \tilde{\mathbf{U}}_{[.,j]}$, for $j \neq \Re$ and 0 for $j = \Re$, since individuals in $\Re$ have already been absorbed. The second row of $\tilde{\mathbf{M}}'$ holds the probability of reaching $\Re$ before death, i.e. $\sum \tilde{\mathbf{U}}_{[\Re,j]}$ for $j \neq \Re$ and 1 for $j = \Re$, since individuals in $\Re$ have already been absorbed.

The conditional fundamental matrix $\tilde{\mathbf{N}}^c$ is given by

$$\tilde{\mathbf{N}}^c = \mathbf{D}^{-1}\tilde{\mathbf{N}}\mathbf{D} \tag{B.14}$$

where, with $\text{diag}(\mathbf{b}_{k.})$ denoting the k^{th} row of $\mathbf{B}$,

$$\mathbf{D} = \text{diag}(\mathbf{b}_{k.}) = \begin{pmatrix} b_{k1} & & \\ & b_{k2} & \\ & & \ddots \end{pmatrix} \tag{B.15}$$

and

$$\mathbf{B} = \mathbf{M}\tilde{\mathbf{N}} \tag{B.16}$$

and

$$\tilde{\mathbf{N}} = (\mathbf{I}_{SG} - \tilde{\mathbf{U}})^{-1} \tag{B.17}$$

$\tilde{\mathbf{N}}^{\mathbf{c}}$ can be analysed like any other fundamental matrix. Thus, the time to abosorbtion in the states of interest (passage times), $\Re$ are given by the column sums of $\tilde{\mathbf{N}}^{\mathbf{c}}$, while the variance and skew of passage times can be calculated from the second and third moments.

B.6 R code

B.6.1 Occupancy times

Occupancy times can be calculated with the `get.occupancy.times` function. This returns the fundamental matrix $\tilde{\mathbf{N}}$, `Ntilde`, which gives the expected occupancy time for each state, conditional on starting state, eq (B.1) and eq (B.2). There is also the option to specify a set of sizes and/or growth classes by setting `size.range` and `G.int` to the size

range and growth classes of interest. The size range should be given as the minimum and maximum DBH measurements of interest, as these will be translated into size classes within the function. Occupancy times for each growth class, summed over the size classes of interest are in the object `o.sizes`, eq (B.3), while occupancy times for each size, summed over the growth classes of interest are returned in the object `o.growth`, eq (B.4). Occupancy times for the specified sizes and growth groups of interest are returned in the object `o.both`, eq (B.5).

```
get.occupancy.times <- function(size.range = c(Y[1], Y[2]),
                                Utilde, S, G, Y,
                                G.int = seq(G)){

  I <- diag(S*G)  # Identity matrix
  Utilde <- as.matrix(Utilde)
  Ntilde <- ginv(I - Utilde)  # Fundamental matrix of Utilde -
  # Ntilde[i,j] is expected occupancy time in state i |
  # starting in state j

  # size bins corresponding to size ranges of interest
  min.c <- which(abs(Y- size.range[1]) ==
                   min(abs(Y- size.range[1])))
  max.c <- which(abs(Y - size.range[length(size.range)])
                 == min(abs(Y - size.range[length(size.range)])))

  # S x 1 vector indicating which sizes classes of interest
  cs <- rep(0, S)
  cs[seq(min.c, max.c, 1)] <- 1

  # o.sizes[i,j] is the sum of occupancy in each size
  # class of interest for growth group i, given starting
  # state j (combination of sizes and growth)
  o.sizes <- kronecker(Diagonal(G), t(cs)) %*% Ntilde  # G x SG

  cg <- rep(0, G)
  cg[G.int] <- 1  # G x 1 vector indicating groups of interest

  # o.growth[i,j] is the sum of occupancy in each growth
```

```
  # class of interest for size
  # class i, given starting state j
  # (combination of sizes and growth)
  o.growth <- kronecker(t(cg), Diagonal(S)) %*% Ntilde

  # occupancy in each size/growth group of interest
  o.both <- kronecker(t(cg), t(cs)) %*% Ntilde

  return(list(Ntilde = Ntilde, o.sizes = o.sizes,
              o.growth = o.growth,
              o.both = o.both))
}
```

The function `get.occupancy.mixed` calculates the occupancy times for each state for a cohort with mixed starting states.

```
get.occupancy.mixed <- function(size.vec, S, b, Utilde, quant){

  n.vec <- get.observed.size.dist(size.vec, S, b)
  # separate into growth classes
  n.vec <- c(n.vec*quant, n.vec*(1 - quant))
  n.vec <- n.vec/sum(n.vec)  # normalise
  I <- diag(S*G)  # Identity matrix
  Utilde <- as.matrix(Utilde)
  Ntilde <- ginv(I - Utilde)  # Fundamental matrix of Utilde
  o.mix <- Ntilde %*% n.vec  # occupancy in each state
  return(o.mix)
}

# Find the population size distribution, given a vector of
# observed sizes
get.observed.size.dist <- function(size.vec, S, b){
  complete.size <- size.vec[!is.na(size.vec)]
  tmp <- cut(complete.size, breaks = c(0,b, Inf),
             labels = FALSE,
             include.lowest = TRUE)
  S.y <- rep(0, S)  # observed size distribution
```

```
  S.y[as.numeric(names(table(tmp)))] <- as.numeric(table(tmp))
  return(S.y)
}
```

This calls the function `get.observed.size.dist` which transforms a vector of observed sizes, `size.vec` into $\tilde{\mathbf{n}}$ of length SxG, which holds the distribution of sizes within growth classes. The occupancy times of this mixed state cohort is calculated as the fundamental matrix multiplied by $\tilde{\mathbf{n}}$, eq (B.6).

B.6.2 Survivorship

The survivorship of a cohort after x years is found with the function `get.survivorship`. The returns a vector of length SxG in which the i^{th} value is the survivors to age x, starting in state i at time 0.

```
get.survivorship <- function(x, S, G, Utilde){

  Utilde <- as.matrix(Utilde)
  l.tilde <- t(t(rep(1, (S*G))) %*% as.matrix(Utilde%^%x,
                                              (S*G), (S*G)))
  # ith entry is survivors to age x of a cohort in state
  # i at time 0.
  return(l.tilde)

}
```

To get the survivorship of a mixed cohort, use the `get.mixed.survivorship` function. This calls `get.observed.size.dist` to transform `size.vec`, a vector of observed sizes, into a vector of length S giving the size distribution of the population. The Kronecker product of this vector, multiplied by a survivorship vector, `l.tilde`, is the survivorship of the mixed cohort, after x years.

```
get.mixed.survivorship <- function(x, size.vec, S, G, b,
                                   quant, Utilde){

  Utilde <- as.matrix(Utilde)
  # survivorship of cohort from state j after x years
```

```
  l.tilde <- t(t(rep(1, (S*G))) %*% as.matrix(Utilde%^%x,
                                              (S*G), (S*G)))

  n.vec <- get.observed.size.dist(size.vec, S, b)  # size distribution
  n.vec <- n.vec/sum(n.vec)
  # survivorship of mixed cohort after x years, by growth class
  mixed.surv <- t(kronecker(diag(G), n.vec)) %*% l.tilde[,1]

  return(mixed.surv)

}
```

B.6.3 Longevity Statistics

Longevity statistics can be calculated with the function `get.longevity`. This returns the mean, `mu`, variance `var`, and third moment, `m3` of longevity. From the third moment we can calculate the skewness in the distribution of longevities. See equations (B.9) to (B.12).

```
get.longevity <- function(S, G, Utilde){
  I <- diag(S*G)  # Identity matrix dimensions of Utilde
  Utilde <- as.matrix(Utilde)
  Ntilde <- ginv(I - Utilde)  # Fundamental matrix of Utilde
  # moments
  m1 <- t(rep(1, S*G)) %*% Ntilde
  m2 <- m1 %*% (2*Ntilde - diag(S*G))
  m3 <- m1 %*% (6*(Ntilde%*%Ntilde) - 6*Ntilde + diag(S*G))
  # variance
  var <- colSums(2 * Ntilde %*% Ntilde - Ntilde) -
    colSums(Ntilde) * colSums(Ntilde)

  return(list(mu = m1, var = var, m3 = m3))
}
```

The function `get.longevity.prob.dist` returns the whole probability distribution of longevities for cohorts starting in each state. Each row of the matrix `p.eta` is the probability distribution of longevities given a starting state.

```
get.longevity.prob.dist <- function(ns, S, G, Utilde){
  Utilde <- as.matrix(Utilde)
  p.eta <- sapply(ns, function(x)
    t(colSums(diag(S*G) - Utilde) %*% (Utilde %^% (x-1))))
  return(p.eta)
}
```

B.6.4 Passage Times

The function `get.passage.time` returns the passage times to a specified set of states, conditional on starting state and survival to the specified states of interest. The parameters `size.range` and `G.int` are set to the sizes (DBH in mm) and growth classes of interest. The function returns the mean, `mu`, and variance, `var`, of passage times from each state to the states of interest.

```
get.passage.time <- function(size.range, Y, G.int, Utilde){

  # Define the set of states - move from actual sizes
  # to corresponding size bins
  min.c <- which(abs(Y- size.range[1]) ==
                   min(abs(Y- size.range[1])))
  max.c <- which(abs(Y - size.range[length(size.range)]) ==
                   min(abs(Y -
                             size.range[length(size.range)])))

  # vector of states of interest
  R <- c()
  for(g in 1:length(G.int)){
    R <- c(R, seq(min.c, max.c, 1) + S*(g-1))
  }

  Mtilde <- 1 - colSums(Utilde)  # probability of death
  Mtilde[R] <- 0  # already in the absorbing state

  Uprime <- Utilde
  # those in the states of interest are in the absorbing state
```

```
  Uprime[ ,R] <- 0
  Uprime[R, ] <- 0

  Mprime <- Mtilde
  Mprime <- rbind(Mprime, colSums(Utilde[R, ]))
  Mprime[2, R] <- 1

  Uprime <- as.matrix(Uprime)
  Ntilde.prime <- ginv(diag(G*S) - Uprime)
  Bprime <- Mprime %*% Ntilde.prime

  ### CONDITIONAL MARKOV CHAIN
  Utilde.c <- diag(Bprime[2,]) %*% Uprime %*%
    ginv(diag(Bprime[2,]))

  eta1 <- ginv(diag(G*S) - Utilde.c)

  var <- colSums(2 * (eta1 %*% eta1) - eta1) -
    colSums(eta1) * colSums(eta1)

  m1 <- colSums(eta1)
  m1[R] <- 0

  return(list(mu = m1, var = var))
}
```

Appendix C

Chapter 2: Worked example

C.1 Introduction

In this appendix we run through the entire workflow with *Prioria copaifera* as an example species. We demonstrate how to:

- Correct measurement errors in the data
- Fit growth and survival models
- Estimate recruit size
- Construct size-by-growth IPMs
- Inverse model fecundity
- Analyse population dynamics from the IPMs e.g. calculate longevities etc.

Many of the treeIPM functions called in the code below are not described in detail but are provided at the bottom of this appendix. These scripts have been written as if the user has a `treeIPM` directory containing a `Source` folder for R scripts, a `Data` folder for data, and `Outputs` and `Figures` folders for outputs generated by the code. Scripts run as if the working directory is set to the `treeIPM` directory.

In all the scripts below involving random number generation, we set the seed to make our results reproducible.

C.2 Data - loading and cleaning

In this section we load data and correct measurement errors to ensure that DBH increments are positive between all censuses (i.e. trees are not allowed to shrink). The complete R script is `A_data_processing.R`.

We downloaded censuses from 1995, 2000, 2005 and 2010 from the CTFS website. From each census we pulled out data for the three species of interest and stacked them into species specific dataframes (i.e. individuals had multiple rows, corresponding to the multiple censuses). The dataframe for *P. copaifera* is loaded below and is used for demonstrating the workflow. It is saved in a file called `raw_pri2co.Rdata` (but users need to make this file themselves by downloading data from CTFS). Other than combining data from multiple censuses, the data is in the standard CTFS format with respect to column names and codes etc.

We begin by loading libraries, functions and data and removing trees with NAs in all censuses.

C.2.1 Formatting

```
rm(list = ls())
### LIBRARIES ###
library(plyr)
library(foreach)
library(doParallel)
library(SpatialTools)

# Set working directory to the treeIPM folder
#setwd('SET YOUR PATH HERE/treeIPM')

### FUNCTIONS ###
source('Source/Data_processing_functions.R')

# number of cores to use for parallel processing
nproc <- detectCores()-2
registerDoParallel(nproc)

### DATA ###
```

```
sp.name <- 'pri2co'  # choose a species
# load unformatted data
load(sprintf('Data/raw_%s.RData', sp.name))
data.mat <- raw.pri2co
# Remove rows for trees present in earlier censuses
# but dead in censuses loaded here
data.mat <- data.mat[which(!is.na(data.mat$CensusID)), ]
```

Ultimately we want a matrix in which each row is an individual stem, with sizes and survival through time as columns. We therefore split the dataframe up by census and, by matching unique stem tags, create lists in which each element is a vector, holding the variable of interest for each stem in a given census. These can be combined with `cbind` to make the new matrix.

```
# Split the dataframe up so each census is
# a separate element in a list
data.cens <- split(data.mat, data.mat$CensusID)
# unique stems
tags <- unique(data.mat$tag)
```

First, we extract the size (DBH) of each stem in each census, putting an NA if the stem is dead or has not yet recruited. From the list of sizes we can assign each stem a survival value, 0 for dead, 1 for alive and NA if not yet recruited.

```
# Size at each census
sizes <- vector('list', length(data.cens))
for(ii in 1:length(data.cens)){
  sizes[[ii]] <- data.cens[[ii]]$dbh[match(tags,
                                           data.cens[[ii]]$tag)]
}

# Survival between census intervals for each stem
survs <- vector("list", length(data.cens) - 1)
for(ii in 1:length(survs)){
  surv <- rep(NA, length(tags))
  # gets a 1 if present and alive in both years
  surv <- ifelse(!is.na(sizes[[(ii + 1)]]) &
```

```
                    !is.na(sizes[[ii]]), 1, NA)
  # alive in the first and dead in the second - gets a 0
  surv <- ifelse(!is.na(sizes[[ii]]) &
                    is.na(sizes[[ii + 1]]), 0, surv)
  survs[[ii]] <- surv
}
```

Growth increments are the differences between sizes.

```
# Increments between censuses
incrs <- t(apply(do.call(cbind, sizes),
                 1, diff))
```

We need the date at which each stem was measured in order to calculate annual increments and probabilities of survival. We extract dates by matching unique stem tags. From dates we get the time between measurements in years.

```
# Dates
dates <- vector('list', length(data.cens))
for(ii in 1:length(data.cens)){
  tmp <- data.cens[[ii]]$ExactDate[match(tags,
                                         data.cens[[ii]]$tag)]
  dates[[ii]] <- as.Date(tmp, format = '%Y-%m-%d')
}

# Time in years between censuses (date t+1 - date t)
times <- vector("list", length(data.cens) - 1)
for(ii in 1:length(times)){
  # ignore leap years
  times[[ii]] <- (dates[[ii+1]] - dates[[ii]])/365
}
```

Provided the plot is a single rectangle, the code below will divide it into 20 m by 20 m subplots and assign subplot numbers. It can be useful to have this standardised for spatial analysis.

```
#  Coordinates and quadrats - x and y for each unique stem
if(length(which(is.na(data.mat$gx))) > 0){
  data.mat <- data.mat[-(which(is.na(data.mat$gx))), ]
}
x <- data.mat$gx[match(tags, data.mat$tag)]
y <- data.mat$gy[match(tags, data.mat$tag)]

max.x <- signif(max(x, na.rm = TRUE), 1)  # max x coordinate
max.y <- signif(max(y, na.rm = TRUE), 1)  # max y coordinate
no.sub.plot.x <- max.x/20  # subplots are 20 m x 20 m
no.sub.plot.y <- max.y/20

# Subplots
subplot <- rep(NA, length(tags))
counter <- 1
for(j in 1:no.sub.plot.y){
  for(i in 1:no.sub.plot.x){
    tmp <- which((x >= i*20-20) & (x < i*20) &
                   (y >= j*20 - 20) & (y < j*20))
    subplot[tmp] <- counter
    counter <- counter+1
  }
}

quad <- subplot
```

Binding together size, survival, DBH increments and spatial variables gives the new matrix in which each row is a unique stem.

NB: with all data types numeric, we can work with a matrix which is much faster than a dataframe with mixed data types.

```
data.mat <- cbind(as.numeric(tags), quad, x, y,
                  do.call(cbind, sizes), do.call(cbind, survs),
                  do.call(cbind, times), incrs)

# remove stems outside of the plotting area
if(length(which(is.na(subplot))) > 0){
```

```
  data.mat <- data.mat[-which(is.na(subplot)), ]
}

# column names
size.names <- mapply(paste, 'size',
                     seq(length(data.cens)), sep = '.')
surv.names <- mapply(paste, 'surv',
                     seq(length(data.cens) - 1), sep = '.')
time.names <- mapply(paste, 'time',
                     seq(length(data.cens) -1), sep = '.')
incr.names <- mapply(paste, 'incr',
                     seq(length(data.cens) - 1), sep = '.')
colnames(data.mat) <- c('tag', 'quad', 'x', 'y', size.names,
                        surv.names, time.names, incr.names)
```

C.2.2 Correcting measurement errors

The code below finds very obvious anomalies in the DBH data and corrects them by making them the mean of adjacent DBHs. If the first or last measurement are obviously wrong, the code uses the second or penultimate increments to adjust DBHs. See the Data_processing_functions.R script for details. In brief, errors are those trees that shrank more than 25% of their original size or grew $>$ 75 mm in a year, (Rüger *et al.*, 2011). In addition trees in which the maximum increment is $>$ an order of magnitude greater than the second largest increment are also flagged as errors (but only if the largest increment $>$ than 60 mm because small trees could grow e.g. 2 mm one year and 20 mm the next).

```
# - only acts on stems with >2 measurements
# finding errors and correcting them
if(length(grep('size', colnames(data.mat))) > 2){
  errors <- which(apply(data.mat, 1, find.errors) == TRUE)
  if(length(errors) > 1){
    data.mat[errors, ] <- t(apply(data.mat[errors, ], 1,
                                  correct.errors))
  }else{
    if(length(errors) == 1){
      data.mat[errors, ] <- t(correct.errors(data.mat[errors,]))
```

```
    }
  }

  # get new increments
  sizes <- data.mat[ ,grep('size', colnames(data.mat))]
  incrs.ll <- t(apply(sizes, 1, diff))
  data.mat[ ,grep('incr', colnames(data.mat))] <- incrs.ll
}
```

Stems dead in all censuses are removed.

```
#  Remove stems dead in all censuses
bb <- data.mat[ ,grep('size', colnames(data.mat))]
data.mat <- data.mat[which(apply(bb, 1,
                                 function(x)
                                   all(is.na(x)))
                           == FALSE), ]
```

The next part of the code calls the `correct.DBH` function which samples each DBH measurement until increments across all censuses are positive. It samples for `give.up` attempts. If a stem still has one or more negative increments but also multiple positive increments, the negative incrments are made the mean of the positive increments. For stems with negative increments and less than two positive increments, an increment is sampled from the positive increments of all stems. DBHs are adjusted to take into account the new positive increments.

This code is made parallel to speed up sampling. The default is to use one less than the number of available cores, however, this can be changed by adjusting the value of `nproc`.

```
# - propose new sizes so that size monotonically increases
reps <- 1  # keep this at one
give.up <- 20000  #  attempts at getting positive increments

dbhs <- data.mat[ ,grep('size',
                        colnames(data.mat))]  # matrix of sizes
times <- data.mat[ ,grep('time',
                         colnames(data.mat))]  # matrix of times
# split dbhs and times into chuncks for parallel processing
```

```
chunk.size <- dim(dbhs)[1]/nproc
d <- seq(dim(dbhs)[1])
e <- split(d, ceiling(seq_along(d)/chunk.size))
dbh.list <- lapply(e, function(x, y) y[x, ], y = dbhs)
times.list <- lapply(e, function(x, y) y[x, ], y = times)

# to get the same results as reported here set the seed
set.seed(1)

out <- foreach(proc = 1:nproc)%dopar% {
  # growth correction code
  resampled.dbhs <-
    replicate(reps,
              correct.dbh(dbh.list[[proc]],
                          times = times.list[[proc]],
                          give.up = give.up))

  sampled <- unlist(resampled.dbhs[2,])
  dd <- resampled.dbhs[1, ]
  ee <- array(unlist(dd),
              dim = c(nrow(dd[[1]]), ncol(dd[[1]]), length(dd)))
  ff <- aperm(ee)

  # adjust the increments to match the new sizes
  med.corrections <- t(apply(ff, 3,
                             function(x) apply(x, 2, median)))

  return(list(med.correct = med.corrections,
              still.neg = sampled))
}
```

The number of trees which still had negative increments after `give.up` iterations, and therefore had increments sampled from other stems, is given by `sampled`. The new DBH measurements are put in the species matrix and increments are updated. Finally we save the output.

```
# number of trees that the algorithm failed on - these trees
# had increments sampled from positive increments of other trees
sampled <- sum(unlist(lapply(out, '[[', 2)))
print(sprintf('total sampled: %d', sampled))

# corrected sizes
med.corrections <- do.call(rbind, lapply(out, '[[', 1))

# replace the sizes with these corrected ones
data.mat[ ,grep('size', colnames(data.mat))] <- med.corrections
# make sure they are all still monotonically increasing
incrs.lll <- t(apply(med.corrections, 1, diff))

# replace the increment columns with the new positive increments
data.mat[ ,grep('incr', colnames(data.mat))] <- incrs.lll

# save the output
save(data.mat, file = sprintf('Data/%s.RData', sp.name))
```

C.3 Vital rates

In this section we fit growth and survival models to the cleaned up *P. copaifera* data using STAN. These scripts are `B_growth_stan.R` and `C_survival_stan.R`.

C.3.1 Growth

Here we only fit the two growth distribution model.

We begin by loading libraries, functions and data.

```
rm(list = ls())
### LIBRARIES ###
library(rstan)
library(shinystan)
library(RColorBrewer)
```

```
set.seed(1)
### SOURCE THE FUNCTIONS ###
source("Source/growth_functions_stan.R")
cols <- brewer.pal(3, 'Dark2')
cols.hist <- make.ramp(cols, levels = 3, transp = 70)

sp.name <- 'pri2co'
load(file = sprintf("Data/%s.RData", sp.name))
```

Next, we define how many growth distributions to fit and find the size threshold for automatic inclusion in the fast growth distribution. This is 200 mm DBH for canopy species and the 0.8^{th} quantile of size for understory species. We will fit growth models to each census interval and so `g.params` is defined to hold parameter values, log likelihoods and uncertainty for each census interval.

```
G <- 2  # number of growth distributions
sizes <- data.mat[ ,grep('size', colnames(data.mat))]
g.thresh <- ifelse(max(sizes, na.rm = TRUE) > 500, 200,
                   quantile(sizes, 0.8, na.rm = TRUE))

n.censuses <- length(grep('size', colnames(data.mat)))
n.intervals <- n.censuses -1

g.params <- vector('list', 3)
# for parameter values
g.params[[1]] <- matrix(NA, nrow = n.intervals, ncol = 5)
# for loglikelihoods
g.params[[2]] <- rep(NA, n.intervals)
# for MCMC chains
g.params[[3]] <- vector('list', n.intervals)
```

For each census interval we get vectors of size, increments and time and make the increments annual.

```
for(census in 1:n.intervals){
  size <- data.mat[ ,grep('size', colnames(data.mat))[(census)]]
  incr <- data.mat[ ,grep('incr', colnames(data.mat))[(census)]]
```

```
  time <- data.mat[ ,grep('time', colnames(data.mat))[(census)]]
  # remove trees dead in either of the focal census years
  dead <- which(is.na(incr) | is.na(time))
  size <- size[-dead]
  incr <- incr[-dead]
  time <- time[-dead]
  hist(incr, breaks = 200)
  summary(incr)

  # MAKE INCREMENT ANNUAL #
  incr <- incr/time
```

We then divide the population up into growth distributions according to the rules defining the size threshold for fast growth and the quantile of small individuals that contribute to the fast growth distribution. Here we are fitting the two growth distribution model. `dists` defines the distribution to fit. We found gamma distributions to be a good fit to increment data.

```
#######################################################################
### MCMC ###
# quantile of small individuals in the fast growth distribution
quant <- 0.95

dists <- rep('gamma', G)

# INCREMENT GROUPS
# Small trees - slow and fast
small.incr <- incr[which(size < g.thresh)]
quant.incr <- quantile(small.incr, quant[1],
                       na.rm = TRUE)
# divide the data into increment groups based on these
# increment thresholds
small.incr.groups <- cut(small.incr,
                         breaks = c(0, quant.incr, 500),
                         labels = FALSE)

incr.groups <- rep(NA, length(incr))
```

```
incr.groups[which(size < g.thresh)] <- small.incr.groups
# trees over size threshold get fast automatically
incr.groups[which(size >= g.thresh)] <- 2

# check the data
hist(incr[which(incr.groups == 1)], breaks = 50,
     xlim = c(min(incr), max(incr)), col = cols.hist[1])
hist(incr[incr.groups == 2], add = T, col = 'blue', breaks = 50)
hist(small.incr[which(small.incr.groups == 2)], add = T,
     col = cols.hist[2], breaks = 50 )
```

Data is put into a list object and then the STAN file is loaded and run.

```
# put the data into a list object
incr.data <- list(N = length(incr),
                  incr = incr,
                  groups = incr.groups)

# compile the model - choose appropriate stan script for
# the no. distributions
# this may take about 40-60 secs

growth.model <- stan(file = 'Source/gamma_growth.stan',
                     data = incr.data, chains = 0,
                     verbose = TRUE)

# parameter sampling
growth.fit <- stan(fit = growth.model, data = incr.data,
                   verbose = TRUE,
                   iter = 3000, chains = 2,
                   control = list(adapt_delta = 0.97,
                                  max_treedepth = 15))
```

Results from the MCMC can be plotted or `shinystan` can be launched which opens a website with very good diagnostic tools.

```
# check the MCMC results
summary(growth.fit)

#pdf(sprintf('Figures/%s_G%d_pairs.pdf',
# sp.name, G))
#pairs(growth.fit)
#dev.off()

#launch_shinystan(growth.fit)
```

We extract parameter values, the loglikelihood of the model given the data and the thinned chains from the MCMC. When all censuses have run we save the output.

```
# extract the parameters
growth.mcmc <- unlist(lapply(extract(growth.fit,
                                     permuted = TRUE),
                             median))
n.p <- length(growth.mcmc)
ps1 <- growth.mcmc[1:(n.p/2)]
ps2 <- growth.mcmc[(n.p/2 +1):n.p]

g.params[[1]][census, 1:G] <- ps1
g.params[[1]][census, (G+1):(G*2)] <- ps2
g.params[[1]][census, ncol(g.params[[1]])] <- g.thresh

chains <- do.call(cbind, extract(growth.fit))
thin <- round(seq(1, dim(chains)[1],
                  length.out = 100))
chains.t <- chains[thin, ]

g.params[[3]][[census]] <- chains.t


log.like <- get.gr.like.stan(incr, ps1, ps2, quant,
                             dists,
                             G, g.thresh, size)
```

```
g.params[[2]][census] <- log.like

}
save(g.params,
   file = sprintf('Output/gparams_G%d_%s.RData',
                  G, sp.name))
```

C.3.2 Survival

To fit the survival model begin by loading libraries, functions and data.

```
rm(list = ls())
### LIBRARIES ###
library(MASS)
library(rstan)
library(shinystan)

### SOURCE THE FUNCTIONS ###
source("Source/survival_functions_stan.R")

sp.name <- 'pri2co'
load(file = sprintf("Data/%s.RData", sp.name))
```

Define the size threshold - we use the same threshold as for the growth model.

```
sizes <- data.mat[ ,grep('size', colnames(data.mat))]
thresh <- ifelse(max(sizes, na.rm = TRUE) > 500, 200,
                 quantile(sizes, 0.8, na.rm = TRUE))
```

Prepare structures to hold outputs.

```
# make vectors of the most recent sizes and
# increments and time between them
n.censuses <- length(grep('size',
                          colnames(data.mat)))
n.intervals <- n.censuses -1
```

```
s.params <- vector('list', 3)
s.params[[1]] <- matrix(NA,
                        nrow = n.intervals, ncol = 7)
s.params[[2]] <- rep(NA, n.intervals)
s.params[[3]] <- vector('list', n.intervals)
```

For each census interval get vectors of size, survival and time. Put them into a list object, load the STAN file and allow it to run.

```
for(census in 1:n.intervals){

  size <- data.mat[ ,grep('size', colnames(data.mat))[census]]
  surv <- data.mat[ ,grep('surv', colnames(data.mat))[census]]
  time <- data.mat[ ,grep('time', colnames(data.mat))[census]]

  keep <- which(!is.na(size) & !is.na(time))
  size <- size[keep]
  surv <- surv[keep]
  time <- time[keep]

  # check the data
  hist(size[surv == 1], breaks = 50)
  hist(size[surv == 0], breaks = 50, add = T, col = 'red')

  # make the data list to run stan model
  surv.data <- list(N = length(size),
                    dbh = size,
                    surv = surv,
                    time = time,
                    thresh = thresh,
                    lowip1 = -1 * thresh,
                    upip2 = 1.4*max(size, na.rm = T),
                    lowr2 = ifelse(max(size) >= 600, -0.0075,
                                   -0.05),
                    upperr2 = ifelse(max(size) >= 600,
                                     -0.00075, -0.005))
```

```
  # compile the model (it may take 40-60 secs)
  surv.model <- stan(file = 'Source/surv.stan',
                     data = surv.data, chains = 0)

  # run the MCMC
  surv.fit <- stan(fit = surv.model,
                   data = surv.data, iter = 3000,
                   chains = 2,
                   control = list(adapt_delta = 0.97,
                                  max_treedepth = 15))
```

We can look at the MCMC outputs using **shinystan**. If the diagnostics are good we save the outputs.

```
# check the posterior distribution
summary(surv.fit)

#launch_shinystan(surv.fit)

# extract the sampling parameters
surv.mcmc <- lapply(extract(surv.fit), median)

chains <- do.call(cbind, extract(surv.fit))
thin <- round(seq(1, dim(chains)[1], length.out = 100))
surv.chains.t <- chains[thin, ]

s.params[[3]][[census]] <- surv.chains.t

surv.mcmc <- lapply(extract(surv.fit), median)

s.params[[1]][census, 1:3] <- unlist(surv.mcmc)[c(1,2,3)]
s.params[[1]][census, 4:6] <- unlist(surv.mcmc)[c(1,4,5)]
s.params[[1]][census, 7] <- thresh

small.surv <- s.params[[1]][census, 1:3]
big.surv <- s.params[[1]][census, 4:6]
```

```
# likelihoods
log.like.surv <- get.like.s(small.surv, big.surv,
                            thresh, size, surv, time)

s.params[[2]][census] <- log.like.surv

}
save(s.params,
   file = sprintf('Output/sparams_%s.RData', sp.name))
```

C.4 Transitions between growth classes

The full script for this section is `D_transition_matrices.R`.

To construct IPMs in which individuals move between size and growth classes we need estimates of transition probabilities between growth classes.

Individuals above a given size threshold are assumed to be in the faster growth classes and therefore their transition matric, **C2**, has zeros for transitioning into slow growth classes and 1s for remaining in fast growth classes.

For small individuals we assume that the probability of moving into the fast growth class increases with size. For each size class from the smallest, up to the size threshold for automatic fast growth, there is a G x G matrix with the transitions between growth classes. Transitions from slow to fast range from 0.02 to 0.1, from the smallest size class to the size threshold, with the corresponding probability of remaining in slow being one minus these values. Transitions from fast to slow range from 0.14 to 0.01, and again, corresponding probabilities of remaining in the fast growth class are one minus these values.

We have to make additional assumptions about transitions into and out of the very fast growth distribution when there is a third distribution.

```
rm(list = ls())

### LIBRARIES
library(MASS)
library(Matrix)
```

```
# load the data from all censuses
sp.name <- 'pri2co'
load(file = sprintf("Data/%s.RData", sp.name))

# size vector
no.censuses <- length(grep('size', colnames(data.mat)))
size <- data.mat[ ,grep('size',
                        colnames(data.mat))[(no.censuses-1)]]
sizes <- data.mat[ ,grep('size', colnames(data.mat))]
# Set up
S <- 1500  # number of size classes
min.size <- 9  # size that trees enter census
max.size <- max(size, na.rm = TRUE) * 1.5  # above size range

# matrix variables
# boundary points of mesh cells
b <-  min.size + c(0:S)*(max.size

 - min.size)/S
Y <- 0.5* (b[1:S] + b[2:(S+1)])  # mid points of mesh cells
h <- Y[2]-Y[1]  # cell widths

growth.thresh <- ifelse(max(sizes, na.rm = TRUE) > 500,
                        200,
                        quantile(sizes, 0.8, na.rm = TRUE))
### TRANSITIONS ###
G <- 2
g.thresh <- which(abs(Y - growth.thresh) ==
                    min(abs(Y - growth.thresh)))
SS <- seq(0.98, 0.9, length.out = g.thresh)
SF <- 1 - SS
FS <- seq(0.14, 0.01, length.out = length(SS))
FF <- 1 - FS

tmat <- cbind(SS, SF, FS, FF)
C1s <- lapply(split(tmat, row(tmat)),
```

```
              function(x) matrix(x, 2, 2))

M1 <- bdiag(C1s)
I2 <- Diagonal(S - g.thresh)
C2 <- matrix(c(0,1,0,1), 2, 2)
M2 <- kronecker(I2, C2)
Mblock <- bdiag(M1, M2)

save(Mblock, file = sprintf('Output/%s_Mblock_%d.RData',
                            sp.name, G))
```

C.5 Recruit size and growth classes

The R script for this section is `E_offspring_sizes.R`.

In order to construct IPMs describing the full lifecycle of a species, we need to estimate the size distribution of new recruits and their distribution between growth classes.

The size distribution is fairly straightforward. In this workflow we are not modelling seed or seedling stages, rather, new individuals enter the model at the size in which they would be included in the census (i.e. above 10 mm DBH). Therefore, we combine the new recruits from each cenus and then find the probability distribution of offspring being in each size class using the function `get.observed.size.dist`.

```
### OFFSPRING SIZES ###
rm(list = ls())

### LIBRARIES
library(MASS)
library(Matrix)

### FUNCTIONS
get.observed.size.dist <- function(size.vec, S, b){
  complete.size <- size.vec[!is.na(size.vec)]
  tmp <- cut(complete.size, breaks = c(0,b, Inf),
             labels = FALSE, include.lowest = TRUE)
  S.y <- rep(0, S)  # the size distribution
```

```
  S.y[as.numeric(names(table(tmp)))] <-
    as.numeric(table(tmp))
  return(S.y)
}

### DATA
sp.name <- 'pri2co'
load(sprintf("Data/%s.RData", sp.name))

# size vector
no.censuses <- length(grep('size', colnames(data.mat)))
sizes <- data.mat[ ,grep('size', colnames(data.mat))]

# pull out the recruits
r1 <- sizes[which(!is.na(sizes[,2]) & is.na(sizes[,1])), ]
r2 <- sizes[which(!is.na(sizes[,3]) & is.na(sizes[,2])), ]
r3 <- sizes[which(!is.na(sizes[,4]) & is.na(sizes[,3])), ]

# remove any that are over 100 mm -
# these are likely to be stems that were
# missed in earlier censuses.
r1 <- r1[which(r1[,2] < 100), ]
r2 <- r2[which(r2[,3] < 100), ]
r3 <- r3[which(r3[,4] < 100), ]

# now find increment of recruits
r.incr1 <- r1[ ,3] - r1[,2]
r.incr2 <- r2[ ,4] - r2[ ,3]

# combine offspring sizes
rs <-c(r1[,2], r2[,3], r3[,4])

# find the offspring size distribution
min.size <- 9
max.size <- max(sizes, na.rm = TRUE)*1.5
S <- 1500  # number of size bins
# boundary points of mesh cells
```

```
b <-  min.size + c(0:S)*(max.size - min.size)/S
offspring.sizes <- get.observed.size.dist(rs, S, b)
offspring.sizes <- offspring.sizes/sum(offspring.sizes)
```

We also need a matrix with the probabilities of adults from each growth class producing offspring in each growth class. Since it is rare to be able to attribute individual seedlings to adult trees, we assume that distribution of recruits into each growth class is independent of parent growth class. As for the proportion of recruits in each growth class, we assume that 95% are in the slow distribution, and either 5% in the fast or 4% and 1% in fast and very fast if the number of growth distributions is three.

```
### GROWTH CLASSES
G <- 2
C3 <- matrix(rep(c(0.95, 0.05), 2), 2, 2)
save(offspring.sizes, C3,
     file = sprintf('Output/offspring_%s_%d.RData',
                    sp.name, G))
```

C.6 Vec-permutation IPM

In this section we provide code for constructing a vec-permutation IPM. This part of the workflow provides a slight chicken-egg problem since to make full IPMs we need estimates of fecundity parameters, but to estimate fecundity parameters we need to construct IPMs. In the 'real' workflow we run the inverse modelling of fecundity first. But in order to better explain the methods, we first show how to construct IPMs and then in the next section demonstrate how to use these IPMs to inverse model fecundity parameters.

The `F_IPMs.R` script begins by loading libraries, functions and data.

```
rm(list = ls())
### LIBRARIES ###
library(Matrix)
library(MASS)

### FUNCTIONS ###
source(file = 'Source/IPM_construction_functions.R')
```

```
### LOAD THE DATA ###
sp.name <- 'pri2co'
load(sprintf("Data/%s.RData", sp.name))

# size matrix
size.mat <- data.mat[ ,grep('size', colnames(data.mat))]
size <- size.mat[ ,ncol(size.mat)-1]
```

Next define some IPM variables. S is the number of size classes. This needs to be sufficiently large to capture individual differences in growth rates. The minimum and maximum sizes need to be outside of the range of observed sizes to prevent eviction of individuals from the model.

```
# matrix set up
min.size <- 9
max.size <- max(size, na.rm = TRUE)*1.5
S <- 1500  # number of size bins
# boundary points of mesh cells
b <-  min.size + c(0:S)*(max.size - min.size)/S
# mid points of mesh cells
Y <- 0.5* (b[1:S] + b[2:(S+1)])
h <- Y[2]-Y[1]  # cell widths
```

Load vital rate parameters corresponding to the species and number of growth classes.

```
# load vital rate parameters
G <- 2  # no. growth distributions
load(sprintf('Output/sparams_%s.RData', sp.name))
load(file = sprintf('Output/gparams_G%d_%s.RData',
                    G, sp.name))

# which of the modelled censuses to use
# (default is most recent) -
census <- nrow(g.params[[1]])
ps1 <- g.params[[1]][census, 1:G]
ps2 <- g.params[[1]][census, (G+1):(G*2)]
g.params <- cbind(ps1, ps2)
```

```
surv.thresh <- s.params[[1]][census, 7]
small.surv <- s.params[[1]][census, 1:3]
big.surv <- s.params[[1]][census, 4:6]

quant <- 0.95  # quantile in slow growth
dists <- rep('gamma', G)  # growth distributions

# threshold for automatic fast growth
growth.thresh <- ifelse(max(size, na.rm = TRUE) > 500, 200,
                        quantile(size, 0.8, na.rm = TRUE))
```

The next step is to make growth and survival models. The function `make.G.matrices` takes the number of growth classes, `G`, distributions, `dists`, growth parameters, `g.params`, and matrix variables, `Y, b, S` and turns them into transition matrices describing movement of individuals from each size to every other size, with one matrix per growth class. The function `make.survival.vector` makes a vector describing the probability of survival at each size.

```
# growth matrices
Gmats <- make.G.matrices(G, dists, g.params, Y, b, S)

# sizes below survival size threshold
small <- which(Y < surv.thresh)
# sizes above survival size threshold
big <- which(Y >= surv.thresh)
# predicted survival for small sizes
S.small <- predict.surv(params = small.surv,
                        x = Y[small],
                        time = 1)
# predicted survival for large sizes
S.big <- predict.surv(params = big.surv,
                      x = Y[big],
                      time = 1)
S.all <- c(S.small, S.big)  # survival vector
```

We multiply the survival vector by each column of the growth matrices to get matrices describing the growth and survival of individuals. These are then arranged as a block

diagonal matrix.

```
Umats <- vector('list', G)

for(i in 1:G){
  # within growth class growth and survival
  Umats[[i]] <- Gmats[[i]]*S.all
  Umats[[i]][S,S] <- 0
}

Ublock <- bdiag(Umats)
```

We also require a matrix describing movement of individual at each size between growth classes. We made this using the `transitions.R` script and simply load it in here.

```
load(file = sprintf('Output/%s_Mblock_%d.RData',
                    sp.name, G))
```

To combine matrices describing movement of individuals *within* a growth class and those describing movement of individuals *between* growth classes we use the vec permutation matrix `K`. Cohort dynamics such as passage times, longevities and occupancy times can all be calculated from the matrix `Utilde`.

```
# vec permutation matrix
K <- as.matrix(make.K(G, S), 'sparseMatrix')
# growth and survival, transitions
Utilde <- t(K) %*% Mblock %*% K %*% Ublock

save(Utilde, Y, b,
     file = sprintf('Output/%s_Utilde_%d.RData',
                    sp.name, G))
```

To complete the life-cycle, we combine `Utilde` with `Ftilde` which describes production of offspring of each size, by parents of each size, and the offspring distribution between growth classes.

```
### RUN THIS SECTION AFTER RUNNING G ###

# load the fecundity parameter estimated in G
load(sprintf('Output/fparams_%s_%d.RData', sp.name, G))
param.f <- median(theta)

params.f <- c(0, rep(param.f, G-1))

# threshold for fecundity
fec.thresh <- ifelse(max(size, na.rm = TRUE) > 500,
                     0.5*max(size, na.rm = TRUE), 0)

# load the offspring size and growth class distributions
load(sprintf('Output/offspring_%s_%d.RData', sp.name, G))

Fmats <- make.F.matrices(G, Y, offspring.sizes,
                         fec.thresh, params.f)
I <- Diagonal(S)
Fblock <- bdiag(Fmats)
Dblock <- kronecker(I, C3)
Ftilde <- t(K) %*% Dblock %*% K %*% Fblock
Atilde <- Utilde + Ftilde

save(Atilde, Y, b, file = sprintf('Output/%s_Atilde_%d.RData',
                                  sp.name, G))
```

C.7 Inverse modelling fecundity

We use a particle filter to inverse model fecundity. Code is based on Beaumont (2010) and Gonzalez(2016).

We assume a simple model of reproduction, whereby only individuals above a size threshold reproduce, and per capita reproduction scales linearly with BA. The slope of the relationship between BA and per capita reproduction is determined by a fecundity parameter which is sampled by the particle filter. A likelihood function compares population level outputs from IPMs built with each sampled fecundity parameter to time series data, i.e.

census data over 15 years. Specifically, we use the 1995 size distribution as a starting point and multiply iteratively by the IPM (constructed with the proposed fecundity parameter). Every five years the number of individuals in the simulated population and their size distribution is compared to the observed population size and size distribution from the census data, see Gonzalez et al. (2016).

The script `G_particle_filter.R` begins by loading libraries, functions and data and setting the number of cores to allocate to parallel processing.

```
rm(list = ls())
### LIBRARIES ###
library(Matrix)
library(MASS)
library(foreach)
library(doParallel)
library(methods)
library(truncnorm)

set.seed(1)
### FUNCTIONS ###
source('Source/IPM_construction_functions.R')
source("Source/particle_filter_functions.R")

### SET UP ###
# number of processors for parallel code
nproc <- detectCores() - 1

# Choose the species and load its data
sp.name <- 'pri2co'
load(sprintf("Data/%s.RData", sp.name))
```

Next we load `Utilde`, the matrix describing movement of individuals between size and growth classes, made in the section above.

```
# size matrix
size.mat <- data.mat[ ,grep('size', colnames(data.mat))]
# matrix set up
min.size <- 9
```

```
max.size <- max(size.mat, na.rm = TRUE)*1.5
S <- 1500
G <- 2
load(sprintf('Output/%s_Utilde_%d.RData', sp.name, G))
```

We begin to make `Ftilde`, but stop short at the final step. Keeping this section outside of the particle filter sampling speeds up the code.

```
# threshold for automatic fast growth
growth.thresh <- ifelse(max(size.mat, na.rm = TRUE)
                        > 500, 200,
                        quantile(size.mat, 0.8,
                                 na.rm = TRUE))
quant <- 0.95

# load the offspring size distribution -
load(sprintf('Output/offspring_%s_%d.RData', sp.name, G))
BA <- find.BA(Y)  # basal area - scales with fecundity
# distribution of offspring between growth classes
Dblock <- kronecker(Diagonal(S), C3)
# move out of particle filter for speed
# vec permutation matrix
K <- as.matrix(make.K(G, S), sparse = TRUE)
tKDK <- t(K) %*% Dblock %*% K
```

We get the size distribution of the population at each census, as this is what the simulated population will be compared to in the likelihood function.

```
# Observed summary statistic
# - the observed size distributions
S.ys <- apply(size.mat, 2, get.observed.size.dist,
              S, b)
```

Before beginning the particle filter we test a range of parameters as this allows us to chose a starting acceptance value for accepting or rejecting parameters in the particle filter.

```
# now find a starting acceptance value that will
# allow us to zoom in on the 'best'
# parameters
# get range of rhos from a wide range of parameters
fs <- seq(0.00001, 10, length.out = 20)
rhos <- rep(NA, length(fs))

# threshold for fecundity
fec.thresh <- ifelse(max(size.mat, na.rm = TRUE) > 500,
                     0.5*max(size.mat, na.rm = TRUE), 0)

# get a size distribution from the IPM made
# with each of these fecundity values
for(ii in 1:length(fs)){
  rhos[ii] <- get.likelihood(fs[ii],  G,  Y,
                             offspring.sizes, fec.thresh,
                             Utilde, S.ys, t.int = 5, quant)
  print(paste(sp.name, ii))
}

# gives an idea of how sensitive the summary statistic is
# to changes in the parameter of interest
range(rhos)
plot(fs, rhos, type = 'l')
abline(v = fs[which(rhos == max(rhos))], lty = 2)
epsilon <- quantile(rhos, 0.6)
abline(h = epsilon)

range(fs[which(rhos > epsilon)])
```

Next we set up the particle filter, specifying priors, the number of iterations and how many particles to sample each iteration. We also define a level of precision at which sampling will stop.

```
N <- 400 # how many particles to sample at each iteration
T_iters <- 25  # number of iterations
```

```
# fecundity prior - prior knowledge
# regarding the value of the fecundity parameter
l.fec.prior <- 0.0001
u.fec.prior <- 10

t <- 1  # start at iteration one
# holds accepted parameters each iteration - overwritten
theta <- rep(NA, N)
# records elapsed time of each iterations
time.elapsed <- rep(NA, T_iters)
# stop criterion for the particle filtering
theta.precision <- 0.0001
posterior <- matrix(NA, ncol = N, nrow = T_iters)
tol <- 0.6
```

In the first iteration of the particle filter, particles are sampled from the prior distribution until `N` samples have been found which have a likelihood value above the acceptance value `epsilon`. Accepted particles are weighted, in this case equally since the prior is a uniform distribution. Finally, epsilon is updated based on the distribution of likelihood values.

In subsequent iterations, accepted particles from the previous iteration are peturbed by `tau`, twice the empirical variance in particle values. These are then sampled from until there are `N` particles which meet the new acceptance value, `epsilon`. The particle filter stops when all of the accepted values are within a specified distance from each other, set by `theta.precision`.

```
while(t <= T_iters){  # each iteration...

  if(t == 1){  ### INITIALISATION
    rhos <- rep(NA, N)  # to hold loglikelihoods
    sim.n <- N  # how many still to sample

    while(sim.n>0){   # keep sampling until N accepted parameters

      # new thetas from the prior distribution
      theta.t <-runif(sim.n, l.fec.prior, u.fec.prior)
      # get the summary statistic and compare to
      # observed summary stat
```

```
    # to get the likelihood
    theta.t.split <- split(theta.t,
                           ceiling(seq_along(theta.t)/(N/nproc)))
    registerDoParallel(nproc)
    # S.x is a matrix with stable size distributions as columns
    rho <-  foreach(proc = 1:nproc,
                    .packages = c('msm', 'Matrix', 'MASS'))
    %dopar%{
      sapply(as.numeric(unlist(theta.t.split[proc])),
             get.likelihood,
             G,  Y,
             offspring.sizes, fec.thresh,
             Utilde, S.ys, t.int = 5, quant)
    }
    rho <- unlist(rho)
    # keep the theta.ts where rho > acceptance value
    keep <- which(rho > epsilon)
    length(keep)
    if(length(keep)>0){
      new <- which(is.na(theta))[1]  # where to fill in
      theta[new:(new + length(keep)-1)] <- theta.t[keep]
      rhos[new:(new+length(keep)-1)] <- rho[keep]
    }
    sim.n <- length(which(is.na(rhos)))  # how many still to sample
  }

  # set the weights
  w <- rep(1/N, N)  # in iteration 1 these are all equal
  # set the value of Tau - twice the empirical variance
  # of the simulated points
  tausq <- 2*em.var(theta)
  # update the acceptance value
  epsilon <- quantile(rhos, prob = tol)

}else{  # for iterations 2 to N

  theta.new <- rep(NA, N)  # vector to hold new thetas
```

```
  # vector to hold the weights and K distribution value
  t.p <- rep(NA, N)
  rhos <- rep(NA, N)  # vector to hold likelihoods
  sim.n <- N  # reset number of particles still to collect

  while(sim.n>0){  # keep sampling until N accepted points

    # sample old thetas with probabilities given by weights
    theta.star <- sample(theta, sim.n, prob = w, replace = TRUE)
    # index of parent thetas
    theta.prev.index <- match(theta.star, theta)
    # peturb parameters by tau
    theta.t <- rnorm(sim.n, theta.star, sqrt(tausq))

    # we evaluate the priors here since the uniform prior means that
    # those outside of the allowed range will be discarded anyway -
    # this saves evaluating the likelihood for values that would break
    # the code
    prior <- dunif(theta.t, min = l.fec.prior,
                   max = u.fec.prior, log = TRUE)
    if(length(which(is.finite(prior))) == 0){
      next()
    }

    # parameters in the uniform distribuiton are evaluated
    eval <- which(!is.infinite(prior))
    theta.t.eval <- theta.t[eval]
    theta.prev.index <- theta.prev.index[eval]

    # get the simulated summary statistic
    theta.t.split <- split(theta.t.eval,
                           ceiling(seq_along(theta.t.eval)/
                                     (sim.n/nproc)))
    registerDoParallel(nproc)
    rho <-  foreach(proc = 1:nproc,
                    .packages = c('msm', 'Matrix', 'MASS'))
    %dopar% {
```

```
      sapply(as.numeric(unlist(theta.t.split[proc])), get.likelihood,
             G,  Y,
             offspring.sizes, fec.thresh,
             Utilde, S.ys, t.int = 5, quant)
    }
    rho <- unlist(rho)
    # keep the theta.ts where rho > acceptance value
    keep <- which(rho > epsilon)
    if(length(keep)>0){  # add the accepted parameters
      new <- which(is.na(theta.new))[1]
      theta.new[new:(new + length(keep)-1)] <- theta.t.eval[keep]
      t.p[new:(new+length(keep)-1)] <- theta.prev.index[keep]
      # save the comparisons
      rhos[new:(new+length(keep)-1)] <- rho[keep]
    }
    sim.n <- length(which(is.na(rhos)))
    print(sim.n)
  }

  # evaluate the prior for each new theta
  theta.priors <- dunif(theta.new, l.fec.prior,
                        u.fec.prior, log = TRUE)

  # evaluate the kernel
  t.prev <- theta[t.p]
  K <- dnorm(theta.new, mean = t.prev,
             sd = sqrt(tausq), log = TRUE)
  K.w <- sum(K * w)
  w <- theta.priors/K.w  # new weights
  w <- w/sum(w)
  theta <- theta.new  # replace old theta with new values
  # new value of tau- twice variance in summary stats
  tausq <- 2*em.var(theta)
  epsilon <- quantile(rhos, prob = tol)

}
```

```
  # this follows each iteration
  save(theta, file = sprintf('Output/fparams_%s_%d.RData', sp.name, G))
  print(paste(sp.name, t))

  posterior[t, ] <- theta

  t <- t+1

  if(max(theta) - min(theta) < theta.precision){
    break
  }

}

posterior <- posterior[1:(t-1), ]
param.f <- median(theta)
save(theta, param.f, posterior,
     file = sprintf('Output/fparams_%s_%d.RData', sp.name, G))
```

Once we have an estimate of the fecundity parameter we can go back and make the IPM, as described above, ready for analysis in the next section.

C.8 IPM diagnostics

In this section we show how to analyse the population using the size-growth IPM. The full script is `H_diagnostics.R`

C.8.1 Occupancy times

The function `get.occupancy.times` calculates the occupancy in each state (combination of size and growth class) of interest, from each starting state. The size range of interest is provided in mm with the argument `size.range` and the growth class of interest are specified by the argument `G.int`.

```
### 1. Occupancy times
size.range <- c(min.size, growth.thresh)  # size classes of interest
```

```
G.int <- c(1,2)  # growth classes of interest
oc <- get.occupancy.times(size.range, Utilde, S, G, Y, G.int)
```

The occupancy time in this size range, for each of the growth groups, is returned in the object `o.sizes`.

Below, we plot the results for occupancy in the understory (sizes up to 200 mm), in each growth group, given starting in each state.

```
library(wesanderson)
cols <- wes_palette('FantasticFox', 5)[2:5]

# time spent in size classes of interest for each growth
# group (rows) from every size/growth combination (columns)
os <- oc$o.sizes
# plot the results
par(mfrow = c(1,1))
plot(Y, os[1,1:S], type = 'l', xlab = 'DBH',
     ylab = 'Years', col = cols[1], lwd = 2,
     main = sprintf('Occupancy of size range %s to %s mm',
                    siz.range[1], size.range[2]), font.main = 1)
points(Y, os[1, (S+1):(S*2)], type = 'l', col = cols[2], lwd = 2)
points(Y, os[2, 1:S], type = 'l', col = cols[3], lwd = 2)
points(Y, os[2, (S+1):(S*2)], type = 'l', col = cols[4], lwd = 2)

legend('topright', col = cols, lwd = 2, title = 'Growth class',
       legend = c('slow | slow', 'slow | fast',
                  'fast | slow', 'fast | fast'))
```

Occupancy times, summed over the growth classes of interest, for each size, are returned in the object `o.growth`.

```
# time spent in growth classes of interest for each size group
# (rows) from every size/growth combination (columns)
og <- oc$o.growth
# plot the results
og.slow <- og[,1:S]
og.fast <- og[,(S+1): (S*2)]
```

```
par(mfrow = c(2,1))

leg.seq <- seq(1, S, length.out = min(10, S))
cols.ramp <- make.ramp(cols, levels = length(leg.seq))
plot(Y, og.slow[,1], type= 'l', xlab = 'DBH', ylab = 'Years',
     main = 'Occupancy of each size class, starting slow',
     ylim = c(0, max(og.slow)), font.main = 1)
for(ss in round(leg.seq)){
  points(Y, og.slow[,ss], type = 'l',
         col = cols.ramp[which(round(leg.seq) == ss)])
}
plot(Y, og.fast[,1], type= 'l', xlab = 'DBH', ylab = 'Years',
     main = 'Occupancy of each size class, starting fast',
     ylim = c(0, max(og.fast)), font.main = 1)
for(ss in round(leg.seq)){
  points(Y, og.fast[,ss], type = 'l',
         col = cols.ramp[which(round(leg.seq) == ss)])
}
```

The occupancy in both the sizes and growth classes of interest are returned in the object `o.both`.

```
# ob shows the time spent in each size/growth group of interest,
# given starting size/growth combinations
ob <- oc$o.both
plot(Y, ob[1:S], type = 'l', col = cols[1], xlab = 'DBH',
     ylab = 'Years', ylim = c(0,max(ob)),
     font.main = 1, cex.main = 0.9, lwd = 2,
     main = sprintf('Occupancy of size range %s to %s
                    and growth class(es) %s, %s',
                    size.range[1], round(size.range[2]),
                    G.int[1], G.int[2]))
points(Y, ob[(S+1):(S*2)], type = 'l', col = cols[2], lwd = 2)
legend('topright', legend = seq(G), col = cols[1:G],
       title ='Growth group',
       lwd =2, cex = 0.8)
```

Finally, the occupancy in each state, given every starting state is given by `Ntilde`.

```
# occupancy time in every state (rows) from every other state (column)
Ntilde <- oc$Ntilde
```

The occupancy time for a cohort of individuals of mixed starting states can be calculated with the function `get.occupancy.mixed`. This returns an SxG vector giving the occupancy time in each state for the mixed cohort.

```
# mixed distribution -  occupancy times of a cohort of mixed states
# here we use the observed population size distribution, alternatives
# would be a cohort of recruits etc...
# shows the occupancy time in EACH state -
# i.e. each size and growth group combination
quant <- 0.95  # proportion of the population in each growth class
mixed.dist <- get.occupancy.mixed(size, S, b, Utilde, quant)
plot(Y, mixed.dist[1:S], type = 'l', xlab = 'DBH',
     ylab = 'Years', font.main = 1,
     col = cols[1], lwd = 2,
     main = 'Occupancy times of a mixed cohort')
points(Y, mixed.dist[(S+1):(S*2)], type = 'l',
       col = cols[2], lwd = 2)
legend('topright', legend = seq(G),
       col = cols[1:G], title ='Growth group',
       lwd =2, cex = 0.8)
```

C.8.2 Survivorship

We can calculate the proportion of the population that would survive x years, given each starting state with the function `get.survivorship`.

```
### 2. Survivorship
x <- 10  # number of years
ltilde.ten <- get.survivorship(x, S, G, Utilde)
plot(Y, ltilde.ten[1:S, 1], type = 'l', xlab = 'DBH',
     ylab = '% Survival',
     font.main = 1, lwd = 2, col = cols[1],
     main = sprintf('Survivorship after %s years', x))
```

```
points(Y, ltilde.ten[(S+1):(S*2), 1], type = 'l', col = cols[2])
legend('topright', legend = seq(G),
       col = cols[1:G], title ='Growth group',
       lwd =2, cex = 0.8)
```

Survivorship for a mixed cohort is calculated with the function `get.mixed.survivorship`. This returns a 1xG vector giving the proportion of survivors from each growth class.

```
# survivorship of a mixed population
mixed.surv <- get.mixed.survivorship(10, size,
                                     S, G, b, quant, Utilde)
barplot(mixed.surv, beside = TRUE, space = 0.2,
        col = cols[1:2], font.main = 1,
        main = 'Survival of a mixed cohort, by growth classes',
        ylab = '% Survival', xlab  = 'Growth class',
        names.arg = seq(G))
```

C.8.3 Longevities

To calculate the expected longevity of each state, we call the function `get.longevity`, which returns the mean, variance and skew in longevities for each starting state.

```
### 3. Longevity stats
longevity <- get.longevity(S, G, Utilde)
mu.longs <- longevity$mu
var.longs <- longevity$var
skew.longs <- longevity$m3

par(mfrow = c(2,1))
plot(Y, mu.longs[1:S], type = 'l', col = cols[1],
     lwd = 2, xlab = "DBH",
     ylab = 'Years', main = 'Longevity')
points(Y, mu.longs[(S+1):(S*2)], type = 'l',
       col = cols[2], lwd = 2)
legend('topright', legend = seq(G), lwd = 2,
       col = cols[1:G],
```

```
       title = 'Starting growth', cex = 0.8)

plot(Y, var.longs[1:S], type = 'l', col = cols[1],
     lwd = 2, xlab = "DBH",
     ylab = 'Years', main = 'Var Longevity')
points(Y, var.longs[(S+1):(S*2)], type = 'l',
       col = cols[2], lwd = 2)
legend('topright', legend = seq(G), lwd = 2,
       col = cols[1:G],
       title = 'Starting growth', cex = 0.8)

plot(Y, skew.longs[1:S], type = 'l', col = cols[1],
     lwd = 2, xlab = "DBH",
     ylab = 'Years', main = 'Skew Longevity')
points(Y, skew.longs[(S+1):(S*2)], type = 'l',
       col = cols[2], lwd = 2)
legend('topright', legend = seq(G), lwd = 2,
       col = cols[1:G],
       title = 'Starting growth', cex = 0.8)
```

The full probability distribution of longevities can be calculated with the function `get.longevity.prob.dist`.

```
ns <- Y
probs <- get.longevity.prob.dist(ns, S, G, Utilde)
plot(Y, probs[1,], type = 'l')
for(mm in seq(10, 100, 10)){
  points(Y, probs[mm, ], type = 'l', lwd = 2,
         col = cols.ramp[mm/10])
}
```

C.8.4 Passage Times

Passage times are calculated with the function `get.passage.time`. This returns the mean and variance of the time in years taken for a cohort starting in each state to reach the state of interest, specified by `R`.

```
### 4. Passage times
R <- growth.thresh
pts <- get.passage.time(R, Y, G.int, Utilde)
mu.pt <- pts$mu
var.pt <- pts$var

plot(Y, mu.pt[1:S], type = 'l', lwd = 2,
     col = cols[1], main = 'PT',
     xlab = 'DBH (mm)', ylab = 'Years')
points(Y, mu.pt[(S+1):(S*2)], type = 'l',
       col = cols[2], lwd = 2 )
legend('topright', legend = seq(G), lwd = 2, col = cols[1:G],
       title = 'Starting growth', cex = 0.8)
abline(v = R, lty = 2, col = 'grey')

plot(Y, var.pt[1:S], type = 'l', lwd = 2,
     col = cols[1], main = 'Var PT',
     xlab = 'DBH (mm)', ylab = 'Years')
points(Y, var.pt[(S+1):(S*2)], type = 'l',
       col = cols[2], lwd = 2 )
legend('topright', legend = seq(G), lwd = 2,
       col = cols[1:G],
       title = 'Starting growth', cex = 0.8)
abline(v = R, lty = 2, col = 'grey')
```

C.9 Functions

C.9.1 Data processing functions

The code below forms `Data_processing_functions.R`.

```
#### correct dbh measurements for all censuses at once
correct.dbh <- function(dbhs,
                        sd2 = 25.6, times = 5,
                        sda = 0.927, sdb = 0.0038,
                        give.up = 20000){
```

```
dim.col <- dim(dbhs)[2]
# propose new parameters
# size dependent growth correction
suppressWarnings(dbh.stars <-  matrix(rnorm(length(dbhs),
                                            dbhs,s
                                            (sda + sdb * dbhs)),
                                      ncol = dim.col,
                                      byrow = FALSE))

# get the increments
diffs <- t(apply(dbh.stars, 1, diff))
if(dim.col == 2){
  diffs <- t(diffs)
}

# negative increments
neg.incrs <- which(apply(diffs, 1,
                         function(x) any(x <= 0)) == TRUE)
# negative sizes
neg.stems <- which(apply(dbh.stars, 1,
                         function(x) any(x <= 0)) == TRUE)
neg <- unique(c(neg.incrs, neg.stems))  # both

ct <- 0
# while anything is still negative keep going
# until give.up to try and correct them
while(length(neg)>1 & ct < give.up) {

  # propose new sizes for negative stems/increments
  suppressWarnings(dbh.stars[neg, ] <-
                     matrix(rnorm(length(dbhs[neg ,]),
                                  dbhs[neg ,],
                                  (sda + sdb * dbhs[neg ,])),
                            ncol = dim.col, byrow = FALSE))
  # new increments for the new sizes
  diffs[neg, ] <- t(apply(dbh.stars[neg, ], 1, diff))
```

```
  # which ones are still negative
  neg.incrs <- which(apply(diffs, 1, function(x)
    any(x <= 0)) == TRUE)
  neg.stems <- which(apply(dbh.stars, 1, function(x)
    any(x <= 0)) == TRUE)
  neg <- unique(c(neg.incrs, neg.stems))
  ct <- ct + 1

  if(ct %% 25 == 0){
    print(sprintf('%d: Negative stems/increments: %d',
                  ct, length(neg)))
  }
}
# at give up... if there are still
# negative stems/increments
if(length(neg) > 0) {

  # first correct negative sizes
  dbh.stars[which(dbh.stars < 0)] <-
    rnorm(length(which(dbh.stars < 0)),
          10, 0.5)

  # now get new diffs
  diffs <- t(apply(dbh.stars, 1, diff))
  if(dim.col == 2){
    diffs <- t(diffs)
  }

  # which rows still have negative growths
  neg <- which(apply(diffs, 1, function(x)
    any(x <= 0)) == TRUE)
  # if a stem has a negative incrment AND one
  # or more positive increment
  # then make the negative the mean of the positives
  # if it has only negative increments then sample from
  # ALL stems.
  if(length(neg) > 0){
```

```
      tmpll <- matrix(diffs[neg, ], ncol = ncol(diffs))

      diffs[neg, ] <-
        t(apply(tmpll, 1,
                function(x)
                  replace(x, which(x < 0),
                          ifelse(length(which(x > 0))
                                 > 0,
                                 mean(x[x > 0],
                                      na.rm = TRUE),
                                 sample(diffs[diffs > 0 &
                                              !is.na(diffs)],
                                        length(which(x<=0)),
                                        replace = TRUE)))))
      # adjust the sizes to take account
      # of the new increments
      # NB some don't have a size in the first few years
      dbh.stars <- t(mapply(make.new.sizes,
                            sizes = split(dbh.stars,
                                          row(dbh.stars)),
                            incrs = split(diffs,
                                          row(diffs))))

    }
  }
  # how many were not corrected before give.up
  n.sampled <- length(neg)
  return(list(dbh.stars = dbh.stars,
              n.sampled = n.sampled))
}

# get new dbh measurements based on
# estimates of error rates
propose.incr <- function(dbhs, sda = 0.927,
                         sdb = 0.0038) {
  dbhs.star <- rnorm(length(dbhs), dbhs,
                     (sda + sdb*dbhs))
```

```
  return(dbhs.star)
}



# find obvious outliers - those that
# are very different
# from the other measurements
find.errors <- function(stem.vec){
  stem <- stem.vec[grep('size', names(stem.vec))]
  diffs <- stem.vec[grep('incr', names(stem.vec))]
  time.vec <- stem.vec[grep('time', names(stem.vec))]
  # make the increments annual
  diffs <- diffs/time.vec
  # second largest difference
  second.diff <- sort(diffs)[length(diffs)-1]

  # returns a true if the largest difference
  # is more than 10 x larger
  # than the second largest difference and also over
  # 60 (because something that
  # grew 2 mm could conceivably grow 20mm the next).
  # also returns true if the stem shrank more than 25%
  # of original size
  # or grew more than 75 mm in a single year
  out <- ifelse(max(diffs) > second.diff*10 &
                  max(diffs) > 60
                | any(diffs > 75, na.rm = TRUE),
                TRUE, FALSE)

  tmp.ll <- cbind(stem[1:(length(stem)-1)],
                  stem[2:length(stem)])
  out <- ifelse(any(tmp.ll[,2] < 0.75*tmp.ll[,1],
                    na.rm = TRUE), TRUE, out)

  # can't correct if there are only 2 measurements
  if(length(which(!is.na(diffs))) < 2){
    out <- FALSE
```

```
  }
  return(out)
}


# correct those obvious outliers -
# make them the mean of measurements either side
# or if they are first or last make them
# second/penultimate -/+ growth from closest
# census - only works when there are >2 measurements
correct.errors <- function(stem.vec){
  full <- stem.vec
  start <- as.numeric(stem.vec[grep('size',
                                    names(stem.vec))])
  stem <- start[!(is.na(start))]  # get rid of NAs
  # can only correct if there are more than two measurements
  if(length(stem) > 2){
    # get the difference between each measurement
    # and every other measurement
    co <- cbind(stem, rep(1, length(stem)))
    dists <- dist1(co)
    outlier <- which(rowMeans(dists) ==
                       max(rowMeans(dists)))[1]

    if(outlier == 1){
      stem[outlier] <- stem[2] - diff(stem)[2]
    }else{
      if(outlier == length(stem)){
        stem[outlier] <- stem[length(stem) -1] +
          diff(stem)[length(stem) - 2]
      }else{
        stem[outlier] <- mean(c(stem[outlier- 1],
                                stem[outlier + 1]))
      }
    }
  }
```

```
  start[!is.na(start)] <- stem
  full[grep('size', names(full))] <- start
  return(full)
}


make.new.sizes <- function(sizes, incrs){
  first <- which(!is.na(sizes))[1]
  if(first != length(sizes)){
    out <- cumsum(c(sizes[first],
                    incrs[first:length(incrs)]))
    out <- c(rep(NA, first-1), out)
  }else{
    out <- sizes
  }
  return(out)
}


fill.in <- function(sizes){
  missing <- which(is.na(sizes[2:3]))
  if(missing == 1){
    sizes[2] <- mean(c(sizes[1], sizes[3]))
  }else{
    sizes[3] <- mean(c(sizes[2], sizes[4]))
  }
  return(sizes)
}

# fill in random NAs where trees have been missed.
find.missing.sizes <- function(tree){
  missing <- which(is.na(tree))

  if(length(missing) > 0){
    for(mm in 1:length(missing)){
      miss <- missing[mm]
```

```
      if(miss != 1 & miss != length(tree)){

        if(!is.na(tree[miss-1]) & !is.na(tree[miss+1])){
          tree[miss] <- mean(c(as.numeric(tree[miss-1]),
                               as.numeric(tree[miss+1])))
        }

      }
    }
  }
  return(tree)
}



remove.too.big <- function(sp.df){
  sizes <- sp.df[ ,grep('size', colnames(sp.df))]
  q.99 <- quantile(sizes, prob = 0.99, na.rm = TRUE)
  too.big <- which(apply(sizes, 1, function(x)
    ifelse(any(x > q.99*2, na.rm = TRUE),
           TRUE, FALSE)) == TRUE)
  if(length(too.big) > 0){
    sp.df <- sp.df[-too.big, ]
  }
  return(sp.df)
}



correct.surv <- function(x){
  x[x == 0] <- NA
  x[which(is.na(x))[1]] <- 0
  return(x)
}
```

C.9.2 Diagnostic functions

The code below forms `Diagnostic_functions.R`.

```
# make nice colour palettes
make.ramp <- function(tmpcol, levels = 10,
                      transp = NA) {
  col.out <- colorRampPalette(tmpcol)(levels)
  if(!is.na(transp)) {
    col.out <- paste(col.out, transp, sep = "")
  }
  return(col.out)
}

### 1. OCCUPANCY TIMES
get.occupancy.times <- function(size.range =
                                  c(Y[1], Y[2]),
                                Utilde, S, G, Y,
                                G.int = seq(G)){

  I <- diag(S*G)  # Identity matrix
  Utilde <- as.matrix(Utilde)
  Ntilde <- ginv(I - Utilde)  # Fundamental matrix of Utilde
  # Ntilde[i,j] is expected occupancy time
  # in state i | starting in state j

  # size bins corresponding to size ranges of interest
  min.c <- which(abs(Y- size.range[1]) ==
                   min(abs(Y- size.range[1])))
  max.c <- which(abs(Y - size.range[length(size.range)]) ==
                   min(abs(Y -
                             size.range[length(size.range)])))
  # S x 1 vector indicating which sizes classes of interest
  cs <- rep(0, S)
  cs[seq(min.c, max.c, 1)] <- 1

  # o.sizes[i,j] is the sum of occupancy in each
  # size class of interest for growth
  # group i, given starting state j
  # (combination of sizes and growth)
  o.sizes <- kronecker(Diagonal(G), t(cs)) %*% Ntilde
```

```
  cg <- rep(0, G)
  # G x 1 vector indicating groups of interest
  cg[G.int] <- 1
  # o.growth[i,j] is the sum of occupancy in
  # each growth class of interest for size
  # class i, given starting state j
  # (combination of sizes and growth)
  o.growth <- kronecker(t(cg), Diagonal(S)) %*% Ntilde

  # occupancy in each size/growth group of interest
  o.both <- kronecker(t(cg), t(cs)) %*% Ntilde

  return(list(Ntilde = Ntilde, o.sizes = o.sizes,
              o.growth = o.growth,
              o.both = o.both))
}


# get observed size distributions
get.observed.size.dist <- function(size.vec, S, b){
  complete.size <- size.vec[!is.na(size.vec)]
  tmp <- cut(complete.size, breaks = c(0,b, Inf),
             labels = FALSE,
             include.lowest = TRUE)
  S.y <- rep(0, S)  # observed size distribution
  S.y[as.numeric(names(table(tmp)))] <-
    as.numeric(table(tmp))
  return(S.y)
}

### 2. Mixed distribution
# i.e. occupancy times for a set of
# individuals mixed among sizes
# and/or groups
```

```r
# gets the occupancy times of a cohort
# i.e. individuals start in different growth/size groups
get.occupancy.mixed <- function(size.vec, S,
                                b, Utilde, quant){

  n.vec <- get.observed.size.dist(size.vec, S, b)
  # separate into growth classes
  n.vec <- c(n.vec*quant, n.vec*(1 - quant))
  n.vec <- n.vec/sum(n.vec)  # normalise
  I <- diag(S*G)  # Identity matrix
  Utilde <- as.matrix(Utilde)
  # Fundamental matrix of Utilde
  Ntilde <- ginv(I - Utilde)
  # occupancy in each state
  o.mix <- Ntilde %*% n.vec
  return(o.mix)
}


### SURVIVORSHIP
get.survivorship <- function(x, S, G, Utilde){

  Utilde <- as.matrix(Utilde)
  l.tilde <- t(t(rep(1, (S*G))) %*%
                 as.matrix(Utilde%^%x, (S*G), (S*G)))
  # ith entry is survivors to age x of a cohort
  # in state i at time 0.
  return(l.tilde)

}

# survivorship of a cohort with mixed
# distribution of sizes and growth classes
get.mixed.survivorship <- function(x, size.vec,
                                   S, G, b,
                                   quant, Utilde){
```

```
  Utilde <- as.matrix(Utilde)
  # survivorship of cohort from state j after x years
  l.tilde <- t(t(rep(1, (S*G))) %*%
                 as.matrix(Utilde%^%x,
                           (S*G), (S*G)))
  # size distribution
  n.vec <- get.observed.size.dist(size.vec, S, b)
  n.vec <- n.vec/sum(n.vec)
  # survivorship of mixed cohort after x years,
  # by growth class
  mixed.surv <- t(kronecker(diag(G), n.vec))
  %*% l.tilde[,1]

  return(mixed.surv)

}


# longevity statistics
get.longevity <- function(S, G, Utilde){
  I <- diag(S*G)  # Identity matrix dimensions of Utilde
  Utilde <- as.matrix(Utilde)
  Ntilde <- ginv(I - Utilde)  # Fundamental matrix of Utilde
  # moments
  m1 <- t(rep(1, S*G)) %*% Ntilde
  m2 <- m1 %*% (2*Ntilde - diag(S*G))
  m3 <- m1 %*% (6*(Ntilde%*%Ntilde) - 6*Ntilde + diag(S*G))
  # variance
  var <- colSums(2 * Ntilde %*% Ntilde - Ntilde) -
    colSums(Ntilde) * colSums(Ntilde)

  return(list(mu = m1, var = var, m3 = m3))
}

### probability distribution of longevity
get.longevity.prob.dist <- function(ns, S, G, Utilde){
  Utilde <- as.matrix(Utilde)
```

```
  p.eta <- sapply(ns, function(x)
    t(colSums(diag(S*G) - Utilde) %*% (Utilde %^% (x-1))))
  return(p.eta)
}



### passage times to sets of states
get.passage.time <- function(size.range, Y,
                             G.int, Utilde){

  # Define the set of states - move from actual
  # sizes to corresponding size bins
  min.c <- which(abs(Y- size.range[1]) ==
                   min(abs(Y- size.range[1])))
  max.c <- which(abs(Y -
                       size.range[length(size.range)]) ==
                   min(abs(Y -
                             size.range[length(size.range)])))

  # vector of states of interest
  R <- c()
  for(g in 1:length(G.int)){
    R <- c(R, seq(min.c, max.c, 1) + S*(g-1))
  }

  Mtilde <- 1 - colSums(Utilde)  # probability of death
  Mtilde[R] <- 0  # already in the absorbing state

  Uprime <- Utilde
  # those in the states of interest are
  # in the absorbing state
  Uprime[ ,R] <- 0
  Uprime[R, ] <- 0

  Mprime <- Mtilde
  Mprime <- rbind(Mprime, colSums(Utilde[R, ]))
```

```
  Mprime[2, R] <- 1

  Uprime <- as.matrix(Uprime)
  Ntilde.prime <- ginv(diag(G*S) - Uprime)
  Bprime <- Mprime %*% Ntilde.prime

  ### CONDITIONAL MARKOV CHAIN
  Utilde.c <- diag(Bprime[2,]) %*% Uprime %*%
    ginv(diag(Bprime[2,]))

  eta1 <- ginv(diag(G*S) - Utilde.c)

  var <- colSums(2 * (eta1 %*% eta1) - eta1) -
    colSums(eta1) * colSums(eta1)

  m1 <- colSums(eta1)
  m1[R] <- 0

  return(list(mu = m1, var = var))
}
```

C.9.3 Growth functions

The code below forms `Growth_functions.R`.

```
get.gr.like.stan <- function(incr, ps1, ps2, quant,
                             dists ,
                             G, g.thresh, size){

  # if G == 3 find increment of top 1%
  if(G == 3){
    incr.g3.thresh <- quantile(incr, quant[2])
  }

  # start with small sizes
  # find the increment corresponding to each quantile
```

```
  small.incr <- incr[which(size < g.thresh)]
  quant.incr <- quantile(small.incr, quant[1],
                         na.rm = TRUE)
  # divide the data into increment groups based on
  # these increment thresholds
  small.incr.groups <- cut(small.incr,
                           breaks = c(0, quant.incr, 500),
                           labels = FALSE)

  incr.groups <- rep(NA, length(incr))
  incr.groups[which(size < g.thresh)] <- small.incr.groups
  incr.groups[which(size >= g.thresh)] <- 2
  if(G == 3){
    incr.groups[which(incr >= incr.g3.thresh)] <- 3
  }

  fits <- vector('list', G) # for each growth distribution...
  for(i in 1:G){
    dist <- dists[i] # define which distribution to fit
    # define the data in that group
    inc <- incr[which(incr.groups == i)]
    fits[[i]] <- dgamma(inc, ps1[i], ps2[i], log = TRUE)
  }
  final <- unlist(fits)
  return(sum(final, na.rm = TRUE))
}

# for making colour gradients
make.ramp <- function(tmpcol, levels = 10,
                      transp = NA) {
  col.out <- colorRampPalette(tmpcol)(levels)
  if(!is.na(transp)) {
    col.out <- paste(col.out, transp, sep = "")
  }
  return(col.out)
}
```

```
dmode <- function(x) {
  den <- density(x, kernel = c("gaussian"))
  ps <- ( den$x[den$y == max(den$y)] )
  return(ps)
}
```

C.9.4 Survival functions

The code below forms `Survival_functions.R`.

```
## four parameter survival curve
predict.surv <- function(x, params, time = 1) {
  K <- params[1]
  ip <- params[2]
  r <- params[3]
  # Linear predictor parameters
  pred.y <-  (K /
                (1 + exp(-(r * ((x - ip) ))))  ^ (time)
  return(pred.y)
}

get.like.s <-  function(params1, params2,
                        thresh, size, surv,
                        time) {
  size.s <- size[size < thresh]
  size.b <- size[size >= thresh]
  time.s <- time[size < thresh]
  time.b <- time[size >= thresh]
  pred.y <- rep(NA, length(size))
  pred.y[size < thresh] <-
    predict.surv(size.s, params1, time = time.s)
  pred.y[size >= thresh] <-
    predict.surv(size.b, params2, time = time.b)
  # if nan give it the upper survival limit
  pred.y[is.nan(pred.y)] <- params1[2]
  # compare to acual observed data
```

```
  like.vec <- dbinom(surv, 1, pred.y, log = TRUE)
  like.vec[which(like.vec == -Inf)] <- -20000
  # total likelihood for all trees
  sum.like <- sum(like.vec, na.rm = TRUE)

  return(sum.like)
}
```

C.9.5 IPM construction functions

The code below forms `IPM_construction_functions.R`.

```
# Makes the vec-permutation matrix
make.K <- function(G, S) {
  n.t <- matrix(seq(G * S), ncol = 1) # ex. pop vector
  n.tk <- matrix(n.t, ncol = G, byrow = FALSE)
  n.tk.new <- matrix(t(n.tk), ncol = 1, byrow = FALSE)
  # this creates the index to move from one to the other.
  comp <- cbind(n.t, n.tk.new)
  K.tmp <- matrix(0, G*S, G*S)   # empty transition matrix
  K <- replace(K.tmp, comp, 1)
  return(K)
}


# cumulative probability of moving from one size to another
grow.prob <- function(size, size.next,
                      params, dist = "gamma") {
  if(dist == "TN") {
    u <- ptruncnorm((size.next - size), a = 0, b = Inf,
                    mean = params[1], sd = params[2])
  } else if(dist == "LN") {  # log normal
    u <- plnorm((size.next - size), mean = params[1],
                sd = params[2])
  } else if(dist == 'N'){  # regular normal
    u <- pnorm((size.next - size), mean = params[1],
```

```
                sd = params[2])
  } else if(dist == 'gamma'){
    u <- pgamma((size.next - size), params[1], params[2])
  }

}

make.G.matrices <- function(G, dists, params.g, Y, b, S){

  Gmats <- vector('list', G)

  for(i in 1:G){
    Gmat <- t(outer(Y, b, grow.prob,
                    params = params.g[i, ],
                    dist = dists[i]))
    get.matrix <- Gmat[2:(S + 1), ] - Gmat[1:S, ] #
    nvals <- colSums(get.matrix, na.rm = TRUE)
    get.matrix <- t((t(get.matrix)/nvals))
    get.matrix[is.na(get.matrix)] <- 0
    Gmats[[i]] <- get.matrix
  }
  return(Gmats)
}

# find the BA of an individual
find.BA <- function(sizes){
  r <- sizes/2
  BA <- (pi * (r ^ 2)) / 100000
  return(BA)
}

# make the F matrices
make.F.matrices <- function(G, Y, offspring.sizes,
                            fec.thresh, f.params){
  BA <- find.BA(Y)
  # inedx of Y that is closest to fec.thresh
  f.thresh <- which(abs(Y - fec.thresh) ==
```

```
                      min(abs(Y - fec.thresh)))
  # those trees with DBH < threshold get 0 fecundity
  BA[1:f.thresh] <- 0

  Fmats <- vector('list', G)
  for(i in 1:G){
    repro <- BA * f.params[i]
    # make a matrix - prob of each adult size
    # producing each offspring size
    Fmats[[i]] <- t(repro %o% offspring.sizes)
  }
  return(Fmats)
}

# predict survival
predict.surv <- function(x, params, time = 1) {
  K <- params[1]
  ip <- params[2]
  r <- params[3]
  # Linear predictor parameters
  pred.y <-  (K /
                (1 + exp(-(r * ((x - ip) ))))  ^ (time)
  return(pred.y)
}

# make a survival vector
make.survival.vector <- function(Y, time,
                                 small.params, big.params,
                                 surv.thresh){

  small <- Y[which(Y < surv.thresh)]
  big <- Y[which(Y >= surv.thresh)]

  prob.small <- predict.surv(small, small.params, time)
  prob.big <- predict.surv(big, big.params, time)

  surv <- c(prob.small, prob.big)
```

```
  return(surv)
}


# Takes an eigenvector from the mega matrix
# and converts it into an IPM style -
# adds the proportion of individuals in each size
#class from each growth environment
# together to give the total proportion of
# individuals in each size class
correct <- function(eigenvec, S, G){
  eigens <- vector('list', G)
  for(i in 1:G){
    eigens[[i]] <- eigenvec[(((i-1)*S)+1):(i*S)]
  }
  w.eigen <- do.call(rbind, eigens)
  w.eigen <- colSums(w.eigen)
  w.eigen <- w.eigen/sum(w.eigen)
  return(w.eigen)
}
```

C.9.6 Particle filter functions

The code below forms `particle_filter_functions.R`.

```
em.var <- function(vec){
  xbar <- sum(vec)/length(vec)
  ssq <- sum((vec - xbar)^2)
  empirical.var <- ssq/length(vec)
  return(empirical.var)
}

get.likelihood <- function(f.params, G, Y,
                           offspring.sizes, fec.thresh,
                           Utilde, S.ys, t.int = 5, quant){
```

```
f.params <- c(0, rep(f.params, G-1))
# make new Ftilde
Fmats <- make.F.matrices(G, Y, offspring.sizes,
                         fec.thresh, f.params)

Fblock <- bdiag(Fmats)

Ftilde <- tKDK %*% Fblock

# make new Atilde
Atilde <- Utilde + Ftilde

# population projection
no.census <- dim(S.ys)[2] - 1
n.yrs <- no.census*t.int
results <- matrix(NA, ncol = S*G, nrow = n.yrs)
# break the population up into growth classes
xx <- S.ys[ ,1]
y.thresh <- max(which(abs(Y - growth.thresh) ==
                        min(abs(Y-growth.thresh))))
start.dist <- rep(0, S*G)
if(G == 2){
  if(y.thresh == S){
    start.dist[1:S] <- round(xx*quant)
    start.dist[(S+1):(length(start.dist))] <-
      round(xx*(1-quant))
  }else{
    start.dist[1:y.thresh] <-
      round(xx[1:y.thresh]*quant)
    start.dist[(S+1):(S+y.thresh)] <-
      round(xx[1:y.thresh]*(1-quant))
    start.dist[(S+y.thresh+1):(length(start.dist))] <-
      xx[(y.thresh+1):length(xx)]
  }
}else{  # i.e if G=3

  if(y.thresh== S){
```

```
    start.dist[1:S] <- round(xx*quant[1])
    start.dist[(S+1):(length(start.dist))] <-
      round(xx*(1-quant[1]))
    start.dist[((S*2 + 1)):(S*3)] <- xx*(1-quant[2])
  }else{
    sonic <- xx*(1 -quant[2])
    no.sonic <- xx*quant[2]
    start.dist[(S*2 + 1):(S*3)] <- sonic

    start.dist[1:y.thresh] <-
      round(no.sonic[1:y.thresh]*quant[1])
    start.dist[(S+1):(S+y.thresh)] <-
      round(no.sonic[1:y.thresh]*(1-quant[1]))
    start.dist[(S+y.thresh+1):(S*2)] <-
      no.sonic[(y.thresh+1):length(no.sonic)]
  }
}

results[1,] <- start.dist

yr <- 2
while(yr  <= n.yrs){
  # move individuals between size classes
  # and light environments
  results[yr, ] <- as.numeric(Atilde %*%
                              as.numeric(results[yr-1, ]))
  yr <- yr + 1
}

# likelihood
# compare the size distributions
sim.sizes <- results[(seq(t.int, no.census*t.int, t.int)), ]
sim.sizes <- t(apply(sim.sizes, 1, correct, S, G))
like.1 <- sum(apply(sim.sizes, 1,
                    compare.size.dists, obs = S.ys[,1]))
# compare population sizes
sim.N <- rowSums(results)[(seq(t.int,
```

```
                                    no.census*t.int, t.int))]
  real.N <- colSums(S.ys)[2:dim(S.ys)[2]]
  like.2 <- sum(dpois(real.N, sim.N, log = TRUE))

  loglike <- sum(like.1, like.2)
  return(loglike)

}

# get observed size distributions
get.observed.size.dist <- function(size.vec, S, b){
  complete.size <- size.vec[!is.na(size.vec)]
  tmp <- cut(complete.size, breaks = c(0,b, Inf),
             labels = FALSE,
             include.lowest = TRUE)
  # observed summary statistic - the size distribution
  S.y <- rep(0, S)
  S.y[as.numeric(names(table(tmp)))] <-
    as.numeric(table(tmp))
  return(S.y)
}

# compare size distributions
compare.size.dists <- function(obs, model){
  log.like <- dmultinom(obs, prob = model,
                        log = TRUE)
  return(log.like)
}



get.likelihood.ll <- function(f.params, G, Y,
                              offspring.sizes, fec.thresh,
                              Utilde, S.ys, t.int = 5){

  f.params <- c(0, rep(f.params, G-1))
  # make new Ftilde
```

```
Fmats <- make.F.matrices(G, Y, offspring.sizes,
                         fec.thresh, f.params)

Fblock <- bdiag(Fmats)

Ftilde <- tKDK %*% Fblock

# make new Atilde
Atilde <- Utilde + Ftilde

# population projection
no.census <- dim(S.ys)[2]
n.yrs <- no.census*t.int
results <- matrix(NA, ncol = S*G, nrow = n.yrs)
# break the population up into growth classes
xx <- S.ys[ ,1]
y.thresh <- max(which(abs(Y - growth.thresh) ==
                        min(abs(Y-growth.thresh))))
start.dist <- rep(0, S*G)
if(G == 2){
  if(y.thresh == S){
    start.dist[1:S] <- round(xx*quant)
    start.dist[(S+1):(length(start.dist))] <-
      round(xx*(1-quant))
  }else{
    start.dist[1:y.thresh] <- round(xx[1:y.thresh]*quant)
    start.dist[(S+1):(S+y.thresh)] <-
      round(xx[1:y.thresh]*(1-quant))
    start.dist[(S+y.thresh+1):(length(start.dist))] <-
      xx[(y.thresh+1):length(xx)]
  }
}else{  # i.e if G=3

  if(y.thresh== S){
    start.dist[1:S] <- round(xx*quant[1])
    start.dist[(S+1):(length(start.dist))] <-
      round(xx*(1-quant[1]))
```

```
    start.dist[((S*2 + 1)):(S*3)] <- xx*(1-quant[2])
  }else{
    sonic <- xx*(1 -quant[2])
    no.sonic <- xx*quant[2]
    start.dist[(S*2 + 1):(S*3)] <- sonic

    start.dist[1:y.thresh] <-
      round(no.sonic[1:y.thresh]*quant[1])
    start.dist[(S+1):(S+y.thresh)] <-
      round(no.sonic[1:y.thresh]*(1-quant[1]))
    start.dist[(S+y.thresh+1):(S*2)] <-
      no.sonic[(y.thresh+1):length(no.sonic)]
  }
}

results[1,] <- start.dist

yr <- 2
while(yr  <= n.yrs){
  # move individuals between size classes
  # and light environments
  results[yr, ] <- as.numeric(Atilde %*%
                              as.numeric(results[yr-1, ]))
  yr <- yr + 1
}

# likelihood
# compare the size distributions
sim.sizes <- results[(seq(t.int,
                          no.census*t.int, t.int)), ]
sim.sizes <- t(apply(sim.sizes, 1, correct, S, G))
like.1 <- sum(apply(sim.sizes, 1,
                    compare.size.dists, obs = S.ys[,1]))
# compare population sizes
sim.N <- rowSums(results)[(seq(t.int,
                               no.census*t.int, t.int))]
real.N <- colSums(S.ys)[2:dim(S.ys)[2]]
```

```
  like.2 <- sum(dpois(real.N, sim.N, log = TRUE))

  loglike <- sum(like.1, like.2)
  size.d <- results[n.yrs, ]
  size.d <- size.d[1:S] + size.d[(S+1):(S*2)]

  return(list(size.d = size.d, loglike = loglike))

}
```

C.10 Stan files

C.10.1 Growth

The code below forms the `gamma_growth.stan` file.

```
data {
  int<lower=0> N;        // no. of trees
  real incr[N];          // diameter increment in mm
  real groups[N];    // which growth groups
}

parameters {
  real<lower=0, upper=1000> alpha1;
  real<lower=0, upper=1000> alpha2;
  real<lower=0, upper=1000> beta1;
  real<lower=0, upper=1000> beta2;
}

model {
  for(i in 1:N)
  {
    if(groups[i] == 1)
      increment_log_prob(gamma_log(incr[i], alpha1, beta1));
    else
      increment_log_prob(gamma_log(incr[i], alpha2, beta2));
```

```
  }
}
```

C.10.2 Survival

The code below forms the `surv.stan` file.

```
data {
  int<lower=0> N;                    // no. of trees
  real<lower=0> dbh[N];              // diameter in mm
  int<lower=0, upper=1> surv[N];     // survival of each tree, 1 for alive, 0 for dead
  real time[N];                      // time interval between two censuses
  real lowip1;                       // ??
  real<lower=0> upip2;
  real<lower=0> thresh;
  real lowr2;
  real upperr2;
}

parameters {
  real<lower=0.01, upper=0.995> K;
  real<lower=lowip1, upper=thresh> ip1;
  real<lower=0.0001, upper=0.25> r1;

  real<lower=thresh, upper=upip2> ip2;
  real<lower=lowr2, upper=upperr2> r2;
}

model {
  real p;
  real theta;

  for(i in 1:N)
  {
    if(dbh[i] < thresh)
    {
```

```
      p <- (K) / (1 + exp(-r1 * (dbh[i] - ip1)));
      theta <- p^time[i];
    }
    else
    {
      p <-  (K) / (1 + exp(-r2 * (dbh[i] - ip2)));
      theta <- p^time[i];
    }
    surv[i] ~ bernoulli(theta);
  }
}
```

Appendix D

Chapter 3: Supplementary material

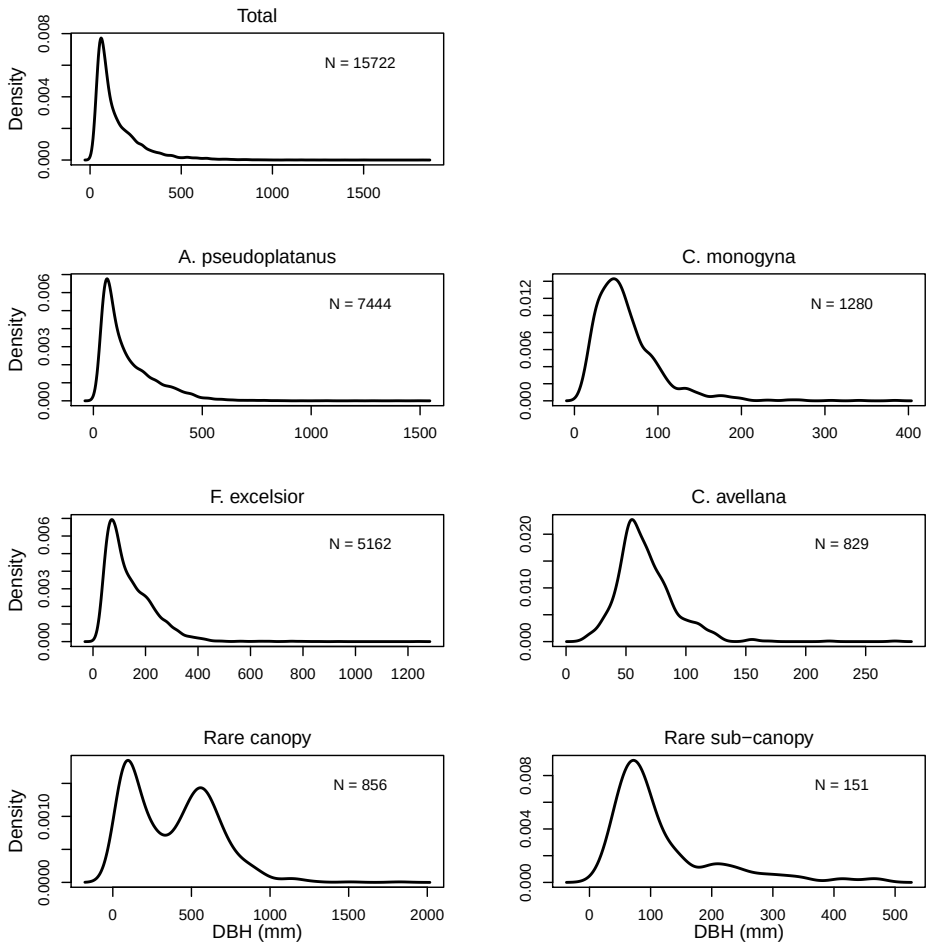


Figure D.1: Density plots showing the size distributions of each species. N shows the number of individuals. There is a lack of small individuals in each species.

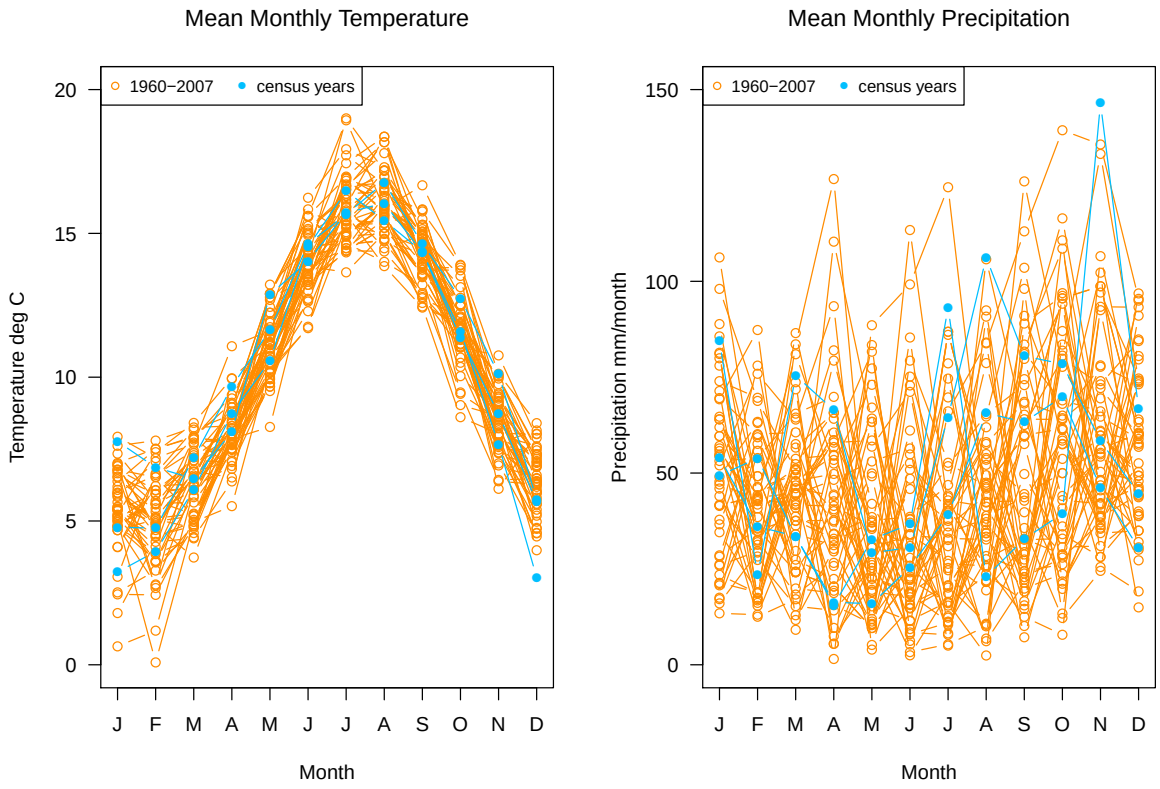


Figure D.2: Mean monthly temperatures and precipitation for Wytham Woods for the thirty years up to, and including the census interval. With the exception of December 2010 and November 2009, mean monthly temperature and precipitation during the census interval were within the range of the preceding thirty years. Data is from CRU CL 2.0 produced by Climatic Research Unit, University of East Anglia, via FetchClimate, Microsoft Research.

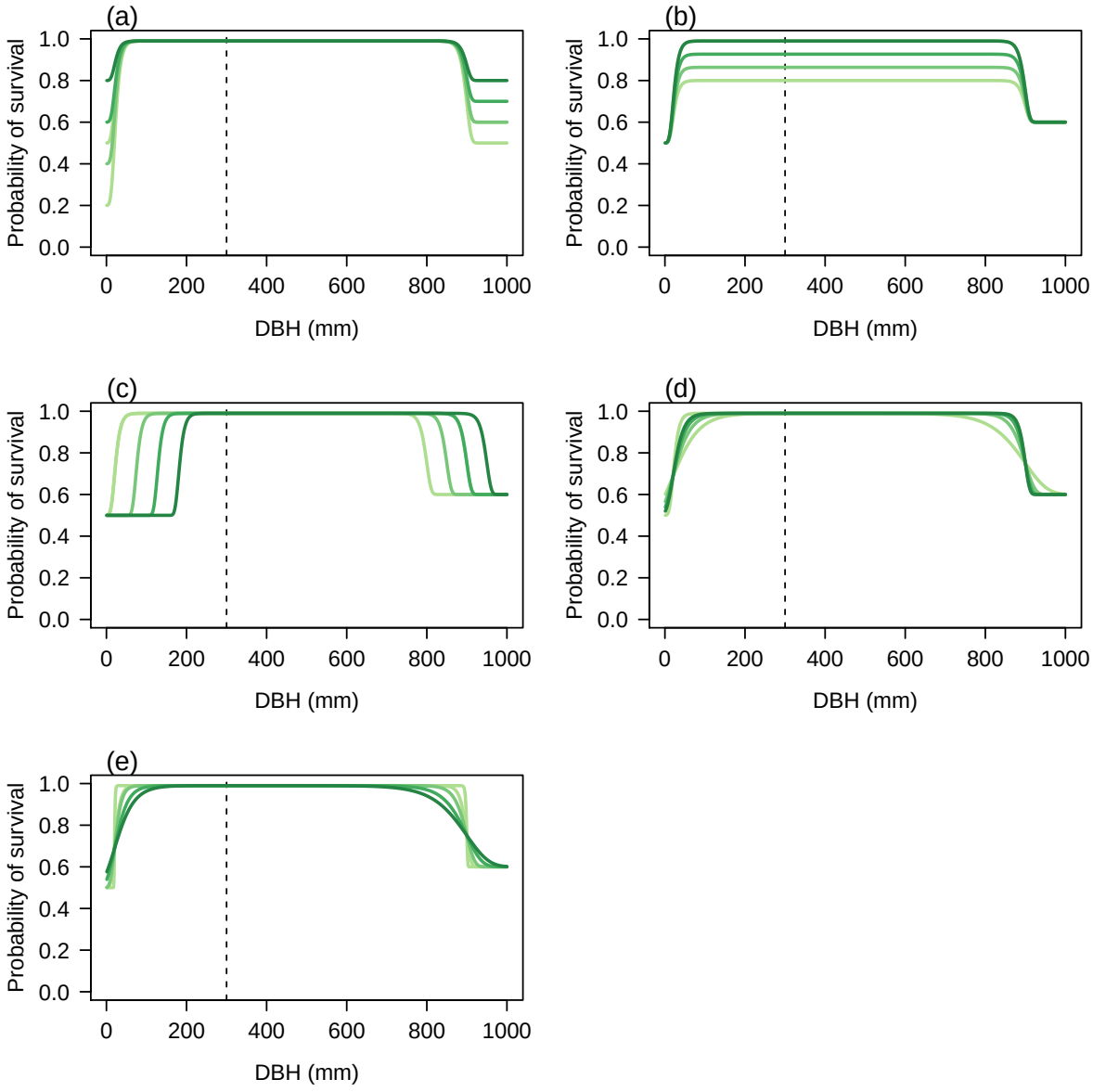


Figure D.3: Schematic of the survival function showing the effect of altering each parameter. The survival function is formed from two five-parameter logisitic regressions that meet at a species-specific size threshold, shown here with a dashed vertical line. Parameters are a) L - lower asymptote, b) K - upper asymptote, c) p -inflection point d) r - rate of change and e) theta - asymmetry of change.

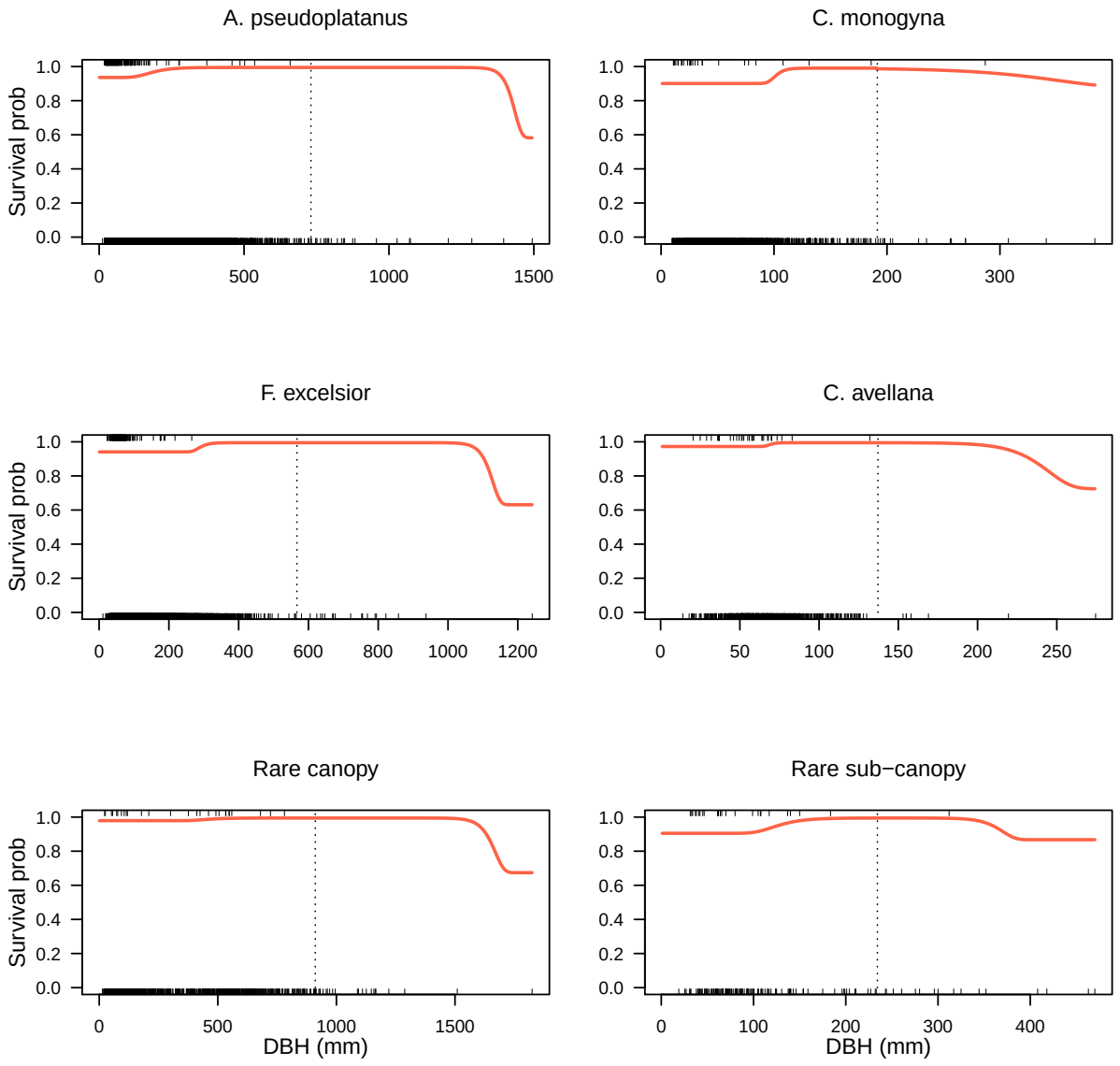


Figure D.4: Survival probability for each species. Survival is a mix of two five-parameter logistic regressions that meet at a senesence threshold. Rugs along the bottom and top axes show the survival and mortality data respectively.

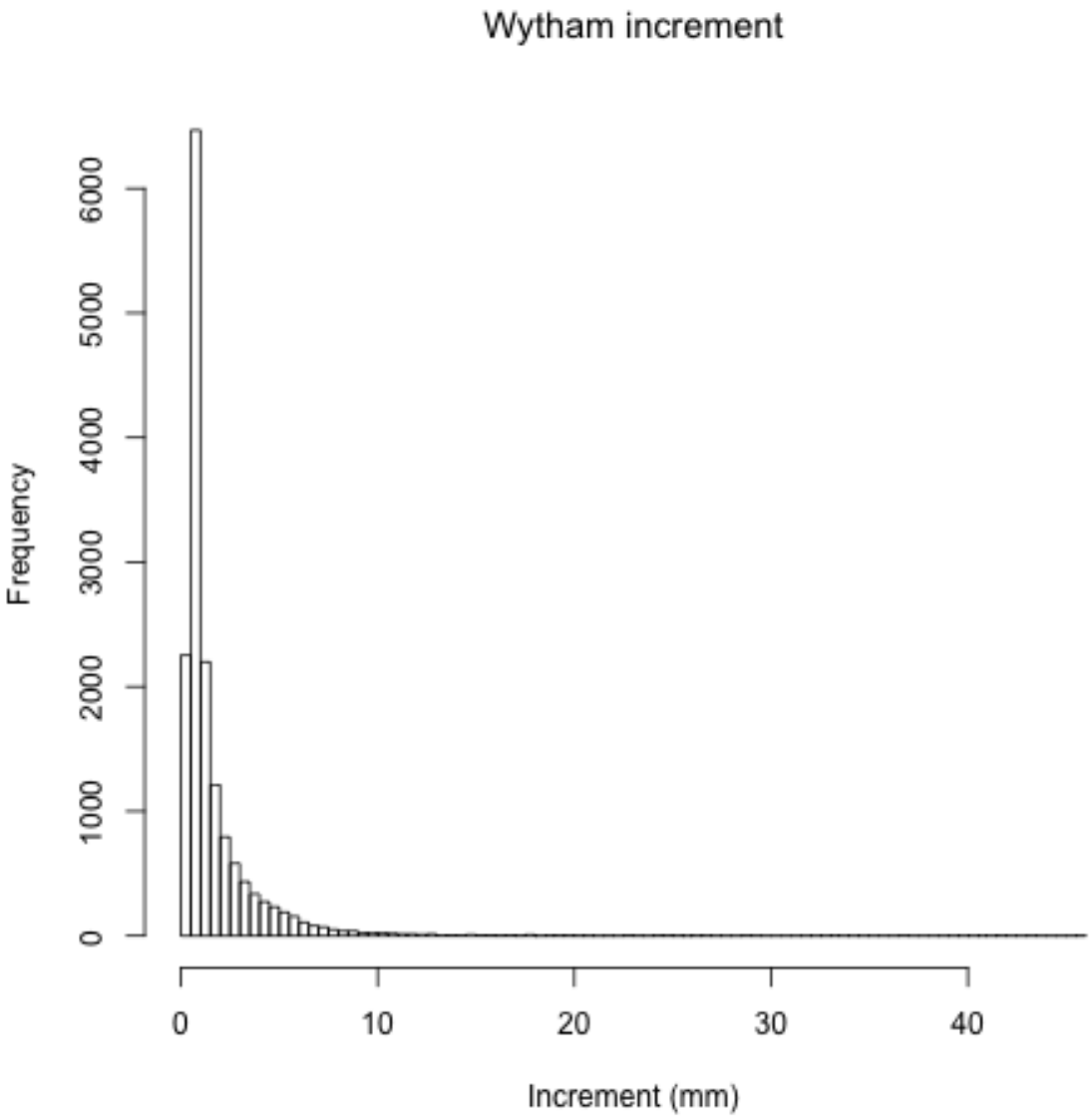


Figure D.5: Histogram of the annual growth increment data from the Wytham census data. The majority of individuals grew a very small amount each year, with a small minority growing a much larger amount.

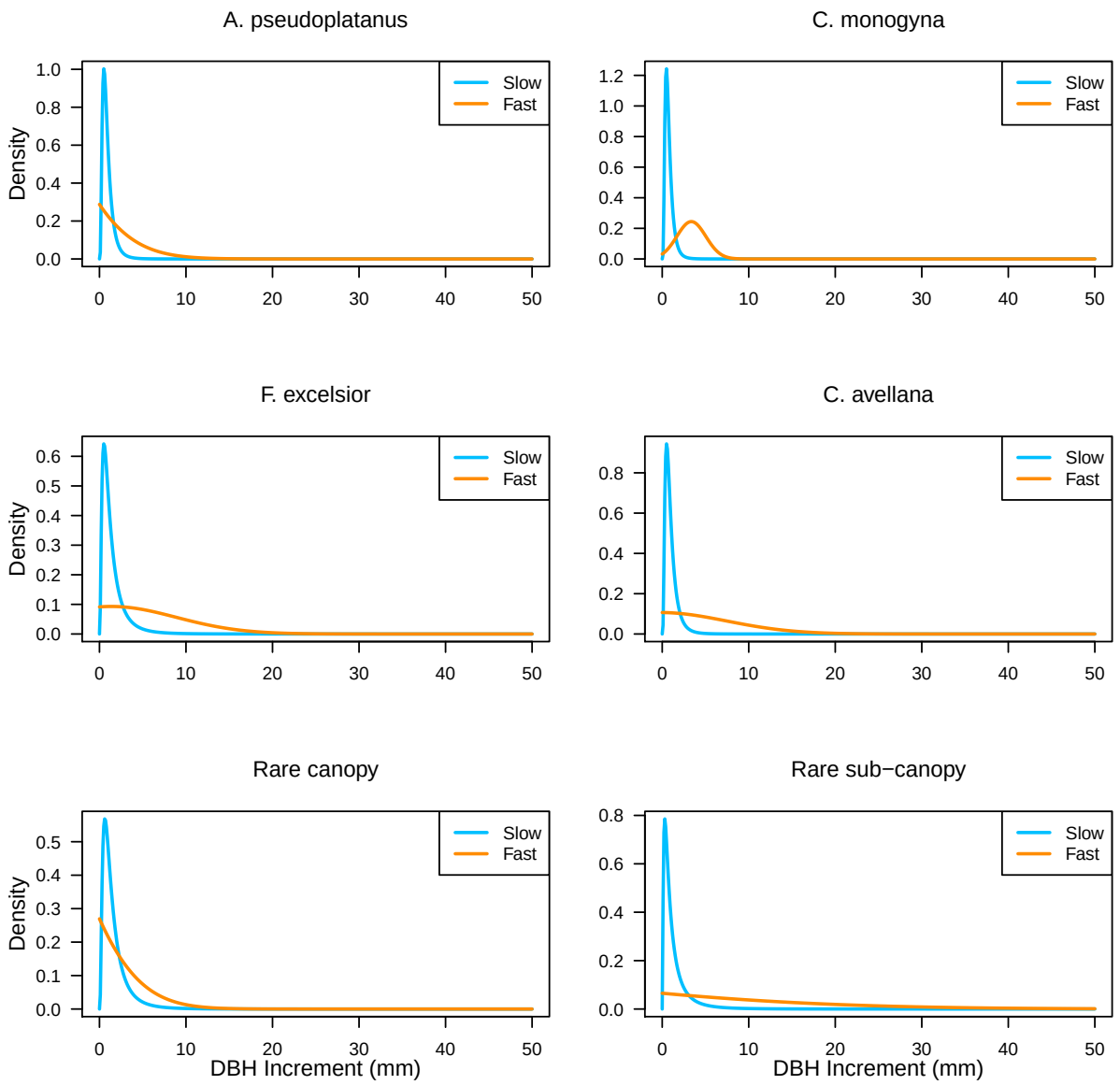


Figure D.6: Growth distributions for each species. Growth is modelled by a lognormal distribution describing slow growth and a truncated normal distribution describing fast growth. Slow and fast growth are assumed to correspond to growth in low and high light respectively. For each species, the slow growth distribution was fit to the slowest 95% of increment data, and the fast growth to the fastest 5%, with the exception that increments corresponding to individuals > 250 mm DBH automatically contributed to the fast growth distribution, since these individuals are assumed to be large enough to have reached the canopy.

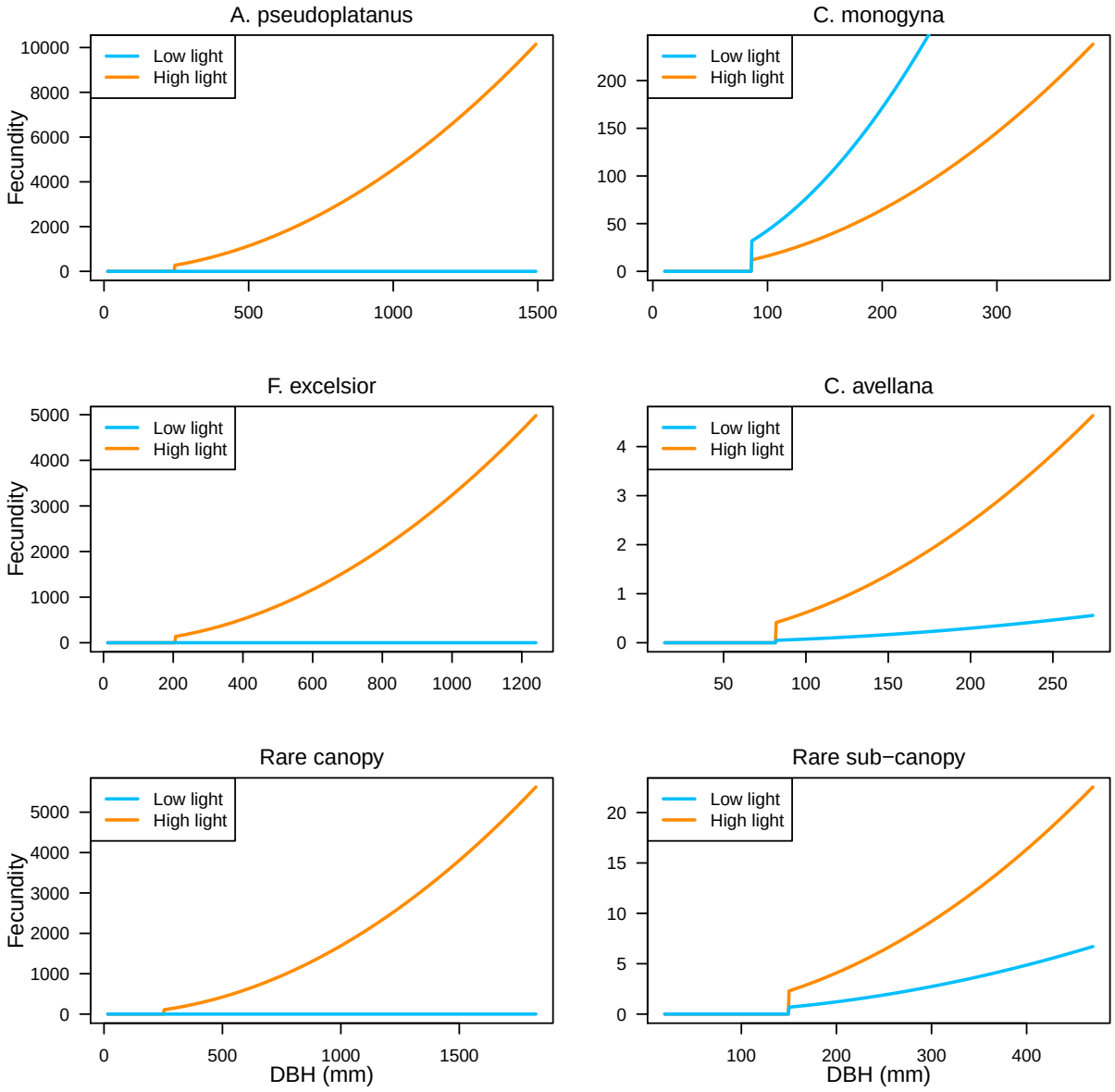


Figure D.7: Fecundity function for each species. Per capita reproductive rate scales with BA and depends on light environment. There is a reproductive threshold below which individuals cannot reproduce, calculated as the 0.8th quantile of the DBH data for each species. Individuals of species capable of reaching the canopy (*A. pseudoplatanus*, *F. excelsior* and 'rare canopy') only reproduce in the high light.

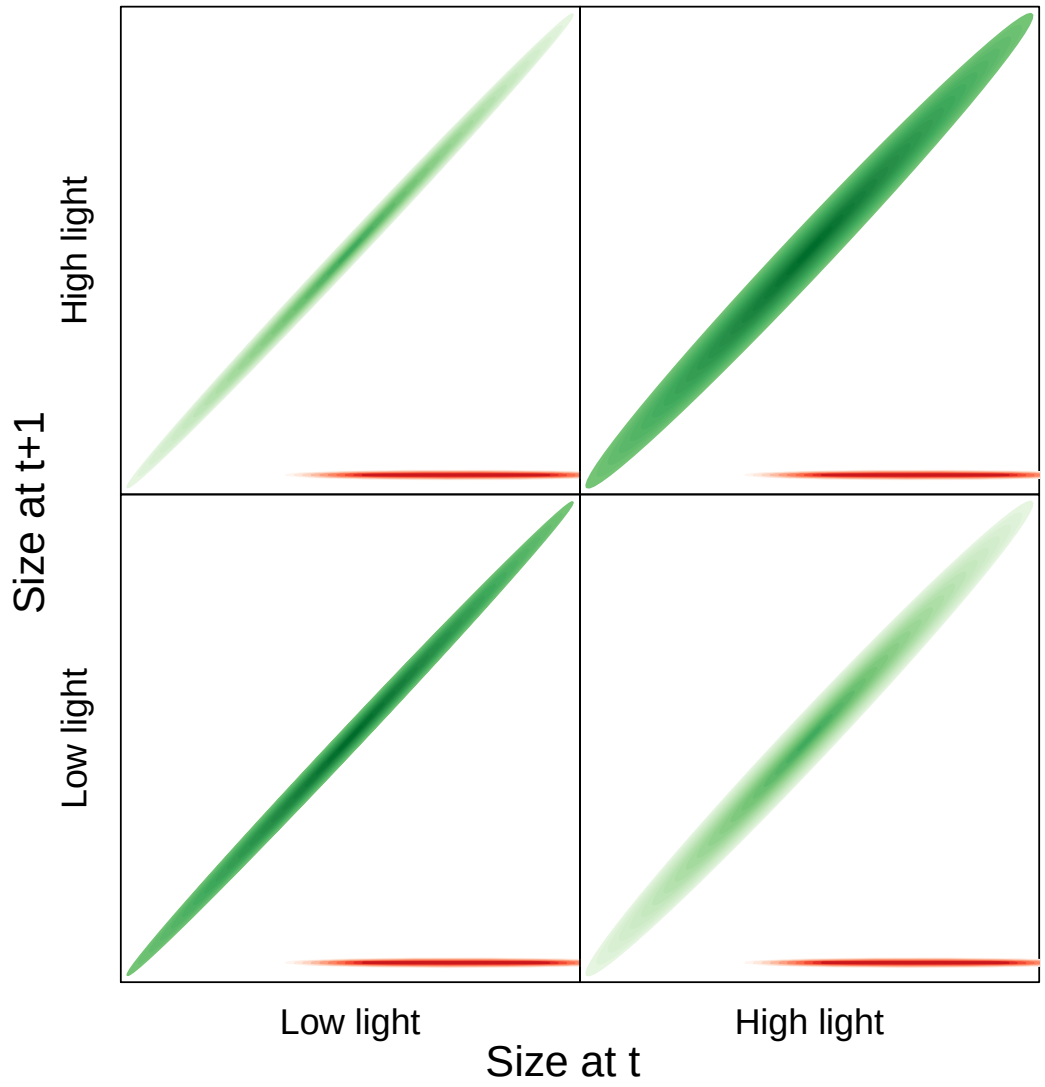


Figure D.8: Schematic of the megamatrix that moves individuals between sizes and light environments. High probabilities are shown with darker colours. Each year individuals increase in size, shown by the green diagonal lines. Individuals in the high light environment grow faster, with greater variance, shown by the wider ellipse. Most individuals remain in their light environment, but can move between light environments, shown by the paler ellipses in the top left and bottom right panels. Individuals larger than a reproductive size threshold produce offspring of small sizes, shown by the red ellipses. Offspring are distributed between light environments with probabilities equal to transition probabilities of adults between light environments.

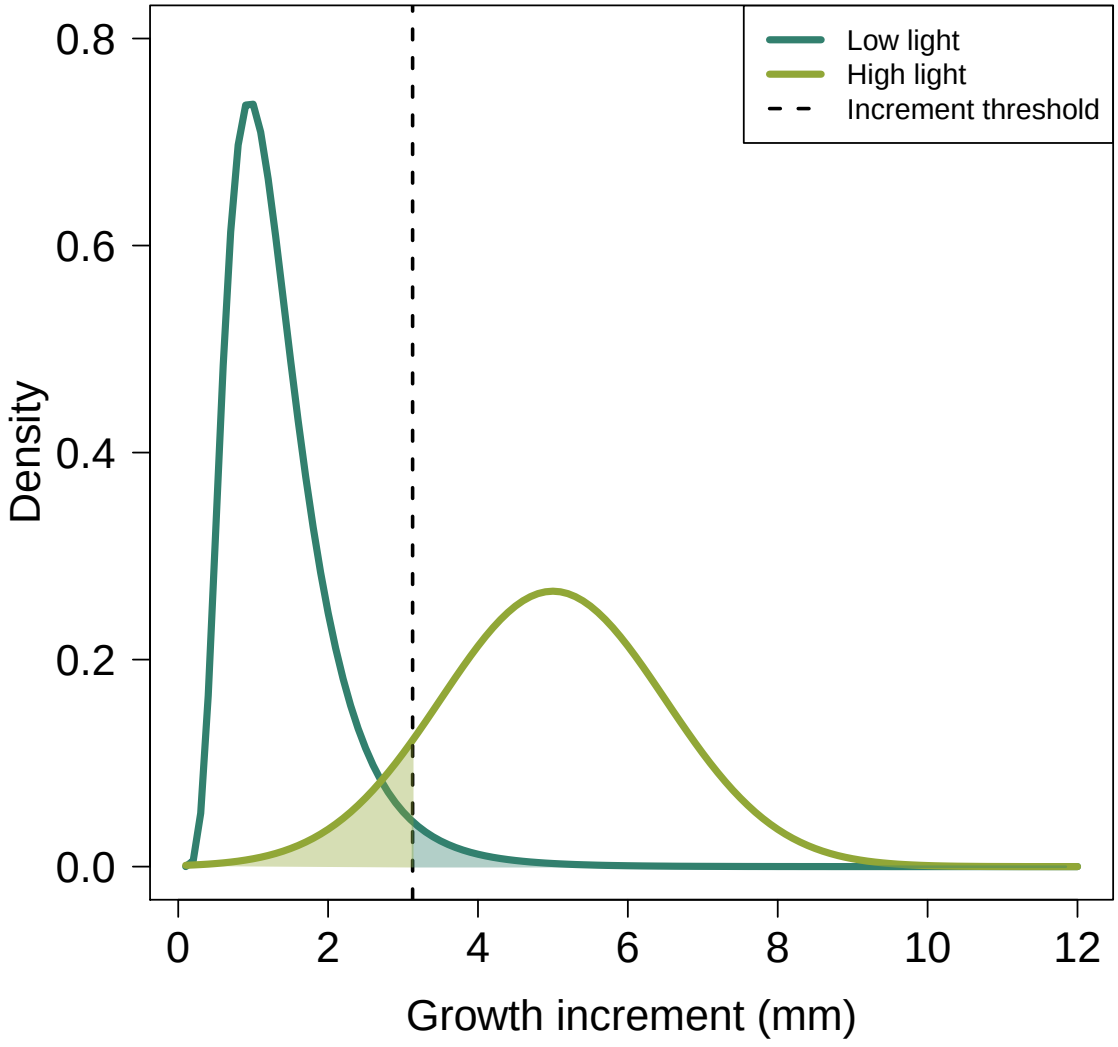


Figure D.9: Schematic of the transition probabilities between light environments used to construct the megamatrices. The transition probabilities between light environments are given by the overlap of each growth distribution with the 95th percentile of all increment data.

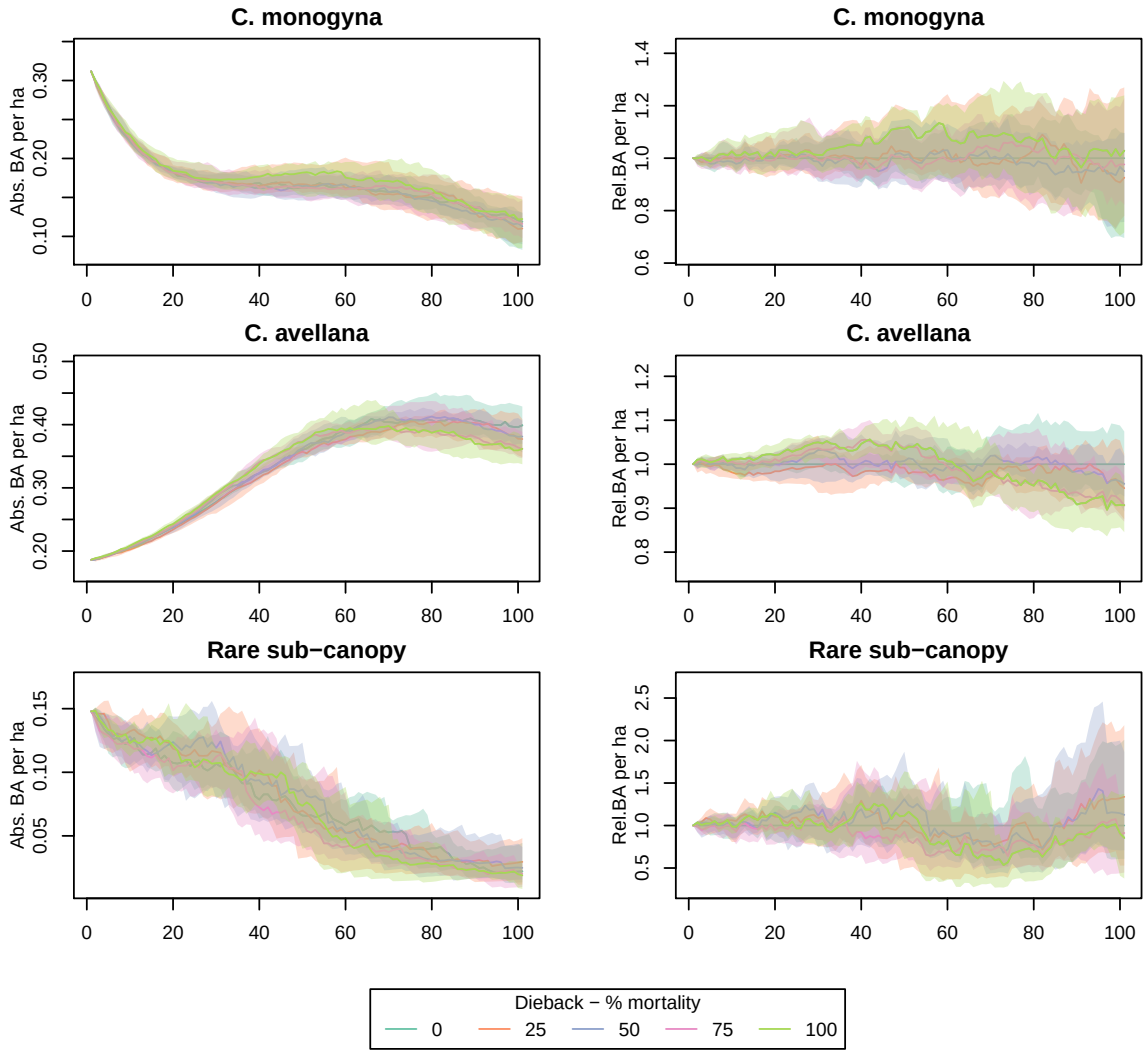


Figure D.10: Basal area (BA m^2 ha^{-1}) of the sub-canopy species through time under each mortality scenario. Left hand panels show absolute BA m^2 ha^{-1}), while right hand panels show BA m^2 ha^{-1}) relative to the 0% mortality scenario (i.e. scenario / 0% mortality). Shading depicts the 5th and 95th percentiles from 10 runs of each scenario. Medians are shown by darker lines. Mortality scenarios did not have much effect on the BA of sub-canopy species, unlike the remaining canopy species.

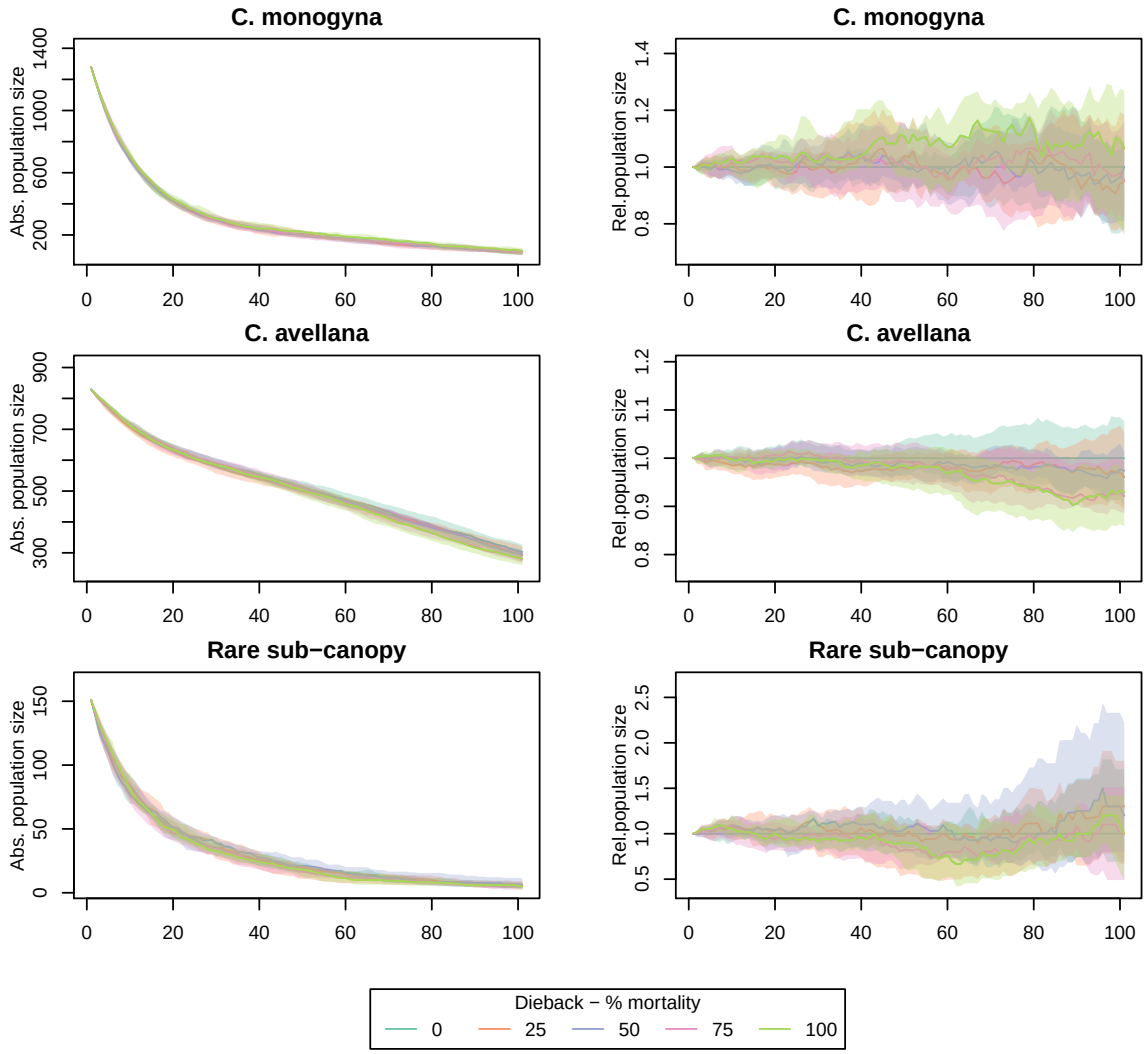


Figure D.11: Population size of sub-canopy species through time under each mortality scenario. Left hand panels show absolute population size while right hand panels show population size relative to the 0% mortality scenario (i.e. scenario / 0% mortality). Shading depicts the 5th and 95th percentiles from 10 simulations of each scenario. Medians are shown by darker lines. The population of sub-canopy species decreased in all mortality simulations.

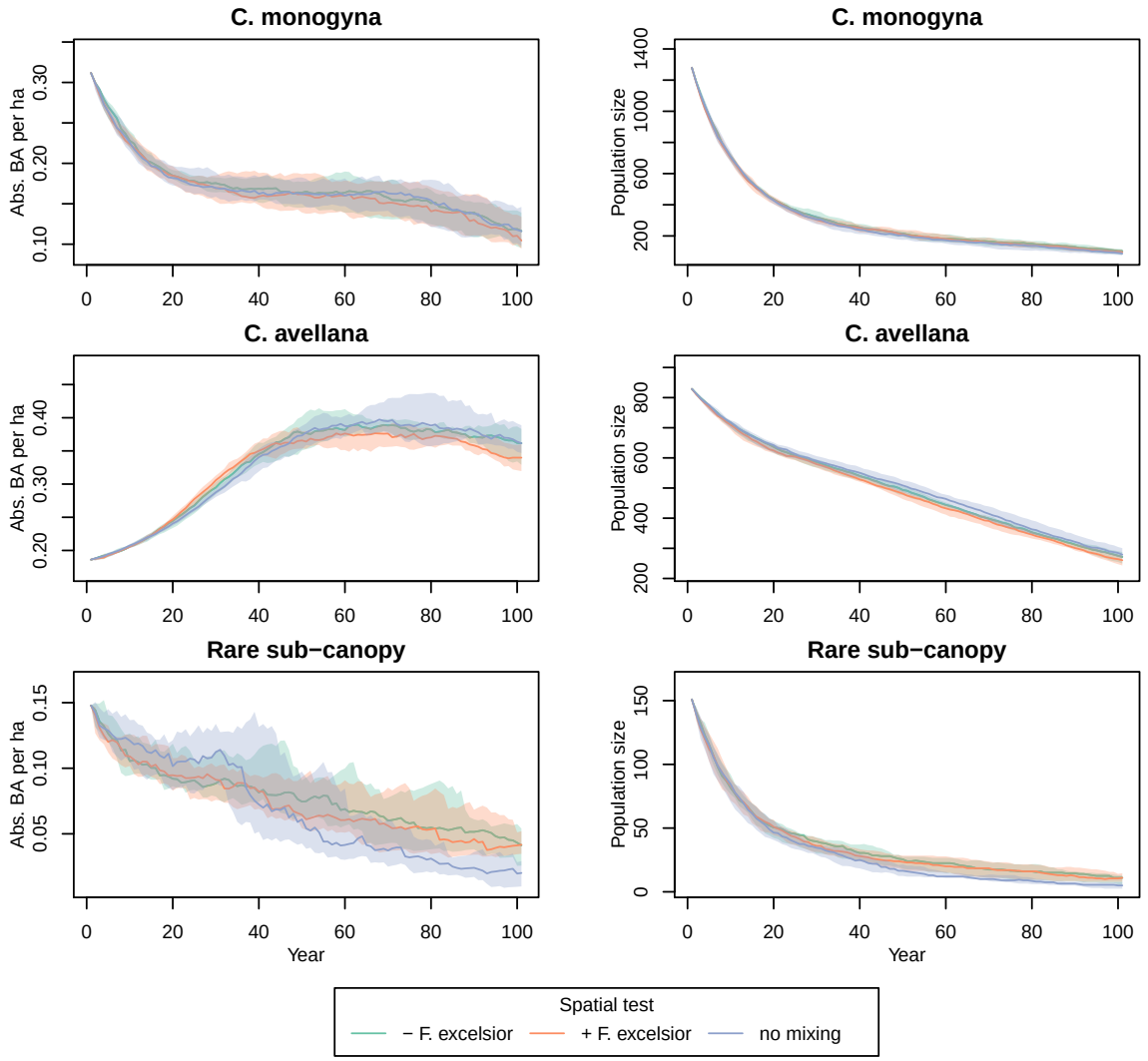


Figure D.12: Results of the spatial randomisation tests showing basal area (BA m^2 ha^{-1}) (left hand panels) and population size (right hand panels) of sub-canopy species through time. Individuals were reassigned paired coordinates, with *F. excelsior* either included in the mixing (+ *F. excelsior*) or excluded (- *F. excelsior*). Spatial tests were run at 75% *F. excelsior* mortality which is also plotted for comparison (no mixing). Shading depicts the 5th and 95th percentiles from 10 runs of each scenario. Medians are shown by darker lines. Spatial randomisation had very little effect on the dynamics of sub-canopy species.

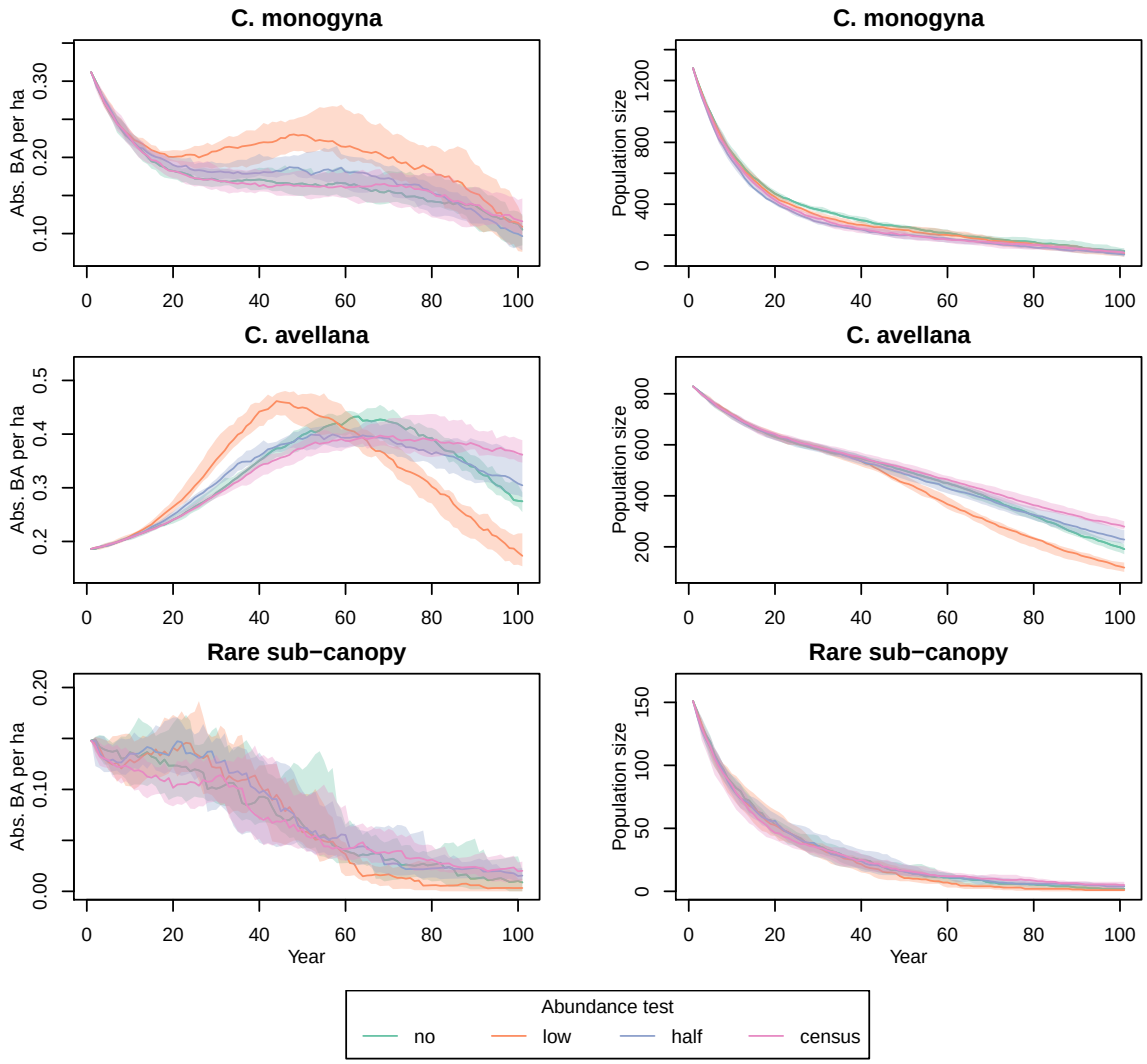


Figure D.13: Results of the abundance tests showing basal area (BA m^2 ha^{-1}) (left hand panel) and population size (right hand panel) of sub-canopy species through time. Shading depicts the 5th and 95th percentiles from 10 runs of each scenario. Medians are shown by darker lines. The coordinates of stems remained unchanged from the census data in order to maintain the size and spatial distribution of the forest but the species identity of *A. pseudoplatanus* and 'rare canopy' species were mixed to test the invasion potential of *A. pseudoplatanus*. The ratio of *A. pseudoplatanus* to 'rare canopy' was no (0:1), low (1:9) or half (1:1). The abundance tests were run at 75% *F. excelsior* mortality, which is also plotted for comparison (census). The population size of all sub-sub canopy species declined through time. *Corylus avellana* individuals grew for the first 50 years (shown by the increase in BA) but the continuous population decline shows that recruitment was low.

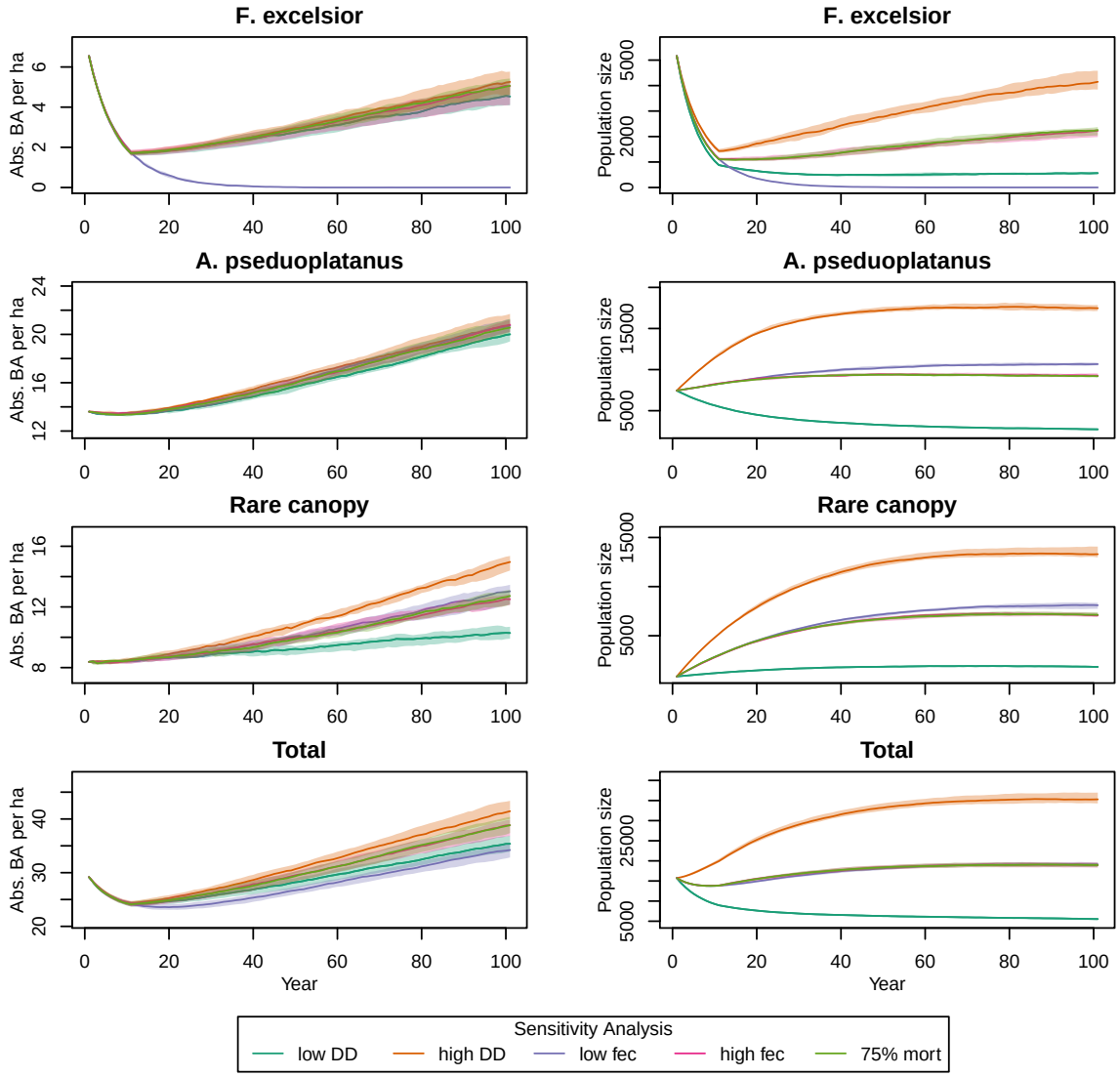


Figure D.14: Results of the sensitivity analysis, showing the basal area (BA m^2 ha^{-1}) and population size of canopy species through time. Shading depicts the 5th and 95th percentiles from 10 runs of each scenario. Medians are shown with darker lines. With the exception of *F. excelsior*, density dependence has a greater impact on BA than fecundity parameters.

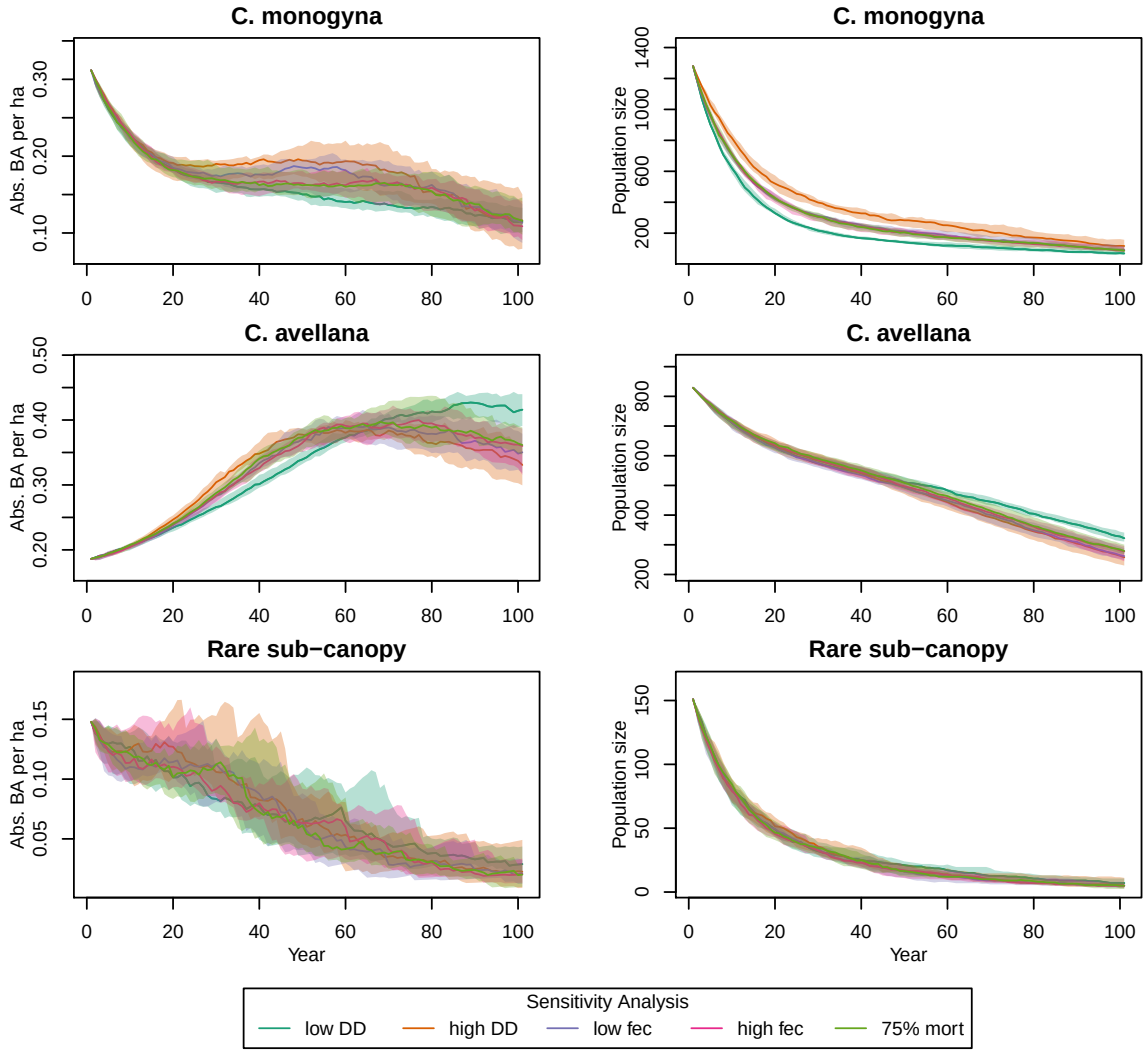


Figure D.15: Results of the sensitivity analysis, showing the basal area (BA m^2 ha^{-1}) and population size of sub-canopy species through time. Shading depicts the 5th and 95th percentiles from 10 runs of each scenario. Medians are shown by darker lines. Density dependence has a greater impact on BA than fecundity parameters but neither treatment influenced sub-canopy species as much as canopy species.

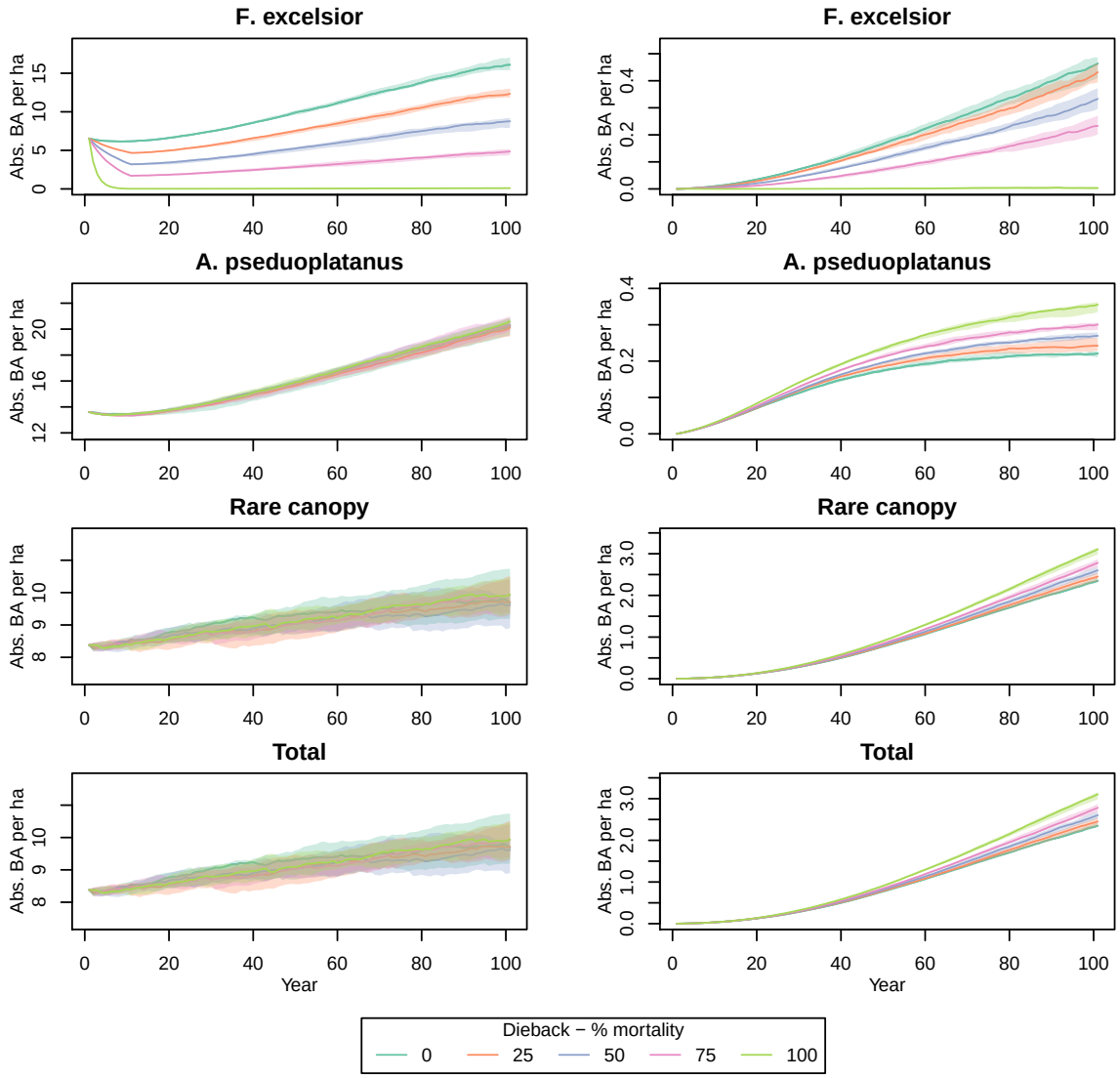


Figure D.16: Basal area (BA m^2 ha^{-1}) of the canopy species under each mortality scenario separated by recruits (right hand panel) and existing individuals (left hand panel). Shading depicts the 5th and 95th percentiles from 10 runs of each scenario. Medians are shown by darker lines. Total refers to the total BA of canopy and sub-canopy species. Over the course of 100 years the BA of the plot increases by 3 m^2 ha^{-1} due to the addition and growth of new recruits. The contribution to BA by *A. pseudoplatanus* and 'rare canopy' recruits is greater in high ash mortality scenarios.

	Number of individuals	**Pooled group**
Acer campestre	120	Canopy
Acer pseudoplatanus	7444	-
Betula spp.	79	Canopy
Carpinus betulus	1	Sub-canopy
Castanea sativa	1	Canopy
Cornus sanguinea	3	Sub-canopy
Corylus avellana	829	-
Crataegus monogyna	1280	-
Euonymus europaeus	22	Sub-canopy
Fagus sylvatica	197	Canopy
Frangula alnus	3	Sub-canopy
Fraxinus excelsior	5162	-
Ilex aquifolium	5	Sub-canopy
Larix decidua	83	Canopy
Picea abies	9	Canopy
Pinus sylvestris	1	Canopy
Prunus avium	3	Sub-canopy
Prunus spinosa	26	Sub-canopy
Pseudotsuga menziesii	1	Canopy
Quercus robur	362	Canopy
Salix spp.	28	Sub-canopy
Sambucus nigra	59	Sub-canopy
Taxus baccata	1	Sub-canopy
Tilia x europaea	3	Canopy

Table D.1: Population size and species groupings

	Slope	Significance
A. pseduoplatanus	-94.21	***
C. monogyna	-69.9	***
F. excelsior	-354.37	***
C. avellana	-62.52	**
Canopy	-264.37	***
Sub-canopy	-158.42	*

Table D.2: Slopes and statistical significance of the relationship between competition and growth for each species. Significance codes: 0 ***, 0.001 **, 0.01 *, 0.05, >0.05 -

D.0.1 Vital rates parameters

	L1	K1	ip1	r1	theta1	L2	K2	ip2	r2	theta2	surv.thresh
A. pseduoplatanus	0.94	0.99	165.78	1.11	49.99	0.58	0.99	1435.09	-10.31	246.08	730.84
C. monogyna	0.90	0.99	99.96	0.97	4.94	0.87	0.99	352.29	-6.82	323.00	191.42
F.excelsior	0.94	0.99	283.92	1.01	16.71	0.63	0.99	1128.57	-8.56	182.29	567.03
C. avellana	0.97	0.99	68.38	1.30	2.96	0.72	0.99	245.24	-17.34	248.63	137.12
Rare canopy	0.98	0.99	437.88	1.08	59.64	0.67	0.99	1670.72	-6.82	251.63	910.80
Rare sub-canopy	0.90	0.99	120.00	0.82	15.20	0.87	0.99	370.58	-14.69	200.70	234.29

Table D.3: Survival Parameters. L = lower asymptote, K = upper asymptote, p = inflection point, theta = symmetry of change, r = rate of change, S.thresh = the meeting point of the two curves. 1 denotes the small survival curve, 2 denotes the large survival curve

	Lognorm Mean	Lognorm SD	Truncnom Mean	Truncnorm SD	Fast growth quantile
A. pseduoplatanus	-0.26	0.63	-13.90	7.67	0.95
C. monogyna	-0.42	0.57	3.37	1.67	0.95
F.excelsior	0.05	0.84	1.37	7.50	0.95
C. avellana	-0.23	0.66	-0.27	7.70	0.95
Rare canopy	0.19	0.81	-11.71	7.43	0.95
Rare sub-canopy	-0.18	1.02	-39.30	28.29	0.95

Table D.4: Growth Parameters. LN mean = lognormal mean, LN SD = lognormal standard deviation, TN Mean = truncated normal mean, TN SD = truncated normal standard deviation, Quantile = quantile for dividing the population in order to fit the two curves

	Low light fec	High light fec	Reproductive threshold
A. pseduoplatanus	0.00	579.54	242.50
C. monogyna	545.82	205.99	250.00
F.excelsior	0.00	412.19	81.50
C. avellana	0.94	7.84	86.00
Rare canopy	0.00	215.38	205.00
Rare sub-canopy	3.87	13.01	149.20

Table D.5: Fecundity Parameters. Parameters get multiplied by BA to give per capita reproductive output. The reproductive threshold represents the size at which individuals begin to produce offspring

D.0.2 Population sizes

	1	25	50	75	100
A. pseduoplatanus	7444.00	8294.50	7855.00	7457.50	7099.50
C. monogyna	1280.00	346.50	199.50	138.50	93.00
F.excelsior	5162.00	3426.00	4071.50	4799.50	5300.50
C. avellana	829.00	608.00	512.00	407.50	305.00
Canopy	856.00	4715.00	6142.00	6330.00	6010.50
Sub-canopy	151.00	42.00	20.00	11.00	5.00
Total	15722.00	17409.00	18836.00	19100.00	18760.00

Table D.6: Population size of each species every 25 years in the 0 percent mortality scenario

	1	25	50	75	100
A. pseduoplatanus	7444.00	8490.00	8250.50	7908.50	7599.00
C. monogyna	1280.00	341.00	207.50	132.50	87.50
F.excelsior	5162.00	2764.50	3403.00	4086.50	4596.50
C. avellana	829.00	601.50	501.50	405.50	296.00
Canopy	856.00	4799.50	6228.00	6495.50	6340.00
Sub-canopy	151.00	44.00	19.50	10.50	6.50
Total	15722.00	16988.50	18656.50	19058.00	18871.00

Table D.7: Population size of each species every 25 years in the 25 percent mortality scenario

	1	25	50	75	100
A. pseduoplatanus	7444.00	8675.00	8779.00	8571.00	8364.00
C. monogyna	1280.00	350.00	199.50	136.00	89.50
F.excelsior	5162.00	2026.50	2512.50	3107.00	3583.00
C. avellana	829.00	607.50	508.50	400.00	298.00
Canopy	856.00	4978.50	6508.50	6804.00	6556.00
Sub-canopy	151.00	43.50	21.00	10.00	6.50
Total	15722.00	16594.00	18497.50	19064.00	18910.00

Table D.8: Population size of each species every 25 years in the 50 percent mortality scenario

	1	25	50	75	100
A. pseduoplatanus	7444.00	9017.00	9376.00	9306.50	9223.50
C. monogyna	1280.00	357.00	205.00	140.50	91.00
F.excelsior	5162.00	1146.50	1564.50	1929.00	2224.50
C. avellana	829.00	613.00	508.50	390.00	284.50
Canopy	856.00	5059.00	6707.50	7180.50	7144.50
Sub-canopy	151.00	39.00	16.50	9.00	5.00
Total	15722.00	16210.50	18347.00	18960.00	18984.00

Table D.9: Population size of each species every 25 years in the 75 percent mortality scenario

	1	25	50	75	100
A. pseduoplatanus	7444.00	9538.00	10359.00	10605.50	10691.00
C. monogyna	1280.00	358.50	221.00	159.00	101.50
F.excelsior	5162.00	14.00	27.00	43.50	51.50
C. avellana	829.00	604.50	504.00	387.50	284.50
Canopy	856.00	5337.00	7217.00	7940.00	8106.00
Sub-canopy	151.00	39.00	18.00	8.50	5.50
Total	15722.00	15887.50	18353.00	19168.00	19229.00

Table D.10: Population size of each species every 25 years in the 100 percent mortality scenario

	1	25	50	75	100
A. pseduoplatanus	7444.00	10636.00	10975.00	10812.00	10567.00
C. monogyna	1280.00	322.00	199.00	136.00	94.00
F.excelsior	5162.00	1330.00	1644.00	1970.00	2093.00
C. avellana	829.00	566.00	448.00	332.00	235.00
Canopy	856.00	2158.00	2746.00	2925.00	3032.00
Sub-canopy	151.00	25.00	9.00	4.00	4.00
Total	15722.00	15062.00	16104.00	16265.00	16134.00

Table D.11: Population size of each species every 25 years in the spatial randomisation test including *F. excelsior* in the mixing

	1	25	50	75	100
A. pseduoplatanus	7444.00	10982.00	11342.00	11036.00	10626.00
C. monogyna	1280.00	342.00	202.00	138.00	90.00
F.excelsior	5162.00	1008.00	1325.00	1697.00	2030.00
C. avellana	829.00	560.00	432.00	332.00	234.00
Canopy	856.00	2197.00	2850.00	3152.00	3217.00
Sub-canopy	151.00	22.00	10.00	7.00	4.00
Total	15722.00	15144.00	16184.00	16372.00	16254.00

Table D.12: Population size of each species every 25 years in the spatial randomisation test excluding *F. excelsior* from the mixing

	1	25	50	75	100
A. pseduoplatanus	4140.00	8324.00	8862.00	8687.00	8339.00
C. monogyna	1280.00	338.00	198.00	135.00	78.00
F.excelsior	5162.00	1186.00	1639.00	2078.00	2425.00
C. avellana	829.00	612.00	486.00	348.00	232.00
Canopy	4160.00	6174.00	7110.00	7500.00	7708.00
Sub-canopy	151.00	42.00	16.00	6.00	4.00
Total	15722.00	16637.00	18352.00	18788.00	18826.00

Table D.13: Population size of each species every 25 years in the abundance test with equal starting population sizes of *A. pseudoplatanus* and 'rare canopy' species

	1	25	50	75	100
A. pseduoplatanus	838.00	2326.00	2637.00	2636.00	2526.00
C. monogyna	1280.00	381.00	232.00	154.00	80.00
F.excelsior	5162.00	1628.00	2438.00	3036.00	3466.00
C. avellana	829.00	612.00	450.00	264.00	123.00
Canopy	7462.00	14410.00	18041.00	19796.00	20379.00
Sub-canopy	151.00	42.00	10.00	3.00	1.00
Total	15722.00	19383.00	23698.00	25754.00	26558.00

Table D.14: Population size of each species every 25 years in the abundance test with *A. pseudoplatanus* and 'rare canopy' species starting in the ratio 1:9

	1	25	50	75	100
C. monogyna	1280.00	409.00	252.00	162.00	100.00
F.excelsior	5162.00	1580.00	2278.00	2904.00	3421.00
C. avellana	829.00	604.00	499.00	354.00	198.00
Canopy	8300.00	17924.00	23392.00	25924.00	26890.00
Sub-canopy	151.00	44.00	16.00	6.00	2.00
Total	15722.00	20525.00	26407.00	29304.00	30542.00

Table D.15: Population size of each species every 25 years in the abundance test with *A. pseudoplatanus* absent

D.0.3 Basal areas

	1	25	50	75	100
A. pseduoplatanus	13.61	14.12	16.01	18.29	20.35
C. monogyna	0.31	0.17	0.16	0.15	0.12
F.excelsior	6.55	7.06	10.08	13.43	16.48
C. avellana	0.19	0.26	0.36	0.41	0.40
Canopy	8.38	9.04	10.09	11.07	12.15
Sub-canopy	0.15	0.11	0.07	0.04	0.02
Total	29.18	30.66	36.82	43.43	49.98

Table D.16: Basal Area of each species every 25 years in the 0 percent mortality scenario

	1	25	50	75	100
A. pseduoplatanus	13.61	14.01	15.82	17.96	20.21
C. monogyna	0.31	0.18	0.17	0.15	0.11
F.excelsior	6.55	5.36	7.68	10.27	12.62
C. avellana	0.19	0.25	0.36	0.40	0.38
Canopy	8.38	8.92	9.84	10.99	12.13
Sub-canopy	0.15	0.12	0.07	0.04	0.03
Total	29.18	28.74	33.90	39.80	45.55

Table D.17: Basal Area of each species every 25 years in the 25 percent mortality scenario

	1	25	50	75	100
A. pseduoplatanus	13.61	14.14	16.03	18.44	20.51
C. monogyna	0.31	0.17	0.16	0.15	0.12
F.excelsior	6.55	3.71	5.35	7.33	9.05
C. avellana	0.19	0.26	0.36	0.41	0.38
Canopy	8.38	8.94	9.85	10.91	12.09
Sub-canopy	0.15	0.12	0.09	0.04	0.03
Total	29.18	27.34	31.98	37.52	42.39

Table D.18: Basal Area of each species every 25 years in the 50 percent mortality scenario

	1	25	50	75	100
A. pseduoplatanus	13.61	14.09	15.97	18.35	20.50
C. monogyna	0.31	0.17	0.16	0.16	0.12
F.excelsior	6.55	1.98	2.91	4.00	5.02
C. avellana	0.19	0.26	0.37	0.39	0.36
Canopy	8.38	8.86	9.88	11.25	12.65
Sub-canopy	0.15	0.11	0.06	0.03	0.02
Total	29.18	25.46	29.32	33.97	38.72

Table D.19: Basal Area of each species every 25 years in the 75 percent mortality scenario

	1	25	50	75	100
A. pseduoplatanus	13.61	14.17	16.14	18.46	20.81
C. monogyna	0.31	0.18	0.18	0.17	0.12
F.excelsior	6.55	0.02	0.05	0.07	0.11
C. avellana	0.19	0.27	0.37	0.39	0.36
Canopy	8.38	8.91	10.00	11.57	12.92
Sub-canopy	0.15	0.10	0.07	0.03	0.02
Total	29.18	23.70	27.05	30.61	34.13

Table D.20: Basal Area of each species every 25 years in the 100 percent mortality scenario

	1	25	50	75	100
A. pseduoplatanus	16.88	17.49	19.60	21.71	23.89
C. monogyna	0.37	0.19	0.18	0.16	0.11
F.excelsior	6.55	1.95	2.89	3.97	5.06
C. avellana	0.23	0.26	0.33	0.34	0.30
Canopy	5.10	5.23	5.70	6.26	6.87
Sub-canopy	0.05	0.03	0.02	0.02	0.01
Total	29.18	25.15	28.43	32.47	35.97

Table D.21: Basal Area of each species every 25 years in spatial randomisation test including *F. excelsior*

	1	25	50	75	100
A. pseduoplatanus	15.59	16.12	18.21	20.36	22.55
C. monogyna	0.37	0.18	0.17	0.15	0.12
F.excelsior	8.33	2.49	3.37	4.36	4.39
C. avellana	0.23	0.27	0.34	0.34	0.30
Canopy	4.71	4.76	5.11	5.68	6.45
Sub-canopy	0.04	0.04	0.03	0.01	0.01
Total	29.18	23.83	27.25	30.82	34.08

Table D.22: Basal Area of each species every 25 years in spatial randomisation test excluding *F. excelsior*

	1	25	50	75	100
A. pseduoplatanus	11.04	11.56	12.93	14.24	15.29
C. monogyna	0.31	0.18	0.18	0.16	0.10
F.excelsior	6.55	1.98	2.96	4.19	5.28
C. avellana	0.19	0.28	0.39	0.38	0.31
Canopy	10.94	11.42	12.37	13.63	15.05
Sub-canopy	0.15	0.13	0.06	0.02	0.02
Total	29.18	25.68	29.03	33.09	36.52

Table D.23: Basal Area of each species every 25 years in the abundance test with *A. pseudoplatanus* and 'rare-canopy' species having equal starting population sizes

	1	25	50	75	100
A. pseduoplatanus	2.25	2.33	2.66	2.98	3.19
C. monogyna	0.31	0.20	0.23	0.19	0.11
F.excelsior	6.55	2.20	3.43	4.86	6.02
C. avellana	0.19	0.30	0.45	0.33	0.18
Canopy	19.73	20.83	23.27	26.53	30.24
Sub-canopy	0.15	0.14	0.06	0.01	0.00
Total	29.18	25.99	30.19	34.92	39.71

Table D.24: Basal Area of each species every 25 years in the abundance test with *A. pseudoplatanus* and 'rare canopy' species having starting populations sizes in the ratio 1:9

	1	25	50	75	100
C. monogyna	0.31	0.17	0.17	0.15	0.11
F.excelsior	6.55	2.01	2.91	4.03	4.98
C. avellana	0.19	0.26	0.40	0.41	0.28
Canopy	21.98	23.26	26.01	29.82	33.78
Sub-canopy	0.15	0.12	0.07	0.03	0.01
Total	29.18	25.82	29.61	34.52	39.35

Table D.25: Basal Area of each species every 25 years in the abundance test with *A. pseudoplatanus* absent

Appendix E

Chapter 4: Supplementary material

E.1 Vital rate parameter values for abundant Wytham species

Species	Census interval	K	p1	r1	p2	r2	Size threshold
Acer pseudoplatanus	2008 - 2010	0.99	-116.18	0.02	1931.72	-0.01	200.00
Corylus avellana	2008 - 2010	0.98	-35.83	0.07	346.46	-0.04	81.86
Crataegus monogyna	2008 - 2010	0.99	-7.59	0.13	459.57	-0.03	85.81
Fraxinus excelsior	2008 - 2010	0.99	-35.45	0.04	1627.68	-0.01	200.00
Quercus robur	2008 - 2010	0.98	-85.27	0.13	1955.99	-0.01	200.00

Table E.1: Parameters for the survival function fit to each Wytham species. K = upper asymptote, p = inflection point, r = rate of change. 1 and 2 denote the small and large survival curve respectively. The small and large curve meet at the size threshold

Species	Census interval	Alpha 1	Alpha 2	Beta 1	Beta 2	Size threshold
Acer pseudoplatanus	2008 - 2010	1.22	1.08	1.38	0.37	200.00
Corylus avellana	2008 - 2010	1.41	0.89	1.46	0.34	200.00
Crataegus monogyna	2008 - 2010	1.28	1.05	1.77	0.57	152.15
Fraxinus excelsior	2008 - 2010	1.20	1.74	1.00	0.33	82.23
Quercus robur	2008 - 2010	0.95	1.20	2.83	0.42	85.98

Table E.2: Parameters for the growth model fit to the Wytham species. Alpha and Beta are the shape and rate parameters of gramma distributions for the slow (1) and fast (2) distributions. The fast distribution was fit to individuals above the size threshold and the fastest 5% of individuals below the size threshold

E.2 Inferred effect of deer on abundant Wytham species

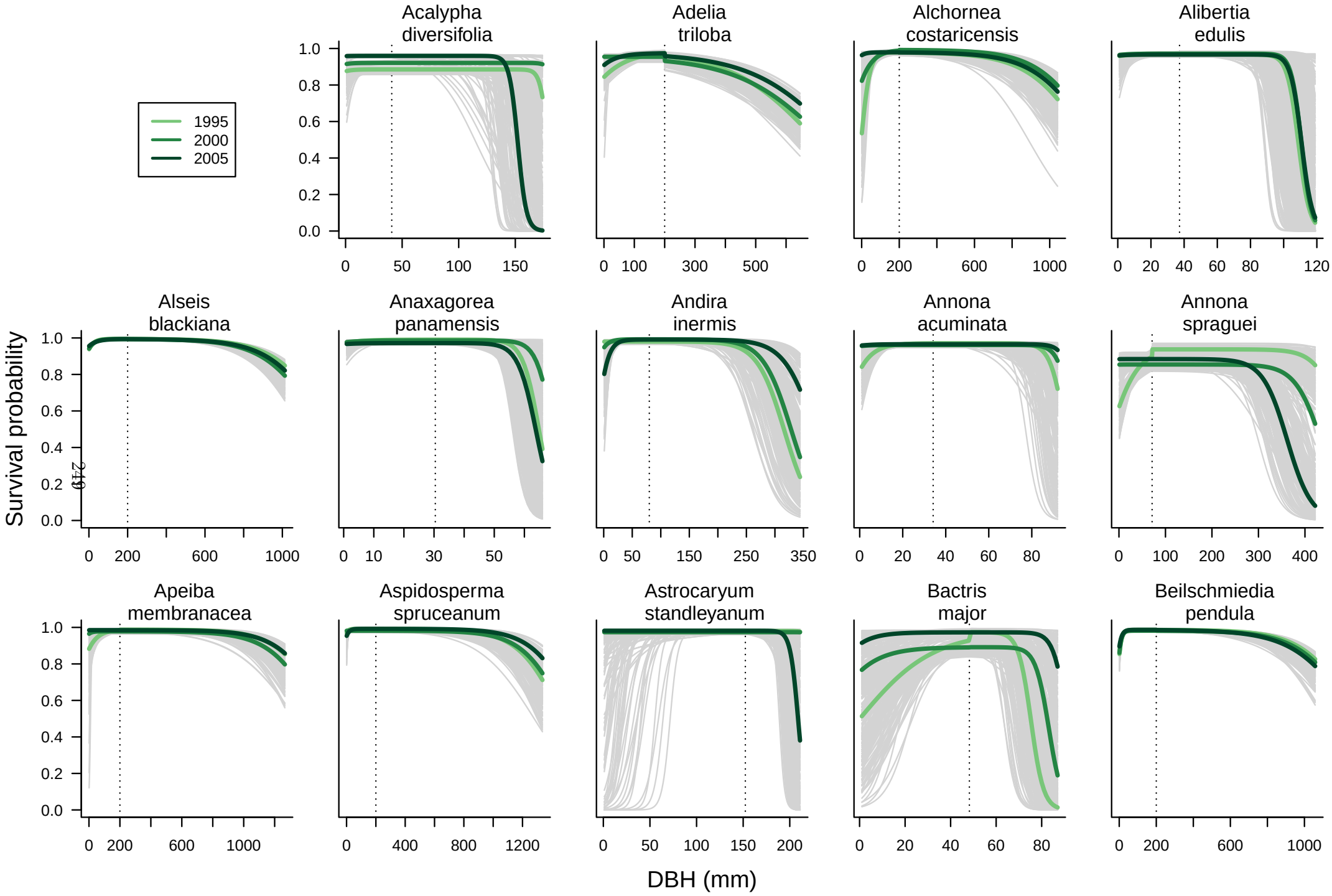
Species	Periodicity	Deer effect	Min survival	Max survival
Acer pseudoplatanus	183.0000	0.1600	0.7733	0.9918
Corylus avellana	30.0000	0.1400	0.7251	0.9996
Crataegus monogyna	32.0000	0.2500	0.5097	0.9990
Fraxinus excelsior	32.0000	0.1200	0.7669	0.9995
Quercus robur	14.0000	0.4500	0.1059	0.9942

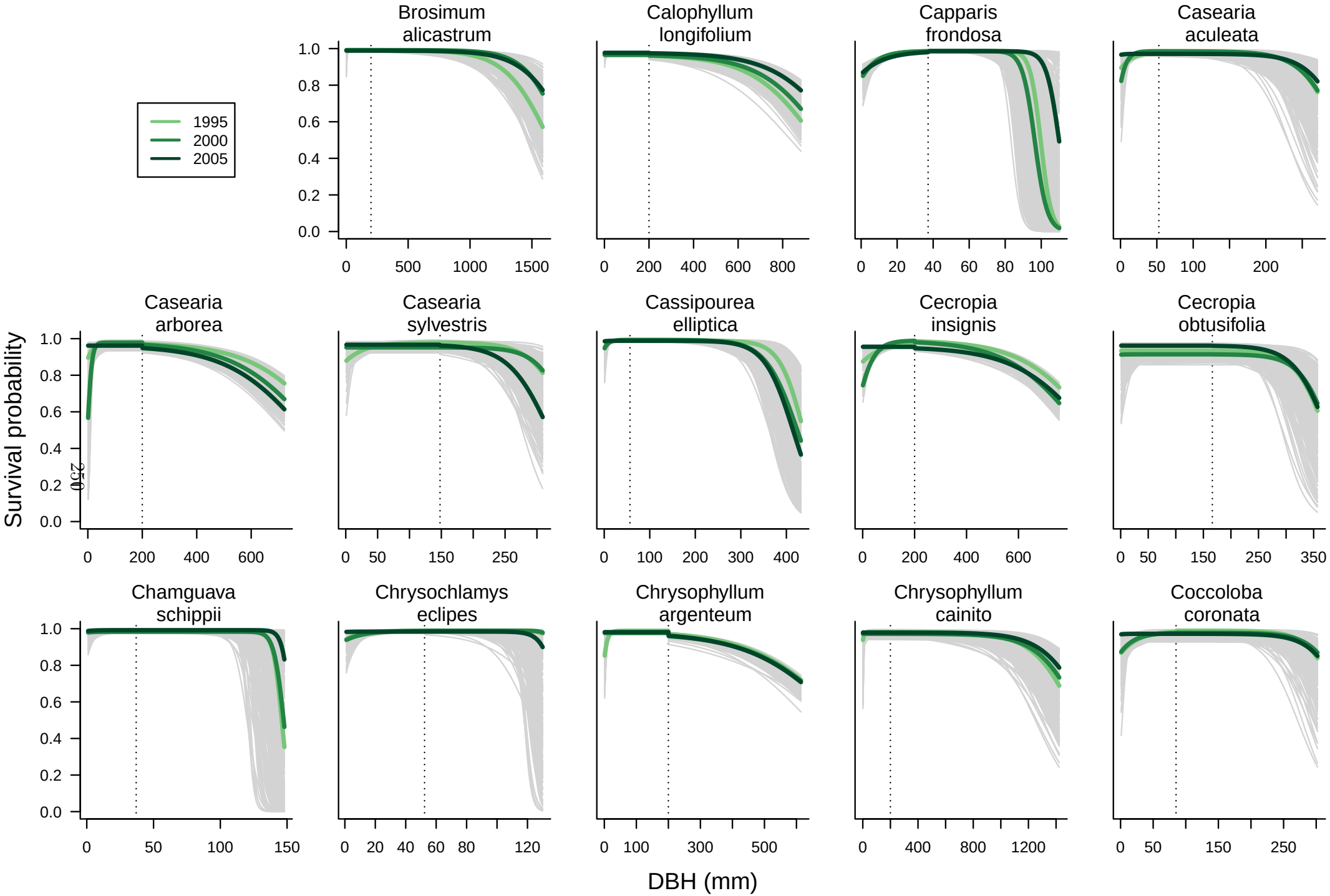
Table E.3: Inferred impact of deer browsing on juvenile survival over fifty years. The impact of deer was modelled with a sine wave with period defined by the Periodicity parameter and the amplitude defined by the Deer effect parameter. Survival of the smallest modelled size is inversely proportional to the sine wave of deer impact.

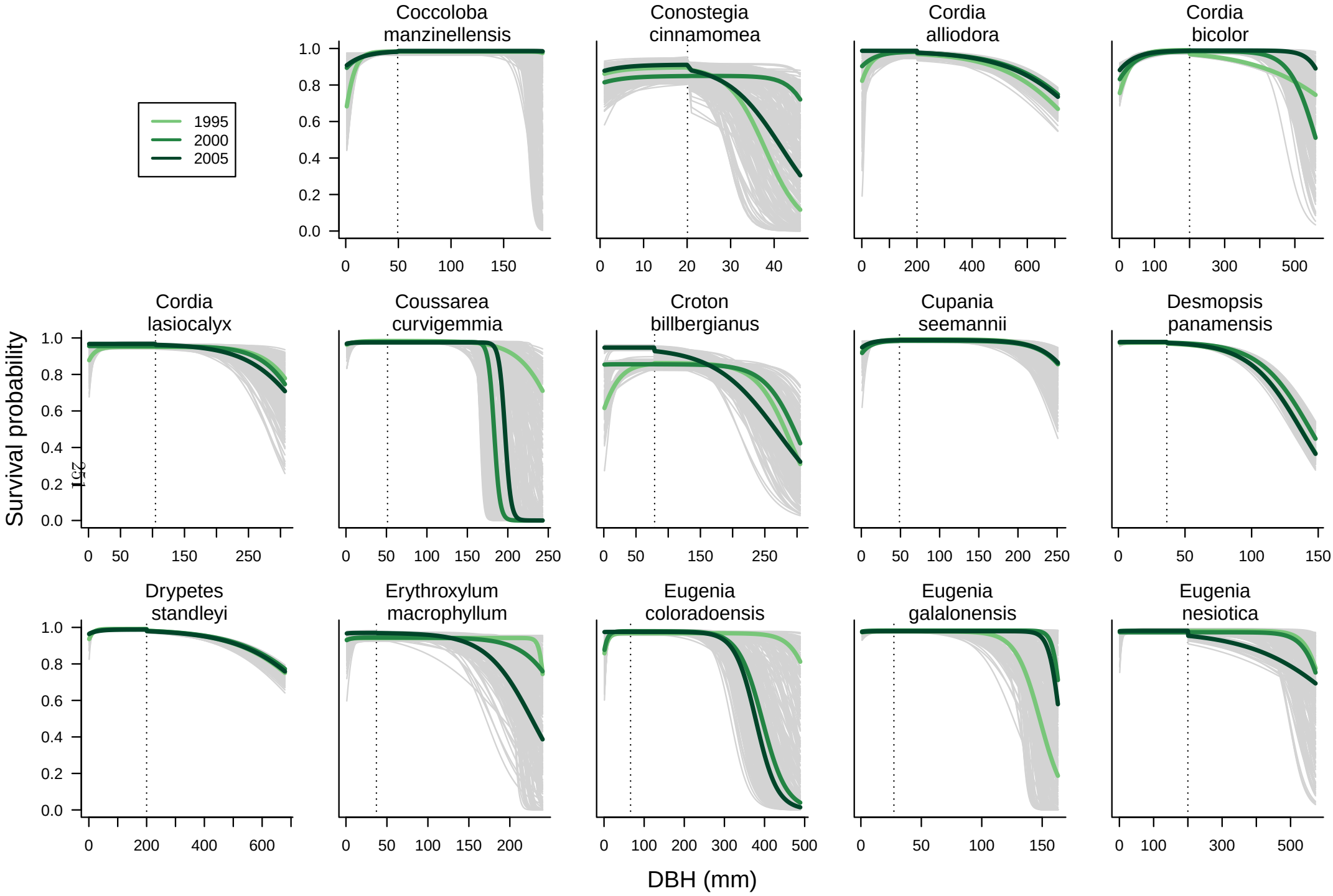
Appendix F

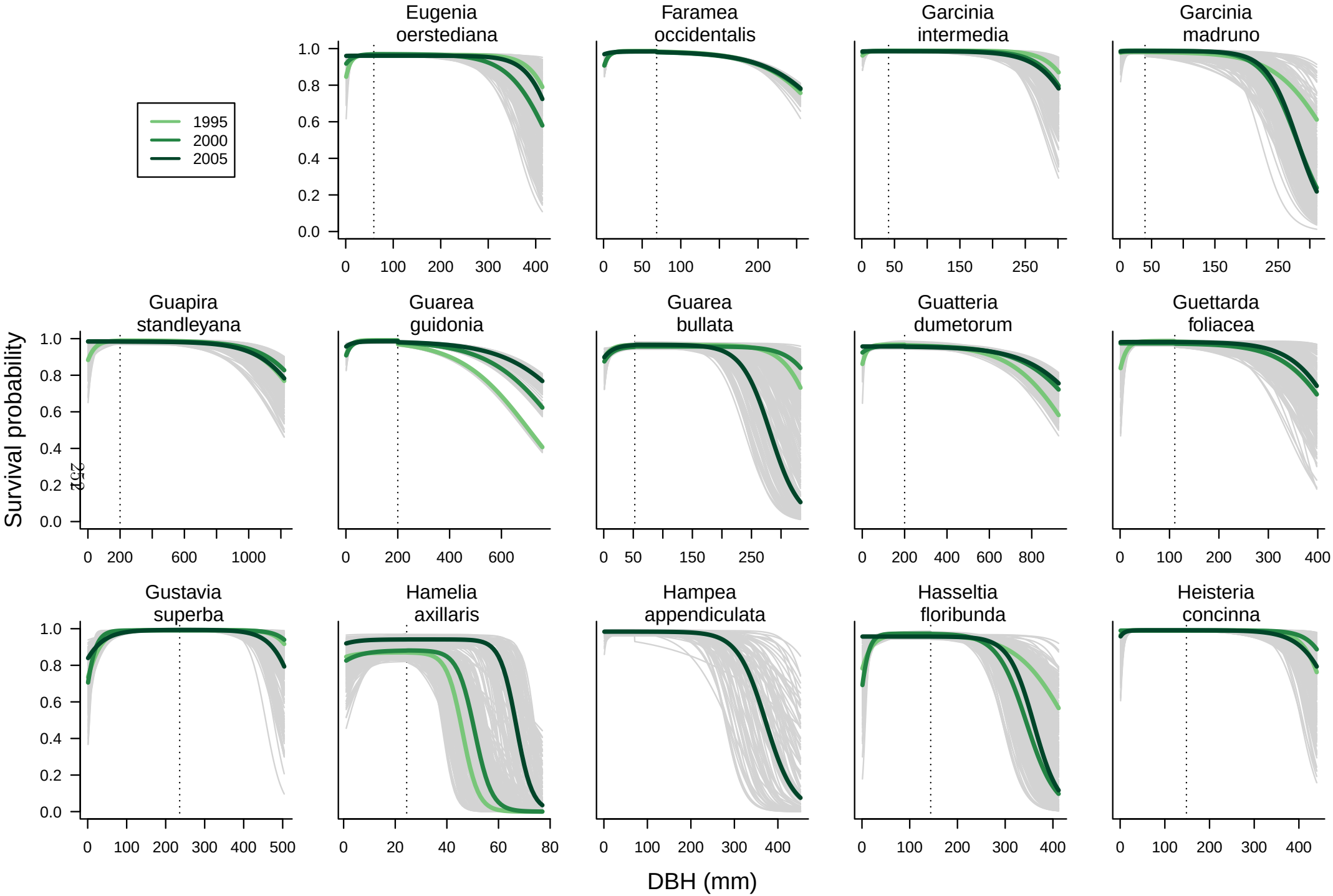
Chapter 5: Supplementary material

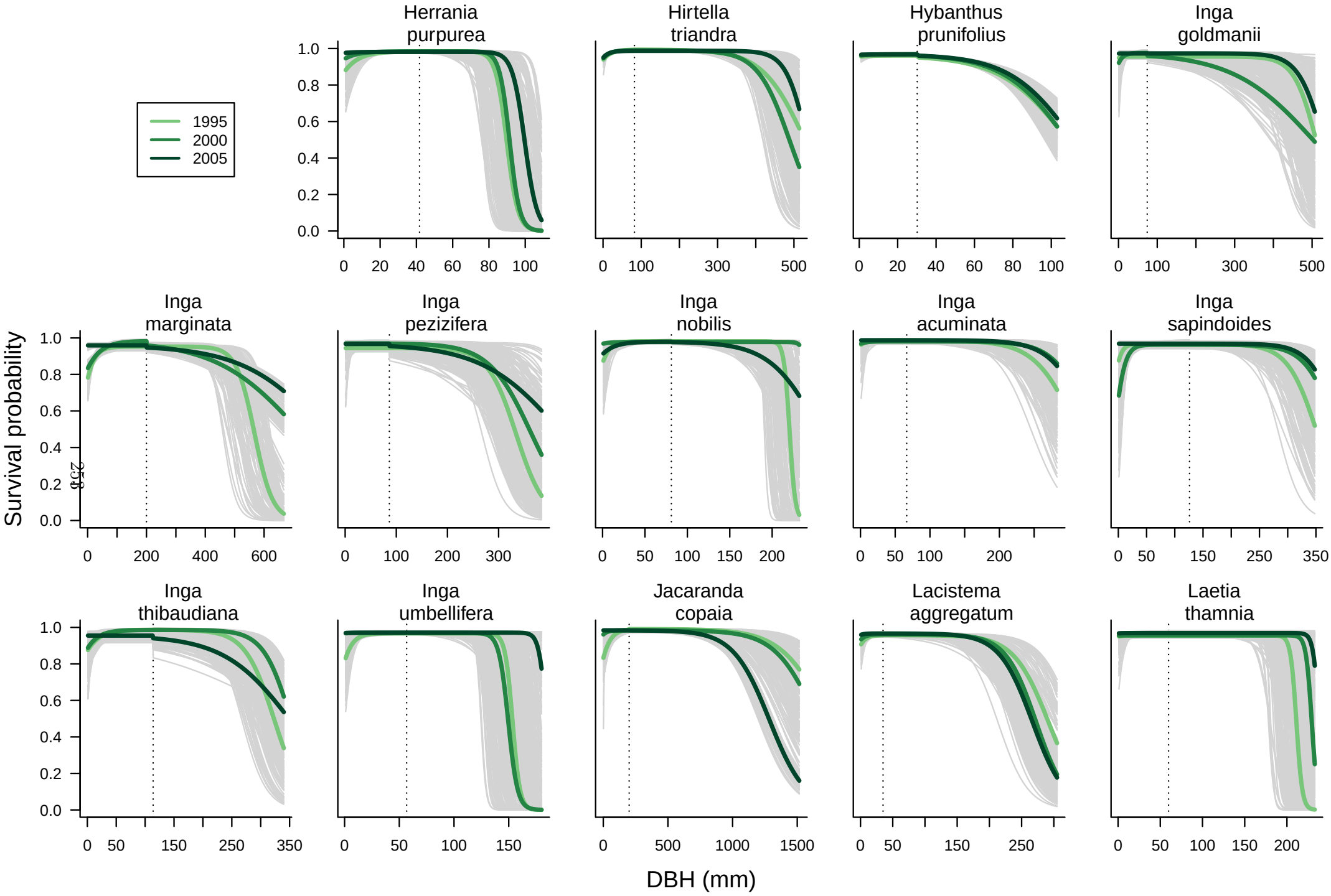
F.1 Diversity of growth and survival across species and through time

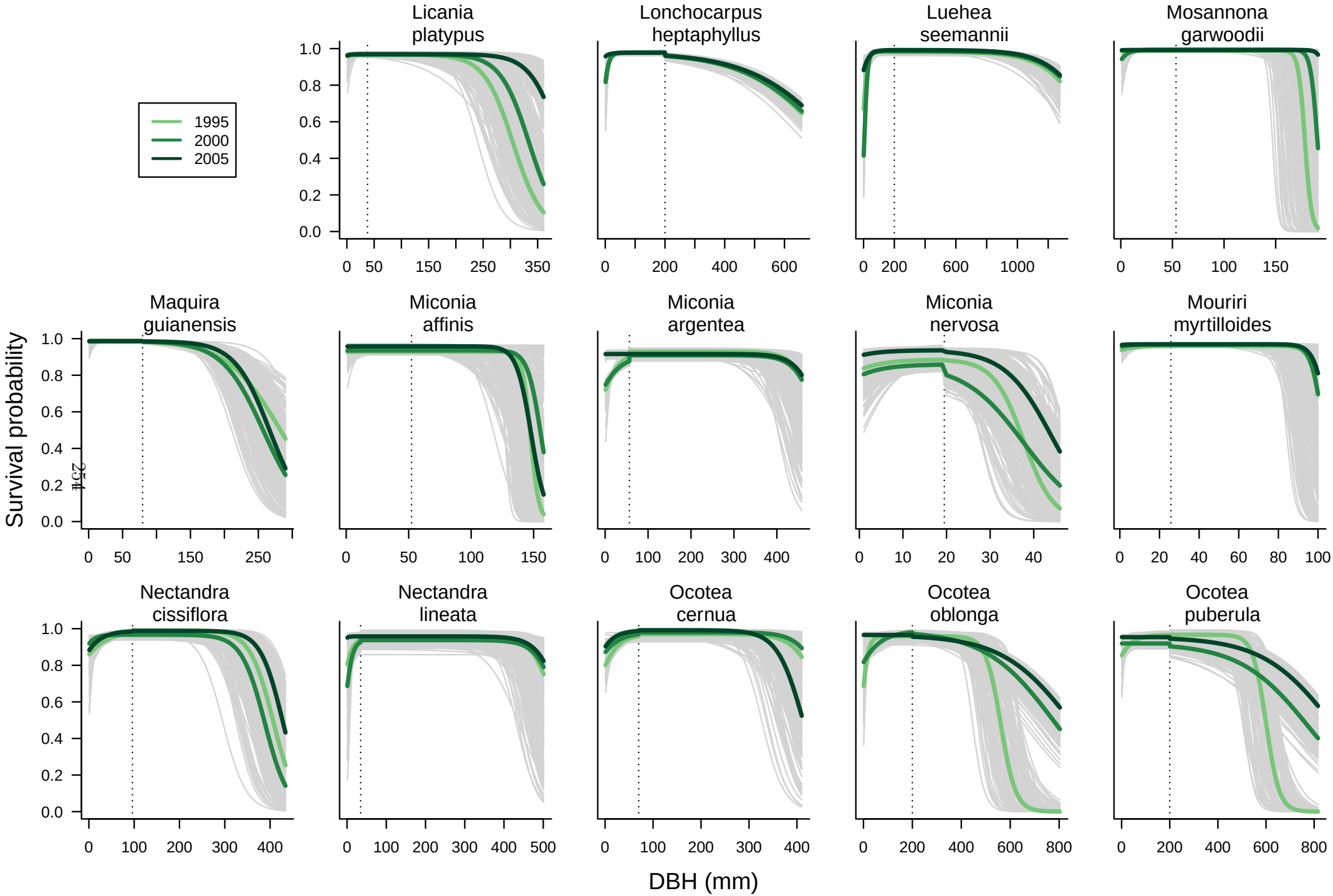

1995
2000
2005
Acalypha diversifolia
Adelia triloba
Alchornea costaricensis
Alibertia edulis
Alseis blackiana
Anaxagorea panamensis
Andira inermis
Annona acuminata
Annona spraguei
Apeiba membranacea
Aspidosperma spruceanum
Astrocaryum standleyanum
Bactris major
Beilschmiedia pendula
Survival probability
DBH (mm)

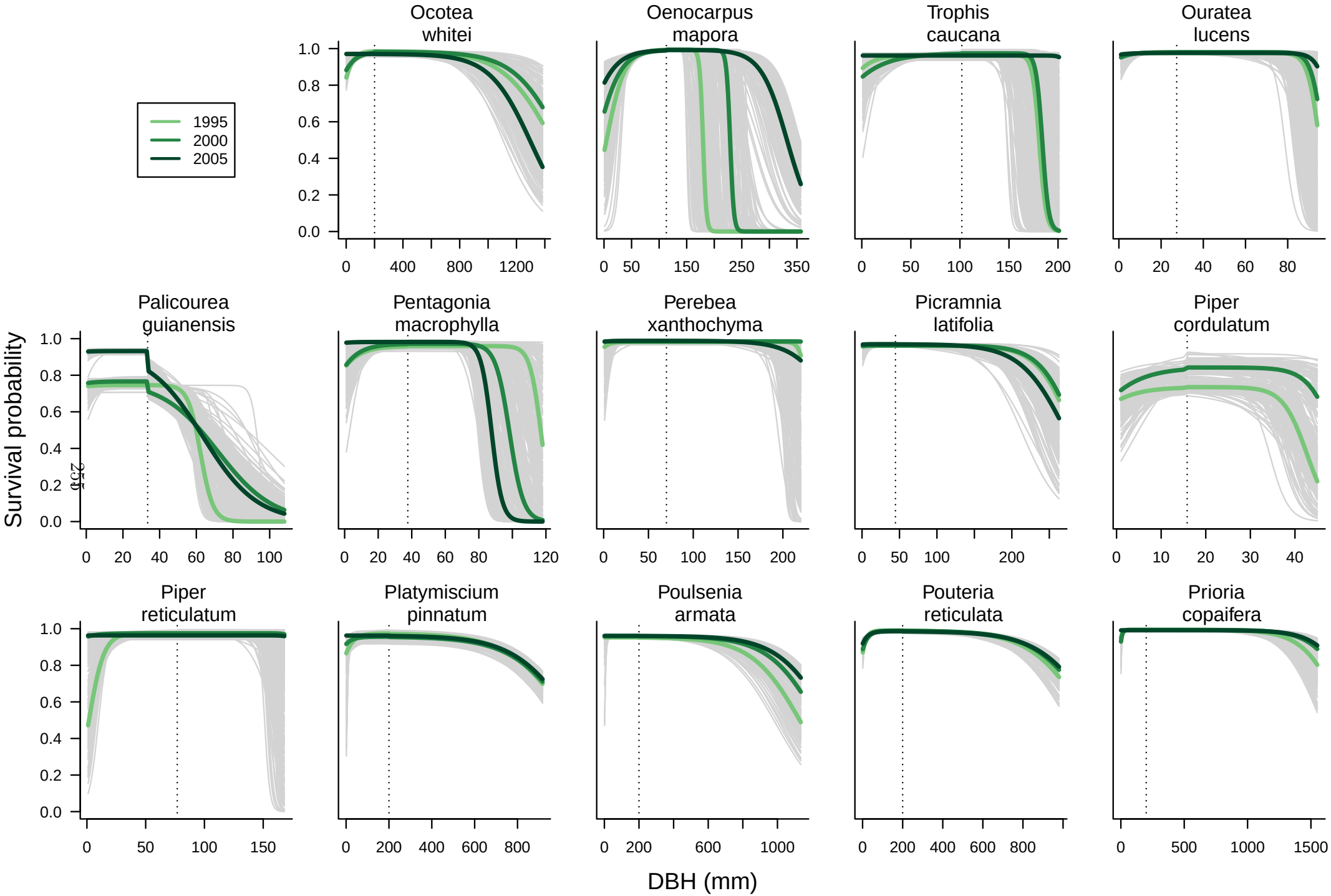

1995
2000
2005
Brosimum alicastrum
Calophyllum longifolium
Capparis frondosa
Casearia aculeata
Casearia arborea
Casearia sylvestris
Cassipourea elliptica
Cecropia insignis
Cecropia obtusifolia
Chamguava schippii
Chrysochlamys eclipes
Chrysophyllum argenteum
Chrysophyllum cainito
Coccoloba coronata
Survival probability
DBH (mm)

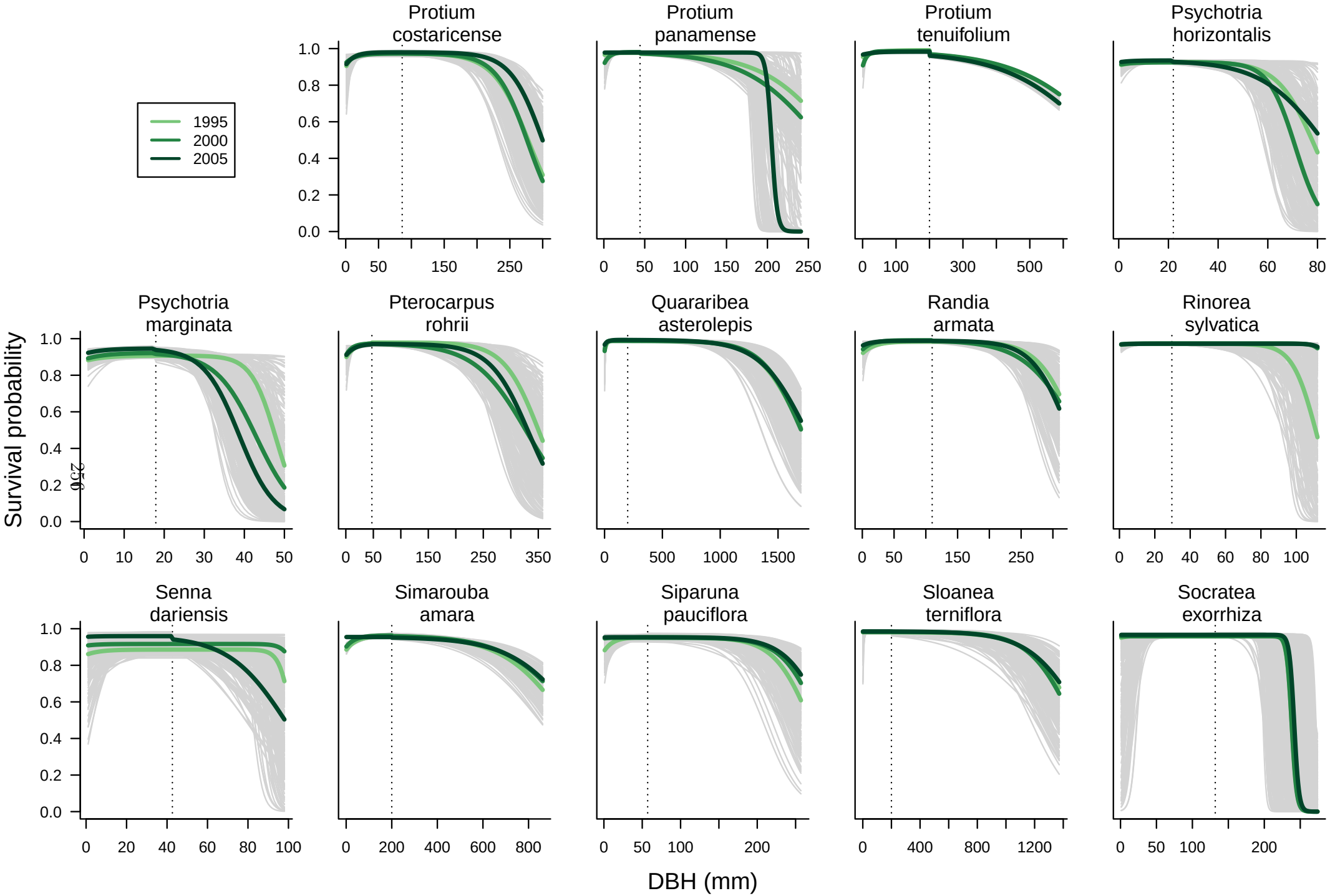

1995
2000
2005
Coccoloba manzinellensis
Conostegia cinnamomea
Cordia alliodora
Cordia bicolor
Cordia lasiocalyx
Coussarea curvigemmia
Croton billbergianus
Cupania seemannii
Desmopsis panamensis
Drypetes standleyi
Erythroxylum macrophyllum
Eugenia coloradoensis
Eugenia galalonensis
Eugenia nesiotica
Survival probability
DBH (mm)
251

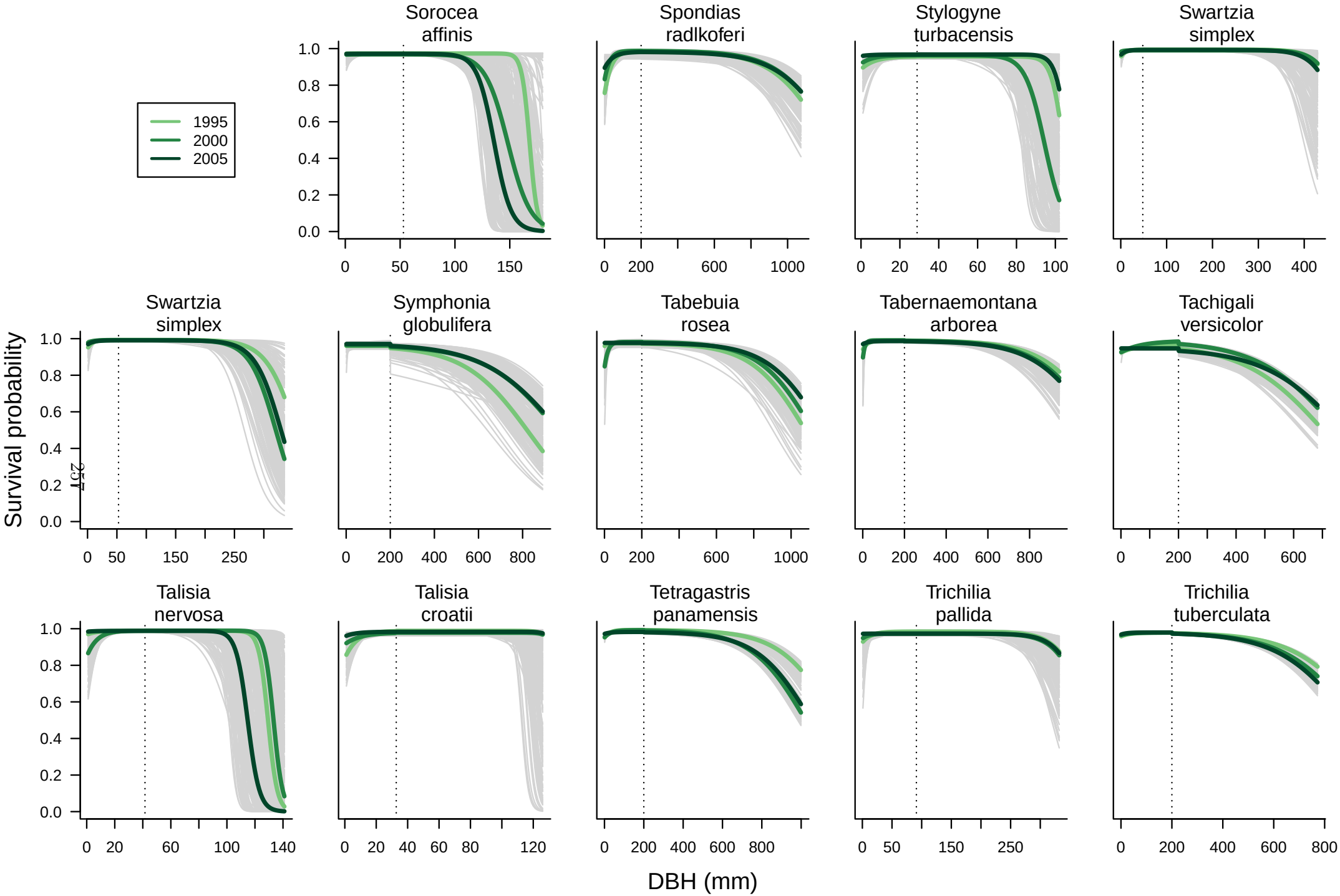

1995
2000
2005
Eugenia oerstediana
Faramea occidentalis
Garcinia intermedia
Garcinia madruno
Guapira standleyana
Guarea guidonia
Guarea bullata
Guatteria dumetorum
Guettarda foliacea
Gustavia superba
Hamelia axillaris
Hampea appendiculata
Hasseltia floribunda
Heisteria concinna
Survival probability
DBH (mm)
252


1995
2000
2005
Herrania purpurea
Hirtella triandra
Hybanthus prunifolius
Inga goldmanii
Inga marginata
Inga pezizifera
Inga nobilis
Inga acuminata
Inga sapindoides
Inga thibaudiana
Inga umbellifera
Jacaranda copaia
Lacistema aggregatum
Laetia thamnia
Survival probability
DBH (mm)


1995
2000
2005
Licania platypus
Lonchocarpus heptaphyllus
Luehea seemannii
Mosannona garwoodii
Maquira guianensis
Miconia affinis
Miconia argentea
Miconia nervosa
Mouriri myrtilloides
Nectandra cissiflora
Nectandra lineata
Ocotea cernua
Ocotea oblonga
Ocotea puberula
Survival probability
DBH (mm)


1995
2000
2005
Ocotea whitei
Oenocarpus mapora
Trophis caucana
Ouratea lucens
Palicourea guianensis
Pentagonia macrophylla
Perebea xanthochyma
Picramnia latifolia
Piper cordulatum
Piper reticulatum
Platymiscium pinnatum
Poulsenia armata
Pouteria reticulata
Prioria copaifera
Survival probability
DBH (mm)
253


1995
2000
2005
Protium costaricense
Protium panamense
Protium tenuifolium
Psychotria horizontalis
Psychotria marginata
Pterocarpus rohrii
Quararibea asterolepis
Randia armata
Rinorea sylvatica
Senna dariensis
Simarouba amara
Siparuna pauciflora
Sloanea terniflora
Socratea exorrhiza
Survival probability
DBH (mm)


1995
2000
2005
Sorocea affinis
Spondias radlkoferi
Stylogyne turbacensis
Swartzia simplex
Swartzia simplex
Symphonia globulifera
Tabebuia rosea
Tabernaemontana arborea
Tachigali versicolor
Talisia nervosa
Talisia croatii
Tetragastris panamensis
Trichilia pallida
Trichilia tuberculata
Survival probability
DBH (mm)
257

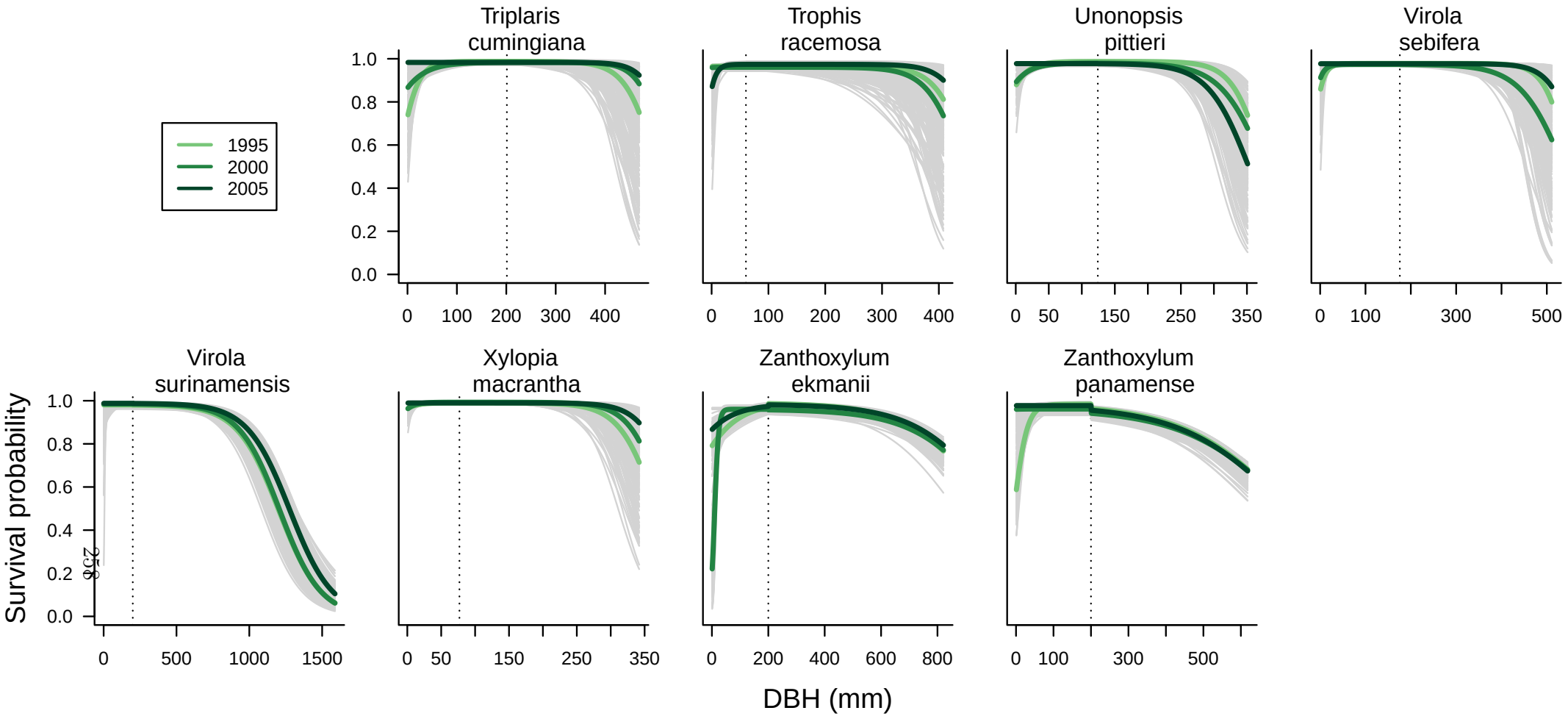
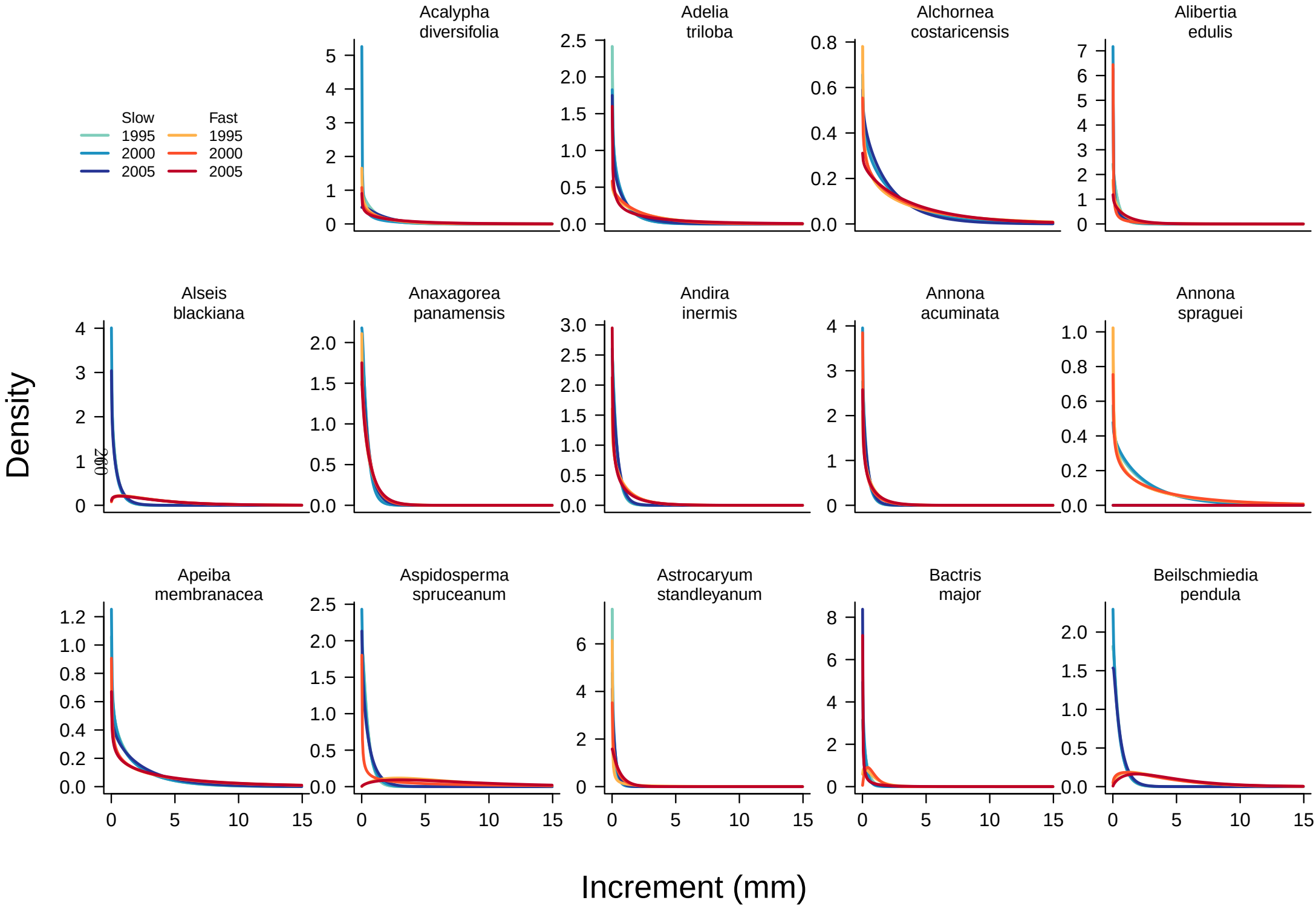
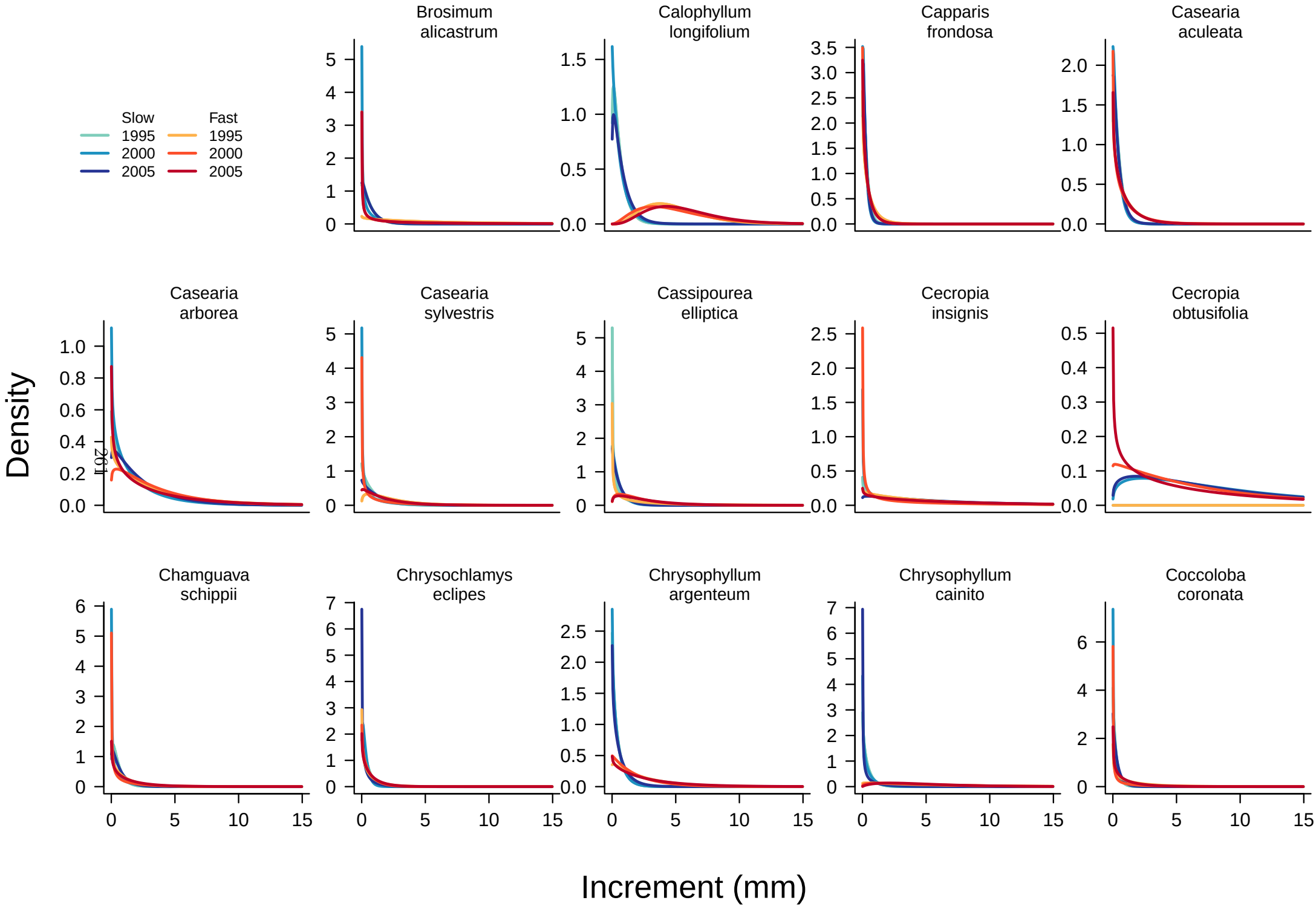
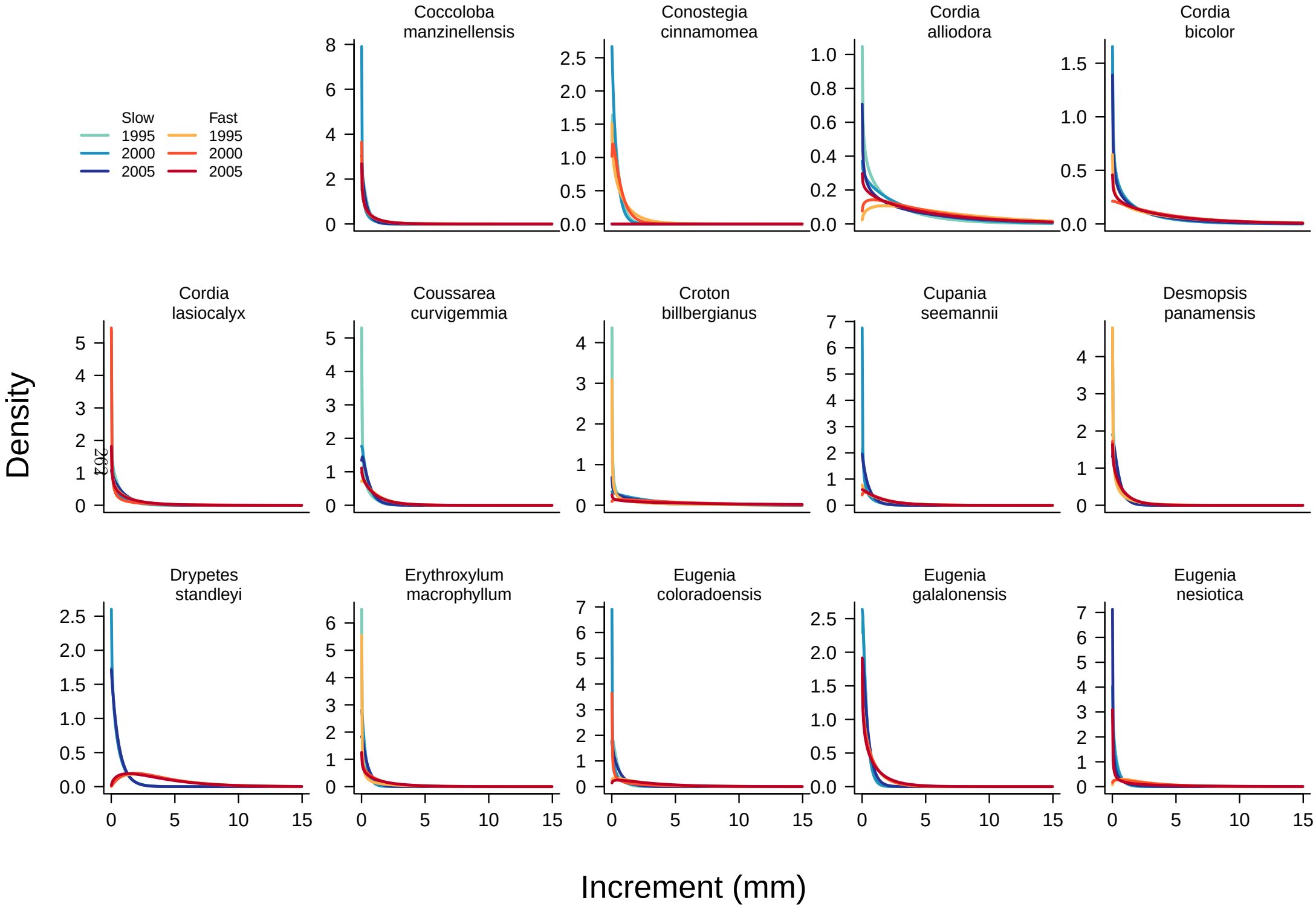
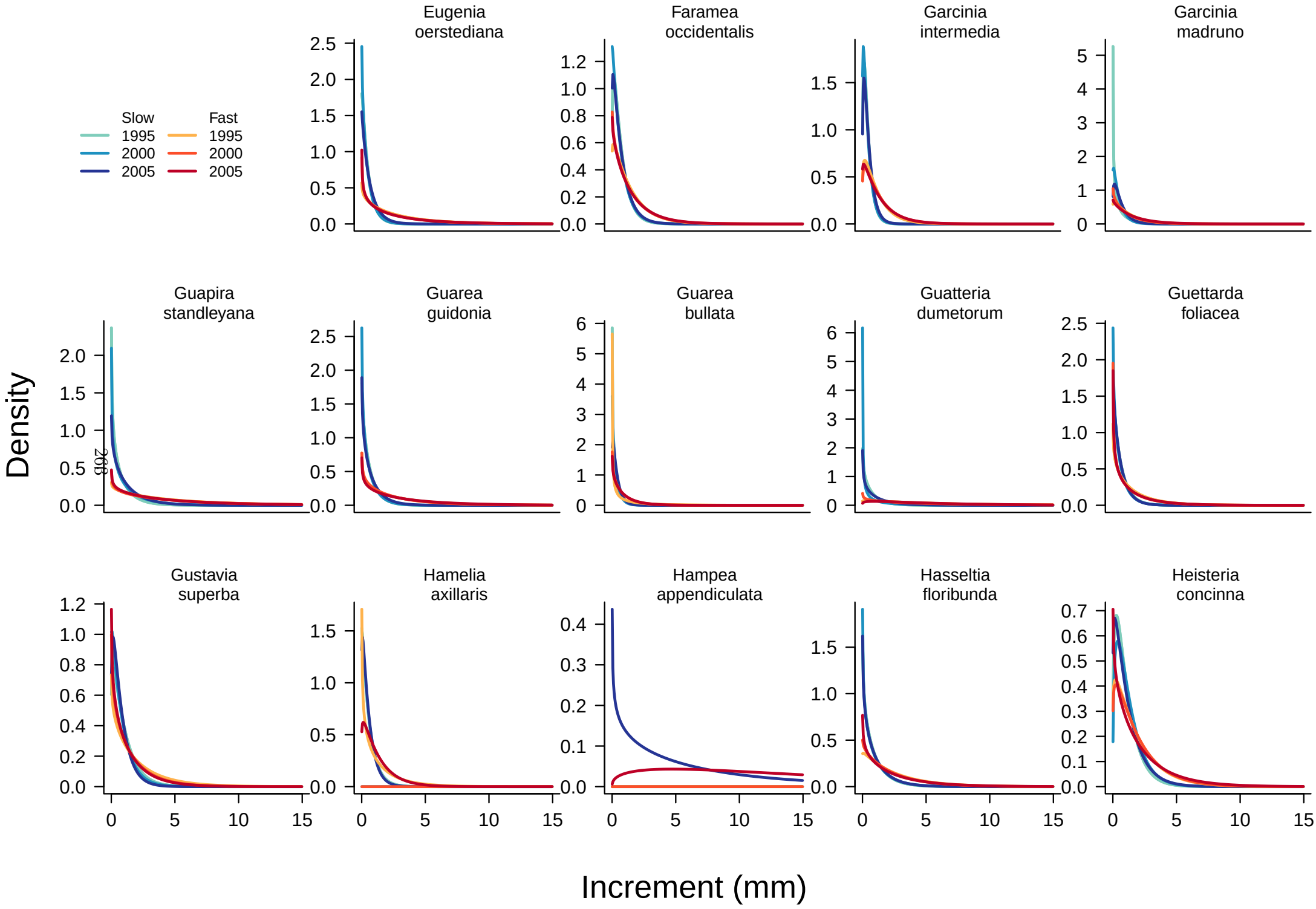

1995
2000
2005
Triplaris cumingiana
Trophis racemosa
Unonopsis pittieri
Virola sebifera
Virola surinamensis
Xylopia macrantha
Zanthoxylum ekmanii
Zanthoxylum panamense
Survival probability
DBH (mm)
256

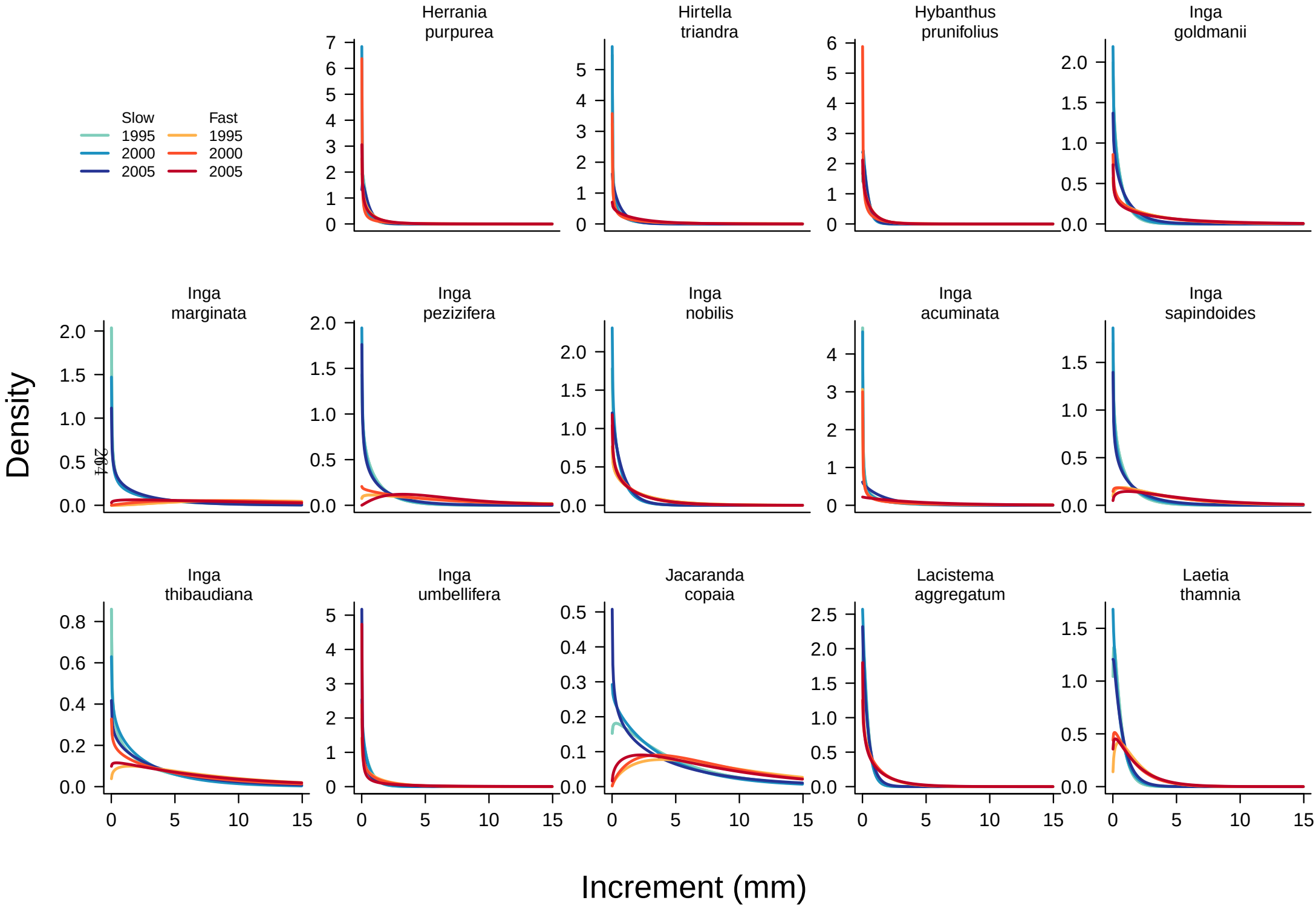
Figure F.1: Survival models for BCI species. Survival was modelled with two logistic regressions that meet at a fixed threshold, with five free parameters in total. BCI species showed high diversity in survival rates, with both high and low juvenile survival, rapid and gradual senescence and high and low upper asymptotes. Species differed in the degree of variation in survival probabilities between censuses.

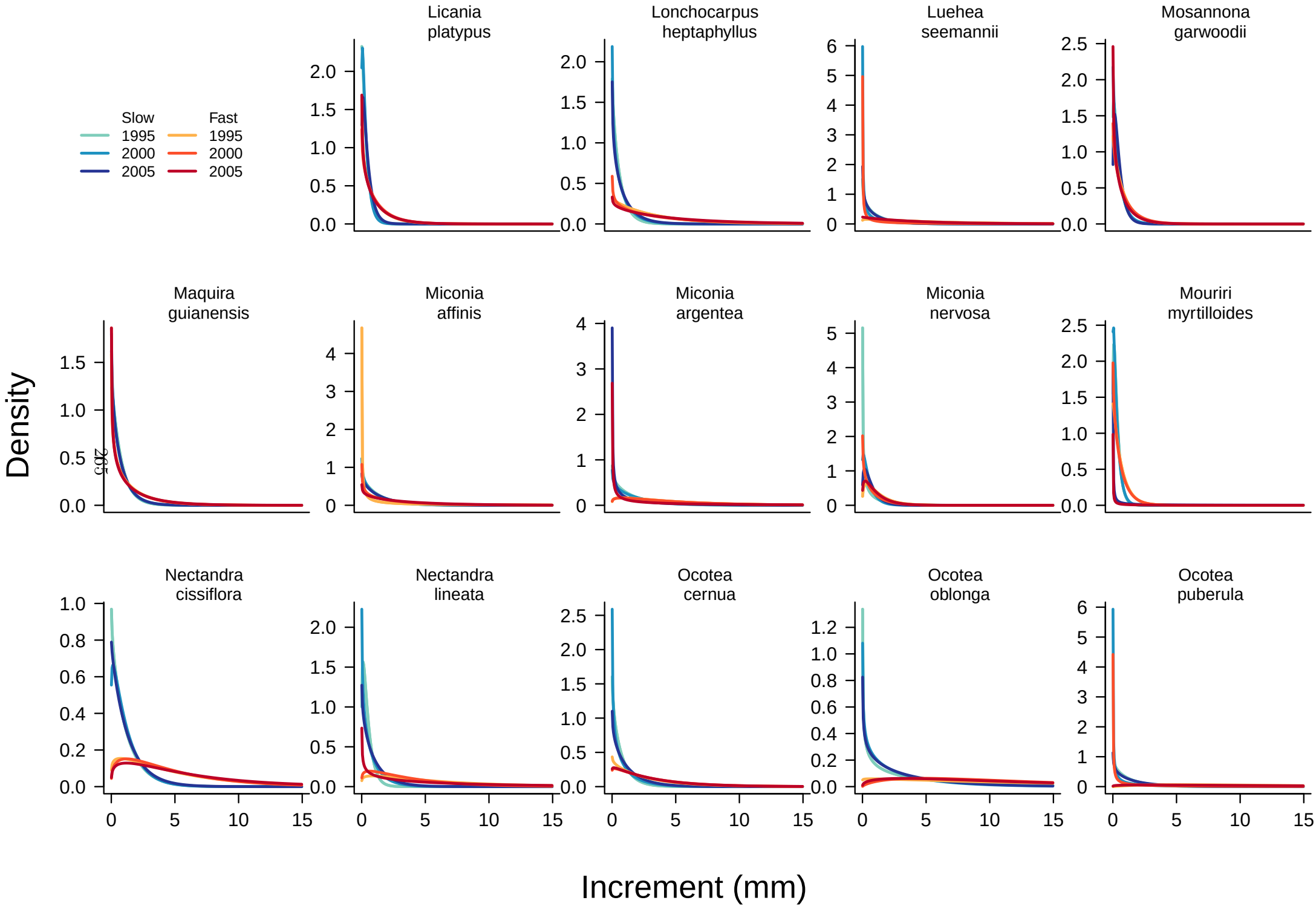

Slow
1995
2000
2005
Fast
1995
2000
2005
Acalypha diversifolia
Adelia triloba
Alchornea costaricensis
Alibertia edulis
Alseis blackiana
Anaxagorea panamensis
Andira inermis
Annona acuminata
Annona spraguei
Apeiba membranacea
Aspidosperma spruceanum
Astrocaryum standleyanum
Bactris major
Beilschmiedia pendula
Density
Increment (mm)

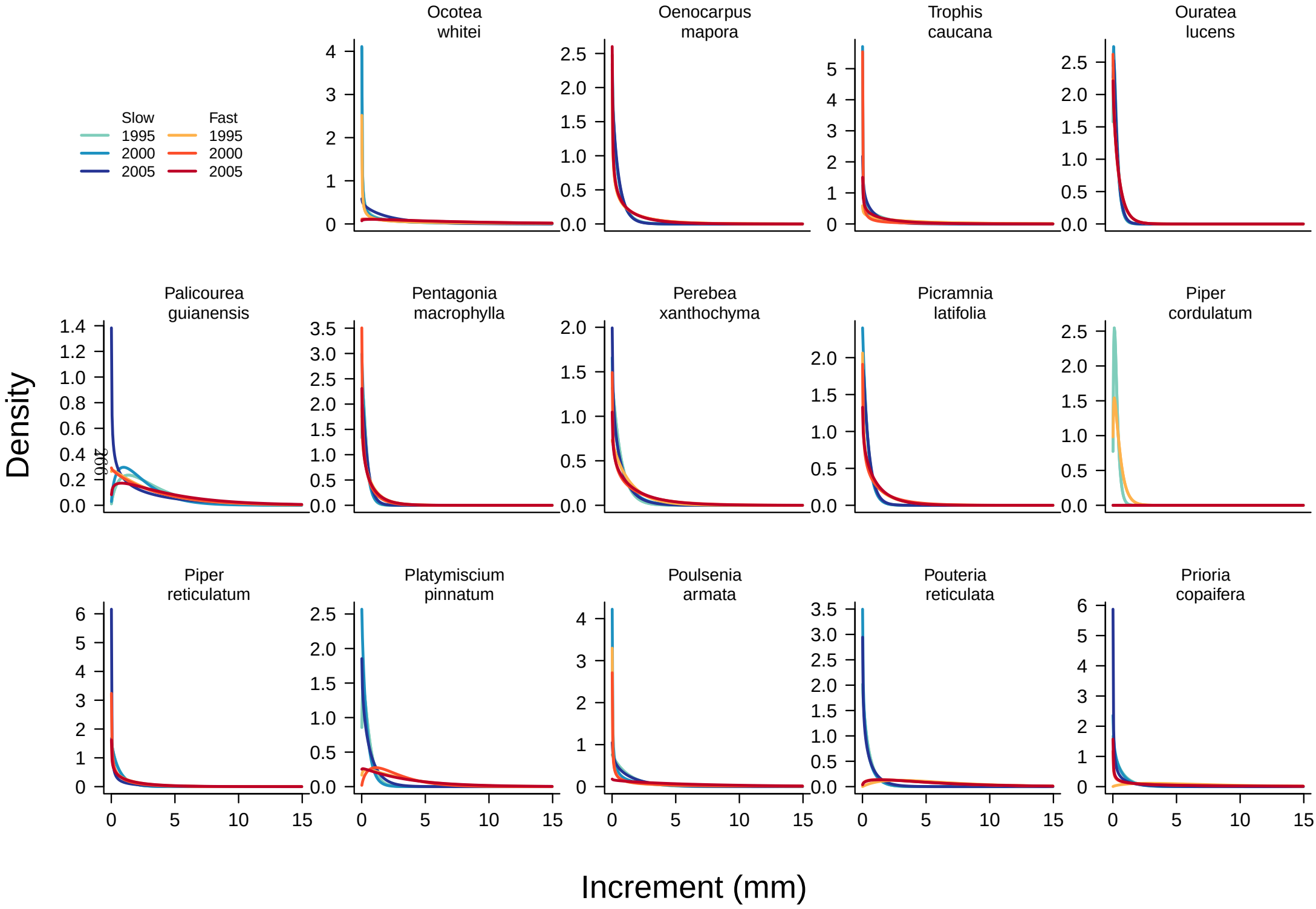

Slow
1995
2000
2005
Fast
1995
2000
2005
Brosimum alicastrum
Calophyllum longifolium
Capparis frondosa
Casearia aculeata
Casearia arborea
Casearia sylvestris
Cassipourea elliptica
Cecropia insignis
Cecropia obtusifolia
Chamguava schippii
Chrysochlamys eclipes
Chrysophyllum argenteum
Chrysophyllum cainito
Coccoloba coronata
Density
Increment (mm)

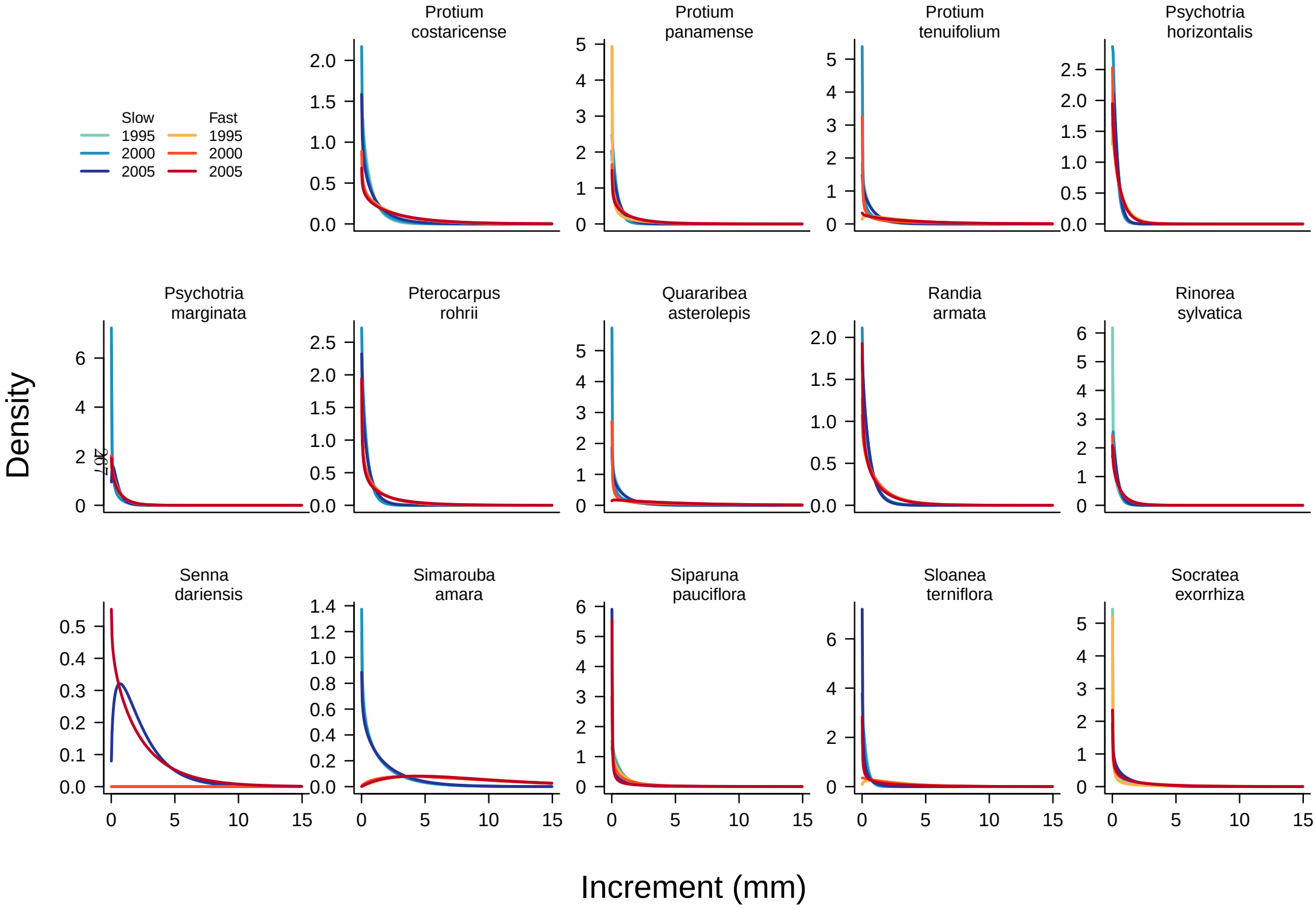

Slow
1995
2000
2005
Fast
1995
2000
2005
Coccoloba manzinellensis
Conostegia cinnamomea
Cordia alliodora
Cordia bicolor
Cordia lasiocalyx
Coussarea curvigemmia
Croton billbergianus
Cupania seemannii
Desmopsis panamensis
Drypetes standleyi
Erythroxylum macrophyllum
Eugenia coloradoensis
Eugenia galalonensis
Eugenia nesiotica
Density
Increment (mm)

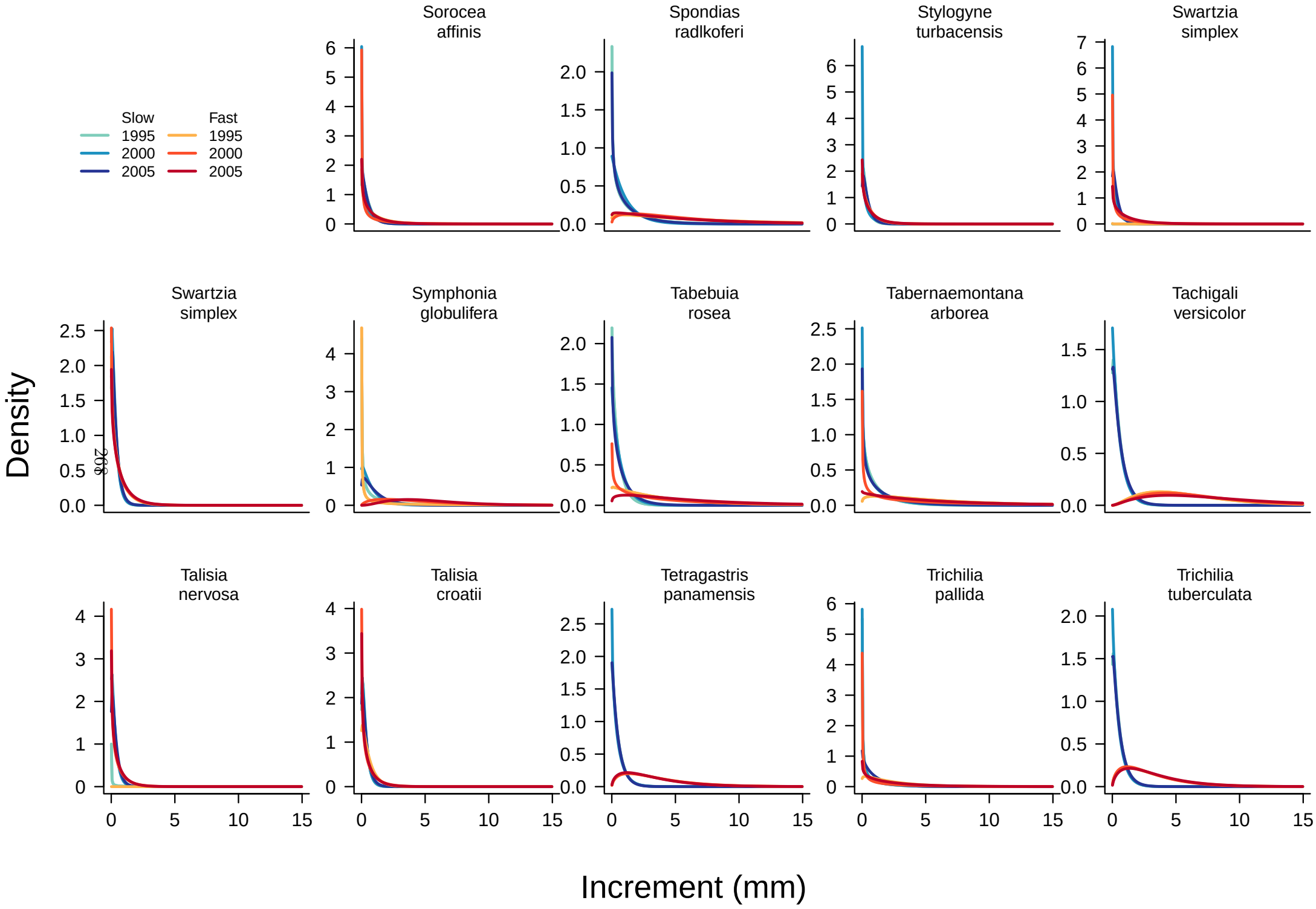

Slow
1995
2000
2005
Fast
1995
2000
2005
Eugenia oerstediana
Faramea occidentalis
Garcinia intermedia
Garcinia madruno
Guapira standleyana
Guarea guidonia
Guarea bullata
Guatteria dumetorum
Guettarda foliacea
Gustavia superba
Hamelia axillaris
Hampea appendiculata
Hasseltia floribunda
Heisteria concinna
Density
Increment (mm)


Slow
1995
2000
2005
Fast
1995
2000
2005
Herrania purpurea
Hirtella triandra
Hybanthus prunifolius
Inga goldmanii
Inga marginata
Inga pezizifera
Inga nobilis
Inga acuminata
Inga sapindoides
Inga thibaudiana
Inga umbellifera
Jacaranda copaia
Lacistema aggregatum
Laetia thamnia
Density
Increment (mm)


Slow
1995
2000
2005
Fast
1995
2000
2005
Licania platypus
Lonchocarpus heptaphyllus
Luehea seemannii
Mosannona garwoodii
Maquira guianensis
Miconia affinis
Miconia argentea
Miconia nervosa
Mouriri myrtilloides
Nectandra cissiflora
Nectandra lineata
Ocotea cernua
Ocotea oblonga
Ocotea puberula
Density
Increment (mm)


Slow
1995
2000
2005
Fast
1995
2000
2005
Ocotea whitei
Oenocarpus mapora
Trophis caucana
Ouratea lucens
Palicourea guianensis
Pentagonia macrophylla
Perebea xanthochyma
Picramnia latifolia
Piper cordulatum
Piper reticulatum
Platymiscium pinnatum
Poulsenia armata
Pouteria reticulata
Prioria copaifera
Density
Increment (mm)


Slow
1995
2000
2005
Fast
1995
2000
2005
Protium costaricense
Protium panamense
Protium tenuifolium
Psychotria horizontalis
Psychotria marginata
Pterocarpus rohrii
Quararibea asterolepis
Randia armata
Rinorea sylvatica
Senna dariensis
Simarouba amara
Siparuna pauciflora
Sloanea terniflora
Socratea exorrhiza
Density
Increment (mm)


Slow
1995
2000
2005
Fast
1995
2000
2005
Sorocea affinis
Spondias radlkoferi
Stylogyne turbacensis
Swartzia simplex
Swartzia simplex
Symphonia globulifera
Tabebuia rosea
Tabernaemontana arborea
Tachigali versicolor
Talisia nervosa
Talisia croatii
Tetragastris panamensis
Trichilia pallida
Trichilia tuberculata
Density
Increment (mm)

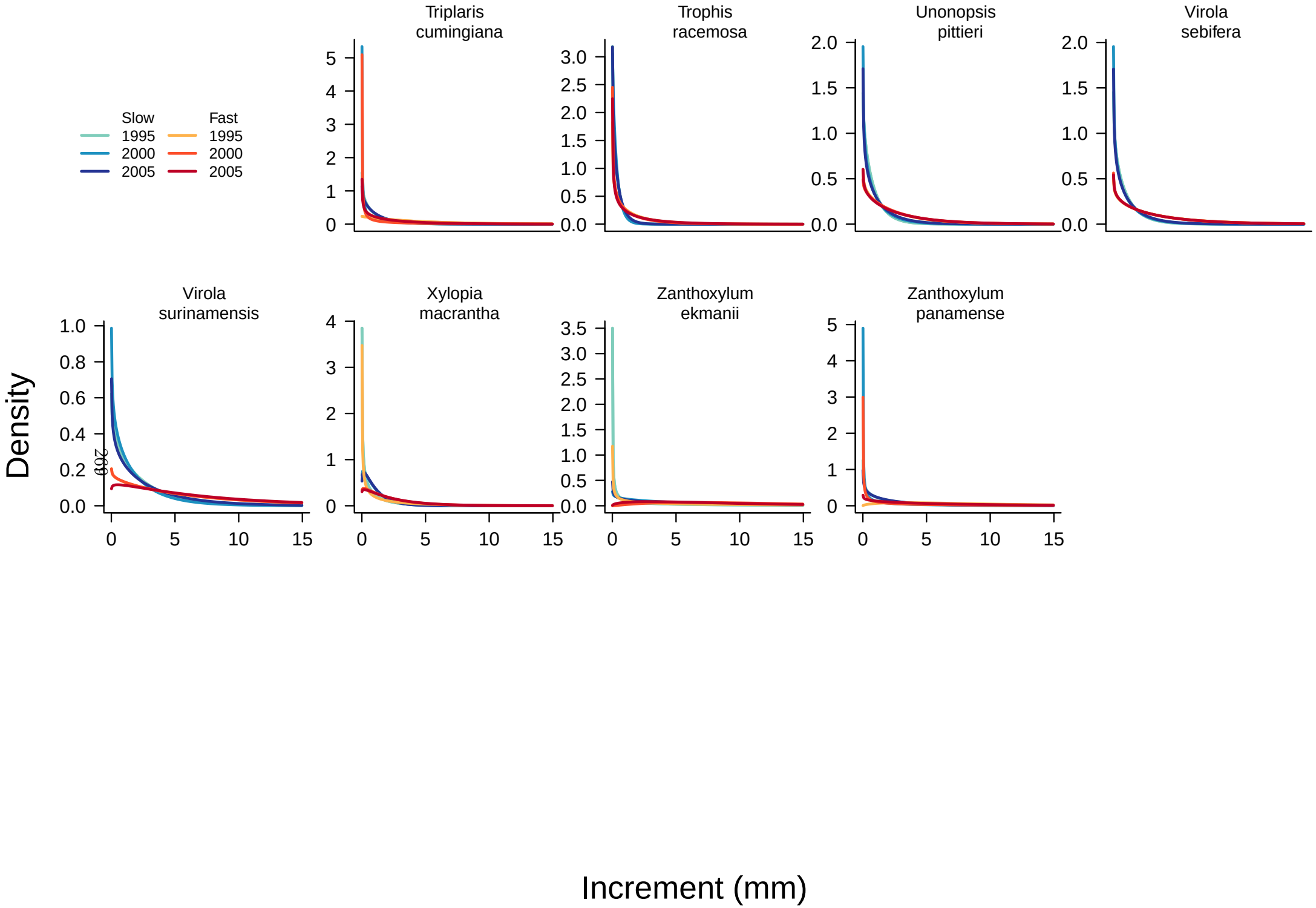
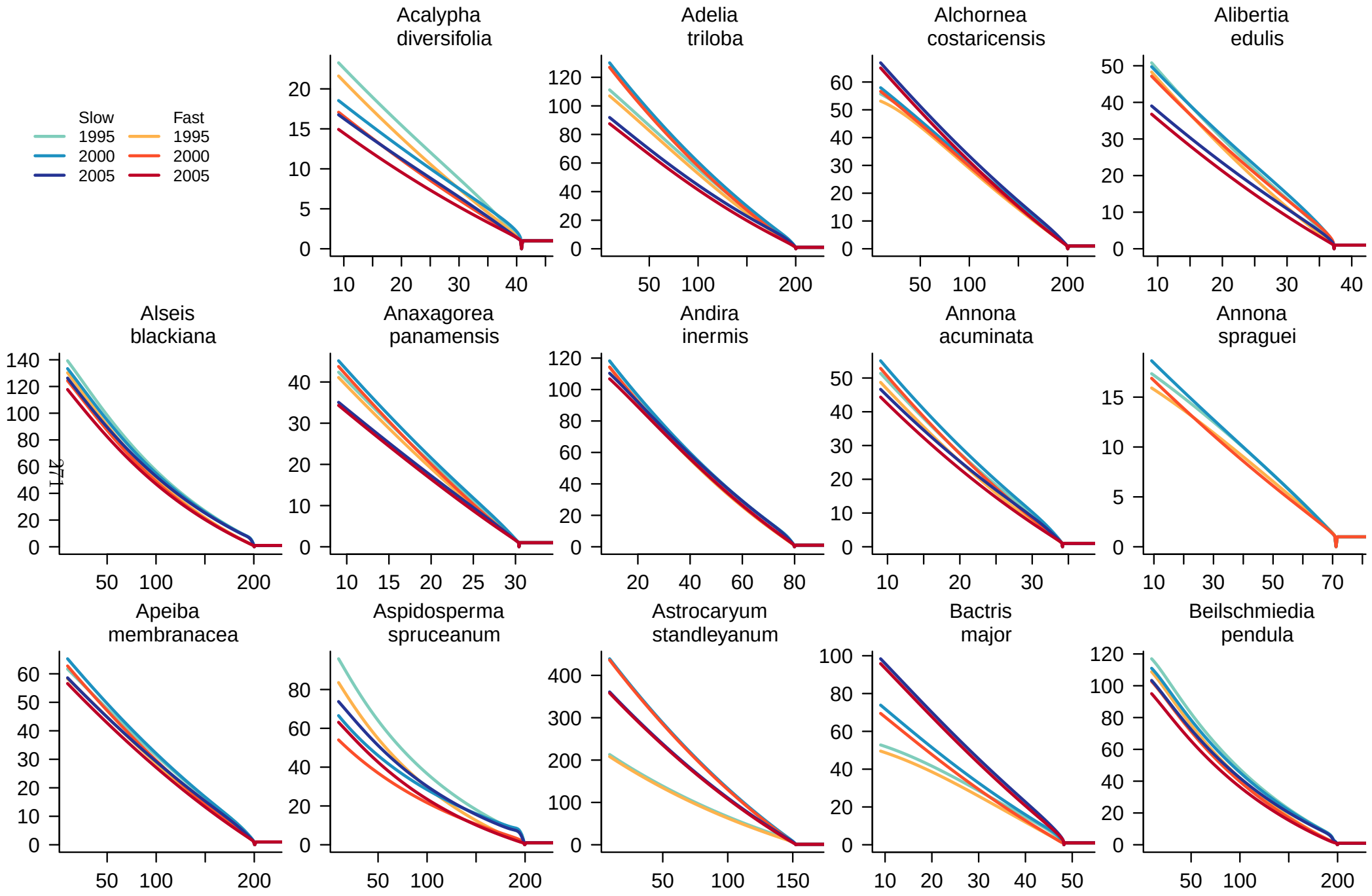
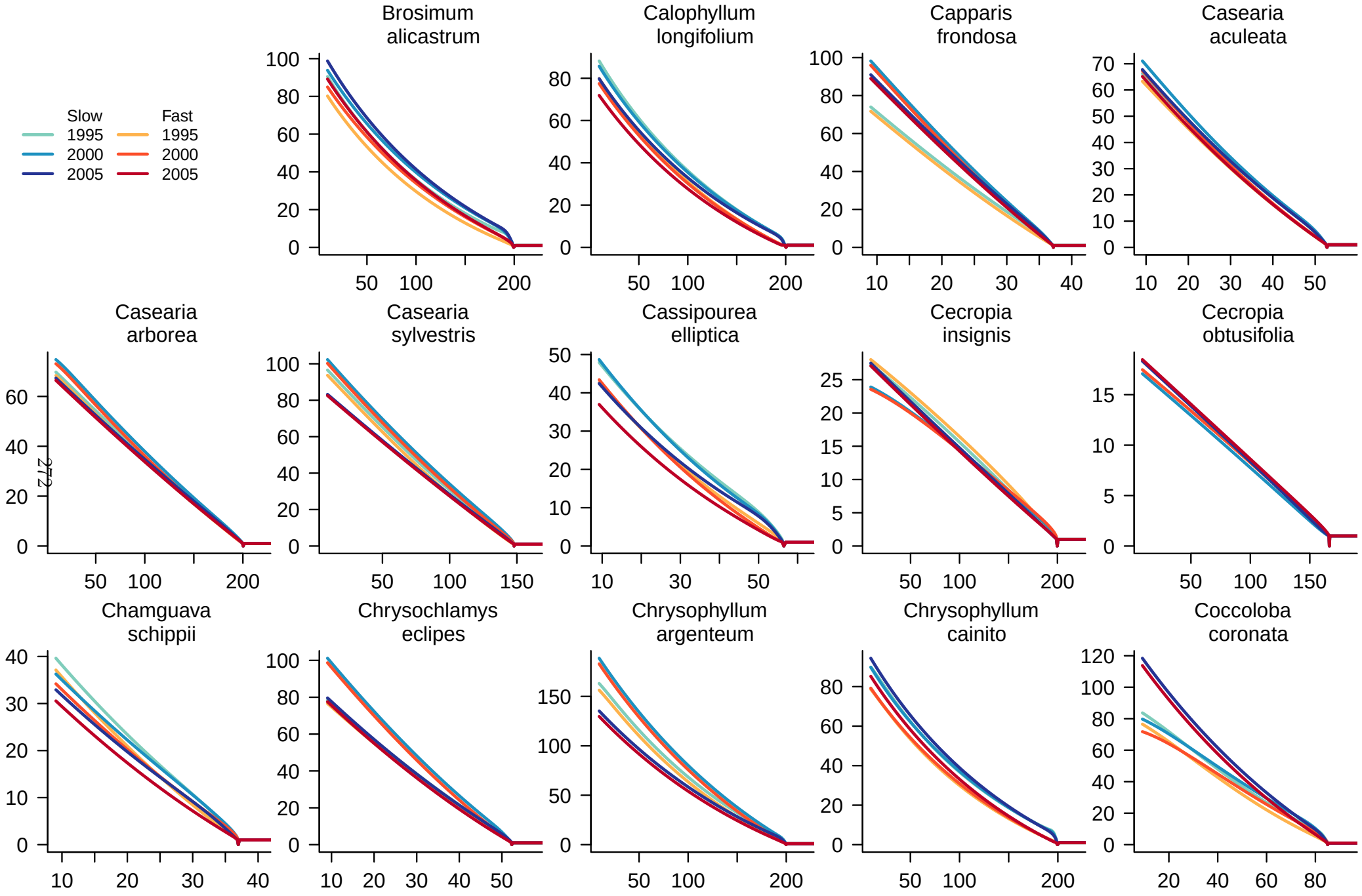
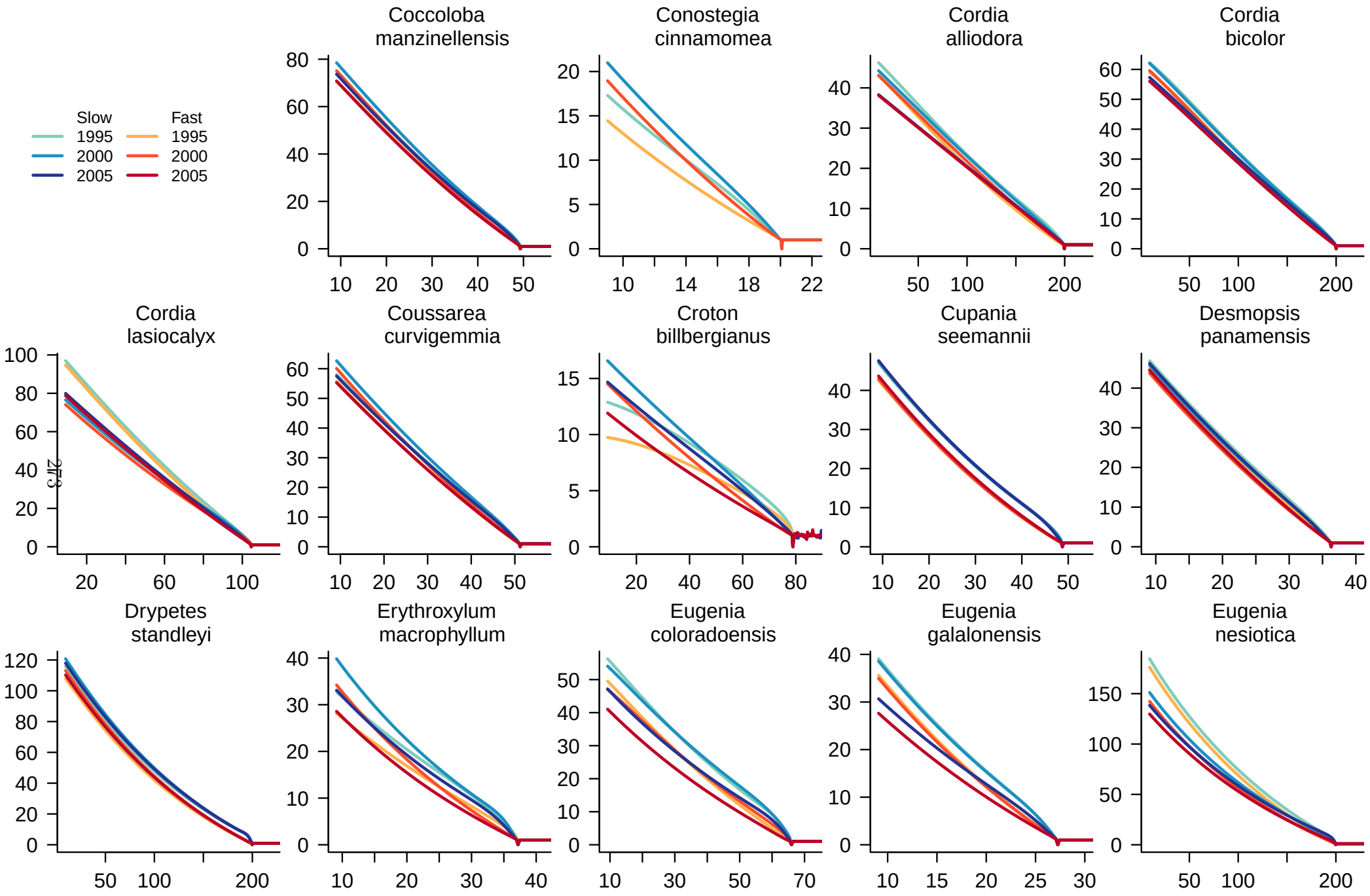

Slow
1995
2000
2005
Fast
1995
2000
2005
Triplaris cumingiana
Trophis racemosa
Unonopsis pittieri
Virola sebifera
Virola surinamensis
Xylopia macrantha
Zanthoxylum ekmanii
Zanthoxylum panamense
Density
Increment (mm)

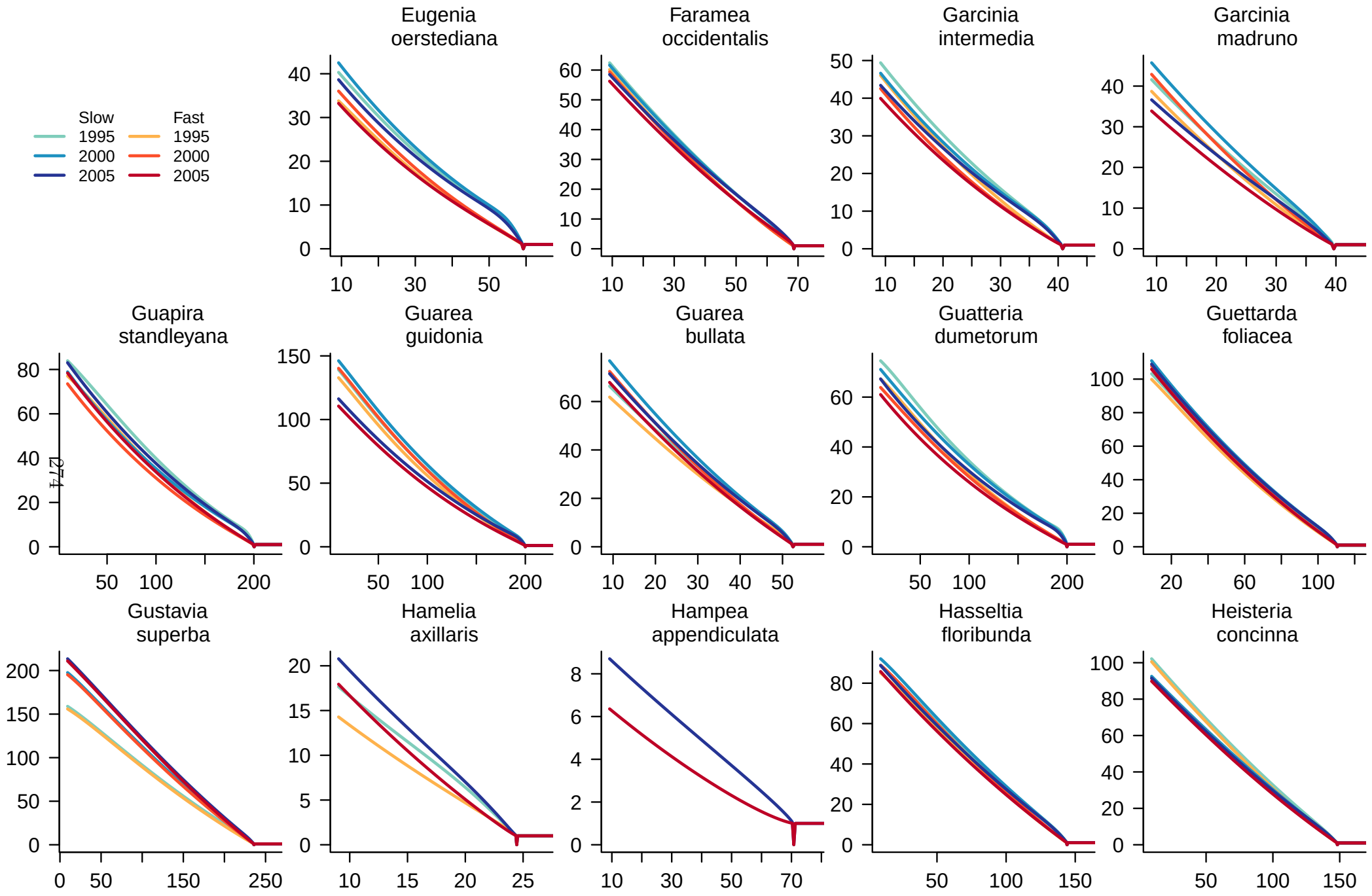
Figure F.2: Growth models for BCI species. For each census interval growth was modelled with a mixture of gamma distributions. The fast growth distribution was fit to individuals above a fixed size threshold, along with the fastest 5% of individuals below the threshold, and the slow distribution was fit to remaining individuals. Growth rates were generally low and most species showed little variation between years.

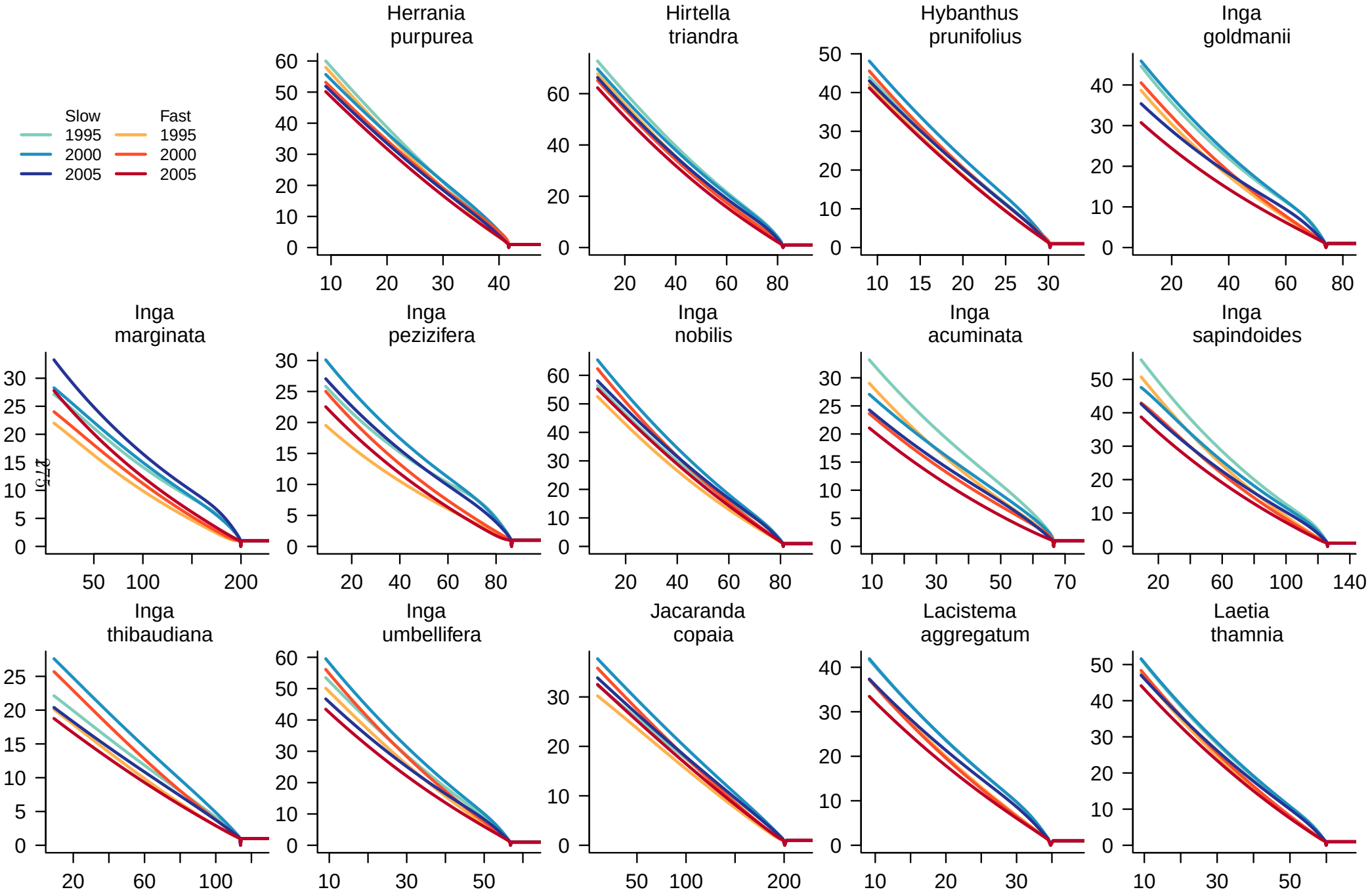
F.2 Shifts in demographic metrics through time

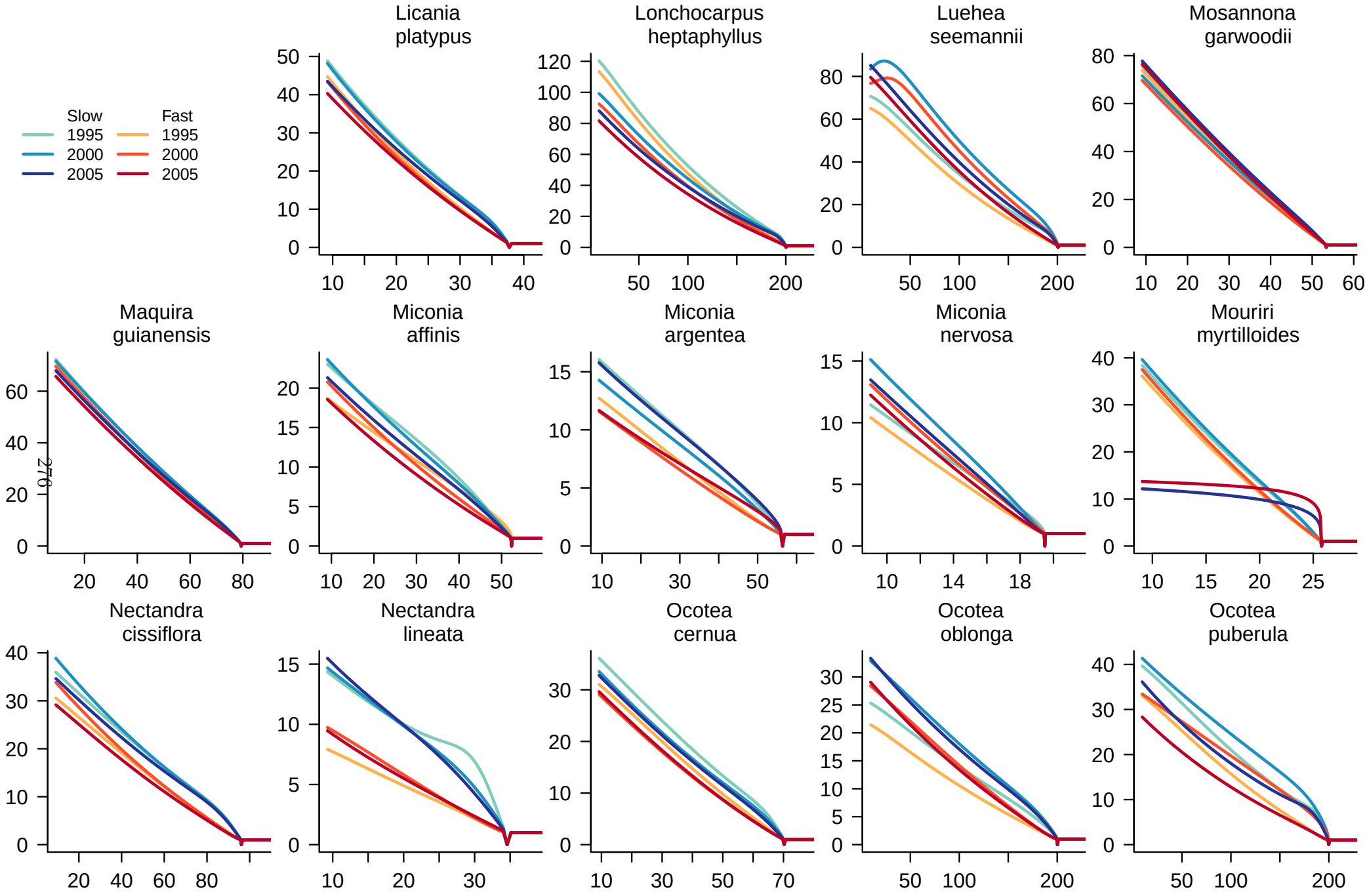

Slow
1995
2000
2005
Fast
1995
2000
2005
Acalypha diversifolia
Adelia triloba
Alchornea costaricensis
Alibertia edulis
Alseis blackiana
Anaxagorea panamensis
Andira inermis
Annona acuminata
Annona spraguei
Apeiba membranacea
Aspidosperma spruceanum
Astrocaryum standleyanum
Bactris major
Beilschmiedia pendula
271

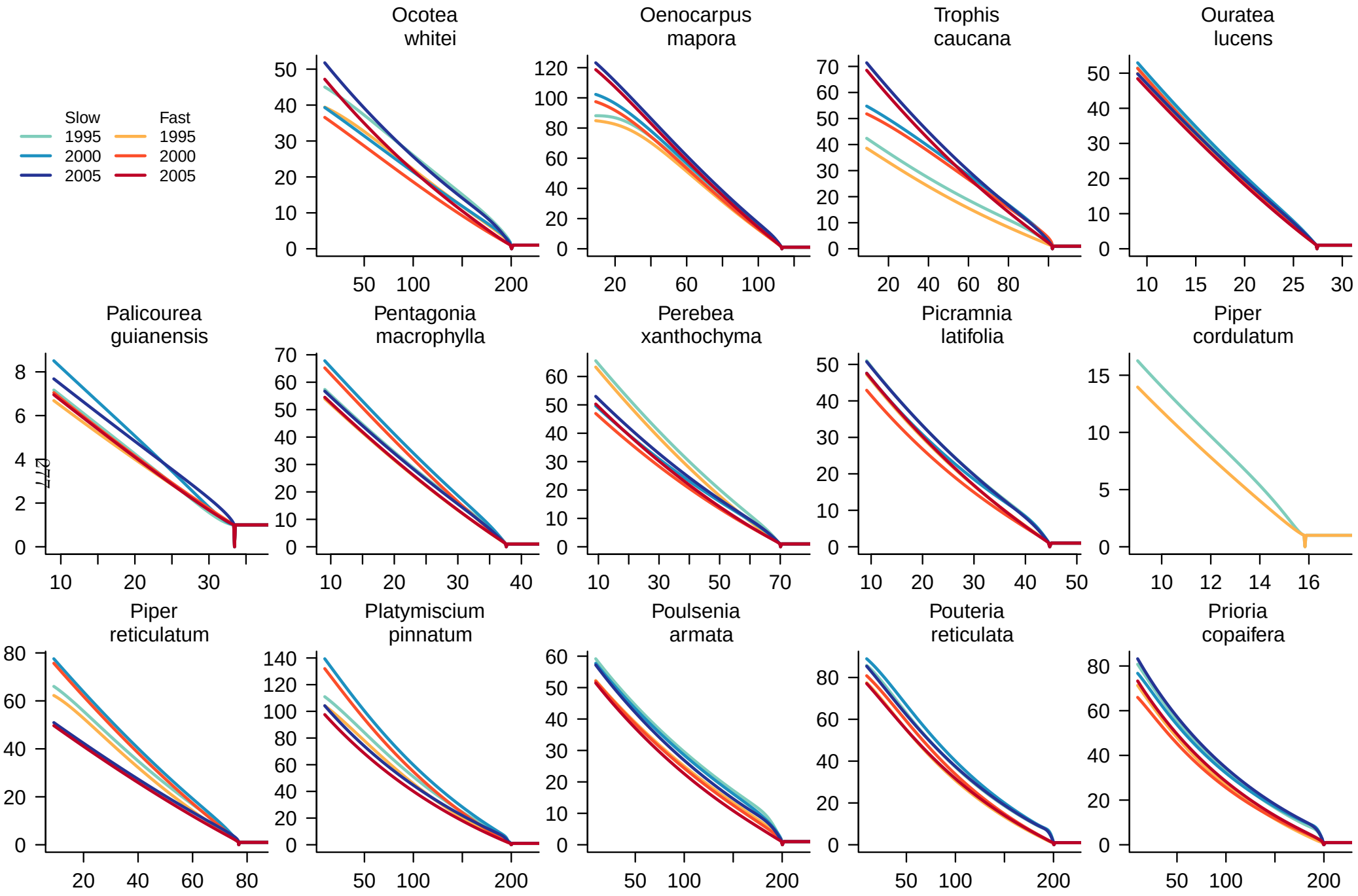

Slow
1995
2000
2005
Fast
1995
2000
2005
Brosimum alicastrum
Calophyllum longifolium
Capparis frondosa
Casearia aculeata
Casearia arborea
Casearia sylvestris
Cassipourea elliptica
Cecropia insignis
Cecropia obtusifolia
Chamguava schippii
Chrysochlamys eclipes
Chrysophyllum argenteum
Chrysophyllum cainito
Coccoloba coronata
272

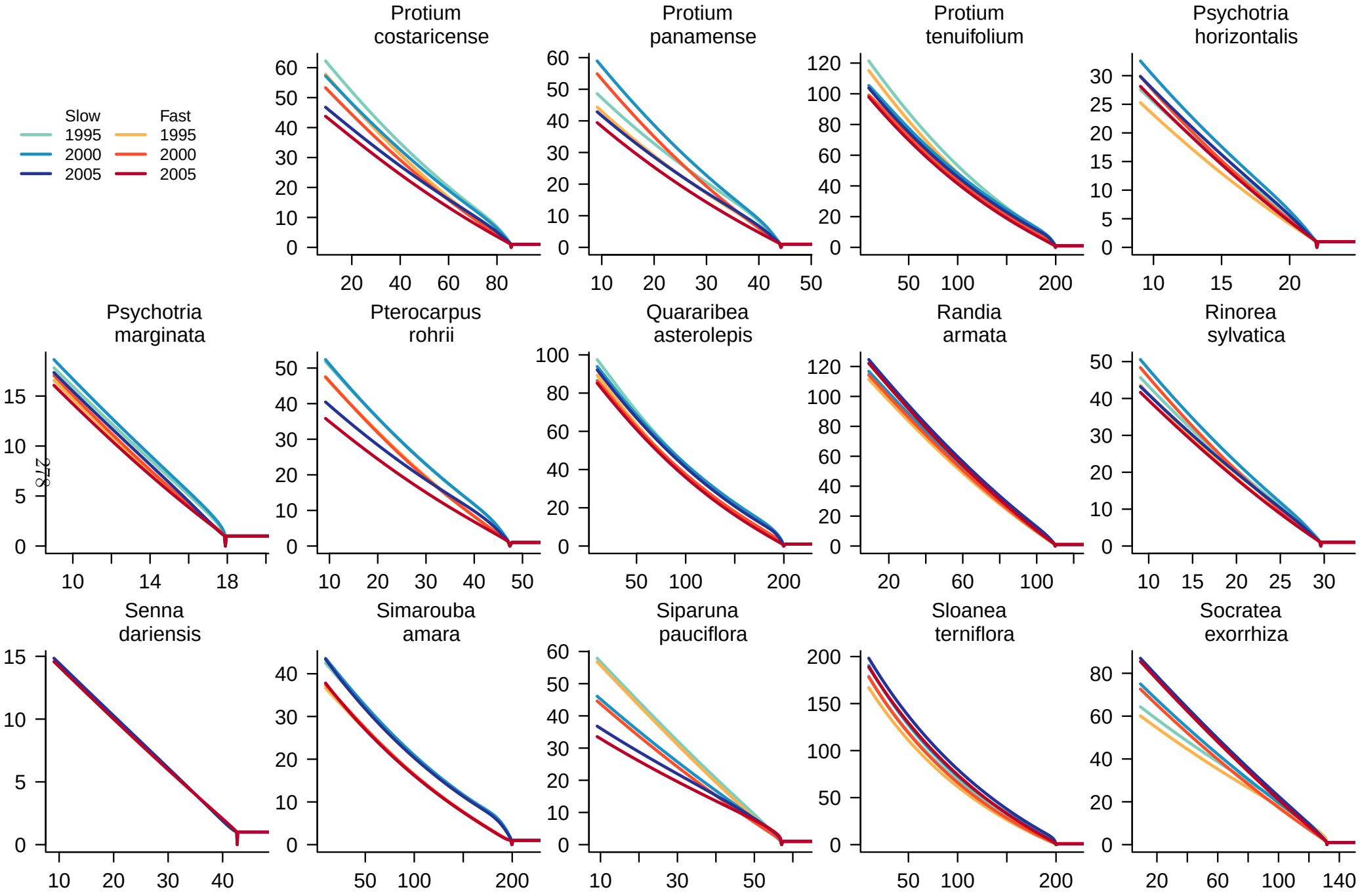

Slow
1995
2000
2005
Fast
1995
2000
2005
Coccoloba manzinellensis
Conostegia cinnamomea
Cordia alliodora
Cordia bicolor
Cordia lasiocalyx
Coussarea curvigemmia
Croton billbergianus
Cupania seemannii
Desmopsis panamensis
Drypetes standleyi
Erythroxylum macrophyllum
Eugenia coloradoensis
Eugenia galalonensis
Eugenia nesiotica
27.3

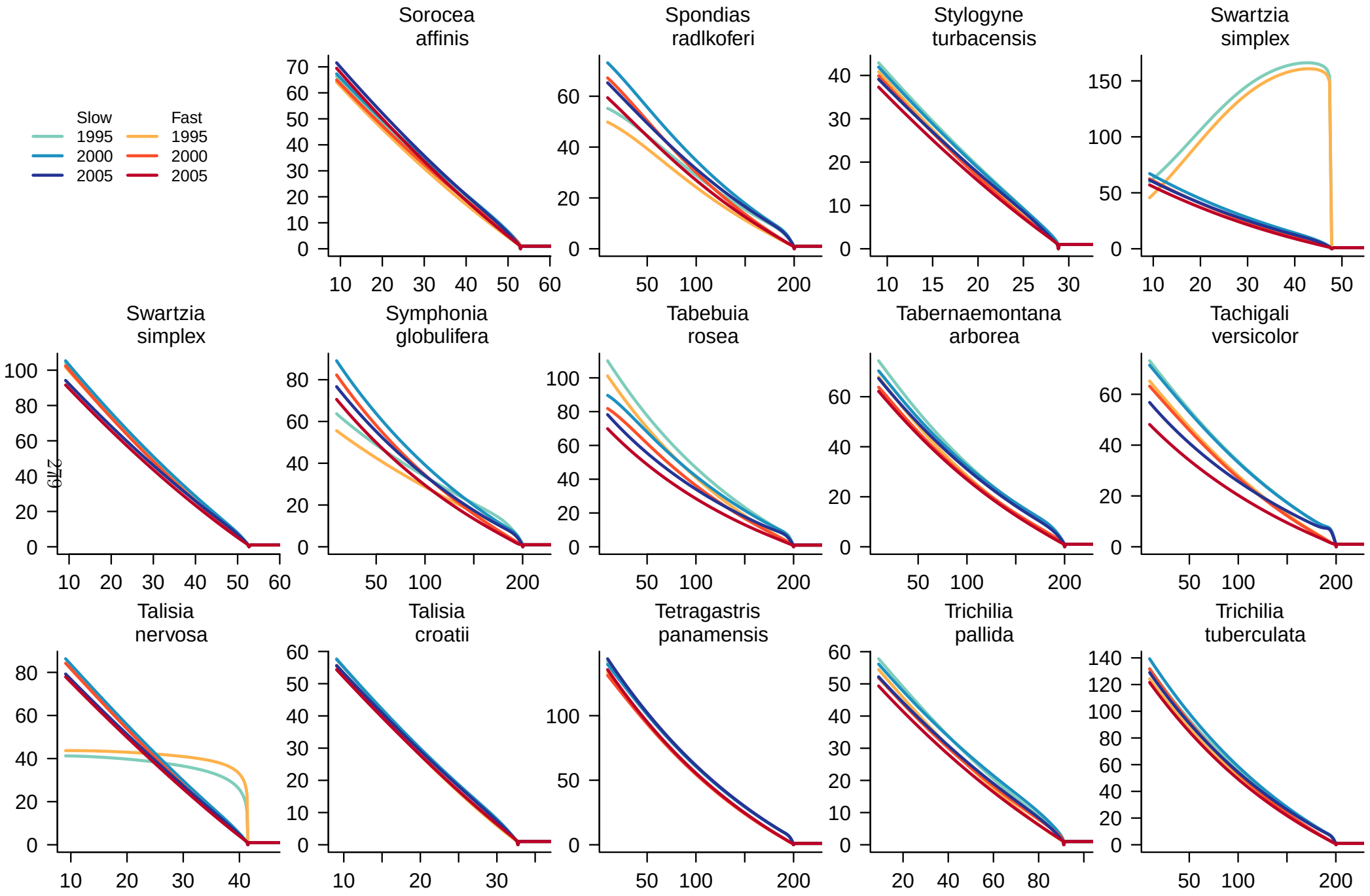

Slow
1995
2000
2005
Fast
1995
2000
2005
Eugenia oerstediana
Faramea occidentalis
Garcinia intermedia
Garcinia madruno
Guapira standleyana
Guarea guidonia
Guarea bullata
Guatteria dumetorum
Guettarda foliacea
Gustavia superba
Hamelia axillaris
Hampea appendiculata
Hasseltia floribunda
Heisteria concinna
1274


Slow
1995
2000
2005
Fast
1995
2000
2005
Herrania purpurea
Hirtella triandra
Hybanthus prunifolius
Inga goldmanii
Inga marginata
Inga pezizifera
Inga nobilis
Inga acuminata
Inga sapindoides
Inga thibaudiana
Inga umbellifera
Jacaranda copaia
Lacistema aggregatum
Laetia thamnia


Slow
1995
2000
2005
Fast
1995
2000
2005
Licania platypus
Lonchocarpus heptaphyllus
Luehea seemannii
Mosannona garwoodii
Maquira guianensis
Miconia affinis
Miconia argentea
Miconia nervosa
Mouriri myrtilloides
Nectandra cissiflora
Nectandra lineata
Ocotea cernua
Ocotea oblonga
Ocotea puberula


Slow
1995
2000
2005
Fast
1995
2000
2005
Ocotea whitei
Oenocarpus mapora
Trophis caucana
Ouratea lucens
Palicourea guianensis
Pentagonia macrophylla
Perebea xanthochyma
Picramnia latifolia
Piper cordulatum
Piper reticulatum
Platymiscium pinnatum
Poulsenia armata
Pouteria reticulata
Prioria copaifera


Slow
1995
2000
2005
Fast
1995
2000
2005
Protium costaricense
Protium panamense
Protium tenuifolium
Psychotria horizontalis
Psychotria marginata
Pterocarpus rohrii
Quararibea asterolepis
Randia armata
Rinorea sylvatica
Senna dariensis
Simarouba amara
Siparuna pauciflora
Sloanea terniflora
Socratea exorrhiza
278


Slow
1995
2000
2005
Fast
1995
2000
2005
Sorocea affinis
Spondias radlkoferi
Stylogyne turbacensis
Swartzia simplex
Swartzia simplex
Symphonia globulifera
Tabebuia rosea
Tabernaemontana arborea
Tachigali versicolor
Talisia nervosa
Talisia croatii
Tetragastris panamensis
Trichilia pallida
Trichilia tuberculata
AMB

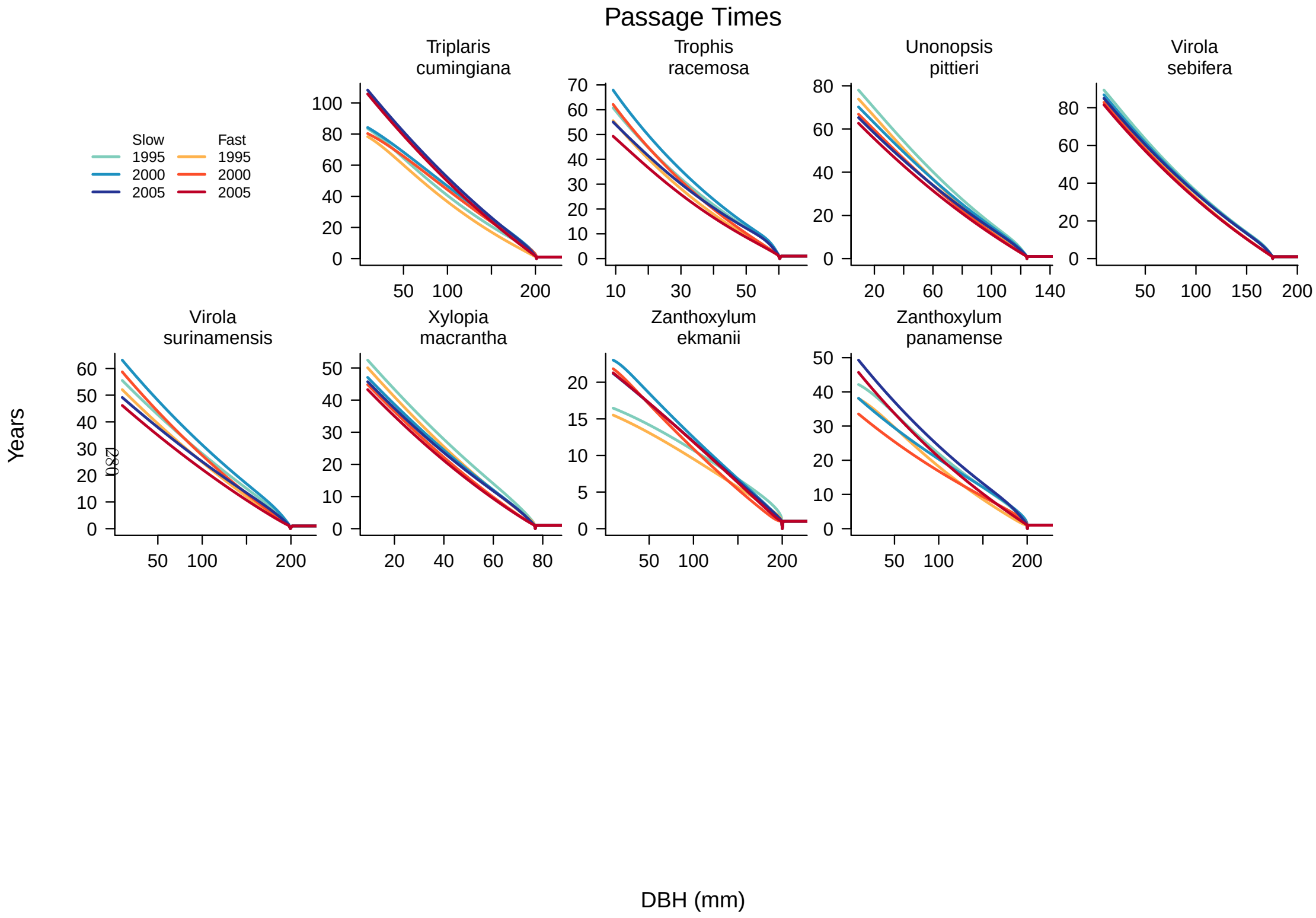
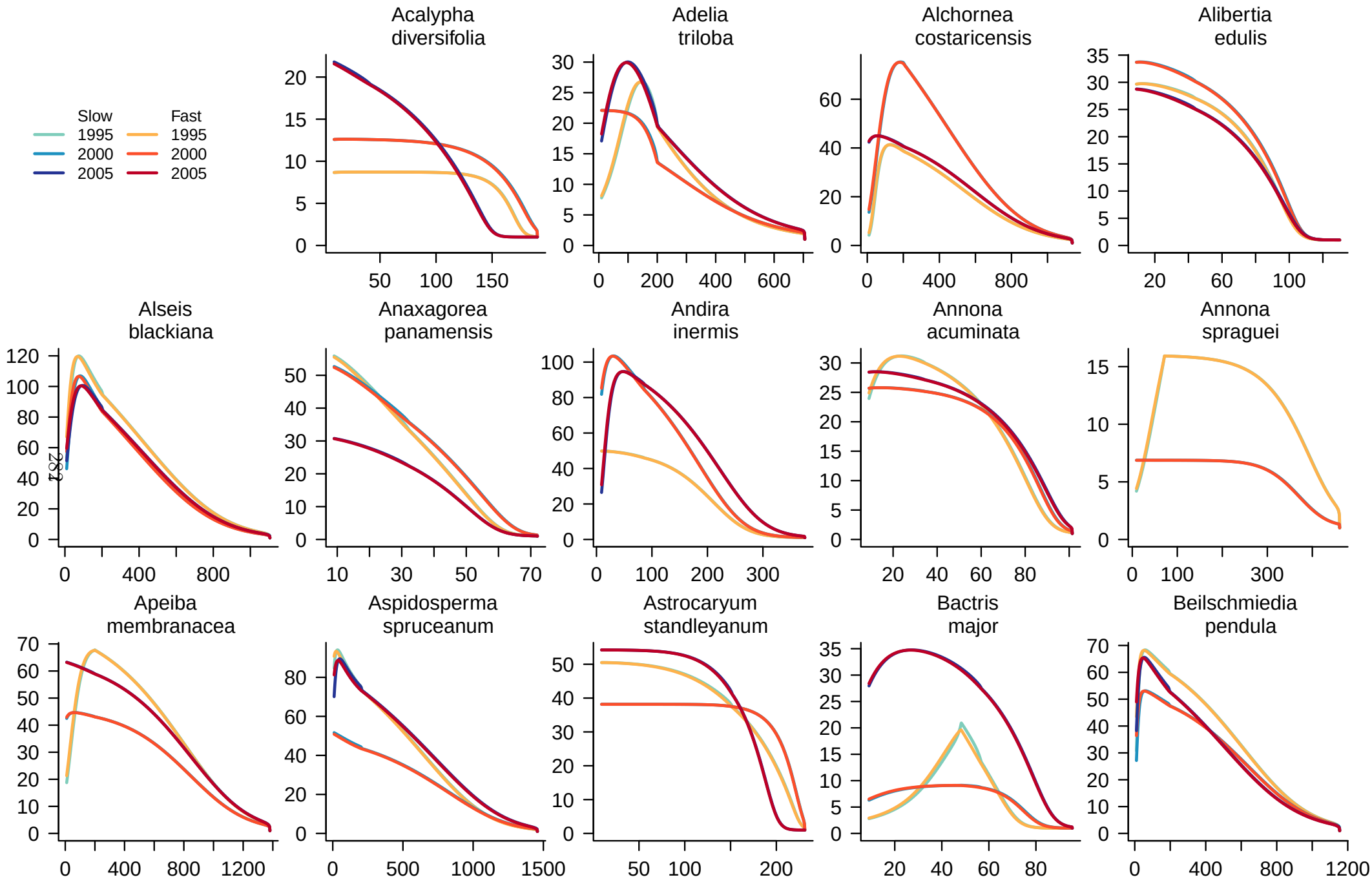
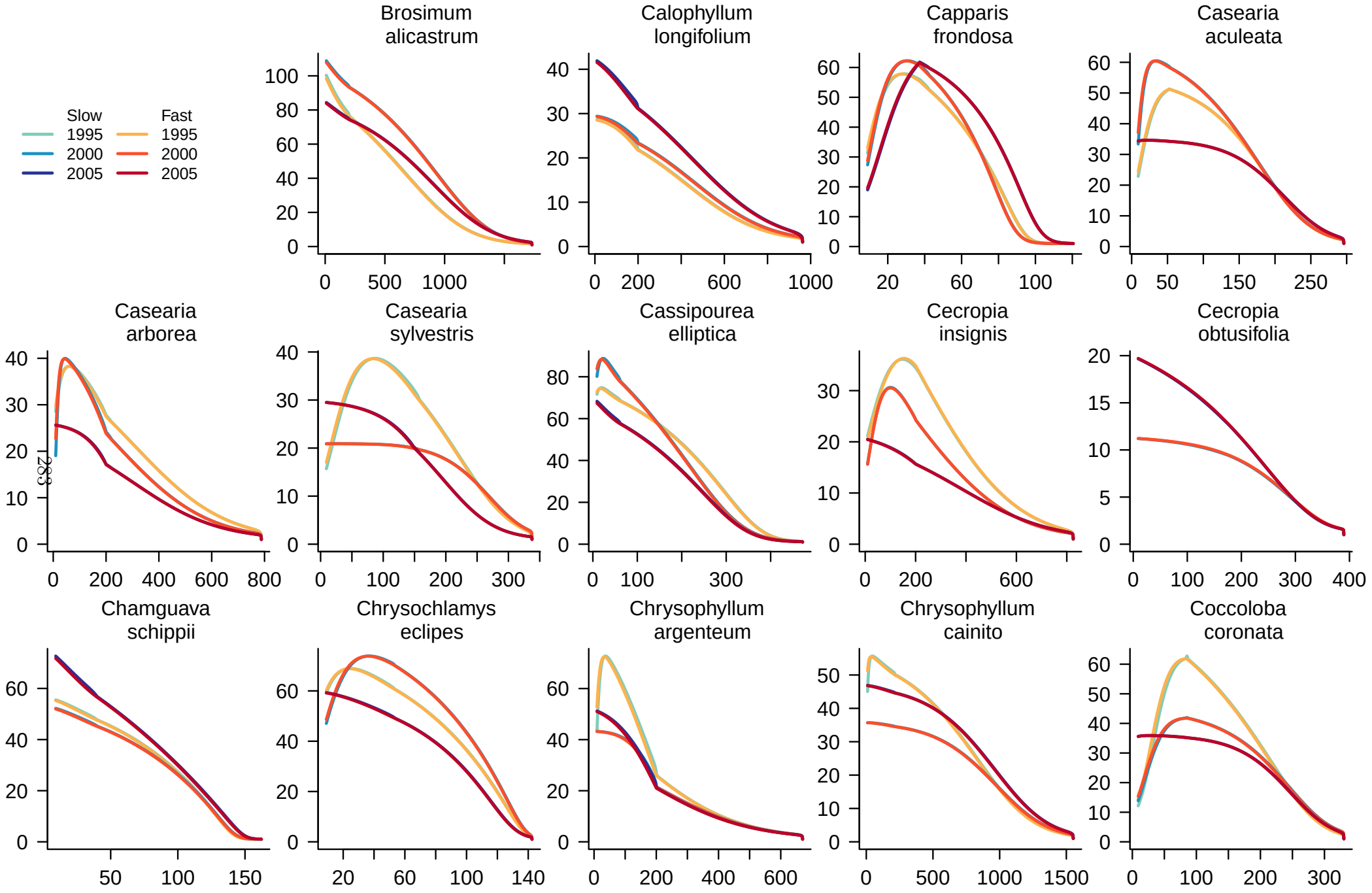
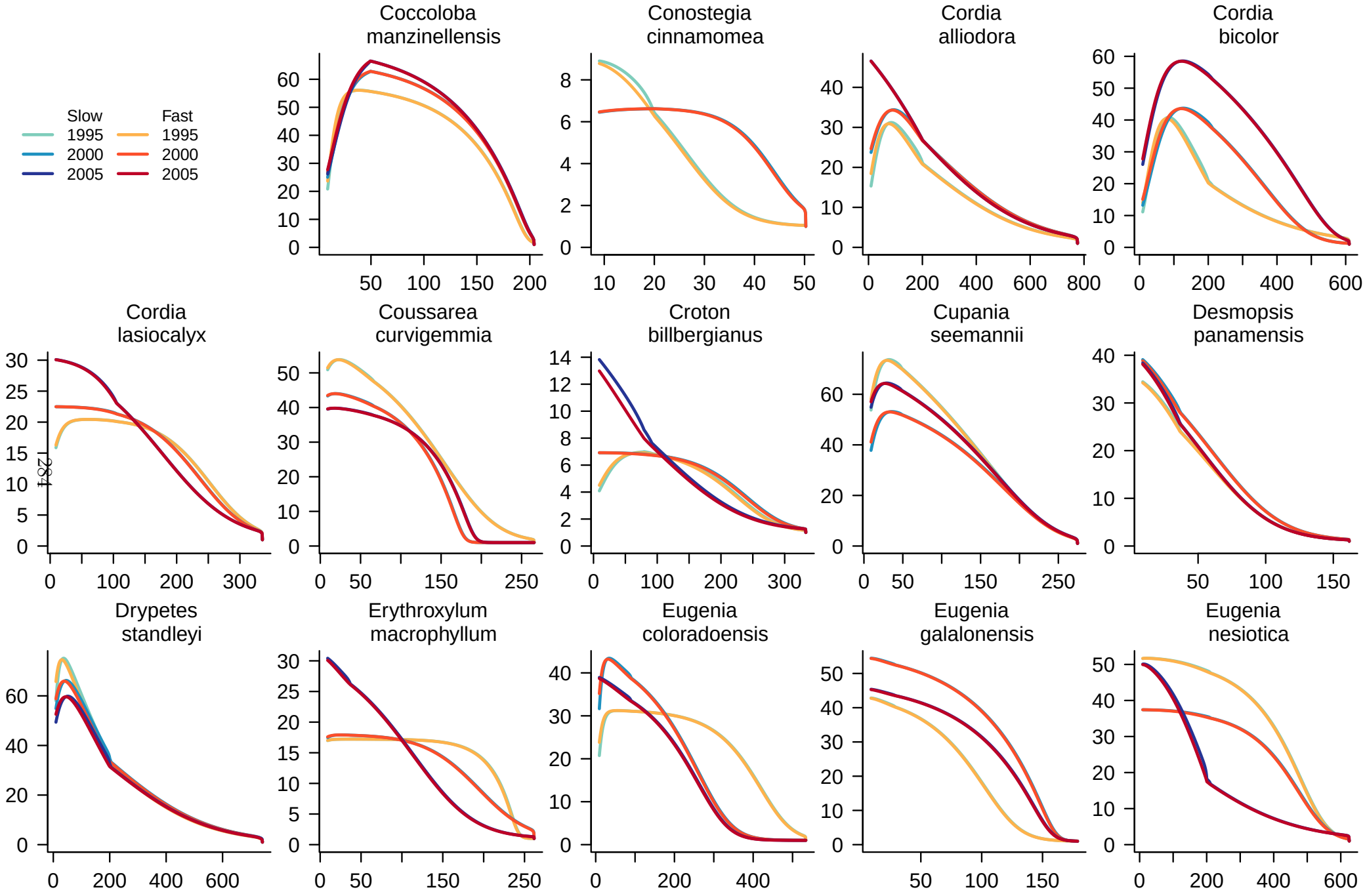
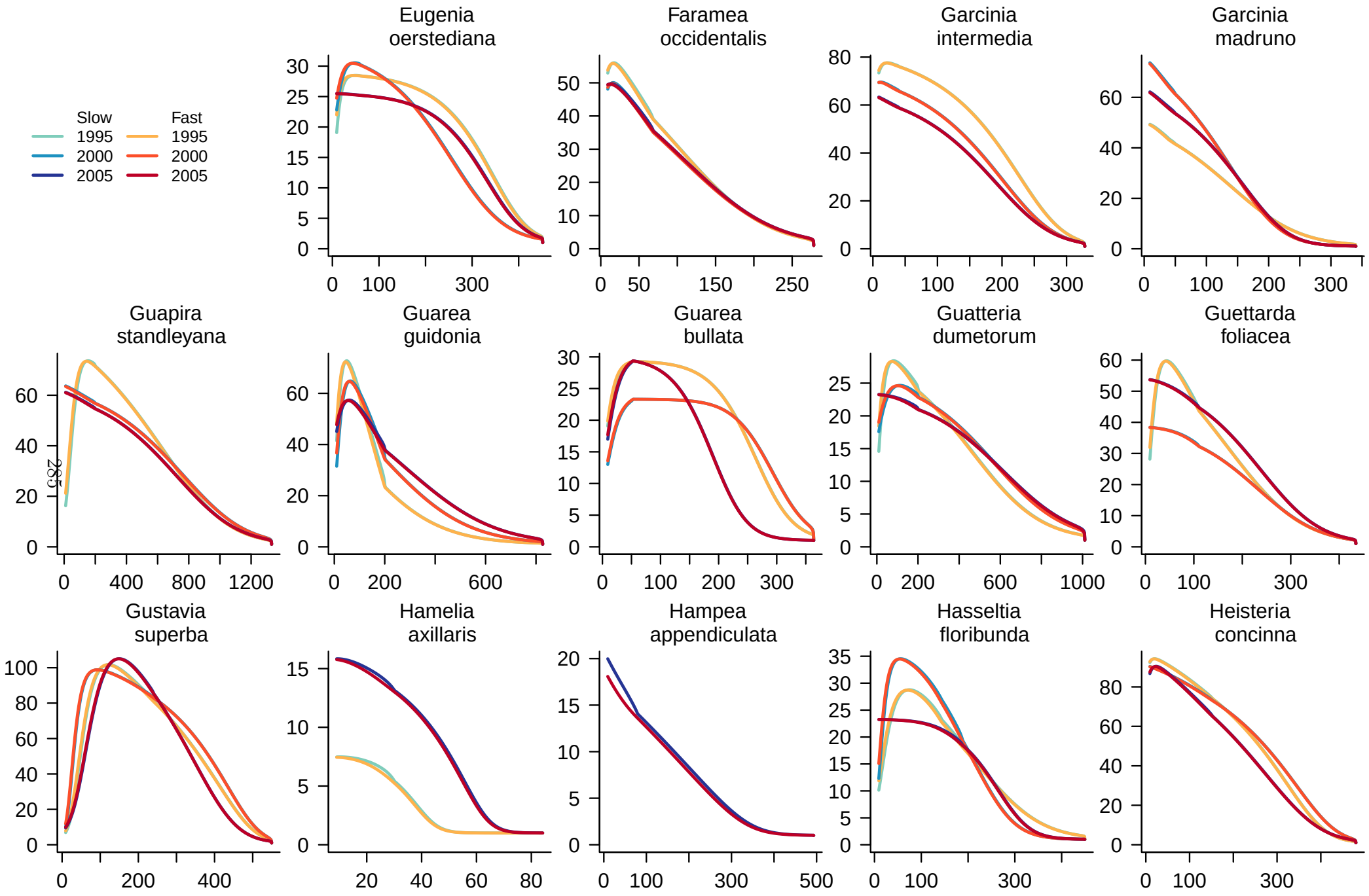

Passage Times
Slow
1995
2000
2005
Fast
1995
2000
2005
Triplaris cumingiana
Trophis racemosa
Unonopsis pittieri
Virola sebifera
Virola surinamensis
Xylopia macrantha
Zanthoxylum ekmanii
Zanthoxylum panamense
Years
DBH (mm)

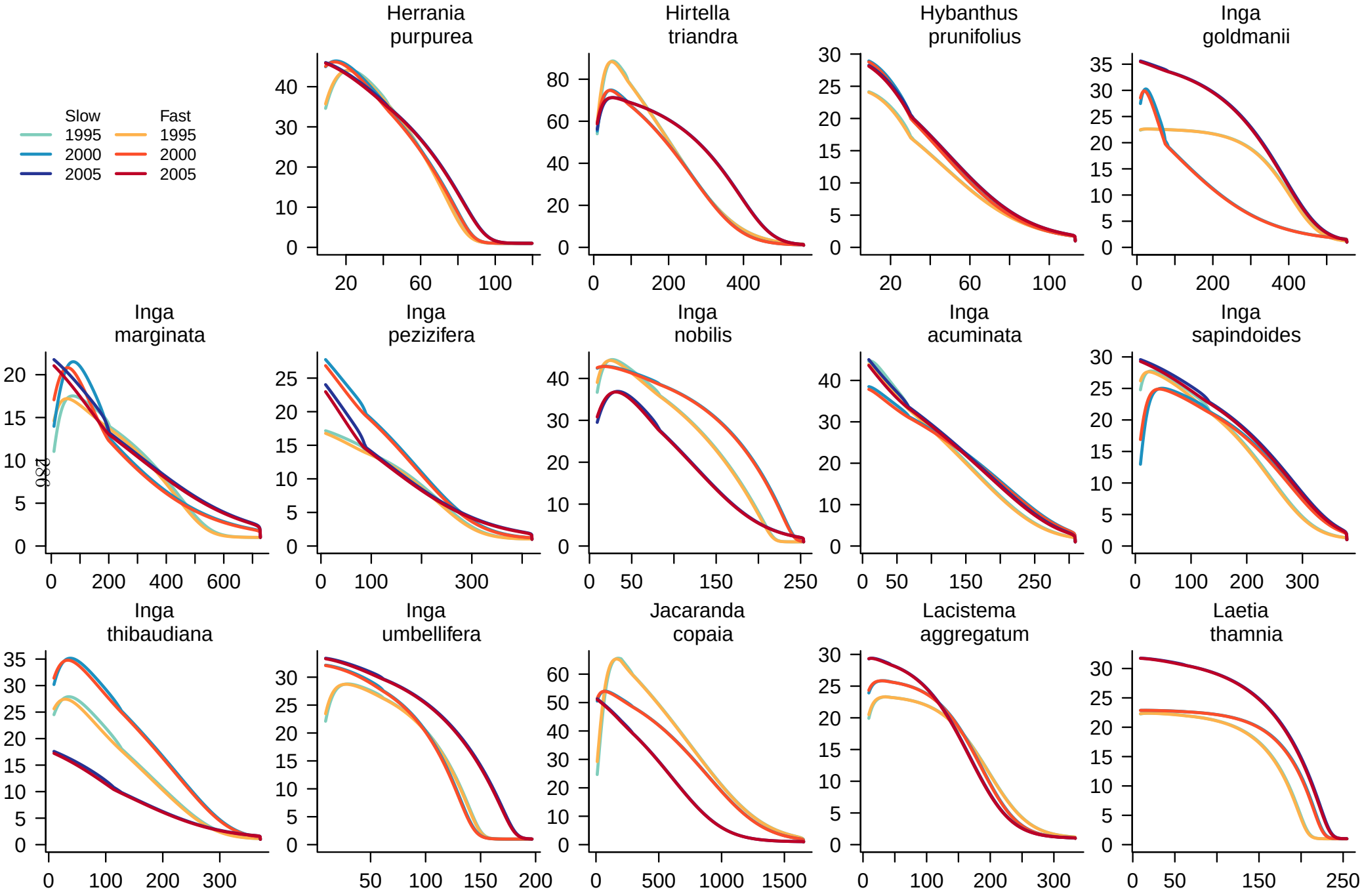
Figure F.3: Passage times to the size threshold for fast growth for each BCI species conditional on growth distribution. For species with a maximum observed size above 500 mm this was set to 200 mm, otherwise it was the 0.8^{th} quantile of the size distribution. Passage times were lower for individuals in the fast growth distribution, although the between census variation meant that in some cases, a slow growing individual in one census had a lower passage time than a fast growing individual from another census.

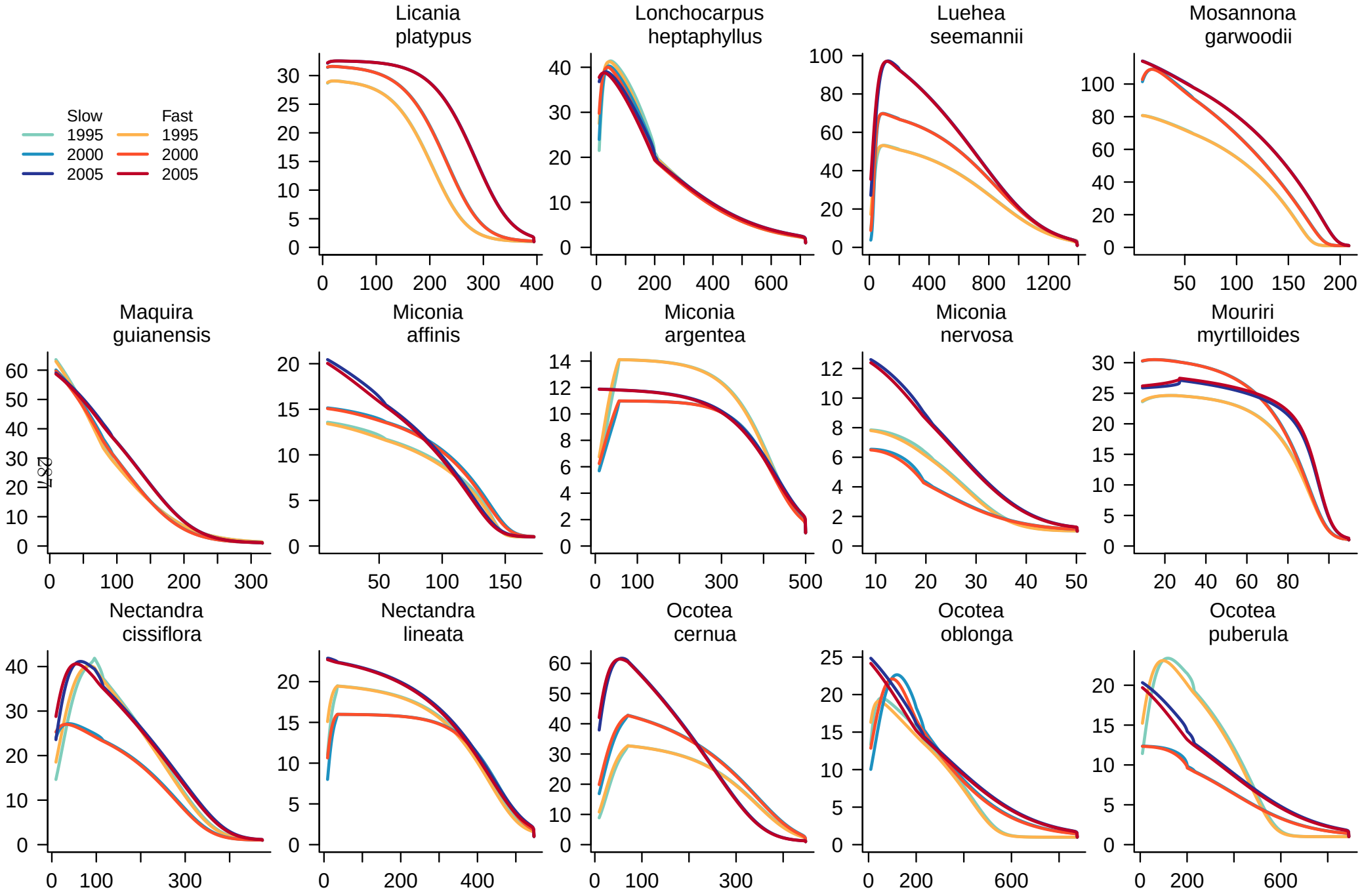

Slow
1995
2000
2005
Fast
1995
2000
2005
Acalypha diversifolia
Adelia triloba
Alchornea costaricensis
Alibertia edulis
Alseis blackiana
Anaxagorea panamensis
Andira inermis
Annona acuminata
Annona spraguei
Apeiba membranacea
Aspidosperma spruceanum
Astrocaryum standleyanum
Bactris major
Beilschmiedia pendula

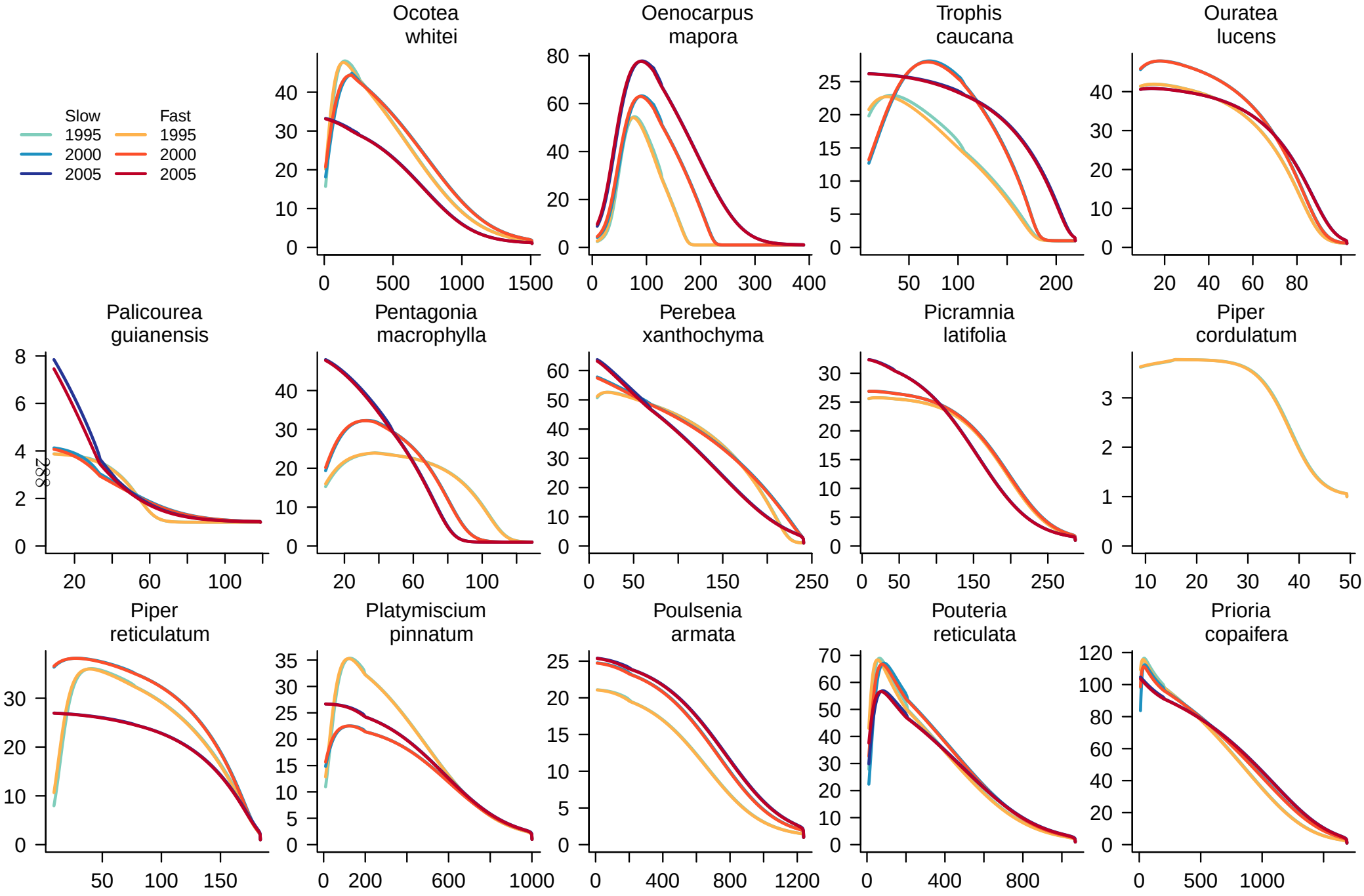

Slow
1995
2000
2005
Fast
1995
2000
2005
Brosimum alicastrum
Calophyllum longifolium
Capparis frondosa
Casearia aculeata
Casearia arborea
Casearia sylvestris
Cassipourea elliptica
Cecropia insignis
Cecropia obtusifolia
Chamguava schippii
Chrysochlamys eclipes
Chrysophyllum argenteum
Chrysophyllum cainito
Coccoloba coronata

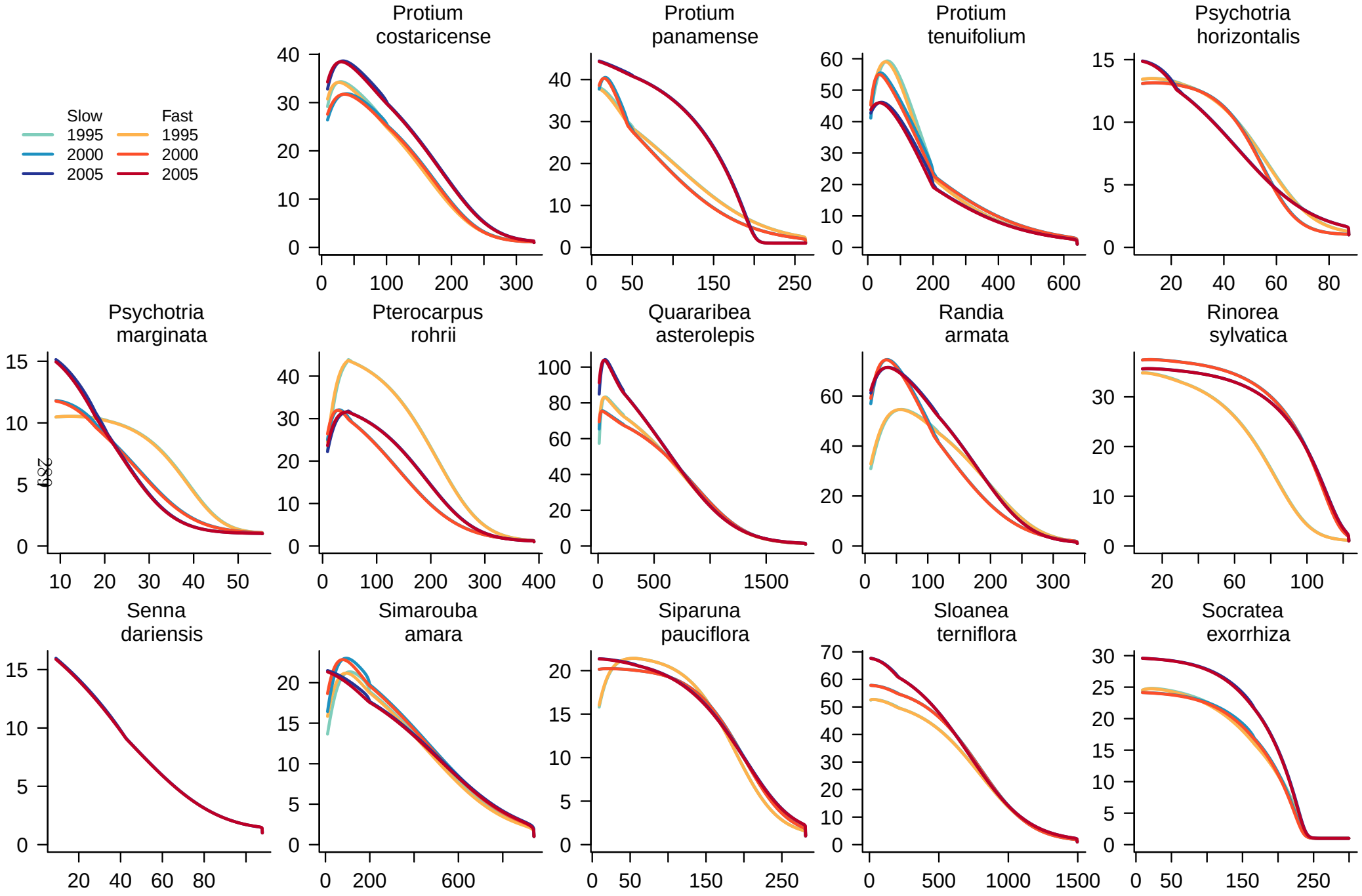

Slow
1995
2000
2005
Fast
1995
2000
2005
Coccoloba manzinellensis
Conostegia cinnamomea
Cordia alliodora
Cordia bicolor
Cordia lasiocalyx
Coussarea curvigemmia
Croton billbergianus
Cupania seemannii
Desmopsis panamensis
Drypetes standleyi
Erythroxylum macrophyllum
Eugenia coloradoensis
Eugenia galalonensis
Eugenia nesiotica
284

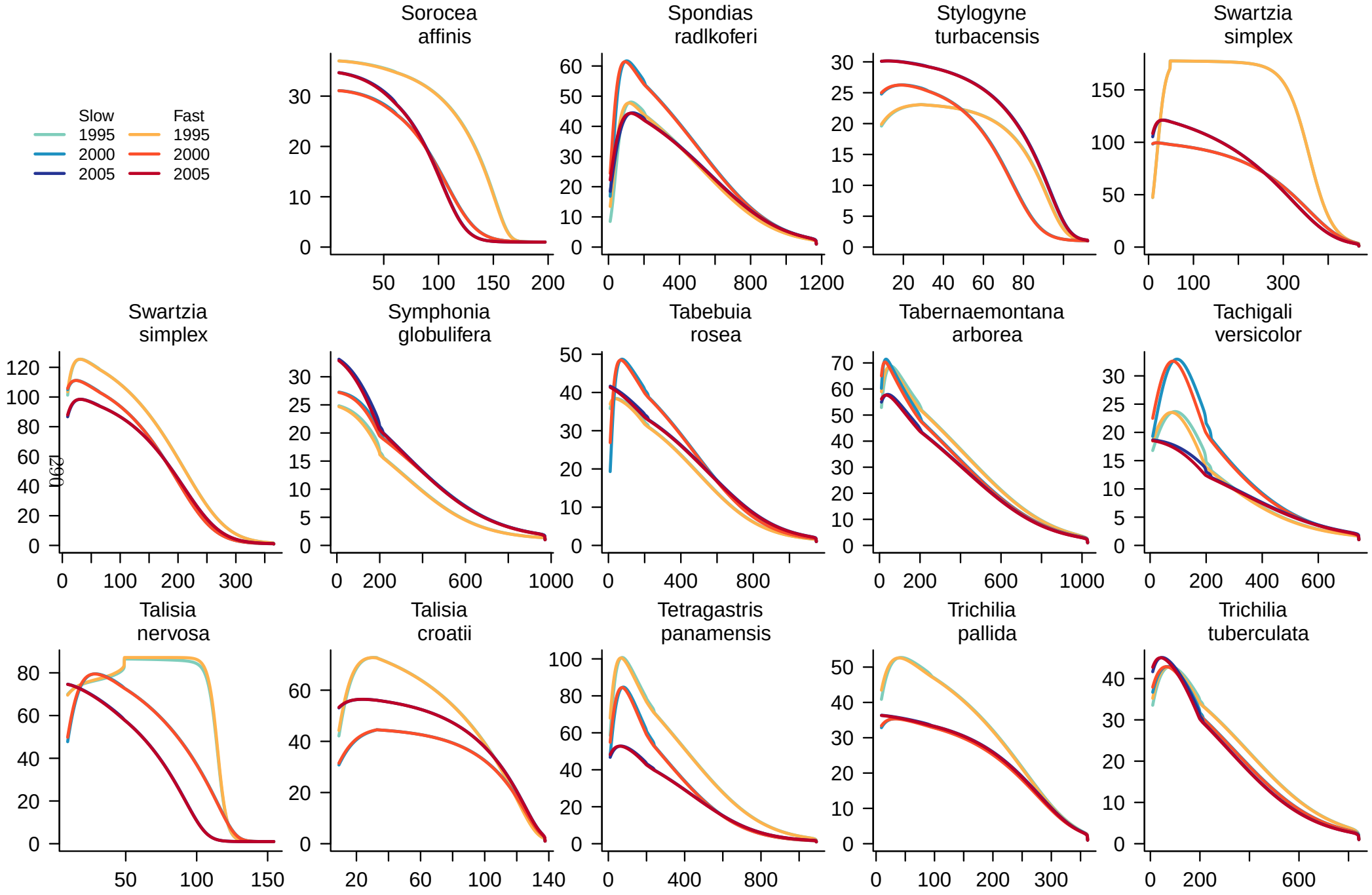

Slow
1995
2000
2005
Fast
1995
2000
2005
Eugenia oerstediana
Faramea occidentalis
Garcinia intermedia
Garcinia madruno
Guapira standleyana
Guarea guidonia
Guarea bullata
Guatteria dumetorum
Guettarda foliacea
Gustavia superba
Hamelia axillaris
Hampea appendiculata
Hasseltia floribunda
Heisteria concinna
285


Slow
1995
2000
2005
Fast
1995
2000
2005
Herrania purpurea
Hirtella triandra
Hybanthus prunifolius
Inga goldmanii
Inga marginata
Inga pezizifera
Inga nobilis
Inga acuminata
Inga sapindoides
Inga thibaudiana
Inga umbellifera
Jacaranda copaia
Lacistema aggregatum
Laetia thamnia
286


Slow
1995
2000
2005
Fast
1995
2000
2005
Licania platypus
Lonchocarpus heptaphyllus
Luehea seemannii
Mosannona garwoodii
Maquira guianensis
Miconia affinis
Miconia argentea
Miconia nervosa
Mouriri myrtilloides
Nectandra cissiflora
Nectandra lineata
Ocotea cernua
Ocotea oblonga
Ocotea puberula
log(RGR)


Slow
1995
2000
2005
Fast
1995
2000
2005
Ocotea whitei
Oenocarpus mapora
Trophis caucana
Ouratea lucens
Palicourea guianensis
Pentagonia macrophylla
Perebea xanthochyma
Picramnia latifolia
Piper cordulatum
Piper reticulatum
Platymiscium pinnatum
Poulsenia armata
Pouteria reticulata
Prioria copaifera


Slow
1995
2000
2005
Fast
1995
2000
2005
Protium costaricense
Protium panamense
Protium tenuifolium
Psychotria horizontalis
Psychotria marginata
Pterocarpus rohrii
Quararibea asterolepis
Randia armata
Rinorea sylvatica
Senna dariensis
Simarouba amara
Siparuna pauciflora
Sloanea terniflora
Socratea exorrhiza
289


Slow
1995
2000
2005
Fast
1995
2000
2005
Sorocea affinis
Spondias radlkoferi
Stylogyne turbacensis
Swartzia simplex
Swartzia simplex
Symphonia globulifera
Tabebuia rosea
Tabernaemontana arborea
Tachigali versicolor
Talisia nervosa
Talisia croatii
Tetragastris panamensis
Trichilia pallida
Trichilia tuberculata
l290

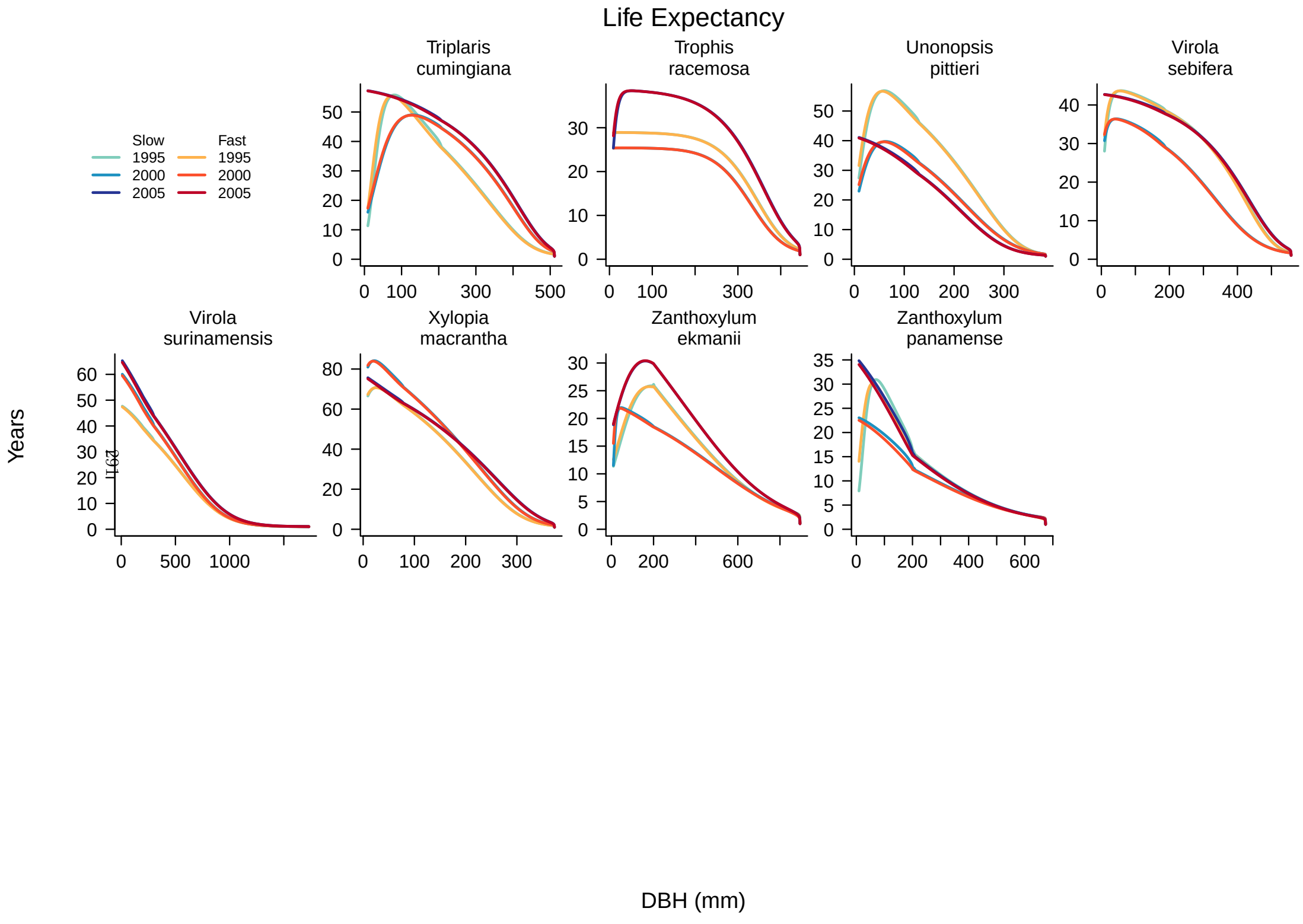

Life Expectancy
Slow
1995
2000
2005
Fast
1995
2000
2005
Triplaris cumingiana
Trophis racemosa
Unonopsis pittieri
Virola sebifera
Virola surinamensis
Xylopia macrantha
Zanthoxylum ekmanii
Zanthoxylum panamense
Years
DBH (mm)

Figure F.4: Life expectancies for BCI species conditional on growth distribution. For any given size there was considerable variation in life expectancy between species but generally very little effect of growth distribution. However, life expectancies differed between years for many species.

F.3 Vital rate parameter tables for 134 BCI species

Table F.1: Survival parameters for BCI species

Species	Census Interval	K	p1	r1	p2	r2	thresh
Acalypha diversifolia	1995-2000	0.885	-24.898	0.178	179.275	-0.298	40.82
	2000-2005	0.921	-26.321	0.185	190.514	-0.291	40.82
	2005-2010	0.96	-31.39	0.207	152.271	-0.266	40.82
Adelia triloba	1995-2000	0.985	-127.363	0.014	701.725	-0.007	200
	2000-2005	0.955	-112.832	0.136	740.273	-0.007	200
	2005-2010	0.974	-113	0.023	777.853	-0.007	200
Alchornea costaricensis	1995-2000	0.979	-3.328	0.043	1201.447	-0.006	200
	2000-2005	0.993	-78.781	0.02	1244.558	-0.007	200
	2005-2010	0.979	-96.199	0.042	1230.676	-0.007	200
Alibertia edulis	1995-2000	0.967	-24.981	0.183	108.894	-0.298	37.235
	2000-2005	0.972	-25.359	0.186	110.682	-0.33	37.235
	2005-2010	0.967	-26.157	0.192	110.819	-0.305	37.235
Alseis blackiana	1995-2000	0.995	-64.875	0.043	1258.027	-0.007	200
	2000-2005	0.994	-80.28	0.035	1206.568	-0.007	200
	2005-2010	0.994	-121.417	0.026	1232.668	-0.007	200
Anaxagorea panamensis	1995-2000	0.99	-21.191	0.182	64.85	-0.371	30.425
	2000-2005	0.986	-22.813	0.196	69.484	-0.367	30.425
	2005-2010	0.972	-24.203	0.21	63.93	-0.333	30.425
Andira inermis	1995-2000	0.98	-49.866	0.149	316.781	-0.042	79.912
	2000-2005	0.992	-28.283	0.105	328.528	-0.04	79.912
	2005-2010	0.991	-12.775	0.105	370.02	-0.037	79.912
Annona acuminata	1995-2000	0.971	-9.432	0.18	95.63	-0.292	34.141
	2000-2005	0.962	-24.998	0.199	99.156	-0.323	34.141
	2005-2010	0.966	-24.664	0.19	102.022	-0.337	34.141
Annona spraguei	1995-2000	0.937	-19.458	0.034	485.148	-0.036	71.262
	2000-2005	0.855	-42.601	0.167	436.039	-0.035	71.262
	2005-2010	0.884	-46.634	0.171	361.678	-0.038	71.262
Apeiba membranacea	1995-2000	0.988	-113.02	0.019	1539.073	-0.007	200
	2000-2005	0.978	-83.138	0.051	1492.509	-0.007	200
	2005-2010	0.985	-115.528	0.149	1547.52	-0.007	200
Aspidosperma spruceanum	1995-2000	0.992	-45.464	0.082	1474.246	-0.007	200
	2000-2005	0.982	-95.655	0.114	1508.132	-0.007	200
	2005-2010	0.992	-53.508	0.059	1580.379	-0.007	200
Astrocaryum standleyanum	1995-2000	0.98	-53.324	0.146	229.885	-0.302	152.329
	2000-2005	0.974	-82.738	0.142	236.165	-0.303	152.329
	2005-2010	0.982	-79.235	0.143	209.061	-0.236	152.329
Bactris major	1995-2000	0.974	-0.776	0.061	75.333	-0.364	48.238
	2000-2005	0.892	-16.764	0.102	83.169	-0.342	48.238
	2005-2010	0.973	-18.432	0.142	91.155	-0.344	48.238
Beilschmiedia pendula	1995-2000	0.986	-19.457	0.091	1288.432	-0.007	200
	2000-2005	0.982	-20.024	0.093	1281.222	-0.007	200
	2005-2010	0.987	-27.539	0.08	1277.532	-0.006	200
Brosimum alicastrum	1995-2000	0.992	-122.028	0.149	1641.796	-0.006	200
	2000-2005	0.992	-106.419	0.145	1758.414	-0.007	200
	2005-2010	0.989	-116.356	0.151	1817.483	-0.006	200
Calophyllum longifolium	1995-2000	0.965	-116.731	0.156	957.43	-0.007	200
	2000-2005	0.966	-119.555	0.155	999.478	-0.007	200
	2005-2010	0.977	-124.334	0.159	1076.68	-0.007	200
Capparis frondosa	1995-2000	0.987	-13.527	0.131	99.744	-0.345	37.186
	2000-2005	0.987	-12.569	0.135	96.441	-0.293	37.186
	2005-2010	0.986	-22.123	0.087	109.991	-0.282	37.186
Casearia aculeata	1995-2000	0.982	-33.721	0.067	302.205	-0.04	52.789
	2000-2005	0.985	-10.064	0.147	305.593	-0.037	52.789
	2005-2010	0.971	-32.296	0.161	314.55	-0.039	52.789
Casearia arborea	1995-2000	0.978	-44.8	0.052	893.991	-0.007	200
	2000-2005	0.979	-1.621	0.122	832.692	-0.007	200
	2005-2010	0.962	-114.647	0.142	802.492	-0.007	200
Casearia sylvestris	1995-2000	0.98	-60.209	0.035	355.761	-0.034	147.934
	2000-2005	0.952	-65.04	0.117	356.813	-0.039	147.934
	2005-2010	0.967	-90.532	0.155	320.849	-0.031	147.934
Cassipourea elliptica	1995-2000	0.989	-18.858	0.164	437.878	-0.038	56.568
	2000-2005	0.993	-25.305	0.115	424.355	-0.029	56.568
	2005-2010	0.988	-36.169	0.162	415.259	-0.032	56.568
Cecropia insignis	1995-2000	0.992	-156.734	0.013	900.182	-0.007	200
	2000-2005	0.99	-38.639	0.028	845.524	-0.007	200
	2005-2010	0.955	-122.151	0.148	883.525	-0.007	200
Cecropia obtusifolia	1995-2000	0.934	-89.837	0.15	374.117	-0.036	166.301
	2000-2005	0.914	-65.31	0.095	381.692	-0.036	166.301
	2005-2010	0.962	-90.642	0.152	376.487	-0.032	166.301
Chamguava schippii	1995-2000	0.985	-25.957	0.199	146.113	-0.308	37

Continued on next page

Table F.1 –continued from previous page

Species	Census Interval	K	p1	r1	p2	r2	thresh
	2000-2005	0.984	-26.876	0.198	147.567	-0.273	37
	2005-2010	0.992	-27.39	0.194	153.097	-0.323	37
Chrysochlamys eclipes	1995-2000	0.988	-23.8	0.122	143.441	-0.312	52.362
	2000-2005	0.989	-34.191	0.083	144.592	-0.312	52.362
	2005-2010	0.984	-35.242	0.178	142.113	-0.195	52.362
Chrysophyllum argenteum	1995-2000	0.989	-13.83	0.124	749.088	-0.007	200
	2000-2005	0.977	-57.52	0.135	751.64	-0.007	200
	2005-2010	0.981	-104.024	0.124	747.87	-0.007	200
Chrysophyllum cainito	1995-2000	0.983	-27.669	0.106	1556.378	-0.006	200
	2000-2005	0.972	-65.204	0.114	1599.636	-0.006	200
	2005-2010	0.979	-99.262	0.135	1647.119	-0.006	200
Coccoloba coronata	1995-2000	0.989	-48.747	0.04	343.049	-0.042	85.085
	2000-2005	0.978	-41.262	0.05	355.064	-0.039	85.085
	2005-2010	0.972	-42.291	0.134	353.138	-0.038	85.085
Coccoloba manzinellensis	1995-2000	0.983	-3.751	0.173	202.958	-0.304	49.334
	2000-2005	0.985	-27.757	0.079	207.591	-0.302	49.334
	2005-2010	0.986	-37.557	0.064	208.075	-0.308	49.334
Conostegia cinnamomea	1995-2000	0.897	-14.592	0.204	37.977	-0.237	20.085
	2000-2005	0.85	-14.585	0.202	51.055	-0.34	20.085
	2005-2010	0.911	-15.026	0.204	41.719	-0.16	20.085
Cordia alliodora	1995-2000	0.981	-48.501	0.033	817.019	-0.007	200
	2000-2005	0.984	-113.577	0.021	873.065	-0.007	200
	2005-2010	0.987	-116.429	0.156	867.981	-0.007	200
Cordia bicolor	1995-2000	0.991	-30.755	0.037	708.695	-0.007	200
	2000-2005	0.985	-65.771	0.025	561.836	-0.026	200
	2005-2010	0.989	-84.574	0.025	618.24	-0.037	200
Cordia lasiocalyx	1995-2000	0.951	-23.025	0.103	352.12	-0.033	104.671
	2000-2005	0.956	-57.596	0.15	347.997	-0.031	104.671
	2005-2010	0.967	-61.071	0.148	354.32	-0.021	104.671
Coussarea curvigemmia	1995-2000	0.983	-35.145	0.106	265.33	-0.043	51.347
	2000-2005	0.978	-29.279	0.148	183.106	-0.282	51.347
	2005-2010	0.975	-31.017	0.155	196.54	-0.274	51.347
Croton billbergianus	1995-2000	0.863	-15.352	0.056	289.652	-0.038	78.906
	2000-2005	0.856	-39.138	0.155	304.34	-0.037	78.906
	2005-2010	0.947	-52.598	0.179	271.872	-0.02	78.906
Cupania seemannii	1995-2000	0.992	-29.729	0.086	293.81	-0.043	48.725
	2000-2005	0.985	-27.409	0.092	295.351	-0.043	48.725
	2005-2010	0.988	-35.347	0.087	297.314	-0.042	48.725
Desmopsis panamensis	1995-2000	0.974	-28.583	0.213	138.217	-0.051	36.326
	2000-2005	0.978	-29.028	0.215	144.745	-0.052	36.326
	2005-2010	0.978	-31.039	0.224	137.766	-0.051	36.326
Drypetes standleyi	1995-2000	0.991	-35.626	0.077	835.244	-0.007	200
	2000-2005	0.989	-81.579	0.044	852.287	-0.007	200
	2005-2010	0.988	-105.902	0.035	842.219	-0.007	200
Erythroxylum macrophyllum	1995-2000	0.942	-24.706	0.179	244.512	-0.294	37.158
	2000-2005	0.944	-23.189	0.173	275.185	-0.04	37.158
	2005-2010	0.97	-27.803	0.2	228.279	-0.035	37.158
Eugenia coloradoensis	1995-2000	0.968	-15.891	0.121	536.935	-0.034	66.119
	2000-2005	0.979	-15.357	0.131	394.791	-0.034	66.119
	2005-2010	0.975	-41.245	0.169	378.846	-0.038	66.119
Eugenia galalonensis	1995-2000	0.978	-22.644	0.221	148.387	-0.099	27.322
	2000-2005	0.983	-23.167	0.221	166.401	-0.284	27.322
	2005-2010	0.979	-23.511	0.225	164.692	-0.219	27.322
Eugenia nesiotica	1995-2000	0.981	-64.195	0.113	609.631	-0.036	200
	2000-2005	0.973	-108.491	0.134	612.017	-0.031	200
	2005-2010	0.981	-73.581	0.082	695.017	-0.007	200
Eugenia oerstediana	1995-2000	0.965	-15.407	0.119	456.439	-0.035	59.194
	2000-2005	0.97	-39.511	0.071	431.338	-0.023	59.194
	2005-2010	0.961	-40.588	0.169	448.013	-0.033	59.194
Faramea occidentalis	1995-2000	0.987	-12.433	0.181	304.405	-0.024	68.756
	2000-2005	0.984	-11.279	0.201	314.3	-0.022	68.756
	2005-2010	0.984	-39.031	0.104	314.504	-0.023	68.756
Garcinia intermedia	1995-2000	0.988	-22.745	0.151	347.727	-0.043	40.933
	2000-2005	0.987	-30.806	0.153	340.674	-0.036	40.933
	2005-2010	0.985	-33.26	0.212	342.823	-0.032	40.933
Garcinia madruno	1995-2000	0.982	-26.908	0.191	332.62	-0.023	39.613
	2000-2005	0.989	-29.264	0.199	280.074	-0.037	39.613
	2005-2010	0.986	-28.436	0.195	280.704	-0.041	39.613
Guapira standleyana	1995-2000	0.99	-85.462	0.024	1404.746	-0.007	200
	2000-2005	0.985	-100.467	0.132	1466.194	-0.007	200
	2005-2010	0.984	-107.875	0.141	1426.027	-0.007	200
Guarea guidonia	1995-2000	0.991	-38.214	0.062	709.269	-0.007	200
	2000-2005	0.988	-44.249	0.054	830.55	-0.007	200
	2005-2010	0.986	-88.229	0.039	934.507	-0.007	200
Guarea bullata	1995-2000	0.966	-26.729	0.092	363.703	-0.037	52.56
	2000-2005	0.957	-31.32	0.073	386.04	-0.037	52.56
	2005-2010	0.967	-36.801	0.068	282.064	-0.041	52.56
Guatteria dumetorum	1995-2000	0.967	-38.925	0.053	983.824	-0.007	200
	2000-2005	0.962	-117.442	0.027	1084.315	-0.007	200
	2005-2010	0.957	-117.811	0.149	1120.183	-0.007	200
Guettarda foliacea	1995-2000	0.987	-17.569	0.093	448.886	-0.017	110.724
	2000-2005	0.974	-58.339	0.152	446.92	-0.019	110.724
	2005-2010	0.982	-48.026	0.141	451.406	-0.021	110.724
Gustavia superba	1995-2000	0.993	-24.873	0.04	570	-0.038	235.898
	2000-2005	0.991	-12.547	0.067	580.126	-0.038	235.898
	2005-2010	0.994	-60.885	0.027	551.234	-0.029	235.898
Hamelia axillaris	1995-2000	0.871	-17.095	0.197	46.076	-0.326	24.436
	2000-2005	0.881	-15.018	0.168	50.75	-0.301	24.436
	2005-2010	0.941	-17.817	0.198	66.881	-0.321	24.436
Hampea appendiculata	1995-2000						
	2000-2005						
	2005-2010	0.984	-45.826	0.176	371.924	-0.031	70.903

Continued on next page

Table F.1 –continued from previous page

Species	Census Interval	K	p1	r1	p2	r2	thresh
Hasseltia floribunda	1995-2000	0.968	-23.113	0.06	429.952	-0.019	143.967
	2000-2005	0.973	-8.207	0.098	344.651	-0.033	143.967
	2005-2010	0.957	-79.244	0.122	360.198	-0.038	143.967
Heisteria concinna	1995-2000	0.991	-23.523	0.149	471.57	-0.038	148.328
	2000-2005	0.99	-42.69	0.176	500.01	-0.036	148.328
	2005-2010	0.992	-27.702	0.117	493.61	-0.026	148.328
Herrania purpurea	1995-2000	0.984	-14.373	0.14	89.785	-0.327	41.72
	2000-2005	0.984	-20.855	0.147	91.406	-0.361	41.72
	2005-2010	0.981	-27.372	0.185	99.706	-0.295	41.72
Hirtella triandra	1995-2000	0.994	-54.329	0.051	528.638	-0.018	82.24
	2000-2005	0.99	-48.034	0.063	488.783	-0.024	82.24
	2005-2010	0.987	-45.959	0.07	534.464	-0.036	82.24
Hybanthus prunifolius	1995-2000	0.961	-24.089	0.21	109.747	-0.057	30.191
	2000-2005	0.969	-24.129	0.198	109.148	-0.06	30.191
	2005-2010	0.968	-27.514	0.232	112.441	-0.06	30.191
Inga goldmanii	1995-2000	0.956	-30.741	0.155	512.684	-0.034	74.088
	2000-2005	0.976	-30.24	0.091	507.39	-0.01	74.088
	2005-2010	0.973	-47.234	0.174	530.506	-0.031	74.088
Inga marginata	1995-2000	0.953	-31.58	0.047	567.617	-0.032	200
	2000-2005	0.983	-65.881	0.026	719.534	-0.007	200
	2005-2010	0.959	-119.949	0.153	811.917	-0.007	200
Inga pezizifera	1995-2000	0.945	-48.799	0.152	334.438	-0.036	86.424
	2000-2005	0.97	-51.276	0.159	362.544	-0.025	86.424
	2005-2010	0.967	-52.109	0.163	422.076	-0.013	86.424
Inga nobilis	1995-2000	0.982	-14.527	0.136	220.532	-0.3	81.129
	2000-2005	0.978	-38.694	0.118	245.775	-0.297	81.129
	2005-2010	0.98	-35.137	0.073	255.858	-0.035	81.129
Inga acuminata	1995-2000	0.986	-29.806	0.121	311.858	-0.034	66.589
	2000-2005	0.981	-32.516	0.131	334.137	-0.038	66.589
	2005-2010	0.987	-45.004	0.179	332.292	-0.036	66.589
Inga sapindoides	1995-2000	0.966	-14.816	0.144	351.845	-0.039	126.075
	2000-2005	0.963	-7.229	0.109	387.609	-0.037	126.075
	2005-2010	0.969	-68.109	0.138	393.336	-0.039	126.075
Inga thibaudiana	1995-2000	0.987	-38.649	0.052	323.599	-0.04	113.861
	2000-2005	0.986	-37.95	0.057	352.63	-0.042	113.861
	2005-2010	0.955	-69.25	0.163	354.241	-0.017	113.861
Inga umbellifera	1995-2000	0.967	-10.492	0.157	153.515	-0.297	56.727
	2000-2005	0.97	-34.892	0.181	149.586	-0.236	56.727
	2005-2010	0.971	-36.238	0.167	184.591	-0.298	56.727
Jacaranda copaia	1995-2000	0.991	-81.251	0.02	1736.881	-0.006	200
	2000-2005	0.984	-117.115	0.032	1653.135	-0.006	200
	2005-2010	0.984	-113.154	0.132	1285.572	-0.007	200
Lacistema aggregatum	1995-2000	0.958	-20.803	0.133	292.025	-0.037	34.951
	2000-2005	0.962	-24.697	0.138	272.561	-0.042	34.951
	2005-2010	0.967	-25.654	0.185	266.783	-0.039	34.951
Laetia thamnia	1995-2000	0.956	-30.971	0.164	211.27	-0.29	59.851
	2000-2005	0.956	-39.774	0.17	229.474	-0.294	59.851
	2005-2010	0.969	-39.534	0.165	238.121	-0.29	59.851
Licania platypus	1995-2000	0.966	-25.015	0.181	305.042	-0.038	37.782
	2000-2005	0.968	-27.089	0.194	334.403	-0.038	37.782
	2005-2010	0.969	-25.946	0.181	392.277	-0.037	37.782
Lonchocarpus heptaphyllus	1995-2000	0.978	-15.947	0.099	749.121	-0.007	200
	2000-2005	0.978	-14.29	0.106	759.022	-0.007	200
	2005-2010	0.977	-58.245	0.065	782.238	-0.007	200
Luehea seemannii	1995-2000	0.982	-10.842	0.065	1514.768	-0.007	200
	2000-2005	0.986	4.596	0.089	1537.721	-0.007	200
	2005-2010	0.992	-62.324	0.033	1543.78	-0.007	200
Mosannona garwoodii	1995-2000	0.989	-32.59	0.17	178.342	-0.314	53.468
	2000-2005	0.994	-16.742	0.165	190.444	-0.301	53.468
	2005-2010	0.992	-36.23	0.183	203.299	-0.295	53.468
Maquira guianensis	1995-2000	0.988	-51.318	0.17	283.415	-0.025	79.488
	2000-2005	0.987	-42.009	0.161	257.855	-0.033	79.488
	2005-2010	0.986	-51.883	0.165	267.249	-0.038	79.488
Miconia affinis	1995-2000	0.929	-33.474	0.183	147.579	-0.298	52.312
	2000-2005	0.936	-37.073	0.183	155.949	-0.187	52.312
	2005-2010	0.958	-36.784	0.194	148.034	-0.171	52.312
Miconia argentea	1995-2000	0.929	-30.33	0.039	504.306	-0.037	56.463
	2000-2005	0.909	-48.038	0.031	505.634	-0.037	56.463
	2005-2010	0.916	-39.968	0.188	512.47	-0.036	56.463
Miconia nervosa	1995-2000	0.886	-13.39	0.198	37.674	-0.291	19.483
	2000-2005	0.859	-12.929	0.194	37.735	-0.147	19.483
	2005-2010	0.937	-15.59	0.217	44.049	-0.189	19.483
Mouriri myrtilloides	1995-2000	0.96	-20.259	0.175	102.858	-0.334	25.754
	2000-2005	0.968	-20.79	0.207	102.801	-0.339	25.754
	2005-2010	0.969	-23.497	0.233	105.472	-0.297	25.754
Nectandra cissiflora	1995-2000	0.99	-70.448	0.026	406.783	-0.039	96.152
	2000-2005	0.967	-39.553	0.073	388.561	-0.039	96.152
	2005-2010	0.988	-54.684	0.038	427.843	-0.041	96.152
Nectandra lineata	1995-2000	0.95	-20.516	0.08	537.65	-0.036	34.677
	2000-2005	0.938	-8.92	0.102	550.245	-0.034	34.677
	2005-2010	0.958	-25.107	0.19	557.071	-0.032	34.677
Ocotea cernua	1995-2000	0.971	-35.103	0.043	463.126	-0.036	70.133
	2000-2005	0.98	-56.764	0.036	473.187	-0.037	70.133
	2005-2010	0.992	-49.349	0.046	413.077	-0.037	70.133
Ocotea oblonga	1995-2000	0.959	-11.493	0.074	561.216	-0.033	200
	2000-2005	0.988	-91.72	0.017	778.893	-0.007	200
	2005-2010	0.966	-115.14	0.137	854.252	-0.007	200
Ocotea puberula	1995-2000	0.967	-80.821	0.025	600.167	-0.036	200
	2000-2005	0.919	-123.9	0.111	779.593	-0.007	200
	2005-2010	0.954	-105.768	0.141	877.963	-0.007	200
Ocotea whitei	1995-2000	0.986	-73.753	0.024	1456.402	-0.006	200
	2000-2005	0.982	-138.17	0.016	1518.494	-0.006	200

Continued on next page

Table F.1 –continued from previous page

Species	Census Interval	K	p1	r1	p2	r2	thresh
	2005-2010	0.971	-133.68	0.071	1302.555	-0.007	200
Oenocarpus mapora	1995-2000	0.995	4.46	0.06	179.617	-0.328	113.079
	2000-2005	0.992	-13.18	0.047	228.823	-0.301	113.079
	2005-2010	0.993	-36.178	0.041	332.243	-0.042	113.079
Trophis caucana	1995-2000	0.965	-33.093	0.074	180.897	-0.289	101.947
	2000-2005	0.974	-45.124	0.041	184.04	-0.314	101.947
	2005-2010	0.962	-58.041	0.157	217.161	-0.291	101.947
Ouratea lucens	1995-2000	0.977	-19.882	0.201	95.087	-0.354	27.383
	2000-2005	0.98	-17.611	0.188	96.928	-0.354	27.383
	2005-2010	0.976	-21.672	0.208	102.314	-0.302	27.383
Palicourea guianensis	1995-2000	0.746	-23.688	0.198	62.331	-0.293	33.461
	2000-2005	0.766	-22.665	0.189	71.738	-0.066	33.461
	2005-2010	0.932	-26.859	0.21	63.508	-0.068	33.461
Pentagonia macrophylla	1995-2000	0.959	-16.693	0.118	117.153	-0.299	37.645
	2000-2005	0.972	-15.418	0.123	98.312	-0.242	37.645
	2005-2010	0.982	-27.175	0.196	87.624	-0.321	37.645
Perebea xanthochyma	1995-2000	0.982	-21.781	0.156	229.661	-0.258	70.091
	2000-2005	0.985	-45.495	0.179	244.238	-0.286	70.091
	2005-2010	0.988	-35.528	0.144	267.576	-0.044	70.091
Picramnia latifolia	1995-2000	0.961	-29.729	0.17	281.842	-0.043	44.624
	2000-2005	0.963	-31.432	0.185	285.175	-0.043	44.624
	2005-2010	0.97	-32.531	0.194	273.006	-0.033	44.624
Piper cordulatum	1995-2000	0.735	-10.631	0.201	42.71	-0.371	15.832
	2000-2005	0.842	-8.887	0.177	49.479	-0.323	15.832
	2005-2010						
Piper reticulatum	1995-2000	0.975	1.424	0.155	185.644	-0.299	76.871
	2000-2005	0.975	-37.301	0.105	185.273	-0.298	76.871
	2005-2010	0.963	-47.456	0.161	186.324	-0.298	76.871
Platymiscium pinnatum	1995-2000	0.974	-65.041	0.031	1046.791	-0.007	200
	2000-2005	0.956	-95.483	0.033	1064.432	-0.007	200
	2005-2010	0.963	-109.539	0.104	1071.365	-0.007	200
Poulsenia armata	1995-2000	0.953	-111.116	0.15	1142.667	-0.007	200
	2000-2005	0.96	-113.293	0.153	1246.129	-0.007	200
	2005-2010	0.961	-108.868	0.147	1306.419	-0.007	200
Pouteria reticulata	1995-2000	0.99	-32.238	0.06	1127.608	-0.007	200
	2000-2005	0.99	-52.461	0.041	1159.181	-0.007	200
	2005-2010	0.986	-64.057	0.04	1180.828	-0.007	200
Prioria copaifera	1995-2000	0.994	-34.154	0.087	1765.845	-0.007	200
	2000-2005	0.993	-28.429	0.091	1860.455	-0.007	200
	2005-2010	0.992	-100.558	0.085	1898.224	-0.007	200
Protium costaricense	1995-2000	0.974	-21.463	0.114	279.191	-0.037	85.995
	2000-2005	0.973	-41.313	0.07	277.503	-0.041	85.995
	2005-2010	0.98	-31.09	0.082	300.846	-0.04	85.995
Protium panamense	1995-2000	0.977	-25.36	0.169	285.002	-0.023	44.246
	2000-2005	0.981	-16.34	0.158	266.826	-0.022	44.246
	2005-2010	0.978	-34.934	0.212	205.153	-0.289	44.246
Protium tenuifolium	1995-2000	0.991	-115.216	0.028	705.541	-0.007	200
	2000-2005	0.986	-27.68	0.086	743.994	-0.007	200
	2005-2010	0.983	-128.492	0.032	710.317	-0.007	200
Psychotria horizontalis	1995-2000	0.927	-17.53	0.216	78.995	-0.133	21.97
	2000-2005	0.925	-19.01	0.223	71.1	-0.185	21.97
	2005-2010	0.935	-19.479	0.231	83.789	-0.078	21.97
Psychotria marginata	1995-2000	0.907	-15.064	0.222	47.922	-0.324	17.904
	2000-2005	0.922	-14.618	0.218	43.023	-0.197	17.904
	2005-2010	0.946	-15.43	0.223	38.696	-0.227	17.904
Pterocarpus rohrii	1995-2000	0.979	-35.145	0.067	351.708	-0.031	47.394
	2000-2005	0.974	-28.215	0.093	329.849	-0.021	47.394
	2005-2010	0.971	-38.658	0.068	332.677	-0.029	47.394
Quararibea asterolepis	1995-2000	0.99	-46.51	0.061	1709.351	-0.005	200
	2000-2005	0.988	-22.414	0.121	1704.611	-0.006	200
	2005-2010	0.993	-91.225	0.039	1741.631	-0.005	200
Randia armata	1995-2000	0.984	-46.201	0.057	335.222	-0.035	109.993
	2000-2005	0.991	-39.707	0.072	337.498	-0.025	109.993
	2005-2010	0.988	-52.213	0.069	324.488	-0.035	109.993
Rinorea sylvatica	1995-2000	0.972	-23.34	0.213	111.309	-0.149	29.655
	2000-2005	0.974	-24.344	0.213	123.704	-0.307	29.655
	2005-2010	0.972	-24.456	0.216	125.203	-0.306	29.655
Senna dariensis	1995-2000	0.886	-22.403	0.152	102.415	-0.321	42.646
	2000-2005	0.916	-26.648	0.173	107.949	-0.31	42.646
	2005-2010	0.959	-28.921	0.189	99.439	-0.07	42.646
Simarouba amara	1995-2000	0.961	-104.316	0.023	975.05	-0.007	200
	2000-2005	0.963	-99.457	0.027	1016.594	-0.007	200
	2005-2010	0.955	-120.502	0.158	1028.179	-0.007	200
Siparuna pauciflora	1995-2000	0.954	-27.243	0.089	270.778	-0.041	57.088
	2000-2005	0.951	-36.316	0.149	282.306	-0.041	57.088
	2005-2010	0.954	-38.839	0.173	290.674	-0.038	57.088
Sloanea terniflora	1995-2000	0.981	-66.344	0.104	1504.91	-0.006	200
	2000-2005	0.983	-83.548	0.139	1470.557	-0.007	200
	2005-2010	0.985	-115.264	0.141	1543.642	-0.005	200
Socratea exorrhiza	1995-2000	0.961	-35.493	0.124	238.153	-0.28	131.8
	2000-2005	0.959	-64.373	0.144	238.095	-0.293	131.8
	2005-2010	0.966	-66.611	0.147	241.597	-0.305	131.8
Sorocea affinis	1995-2000	0.973	-37.935	0.19	168.06	-0.283	53.002
	2000-2005	0.968	-36.016	0.175	148.235	-0.097	53.002
	2005-2010	0.972	-38.212	0.193	135.752	-0.13	53.002
Spondias radlkoferi	1995-2000	0.985	-35.119	0.033	1217.379	-0.007	200
	2000-2005	0.988	-42.033	0.039	1254.36	-0.007	200
	2005-2010	0.982	-96.574	0.024	1265.432	-0.007	200
Stylogyne turbacensis	1995-2000	0.957	-16.512	0.154	104.111	-0.323	28.868
	2000-2005	0.964	-16.783	0.178	94.379	-0.201	28.868
	2005-2010	0.968	-22.629	0.208	106.244	-0.331	28.868
Swartzia simplex	1995-2000	0.994	-30.259	0.105	492.362	-0.038	48.037

Continued on next page

Table F.1 –continued from previous page

Species	Census Interval	K	p1	r1	p2	r2	thresh
	2000-2005	0.99	-30.03	0.161	495.518	-0.038	48.037
	2005-2010	0.993	-34.141	0.103	489.443	-0.034	48.037
Swartzia simplex	1995-2000	0.993	-23.334	0.13	354.884	-0.039	52.76
	2000-2005	0.992	-34.429	0.122	320.736	-0.045	52.76
	2005-2010	0.991	-35.07	0.106	329.548	-0.045	52.76
Symphonia globulifera	1995-2000	0.961	-112.906	0.142	832.216	-0.007	200
	2000-2005	0.964	-110.597	0.152	967.339	-0.006	200
	2005-2010	0.971	-117.188	0.148	974.748	-0.006	200
Tabebuia rosea	1995-2000	0.975	-48.107	0.084	1083.38	-0.007	200
	2000-2005	0.982	-29.711	0.06	1120.141	-0.007	200
	2005-2010	0.977	-111.365	0.147	1174.451	-0.007	200
Tabernaemontana arborea	1995-2000	0.99	-61.931	0.047	1162.895	-0.007	200
	2000-2005	0.991	-19.451	0.111	1137.621	-0.007	200
	2005-2010	0.987	-105.808	0.038	1121.927	-0.007	200
Tachigali versicolor	1995-2000	0.969	-168.524	0.018	711.056	-0.007	200
	2000-2005	0.988	-182.486	0.015	755.833	-0.007	200
	2005-2010	0.947	-123.073	0.157	782.747	-0.007	200
Talisia nervosa	1995-2000	0.989	-23.393	0.162	129.394	-0.306	41.569
	2000-2005	0.989	-11.605	0.155	133.319	-0.31	41.569
	2005-2010	0.988	-28.429	0.189	114.882	-0.242	41.569
Talisia croatii	1995-2000	0.988	-11.57	0.15	138.374	-0.317	32.744
	2000-2005	0.978	-24.968	0.107	140.194	-0.322	32.744
	2005-2010	0.983	-24.106	0.151	140.995	-0.32	32.744
Tetragastris panamensis	1995-2000	0.993	-78.297	0.04	1175.235	-0.007	200
	2000-2005	0.992	-103.091	0.031	1023.965	-0.007	200
	2005-2010	0.982	-137.596	0.033	1053.668	-0.007	200
Trichilia pallida	1995-2000	0.984	-38.509	0.071	386.153	-0.038	91.102
	2000-2005	0.973	-38.988	0.092	380.373	-0.041	91.102
	2005-2010	0.973	-56.058	0.125	381.118	-0.043	91.102
Trichilia tuberculata	1995-2000	0.979	-130.15	0.03	969.503	-0.007	200
	2000-2005	0.979	-144.011	0.029	931.758	-0.007	200
	2005-2010	0.979	-98.633	0.045	903.932	-0.007	200
Triplaris cumingiana	1995-2000	0.988	-19.589	0.053	504.949	-0.032	201.17
	2000-2005	0.983	-68.892	0.029	525.012	-0.039	201.17
	2005-2010	0.983	-103.939	0.105	539.111	-0.039	201.17
Trophis racemosa	1995-2000	0.965	-37.66	0.172	456.49	-0.034	60.395
	2000-2005	0.961	-37.795	0.163	444.985	-0.032	60.395
	2005-2010	0.974	-16.631	0.121	477.161	-0.036	60.395
Unonopsis pittieri	1995-2000	0.987	-36.306	0.056	376.523	-0.042	124.246
	2000-2005	0.98	-47.069	0.049	377.977	-0.03	124.246
	2005-2010	0.978	-73.434	0.152	354.075	-0.032	124.246
Virola sebifera	1995-2000	0.978	-21.298	0.089	551.197	-0.037	175.748
	2000-2005	0.974	-26.886	0.097	539.165	-0.021	175.748
	2005-2010	0.977	-96.737	0.15	576.717	-0.032	175.748
Virola surinamensis	1995-2000	0.981	-110.708	0.102	1203.394	-0.007	200
	2000-2005	0.985	-106.939	0.102	1208.22	-0.007	200
	2005-2010	0.988	-108.111	0.15	1277.291	-0.007	200
Xylopia macrantha	1995-2000	0.99	-47.173	0.075	368.125	-0.037	76.896
	2000-2005	0.993	-37.024	0.092	380.317	-0.039	76.896
	2005-2010	0.99	-54.308	0.18	398.264	-0.04	76.896
Zanthoxylum ekmanii	1995-2000	0.99	-110.551	0.012	993.407	-0.007	200
	2000-2005	0.96	9.586	0.141	1017.81	-0.007	200
	2005-2010	0.984	-155.582	0.013	1021.119	-0.007	200
Zanthoxylum panamense	1995-2000	0.984	-5.927	0.057	730.802	-0.007	200
	2000-2005	0.962	-104.249	0.063	739.854	-0.007	200
	2005-2010	0.977	-111.664	0.137	729.733	-0.007	200

Table F.2: Growth parameters for BCI species

Species	Census Interval	Alpha1	Alpha2	Beta1	Beta2	thresh
Acalypha diversifolia	1995-2000	0.951	0.705	0.89	0.428	40.82
	2000-2005	0.316	0.76	0.243	0.334	40.82
	2005-2010	1.06	0.751	0.644	0.25	40.82
Adelia triloba	1995-2000	0.714	0.9	0.775	0.349	200
	2000-2005	0.818	0.927	0.896	0.413	200
	2005-2010	0.761	0.582	0.635	0.172	200
Alchornea costaricensis	1995-2000	0.9	0.721	0.349	0.166	200
	2000-2005	0.852	0.815	0.312	0.202	200
	2005-2010	0.927	0.944	0.416	0.23	200
Alibertia edulis	1995-2000	0.988	0.836	2.386	0.936	37.235
	2000-2005	0.35	0.218	0.796	0.25	37.235
	2005-2010	0.399	0.9	0.732	0.784	37.235
Alseis blackiana	1995-2000	0.893	1.267	2.057	0.364	200
	2000-2005	0.736	1.287	1.741	0.355	200
	2005-2010	0.803	1.208	1.582	0.327	200
Anaxagorea panamensis	1995-2000	1.182	0.848	2.706	1.22	30.425
	2000-2005	1.051	0.994	2.623	1.508	30.425
	2005-2010	1.069	0.901	1.916	1.226	30.425
Andira inermis	1995-2000	1.038	0.813	2.864	0.742	79.912
	2000-2005	0.99	0.714	2.592	0.644	79.912
	2005-2010	1.017	0.609	2.295	0.583	79.912
Annona acuminata	1995-2000	1.01	0.825	2.921	1.096	34.141
	2000-2005	0.836	0.615	2.497	0.934	34.141
	2005-2010	0.983	0.725	2.463	0.897	34.141
Annona spraguei	1995-2000	0.882	0.683	0.317	0.185	71.262
	2000-2005	0.943	0.741	0.361	0.183	71.262
	2005-2010					

Continued on next page

Table F.2 –continued from previous page

Species	Census Interval	Alpha1	Alpha2	Beta1	Beta2	thresh
Apeiba membranacea	1995-2000	0.789	0.692	0.387	0.143	200
	2000-2005	0.735	0.679	0.349	0.15	200
	2005-2010	0.894	0.737	0.355	0.151	200
Aspidosperma spruceanum	1995-2000	1.132	1.859	2.602	0.3	200
	2000-2005	0.925	0.432	1.934	0.048	200
	2005-2010	0.89	1.643	1.464	0.211	200
Astrocaryum standleyanum	1995-2000	0.393	0.177	1.103	0.164	152.329
	2000-2005	0.955	0.739	4.464	1.478	152.329
	2005-2010	0.916	1.009	3.381	1.658	152.329
Bactris major	1995-2000	0.965	1.219	2.931	1.379	48.238
	2000-2005	0.898	1.996	3.954	2.463	48.238
	2005-2010	0.248	0.232	0.878	0.423	48.238
Beilschmiedia pendula	1995-2000	1.036	1.525	2.087	0.393	200
	2000-2005	0.934	1.355	1.875	0.337	200
	2005-2010	1.046	1.74	1.831	0.391	200
Brosimum alicastrum	1995-2000	1.088	0.934	1.638	0.157	200
	2000-2005	0.418	0.311	0.565	0.057	200
	2005-2010	1.055	0.318	1.546	0.062	200
Calophyllum longifolium	1995-2000	1.211	4.168	1.966	0.848	200
	2000-2005	0.975	2.843	1.499	0.564	200
	2005-2010	1.168	4.085	1.476	0.725	200
Capparis frondosa	1995-2000	1.232	0.822	4.223	1.43	37.186
	2000-2005	1.138	0.8	5.216	1.871	37.186
	2005-2010	1.153	0.831	4.776	1.918	37.186
Casearia aculeata	1995-2000	1.221	0.841	2.7	0.819	52.789
	2000-2005	1.049	0.716	2.673	0.674	52.789
	2005-2010	1.061	0.826	2.333	0.825	52.789
Casearia arborea	1995-2000	0.921	0.899	0.403	0.25	200
	2000-2005	0.778	1.132	0.387	0.319	200
	2005-2010	1.074	0.738	0.433	0.218	200
Casearia sylvestris	1995-2000	0.944	1.319	0.98	0.589	147.934
	2000-2005	0.385	0.368	0.403	0.215	147.934
	2005-2010	0.974	1.039	0.658	0.538	147.934
Cassipourea elliptica	1995-2000	0.494	0.451	0.866	0.195	56.568
	2000-2005	1.013	1.362	1.88	0.612	56.568
	2005-2010	0.98	1.277	1.616	0.48	56.568
Cecropia insignis	1995-2000	0.776	0.943	0.105	0.171	200
	2000-2005	0.463	0.353	0.06	0.044	200
	2005-2010	1.064	0.872	0.162	0.114	200
Cecropia obtusifolia	1995-2000					
	2000-2005	1.329	1.021	0.14	0.13	166.301
	2005-2010	1.255	0.711	0.14	0.086	166.301
Chamguava schippii	1995-2000	1.276	0.816	2.382	0.686	37
	2000-2005	0.4	0.341	0.628	0.275	37
	2005-2010	1.116	0.759	1.66	0.518	37
Chrysochlamys eclipes	1995-2000	1.081	0.681	2.495	0.86	52.362
	2000-2005	1.293	0.828	4.195	1.268	52.362
	2005-2010	0.436	0.818	1.074	1.009	52.362
Chrysophyllum argenteum	1995-2000	0.901	1.028	1.806	0.406	200
	2000-2005	0.852	1.004	1.774	0.508	200
	2005-2010	0.829	0.922	1.226	0.327	200
Chrysophyllum cainito	1995-2000	0.885	1.044	2.044	0.171	200
	2000-2005	0.66	1.277	1.406	0.233	200
	2005-2010	0.275	1.736	0.467	0.339	200
Coccoloba coronata	1995-2000	0.928	0.676	3.478	0.391	85.085
	2000-2005	0.375	0.196	0.976	0.133	85.085
	2005-2010	0.96	0.651	2.76	0.569	85.085
Coccoloba manzinellensis	1995-2000	1.244	0.669	3.259	0.809	49.334
	2000-2005	0.368	0.585	1.152	0.723	49.334
	2005-2010	0.921	0.701	2.464	0.842	49.334
Conostegia cinnamomea	1995-2000	1.223	0.856	2.642	0.847	20.085
	2000-2005	0.992	1.142	2.674	1.721	20.085
	2005-2010					
Cordia alliodora	1995-2000	0.74	1.357	0.282	0.198	200
	2000-2005	0.93	1.182	0.257	0.215	200
	2005-2010	0.723	0.903	0.147	0.171	200
Cordia bicolor	1995-2000	0.668	0.749	0.32	0.158	200
	2000-2005	0.649	1.008	0.3	0.223	200
	2005-2010	0.654	0.846	0.237	0.197	200
Cordia lasiocalyx	1995-2000	0.909	0.749	1.3	0.561	104.671
	2000-2005	0.384	0.253	0.445	0.16	104.671
	2005-2010	0.975	0.696	0.982	0.466	104.671
Coussarea curvigemmia	1995-2000	0.498	1.047	0.89	0.877	51.347
	2000-2005	1.039	0.96	2.053	0.848	51.347
	2005-2010	1.096	0.914	1.907	0.786	51.347
Croton billbergianus	1995-2000	0.293	0.323	0.105	0.05	78.906
	2000-2005	0.987	1.129	0.312	0.195	78.906
	2005-2010	0.771	0.824	0.198	0.087	78.906
Cupania seemannii	1995-2000	0.966	0.926	1.945	0.558	48.725
	2000-2005	0.398	1.122	0.879	0.686	48.725
	2005-2010	0.99	1.018	1.925	0.647	48.725
Desmopsis panamensis	1995-2000	0.622	0.451	1.362	0.53	36.326
	2000-2005	1.045	0.847	2.253	0.949	36.326
	2005-2010	1.196	0.881	2.52	1.045	36.326
Drypetes standleyi	1995-2000	0.988	1.816	1.706	0.451	200
	2000-2005	0.829	1.985	1.452	0.53	200
	2005-2010	0.993	1.553	1.706	0.409	200
Erythroxylum macrophyllum	1995-2000	0.399	0.264	0.802	0.187	37.158
	2000-2005	1.045	0.839	3.295	0.626	37.158
	2005-2010	1.035	0.778	2.102	0.451	37.158
Eugenia coloradoensis	1995-2000	1.106	1.112	2.493	0.456	66.119
	2000-2005	0.337	0.371	0.661	0.14	66.119

Continued on next page

Table F.2 –continued from previous page

Species	Census Interval	Alpha1	Alpha2	Beta1	Beta2	thresh
	2005-2010	0.953	1.195	1.519	0.389	66.119
Eugenia galalonensis	1995-2000	1.149	0.857	3.63	0.978	27.322
	2000-2005	1.073	0.845	3.367	0.919	27.322
	2005-2010	1.085	0.751	2.479	0.682	27.322
Eugenia nesiotica	1995-2000	0.941	1.43	2.665	0.592	200
	2000-2005	0.789	1.171	2.155	0.403	200
	2005-2010	0.352	0.403	0.79	0.128	200
Eugenia oerstediana	1995-2000	1.032	0.892	2.047	0.33	59.194
	2000-2005	0.905	0.778	1.82	0.304	59.194
	2005-2010	0.988	0.741	1.511	0.276	59.194
Faramea occidentalis	1995-2000	1.208	1.066	1.721	0.727	68.756
	2000-2005	1.02	0.939	1.434	0.636	68.756
	2005-2010	1.094	0.945	1.445	0.619	68.756
Garcinia intermedia	1995-2000	1.382	1.185	3.252	1.024	40.933
	2000-2005	1.182	1.145	2.843	0.855	40.933
	2005-2010	1.316	1.069	2.738	0.79	40.933
Garcinia madruno	1995-2000	0.508	1.071	0.927	0.803	39.613
	2000-2005	1.079	0.92	2.127	0.752	39.613
	2005-2010	1.235	0.975	1.915	0.639	39.613
Guapira standleyana	1995-2000	0.759	0.922	0.941	0.198	200
	2000-2005	0.693	0.821	0.563	0.164	200
	2005-2010	0.867	0.833	0.678	0.187	200
Guarea guidonia	1995-2000	0.932	0.8	1.438	0.28	200
	2000-2005	0.791	0.82	1.251	0.315	200
	2005-2010	0.846	0.796	1.06	0.24	200
Guarea bullata	1995-2000	0.553	0.32	1.43	0.316	52.56
	2000-2005	0.924	0.835	2.993	0.928	52.56
	2005-2010	1.144	0.846	3.042	0.881	52.56
Guatteria dumetorum	1995-2000	0.85	1.056	1.134	0.197	200
	2000-2005	0.303	0.828	0.369	0.155	200
	2005-2010	0.743	1.195	0.649	0.211	200
Guettarda foliacea	1995-2000	0.971	0.831	1.504	0.522	110.724
	2000-2005	0.844	0.678	1.428	0.464	110.724
	2005-2010	0.962	0.688	1.554	0.455	110.724
Gustavia superba	1995-2000	1.151	0.889	1.126	0.435	235.898
	2000-2005	1.035	0.864	1.179	0.545	235.898
	2005-2010	1.185	0.837	1.496	0.567	235.898
Hamelia axillaris	1995-2000	1.021	0.728	1.669	0.513	24.436
	2000-2005					
	2005-2010	1.104	1.101	1.925	0.821	24.436
Hampea appendiculata	1995-2000					
	2000-2005					
	2005-2010	0.778	1.381	0.116	0.081	70.903
Hasseltia floribunda	1995-2000	0.849	1.019	0.893	0.392	143.967
	2000-2005	0.775	0.951	0.768	0.396	143.967
	2005-2010	0.825	0.834	0.796	0.339	143.967
Heisteria concinna	1995-2000	1.343	1.122	1.237	0.586	148.328
	2000-2005	1.44	1.134	1.143	0.57	148.328
	2005-2010	1.134	0.885	0.942	0.407	148.328
Herrania purpurea	1995-2000	1.084	0.739	2.573	0.934	41.72
	2000-2005	0.386	0.215	0.852	0.234	41.72
	2005-2010	1.157	0.63	2.27	0.698	41.72
Hirtella triandra	1995-2000	0.47	0.447	0.807	0.219	82.24
	2000-2005	0.414	0.413	0.645	0.2	82.24
	2005-2010	0.949	0.893	1.366	0.425	82.24
Hybanthus prunifolius	1995-2000	1.282	0.892	3.412	1.288	30.191
	2000-2005	1.109	0.385	3.361	0.569	30.191
	2005-2010	1.186	0.841	3.028	1.188	30.191
Inga goldmanii	1995-2000	0.88	0.862	1.304	0.279	74.088
	2000-2005	0.805	0.762	1.058	0.25	74.088
	2005-2010	0.863	0.752	0.781	0.189	74.088
Inga marginata	1995-2000	0.538	2.895	0.182	0.191	200
	2000-2005	0.591	1.971	0.16	0.145	200
	2005-2010	0.712	1.18	0.256	0.095	200
Inga pezizifera	1995-2000	0.814	1.12	0.649	0.154	86.424
	2000-2005	0.686	0.961	0.483	0.165	86.424
	2005-2010	0.683	2.097	0.411	0.341	86.424
Inga nobilis	1995-2000	0.87	0.849	1.095	0.366	81.129
	2000-2005	0.797	0.816	1.091	0.442	81.129
	2005-2010	0.983	0.764	1.141	0.384	81.129
Inga acuminata	1995-2000	0.398	0.383	0.348	0.101	66.589
	2000-2005	0.356	0.373	0.229	0.085	66.589
	2005-2010	0.981	0.994	0.567	0.212	66.589
Inga sapindoides	1995-2000	0.804	1.209	0.764	0.291	126.075
	2000-2005	0.722	1.089	0.562	0.238	126.075
	2005-2010	0.755	1.289	0.456	0.25	126.075
Inga thibaudiana	1995-2000	0.717	1.239	0.185	0.161	113.861
	2000-2005	0.833	0.862	0.264	0.147	113.861
	2005-2010	0.864	1.058	0.198	0.14	113.861
Inga umbellifera	1995-2000	0.932	0.775	1.579	0.521	56.727
	2000-2005	0.871	0.624	1.66	0.454	56.727
	2005-2010	0.425	0.277	0.537	0.117	56.727
Jacaranda copaia	1995-2000	1.07	1.732	0.226	0.185	200
	2000-2005	0.953	1.785	0.227	0.222	200
	2005-2010	0.795	1.39	0.159	0.172	200
Lacistema aggregatum	1995-2000	1.194	0.773	3.064	0.647	34.951
	2000-2005	1.01	0.852	2.722	0.668	34.951
	2005-2010	0.952	0.719	2.025	0.523	34.951
Laetia thamnia	1995-2000	1.184	1.379	2.016	0.788	59.851
	2000-2005	0.967	1.092	1.519	0.669	59.851
	2005-2010	1.033	1.121	1.385	0.622	59.851
Licania platypus	1995-2000	1.068	0.809	2.942	0.744	37.782

Continued on next page

Table F.2 –continued from previous page

Species	Census Interval	Alpha1	Alpha2	Beta1	Beta2	thresh
	2000-2005	1.162	0.876	3.397	0.738	37.782
	2005-2010	1.213	0.786	2.636	0.692	37.782
Lonchocarpus heptaphyllus	1995-2000	0.955	0.981	1.55	0.291	200
	2000-2005	0.792	0.8	0.995	0.197	200
	2005-2010	0.832	0.902	0.909	0.193	200
Luehea seemannii	1995-2000	0.829	1.083	0.742	0.203	200
	2000-2005	0.316	0.173	0.366	0.047	200
	2005-2010	0.748	0.993	0.679	0.224	200
Mosannona garwoodii	1995-2000	1.145	0.983	2.438	1.151	53.468
	2000-2005	0.965	0.906	1.973	0.967	53.468
	2005-2010	1.376	0.751	2.866	0.955	53.468
Maquira guianensis	1995-2000	1.026	0.727	1.38	0.463	79.488
	2000-2005	0.875	0.685	1.133	0.451	79.488
	2005-2010	0.902	0.669	1.126	0.408	79.488
Miconia affinis	1995-2000	0.972	0.224	0.711	0.061	52.312
	2000-2005	0.844	0.706	0.628	0.235	52.312
	2005-2010	0.922	0.84	0.592	0.232	52.312
Miconia argentea	1995-2000	0.878	1.202	0.498	0.257	56.463
	2000-2005	0.859	1.179	0.392	0.241	56.463
	2005-2010	0.387	0.36	0.198	0.054	56.463
Miconia nervosa	1995-2000	0.443	1.348	0.599	1.126	19.483
	2000-2005	1.122	0.779	2.045	0.841	19.483
	2005-2010	1.311	1.235	1.857	1.14	19.483
Mouriri myrtilloides	1995-2000	1.314	1.02	3.975	1.539	25.754
	2000-2005	1.107	0.901	3.397	1.402	25.754
	2005-2010	0.051	0.016	0	0	25.754
Nectandra cissiflora	1995-2000	0.949	1.163	0.787	0.226	96.152
	2000-2005	1.112	1.324	0.897	0.27	96.152
	2005-2010	0.982	1.251	0.735	0.212	96.152
Nectandra lineata	1995-2000	1.299	1.171	2.715	0.2	34.677
	2000-2005	0.781	1.183	0.966	0.294	34.677
	2005-2010	0.901	0.664	0.856	0.097	34.677
Ocotea cernua	1995-2000	0.918	0.941	1.192	0.322	70.133
	2000-2005	0.671	1.052	0.679	0.315	70.133
	2005-2010	0.891	1.04	0.695	0.319	70.133
Ocotea oblonga	1995-2000	0.578	1.05	0.122	0.07	200
	2000-2005	0.702	1.685	0.23	0.146	200
	2005-2010	0.746	1.372	0.214	0.115	200
Ocotea puberula	1995-2000	0.869	1.893	0.64	0.169	200
	2000-2005	0.243	0.198	0.204	0.034	200
	2005-2010	0.814	1.238	0.486	0.09	200
Ocotea whitei	1995-2000	0.342	0.358	0.144	0.043	200
	2000-2005	0.302	1.024	0.095	0.127	200
	2005-2010	0.933	1.115	0.424	0.145	200
Oenocarpus mapora	1995-2000	0.899	0.583	1.624	0.369	113.079
	2000-2005	0.886	0.612	1.71	0.406	113.079
	2005-2010	0.978	0.601	1.861	0.449	113.079
Trophis caucana	1995-2000	0.838	0.81	0.614	0.209	101.947
	2000-2005	0.27	0.17	0.219	0.088	101.947
	2005-2010	0.768	0.692	0.884	0.345	101.947
Ouratea lucens	1995-2000	1.385	0.946	4.753	1.91	27.383
	2000-2005	1.182	0.886	4.182	1.826	27.383
	2005-2010	1.18	0.952	3.829	1.919	27.383
Palicourea guianensis	1995-2000	1.777	1.025	0.575	0.302	33.461
	2000-2005	1.652	0.985	0.677	0.271	33.461
	2005-2010	0.627	1.218	0.192	0.273	33.461
Pentagonia macrophylla	1995-2000	1.369	0.837	4.038	1.011	37.645
	2000-2005	1.009	0.662	3.167	1.025	37.645
	2005-2010	1.152	0.764	2.877	0.932	37.645
Perebea xanthochyma	1995-2000	1.034	0.99	1.511	0.705	70.091
	2000-2005	0.865	0.692	0.985	0.342	70.091
	2005-2010	0.821	0.806	1.008	0.422	70.091
Picramnia latifolia	1995-2000	1.056	0.706	2.48	0.593	44.624
	2000-2005	0.998	0.694	2.448	0.495	44.624
	2005-2010	1.057	0.857	2.278	0.732	44.624
Piper cordulatum	1995-2000	1.755	1.301	6.188	2.684	15.832
	2000-2005					
	2005-2010					
Piper reticulatum	1995-2000	0.974	0.736	1.467	0.47	76.871
	2000-2005	0.947	0.541	1.4	0.445	76.871
	2005-2010	0.242	0.702	0.238	0.409	76.871
Platymiscium pinnatum	1995-2000	1.314	1.141	2.502	0.346	200
	2000-2005	0.97	1.723	2.392	0.654	200
	2005-2010	0.888	1.024	1.239	0.288	200
Poulsenia armata	1995-2000	0.994	0.313	0.745	0.053	200
	2000-2005	0.387	0.367	0.242	0.06	200
	2005-2010	0.856	0.959	0.552	0.142	200
Pouteria reticulata	1995-2000	0.964	1.948	1.818	0.334	200
	2000-2005	0.742	1.323	1.478	0.249	200
	2005-2010	0.735	1.335	1.132	0.243	200
Prioria copaifera	1995-2000	0.912	1.739	1.211	0.264	200
	2000-2005	0.819	0.548	1.234	0.072	200
	2005-2010	0.379	0.497	0.544	0.076	200
Protium costaricense	1995-2000	0.934	0.878	1.276	0.365	85.995
	2000-2005	0.778	0.795	0.922	0.322	85.995
	2005-2010	0.799	0.832	0.682	0.291	85.995
Protium panamense	1995-2000	1.061	0.33	2.217	0.227	44.246
	2000-2005	1.016	0.787	2.677	0.679	44.246
	2005-2010	0.932	0.75	1.634	0.483	44.246
Protium tenuifolium	1995-2000	0.897	1.163	1.275	0.345	200
	2000-2005	0.385	0.365	0.448	0.098	200
	2005-2010	0.912	0.943	1.069	0.246	200

Continued on next page

Table F.2 –continued from previous page

Species	Census Interval	Alpha1	Alpha2	Beta1	Beta2	thresh
Psychotria horizontalis	1995-2000	1.342	0.921	3.698	1.32	21.97
	2000-2005	1.089	0.823	3.81	1.37	21.97
	2005-2010	1.26	0.931	3.563	1.551	21.97
Psychotria marginata	1995-2000	0.472	0.968	1.182	1.495	17.904
	2000-2005	0.403	0.875	1.075	1.306	17.904
	2005-2010	1.336	0.879	2.869	1.243	17.904
Pterocarpus rohrii	1995-2000	1.074	0.709	2.422	0.515	47.394
	2000-2005	0.925	0.692	2.193	0.483	47.394
	2005-2010	0.88	0.633	1.551	0.345	47.394
Quararibea asterolepis	1995-2000	0.86	1.069	1.081	0.21	200
	2000-2005	0.334	0.389	0.369	0.078	200
	2005-2010	0.789	1.059	0.796	0.207	200
Randia armata	1995-2000	0.962	0.817	1.65	0.568	109.993
	2000-2005	0.882	0.886	1.404	0.657	109.993
	2005-2010	0.982	0.715	1.682	0.564	109.993
Rinorea sylvatica	1995-2000	0.565	0.851	1.666	1.259	29.655
	2000-2005	1.146	0.833	3.727	1.357	29.655
	2005-2010	1.186	0.871	3.044	1.32	29.655
Senna dariensis	1995-2000					
	2000-2005					
	2005-2010	1.43	0.916	0.628	0.367	42.646
Simarouba amara	1995-2000	0.793	2.046	0.462	0.224	200
	2000-2005	0.757	1.652	0.452	0.18	200
	2005-2010	0.848	1.943	0.434	0.217	200
Siparuna pauciflora	1995-2000	1.024	0.857	1.473	0.858	57.088
	2000-2005	0.965	0.554	1.132	0.417	57.088
	2005-2010	0.304	0.168	0.322	0.087	57.088
Sloanea terniflora	1995-2000	1.281	1.327	4.044	0.459	200
	2000-2005	0.918	1.011	3.095	0.372	200
	2005-2010	0.425	0.473	1.187	0.202	200
Socratea exorrhiza	1995-2000	0.305	0.146	0.245	0.052	131.8
	2000-2005	0.746	0.613	0.623	0.25	131.8
	2005-2010	0.737	0.569	0.641	0.302	131.8
Sorocea affinis	1995-2000	1.162	0.78	2.324	0.761	53.002
	2000-2005	0.455	0.302	0.924	0.321	53.002
	2005-2010	1.056	0.749	2.238	0.816	53.002
Spondias radlkoferi	1995-2000	0.638	1.129	0.477	0.168	200
	2000-2005	1	1.415	0.9	0.26	200
	2005-2010	0.701	1.072	0.544	0.183	200
Stylogyne turbacensis	1995-2000	1.175	0.892	3.272	1.33	28.868
	2000-2005	0.481	0.887	1.339	1.263	28.868
	2005-2010	1.226	0.773	2.964	1.043	28.868
Swartzia simplex	1995-2000	0	0	500.006	0	48.037
	2000-2005	0.485	0.365	1.407	0.309	48.037
	2005-2010	1.159	0.811	3.059	0.648	48.037
Swartzia simplex	1995-2000	1.284	0.846	3.924	1.223	52.76
	2000-2005	1.147	0.763	3.678	1.055	52.76
	2005-2010	1.197	0.843	3.385	1.079	52.76
Symphonia globulifera	1995-2000	0.43	0.163	0.379	0.03	200
	2000-2005	1.072	1.679	1.283	0.367	200
	2005-2010	1.167	3.084	1.068	0.571	200
Tabebuia rosea	1995-2000	0.924	1.019	1.72	0.243	200
	2000-2005	0.979	0.706	1.366	0.144	200
	2005-2010	0.802	1.227	0.975	0.201	200
Tabernaemontana arborea	1995-2000	0.742	1.225	0.657	0.208	200
	2000-2005	0.624	0.494	0.493	0.077	200
	2005-2010	0.677	0.97	0.454	0.163	200
Tachigali versicolor	1995-2000	1.104	2.618	1.868	0.436	200
	2000-2005	0.997	2.696	1.722	0.408	200
	2005-2010	1.053	2.307	1.614	0.293	200
Talisia nervosa	1995-2000	0.017	0	0	0	41.569
	2000-2005	1.129	0.624	3.76	1.116	41.569
	2005-2010	1.221	0.746	3.486	1.325	41.569
Talisia croatii	1995-2000	1.288	1.105	4.069	1.846	32.744
	2000-2005	1.194	0.63	3.768	1.068	32.744
	2005-2010	1.175	0.711	3.247	1.262	32.744
Tetragastris panamensis	1995-2000	1.003	1.614	1.945	0.454	200
	2000-2005	0.859	1.578	1.727	0.437	200
	2005-2010	1.015	1.555	2.041	0.463	200
Trichilia pallida	1995-2000	0.363	1.104	0.406	0.441	91.102
	2000-2005	0.331	0.301	0.377	0.116	91.102
	2005-2010	0.915	0.803	0.838	0.311	91.102
Trichilia tuberculata	1995-2000	1.105	1.572	2.086	0.482	200
	2000-2005	0.969	1.604	1.911	0.518	200
	2005-2010	1.054	1.668	1.866	0.495	200
Triplaris cumingiana	1995-2000	0.815	0.996	0.715	0.231	201.17
	2000-2005	0.274	0.188	0.177	0.062	201.17
	2005-2010	0.888	0.662	0.706	0.241	201.17
Trophis racemosa	1995-2000	0.844	0.681	1.964	0.426	60.395
	2000-2005	0.945	0.61	2.671	0.431	60.395
	2005-2010	0.82	0.587	1.792	0.32	60.395
Unonopsis pittieri	1995-2000	0.912	0.882	1.031	0.334	124.246
	2000-2005	0.755	0.927	0.716	0.342	124.246
	2005-2010	0.759	0.867	0.611	0.308	124.246
Virola sebifera	1995-2000	0.859	0.862	0.819	0.25	175.748
	2000-2005	0.738	0.844	0.653	0.248	175.748
	2005-2010	0.759	0.855	0.611	0.252	175.748
Virola surinamensis	1995-2000	0.891	0.934	0.363	0.139	200
	2000-2005	0.816	0.937	0.414	0.141	200
	2005-2010	0.819	1.073	0.28	0.146	200
Xylopia macrantha	1995-2000	0.515	0.422	0.521	0.204	76.896
	2000-2005	1.1	1.064	1.003	0.464	76.896

Continued on next page

Table F.2 –continued from previous page

Species	Census Interval	Alpha1	Alpha2	Beta1	Beta2	thresh
	2005-2010	1.165	1.073	1.059	0.44	76.896
Zanthoxylum ekmanii	1995-2000	0.257	0.481	0.029	0.035	200
	2000-2005	0.872	2.168	0.131	0.193	200
	2005-2010	0.721	1.475	0.083	0.165	200
Zanthoxylum panamense	1995-2000	0.709	1.602	0.295	0.187	200
	2000-2005	0.229	0.299	0.08	0.032	200
	2005-2010	0.77	0.853	0.311	0.121	200

F.4 Demographic metrics for 134 BCI species

Table F.3: Passage times from 9mm to the size threshold for fast growth

Species	Census	PT Slow	PT Fast	Growth Threshold	LE Slow	LE Fast
Acalypha diversifolia	1995-2000	23.26	21.61	40.82	8.66	8.67
	2000-2005	18.54	17.08	40.82	12.58	12.59
	2005-2010	16.76	14.93	40.82	21.80	21.57
Adelia triloba	1995-2000	111.19	106.96	200.00	7.78	8.12
	2000-2005	130.15	126.96	200.00	22.10	22.10
	2005-2010	91.86	87.52	200.00	17.09	18.23
Alchornea costaricensis	1995-2000	55.69	53.12	200.00	4.21	5.22
	2000-2005	57.95	56.62	200.00	13.62	14.77
	2005-2010	66.92	65.06	200.00	42.36	42.80
Alibertia edulis	1995-2000	50.81	48.30	37.23	29.65	29.68
	2000-2005	49.74	47.16	37.23	33.70	33.68
	2005-2010	39.03	36.78	37.23	28.77	28.73
Alseis blackiana	1995-2000	139.25	130.28	200.00	53.44	67.06
	2000-2005	133.40	124.32	200.00	46.21	57.44
	2005-2010	126.30	117.74	200.00	51.47	59.52
Anaxagorea panamensis	1995-2000	42.39	41.10	30.43	55.90	55.52
	2000-2005	45.15	43.76	30.43	52.67	52.39
	2005-2010	35.07	34.32	30.43	30.77	30.69
Andira inermis	1995-2000	118.30	114.27	79.91	49.86	49.85
	2000-2005	118.14	114.27	79.91	81.80	85.25
	2005-2010	110.36	106.81	79.91	26.48	30.79
Annona acuminata	1995-2000	51.38	48.71	34.14	23.95	24.89
	2000-2005	55.11	52.86	34.14	25.69	25.71
	2005-2010	46.65	44.35	34.14	28.43	28.45
Annona spraguei	1995-2000	17.35	15.92	71.26	4.19	4.42
	2000-2005	18.64	16.89	71.26	6.87	6.87
	2005-2010					
Apeiba membranacea	1995-2000	61.68	58.29	200.00	18.76	21.32
	2000-2005	65.28	62.76	200.00	42.48	42.91
	2005-2010	58.60	56.59	200.00	63.26	63.16
Aspidosperma spruceanum	1995-2000	95.85	83.58	200.00	84.63	90.75
	2000-2005	66.54	54.03	200.00	51.66	50.86
	2005-2010	73.78	63.10	200.00	70.10	81.24
Astrocaryum standleyanum	1995-2000	213.14	208.25	152.33	50.49	50.48
	2000-2005	439.24	436.27	152.33	38.16	38.16
	2005-2010	360.94	358.32	152.33	54.22	54.22
Bactris major	1995-2000	52.81	49.56	48.24	2.80	2.91
	2000-2005	73.88	69.49	48.24	6.30	6.51
	2005-2010	98.40	95.82	48.24	27.95	28.39
Beilschmiedia pendula	1995-2000	116.97	108.79	200.00	30.80	43.45
	2000-2005	110.99	102.70	200.00	27.16	36.43
	2005-2010	103.36	95.03	200.00	38.29	48.97
Brosimum alicastrum	1995-2000	90.50	80.19	200.00	100.32	98.44
	2000-2005	93.84	84.97	200.00	108.85	107.86
	2005-2010	98.78	89.19	200.00	84.39	83.86
Calophyllum longifolium	1995-2000	88.20	79.91	200.00	28.62	28.53
	2000-2005	85.72	77.50	200.00	29.42	29.32
	2005-2010	79.80	71.91	200.00	41.92	41.54
Capparis frondosa	1995-2000	73.99	71.70	37.19	31.34	33.01
	2000-2005	98.25	95.94	37.19	27.37	28.75
	2005-2010	90.98	88.98	37.19	18.98	19.66
Casearia aculeata	1995-2000	66.29	63.31	52.79	22.86	24.32
	2000-2005	71.08	67.30	52.79	33.40	37.09
	2005-2010	67.78	65.17	52.79	34.34	34.39
Casearia arborea	1995-2000	69.74	68.40	200.00	28.57	29.63
	2000-2005	74.78	73.11	200.00	19.02	22.70
	2005-2010	67.34	66.45	200.00	25.63	25.61
Casearia sylvestris	1995-2000	96.56	93.67	147.93	15.70	17.00
	2000-2005	102.30	100.23	147.93	20.89	20.89
	2005-2010	83.22	82.52	147.93	29.50	29.48
Cassipourea elliptica	1995-2000	47.92	42.63	56.57	71.60	72.73
	2000-2005	48.67	43.42	56.57	80.16	83.72
	2005-2010	42.43	36.96	56.57	68.29	67.35
Cecropia insignis	1995-2000	27.35	28.03	200.00	21.12	20.42
	2000-2005	23.91	23.56	200.00	15.61	15.64
	2005-2010	27.50	27.08	200.00	20.48	20.44
Cecropia obtusifolia	1995-2000					
	2000-2005	17.08	17.48	166.30	11.20	11.22
	2005-2010	18.32	18.48	166.30	19.67	19.71

Continued on next page

Table F.3 –continued from previous page

Species	Census	PT Slow	PT Fast	Growth Threshold	LE Slow	LE Fast
Chamguava schippii	1995-2000	39.63	37.12	37.00	55.52	55.24
	2000-2005	36.26	34.19	37.00	52.20	51.95
	2005-2010	32.92	30.55	37.00	72.67	71.75
Chrysochlamys eclipes	1995-2000	78.44	76.59	52.36	59.12	60.11
	2000-2005	101.17	98.71	52.36	47.08	48.63
	2005-2010	79.62	77.56	52.36	59.30	59.20
Chrysophyllum argenteum	1995-2000	163.07	156.35	200.00	43.37	52.69
	2000-2005	188.63	182.92	200.00	43.21	43.19
	2005-2010	135.30	129.74	200.00	51.21	50.95
Chrysophyllum cainito	1995-2000	89.91	78.65	200.00	45.05	51.21
	2000-2005	89.81	79.24	200.00	35.67	35.68
	2005-2010	94.37	85.23	200.00	46.87	46.80
Coccoloba coronata	1995-2000	83.71	76.55	85.08	12.16	14.21
	2000-2005	79.75	71.78	85.08	13.87	15.35
	2005-2010	118.41	113.80	85.08	35.56	35.63
Coccoloba manzinellensis	1995-2000	73.64	70.55	49.33	20.82	23.67
	2000-2005	78.49	75.16	49.33	25.02	26.83
	2005-2010	73.71	70.81	49.33	26.20	27.70
Conostegia cinnamomea	1995-2000	17.30	14.44	20.09	8.90	8.78
	2000-2005	20.99	18.95	20.09	6.45	6.47
	2005-2010					
Cordia alliodora	1995-2000	46.24	43.00	200.00	15.32	18.44
	2000-2005	44.26	43.09	200.00	23.72	24.65
	2005-2010	38.30	38.14	200.00	46.60	46.54
Cordia bicolor	1995-2000	62.21	59.02	200.00	11.13	13.99
	2000-2005	62.03	59.59	200.00	13.22	15.10
	2005-2010	57.30	56.02	200.00	26.03	27.76
Cordia lasiocalyx	1995-2000	96.95	94.66	104.67	15.86	16.29
	2000-2005	76.56	74.06	104.67	22.49	22.48
	2005-2010	79.92	78.72	104.67	30.09	30.07
Coussarea curvigemmia	1995-2000	58.07	55.75	51.35	50.90	51.45
	2000-2005	62.67	60.08	51.35	43.33	43.49
	2005-2010	57.51	55.31	51.35	39.53	39.59
Croton billbergianus	1995-2000	12.88	9.74	78.91	4.09	4.50
	2000-2005	16.57	14.51	78.91	6.92	6.92
	2005-2010	14.67	11.91	78.91	13.82	12.98
Cupania seemannii	1995-2000	46.93	42.56	48.73	53.75	58.09
	2000-2005	47.49	42.93	48.73	37.81	41.08
	2005-2010	47.57	43.67	48.73	54.86	57.03
Desmopsis panamensis	1995-2000	46.89	44.90	36.33	34.44	34.23
	2000-2005	45.74	43.75	36.33	39.09	38.83
	2005-2010	46.23	44.52	36.33	38.38	38.12
Drypetes standleyi	1995-2000	115.78	107.87	200.00	58.04	65.76
	2000-2005	120.78	113.08	200.00	54.86	58.80
	2005-2010	117.93	110.23	200.00	49.37	52.56
Erythroxylum macrophyllum	1995-2000	32.78	28.12	37.16	16.98	17.02
	2000-2005	39.84	34.22	37.16	17.47	17.60
	2005-2010	33.10	28.57	37.16	30.43	30.10
Eugenia coloradoensis	1995-2000	56.31	49.54	66.12	20.74	23.81
	2000-2005	54.09	47.01	66.12	31.65	35.18
	2005-2010	47.18	41.05	66.12	38.95	38.69
Eugenia galalonensis	1995-2000	39.09	35.61	27.32	42.84	42.75
	2000-2005	38.58	34.97	27.32	54.45	54.39
	2005-2010	30.67	27.62	27.32	45.39	45.29
Eugenia nesiotica	1995-2000	184.64	176.31	200.00	51.63	51.67
	2000-2005	151.14	142.28	200.00	37.43	37.43
	2005-2010	138.42	129.78	200.00	50.09	49.95
Eugenia oerstediana	1995-2000	40.31	33.81	59.19	19.08	22.00
	2000-2005	42.51	36.04	59.19	22.79	24.73
	2005-2010	38.64	33.24	59.19	25.49	25.48
Faramea occidentalis	1995-2000	62.44	60.16	68.76	52.93	53.79
	2000-2005	61.65	59.38	68.76	48.08	48.64
	2005-2010	58.52	56.26	68.76	49.44	49.44
Garcinia intermedia	1995-2000	49.40	46.04	40.93	73.39	74.43
	2000-2005	46.63	42.55	40.93	69.40	69.44
	2005-2010	43.41	39.94	40.93	63.34	63.07
Garcinia madruno	1995-2000	41.59	38.71	39.61	49.32	49.11
	2000-2005	45.73	42.89	39.61	73.71	73.30
	2005-2010	36.62	33.88	39.61	62.18	61.84
Guapira standleyana	1995-2000	83.93	77.05	200.00	16.24	21.18
	2000-2005	78.92	73.54	200.00	63.72	63.47
	2005-2010	83.05	78.42	200.00	61.19	61.01
Guarea guidonia	1995-2000	139.06	132.85	200.00	41.48	48.41
	2000-2005	146.17	140.27	200.00	31.48	36.63
	2005-2010	116.26	110.57	200.00	45.09	47.71
Guarea bullata	1995-2000	66.35	61.83	52.56	19.07	19.86
	2000-2005	76.84	72.43	52.56	13.01	13.58
	2005-2010	71.52	67.90	52.56	16.99	17.70
Guatteria dumetorum	1995-2000	74.56	67.30	200.00	14.57	18.41
	2000-2005	71.09	63.86	200.00	17.58	19.02
	2005-2010	67.28	61.01	200.00	23.27	23.24
Guettarda foliacea	1995-2000	103.21	99.86	110.72	28.16	31.91
	2000-2005	110.94	107.79	110.72	38.38	38.36
	2005-2010	108.92	105.92	110.72	53.72	53.67
Gustavia superba	1995-2000	158.93	155.90	235.90	6.89	7.88
	2000-2005	197.64	195.26	235.90	10.01	11.81
	2005-2010	213.52	211.01	235.90	9.46	9.94
Hamelia axillaris	1995-2000	17.65	14.28	24.44	7.47	7.45
	2000-2005					
	2005-2010	20.79	17.94	24.44	15.84	15.77
Hampea appendiculata	1995-2000					

Continued on next page

Table F.3 –continued from previous page

Species	Census	PT Slow	PT Fast	Growth Threshold	LE Slow	LE Fast
	2000-2005					
	2005-2010	8.70	6.36	70.90	19.98	18.08
Hasseltia floribunda	1995-2000	88.97	85.06	143.97	10.13	11.87
	2000-2005	92.09	88.89	143.97	12.30	15.08
	2005-2010	88.77	85.77	143.97	23.26	23.25
Heisteria concinna	1995-2000	102.17	100.55	148.33	92.32	92.77
	2000-2005	92.54	91.29	148.33	90.36	90.23
	2005-2010	91.57	89.84	148.33	86.72	87.51
Herrania purpurea	1995-2000	60.01	57.97	41.72	34.60	35.71
	2000-2005	55.68	53.15	41.72	44.96	45.07
	2005-2010	51.87	50.16	41.72	46.01	45.84
Hirtella triandra	1995-2000	72.74	67.68	82.24	54.02	59.11
	2000-2005	69.64	65.13	82.24	55.31	58.56
	2005-2010	66.29	62.31	82.24	56.17	58.88
Hybanthus prunifolius	1995-2000	43.98	42.06	30.19	24.15	24.05
	2000-2005	48.15	45.56	30.19	28.93	28.77
	2005-2010	43.02	41.19	30.19	28.25	28.11
Inga goldmanii	1995-2000	44.62	38.66	74.09	22.39	22.49
	2000-2005	45.89	40.54	74.09	27.48	28.55
	2005-2010	35.40	30.74	74.09	35.62	35.47
Inga marginata	1995-2000	27.13	21.99	200.00	11.04	14.60
	2000-2005	28.30	24.02	200.00	13.97	17.07
	2005-2010	33.28	27.78	200.00	21.76	21.05
Inga pezizifera	1995-2000	25.84	19.52	86.42	17.16	16.78
	2000-2005	30.10	25.01	86.42	27.76	26.85
	2005-2010	27.05	22.53	86.42	24.02	22.97
Inga nobilis	1995-2000	56.35	52.55	81.13	36.68	39.04
	2000-2005	65.43	62.34	81.13	42.43	42.57
	2005-2010	58.11	55.22	81.13	29.51	30.80
Inga acuminata	1995-2000	33.19	29.02	66.59	44.65	43.88
	2000-2005	27.06	23.62	66.59	38.50	37.85
	2005-2010	24.28	21.07	66.59	45.03	43.62
Inga sapindoides	1995-2000	55.84	50.74	126.08	24.78	26.20
	2000-2005	47.60	42.95	126.08	12.97	16.88
	2005-2010	42.68	38.75	126.08	29.57	29.29
Inga thibaudiana	1995-2000	22.12	20.11	113.86	24.51	25.62
	2000-2005	27.61	25.69	113.86	30.20	31.40
	2005-2010	20.39	18.76	113.86	17.59	17.23
Inga umbellifera	1995-2000	53.50	50.13	56.73	22.11	23.45
	2000-2005	59.55	56.13	56.73	32.15	32.08
	2005-2010	46.73	43.42	56.73	33.39	33.30
Jacaranda copaia	1995-2000	32.30	30.22	200.00	24.66	29.21
	2000-2005	37.72	35.82	200.00	50.50	51.38
	2005-2010	33.86	32.52	200.00	51.30	51.06
Lacistema aggregatum	1995-2000	41.64	37.29	34.95	19.91	20.50
	2000-2005	41.92	37.19	34.95	23.92	24.34
	2005-2010	37.35	33.45	34.95	29.30	29.33
Laetia thamnia	1995-2000	51.44	47.59	59.85	22.27	22.31
	2000-2005	51.61	48.39	59.85	22.86	22.87
	2005-2010	47.04	44.15	59.85	31.75	31.73
Licania platypus	1995-2000	48.82	44.73	37.78	28.68	28.78
	2000-2005	48.16	43.43	37.78	31.44	31.49
	2005-2010	43.45	40.31	37.78	32.16	32.23
Lonchocarpus heptaphyllus	1995-2000	120.28	113.36	200.00	21.51	27.48
	2000-2005	99.19	92.50	200.00	23.96	29.76
	2005-2010	88.14	81.62	200.00	36.79	37.75
Luehea seemannii	1995-2000	70.63	65.08	200.00	9.38	17.19
	2000-2005	83.46	76.73	200.00	3.76	8.80
	2005-2010	85.12	79.54	200.00	27.14	35.46
Mosannona garwoodii	1995-2000	75.65	73.92	53.47	80.78	80.71
	2000-2005	71.61	69.67	53.47	101.42	102.79
	2005-2010	77.79	76.42	53.47	114.13	113.97
Maquira guianensis	1995-2000	72.25	69.95	79.49	63.60	62.99
	2000-2005	71.61	69.57	79.49	60.09	59.69
	2005-2010	67.92	65.71	79.49	59.02	58.67
Miconia affinis	1995-2000	23.02	18.67	52.31	13.57	13.41
	2000-2005	23.60	20.77	52.31	15.15	15.08
	2005-2010	21.32	18.56	52.31	20.45	20.04
Miconia argentea	1995-2000	16.05	12.72	56.46	5.75	6.74
	2000-2005	14.28	11.58	56.46	5.69	6.24
	2005-2010	15.77	11.67	56.46	11.88	11.87
Miconia nervosa	1995-2000	11.45	10.41	19.48	7.85	7.80
	2000-2005	15.12	13.08	19.48	6.54	6.49
	2005-2010	13.47	12.24	19.48	12.60	12.39
Mouriri myrtilloides	1995-2000	38.36	36.12	25.75	23.60	23.73
	2000-2005	39.61	37.47	25.75	30.25	30.30
	2005-2010	12.16	13.70	25.75	25.88	26.19
Nectandra cissiflora	1995-2000	35.95	30.57	96.15	14.63	18.53
	2000-2005	38.88	33.82	96.15	23.98	25.29
	2005-2010	34.64	29.15	96.15	23.58	28.78
Nectandra lineata	1995-2000	14.36	7.92	34.68	11.00	15.09
	2000-2005	14.68	9.74	34.68	8.00	10.64
	2005-2010	15.49	9.46	34.68	22.87	22.69
Ocotea cernua	1995-2000	36.11	31.05	70.13	8.88	10.79
	2000-2005	33.54	29.10	70.13	16.86	19.86
	2005-2010	32.79	29.63	70.13	37.92	42.04
Ocotea oblonga	1995-2000	25.32	21.44	200.00	13.34	16.30
	2000-2005	32.87	28.38	200.00	10.03	12.85
	2005-2010	33.35	29.05	200.00	24.84	24.15
Ocotea puberula	1995-2000	39.64	33.11	200.00	11.43	15.23
	2000-2005	41.37	33.43	200.00	12.36	12.34

Continued on next page

Table F.3 –continued from previous page

Species	Census	PT Slow	PT Fast	Growth Threshold	LE Slow	LE Fast
	2005-2010	36.13	28.33	200.00	20.33	19.70
Ocotea whitei	1995-2000	45.02	39.42	200.00	15.71	20.18
	2000-2005	39.31	36.57	200.00	18.15	20.76
	2005-2010	51.77	47.20	200.00	33.24	33.12
Oenocarpus mapora	1995-2000	88.16	84.86	113.08	2.45	2.65
	2000-2005	102.28	97.46	113.08	4.14	4.52
	2005-2010	123.23	118.69	113.08	8.82	9.67
Trophis caucana	1995-2000	42.40	38.60	101.95	19.82	20.78
	2000-2005	54.77	51.79	101.95	12.69	13.21
	2005-2010	71.39	68.52	101.95	26.19	26.17
Ouratea lucens	1995-2000	51.49	49.93	27.38	41.33	41.41
	2000-2005	52.96	51.37	27.38	45.66	45.89
	2005-2010	49.80	48.44	27.38	40.57	40.60
Palicourea guianensis	1995-2000	7.17	6.68	33.46	3.88	3.87
	2000-2005	8.51	7.05	33.46	4.13	4.07
	2005-2010	7.68	6.95	33.46	7.84	7.45
Pentagonia macrophylla	1995-2000	57.38	53.93	37.65	15.27	15.99
	2000-2005	67.82	65.23	37.65	19.37	20.17
	2005-2010	56.73	54.51	37.65	47.95	47.72
Perebea xanthochyma	1995-2000	65.53	63.31	70.09	50.74	51.15
	2000-2005	49.63	46.97	70.09	57.81	57.46
	2005-2010	52.99	50.30	70.09	63.75	63.23
Picramnia latifolia	1995-2000	51.00	47.22	44.62	25.56	25.61
	2000-2005	47.62	42.92	44.62	26.85	26.86
	2005-2010	50.75	47.58	44.62	32.37	32.33
Piper cordulatum	1995-2000	16.26	13.96	15.83	3.62	3.63
	2000-2005					
	2005-2010					
Piper reticulatum	1995-2000	66.05	62.26	76.87	7.97	10.67
	2000-2005	77.57	75.69	76.87	36.37	36.57
	2005-2010	50.95	49.67	76.87	26.96	26.94
Platymiscium pinnatum	1995-2000	110.96	104.21	200.00	10.97	12.85
	2000-2005	139.41	132.02	200.00	14.84	15.68
	2005-2010	104.21	97.58	200.00	26.68	26.68
Poulsenia armata	1995-2000	59.17	52.25	200.00	21.09	21.07
	2000-2005	57.73	52.05	200.00	24.76	24.73
	2005-2010	57.20	51.46	200.00	25.39	25.36
Pouteria reticulata	1995-2000	85.77	77.47	200.00	27.87	42.96
	2000-2005	88.95	80.83	200.00	22.35	32.67
	2005-2010	85.38	77.09	200.00	29.88	37.58
Prioria copaifera	1995-2000	80.79	71.31	200.00	98.01	109.20
	2000-2005	76.75	65.95	200.00	83.73	98.64
	2005-2010	83.24	73.31	200.00	104.72	103.61
Protium costaricense	1995-2000	62.24	57.82	86.00	29.16	30.73
	2000-2005	57.22	53.29	86.00	26.39	27.59
	2005-2010	46.78	43.76	86.00	32.81	34.26
Protium panamense	1995-2000	48.61	44.34	44.25	38.01	37.74
	2000-2005	58.95	54.89	44.25	37.73	38.58
	2005-2010	42.86	39.44	44.25	44.43	44.28
Protium tenuifolium	1995-2000	121.37	115.14	200.00	42.56	45.99
	2000-2005	105.40	99.12	200.00	41.10	45.20
	2005-2010	103.76	97.87	200.00	42.70	43.78
Psychotria horizontalis	1995-2000	27.57	25.30	21.97	13.42	13.44
	2000-2005	32.57	29.88	21.97	13.08	13.10
	2005-2010	29.86	28.13	21.97	14.90	14.87
Psychotria marginata	1995-2000	17.82	16.58	17.90	10.46	10.48
	2000-2005	18.65	17.06	17.90	11.81	11.76
	2005-2010	17.35	16.07	17.90	15.14	14.95
Pterocarpus rohrii	1995-2000	51.81	47.29	47.39	22.55	24.53
	2000-2005	52.37	47.53	47.39	25.02	26.39
	2005-2010	40.45	35.83	47.39	22.21	23.65
Quararibea asterolepis	1995-2000	97.53	89.37	200.00	57.39	66.80
	2000-2005	93.94	86.52	200.00	65.35	69.38
	2005-2010	92.16	85.23	200.00	84.89	91.20
Randia armata	1995-2000	114.63	111.39	109.99	30.91	32.81
	2000-2005	116.75	114.29	109.99	56.91	59.04
	2005-2010	124.61	122.09	109.99	61.13	62.29
Rinorea sylvatica	1995-2000	45.68	43.56	29.66	34.83	34.82
	2000-2005	50.54	48.37	29.66	37.40	37.42
	2005-2010	43.22	41.66	29.66	35.63	35.64
Senna dariensis	1995-2000					
	2000-2005					
	2005-2010	14.85	14.57	42.65	15.97	15.88
Simarouba amara	1995-2000	42.50	36.64	200.00	13.65	15.85
	2000-2005	43.63	37.47	200.00	16.43	18.66
	2005-2010	43.41	37.82	200.00	21.50	21.34
Siparuna pauciflora	1995-2000	57.90	56.77	57.09	15.80	16.04
	2000-2005	46.10	44.62	57.09	20.14	20.15
	2005-2010	36.80	33.55	57.09	21.36	21.34
Sloanea terniflora	1995-2000	179.24	167.00	200.00	52.46	52.59
	2000-2005	190.34	178.23	200.00	57.85	57.83
	2005-2010	198.21	188.81	200.00	67.68	67.64
Socratea exorrhiza	1995-2000	64.37	60.10	131.80	24.52	24.52
	2000-2005	75.04	72.61	131.80	24.15	24.14
	2005-2010	87.02	85.50	131.80	29.59	29.58
Sorocea affinis	1995-2000	66.43	64.14	53.00	37.00	36.98
	2000-2005	67.32	64.98	53.00	31.09	31.07
	2005-2010	71.56	69.46	53.00	34.67	34.63
Spondias radlkoferi	1995-2000	55.23	49.83	200.00	8.48	13.46
	2000-2005	73.16	67.22	200.00	16.83	24.39
	2005-2010	65.29	59.41	200.00	18.45	22.24

Continued on next page

Table F.3 –continued from previous page

Species	Census	PT Slow	PT Fast	Growth Threshold	LE Slow	LE Fast
Stylogyne turbacensis	1995-2000	42.92	40.86	28.87	19.60	19.89
	2000-2005	41.93	39.92	28.87	24.78	25.00
	2005-2010	39.12	37.31	28.87	30.09	30.11
Swartzia simplex	1995-2000	59.77	45.53	48.04	47.30	47.41
	2000-2005	67.16	62.51	48.04	98.32	98.64
	2005-2010	61.38	56.98	48.04	105.25	108.41
Swartzia simplex	1995-2000	104.13	101.69	52.76	101.23	103.55
	2000-2005	105.32	102.52	52.76	104.97	105.79
	2005-2010	94.20	91.61	52.76	86.65	87.87
Symphonia globulifera	1995-2000	63.69	55.58	200.00	24.84	24.68
	2000-2005	89.07	82.30	200.00	27.27	27.21
	2005-2010	76.68	70.58	200.00	33.12	32.86
Tabebuia rosea	1995-2000	110.11	101.14	200.00	35.78	36.96
	2000-2005	89.64	81.86	200.00	19.31	26.87
	2005-2010	78.23	69.90	200.00	41.64	41.34
Tabernaemontana arborea	1995-2000	74.37	67.90	200.00	52.88	58.94
	2000-2005	70.33	63.79	200.00	60.25	64.99
	2005-2010	67.32	62.17	200.00	54.97	56.15
Tachigali versicolor	1995-2000	73.18	65.22	200.00	16.79	18.46
	2000-2005	71.45	63.18	200.00	19.29	22.48
	2005-2010	56.79	48.12	200.00	18.68	18.55
Talisia nervosa	1995-2000	41.25	43.69	41.57	69.93	69.55
	2000-2005	86.31	84.24	41.57	47.74	49.82
	2005-2010	79.25	77.92	41.57	74.67	74.59
Talisia croatii	1995-2000	57.74	55.74	32.74	42.10	44.25
	2000-2005	57.56	55.47	32.74	30.77	31.46
	2005-2010	55.62	54.34	32.74	53.06	53.29
Tetragastris panamensis	1995-2000	142.10	133.76	200.00	58.55	67.90
	2000-2005	139.72	131.21	200.00	47.76	54.86
	2005-2010	144.08	135.63	200.00	46.73	48.18
Trichilia pallida	1995-2000	57.80	54.44	91.10	40.86	43.46
	2000-2005	56.14	51.88	91.10	32.84	33.38
	2005-2010	52.19	49.35	91.10	36.35	36.30
Trichilia tuberculata	1995-2000	131.91	124.36	200.00	33.54	35.23
	2000-2005	139.32	131.74	200.00	36.69	37.92
	2005-2010	128.99	121.58	200.00	41.66	42.74
Triplaris cumingiana	1995-2000	83.50	78.33	201.17	11.35	17.24
	2000-2005	84.23	80.31	201.17	15.97	17.35
	2005-2010	108.23	105.73	201.17	57.23	57.16
Trophis racemosa	1995-2000	60.77	55.59	60.40	28.86	28.88
	2000-2005	67.92	62.16	60.40	25.31	25.33
	2005-2010	55.06	49.32	60.40	25.39	28.13
Unonopsis pittieri	1995-2000	78.00	73.87	124.25	27.39	31.58
	2000-2005	70.20	66.84	124.25	22.96	25.14
	2005-2010	65.28	62.65	124.25	41.09	40.88
Virola sebifera	1995-2000	89.30	84.75	175.75	28.03	31.93
	2000-2005	86.83	82.81	175.75	30.73	32.35
	2005-2010	84.94	81.51	175.75	42.75	42.69
Virola surinamensis	1995-2000	55.52	52.08	200.00	47.68	47.39
	2000-2005	63.14	58.74	200.00	60.05	59.48
	2005-2010	49.15	46.16	200.00	65.28	64.63
Xylopia macrantha	1995-2000	52.46	50.08	76.90	66.54	67.31
	2000-2005	47.08	44.83	76.90	80.94	81.83
	2005-2010	45.74	43.28	76.90	75.66	75.12
Zanthoxylum ekmanii	1995-2000	16.46	15.52	200.00	11.35	12.56
	2000-2005	23.03	21.85	200.00	11.52	15.48
	2005-2010	21.21	21.29	200.00	18.85	18.99
Zanthoxylum panamense	1995-2000	42.15	38.05	200.00	7.92	14.03
	2000-2005	38.13	33.54	200.00	23.04	22.52
	2005-2010	49.29	45.70	200.00	34.83	34.05

Table F.4: Passage Times and Life Expectancies for BCI species

Species	Slow PT			Fast PT			Slow LE			Fast LE		
	100 mm	150 mm	200 mm	100 mm	150 mm	200 mm	10 mm	50 mm	100 mm	10 mm	50 mm	100 mm
Acalypha diversifolia	53.59	79.13	1.00	51.93	77.46	1.00	8.67	8.72	8.67	8.68	8.72	8.67
Adelia triloba	59.08	87.06	111.19	54.85	82.84	106.96	7.85	13.14	22.49	8.20	13.80	23.15
Alchornea costaricensis	27.07	41.89	55.69	24.51	39.33	53.13	4.21	24.16	40.21	5.22	25.97	40.43
Alibertia edulis	119.36	1.00	1.00	116.85	1.00	1.00	29.70	26.23	5.27	29.71	26.15	5.00
Alseis blackiana	88.77	118.23	139.26	79.80	109.25	130.28	53.44	113.82	117.33	67.06	116.57	115.56
Anaxagorea panamensis	90.78	90.78	90.78	89.49	89.49	89.49	55.37	14.00	1.00	54.94	13.70	1.00
Andira inermis	137.27	181.94	226.46	133.24	177.91	222.43	49.86	48.69	44.78	49.84	48.57	44.70
Annona acuminata	128.15	128.66	128.66	125.48	126.00	126.00	25.14	26.61	1.24	25.97	26.49	1.23
Annona spraguei	25.31	37.62	49.99	23.83	36.14	48.51	4.30	11.31	15.89	4.53	11.70	15.89
Apeiba membranacea	33.69	48.61	61.68	30.31	45.23	58.29	18.76	37.28	56.57	21.33	40.10	58.20
Aspidosperma spruceanum	66.64	83.99	95.85	54.38	71.73	83.58	84.63	92.81	86.05	90.75	90.81	83.94
Astrocaryum standleyanum	156.57	211.11	252.22	151.68	206.22	247.32	50.49	49.95	47.06	50.48	49.89	46.80
Bactris major	1.00	1.00	1.00	1.00	1.00	1.00	2.91	19.74	1.00	3.03	18.31	1.00
Beilschmiedia pendula	75.90	100.20	116.97	67.72	92.03	108.79	30.80	68.02	66.41	43.45	68.16	65.77
Brosimum alicastrum	62.28	78.79	90.50	51.97	68.49	80.19	100.32	94.37	87.78	98.44	92.51	85.99
Calophyllum longifolium	57.74	75.18	88.20	49.45	66.89	79.91	28.61	28.16	26.99	28.52	27.96	26.58
Capparis frondosa	179.03	1.00	1.00	176.74	1.00	1.00	33.93	48.13	1.73	35.55	47.95	1.68
Casearia aculeata	111.35	159.13	206.55	108.38	156.16	203.57	23.91	50.84	46.11	25.38	50.97	46.02
Casearia arborea	35.63	53.25	69.74	34.28	51.90	68.40	28.96	38.04	36.95	30.00	38.09	36.72
Casearia sylvestris	68.64	97.58	119.86	65.75	94.70	116.98	16.18	33.91	38.27	17.50	34.66	37.98
Cassipourea elliptica	66.29	87.44	108.58	61.00	82.15	103.29	72.31	70.74	64.15	73.17	69.92	63.93
Cecropia insignis	12.80	19.85	27.35	13.47	20.52	28.03	21.28	28.51	34.38	20.58	27.95	34.16
Cecropia obtusifolia	1.00	1.00	1.00	1.00	1.00	1.00	1.00	1.00	1.00	1.00	1.00	1.00
Chamguava schippii	91.89	128.75	1.00	89.38	126.25	1.00	55.37	45.30	27.38	55.07	45.13	27.06
Chrysochlamys eclipes	137.87	189.03	189.03	136.01	187.17	187.17	60.55	62.34	36.62	61.43	61.88	36.35
Chrysophyllum argenteum	100.35	136.31	163.07	93.63	129.59	156.35	45.30	71.37	59.60	54.20	70.39	57.98
Chrysophyllum cainito	61.19	78.00	89.91	49.94	66.74	78.65	45.05	55.65	54.23	51.21	55.29	53.69
Coccoloba coronata	92.05	120.48	149.06	84.88	113.32	141.89	12.71	49.97	59.21	14.88	52.55	58.92
Coccoloba manzinellensis	133.40	192.46	249.69	130.31	189.37	246.61	24.03	55.65	50.62	26.86	55.62	50.55
Conostegia cinnamomea	1.00	1.00	1.00	1.00	1.00	1.00	8.85	1.05	1.00	8.69	1.05	1.00
Cordia alliodora	25.83	36.99	46.24	22.60	33.75	43.00	15.64	28.47	30.84	18.74	29.47	30.04
Cordia bicolor	32.85	48.62	62.21	29.66	45.43	59.02	11.43	34.35	40.08	14.32	35.94	39.04
Cordia lasiocalyx	93.33	128.87	163.83	91.04	126.58	161.54	16.24	20.41	20.20	16.64	20.41	20.17
Coussarea curvigemmia	101.21	142.42	182.78	98.89	140.10	180.46	51.28	50.88	40.54	51.77	50.51	40.37
Croton billbergianus	15.14	20.09	24.75	11.56	16.31	20.96	4.18	6.67	6.79	4.59	6.73	6.74
Cupania seemannii	77.15	106.99	136.62	72.78	102.62	132.25	55.45	69.93	54.84	59.56	69.61	54.45
Desmopsis panamensis	112.02	1.00	1.00	110.02	1.00	1.00	34.24	19.96	5.81	34.02	19.84	5.74
Drypetes standleyi	74.56	98.38	115.78	66.65	90.47	107.87	59.19	73.74	60.49	66.50	71.75	57.76
Erythroxylum macrophyllum	67.72	95.96	124.20	63.03	91.27	119.50	17.01	17.21	17.15	17.05	17.21	17.15
Eugenia coloradoensis	72.53	92.43	112.33	65.76	85.66	105.56	21.26	31.21	31.04	24.22	31.22	31.03
Eugenia galalonensis	119.99	165.96	1.00	116.52	162.49	1.00	42.80	36.78	18.32	42.69	36.66	18.02
Eugenia nesiotica	116.40	155.30	184.64	108.07	146.96	176.31	51.64	51.60	51.02	51.68	51.56	50.92
Eugenia oerstediana	54.35	72.18	90.01	47.85	65.68	83.51	19.88	28.48	28.03	22.61	28.45	28.00
Faramea occidentalis	83.30	116.65	149.02	81.01	114.37	146.74	53.64	46.64	31.10	54.33	45.73	30.90
Garcinia intermedia	99.82	142.78	185.45	96.46	139.42	182.09	74.20	75.12	68.52	75.08	75.05	68.40
Garcinia madruno	87.94	124.57	160.57	85.06	121.69	157.69	49.23	41.63	33.00	48.99	41.46	32.84
Guapira standleyana	50.18	69.43	83.93	43.30	62.54	77.05	16.24	43.28	68.14	21.18	49.10	70.03
Guarea guidonia	84.19	115.34	139.06	77.99	109.14	132.85	42.90	72.73	60.54	49.67	72.05	58.39
Guarea bullata	108.62	153.36	197.97	104.10	148.84	193.45	19.57	29.18	29.02	20.34	29.21	29.02
Guatteria dumetorum	47.01	62.65	74.56	39.76	55.40	67.30	14.57	26.96	28.22	18.41	27.65	27.88
Guettarda foliacea	95.35	127.50	158.04	92.00	124.15	154.69	29.92	59.43	47.82	33.61	59.05	46.81
Gustavia superba	69.74	105.58	138.18	66.70	102.54	135.15	7.10	53.34	99.10	8.13	56.77	99.61
Hamelia axillaris	1.00	1.00	1.00	1.00	1.00	1.00	7.48	1.18	1.00	7.44	1.16	1.00
Hampea appendiculata	10.49	13.40	16.32	7.79	10.68	13.60	19.89	16.64	13.13	18.00	15.14	12.65
Hasseltia floribunda	64.40	91.82	113.32	60.49	87.91	109.42	10.59	27.17	27.86	12.36	27.59	27.51
Heisteria concinna	71.45	103.27	129.31	69.83	101.65	127.70	92.73	91.30	83.73	93.09	91.01	83.29
Herrania purpurea	1.00	1.00	1.00	1.00	1.00	1.00	36.26	31.28	1.03	37.24	31.04	1.03

Continued on next page

Table F.4 –continued from previous page

Species		Slow PT: 9mm -			Fast PT: 9mm -			Slow LE			Fast LE	
	100 mm	150 mm	200 mm	100 mm	150 mm	200 mm	10 mm	50 mm	100 mm	10 mm	50 mm	100 mm
Hirtella triandra	81.99	106.33	130.62	76.93	101.28	125.56	55.06	88.68	77.25	60.08	88.25	76.89
Hybanthus prunifolius	1.00	1.00	1.00	1.00	1.00	1.00	24.04	11.72	2.46	23.93	11.64	2.44
Inga goldmanii	52.62	67.85	83.25	46.66	61.89	77.28	22.41	22.59	22.44	22.50	22.57	22.43
Inga marginata	17.81	23.17	27.13	12.70	18.03	21.99	11.22	17.02	17.25	14.70	17.19	16.43
Inga pezizifera	26.96	33.52	40.01	20.64	27.21	33.70	17.14	15.97	13.73	16.75	15.36	13.52
Inga nobilis	64.10	85.28	106.34	60.30	81.48	102.54	37.82	42.01	33.36	39.89	41.28	33.10
Inga acuminata	41.23	53.81	66.18	37.05	49.63	62.00	44.69	37.67	28.52	43.84	36.10	28.10
Inga sapindoides	47.94	61.29	72.89	42.84	56.19	67.79	25.12	27.14	24.37	26.39	26.75	23.66
Inga thibaudiana	19.82	26.99	33.41	17.81	24.96	31.39	24.72	27.32	21.99	25.77	26.30	20.68
Inga umbellifera	81.52	112.87	1.00	78.15	109.50	1.00	23.02	27.61	20.48	24.21	27.33	20.27
Jacaranda copaia	16.52	24.55	32.30	14.48	22.47	30.22	24.66	44.16	60.01	29.21	47.85	61.45
Lacistema aggregatum	94.91	134.49	173.41	90.56	130.14	169.06	20.33	23.16	21.97	20.85	23.15	21.94
Laetia thamnia	73.51	101.22	128.74	69.66	97.37	124.89	22.29	22.18	21.11	22.33	22.13	21.06
Licania platypus	104.02	148.40	192.36	99.93	144.30	188.27	28.75	28.79	27.50	28.83	28.78	27.46
Lonchocarpus heptaphyllus	73.94	100.00	120.28	67.02	93.08	113.36	22.46	41.40	37.67	28.27	41.14	36.77
Luehea seemannii	41.63	57.97	70.63	36.08	52.41	65.08	9.38	46.33	53.20	17.19	49.09	53.05
Mosannona garwoodii	130.54	188.38	1.00	128.81	186.65	1.00	80.72	72.16	55.11	80.63	71.79	54.93
Maquira guianensis	86.56	117.06	145.83	84.25	114.76	143.53	63.31	48.20	27.59	62.69	47.16	27.36
Miconia affinis	31.54	39.19	38.25	26.87	34.51	33.57	13.56	12.14	8.98	13.39	11.85	8.72
Miconia argentea	24.55	34.63	44.62	21.22	31.30	41.29	5.92	12.85	14.07	6.92	13.49	14.06
Miconia nervosa	1.00	1.00	1.00	1.00	1.00	1.00	7.82	1.02	1.00	7.75	1.02	1.00
Mouriri myrtilloides	144.85	1.00	1.00	142.61	1.00	1.00	23.79	23.49	2.56	23.90	23.46	2.45
Nectandra cissiflora	36.94	46.79	56.39	31.57	41.42	51.01	15.06	33.66	41.21	19.00	36.05	39.11
Nectandra lineata	24.25	32.42	40.60	17.82	25.99	34.17	11.30	19.41	19.15	15.31	19.39	19.12
Ocotea cernua	45.61	62.22	78.84	40.55	57.17	73.78	9.22	27.43	32.19	11.19	29.01	32.15
Ocotea oblonga	14.94	20.69	25.32	11.39	16.86	21.44	13.66	19.52	18.67	16.49	19.08	17.82
Ocotea puberula	25.59	33.40	39.64	19.05	26.86	33.11	11.62	19.23	23.19	15.40	21.25	23.09
Ocotea whitei	25.22	35.70	45.02	19.96	30.13	39.42	15.71	32.52	45.21	20.18	35.86	46.02
Oenocarpus mapora	76.84	113.25	1.00	73.55	109.95	1.00	2.52	32.55	47.68	2.74	35.84	45.74
Trophis caucana	41.85	54.05	61.36	38.05	50.25	57.57	20.09	22.09	15.98	20.98	21.40	15.00
Ouratea lucens	1.00	1.00	1.00	1.00	1.00	1.00	41.52	36.29	1.15	41.58	36.22	1.14
Palicourea guianensis	1.00	1.00	1.00	1.00	1.00	1.00	3.87	2.47	1.00	3.87	2.44	1.00
Pentagonia macrophylla	131.42	1.00	1.00	127.97	1.00	1.00	16.01	23.29	10.57	16.70	23.26	10.26
Perebea xanthochyma	86.40	121.31	156.37	84.19	119.09	154.15	51.10	50.64	44.70	51.45	50.41	44.59
Picramnia latifolia	94.71	134.47	173.40	90.92	130.69	169.62	25.60	25.49	24.25	25.64	25.48	24.22
Piper cordulatum	1.00	1.00	1.00	1.00	1.00	1.00	3.65	1.00	1.00	3.65	1.00	1.00
Piper reticulatum	80.16	111.02	132.42	76.37	107.24	128.64	9.24	35.66	29.28	12.09	35.42	29.13
Platymiscium pinnatum	66.12	92.07	110.96	59.37	85.32	104.21	11.27	25.33	34.52	13.18	27.19	34.85
Poulsenia armata	39.24	50.28	59.17	32.36	43.36	52.25	21.09	21.00	20.78	21.07	20.95	20.69
Pouteria reticulata	55.84	73.14	85.77	47.54	64.84	77.47	27.87	67.42	65.52	42.96	68.21	63.34
Prioria copaifera	54.97	69.84	80.79	45.49	60.36	71.31	98.01	115.90	109.51	109.20	114.09	107.50
Protium costaricense	69.20	89.03	108.79	64.78	84.61	104.37	29.81	32.92	25.47	31.21	32.37	24.92
Protium panamense	83.69	113.30	138.30	79.43	109.04	134.03	37.99	28.74	20.30	37.69	28.36	20.13
Protium tenuifolium	73.45	100.58	121.37	67.22	94.35	115.14	42.99	58.72	53.80	46.38	58.92	51.87
Psychotria horizontalis	1.00	1.00	1.00	1.00	1.00	1.00	13.45	8.78	1.00	13.46	8.68	1.00
Psychotria marginata	1.00	1.00	1.00	1.00	1.00	1.00	10.50	1.37	1.00	10.51	1.35	1.00
Pterocarpus rohrii	89.67	124.99	160.13	85.14	120.46	155.60	23.35	43.73	39.93	25.32	43.54	39.83
Quararibea asterolepis	61.42	81.93	97.53	53.26	73.77	89.37	57.39	82.68	81.73	66.80	82.98	80.89
Randia armata	106.27	142.67	176.52	103.03	139.43	173.28	32.01	54.27	49.40	33.88	54.37	48.77
Rinorea sylvatica	144.59	1.00	1.00	142.47	1.00	1.00	34.83	29.33	4.38	34.81	29.23	4.27
Senna dariensis	1.00	1.00	1.00	1.00	1.00	1.00	1.00	1.00	1.00	1.00	1.00	1.00
Simarouba amara	27.10	35.88	42.50	21.24	30.02	36.64	13.81	19.04	21.30	15.98	20.03	21.17
Siparuna pauciflora	99.10	146.30	192.67	97.97	145.17	191.54	16.14	21.39	20.49	16.36	21.39	20.48
Sloanea terniflora	118.23	153.05	179.24	105.99	140.81	167.00	52.46	52.64	52.11	52.59	52.59	51.99
Socratea exorrhiza	52.40	70.33	83.94	48.24	66.04	79.65	24.57	24.43	22.64	24.56	24.30	22.30
Sorocea affinis	112.23	159.33	1.00	109.94	157.04	1.00	36.99	35.58	30.05	36.97	35.47	29.95
Spondias radlkoferi	31.97	45.09	55.23	26.57	39.69	49.83	8.48	30.62	46.78	13.46	35.95	47.37
Stylogyne turbacensis	143.62	1.00	1.00	141.56	1.00	1.00	20.06	22.25	3.05	20.32	22.23	2.92

Continued on next page

Table F.4 –continued from previous page

Species		Slow PT: 9mm -			Fast PT: 9mm -			Slow LE			Fast LE	
	100 mm	150 mm	200 mm	100 mm	150 mm	200 mm	10 mm	50 mm	100 mm	10 mm	50 mm	100 mm
Swartzia simplex	72.08	76.05	78.75	57.84	61.80	64.50	50.69	177.68	177.44	50.81	177.67	177.43
Swartzia simplex	176.90	249.41	321.84	174.46	246.98	319.41	103.56	122.53	108.75	105.72	122.23	108.63
Symphonia globulifera	45.34	55.54	63.69	37.46	47.46	55.58	24.83	24.25	22.96	24.66	23.97	22.45
Tabebuia rosea	70.42	92.89	110.11	61.46	83.92	101.14	35.78	38.41	37.22	36.96	38.26	36.85
Tabernaemontana arborea	46.80	62.55	74.37	40.32	56.08	67.90	52.88	68.63	65.28	58.94	68.29	63.65
Tachigali versicolor	46.47	61.53	73.18	38.52	53.58	65.22	16.91	22.01	23.58	18.57	22.77	23.00
Talisia nervosa	28.72	27.62	27.57	31.16	30.06	30.01	70.59	86.49	84.32	70.29	87.18	86.26
Talisia croatii	168.97	229.51	229.51	166.97	227.51	227.51	45.49	67.76	39.48	47.54	67.66	39.22
Tetragastris panamensis	87.44	118.39	142.10	79.10	110.05	133.76	58.55	97.13	98.18	67.90	98.79	96.71
Trichilia pallida	61.39	81.17	100.81	58.03	77.81	97.45	41.52	52.50	46.88	44.02	52.15	46.71
Trichilia tuberculata	81.91	110.25	131.91	74.36	102.70	124.36	33.81	41.63	42.59	35.47	42.08	42.28
Triplaris cumingiana	47.81	67.58	83.09	42.64	62.42	77.92	11.75	49.33	54.61	17.73	51.69	53.52
Trophis racemosa	84.17	114.13	143.84	78.98	108.95	138.65	28.87	28.89	28.77	28.89	28.89	28.76
Unonopsis pittieri	66.03	87.72	106.36	61.90	83.59	102.23	28.32	56.24	52.27	32.48	56.43	51.24
Virola sebifera	57.70	79.83	96.42	53.15	75.29	91.88	28.63	43.60	42.75	32.42	43.62	42.50
Virola surinamensis	30.28	43.68	55.53	26.85	40.23	52.08	47.68	46.43	44.53	47.39	46.05	44.05
Xylopia macrantha	63.36	86.98	110.55	60.99	84.60	108.18	66.96	68.25	58.07	67.67	67.60	57.85
Zanthoxylum ekmanii	8.84	12.70	16.46	7.97	11.78	15.52	11.47	16.73	22.29	12.68	17.90	22.99
Zanthoxylum panamense	24.13	34.17	42.15	20.04	30.06	38.05	8.25	28.92	29.00	14.43	29.79	27.02

Bibliography

Ackerly, D. (2003). Community Assembly, Niche Conservatism, and Adaptive Evolution in Changing Environments. *International Journal of Plant Sciences*, 164, S165–S184.

Adams, T., Purves, D. & Pacala, S. (2007). Understanding height-structured competition in forests: is there an R* for light? *Proceedings of the Royal Society of London B: Biological Sciences*, 274, 3039–3048.

Alder, D. & Silva, J. (2000). An empirical cohort model for management of Terra Firme forests in the Brazilian Amazon. *Forest Ecology and Management*, 130, 141 – 157.

Alvarez-Buylla, E.R. & Martinez-Ramos, M. (1992). Demography and Allometry of *Cecropia Obtusifolia*, a Neotropical Pioneer Tree - An Evaluation of the Climax-Pioneer Paradigm for Tropical Rain Forests. *Journal of Ecology*, 80, 275–290.

Anderson-Teixeira, K.J., Davies, S.J., Bennett, A.C., Gonzalez-Akre, E.B., Muller-Landau, H.C., Wright, J.S., K., A.S., Almeyda Z., A.M., Alonso, A., Baltzer, J., Basset, Y., Bourg, N., Broadbent, E., Brockelman, W., Bunyavejchewin, S., Burslem, D., Butt, N., Cao, M., Cardenas, D., Chuyong, G., Clay, K., Cordell, S., Dattaraja, H., Deng, X., Detto, M., Du, X., Duque, A., Erikson, D., Ewango, C., Fischer, G.A., Fletcher, C., Foster, R., Giardina, C., Gilbert, G., Gunatilleke, N., Gunatilleke, S., Hao, Z., Hargrove, W.W., Hart, T., Hau, B., He, F., Hoffman, F., Howe, R., Hubbell, S., Inman-Narahari, F., Jansen, P., Jiang, M., Johnson, D., Kanzaki, M., Kassim, A., Kenfack, D., Kibet, S., Kinnaird, M.F., Korte, L., Kral, K., Kumar, J., Larson, A., Li, Y., Li, X., Liu, S., Lum, S., Lutz, J., Ma, K., Maddalena, D., Makana, J., Malhi, Y., Marthews, T., S.R., M., McMahon, S., McShea, W., Memiaghe, H., Mi, X., Mizuno, T., Morecroft, M., Myers, J., Novotny, V., de Oliveira, A., Ong, P.S., Orwig, D., Ostertag, R., den Ouden, J., Parker, G., Phillips, R., Sack, L., Sainge, M., Sang, W., Sri-ngernyuang, K., Sukumar, R., Sun, I., Sungpalee, W., Suresh, H., Tan, S., Thomas, S., Thomas, D., Thompson, J., Turner, B., Uriarte, M., Valencia, R., Vallejo, M., Vicentini, A., Vrska, T., Wang, X., Wang, X., Weiblen, G., Wolf, A., Xu, H., Yap, S. & Zimmerman, J. (2015). CTFS-forestGEO: a worldwide network monitoring forests in an era of global change. *Global Change Biology*, 21, 528–549.

Augustine, D. & McNaughton, S. (1998). Ungulate effects on the functional species composition of plant communities: herbivore selectivity and plant tolerance. *Journal of wildlife management*, 62, 1165 – 1183.

Bale, J.S., Masters, G.J., Hodkinson, I.D., Awmack, C., Bezemer, T.M., Brown, V.K., Butterfield, J., Buse, A., Coulson, J.C., Farrar, J., Good, J.E.G., Harrington, R., Hartley, S., Jones, T.H., Lindroth, R.L., Press, M.C., Symrnioudis, I., Watt, A.D. & Whittaker, J.B. (2002). Herbivory in global climate change research: direct effects of rising temperature on insect herbivores. *Global Change Biology*, 8, 1–16.

Bates, D. & Maechler, M. (2015). *Matrix: Sparse and Dense Matrix Classes and Methods*. R package version 1.2-3.

Battisti, A., Stastny, M., Netherer, S., Robinet, C., Schopf, A., Roques, A. & Larsson, S. (2005). Expansion of geographic range in the pine processionary moth caused by increased winter temperatures. *Ecological Applications*, 15, 2084–2096.

Beaumont, M.A. (2010). Approximate Bayesian Computation in Evolution and Ecology. In: *Annual Review of Ecology, Evolution, and Systematics* (ed. Futuyma, DJ and Shafer, HB and Simberloff, D). vol. 41 of *Annual Review of Ecology Evolution and Systematics*, pp. 379–406.

Bennett, A.C., McDowell, N.G., Allen, C.D. & Anderson-Teixeira, K.J. (2015). Larger trees suffer most during drought in forests worldwide. *Nature Plants*, 1, 15139–15144.

Besbeas, P., Lebreton, J.D. & Morgan, B.J.T. (2003). The efficient integration of abundance and demographic data. *Journal of the Royal Statistical Society: Series C (Applied Statistics)*, 52, 95–102.

Bossel, H. & Krieger, H. (1991). Simulation model of natural tropical forest dynamics. *Ecological Modelling*, 59, 37 – 71.

Bossel, H. & Krieger, H. (1994). Simulation of multi-species tropical forest dynamics using a vertically and horizontally structured model. In: *Contrasts between Biologically-based Process Models and Management-oriented Growth and Yield Models* (eds. Mohren, G., Bartelink, H. & Jansen, J.). IUFRO, Forest Ecology and Management, Wageningen, Netherlands, vol. 69, pp. 123–144.

Botkin, D.B., Janak, J. & Wallis, J.R. (1972). Some Ecological Consequences of a Computer Model of Forest Growth. *Journal of Ecology*, 60, 849–872.

Brasier, C. & Buck, K. (2001). Rapid Evolutionary Changes in a Globally Invading Fungal Pathogen (Dutch Elm Disease). *Biological Invasions*, 3, 223–233.

Brasier, C.M. (2008). The biosecurity threat to the UK and global environment from international trade in plants. *Plant Pathology*, 57, 792–808.

Brienen, R. & Zuidema, P. (2006). Lifetime growth patterns and ages of Bolivian rain forest trees obtained by tree ring analysis. *Journal of Ecology*, 94, 481–493.

Brunet, J., Bukina, Y., Hedwall, P.O., Holmström, E. & von Oheimb, G. (2014). Pathogen induced disturbance and succession in temperate forests: Evidence from a 100-year data set in southern Sweden. *Basic and Applied Ecology*, 15, 114 – 121.

Bugmann, H. (1994). *On the Ecology of Mountainous Forests in a changing Climate: A simulation Study*. Ph.D. thesis, Swiss Federal Institute of Technology, Zurich, Switzerland.

Bugmann, H., Grote, R., Lasch, P., Lindner, M. & Suckow, F. (1997). A new forest gap model to study the effects of environmental change on forest structure and functioning. In: *Impacts of Global Change on Tree Physiology and Forest Ecosystems: Proceedings of the International Conference on Impacts of Global Change on Tree Physiology and Forest Ecosystems, held 26–29 November 1996, Wageningen, The Netherlands* (eds. Mohren, G., Kramer, K. & Sabaté, S.). Springer Netherlands, Dordrecht, pp. 255–261.

Bugmann, H. & Weisberg, P.J. (2003). Forest-ungulate interactions: monitoring, modeling and management. *Journal for Nature Conservation*, 10, 193 – 201.

Butt, N., Campbell, G., Malhi, Y., Morecroft, M., Fenn, K., Campbell, G., Butt, S.A., Sherlock, L. & Zakiuddin, Y. (2009). Initial Results from Establishment of a Long-term Broadleaf Monitoring Plot at Wytham Woods, Oxford, UK.

Buzzard, V., Hulshof, C.M., Birt, T., Violle, C. & Enquist, B.J. (2016). Re-growing a tropical dry forest: functional plant trait composition and community assembly during succession. *Functional Ecology*, 30, 1006–1013.

Canham, C.D. (1988). Growth and Canopy Architecture of Shade-Tolerant Trees: Response to Canopy Gaps. *Ecology*, 69, 786–795.

Cao, M. & Woodward, F. (1998). Dynamic responses of terrestrial ecosystem carbon cycling to global climate change. *Nature*, 393, 249 – 252.

Caswell, H. (2000). *Matrix Population Models: Construction, Analysis and Interpretation*. Sinauer Associates, Sunderland, Massachusetts.

Caswell, H. (2012). Matrix models and sensitivity analysis of populations classified by age and stage: a vec-permutation matrix approach. *Theoretical Ecology*, 5, 404–417.

Caswell, H. & Salguero-Gómez, R. (2013). Age, stage and senescence in plants. *Journal of Ecology*, 101, 585–595.

Chang-Yang, C.H., Lu, C.L., Sun, I.F. & Hsieh, C.F. (2013). Long-term Seedling Dynamics of Tree Species in a Subtropical Rain Forest, Taiwan. *Taiwania*, 58, 35–43.

Childs, D.Z., Rees, M., Rose, K.E., Grubb, P.J. & Ellner, S.P. (2003). Evolution of Complex Flowering Strategies: An Age- and Size-Structured Integral Projection Model. *Proceedings: Biological Sciences*, 270, 1829–1838.

Clark, D.A. & Clark, D.B. (1992). Life History Diversity of Canopy and Emergent Trees in a Neotropical Rain Forest. *Ecological Monographs*, 62, 315–344.

Clark, D.B., Mercado, L.M., Sitch, S., Jones, C.D., Gedney, N., Best, M.J., Pryor, M., Rooney, G.G., Essery, R.L.H., Blyth, E., Boucher, O., Harding, R.J., Huntingford, C. & Cox, P.M. (2011). The joint UK Land Environment Simulator (JULES), model description Part 2: Carbon fluxes and vegetation dynamics. *Geoscientific Model Development*, 4, 701–722.

Clark, J.S. (2010). Individuals and the Variation Needed for High Species Diversity in Forest Trees. *Science*, 327, 1129–1132.

Clark, J.S., Bell, D., Chu, C., Courbaud, B., Dietze, M., Hersh, M., HilleRisLambers, J., Ibasez, I., LaDeau, S., McMahon, S., Metcalf, J., Mohan, J., Moran, E., Pangle, L., Pearson, S., Salk, C., Shen, Z., Valle, D. & Wyckoff, P. (2010). High-dimensional coexistence based on individual variation: a synthesis of evidence. *Ecological Monographs*, 80, 569–608.

Clark, J.S., Bell, D.M., Kwit, M.C. & Zhu, K. (2014). Competition-interaction landscapes for the joint response of forests to climate change. *Global Change Biology*, 20, 1979–1991.

Clebsch, E. & Busing, R. (1989). Secondary Succession, Gap Dynamics, and Community Structure in a Southern Appalachian Cove Forest. *Ecology*, 70, 728–735.

Cobb, R.C., Filipe João, A.N., Meentemeyer, R.K., Gilligan, C.A. & Rizzo, D.M. (2012). Ecosystem transformation by emerging infectious disease: loss of large tanoak from California forests. *Journal of Ecology*, 100, 712–722.

Comita, L.S., Aguilar, S., Pérez, R., Lao, L. & Hubell, S.P. (2007). Patterns of woody plant species abundance and diversity in the seedling layer of a tropical forest. *Journal of Vegetation Science*, 18, 163–174.

Condit, R. (1998). *Tropical Forest Census Plots: Methods and Results from Barro Colorado Island, Panama and a Comparison with Other Plots*. Springer-Verlag, Berlin Heidelberg.

Condit, R., Aguilar, S., Hernandez, A., Perez, R., Lao, S., Angehr, G., Hubbell, S.P. & Foster, R.B. (2004). Tropical forest dynamics across a rainfall gradient and the impact of an El Niño dry season. *Journal of Tropical Ecology*, 20, 51–72.

Condit, R., Ashton, P., Bunyavejchewin, S., Dattaraja, H.S., Davies, S., Esufali, S., Ewango, C., Foster, R., Gunatilleke, I.A.U.N., Gunatilleke, C.V.S., Hall, P., Harms, K.E., Hart, T., Hernandez, C., Hubbell, S., Itoh, A., Kiratiprayoon, S., LaFrankie, J., de Lao, S.L., Makana, J.R., Noor, M.N.S., Kassim, A.R., Russo, S., Sukumar, R., Samper, C., Suresh, H.S., Tan, S., Thomas, S., Valencia, R., Vallejo, M., Villa, G. & Zillio, T. (2006). The importance of demographic niches to tree diversity. *Science*, 313, 98–101.

Condit, R., Hubbell, S.P. & Foster, R.B. (1992). Short-Term Dynamics of a Neotropical Forest. *BioScience*, 42, 822–828.

Condit, R., Hubbell, S.P. & Foster, R.B. (1993). Mortality and growth of a commercial hardwood 'el cativo', *Prioria copaifera*, in Panama. *Forest Ecology and Management*, 62, 107–122.

Condit, R., Hubbell, S.P. & Foster, R.B. (1995). Mortality Rates of 205 Neotropical Tree and Shrub Species and the Impact of a Severe Drought. *Ecological Monographs*, 65, 419–439.

Coomes, D.A. & Allen, R.B. (2007). Mortality and tree-size distributions in natural mixed-age forests. *Journal of Ecology*, 95, 27–40.

Coomes, D.A. & Allen, R.B. (2009). Testing the Metabolic Scaling Theory of tree growth. *Journal of Ecology*, 97, 1369–1373.

Cox, P. (2001). Description of the TRIFFID dynamic global vegetation model. Tech. Rep. 24, Met Office, Hadley Centre.

Cramer, W., Bondeau, A., Woodward, F.I., Prentice, I.C., Betts, R.A., Brovkin, V., Cox, P.M., Fisher, V., Foley, J.A., Friend, A.D., Kucharik, C., Lomas, M.R., Ramankutty, N., Sitch, S., Smith, B., White, A. & Young-Molling, C. (2001). Global response of

terrestrial ecosystem structure and function to CO_2 and climate change: results from six dynamic global vegetation models. *Global Change Biology*, 7, 357–373.

Croat, T.B. (1978). *Flora of Barro Colorado Island*. Stanford University Press, Stanford, CA.

Csardi, G. & Nepusz, T. (2006). The igraph software package for complex network research. *InterJournal*, Complex Systems, 1695.

Cudmore, T., Björklund, N., Carroll, A. & Lindgren, B. (2010). Climate change and range expansion of an aggressive bark beetle: evidence of higher beetle reproduction in naïve host tree populations. *Journal of Applied Ecology*, 47, 1036–1043.

Davies, S.J. (2001). Tree mortality and growth in 11 sympatric Macaranga species in Borneo. *Ecology*, 82, 920–932.

Díaz, S. & Cabido, M. (1997). Plant Functional Types and Ecosystem Function in Relation to Global Change. *Journal of Vegetation Science*, 8, 463–474.

Didion, M., Kupferschmid, A. & Bugmann, H. (2009). Long-term effects of ungulate browsing on forest composition and structure. *Forest Ecology and Management*, 258, Supplement, S44 – S55. {IUFRO} Conference on Biodiversity in Forest Ecosystems and Landscapes.

Dislich, C., Gunter, S., Homeier, J., Schroder, B. & Huth, A. (2009). Simulating forest dynamics of a tropical montane forest in South Ecuador. *Erdkunde*, 63, 347 – 364.

Dobrowski, S.Z., Swanson, A.K., Abatzoglou, J.T., Holden, Z.A., Safford, H.D., Schwartz, M.K. & Gavin, D.G. (2015). Forest structure and species traits mediate projected recruitment declines in western US tree species. *Global Ecology and Biogeography*, 24, 917–927.

Doyle, T.W. (1981). The Role of Disturbance in the Gap Dynamics of a Montane Rain Forest: An Application of a Tropical Forest Succession Model. In: *Forest Succession: Concepts and Application* (eds. West, D.C., Shugart, H.H. & Botkin, D.B.). Springer New York, New York, NY, pp. 56–73.

Duboz, R., Versmisse, D., Travers, M., Ramat, E. & Shin, Y.J. (2010). Application of an evolutionary algorithm to the inverse parameter estimation of an individual-based model. *Ecological Modelling*, 221, 840–849.

Easterling, M.R., Ellner, S.P. & Dixon, P.M. (2000). Size-Specific Sensitivity: Applying a New Structured Population Model. *Ecology*, 81, 694–708.

Ellison, A.M., Bank, M.S., Clinton, B.D., Colburn, E.A., Elliott, K., Ford, C.R., Foster, D.R., Kloeppel, B.D., Knoepp, J.D., Lovett, G.M., Mohan, J., Orwig, D.A., Rodenhouse, N.L., Sobczak, W.V., Stinson, K.A., Stone, J.K., Swan, C.M., Thompson, J., Von Holle, B. & Webster, J.R. (2005). Loss of foundation species: consequences for the structure and dynamics of forested ecosystems. *Frontiers in Ecology and the Environment*, 3, 479–486.

Ellner, S. & Rees, M. (2006). Integral projection models for species with complex demography. *American Naturalist*, 167, 410–428.

Ennos, R.A. (2015). Resilience of forests to pathogens: an evolutionary ecology perspective. *Forestry*, 88, 41–52.

Enquist, B., Tiffney, B. & Niklas, K. (2007). Metabolic Scaling and the Evolutionary Dynamics of Plant Size, Form, and Diversity: Toward a Synthesis of Ecology, Evolution, and Paleontology. *International Journal of Plant Sciences*, 168, 729–749.

Enquist, B.J. & Niklas, K.J. (2001). Invariant scaling relations across tree-dominated communities. *Nature*, 410, 655–660.

Eschtruth, A.K., Cleavitt, N.L., Battles, J.J., Evans, R.A. & Fahey, T.J. (2006). Vegetation dynamics in declining eastern hemlock stands: 9 years of forest response to hemlock woolly adelgid infestation. *Canadian Journal of Forest Research-Revue Canadienne De Recherche Forestiere*, 36, 1435–1450.

Fajvan, M. & Wood, J. (1996). Stand structure and development after gypsy moth defoliation in the Appalachian Plateau. *Forest Ecology and Management*, 89, 79 – 88.

FAO (2010). Global forest resources assessment 2010. Tech. rep., Food and Agricultural Organization of the United Nations.

Fischer, R., Bohn, F., de Paula, M.D., Dislich, C., Groeneveld, J., Gutiérrez, A.G., Kazmierczak, M., Knapp, N., Lehmann, S., Paulick, S., Pütz, S., Rödig, E., Taubert, F., Köhler, P. & Huth, A. (2016). Lessons learned from applying a forest gap model to understand ecosystem and carbon dynamics of complex tropical forests. *Ecological Modelling*, 326, 124 – 133.

Foley, J.A., Prentice, I.C., Ramankutty, N., Levis, S., Pollard, D., Sitch, S. & Haxeltine, A. (1996). An integrated biosphere model of land surface processes, terrestrial carbon balance, and vegetation dynamics. *Global Biogeochemical Cycles*, 10, 603–628.

Ford, C.R., Elliott, K.J., Clinton, B.D., Kloeppel, B.D. & Vose, J.M. (2012). Forest dynamics following eastern hemlock mortality in the southern Appalachians. *Oikos*, 121, 523–536.

Foster, R.B. & Brokaw, N.V. (1982). Structure and history of the vegetation of Barro Colorado Island. In: *The Ecology of a Tropical Forest: Seasonal Rhythms and Long-Term Changes* (eds. Leigh, E.G., Rand, A.S. & Windsor, D.M.). Smithsonian Institution Press, Washington, D.C., pp. 67–81.

Frelich, L.E., Calcote, R.R., Davis, M.B. & Pastor, J. (1993). Patch Formation and Maintenance in an Old-Growth Hemlock-Hardwood Forest. *Ecology*, 74, 513–527.

Frelich, L.E. & Reich, P.B. (1995). Spatial Patterns and Succession in a Minnesota Southern-Boreal Forest. *Ecological Monographs*, 65, 325–346.

French, J. (2014). *SpatialTools: Tools for spatial data analysis*. R package version 0.5.8.

Friedlingstein, P., Cox, P., Betts, R., Bopp, L., Bloh, W.V., Brovkin, V., Cadule, P., Doney, S., Eby, M., Fung, I., Bala, G., John, J., Jones, C., Joos, F., Kato, T., Kawamiya, M., Knorr, W., Lindsay, K., Matthews, H.D., Raddatz, T., Rayner, P., Reick, C., Roeckner, E., Schnitzler, K.G., Schnur, R., Strassmann, K., Weaver, A.J., Yoshikawa, C. & Zeng, N. (2006). Climate-carbon cycle feedback analysis: Results from the (CMIP)-M-4 model intercomparison. *Journal of Climate*, 19, 3337–3353.

Friend, A.D., Lucht, W., Rademacher, T.T., Keribin, R., Betts, R., Cadule, P., Ciais, P., Clark, D.B., Dankers, R., Falloon, P.D., Ito, A., Kahana, R., Kleidon, A., Lomas, M.R., Nishina, K., Ostberg, S., Pavlick, R., Peylin, P., Schaphoff, S., Vuichard, N., Warszawski, L., Wiltshire, A. & Woodward, F.I. (2014). Carbon residence time dominates uncertainty in terrestrial vegetation responses to future climate and atmospheric CO_2. *Proceedings of the National Academy of Sciences*, 111, 3280–3285.

Friend, A.D. & White, A. (2000). Evaluation and analysis of a dynamic terrestrial ecosystem model under preindustrial conditions at the global scale. *Global Biogeochemical Cycles*, 14, 1173–1190.

Galbraith, D., Levy, P.E., Sitch, S., Huntingford, C., Cox, P., Williams, M. & Meir, P. (2010). Multiple mechanisms of Amazonian forest biomass losses in three dynamic global vegetation models under climate change. *New Phytologist*, 187, 647–665.

Gelman, A., Carlin, J., Stern, H., Dunson, D., Vehtari, A. & Rubin, D. (2013). *Bayesian Data Analysis*. 3rd edn. Chapman and Hall/CRC, Boca Raton.

Gelman, A. & Hill, J. (2007). *Data analysis using regression and multi-level/hierarchical models*. Cambridge University Press, New York.

Gibson, L., Lee, T.M., Koh, L.P., Brook, B.W., Gardner, T.A., Barlow, J., Peres, C.A., Bradshaw, C.J.A., Laurance, W.F., Lovejoy, T.E. & Sodhi, N.S. (2011). Primary forests are irreplaceable for sustaining tropical biodiversity. *Nature*, 478, 378–381.

González, E.J. & Martorell, C. (2013). Reconstructing shifts in vital rates driven by long-term environmental change: a new demographic method based on readily available data. *Ecology and Evolution*, 3, 2273–2284.

González, E.J., Martorell, C. & Bolker, B.M. (2016). Inverse estimation of integral projection model parameters using time series of population-level data. *Methods in Ecology and Evolution*, 7, 147–156.

Grimm, V. & Railsback, S.F. (2005). *Individual-based Modeling and Ecology*. Princeton University Press, Princeton, NJ.

Gross, A., Holdenrieder, O., Pautasso, M., Queloz, V. & Sieber, T.N. (2014). *Hymenoscyphus pseudoalbidus*, the causal agent of European ash dieback. *Molecular Plant Pathology*, 15, 5–21.

Grote, S., Condit, R., Hubbell, S., Wirth, C. & Rüger, N. (2013). Response of Demographic Rates of Tropical Trees to Light Availability: Can Position-Based Competition Indices Replace Information from Canopy Census Data? *PLoS One*, 8.

Hansen, M.C., Potapov, P.V., Moore, R., Hancher, M., Turubanova, S.A., Tyukavina, A., Thau, D., Stehman, S.V., Goetz, S.J., Loveland, T.R., Kommareddy, A., Egorov, A., Chini, L., Justice, C.O. & Townshend, J.R.G. (2013). High-Resolution Global Maps of 21st-Century Forest Cover Change. *Science*, 342, 850–853.

Hartig, F., Calabrese, J.M., Reineking, B., Wiegand, T. & Huth, A. (2011). Statistical inference for stochastic simulation models - theory and application. *Ecology Letters*, 14, 816–827.

Hartig, F., Dislich, C., Wiegand, T. & Huth, A. (2014). Technical Note: Approximate Bayesian parameterization of a process-based tropical forest model. *Biogeosciences*, 11, 1261–1272.

Hartig, F., Dyke, J., Hickler, T., Higgins, S.I., O'Hara, R.B., Scheiter, S. & Huth, A. (2012). Connecting dynamic vegetation models to data - an inverse perspective. *Journal of Biogeography*, 39, 2240–2252.

Hastings, W.K. (1970). Monte Carlo Sampling Methods Using Markov Chains and Their Applications. *Biometrika*, 57, 97–109.

Hicke, J.A., Allen, C.D., Desai, A.R., Dietze, M.C., Hall, R.J., (Ted) Hogg, E.H., Kashian, D.M., Moore, D., Raffa, K.F., Sturrock, R.N. & Vogelmann, J. (2012). Effects of biotic disturbances on forest carbon cycling in the United States and Canada. *Global Change Biology*, 18, 7–34.

Hubbell, S., Foster, R., O'Brien, S., Harms, K., Condit, R., Wechsler, B., Wright, S. & de Lao, S. (1999). Light-gap disturbances, recruitment limitation, and tree diversity in a neotropical forest. *Science*, 283, 554–557.

Hubbell, S.P. & Foster, R.B. (1983). Diversity of canopy trees in a neotropical forest and implications for conservation. In: *Tropical rain forest: ecology and management* (eds. Sutton, S.L., Whitmore, T.C. & Chadwick, A.C.). Blackwell Scientific, Oxford, UK, pp. 25–41.

Hulshof, C. & Swenson, N. (2010). Variation in Leaf Functional Trait Values within and across Individuals and Species: An Example from a Costa Rican Dry Forest. *Functional Ecology*, 24, 217–223.

Hurtt, G., Frolking, S., Fearon, M., Moore, B., Shevliakova, E., Malyshev, S., Pacala, S. & Houghton, R. (2006). The underpinnings of land-use history: three centuries of global gridded land-use transitions, wood-harvest activity, and resulting secondary lands. *Global Change Biology*, 12, 1208–1229.

Hurtt, G.C., Moorcroft, P.R., Pacala, S.W. & Levin, S.A. (1998). Terrestrial models and global change: challenges for the future. *Global Change Biology*, 4, 581–590.

Husheer, S.W., Coomes, D.A. & Robertson, A.W. (2003). Long-term influences of introduced deer on the composition and structure of New Zealand Nothofagus forests. *Forest Ecology and Management*, 181, 99 – 117.

Huth, A., Ditzer, T. & Bossel, H. (1998). *The Rain Forest Growth Model FORMIX3 - Model Description and Analysis of Forest Growth and Logging Scenarios for the Deramakot Forest Reserve (Malaysia).* Erich Goltze Publishers, Göttingen.

Hérault, B., Bachelot, B., Poorter, L., Rossi, V., Bongers, F., Chave, J., Paine, C.E.T., Wagner, F. & Baraloto, C. (2011). Functional traits shape ontogenetic growth trajectories of rain forest tree species. *Journal of Ecology*, 99, 1431–1440.

Iida, Y., Kohyama, T.S., Swenson, N.G., Su, S.H., Chen, C.T., Chiang, J.M. & Sun, I.F. (2014). Linking functional traits and demographic rates in a subtropical tree community: the importance of size dependency. *Journal of Ecology*, 102, 641–650.

Ishihara, M.I., Konno, Y., Umeki, K., Ohno, Y. & Kikuzawa, K. (2016). A New Model for Size-Dependent Tree Growth in Forests. *PLoS ONE*, 11, 1–18.

Jactel, H., Petit, J., Desprez-Loustau, M.L., Delzon, S., Piou, D., Battisti, A. & Koricheva, J. (2012). Drought effects on damage by forest insects and pathogens: a meta-analysis. *Global Change Biology*, 18, 267–276.

Janik, D., Adam, D., Vrska, T., Hort, L., Unar, P., Kral, K., Samonil, P. & Horal, D. (2008). Tree layer dynamics of the Cahnov–Soutok near-natural floodplain forest after 33 years (1973–2006). *European Journal of Forest Research*, 127, 337–345.

Jepsen, J.U., Hagen, S.B., Ims, R.A. & Yoccoz, N.G. (2008). Climate change and outbreaks of the geometrids *Operophtera brumata* and *Epirrita autumnata* in subarctic birch forest: evidence of a recent outbreak range expansion. *Journal of Animal Ecology*, 77, 257–264.

Jönsson, M.T. & Thor, G. (2012). Estimating Coextinction Risks from Epidemic Tree Death: Affiliate Lichen Communities among Diseased Host Tree Populations of *Fraxinus excelsior*. *Plos One*, 7.

Jorritsma, I., van Hees, A. & Mohren, G. (1999). Forest development in relation to ungulate grazing: a modeling approach. *Forest Ecology and Management*, 120, 23 – 34.

Jung, V., Violle, C., Mondy, C., Hoffmann, L. & Muller, S. (2010). Intraspecific variability and trait-based community assembly. *Journal of Ecology*, 98, 1134–1140.

Keenan, R., Reams, G.A., Achard, F., de Freitas, J., Grainger, A. & Lindquist, E. (2015). Dynamics of global forest area: Results from the FAO Global Forest Resources Assessment 2015. *Forest Ecology and Management*, 352, 9–20.

Keßler, M., Cech, T., Brandstetter, M. & Kirisits, T. (2012). Dieback of ash (*Fraxinus excelsior* and *Fraxinus angustifolia*) in Eastern Austria: Disease development on monitoring plots from 2007 to 2010. *Journal of Agricultural Extension and Rural Development*, 4, 223–226.

Kienast, F., Fritschi, J., Bissegger, M. & Abderhalden, W. (1999). Modeling successional patterns of high-elevation forests under changing herbivore pressure–responses at the landscape level. *Forest Ecology and Management*, 120, 35 – 46.

King, A., Post, W. & Wullschleger, S. (1997). The potential response of terrestrial carbon storage to changes in climate and atmospheric CO_2. *Climatic Change*, 35, 199–227.

King, K. & Lively, C. (2012). Does genetic diversity limit disease spread in natural host populations? *Heredity*, 109, 199–203.

Kirby, K.J., Bazely, D.R., Goldberg, E.A., Hall, J.E., Isted, R., Perry, S.C. & Thomas, R.C. (2014). Changes in the tree and shrub layer of Wytham Woods (Southern England): local and national trends compared. *Forestry*, 87, 663–673.

Kirisits, T. & Freinschlag, C. (2012). Ash dieback caused by *Hymenoscyphus pseudoalbidus* in a seed plantation of *Fraxinus excelsior* in Austria. *Journal of Agricultural Extension and Rural Development*, 4, 184–191.

Kjær, E.D., McKinney, L.V., Nielsen, L.R., Hansen, L.N. & Hansen, J.K. (2012). Adaptive potential of ash (*Fraxinus excelsior*) populations against the novel emerging pathogen *Hymenoscyphus pseudoalbidus*. *Evolutionary Applications*, 5, 219–228.

Kneeshaw, D. & Bergeron, Y. (1998). Canopy Gap Characteristics and Tree Replacement in the Southeastern Boreal Forest. *Ecology*, 79, 783–794.

Köhler, P. & Huth, A. (1998). The effects of tree species grouping in tropical rain forest modelling - simulations with the individual based model FORMIND. *Ecological Modelling*, 109, 301–321.

Kolbe, A.E., Buongiorno, J. & Vasievich, M. (1999). Geographic extension of an uneven-aged, multi-species matrix growth model for northern hardwood forests. *Ecological Modelling*, 121, 235 – 253.

Kraft, N., Crutsinger, G.M., Forrestel, E.J. & Emery, N. (2014). Functional trait differences and the outcome of community assembly: an experimental test with vernal pool annual plants. *Oikos*, 123, 1391–1399.

Kraft, N., Valencia, R. & Ackerly, D. (2008). Functional Traits and Niche-Based Tree Community Assembly in an Amazonian Forest. *Science*, 322, 580–582.

Kramer, K., Bruinderink, G.G. & Prins, H. (2006). Spatial interactions between ungulate herbivory and forest management. *Forest Ecology and Management*, 226, 238 – 247.

Kurz, W.A., Dymond, C.C., Stinson, G., Ramply, G.J., Neilson, E.T., Carroll, A.T., Ebata, T. & Safranyik, L. (2008). Mountain pine beetle and forest carbon feedback to climate change. *Nature*, 452, 987–90.

Lasky, J.R., Yang, J., Zhang, G., Cao, M., Tang, Y. & Keitt, T.H. (2014). The role of functional traits and individual variation in the co-occurrence of Ficus species. *Ecology*, 95, 978–990.

Lee, H., Davies, S., LaFrankie, J., Tan, S., Itoh, A., Yamakura, T. & Ashton, P. (2002). Floristic and structural diversity of 52 hectares of mixed diptrocarp forest in Lambir Hills National Park, Sarawak, Malaysia. *Journal of Tropical Forest Science*, 14, 379–400.

Leigh, E. (1999). *Tropical forest ecology: a view from Barro Colorado Island*. Oxford University Press, Oxford, UK.

Leigh, E.G.J., Rand, S.A. & Windsor, D.M. (1982). *The Ecology of a Tropical Forest: Seasonal Rhythms and Long-Term Changes*. Smithsonian Institution Press, Washington, D.C.

Lemoine, D., Peltier, J.P. & Marigo, G. (2001). Comparative studies of the water relations and the hydraulic characteristics in *Fraxinus excelsior*, *Acer pseudoplatanus* and *A. opalus* trees under soil water contrasted conditions. *Ann. For. Sci.*, 58, 723–731.

Liang, N., Tang, Y. & Okuda, T. (2001). Is elevation of carbon dioxide concentration beneficial to seedling photosynthesis in the understory of tropical rain forests? *Tree Physiology*, 21, 1047–1055.

Lichstein, J.W., Dushoff, J., Ogle, K., Chen, A., Purves, D.W., Caspersen, J.P. & Pacala, S.W. (2010). Unlocking the forest inventory data: relating individual tree performance to unmeasured environmental factors. *Ecological Applications*, 20, 684–699.

Lim, T.K. (2012). *Edible Medicinal and Non-Medicinal Plants*, Springer, Netherlands, vol. 2, chap. 9, pp. 62–65.

Lines, E.R., Coomes, D.A. & Purves, D.W. (2010). Influences of Forest Structure, Climate and Species Composition on Tree Mortality across the Eastern US. *PLoS ONE*, 5, 1–12.

Logan, J.A. & Powell, J.A. (2001). Ghost forest, global warming and the mountain pine beetle (coleoptera: Scolyttidae). *American entomologist*, 47, 160–173.

Loo, J.A. (2009). Ecological impacts of non-indigenous invasive fungi as forest pathogens. *Biological Invasions*, 11, 81–96.

Lygis, V., Bakys, R., Gustiene, A., Burokiene, D., Matelis, A. & Vasaitis, R. (2014). Forest self-regeneration following clear-felling of dieback-affected *Fraxinus excelsior*: focus on ash. *European Journal of Forest Research*, 133, 501–510.

Malhi, Y., Phillips, O., Lloyd, J., Baker, T., Wright, J., Almeida, S., Arroyo, L., Frederiksen, T., Grace, J., Higuchi, N., Killeen, T., Laurance, W., Leaño, C., Lewis, S., Meir, P., Monteagudo, A., Neill, D., Núñez Vargas, P., Panfil, S., Patiño, S., Pitman, N., Quesada, C., Rudas-Ll., A., Salomão, R., Saleska, S., Silva, N., Silveira, M., Sombroek, W., Valencia, R., Vásquez Martínez, R., Vieira, I. & Vinceti, B. (2002). An international network to monitor the structure, composition and dynamics of Amazonian forests (RAINFOR). *Journal of Vegetation Science*, 13, 439–450.

Martínez, I., Wiegand, T., Julio Camarero, J., Batllori, E. & Gutiérrez, E. (2011). Disentangling the Formation of Contrasting Tree-Line Physiognomies Combining Model Selection and Bayesian Parameterization for Simulation Models. *The American Naturalist*, 177, E136–E152.

McGill, B.J., Enquist, B.J., Weiher, E. & Westoby, M. (2006). Rebuilding community ecology from functional traits. *Trends in Ecology & Evolution*, 21, 178 – 185.

McKinney, L.V., Nielsen, L.R., Collinge, D.B., Thomsen, I.M., Hansen, J.K. & Kjær, E.D. (2014). The ash dieback crisis: genetic variation in resistance can prove a long-term solution. *Plant Pathology*, 63, 485–499.

McKinney, L.V., Thomsen, I.M., Kjaer, E.D., Bengtsson, S.B.K. & Nielsen, L.R. (2012). Rapid invasion by an aggressive pathogenic fungus (*Hymenoscyphus pseudoalbidus*) replaces a native decomposer (*Hymenoscyphus albidus*): a case of local cryptic extinction? *Fungal Ecology*, 5, 663–669.

McMahon, S.M., Metcalf, C.J.E. & Woodall, C.W. (2011). High-Dimensional Coexistence of Temperate Tree Species: Functional Traits, Demographic Rates, Life-History Stages, and Their Physical Context. *PLoS ONE*, 6, 1–11.

McRoberts, R.E., Bechtold, W.A., Patterson, P.L., Scott, C.T. & Reams, G.A. (2005). The Enhanced Forest Inventory and Analysis Program of the USDA Forest Service: Historical Perspective and Announcement of Statistical Documentation. *Journal of Forestry*, 103, 304–308.

Medvigy, D., Wofsy, S.C., Munger, J.W. & Moorcroft, P.R. (2010). Responses of terrestrial ecosystems and carbon budgets to current and future environmental variability. *Proceedings of the National Academy of Sciences*, 107, 8275–8280.

Merow, C., Dahlgren, J.P., Metcalf, C.J., Childs, D.Z., Evans, M.E.K., Jongejans, E., Record, S., Rees, M., Salguero-Gómez, R. & McMahon, M. (2014a). Advancing

population ecology with integral projection models: a practical guide. *Methods in Ecology and Evolution*, 5, 99–110.

Merow, C., Latimer, A.M., Wilson, A.M., McMahon, S.M., Rebelo, A.G. & Silander, J.A. (2014b). On using integral projection models to generate demographically driven predictions of species' distributions: development and validation using sparse data. *Ecography*, 37, 1167–1183.

Metcalf, C.J.E., Horvitz, C.C., Tuljapurkar, S. & Clark, D.A. (2009). A time to grow and a time to die: a new way to analyze the dynamics of size, light, age, and death of tropical trees. *Ecology*, 90, 2766–2778.

Millennium Ecosystem Assessment (2005). Ecosystems and human well-being: Biodiversity synthesis. Tech. rep., Washington, DC.

Mitchell, R., Beaton, J., Bellamy, P., Broome, A., Chetcuti, J., Eaton, S., Ellis, C., Gimona, A., Harmer, R., Hester, A., Hewison, R., Hodgetts, N., Iason, G., Kerr, G., Littlewood, N., Newey, S., Potts, J., Pozsgai, G., Ray, D., Sim, D., Stockan, J., Taylor, A. & Woodward, S. (2014). Ash dieback in the UK: A review of the ecological and conservation implications and potential management options. *Biological Conservation*, 175, 95 – 109.

Moorcroft, P.R. (2006). How close are we to a predictive science of the biosphere? *Trends in Ecology & Evolution*, 21, 400 – 407.

Moorcroft, P.R., Hurtt, G.C. & Pacala, S.W. (2001). A method for scaling vegetation dynamics: the ecosystem demography model (ED). *Ecological Monographs*, 71, 557–586.

Morecroft, M., Taylor, M., Ellwood, S. & Quinn, S. (2001). Impacts of deer herbivory on ground vegetation at Wytham Woods, central England. *Forestry*, 74, 251–257.

Morecroft, M.D., Stokes, V.J., Taylor, M.E. & Morison, J.I. (2008). Effects of climate and management history on the distribution and growth of sycamore (*Acer pseudoplatanus* l.) in a southern British woodland in comparison to native competitors. *Forestry*, 81, 59–74.

Morris, W.F. & Doak, D.F. (2002). *Quantitative Conservation Biology: Theory and Practice of Population Viability Analysis*. Sinauer Associates Inc., US.

Murphy, J., Sexton, D., Jenkins, G., Boorman, P., Booth, B., Brown, C., Clark, R., Collins, M., Harris, G., Kendon, E., Betts, R., Brown, S., Howard, T., Humphrey, K., McMarthy, M., McDonald R.and Stephens, A., Wallace, C., Warren, R., Wilby, R. &

Wood, R. (2009). UK climate projections science report: Climate change projections. Tech. rep., Met Office Hadley Centre, Exeter, UK.

Nakashizuka, T. (2001). Species coexistence in temperate, mixed deciduous forests. *Trends in Ecology & Evolution*, 16, 205 – 210.

National Forest Inventory, F.C. (2012). NFI preliminary estimates of quantities of broadleaved species in British woodlands, with special focus on ash. Tech. rep.

Needham, J., Merow, C., Butt, N., Malhi, Y., Marthews, T.R., Morecroft, M. & McMahon, S.M. (2016). Forest community response to invasive pathogens: the case of ash dieback in a British woodland. *Journal of Ecology*, 104, 315–330.

Obrien, S., Hubbell, S., Spriro, P., Condit, R. & Foster, R. (1995). Diameter, Height, Crown and Age-Relationships in 8 Neotropical Tree Species. *Ecology*, 76, 1926–1939.

Pacala, S.W., Canham, C.D., Saponara, J., Silander, J.A., Kobe, R.K. & Ribbens, E. (1996). Forest Models Defined by Field Measurements: Estimation, Error Analysis and Dynamics. *Ecological Monographs*, 66, 1–43.

Pacala, S.W., Canham, C.D. & Silander-Jr., J.A. (1993). Forest models defined by field measurements: I. The design of a northeastern forest simulator. *Canadian Journal of Forest Research*, 23, 1980–1988.

Paine, C.E.T., Amissah, L., Auge, H., Baraloto, C., Baruffol, M., Bourland, N., Bruelheide, H., Daïnou, K., de Gouvenain, R.C., Doucet, J.L., Doust, S., Fine, P.V.A., Fortunel, C., Haase, J., Holl, K.D., Jactel, H., Li, X., Kitajima, K., Koricheva, J., Martínez-Garza, C., Messier, C., Paquette, A., Philipson, C., Piotto, D., Poorter, L., Posada, J.M., Potvin, C., Rainio, K., Russo, S.E., Ruiz-Jaen, M., Scherer-Lorenzen, M., Webb, C.O., Wright, S.J., Zahawi, R.A. & Hector, A. (2015). Globally, functional traits are weak predictors of juvenile tree growth, and we do not know why. *Journal of Ecology*, 103, 978–989.

Paine, C.E.T., Baraloto, C., Chave, J. & Hérault, B. (2011). Functional traits of individual trees reveal ecological constraints on community assembly in tropical rain forests. *Oikos*, 120, 720–727.

Pautasso, M., Aas, G., Queloz, V. & Holdenrieder, O. (2013). European ash (*Fraxinus excelsior*) dieback – a conservation biology challenge. *Biological Conservation*, 158, 37–49.

Pavlick, R., Drewry, D.T., Bohn, K., Reu, B. & Kleidon, A. (2013). The Jena Diversity-Dynamic Global Vegetation Model (JeDi-DGVM): a diverse approach to representing terrestrial biogeography and biogeochemistry based on plant functional trade-offs. *Biogeosciences*, 10, 4137–4177.

Payandeh, B. & Papadopol, P. (1994). Partial Calibration of "ONTWIGS": A Forest Growth and Yield Projection System Adapted for Ontario. *Northern Journal of Applied Forestry*, 11, 41–46.

Paz, H., Mazer, S.J. & Martinez-Ramos, M. (2005). Comparative Ecology of Seed Mass in *Psychotria* (Rubiaceae): Within- and between-Species Effects of Seed Mass on Early Performance. *Functional Ecology*, 19, 707–718.

Perrins, C. & Overall, R. (2001). Effect of increasing numbers of deer on bird populations in Wytham Woods, central England. *Forestry*, 74, 299–309.

Peterken, G. & Mountford, E. (1998). Long-Term Change in an Unmanaged Population of Wych Elm Subjected to Dutch Elm Disease. *Journal of Ecology*, 86, 205–218.

Peterken, G.P. & Jones, E.W. (1987). Forty Years of Change in Lady Park Wood: The Old-Growth Stands. *Journal of Ecology*, 75, 477–512.

Pfister, C. & Wang, M. (2005). Beyond size: Matrix projection models for populations where size is an incomplete descriptor. *Ecology*, 86, 2673–2683.

Picard, N., Bar-Hen, A. & Guedon, Y. (2003). Modelling diameter class distribution with a second-order matrix model. *Forest Ecology and Management*, 180, 389–400.

Pliura, A., Lygis, V., Suchockas, V. & Bartkevicius, E. (2011). Performance of twenty four European *Fraxinus excelsior* populations in three Lithuanian progeny trials with a special emphasis on resistance to *Chalara fraxinea*. *Baltic Forestry*, 17, 17–34.

Poorter, L. & Bongers, F. (2006). Leaf traits are good predictors of plant performance across 53 rain forest species. *Ecology*, 87, 1733–1743.

Poorter, L., Bongers, L. & Bongers, F. (2006). Architecture of 54 moist-forest tree species: Traits, trade-offs, and functional groups. *Ecology*, 87, 1289–1301.

Poorter, L., Wright, S.J., Paz, H., Ackerly, D.D., Condit, R., Ibarra-Manríquez, G., Harms, K.E., Licona, J.C., Martínez-Ramos, M., Mazer, S.J., Muller-Landau, H.C., Peña-Claros, M., Webb, C.O. & Wright, I.J. (2008). Are functional traits good predictors of demographic rates? evidence from five neotropical forests. *Ecology*, 89, 1908–1920.

Powers, J. & Tiffin, P. (2010). Plant functional type classifications in tropical dry forests in Costa Rica: leaf habit versus taxonomic approaches. *Functional Ecology*, 24, 927–936.

Prentice, I. & Leemans, R. (1990). Pattern and Process and the Dynamics of Forest Structure: A Simulation Approach. *Journal of Ecology*, 78, 340–355.

Przybyl, K. (2002). Fungi associated with necrotic apical parts of *Fraxinus excelsior* shoots. *Forest Pathology*, 32, 387–394.

Purves, D. & Pacala, S. (2008). Predictive Models of Forest Dynamics. *Science*, 320, 1452–1453.

Purves, D.W. (2009). The demography of range boundaries versus range cores in eastern US tree species. *Proceedings of the Royal Society of London B: Biological Sciences*, 276, 1477–1484.

Purves, D.W., Lichstein, J.W. & Pacala, S.W. (2007). Crown Plasticity and Competition for Canopy Space: A New Spatially Implicit Model Parameterized for 250 North American Tree Species. *PlosOne*, 2.

Purves, D.W., Lichstein, J.W., Strigul, N. & Pacala, S.W. (2008). Predicting and understanding forest dynamics using a simple tractable model. *Proceedings of the National Academy of Sciences*, 105, 17018–17022.

Putman, R., Edwards, P., Mann, J., How, R. & Hill, S. (1989). Vegetational and faunal changes in an area of heavily grazed woodland following relief of grazing. *Biological Conservation*, 47, 13 – 32.

R Core Team (2014). *R: A Language and Environment for Statistical Computing*. R Foundation for Statistical Computing, Vienna, Austria.

Rawal, D.S., Kasel, S., Keatley, M.R. & Nitschke, C.R. (2015). Environmental effects on germination phenology of co-occurring eucalypts: implications for regeneration under climate change. *International Journal of Biometeorology*, 59, 1237–1252.

Reyer, C.P.O., Brouwers, N., Rammig, A., Brook, B.W., Epila, J., Grant, R.F., Holmgren, M., Langerwisch, F., Leuzinger, S., Lucht, W., Medlyn, B., Pfeifer, M., Steinkamp, J., Vanderwel, M.C., Verbeeck, H. & Villela, D.M. (2015). Forest resilience and tipping points at different spatio-temporal scales: approaches and challenges. *Journal of Ecology*, 103, 5–15.

Rooney, T.P. & Waller, D.M. (2003). Direct and indirect effects of white-tailed deer in forest ecosystems. *Forest Ecology and Management*, 181, 165 – 176.

Rüger, N., Berger, U., Hubbell, S.P., Vieilledent, G. & Condit, R. (2011). Growth Strategies of Tropical Species: Disentangling Light and Size Effects. *PLoS One*, 6.

Rüger, N. & Condit, R. (2012). Testing metabolic theory with models of tree growth that include light competition. *Functional Ecology*, 26, 759–765.

Russo, S.E., Davies, S., King, D.A. & Tan, S. (2005). Soil-Related Performance Variation and Distributions of Tree Species in a Bornean Rain Forest. *Journal of Ecology*, 93, 879–889.

Sage, R.W., Porter, W.F. & Underwood, H.B. (2003). Windows of opportunity: white-tailed deer and the dynamics of northern hardwood forests of the northeastern US. *Journal for Nature Conservation*, 10, 213 – 220.

Savill, P., Perrins, C., Kirby, K. & Fisher, N. (2010). *Wytham Woods: Oxford's Ecological Laboratory*. Oxford University Press, Oxford.

Schaphoff, S., Heyder, U., Ostberg, S., Gerten, D., Heinke, J. & Lucht, W. (2013). Contribution of permafrost soils to the global carbon budget. *Environmental Research Letters*, 8, 014026.

Seconca, C. & Leisse, N. (1994). Significance of bark beetles Coleoptera Scolytidae in the spread of Dutch elm disease in the area Euskirchen West Germany. *Zeitschrift Angewandte Entomologie*, 98, 413 – 423.

Sitch, S., Huntingford, C., Gedney, N., Levy, P.E., Lomas, M., Piao, S.L., Betts, R., Ciasis, P., Cox, P., Friedlingstein, P., Jones, C.D., Prentice, I.C. & Woodward, F.I. (2008). Evaluation of the terrestrial carbon cycle, future plant geography and climate-carbon cycle feedbacks using five Dynamic Global Vegetation Models (DGVMs). *Global Change Biology*, 14, 2015–2039.

Sitch, S., Smith, B., Prentice, I.C., Arneth, A., Bondeau, A., Cramer, W., Kaplan, J.O., Levis, S., Lucht, W., Sykes, M.T., Thonicke, K. & Venevsky, S. (2003). Evaluation of ecosystem dynamics, plant geography and terrestrial carbon cycling in the LPJ dynamic global vegetation model. *Global Change Biology*, 9, 161–185.

Smith, W. (2002). Forest inventory and analysis: a national inventory and monitoring program. *Environmental Pollution*, 116, Supplement 1, S233 – S242.

Solomon, A.M. (1986). Transient Response of Forests to CO2-Induced Climate Change: Simulation Modeling Experiments in Eastern North America. *Oecologia*, 68, 567–579.

Stark, S.C., Enquist, B.J., Saleska, S.R., Leitold, V., Schietti, J., Longo, M., Alves, L.F., Camargo, P.B. & Oliveira, R.C. (2015). Linking canopy leaf area and light environments with tree size distributions to explain Amazon forest demography. *Ecology Letters*, 18, 636–645.

Strigul, N., Pristinski, D., Purves, D., Dushoff, J. & Pacala, S. (2008). Scaling from trees to forests: Tractable macroscopic equations for forest dynamics. *Ecological Monographs*, 78, 523–545.

Tingley, M.W., Orwig, D.A., Field, R. & Motzkin, G. (2002). Avian response to removal of a forest dominant: consequences of hemlock woolly adelgid infestations. *Journal of Biogeography*, 29, 1505–1516.

Tissier, J., Lambs, L., Peltier, J.P. & Marigo, G. (2004). Relationships between hydraulic traits and habitat preference for six *Acer* species occurring in the French Alps. *Ann. For. Sci.*, 61, 81–86.

Tomppo, E., Geschwantner, T., Lawrence, M. & McRoberts, R. (eds.) (2010). *National Forest Inventories. Pathways for Common Reporting*. Springer, New York.

Umaña, M.N., Forero-Montana, J., Muscarella, R., Nytch, C.J., Thompson, J., Uriarte, M., Zimmerman, J. & Swenson, N.G. (2016). Interspecific Functional Convergence and Divergence and Intraspecific Negative Density Dependence Underlie the Seed-to-Seedling Transition in Tropical Trees. *The American Naturalist*, 187.

Urban, D., Bonan, G., Smith, T. & Shugart, H. (1991). Modelling Forest Succession in Europe Spatial applications of gap models. *Forest Ecology and Management*, 42, 95 – 110.

Uriarte, M., Swenson, N.G., Chazdon, R.L., Comita, L.S., John Kress, W., Erickson, D., Forero-Montana, J., Zimmerman, J.K. & Thompson, J. (2010). Trait similarity, shared ancestry and the structure of neighbourhood interactions in a subtropical wet forest: implications for community assembly. *Ecology Letters*, 13, 1503–1514.

van der Meer, P. & Bongers, F. (1996). Formation and Closure of Canopy Gaps in the Rain Forest at Nouragues, French Guiana. *Vegetatio*, 126, 167–179.

Van Mantgem, P.J. & Stephenson, N.L. (2007). Apparent climatically induced increase of tree mortality rates in a temperate forest. *Ecology Letters*, 10, 909–916.

Vasaitis, R. & Lygis, V. (2008). Emerging Forest Disease in South-eastern Baltic Sea Region. In: *Network of Climate Change Risks on Forests (ForRisk)*. SNS Workshop, Umea, Sweden, pp. 14–15.

Violle, C., Enquist, B.J., McGill, B.J., Jiang, L., Albert, C.H., Hulshof, C., Jung, V. & Messier, J. (2012). The return of the variance: intraspecific variability in community ecology. *Trends in Ecology & Evolution*, 27, 244 – 252.

Visser, M.D., Bruijning, M., Wright, S.J., Muller-Landau, H.C., Jongejans, E., Comita, L.S. & de Kroon, H. (2016). Functional traits as predictors of vital rates across the life cycle of tropical trees. *Functional Ecology*, 30, 168–180.

Visser, M.D., Jongejans, E., van Breugel, M., Zuidema, P.A., Chen, Y.Y., Kassim, A.R. & de Kroon, H. (2011). Strict mast fruiting for a tropical dipterocarp tree: a demographic cost-benefit analysis of delayed reproduction and seed predation. *Journal of Ecology*, 99, 1033–1044.

von Humboldt, A. (1849). *Aspects of nature, in different lands and different climates; with scientific elucidations*. Philadelphia, Lea and Blanchard, London, UK.

Vrška, T., Adam, D., Hort, L., Kovár, T. & Janĭk, D. (2009). European beech (*Fagus sylvatica* l.) and silver fir (*Abies alba* mill.) rotation in the carpathians—a developmental cycle or a linear trend induced by man? *Forest Ecology and Management*, 258, 347 – 356.

Walck, J.L., Hidayai, S.N., Dixon, K.W., Thompson, K. & Poschold, P. (2011). Climate change and plant regeneration from seed. *Global Change Biology*, 17, 2145–2161.

Waters, T.L. & Savill, P.S. (1992). Ash and Sycamore Regeneration and the Phenomenon of their Alternation. *Forestry*, 65, 417–433.

Weisberg, P.J. & Bugmann, H. (2003). Forest dynamics and ungulate herbivory: from leaf to landscape. *Forest Ecology and Management*, 181, 1 – 12.

Westoby, M., Falster, D.S., Moles, A.T., Vesk, P.A., & Wright, I.J. (2002). Plant Ecological Strategies: Some Leading Dimensions of Variation Between Species. *Annual Review of Ecology and Systematics*, 33, 125–159.

Whitmore, F. (1998). *An Introduction to Tropical Rain Forests*. Oxford University Press, Oxford.

Williams, A., Allen, C.D., Macalady, A.K., Griffin, D., Woodhouse, C.A., Meko, D.M., Swetnam, T.W., Rauscher, S.A., Seager, R., Grissino-Mayer, H.D., Dean, J.S., Cook, E.R., Gangodagamage, C., Cai, M. & McDowell, N.G. (2013). Temperature as a potent driver of regional forest drought stress and tree mortality. *Nature Clim. Change*, 3, 292–297.

Williams, J.L., Miller, T.E.X. & Ellner, S.P. (2012). Avoiding unintentional eviction from integral projection models. *Ecology*, 93, 2008–2014.

Williams, M. (1996). A three-dimensional model of forest development and competition. *Ecological Modelling*, 89, 73 – 98.

Wissel, C. (1992). Modelling the mosaic cycle of a Middle European beech forest. *Ecological Modelling*, 63, 29 – 43.

Wood, S.N. (1987). Inverse problems and structured-population dynamics. In: *Structured-Population Models in marine, Terrestrial, and Freshwater Systems* (eds. Tuljapurkar, S. & Caswell, H.). Chapman and Hall, New York, USA, pp. 555–586.

Woodward, F.I. & Lomas, M.R. (2004). Vegetation dynamics - simulating responses to climatic change. *Biological Reviews*, 79, 643–670.

Zhu, K., Woodall, C.W., Ghosh, S., Gelfand, A.E. & Clark, J.S. (2014). Dual impacts of climate change: forest migration and turnover through life history. *Global Change Biology*, 20, 251–264.

Zuidema, P.A., Brienen, R.J.W., During, H.J. & Gueneralp, B. (2009). Do Persistently Fast-Growing Juveniles Contribute Disproportionately to Population Growth? A New Analysis Tool for Matrix Models and Its Application to Rainforest Trees. *The American Naturalist*, 174, 709–719.

Zuidema, P.A., Jongejans, E., Chien, P.D., During, H.J. & Schieving, F. (2010). Integral Projection Models for trees: a new parameterization method and a validation of model output. *Journal of Ecology*, 98, 345–355.